UNIVERSITÄT BAYREUTH

Nanostructured 3d-Metal Catalysts for the Synthesis of Amines

DISSERTATION

zur Erlangung des akademischen Grades eines
Doktors der Naturwissenschaften (Dr. rer. nat.)
an der Fakultät für Biologie, Chemie und Geowissenschaften
der Universität Bayreuth

vorgelegt von

M. Sc. Matthias Klaus Elfinger

geboren in Dachau

Bayreuth, 2023

Die vorliegende Arbeit wurde in der Zeit von August 2020 bis Juli 2023 in Bayreuth am Lehrstuhl Anorganische Chemie II unter Betreuung von Herrn Professor Dr. Rhett Kempe angefertigt.

Vollständiger Abdruck der von der Fakultät für Biologie, Chemie und Geowissenschaften der Universität Bayreuth genehmigten Dissertation zur Erlangung des akademischen Grades eines Doktors der Naturwissenschaften (Dr. rer. nat.).

Form der Dissertation: Kumulative Dissertation
Dissertation eingereicht am: 28.07.2023
Zulassung durch die Promotionskommission: 23.08.2023
Wissenschaftliches Kolloquium: 12.02.2024

Amtierender Dekan: Prof. Dr. Cyrus Samimi

Prüfungsausschuss:

Prof. Dr. Rhett Kempe (Gutachter)
PD Dr. Günter Motz (Gutachter)
Prof. Dr. Rainer Schobert (Vorsitz)
Prof. Dr. Anna Schenk

Meiner Familie in Dankbarkeit gewidmet.

Table of contents

Abbreviations VI

1 Summary / Zusammenfassung 7

1.2 Zusammenfassung 9

2 Introduction 11

2.1 Heterogeneous earth abundant metal catalysts 11

2.2 Polymer-derived ceramics as N-doped catalyst support materials 12

2.3 Heterogeneous cobalt catalysts for the reductive amination 13

2.4 Borrowing Hydrogen / Hydrogen Autotransfer 16

2.5 References 17

3 Overview of thesis results 20

3.1 Synopsis 20

3.2 Individual Contributions to Joint Publications 33

4 Co-Catalyzed Synthesis of Primary Amines via Reductive Amination employing Hydrogen under very mild Conditions 35

5 Synthesis of Secondary Amines via Borrowing Hydrogen employing a Nanostructured Bimetallic 3d-Metal Catalyst 114

6 General Synthesis of Alkyl Amines via Borrowing Hydrogen and Reductive Amination 145

7 List of Publications 295

8 Acknowledgement 296

9 (Eidesstattliche) Versicherungen und Erklärungen 297

Abbreviations

a. u.	arbitrary units
BET	Brunauer Emmett Teller
BH HA	borrowing hydrogen / hydrogen autotransfer
DMSO	dimethyl sulfoxide
EDX	energy dispersive X-ray
EELS	electron energy loss spectroscopy
EtOH	ethanol
FT- IR	fourier transform infrared spectroscopy
GC	gas chromatography
HAADF	high-angle annular dark-field
HMQC	Heteronuclear Single Quantum Coherence
ICP-OES	inductively coupled plasma optical emission spectroscopy
KOH	potassium hydroxide
LC-HRMS	liquid chromatography-high resolution mass spectrometry
mol%	mole fraction
NMR	nuclear magnetic resonance
NP	nanoparticles
N-SiC	nitrogen-doped silicon carbide material
PDC	polymer derived ceramic
PDF	pair distribution function
ppm	parts per million
PXRD	powder X-ray diffraction
SEM	scanning electron microscopy
SMP-10	polycarbosilane
ss-NMR	solid state-nuclear magnetic resonance
STEM	scanning transmission electron microscopy
TEM	transmission electron microscopy
wt%	weight percent
XPS	X-ray photoelectron spectroscopy
ZIF	zeolithic imidazolate framework

1 Summary / Zusammenfassung

1.1 Summary

This thesis deals with the preparation of heterogeneous, nanostructured and reusable catalysts for the synthesis of amines.

The first part focuses on a cobalt catalyst for the synthesis of primary amines by reductive amination under very mild conditions. This catalyst can outperform commercially available noble metal catalysts at 50 °C and 10 bar hydrogen pressure. In addition, easy-to-handle aqueous ammonia can be used as a nitrogen source. The support material was prepared by a method described in the literature, which involved copolymerizing acrylonitrile and SMP-10, a commercially available silicon rich polycarbosilane precursor. The resulting greenbody was then pyrolyzed under nitrogen atmosphere at 1000 °C and activated via base treatment to acquire the N-SiC support. To obtain the active catalyst, the support was wet impregnated with a nitrogen-rich cobalt salt, and the resulting compound had to be pyrolyzed (700 °C, N_2) and reduced (H_2/N_2, 550 °C). Transmission electron microscopy (TEM) revealed that the cobalt nanoparticles are homogeneously distributed with an average particle size of 5.9 nm. The surface area of the support material (545 m^2/g) as well as the catalyst (491 m^2/g) could be determined by argon physisorption measurements. X-ray photoelectron spectroscopy (XPS) as well as powder X-ray diffraction (PXRD) in combination with pair distribution function (PDF) showed the existence of metallic and oxidic cobalt. A broad substrate scope and very good tolerance of functional groups were observed. The high activity and selectivity of the catalyst is attributable to the unique structure of the support material. It contains free N-H_x functionalities in the pores, which could be detected by solid-state nuclear magnetic resonance (ss-NMR) spectroscopy.

The second part of the thesis deals with the further development of the previous cobalt catalyst in order to expand its application area to different reaction pathways. By combining cobalt and scandium on N-SiC following the already established procedure, a new catalyst could be described to mediate the borrowing hydrogen or hydrogen autotransfer (BH HA) reaction of benzyl alcohols and aniline derivatives. In this reaction, the benzyl alcohol is dehydrogenated while the obtained hydrogen is stored on the catalyst. In the second reaction step, the aniline or one of its derivatives condenses with the carbonyl compound to form the corresponding secondary imine, which is hydrogenated using the previously stored hydrogen. In contrast to reductive amination, no additional hydrogen gas is required for this reaction. The catalyst is so active that only 0.5 equivalents of potassium hydroxide are required for complete conversion. The reaction conditions could be adjusted to

1.0 mol% Co, 0.33 mol% Sc, 24 h and a temperature range of 120 - 140 °C to synthesize 13 differently substituted secondary amines.

The last part combines the two previous reactions to one complex amine synthesis approach with a single catalyst. By switching the aniline derivative to gaseous ammonia, primary amines could be formed starting from abundantly available alcohols. By utilizing the ability of the bimetallic Co/Sc catalyst presented above to mediate BH HA and reductive amination, additional reaction steps could be added to generate more complex secondary and tertiary amines. The reaction proceeds sequentially without the need for intervening purification steps. Characterization of the catalyst by scanning transmission electron microscopy combined with high-angle annular dark-field imaging (HAADF-STEM) revealed homogeneously distributed Co nanoparticles with an average diameter of 13.9 nm. The Sc particles are orders of magnitude smaller and finely distributed over the support material, as shown by electron energy loss spectroscopy (EELS). Comparing the signal regions of the Co 2p and Sc 2s regions determined by XPS, it can be seen that the Sc fraction is ten times higher than the Co fraction, albeit the same concentration is expected from the catalyst preparation. Since XPS is a surface method, this indicates that Sc is finely dispersed on the outer layer, while Co is present in the form of larger particles. This observation is consistent with the results from STEM-EELS. Employing the catalyst, a substrate scope consisting of 13 primary, 24 secondary, and eight tertiary amines was established, with five of the latter not known in the literature at the time of synthesis.

1.2 Zusammenfassung

Diese Arbeit befasst sich mit der Herstellung von heterogenen, nanostrukturierten und wiederverwendbaren Katalysatoren für die Synthese von Aminen.
Der erste Teil konzentriert sich auf einen Kobaltkatalysator für die Synthese von primären Aminen durch reduktive Aminierung unter sehr milden Bedingungen. Dieser Katalysator kann bei 50 °C und 10 bar Wasserstoffdruck die Selektivität kommerzieller Edelmetallkatalysatoren übertreffen und mit einfach handhabbarem wässrigem Ammoniak als Stickstoffquelle arbeiten. Das Trägermaterial wurde nach einer in der Literatur beschriebenen Methode hergestellt, bei der Acrylnitril und SMP-10, ein handelsüblicher siliziumreicher Polycarbosilan-Präkursor, copolymerisiert wurden. Der resultierende Grünkörper wurde unter Stickstoffatmosphäre bei 1000 °C pyrolysiert und durch Basenbehandlung aktiviert, um den N-SiC-Träger zu generieren. Um den aktiven Katalysator zu erhalten, wurde der Träger mit einem stickstoffreichen Kobaltsalz nass imprägniert und anschließend pyrolysiert (700 °C, N_2) und reduziert (H_2/N_2, 550 °C). Die Transmissionselektronenmikroskopie (TEM) zeigte, dass die Kobalt-Nanopartikel homogen verteilt sind und eine durchschnittliche Partikelgröße von 5,9 nm aufweisen. Die Oberfläche des Trägermaterials (545 m^2/g) sowie des Katalysators (491 m^2/g) konnte durch Argon-Physisorptionsmessungen bestimmt werden. Röntgen-Photoelektronenspektroskopie (XPS) sowie Pulver-Röntgendiffraktometrie (PXRD) in Kombination mit einer Paarverteilungsfunktion (PDF) zeigten die Existenz von metallischem und oxidischem Kobalt. Es konnte eine umfangreicher Substratbreite und damit auch eine sehr gute Toleranz gegenüber funktionellen Gruppen gezeigt werden. Die hohe Aktivität und Selektivität des Katalysators ist auf die einzigartige Struktur des Trägermaterials zurückzuführen. Es enthält freie N-H_x-Funktionalitäten in den Poren, die durch Festkörper-Kernspinresonanzspektroskopie (ss-NMR) nachgewiesen werden konnten.
Der zweite Teil der Arbeit befasst sich mit der Weiterentwicklung des bisherigen Kobaltkatalysators, um seinen Anwendungsbereich auf weitere Reaktionswege auszuweiten. Durch die Kombination von Kobalt und Scandium auf N-SiC nach dem bereits etablierten Verfahren konnte ein neuer Katalysator beschrieben werden, der die Borrowing Hydrogen- oder Hydrogen Autotransfer-Reaktion (BH HA) von Benzylalkoholen und Anilinderivaten ermöglicht. Bei dieser Reaktion wird der Benzylalkohol dehydriert, während der gewonnene Wasserstoff am Katalysator gespeichert wird. Im zweiten Reaktionsschritt kondensiert das Anilin oder eines seiner Derivate mit der Carbonylverbindung zu dem entsprechenden sekundären Imin, das mit Hilfe des zuvor

gespeicherten Wasserstoffs hydriert wird. Im Gegensatz zur reduktiven Aminierung wird für diese Reaktion kein zusätzliches Wasserstoffgas benötigt. Der Katalysator ist so aktiv, dass für eine vollständige Umsetzung nur 0,5 Äquivalente Kaliumhydroxid benötigt werden. Die Reaktionsbedingungen konnten auf 1,0 mol% Co, 0,33 mol% Sc, 24 h und einen Temperaturbereich von 120 - 140 °C eingestellt werden, um 13 unterschiedlich substituierte sekundäre Amine zu synthetisieren.

Im letzten Teil werden die beiden vorangegangenen Reaktionen kombiniert, um die Synthese komplexer Aminstrukturen mit einem einzigen Katalysator zu ermöglichen. Durch die Verwendung von gasförmigem Ammoniak konnten primäre Amine aus gut zugänglichen Alkoholen gebildet werden. Da der oben vorgestellte, bimetallische Co/Sc-Katalysator sowohl BH HA als auch die reduktive Aminierung katalysieren kann, konnten weitere Reaktionsschritte hinzugefügt werden, um komplexere sekundäre und tertiäre Amine zu erzeugen. Die Reaktion läuft sequenziell ab, ohne dass zwischenzeitliche Aufarbeitungsschritte erforderlich sind. Die Charakterisierung des Katalysators durch Rastertransmissionselektronenmikroskopie in Kombination mit Dunkelfeld-Bildgebung (HAADF-STEM) ergab homogen verteilte Co-Nanopartikel mit einem durchschnittlichen Durchmesser von 13,9 nm. Die Sc-Partikel sind um Größenordnungen kleiner und fein über das Trägermaterial verteilt, wie die Elektronenenergieverlustspektroskopie (EELS) zeigt. Vergleicht man die mittels XPS ermittelten Signalbereiche der Co 2p und Sc 2s-Regionen, so zeigt sich, dass der Sc-Anteil zehnmal höher ist als der Co-Anteil, obwohl bedingt durch die Katalysatorherstellung die gleiche Konzentration zu erwarten ist. Da es sich bei XPS um eine Oberflächenmethode handelt, deutet dies darauf hin, dass Sc in der äußeren Schicht fein verteilt ist, während Co in Form größerer Partikel vorliegt. Mit Hilfe des Katalysators wurde eine Substratbreite von 13 primären, 24 sekundären und acht tertiären Aminen ermittelt, wobei fünf der letzteren zum Zeitpunkt der Synthese literaturunbekannt waren.

2 Introduction

2.1 Heterogeneous earth abundant metal catalysts

The application of supported metal catalysts is observed in a wide range of crucial processes in the modern chemical industry such as petrochemistry, energy storage and the reduction of pollutants.[1] The synthesis of a variety of modern products, such as high-temperature lubricants, high-performance polymers, and also cancer therapeutics, which are required by an advanced society, would be inconceivable without catalysts. The catalysts used can be of homogeneous and heterogeneous nature. The former is in the same phase as the substrates, while the latter is in a different phase. Since heterogeneous catalysts are more easily separable from the reaction solution and thus recyclable and more robust than their homogeneous counterpart, the class of heterogeneous catalysts plays an important role in the industry.[2] These consist of a support material and a catalytically active species, e.g. in the form of metal nanoparticles. Such catalysts are usually prepared from a metal source and a reducing agent supported on metal oxides, carbon or zeolites.[3] The catalytic activity of nanoparticles is due to the concept of the "nano-effect". This states that the properties of metal nanoparticles differ from those of macroscopic metal, as there is a significant increase in surface area compared to volume when the nanometer size is reached.[4] In addition to the surface increase, nanoparticles exhibit quantum size effects which can contribute to their catalytic activity.[5]

Since the consequences of climate change and environmental pollution have become clear, it is even more important to design efficient ways to reduce these threats and preserve our planet for future generations and shift to a greener chemistry. Catalysis permits this through its linkage to the reduction of reaction waste, lower temperature requirements and good reusability.[6] Logically, decades of research have been committed to the development of new catalyst systems to enhance the mentioned properties. To preserve our nature’s resources, it has become a very important task to replace the frequently used noble metals, for example Pt, Pd, Ir and Rh with abundantly available 3d-metals. This step comes with various benefits. On the one hand, 3d-metals show a significantly higher abundance in earth’s crust, which is directly coupled with a lower price. In addition, this can lead to the accessibility of novel selectivity patterns to create new reaction pathways and broader substrate scopes.[7]

2.2 Polymer-derived ceramics as N-doped catalyst support materials

A catalyst support material must have many properties to meet its requirements, such as heat resistance, chemical stability, and excellent mechanical properties. Polymer-derived ceramics (PDCs) are suitable for use as a support material because they are available in a variety of compositions. These include the most commonly used silicon carbide (SiC), silicon oxycarbide (SiO_xC_y), silicon nitride (Si_3N_4), silicon carbonitride ($Si_{3+x}N_4C_{x+y}$) and silicon oxynitride (SiO_xN_y).[8] There's even a way to apply PDCs as dielectric ceramics or bioceramics.[9] In the 1970s, Fritz and Verbeek *et al.* were able to synthesize the first Si_3N_4/SiC fibers from the corresponding organosilicon polymers.[10] After this discovery, the research field of PDCs received constant attention. In general, PDCs are prepared by pyrolysis of organosilicon polymers under an inert atmosphere, usually nitrogen. The resulting ceramic is nanostructured and its properties are variable by changing the polymers used. Adjustable parameters include the polymer structure, the blend of different polymers or components, and the ceramization process itself.[11] Conventional ceramic systems often require the addition of additives, which PDCs eliminate. The large and ever-growing number of available PDC precursors allows scientists to create a suitable material for numerous applications, making them attractive for the development of next-generation materials. The choice of precursors also benefits the number of certain atoms in PDCs, particularly nitrogen, which is responsible for the excellent properties of N-doped carbon materials as catalyst supports.[12] For challenging catalytic reactions and the associated requirement for high selectivities, the choice of support is of great importance, as the interactions between the active phase and the support phase affect the catalytic activity.[13] N-doped carbon materials find application not only in the reduction of oxygen in fuel cells, but also in photocatalytic reactions and CO_2 capturing.[14] Strategies for introducing nitrogen into the carbon-skeleton range from treating the carbon with ammonia at high temperatures to vapor deposition of nitrogen-containing compounds to liquid-phase polymerization, with the aforementioned approach using nitrogen-rich organo-polymer precursors being the most practical.[15] The nitrogen within the ceramic material can occur in various bonding forms, such as pyridine, pyrrole, quaternary form, and pyridine N-oxide.[16] The orbital interactions between metal and nitrogen are responsible for the high stability of metal nanoparticles (NP) on such supports. Nucleation and consequent growth of NP can be prevented by N-inclusions, as they can bind the metal particles due to the free electron pair on the nitrogen.[17] Moreover, nitrogen species increase the binding energy between metal and N-doped carbon by interacting with the metal center, which improves the stability of NP and consequently the corresponding catalysts.[18] This leads

to the stabilization of individual metal atoms such as Pd and Co by N-doped carbon, which acts as a solid ligand.[16] The combination of interfacial charge-transfer at the metal-support bonding site and the good tunability of the support material with respect to the acid/base character of the surface leads to a unique metal-support-reactant interaction.[19] In recent years, non-oxidic PDCs such as SiC, SiCN and N-SiC have been found to be most suitable for heterogeneous catalysts. N-SiC, as the latest development, combines the outstanding properties of N-doped ceramics with excellent nanoparticle accessibility as they are located on the catalyst surface. The synthesis is based on the pioneering work of the Motz group, which reported a novel polyacrylonitrile-silazane hybrid polymer with excellent oxidation resistance.[20] To synthesize N-SiC, the commercially available polycarbosilane precursor SMP-10 is polymerized with acrylonitrile as the nitrogen source. After pyrolysis of the greenbody, the resulting material is activated by base treatment to significantly increase the surface area. Unlike SiCN, where the metal is introduced during ceramic synthesis using a complex, the metal is added to N-SiC only after the ceramic is fully prepared. For this purpose, a metal salt is wet impregnated directly onto the support material by evaporation of a solvent. After pyrolysis and subsequent reduction, this produces metal nanoparticles that are finely distributed over the entire surface of the support material, while SiCN encloses a large proportion of the nanoparticles due to its synthesis process.

2.3 Heterogeneous cobalt catalysts for the reductive amination

Amines represent a group of chemical compounds characterized by sp^3-hybridized nitrogen atoms with three single bonds.[21] Due to their versatile properties, they are important building blocks or precursors of natural products, dyes and polymers.[22] Furthermore, amines are of great pharmaceutical relevance and an important class of compounds for drug development due to their affinity for various receptors in biological systems.[23]

In industrial processes, heterogeneous catalysts are mainly used to produce amines, since they make a complex separation of the catalyst from the reaction product obsolete and thus cost-intensive purification by chromatography, distillation or extraction can be dispensed with.[24] In the following, the use of cobalt in combination with heterogeneous support materials for the catalytic production of primary amines will be discussed. Due to its frequent natural occurrence and the associated low cost, cobalt is an economically advantageous and sustainable alternative to noble metals.[25] A large number of the catalysts developed to date have been designed for the activation of structurally simple

substrates.[26] However, as 170 of the top 200 drugs already contained one or more nitrogen atoms or amino groups in 2022, the ability of converting complex carbonyl substrates to amines has come further to the fore.[27] The method of choice for this approach is the reductive amination, which has already been explored to a certain extent, after it was first described by Mignonac in 1921.[28]

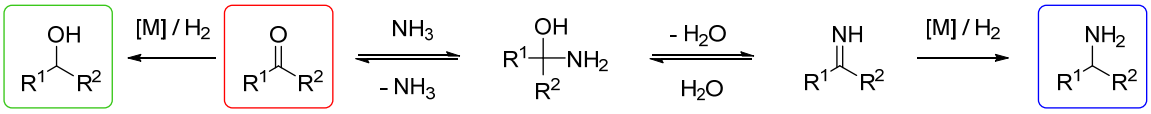

Scheme 1: Reductive amination of ketones to primary amines employing ammonia and a heterogeneous catalyst.

The reductive amination mechanism for ketones with ammonia and a heterogeneous catalyst proceeds as shown in Scheme 1.[29] The formation of the imine competes with the hydrogenation of the carbonyl compound (red outline) to the alcohol (green outline). Therefore, a high selectivity of the catalyst is important in order to suppress this side reaction and thus to favor the formation of the imine via condensation. After that, the catalyst hydrogenates the imine to the corresponding primary amine (blue outline). For the synthesis of secondary and tertiary amines, the ammonia has to be replaced by primary or secondary amines respectively. The reductive amination impresses with cheap and abundantly available starting materials as well as a large variety of substrates that can be converted.

The first catalyst of this type was published in 2014 by Stemmler *et al.*[30] It was prepared by pyrolysis of $Co(OAc)_2$ and 1,10-phenantroline on activated carbon at 800 °C under nitrogen atmosphere, which allowed the formation of Co/Co-oxide nanocomposites coated by a nitrogen-rich graphene layer. The system was first used for reductive coupling of nitroarenes with carbonyl compounds. A year later, reductive amination of aldehydes and ketones at 150-160 °C, 50 bar H_2 and a loading of 3 mol% Co was achieved in moderate to very good yields.[31] Further work by Huang *et al.* in 2016 dealt with the reductive amination of aldehydes and ketones with amines using a Co@NC catalyst.[32] The system was prepared by pyrolysis of $Co(OAc)_2$ and 1-methyl-3-cyanomethyl-1H-imidazolium chloride on activated carbon for 2 h at 800 °C. Primary amines could be prepared at 110 °C, 10 bar H_2 and a loading of 2 mol% Co in good to very good yields, while for secondary amines the reaction conditions had to be adapted (140 °C, 30 bar H_2, 3 mol%). In 2017, Dong's group published a Co catalyst generated by pyrolysis of a homogeneous mixture of melamine, polyacrylonitrile and $Co(NO_3)_2$ at 900 °C under nitrogen

atmosphere.[33] Reductive N-alkylation of nitroarenes with carbonyl compounds could be carried out at 100-120 °C and 10 bar H_2 in up to quantitative yields.

In the same year, Beller's group reported the reductive amination of carbonyl compounds with NH_3, amines and nitro compounds by graphene coated cobalt nanoparticles in a MOF, which was supported on *Vulcan XC 72R* and pyrolyzed.[26] The activity of the catalyst generated was sufficient to produce 140 substrates, including primary, secondary and tertiary amines, as well as to convert important pharmaceuticals in very good yields. In 2019, Chi's group reported pyrolysis of cobalt-coordinated organic polymers at 800 °C to generate nanoparticles.[34] This catalyst showed high activity in selective reductive amination of aldehydes to primary amines with aqueous ammonia. More recent work on the topic of reductive amination with cobalt catalysts was again published by Beller's group in 2020.[35] The group reported the synthesis of *in situ* generated cobalt nanoparticles from molecularly defined cobalt-salen complexes, which achieved particle sizes of 2-4 nm embedded in a carbon nitrogen framework. At 120 °C, 45 bar H_2, 5-7 bar NH_3 and a loading of 6 mol% Co-salen, numerous primary and secondary amines could be produced in good to very good yields. In 2021, Sheng *et al*. published the successful synthesis of single-crystal cobalt phosphide nanorods for the reductive amination of carbonyl compounds.[36] Their catalyst was able to mediate the synthesis of a large number of primary amines under mild conditions (10 mol% Co, 100 °C, 1 bar H_2). Through pyrolysis of the metal organic framework *ZIF-67* at 800 °C, Zheng and coworkers were able to create graphene encapsulated Co nanoparticles and atomically dispersed Co-N_x sites on the support material simultaneously.[37] The obtained catalyst was able to mediate the reductive amination of different substrates at 35 °C employing 14 bar H_2 and 6 bar gaseous NH_3. The most recent work in this research field was published in 2022 by the group of Hara.[38] Their composite of metallic cobalt and silica particles could catalyze the reductive amination carbonyl compounds to primary amines (1 bar NH_3, 5 bar H_2, 50 °C, 15 h) as well as the hydrogenation of nitriles. The striking increase in publication density, especially in recent years, once again underscores the high relevance of reductive amination in current research.

2.4 Borrowing Hydrogen / Hydrogen Autotransfer

The Borrowing Hydrogen or Hydrogen Autotransfer (BH HA) catalysis deals with the N-alkylation of amines with alcohols. It differs from reductive amination in that alcohols can be used as reactants instead of carbonyl compounds, and no external hydrogen needs to be added. This is highly beneficial for sustainable catalysis, since alcohols can be obtained from food waste, that does not interfere with the human food chain and would otherwise be thrown away. Lignin, which occurs in lignocellulose from cell walls of lignified plants at a rate of approx. 10-30%, is used for alcohol production. Hydrogenolysis of lignin leads to a mixture of alcohols that can be processed further.[39] In combination with 3d-metal catalysts, borrowing hydrogen is a sustainable method for amine synthesis, just like the aforementioned reductive amination. It was first described in 1932 by Winans and Adkins and has since sparked the interest of the research field of homogeneous catalysis.[40]

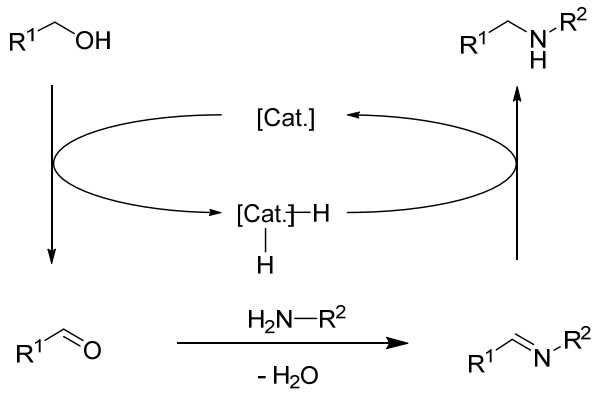

Scheme 2: Borrowing Hydrogen / Hydrogen Autotransfer reaction of a primary alcohol with a primary amine.

The BH HA mechanism is shown in Scheme 2. The first step involves the dehydrogenation of the alcohol to its corresponding carbonyl compound while the obtained hydrogen is stored at the catalyst. Afterwards aniline condenses with the carbonyl compound to an imine, which is then hydrogenated employing the hydrogen stored before.

Many research groups have established homogeneous catalyst systems for BH HA based on transition metal complexes.[41] Heterogeneous systems, which offer better stability and reusability, have only been reported with Fe,[42] Ni,[43] and Cu[44] with the exception of the Beller group, which published a heterogeneous cobalt catalyst in 2021.[45] They were able to generate the catalyst by mixing cobalt salts, nitrogen-containing ligands and silica. After pyrolysis at 800 °C, the remaining silica was removed using ammonium hydrogen fluoride. Employing this catalyst, more than 100 different amines could be synthesized. With this being the only publication at the time, the research field of heterogeneous Co catalysts for BH HA is still quite unexplored and offers multiple opportunities for scientific progress.

2.5 References

[1] a) E. Antolini, *Appl. Catal. B: Environ.* **2010**, *100*, 413; b) S. Chen, C. Pei, J. Gong, *Energy Environ. Sci.* **2019**, *12*, 3473; c) A. K. Datye, M. Votsmeier, *Nat. Mater.* **2021**, *20*, 1049; d) L. Piccolo, *Catal. Today* **2021**, *373*, 80.

[2] J. H. Clark, D. J. Macquarrie, *Org. Process Res. Dev.* **1997**, *1*, 149.

[3] D. Astruc, F. Lu, J. R. Aranzaes, *Angew. Chem. Int. Ed.* **2005**, *44*, 7852.

[4] a) F. Yang, D. Deng, X. Pan, Q. Fu, X. Bao, *Natl. Sci. Rev.* **2015**, *2*, 183; b) G. Seifert, *Cryst. Res. Technol.* **1994**, *29*, 956.

[5] X. Ma, P. Jiang, Y. Qi, J. Jia, Y. Yang, W. Duan, W.-X. Li, X. Bao, S. B. Zhang, Q.-K. Xue, *PNAS* **2007**, *104*, 9204.

[6] A. T. Bell, *Science* **2003**, 1688.

[7] R. M. Bullock, *Science* **2013**, *342*, 1054.

[8] a) H. SCHÖNFELDER, F. ALDINGER, R. RIEDEL, *J. Phys. IV France* **1993**, *03*, C7-1293-C7-1298; b) P. Colombo, G. Mera, R. Riedel, G. D. Sorarù, *J. Am. Ceram. Soc.* **2010**, *93*, 1805-1837.

[9] a) Q. Yu, Y. Han, X. Wang, C. Qin, D. Zhai, Z. Yi, J. Chang, Y. Xiao, C. Wu, *ACS Nano* **2018**, *12*, 2695; b) S. Xu, K. Lin, Z. Wang, J. Chang, L. Wang, J. Lu, C. Ning, *Biomater.* **2008**, *29*, 2588.

[10] R. Riedel, G. Mera, R. HAUSER, A. KLONCZYNSKI, *J. Ceram. Soc. Japan* **2006**, *114*, 425.

[11] Paolo Colombo, Gabriela MERA, Ralf RIEDEL, Gian Domenico Sorarù in *Ceram. Sci. Technol.* John Wiley & Sons, Ltd, **2013**, pp. 245–320.

[12] F. Rodríguez-reinoso, *Carbon* **1998**, *36*, 159.

[13] M. C. Román-Martínez, D. Cazorla-Amorós, A. Linares-Solano, C.-M. de Lecea, H. Yamashita, M. Anpo, *Carbon* **1995**, *33*, 3.

[14] X. Wang, K. Maeda, A. Thomas, K. Takanabe, G. Xin, J. M. Carlsson, K. Domen, M. Antonietti, *Nat. Mater.* **2009**, *8*, 76.

[15] a) J. Przepiórski, M. Skrodzewicz, A. Morawski, *Appl. Surf. Sci* **2004**, *225*, 235; b) Z. Jin, J. Yao, C. Kittrell, J. M. Tour, *ACS Nano* **2011**, *5*, 4112; c) J. S. Lee, X. Wang, H. Luo, G. A. Baker, S. Dai, *J. Am. Chem. Soc.* **2009**, *131*, 4596.

[16] L. He, F. Weniger, H. Neumann, M. Beller, *Angew. Chem.* **2016**, *128*, 12770.

[17] a) B. Choi, H. Yoon, I.-S. Park, J. Jang, Y.-E. Sung, *Carbon* **2007**, *45*, 2496; b) Y.-H. Li, T.-H. Hung, C.-W. Chen, *Carbon* **2009**, *47*, 850.

[18] W. Xia, *Catal. Sci. Technol.* **2016**, *6*, 630.

[19] D. S. Su, S. Perathoner, G. Centi, *Chem. Rev.* **2013**, *113*, 5782.

[20] L. F. B. Ribeiro, O. Flores, P. Furtat, C. Gervais, R. Kempe, R. A. F. Machado, G. Motz, *J. Mater. Chem. A* **2017**, *5*, 720.

[21] S. A. Lawrence, *Amines*. *Synthesis, properties, and applications*, Cambridge University Press, Cambridge, **2004**.

[22] a) T. C. Nugent, M. El-Shazly, *Adv. Synth. Catal.* **2010**, *352*, 753; b) D. B. Bagal, R. A. Watile, M. V. Khedkar, K. P. Dhake, B. M. Bhanage, *Catal. Sci. Technol.* **2012**, *2*, 354.

[23] A. Ricci, *Modern Amination Methods*, Wiley-VCH, Weinheim, **2008**.

[24] V. Polshettiwar, R. S. Varma, *Green Chem.* **2010**, *12*, 743.

[25] *Lexikon der chemischen Elemente*, Hirzel.

[26] R. V. Jagadeesh, K. Murugesan, A. S. Alshammari, H. Neumann, M.-M. Pohl, J. Radnik, M. Beller, *Science* **2017**, *358*, 326.

[27] N. A. McGrath, M. Brichacek, J. T. Njardarson, *J. Chem. Educ.* **2010**, *87*, 1348.

[28] G. Mignonac, *Compt. Rend.* **1921**, 223.

[29] T. Irrgang, R. Kempe, *Chem. Rev.* **2020**, *120*, 9583.

[30] T. Stemmler, F. A. Westerhaus, A.-E. Surkus, M.-M. Pohl, K. Junge, M. Beller, *Green Chem.* **2014**, *16*, 4535.

[31] S. Pisiewicz, T. Stemmler, A.-E. Surkus, K. Junge, M. Beller, *ChemCatChem* **2015**, *7*, 62.

[32] F. Mao, D. Sui, Z. Qi, H. Fan, R. Chen, J. Huang, *RSC Adv.* **2016**, *6*, 94068.

[33] X. Cui, K. Liang, M. Tian, Y. Zhu, J. Ma, Z. Dong, *J. Colloid Interface Sci.* **2017**, *501*, 231.

[34] Z. Yuan, B. Liu, P. Zhou, Z. Zhang, Q. Chi, *J. Catal.* **2019**, *370*, 347.

[35] T. Senthamarai, V. G. Chandrashekhar, M. B. Gawande, N. V. Kalevaru, R. Zbořil, P. C. J. Kamer, R. V. Jagadeesh, M. Beller, *Chem. Sci.* **2020**, *11*, 2973.

[36] M. Sheng, S. Fujita, S. Yamaguchi, J. Yamasaki, K. Nakajima, S. Yamazoe, T. Mizugaki, T. Mitsudome, *JACS Au* **2021**, *1*, 501.

[37] B. Zheng, J. Xu, J. Song, H. Wu, X. Mei, K. Zhang, W. Han, W. Wu, M. He, B. Han, *Chem. Sci.* **2022**, *13*, 9047.

[38] K. Kato, D. Deng, Y. Kita, K. Kamata, M. Hara, *Catal. Sci. Technol.* **2022**, *12*, 5425.

[39] A. M. Ruppert, K. Weinberg, R. Palkovits, *Angew. Chem. Int. Ed.* **2012**, *51*, 2564.

[40] C. F. Winans, H. Adkins, *J. Am. Chem. Soc.* **1932**, *54*, 306.

[41] a) T. Yan, B. L. Feringa, K. Barta, *Nat Commun* **2014**, *5*, 5602; b) M. Vellakkaran, K. Singh, D. Banerjee, *ACS Catal.* **2017**, *7*, 8152; c) M. Vayer, S. P. Morcillo, J. Dupont, V. Gandon, C. Bour, *Angew. Chem. Int. Ed.* **2018**, *57*, 3228; d) A. Quintard, T. Constantieux, J. Rodriguez, *Angew. Chem. Int. Ed.* **2013**, *52*, 12883; e) S. Elangovan, J. Neumann, J.-B. Sortais, K. Junge, C. Darcel, M. Beller, *Nat Commun*

2016, *7*, 12641; f) N. Deibl, R. Kempe, *Angew. Chem. Int. Ed.* **2017**, *56*, 1663; g) N. Deibl, R. Kempe, *J. Am. Chem. Soc.* **2016**, *138*, 10786; h) M. Subaramanian, S. P. Midya, P. M. Ramar, E. Balaraman, *Org. Lett.* **2019**, *21*, 8899.

[42] C. Gonzalez-Arellano, K. Yoshida, R. Luque, P. L. Gai, *Green Chem.* **2010**, *12*, 1281.

[43] a) X. Cui, X. Dai, Y. Deng, F. Shi, *Chem. Eur. J.* **2013**, *19*, 3665; b) A. Tomer, F. Wyrwalski, C. Przybylski, J.-F. Paul, E. Monflier, M. Pera-Titus, A. Ponchel, *J. Catal.* **2017**, *356*, 111; c) K. Shimizu, K. Kon, W. Onodera, H. Yamazaki, J. N. Kondo, *ACS Catal.* **2013**, *3*, 112; d) K. Shimizu, S. Kanno, K. Kon, S. Hakim Siddiki, H. Tanaka, Y. Sakata, *Catal. Today* **2014**, *232*, 134; e) K. Shimizu, N. Imaiida, K. Kon, S. M. A. Hakim Siddiki, A. Satsuma, *ACS Catal.* **2013**, *3*, 998; f) A. Afanasenko, S. Elangovan, M. C. A. Stuart, G. Bonura, F. Frusteri, K. Barta, *Catal. Sci. Technol.* **2018**, *8*, 5498.

[44] a) Y. Wu, Y. Huang, X. Dai, F. Shi, *ChemSusChem* **2019**, *12*, 3185; b) S. Pang, Y. Deng, F. Shi, *Chem. Commun.* **2015**, *51*, 9471; c) F. Santoro, R. Psaro, N. Ravasio, F. Zaccheria, *ChemCatChem* **2012**, *4*, 1249; d) H. Liu, G.-K. Chuah, S. Jaenicke, *J. Catal.* **2015**, *329*, 262; e) M. Dixit, M. Mishra, P. A. Joshi, D. O. Shah, *Catal. Commun.* **2013**, *33*, 80.

[45] Z. Ma, B. Zhou, X. Li, R. G. Kadam, M. B. Gawande, M. Petr, R. Zbořil, M. Beller, R. V. Jagadeesh, *Chem. Sci.* **2021**, *13*, 111.

3 Overview of thesis results

This thesis contains three publications, shown in chapters 4-6. Two of them are published, and one is to be submitted. The synopsis (chapter 3.1) summarizes the results and the individual contributions are described in detail in chapter 3.2.

3.1 Synopsis

As heterogeneous catalysis has become a mainstay of sustainable chemistry, the Kempe group focused on the development of new materials to advance research in this field. The development of new PDCs as catalyst support materials is a key area that has been worked on. Starting with the pioneering work of the Motz group, which began with the copolymerization of SMP-10, a commercially available polycarbosilane precursor, and acrylonitrile, the Kempe group discovered that pyrolysis of this material yields a nitrogen-rich, silicone-doped support material, namely N-SiC, which has extremely good properties in terms of nanoparticle stabilization and overall catalyst activity. Since it is highly desirable to replace noble metals with more earth-abundant 3d-metals in order to preserve nature's resources for future generations, Kempe's group mainly focused on the combination of N-SiC and 3d-metals. Following this principle, Schoenauer *et al.* succeeded in synthesizing a highly active cobalt catalyst for the general synthesis of secondary alkylamines by reductive alkylation of nitriles with aldehydes and ketones. The excellent activity of the Co/N-SiC catalyst used highlighted that this material has great potential for promising reactions.

The first publication deals with the further development of this catalyst and its application for reductive amination for the synthesis of primary amines under very mild conditions. In view of rising energy prices, mild reaction conditions have become even more important to enable economical and environmentally friendly production. For these reasons, we have mainly focused on improving the catalyst activity and thus lowering the reaction temperature and the required hydrogen pressure. An already established process was used to prepare the N-SiC support material (Scheme 3). In the first step, 80 wt% acrylonitrile and 20 wt% commercial SMP-10 are copolymerized (Scheme 3A). After pyrolysis of the resulting greenbody, a Si-rich CN material is obtained (Scheme 3B).

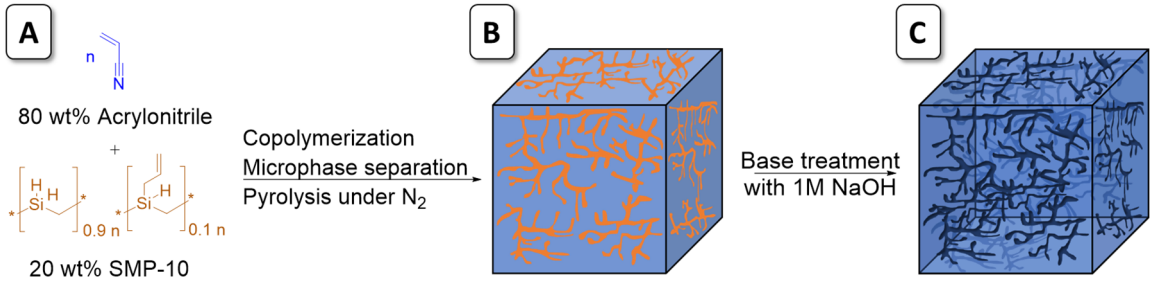

Scheme 3: Synthesis of the N-SiC support material. Copolymerization, microphase separation and pyrolysis of acrylonitrile and SMP-10 (**A**) to give a Si-rich CN-material (**B**). After treatment with 1 M NaOH, the silicon phase is almost completely removed to obtain the N-SiC support material (**C**).

To increase the surface area, treatment with 1 M NaOH solution is required. This leads to N-SiC, a microporous, Si-doped and N-rich carbon support material. In the next step, the metal is deposited on the support material. Wet impregnation of N-SiC with $Co(NO_3)_2 \cdot 6\ H_2O$ in water, pyrolysis (700 °C, N_2) and subsequent reduction (550 °C, N_2/H_2) yields the catalyst. Inductively coupled plasma optical emission spectroscopy (ICP-OES) revealed a Co content of 2.24 wt% as opposed to a theoretical content of 3 wt%. This indicates some losses during the synthesis process.

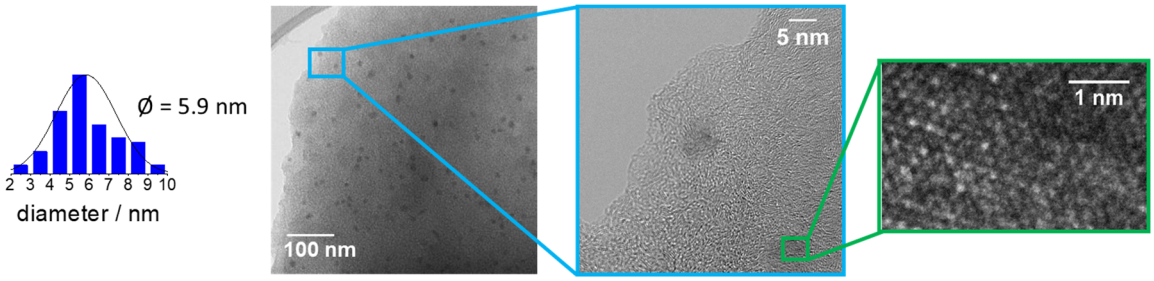

Figure 1: HR-TEM analysis of the Co/N-SiC catalyst suggested the presence of homogeneously distributed Co nanoparticles. The particle diameter averages 5.9 nm. Higher magnifications were able to visualize single Co particles and atomic resolution of a nanoparticle surface.

To obtain more detailed information about the nature of the nanoparticles, TEM analysis was performed (Figure 1). The results showed a homogeneous distribution of Co nanoparticles on the N-SiC support with an average particle diameter of 5.9 nm. The small size of the NP could be attributed to the stabilization ability of the N-SiC support and its free N-H_x functionalities. These resulted from the base treatment of the greenbody due to the hydrolysis of the C-N-Si bonds and could be qualitatively detected by solid-state NMR spectroscopy (Figure 2).

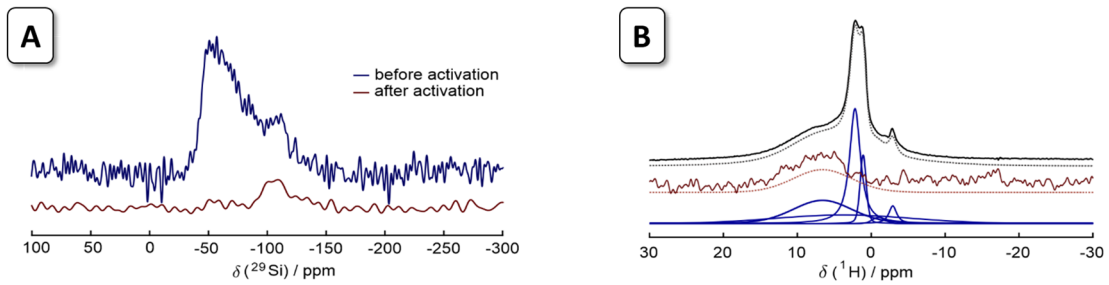

Figure 2: ^{29}Si-SP-MAS NMR spectra of the N-SiC support material (**A**). Blue line: before activation, brown line: after activation. Nitrogen selective ^{1}H-^{14}N HMQC spectra (**B**, blue lines) show the presence of free NH_x-groups.

Figure 2A shows the ss-NMR spectra of the N-SiC support prior to the activation with 1 M NaOH (blue line) and afterwards (brown line). It can be recognized that the majority of silicon could be removed from the support and thus creating the free NH_x-functionalities, which could be proven by ^{1}H-^{14}N heteronuclear multiple quantum correlation (HMQC) spectra (Figure 2B, blue lines). The multiple blue lines indicate different binding modes of the nitrogen, which can be attributed to pyrrolic, pyridinic and graphitic nitrogen. These findings are consistent with the XPS spectra shown in Figure 3, which confirmed the mentioned binding modes through the different binding energies.

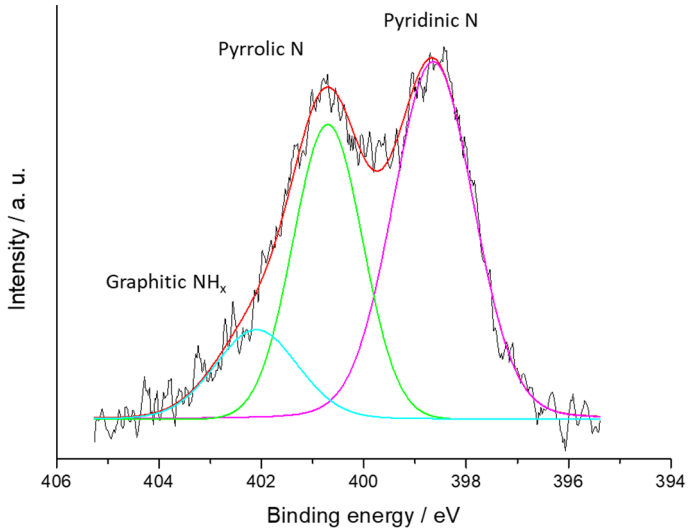

Figure 3: High resolution XPS of the N1s region of the catalyst. Three major peaks are shown, which can be assigned to 16.4 % graphitic nitrogen (401.3 eV), 32.8 % pyrrolic nitrogen (400.05 eV) and 50.8 % pyridinic nitrogen (398.6 eV).

With this catalyst and the optimized reaction conditions, a wide range of substrates could be prepared. The reductive amination of substrates with an aromatic and an aliphatic moiety worked well for sterically demanding, electron donating and electron withdrawing groups in different ring positions as well as for long and short aliphatic moieties

(Scheme 4, substrates **1**-**13**). It is particularly noteworthy that substrates with a doubly substituted ring, two aromatic residues, a heterocycle, and an indanone structure could be converted successfully (substrates **14**-**18**). Reductive amination of various aromatic aldehydes could also be carried out, although the temperature had to be raised to 80 °C to avoid self-coupling products.

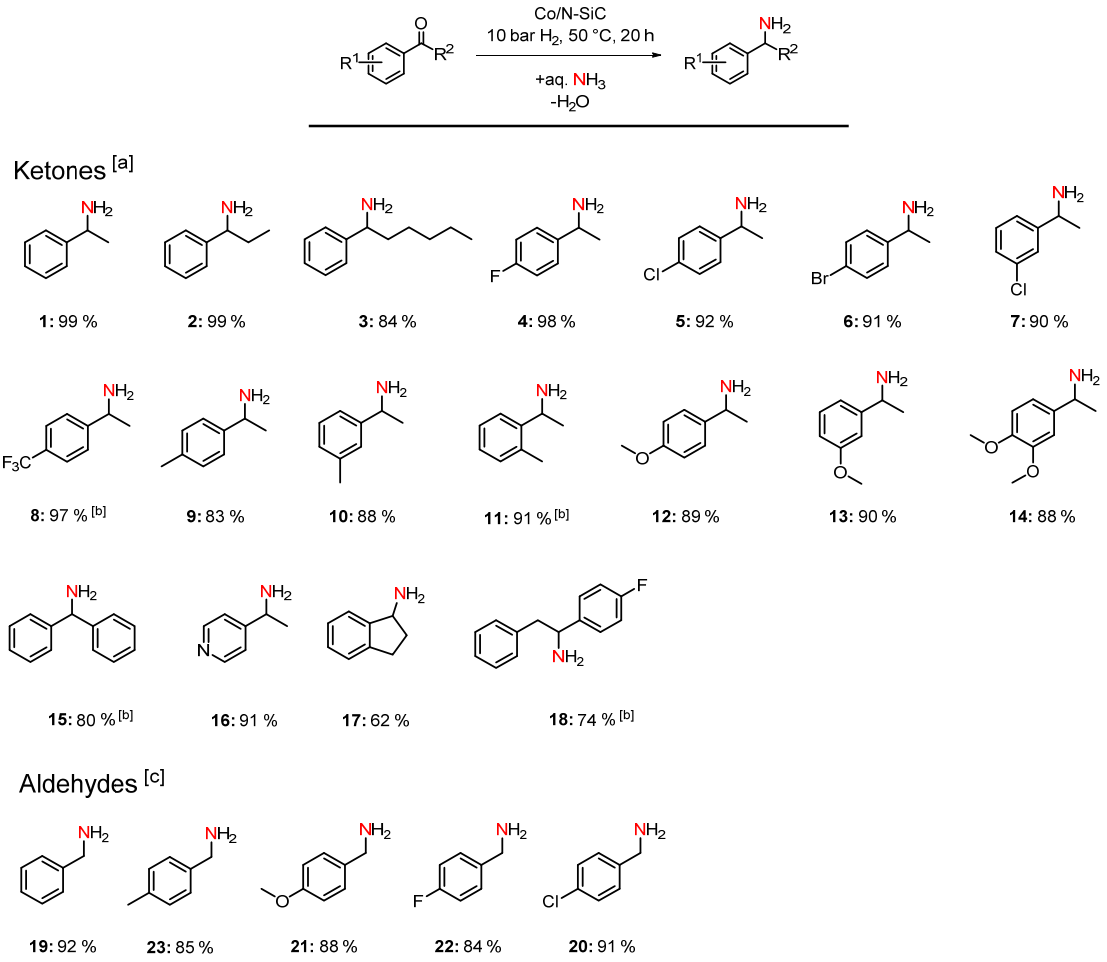

Scheme 4: Reductive amination of aryl substituted ketones and aldehydes to primary amines. [a] Reaction conditions for ketones: 1.5 mol% Co (2.24 wt% Co, 0.0075 mmol Co, 0.44 mg Co), 0.5 mmol ketone, 50 °C, 20 h, 10 bar H_2, 3.5 mL aq. NH_3-32%. [b] 60°C. [c] Reaction conditions for aldehydes: 1.1 mol% Co, 0.5 mmol aldehyde, 80 °C, 20 h, 10 bar H_2, 3.5 mL aq. NH_3-32 %. Isolated yields of the converted hydrochloride salts.

Reductive amination of various fully aliphatic ketones was also possible. Linear, branched and cyclic substrates could be converted into their corresponding amines in moderate to very good yields (Scheme 5, left panel). The conversion of biologically active molecules into their amine counterparts could also be carried out under very mild conditions (Scheme 5, right panel). The challenging stanolone had to be treated at higher temperatures (65 °C), higher catalyst loading (3 mol% Co) and the addition of ethanol to improve its solubility.

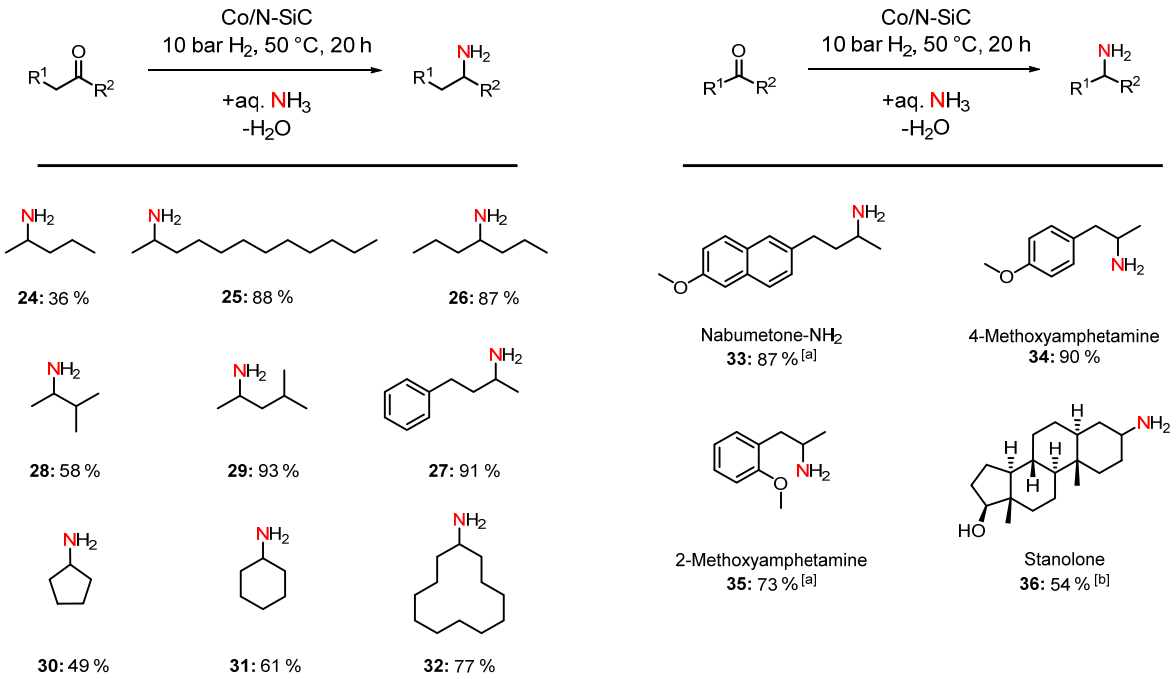

Scheme 5: Reductive amination of purely and partly aliphatic ketones (left) and biologically active molecules (right). Reaction conditions: 1.5 mol% Co (2.24 wt% Co, 0.0075 mmol Co, 0.44 mg Co), 0.5 mmol ketone, 50 °C, 20 h, 10 bar H_2, 3.5 mL aq. NH_3-32%. [a] 60°C. [b] 3 mol% Co, 65 °C, 3.2 mL aq. NH_3-32 %, 0.3 mL EtOH. Isolated yields of the converted hydrochloride salts.

The catalyst could be reused five times without any significant loss of activity for the reductive amination of acetophenone. The same substrate could also be scaled up to 20 times the amount that was initially used and obtained with an excellent yield of 95 %.

Inspired by the outstanding activity of the Co catalyst towards the hydrogenation of imines, another method for the synthesis of amines was targeted. Since not only primary amines, as synthesized in the first publication are important for industrial and pharmaceutical purposes, the second work focuses on the generation of secondary amines. Alcohols were also used to further increase the sustainability of the reaction. Alcohols can be obtained from lignin, which is present in food waste and cells of wooden plants. This provides a viable basis for alternative, environmentally friendly ways of producing carbon to move away from oil and coal. The goal was to modify the existing catalyst as little as possible so that it could be employed in the BH HA reaction of alcohols and aromatic amines. The reaction mechanism was described above and proceeds without external hydrogen (Scheme 2). Since its discovery in 1932, the reaction has been improved for a wide range of applications. However, with the exception of the Beller group in 2021, no one has yet succeeded in using a heterogeneous cobalt catalyst for this reaction. Based on these findings, the Co/N-SiC catalyst used in the first publication was modified with scandium, a metal that is even more abundant than cobalt. Cobalt and scandium proved to be the most

active combination. The use of other rare earth metals as well as cobalt and scandium alone could not match the activity of the Co/Sc catalyst. The resulting bimetallic Co/Sc catalyst was able to mediate the BH HA synthesis of secondary amines under mild conditions and with catalytic amounts of base. The synthesis procedure differs little from the original procedure for the Co catalyst. The only exception is the simultaneous addition of $Sc(NO_3)_3 \cdot 5\ H_2O$ and $Co(NO_3)_2 \cdot 6\ H_2O$ in equal weight percent to the impregnation process. Pyrolysis followed by reduction results in the active catalyst. After optimizing the reaction conditions for the benchmark reaction of benzyl alcohol and aniline, the reaction temperature was set to 120 °C and 0.5 equivalents of KOH was used. The reaction was carried out in toluene under argon atmosphere to suppress any side reactions and to exclude the presence of oxygen as acceptor.

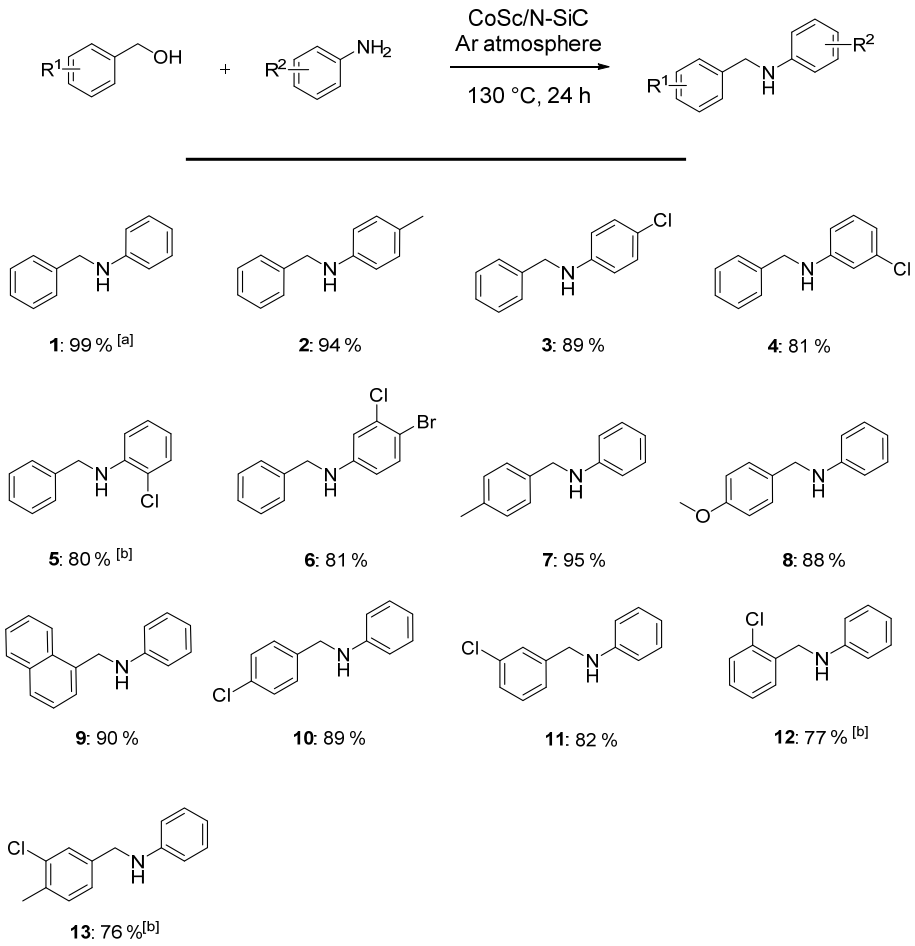

Scheme 6: Substrate scope of the BH HA reaction. Reaction conditions: 1.0 mmol benzyl alcohol, 0.5 mmol amine, 1.0 mol% Co, 0.33 mol% Sc, 0.5 mL toluene, 0.25 mmol KOH, 130 °C, 24 h, argon atmosphere. [a] 120 °C, [b] 140 °C. Isolated yields of the converted hydrochloride salts.

Besides the benchmark substrate (Scheme 6, substrate **1**), the temperature had to be raised for all substituted derivatives. For the aniline-side, various electron donating and withdrawing substituents could be tolerated (substrates **2**-**6**). The same observations could be made for the variation of the benzyl alcohol (substrates **7**-**13**). In both cases, doubly substituted rings could be tolerated well. For the sterically demanding chloride in ortho-position (substrates **5** and **12**), the temperature had to be raised to 140 °C.

In view of the excellent results obtained in both reductive amination and BH HA, the idea arose to combine the two processes to obtain more complex amine structures. This would significantly increase the potential applicability for pharmaceutical products, as these are usually in more complex structures. Since the cobalt catalyst was able to mediate reductive amination, the bimetallic cobalt-scandium catalyst should be able to do the same, apart from its already demonstrated excellent activity for BH HA. With the latter catalyst, the synthesis of primary amines as well as the consecutive synthesis of secondary and tertiary amines could be carried out by combining reductive amination and BH HA reactions. Tertiary amines in particular could be synthesized in a five-component reaction employing gaseous NH_3 and an alcohol for the borrowing hydrogen step and two carbonyl compounds as well as molecular hydrogen for the reductive amination steps (Scheme 7).

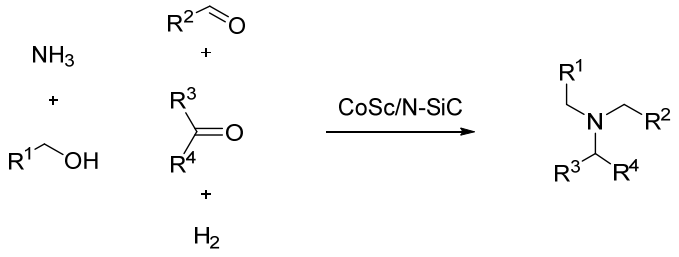

Scheme 7: Consecutive five-component reaction to synthesize tertiary amines mediated by a heterogeneous bimetallic cobalt-scandium catalyst.

The fact that this combination of reactions with the same reusable and heterogeneous catalyst has not yet been published makes this topic particularly interesting. The catalyst synthesis procedure doesn't differ from the above-mentioned process. After the optimization of the reaction conditions for the borrowing hydrogen step (1.5 mol% Co, 0.49 mol% Sc, 0.5 mmol KOH, 160 °C, 20 bar NH_3, 44 h), different catalysts were screened for this particular step (Table 1) to again validate Co/Sc as most active metal combination and N-SiC as the best support material, as it has been for the synthesis of secondary amines via BH HA mentioned above.

Table 1: Catalyst screening for the BH HA reaction of benzyl alcohol and gaseous ammonia.[a]

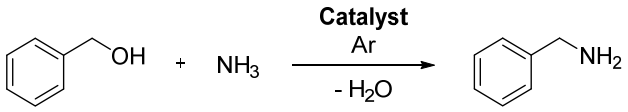

Entry	*Metal(s)*	*Support*	*Yield / %*
1	Co/La	N-SiC	5
2	Co/Gd	N-SiC	9
3	Co/Lu	N-SiC	54
4	**Co/Sc**	**N-SiC**	**99**
5 [b]	Fe/Sc	N-SiC	7
6 [b]	Ni/Sc	N-SiC	33
7 [b]	Fe	N-SiC	0
8 [b]	Ni	N-SiC	12
9 [b]	Co	N-SiC	16
10 [b]	Sc	N-SiC	32
11	Co/Sc	Activated C	67
12	Co/Sc	Al_2O_3	2
13	Co/Sc	TiO_2	0
14	Co/Sc	SiO_2	0
15	-	N-SiC	0

[a] Reaction conditions: 1.5 mol% Co/Fe/Ni, 0.85 mol% La, 0.74 mol% Gd, 0.66 mol% Lu, 0.49 mol% Sc, pyrolyzed at 700 °C, 0.5 mmol benzyl alcohol, 2.0 mL toluene, 0.5 mmol KOH, 160 °C, 44 h, 20 bar NH_3. Yields were determined by GC using *n*-dodecane as an internal standard. [b] 1.5 mol% Fe/Ni/Co/Sc.

It can be seen that all other combinations as well as Co/Sc on different supports do not provide the outstanding activity of the CoSc/N-SiC catalyst. To better understand the catalyst, a HAADF-STEM analysis was performed (Figure 4), which revealed a homogeneous distribution of Co nanoparticles over the support material with an average particle size of 13.9 nm. The Sc particles could be visualized by STEM-EELS and are orders of magnitude smaller than the Co particles and finely distributed over the entire support material including the area of the Co particles. These results are consistent with the XPS measurements, which found a sevenfold higher atomic percentage of Sc compared to Co, indicating a fine distribution of Sc on the outer layer, whereas Co is present as larger particles. In addition, for cobalt, oxidic (Co_2O_3 and $Co(OH)_2$) and metallic species could be identified, with the latter accounting for the smaller fraction. For Sc, only a single species could be found, indicating oxidized Sc. Scanning electron microscopy (SEM)-analysis of the catalyst in combination with energy dispersive X-ray (EDX) imaging revealed a similar distribution of Si and Sc.

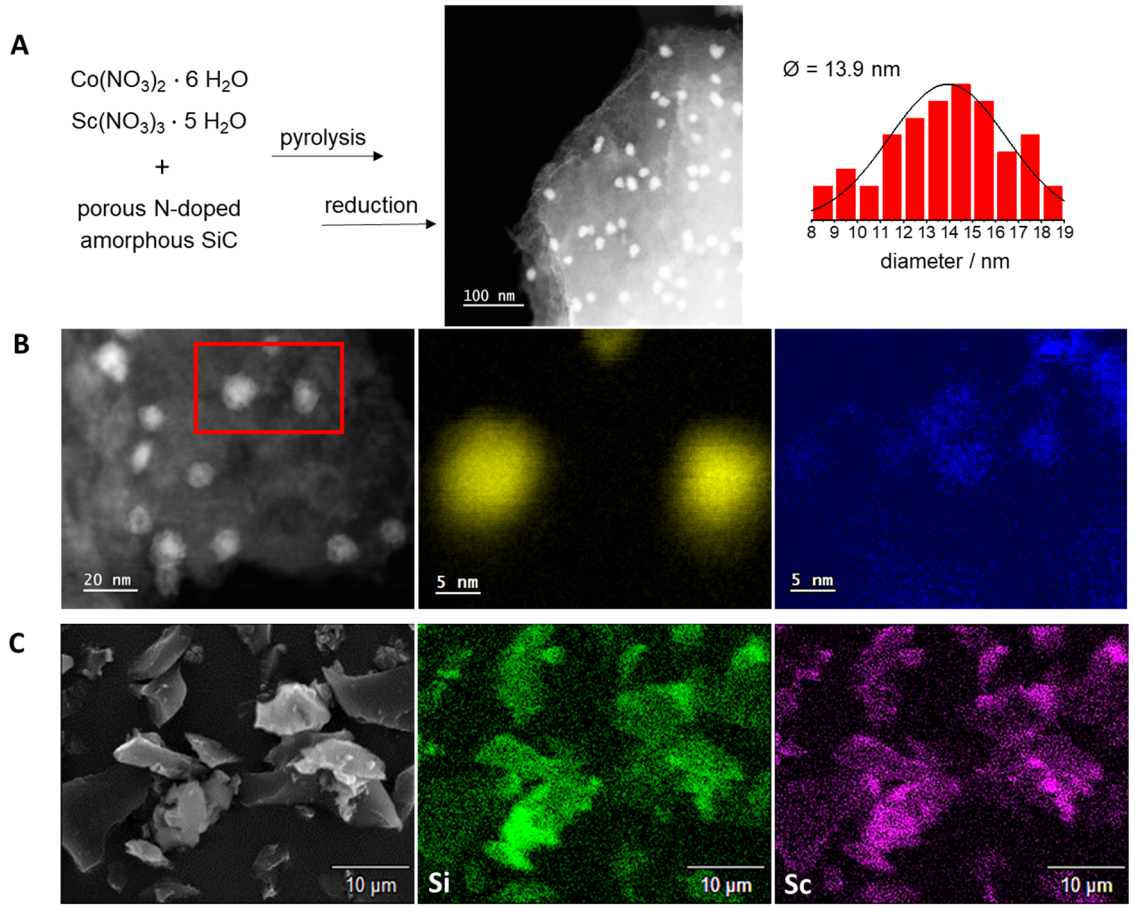

Figure 4: Synthesis and characterization of the Co/Sc catalyst. **A**: Synthesis of the CoSc/N-SiC catalyst and HAADF-STEM image with particle size distribution. **B**: Higher magnification HAADF-STEM image (left panel) with EELS analysis of Co (middle panel) and Sc (right panel). **C**: Scanning electron microscopy (SEM) of the catalyst (left panel) in combination with energy dispersive X-ray (EDX) mapping (middle and right panel).

To demonstrate the selectivity of the catalyst, a broad substrate scope was established. For better clarity, the scope is split in three separate parts for primary, secondary and tertiary amines respectively. For the first part, all synthesized primary amines are shown in Scheme 8. With the BH HA methodology, benzyl alcohols with various substituents (products **2**-**8**) could be converted into the corresponding benzyl amines. A second amine function in the molecule did not pose any problem. The conversion of two aliphatic molecules (**9, 10**) could be accomplished by applying the reductive amination reaction conditions established in the first part (50 °C, 10 bar H_2, aqueous ammonia). The conversion of three biologically active molecules (**11**-**13**) could also be accomplished. Thus, the capability of the bimetallic Co/Sc catalyst to mediate the reductive amination under these conditions could be confirmed.

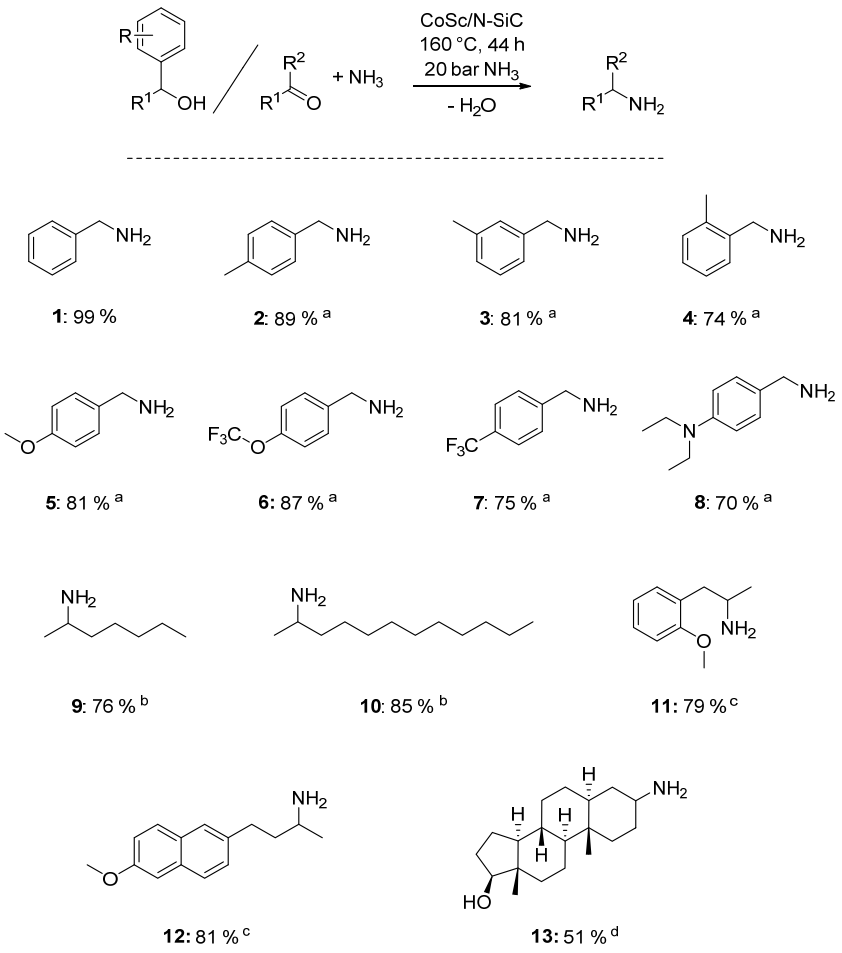

Scheme 8: Synthesis of primary amines employing a Co/Sc-catalyst. Isolated yields of the converted hydrochloride salts. Reaction conditions: 1.5 mol% Co, 0.49 mol% Sc, 0.5 mmol alcohol, 2.0 mL toluene, 0.5 mmol KOH, 160 °C, 44 h, 20 bar NH_3. [a] 180 °C. [b] 0.5 mmol ketone, 50 °C, 20 h, 10 bar H_2, 3.5 mL aq. NH_3-32%. [c] 0.5 mmol ketone, 60 °C, 20 h, 15 bar H_2, 3.5 mL aq. NH_3-32%. [d] 0.25 mmol ketone, 65 °C, 20 h, 15 bar H_2, 3.2 mL aq. NH_3-32%, 0.3 mL EtOH.

To tap the full potential of the Co/Sc catalyst, the combination of BH HA and reductive amination in subsequent manner has been explored. After the BH HA step with the benzyl alcohol to yield a primary amine, the catalyst can be used for the next step without any workup requirements. The neutralization of the reaction milieu and the addition of 0.8 mmol carbonyl compound led to the formation of more complex secondary amines (Scheme 9) while applying 100 °C and 40 bar H_2. This reaction sequence was able to mediate the synthesis of partly aliphatic secondary amines with different chain length and different branching (substrates **14**-**19**). The introduction of a ketone with aromatic ring and an electron withdrawing substituent didn't pose any problem (**20**-**22**). With the temperature increase to 180 °C in the BH HA step, substituted benzyl alcohols could be introduced and combined with an aliphatic ketone (substrates **23**-**26**). When employing aromatic aldehydes instead of ketones for the reductive amination step, another series of secondary

amine substrates could be synthesized (**27**-**35**). By raising the temperature of the reductive amination to 150 °C even benzophenone could be employed to yield a rather bulky secondary amine (substrate **36**).

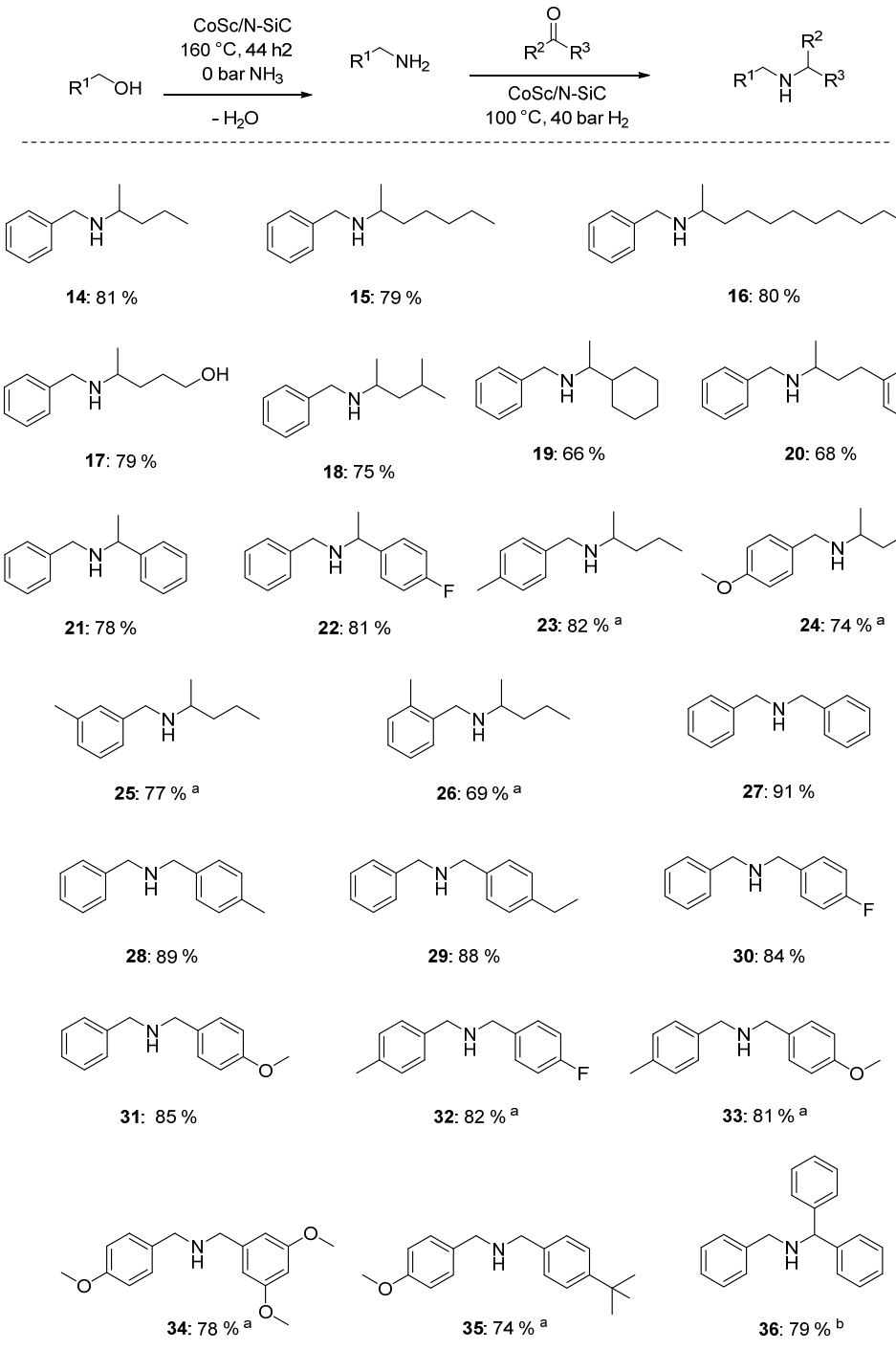

Scheme 9: One pot synthesis of secondary amines employing a Co/Sc-catalyst. Isolated yields of the converted hydrochloride salts. Reaction conditions for first step: 1.5 mol% Co, 0.49 mol% Sc, 0.5 mmol alcohol, 2.0 mL Toluene, 0.5 mmol KOH, 160 °C, 44 h, 20 bar NH_3. [a] 180 °C. Reaction conditions for second step: 1.5 mol% Co, 0.49 mol% Sc, 0.8 mmol carbonyl compound, 2.0 mL Toluene, 100 °C, 20 h, 40 bar H_2, 0.05 mL 32 % HCl. [b] 150 °C.

For the synthesis of tertiary amines with three benzylic substituents, the established synthesis protocol was extended by another reductive amination step. By adding 1.0 mmol of aldehyde and 0.05 mL concentrated hydrochloric acid, three examples could be synthesized at a temperature of 140 °C (Scheme 10, substrates **37**-**39**). Targeting tertiary amines with an unbranched aliphatic moiety, a workaround was needed since the catalyst could not mediate the BH HA reaction or reductive amination of unbranched, purely aliphatic compounds due to side reactions. By switching the gaseous ammonia with *n*-pentylamine, the formation of the imine was accomplished but the compound could not be hydrated to the corresponding amine. Thus, an extra hydrogenation step had to be carried out to obtain the desired product (Scheme 10, substrate **40**). Analogue to the tribenzylamine derivatives before, a third step can be added to this reaction to give tertiary amines. By adding 1.0 mmol of the respective aldehyde, substrates **41**-**45** could be synthesized. The reusability of the catalyst could be demonstrated by repeating the BH HA reaction of the model substrate benzyl alcohol five times without changing the catalyst. The reaction could be carried out every time without any significant loss of activity. Furthermore, the upscaling capabilities of the CoSc/N-SiC catalyst could be confirmed by carrying out the synthesis of product **14** (Scheme 9) with ten times the amount of all components. The secondary amine could be isolated with a yield of 76 %.

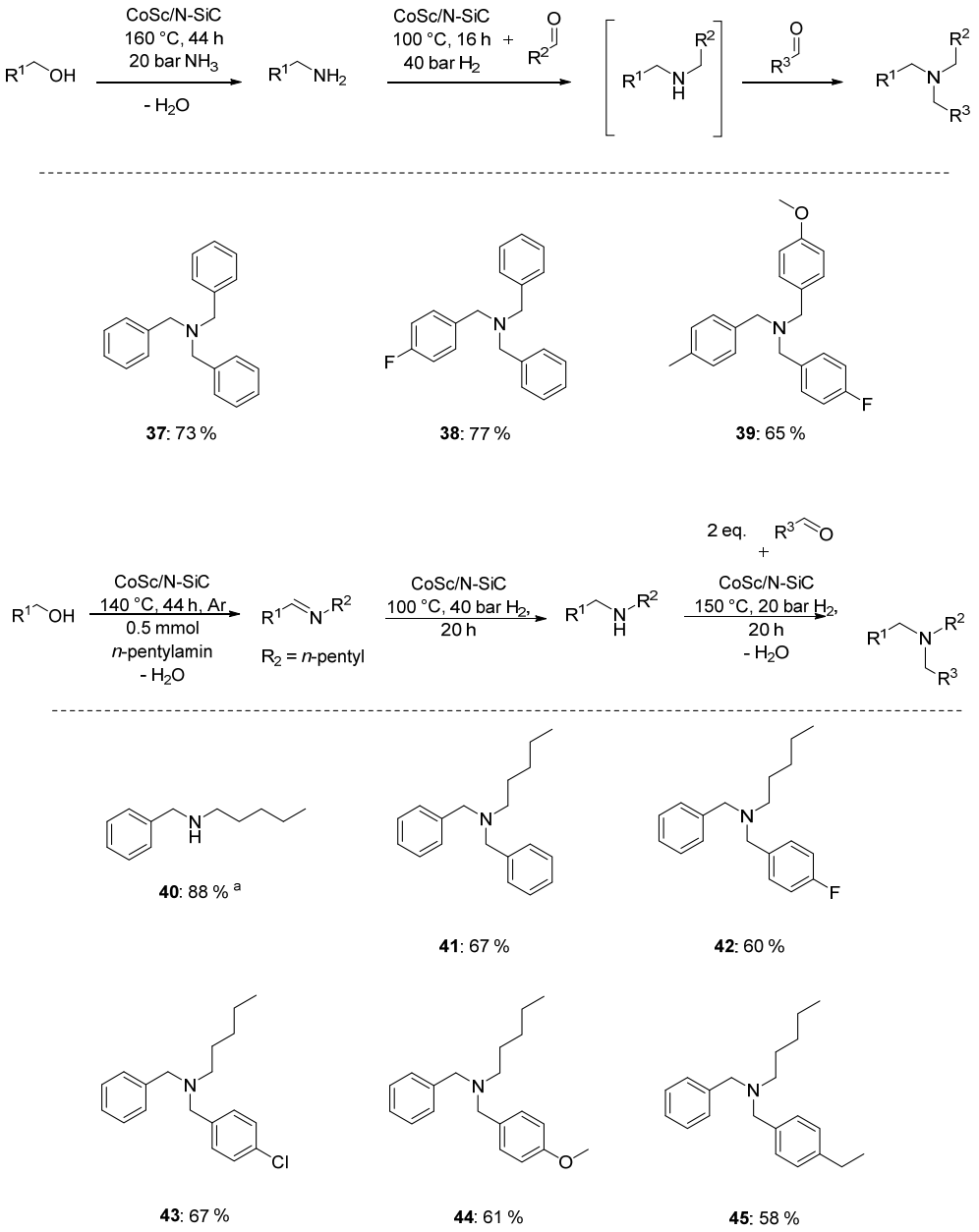

Scheme 10: One pot synthesis of tertiary amines employing a Co/Sc-catalyst. Isolated yields of the converted hydrochloride salts. Substrates 37-39: Reaction conditions for first step: 1.5 mol% Co, 0.49 mol% Sc, 0.5 mmol alcohol, 2.0 mL toluene, 0.5 mmol KOH, 160 °C, 44 h, 20 bar NH_3. Reaction conditions for second step: 1.5 mol% Co, 0.49 mol% Sc, 0.8 mmol aldehyde, 2.0 mL toluene, 100 °C, 20 h, 40 bar H_2, 0.05 mL 32 % HCl. Reaction conditions for third step: 1.5 mol% Co, 0.49 mol% Sc, 1.0 mmol aldehyde, 2.0 mL toluene, 140 °C, 20 h, 40 bar H_2, 0.05 mL 32 % HCl. Substrates 40-45: Reaction conditions for first step: 2.0 mol% Co, 0.65 mol% Sc, 0.5 mmol alcohol, 0.5 mmol *n*-pentylamine, 2.0 mL toluene, 0.5 mmol KOH, 140 °C, 44 h, Ar atmosphere. Reaction conditions for second step: 2.0 mol% Co, 0.65 mol% Sc, 2.0 mL toluene, 100 °C, 20 h, 40 bar H_2. Reaction conditions for third step: 2.0 mol% Co, 0.65 mol% Sc, 1.0 mmol aldehyde, 2.0 mL toluene, 150 °C, 20 h, 20 bar H_2, 0.05 mL 32 % HCl. [a] Product isolated after second step.

3.2 Individual Contributions to Joint Publications

The results presented in this thesis were achieved in collaboration with others and are published or to be submitted as indicated below. The contributions of all co-authors to the respective publication are specified. The corresponding author is annotated by an asterisk (*).

Chapter 4

This work is published in *ChemSusChem* **2021**, *14*, 2360-2366 with the tiltle:

Co-Catalyzed Synthesis of Primary Amines via Reductive Amination employing Hydrogen under very mild Conditions
Matthias Elfinger, Timon Schönauer, Sabrina L. J. Thomä, Robert Stäglich, Markus Drechsler, Mirijam Zobel, Jürgen Senker, Rhett Kempe*

I carried out the catalyst synthesis, catalytic reactions and parts of the catalyst characterization. Sabrina L. J. Thomä and Mirijam Zobel performed XRD analyses and PDF refinement. Timon Schönauer and I co-developed the catalyst. Robert Stäglich and Jürgen Senker carried out solid state NMR analyses. Markus Drechsler recorded the TEM images. Me and Rhett Kempe co-wrote the manuscript. Rhett Kempe supervised the work and was involved in the scientific discussions.

Chapter 5

This work is to be submitted with the title:

Synthesis of Secondary Amines via Borrowing Hydrogen employing a nanostructured bimetallic 3d-metal catalyst
Matthias Elfinger, Marie Bergmann, Rhett Kempe*

I carried out the catalyst synthesis, catalytic reactions and catalyst characterization. Marie Bergmann carried out some substrate syntheses during her bachelor thesis. Me and Rhett Kempe co-wrote the manuscript. Rhett Kempe supervised the work and was involved in the scientific discussions.

Chapter 6

This work is published in *Adv. Synth. Catal*. **2023**, *365*, 4654-4661 with the title:

General Synthesis of Alkyl Amines via Borrowing Hydrogen and Reductive Amination

Matthias Elfinger, Christof Bauer, Jörg Schmauch, Michael Moritz, Christoph Wichmann, Christian Papp, Rhett Kempe*

I carried out the catalyst synthesis, catalytic reactions and parts of the catalyst characterization. Christof Bauer revised the manuscript and supporting information and carried out the necessary experiments as well as co-wrote the manuscript. Jörg Schmauch performed the STEM-EELS measurements. Michael Moritz measured the XPS samples, Michael Moritz, Christian Papp and Christoph Wichmann performed XPS data analysis and evaluation. Me and Rhett Kempe co-wrote the manuscript. Rhett Kempe supervised the work and was involved in the scientific discussions.

4 Co-Catalyzed Synthesis of Primary Amines via Reductive Amination employing Hydrogen under very mild Conditions

Matthias Elfinger, Timon Schönauer, Sabrina L. J. Thomä, Robert Stäglich, Markus Drechsler, Mirijam Zobel, Jürgen Senker, Rhett Kempe*

Co-Catalyzed Synthesis of Primary Amines via Reductive Amination employing Hydrogen under very mild Conditions.

ChemSusChem, **2021**, *14*, 2360-2366

Copyright Wiley-VCH GmbH.
Reproduced with permission (https://creativecommons.org/licences/by/4.0/).

Alterations: Yellow backgrounds in the Supporting Information removed.

Check for updates

ChemSusChem

Full Papers
doi.org/10.1002/cssc.202100553

Chemistry Europe
European Chemical Societies Publishing

VIP *Very Important Paper*

Co-Catalyzed Synthesis of Primary Amines via Reductive Amination employing Hydrogen under very mild Conditions

Matthias Elfinger,[a] Timon Schönauer,[a] Sabrina L. J. Thomä,[b] Robert Stäglich,[c] Markus Drechsler,[d] Mirijam Zobel,[b] Jürgen Senker,[c] and Rhett Kempe*[a]

Nanostructured and reusable 3d-metal catalysts that operate with high activity and selectivity in important chemical reactions are highly desirable. Here, a cobalt catalyst was developed for the synthesis of primary amines via reductive amination employing hydrogen as the reducing agent and easy-to-handle ammonia, dissolved in water, as the nitrogen source. The catalyst operates under very mild conditions (1.5 mol% catalyst loading, 50 °C and 10 bar H_2 pressure) and outperforms commercially available noble metal catalysts (Pd, Pt, Ru, Rh, Ir). A broad scope and a very good functional group tolerance were observed. The key for the high activity seemed to be the used support: an N-doped amorphous carbon material with small and turbostratically disordered graphitic domains, which is microporous with a bimodal size distribution and with basic NH functionalities in the pores.

Introduction

Reductive amination, the reaction of an aldehyde or a ketone and ammonia or an amine in the presence of a reducing agent, is a very important chemical transformation intensively investigated and used in industry and academia.[1] The use of inexpensive and potentially green hydrogen as the reducing agent in the presence of a catalyst is especially attractive.[1] The products of reductive aminations, alkyl amines, are very important bulk and fine chemicals and/or biologically active compounds such as pharmaceuticals or agro chemicals.[2] Especially challenging and important is the synthesis of primary amines. The reaction is challenging since over-alkylation and other unwanted side reactions have to be avoided, and it is crucial since primary amines are important starting materials to synthesize other amines or N-heterocyclic compounds.[3] The replacement of rare elements in key technologies is very important too. Catalysis, a key technology of our century, is often based on rare noble metals such as Pd, Pt, Rh, and Ir. Earth-abundant metal catalysts have played an important role with respect to the development of reductive amination in its early days,[4] in particular Raney Ni. Note that Raney Ni is difficult to handle and its reusability is limited. Very recently, nanostructured and reusable Co catalysts have been introduced for the general synthesis of primary amines from ammonia and ketones or aldehydes and hydrogen (Scheme 1).[5] Unfortunately, these catalysts operate under rather harsh conditions. A general problem with 3d-metal catalysts is their significantly lower activity in many reactions in comparison to noble metal catalysts. Thus, reusable or nanostructured catalysts based on abundantly available elements that operate under very mild conditions and

[a] *M. Elfinger, T. Schönauer, Prof. Dr. R. Kempe*
Inorganic Chemistry II – Catalyst design, Sustainable Chemistry Centre
University of Bayreuth
95440 Bayreuth (Germany)
E-mail: kempe@uni-bayreuth.de
[b] *S. L. J. Thomä, Prof. Dr. M. Zobel*
Solid State Chemistry – Mesostructured Materials
University of Bayreuth
95440 Bayreuth (Germany)
[c] *R. Stäglich, Prof. Dr. J. Senker*
Inorganic Chemistry III and North Bavarian NMR center
University of Bayreuth
95440 Bayreuth (Germany)
[d] *Dr. M. Drechsler*
Bavarian Polymer Institute (BPI), Keylab "Electron and Optical Microscopy"
University of Bayreuth
95440 Bayreuth (Germany)

Supporting information for this article is available on the WWW under https://doi.org/10.1002/cssc.202100553

© 2021 The Authors. ChemSusChem published by Wiley-VCH GmbH. This is an open access article under the terms of the Creative Commons Attribution License, which permits use, distribution and reproduction in any medium, provided the original work is properly cited.

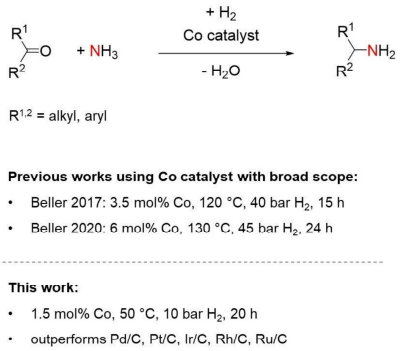

Scheme 1. Reusable and nanostructured Co catalysts for the reductive amination of ketones and aldehydes to primary amines using hydrogen as the reducing agent.

ChemSusChem
Full Papers
doi.org/10.1002/cssc.202100553
Chemistry Europe
European Chemical Societies Publishing

1864564x, 2021, 11, Downloaded from https://chemistry-europe.onlinelibrary.wiley.com/doi/10.1002/cssc.202100553 by Universitaet Bayreuth, Wiley Online Library on [13/07/2023]. See the Terms and Conditions (https://onlinelibrary.wiley.com/terms-and-conditions) on Wiley Online Library for rules of use; OA articles are governed by the applicable Creative Commons License

are competitive with noble metal catalysts are highly desirable. We have recently introduced Ni[6] and Fe[7] catalysts and report here on a highly active and reusable Co catalyst for the selective synthesis of primary amines via reductive amination employing hydrogen as the reducing agent. Our catalyst operates under very mild conditions (1.5 mol% catalyst loading, 50 °C and 10 bar H_2 pressure) and outperforms commercially available noble metal catalysts (Pd, Pt, Ru, Rh, Ir), and ammonia dissolved in water, which is easy to handle and inexpensive, is used. We observe a broad scope with good functional group tolerance that encompasses aryl-alkyl, diaryl, dialkyl ketones and aldehydes, which can be converted into the corresponding primary amines. Furthermore, the amination of biologically active compounds has been demonstrated. The key for the high activity seems to be the used N-SiC support. It is an N-doped (≈7 wt%) amorphous carbon material processed at 1000 °C having graphitic domains smaller than 2 nm with a turbostratic disorder and widened average interlayer distances. The material is microporous with a bimodal pore size distribution, which look as if to be of a chemically different origin. The larger of them seem to contain accessible basic NH functionalities most likely formed via hydrolysis of C–N–Si bonds during NaOH treatment. Besides the above-mentioned two Co catalysts for the synthesis of primary amines from ketones or aldehydes and ammonia, other Co catalyst systems for reductive amination reactions employing hydrogen as the reducing agent have been introduced.[8]

Results and Discussion

Catalyst synthesis and characterization

First, the N-SiC support was synthesized following published procedures by crosslinking the commercially available polycarbosilane precursor SMP 10 and acrylonitrile in dimethylformamide, using azobis-isobutyronitrile as an initiator.[9] The greenbody was pyrolyzed at 1000 °C under inert atmosphere and then treated with 1 M NaOH at 85 °C overnight (see the Supporting Information 2.1). To obtain the active catalyst, the N–SiC support was impregnated with $Co(NO_3)_2 \cdot 6H_2O$ dissolved in water, pyrolyzed (700 °C, N_2) and reduced (550 °C, N_2/H_2). Inductively coupled plasma optical emission spectroscopy (ICP-OES) analysis of the catalyst revealed a cobalt content of 2.24 wt% (see the Supporting Information 3.1). The specific surface area could be determined by argon physisorption measurements (Figure 1C) and showed a decline in surface area from 545 $m^2 g^{-1}$ of the support material to 491 $m^2 g^{-1}$ of the catalyst. A homogeneous distribution of the cobalt nanoparticles over the N-SiC support (Figure 1B) and an average particle size of 5.9 nm could be determined via transmission electron microscopy (TEM). In addition, X-ray photoelectron spectroscopy (XPS) showed the presence of metallic cobalt and cobalt oxi(hydroxide) species as well as different binding modes of nitrogen within the support material at the surface of the catalyst material (see the Supporting Information Figure S2). Scanning electron microscopy (SEM) in combination with energy dispersive X-ray spectroscopy (EDX) confirmed the homogeneous distribution of the cobalt nanoparticles over the N-SiC support (see the Supporting Information Figure S3). Pair distribution function (PDF) studies (Figure 1D) indicate the presence of Co fcc and CoO fcc

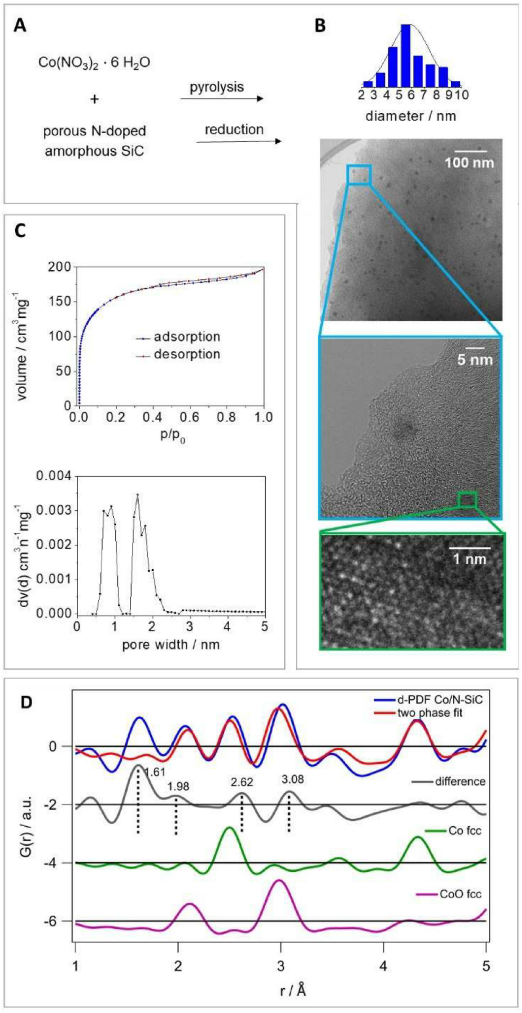

Figure 1. Synthesis and characterization of the Co catalyst: (A) Synthesis of the crosslinked material, followed by pyrolysis and NaOH treatment to obtain the support material; wet impregnation, pyrolysis and reduction led to the active Co catalyst. (B) TEM analysis suggested the presence of homogeneously distributed Co nanoparticles with an average particle size of 5.9 nm. High-resolution (HR)TEM micrograph with atomic resolution of a Co nanoparticle surface. (C) Surface characterization and pore size distribution of the catalyst via argon physisorption measurement [calculation model: Ar at 87 K on carbon (cylindr. pores, NLDFT equilibrium model)]. The specific surface showed a slight decline from 545 $m^2 g^{-1}$ of the support material to 491 $m^2 g^{-1}$ of the catalyst. (D) The differential-PDF of (Co/N-SiC)-(N-SiC) (blue) was fitted with a two-phase fit (red) containing a Co fcc (green) and a CoO fcc (pink) phase. Remaining distance correlations in the difference curve (grey) exist for the short-range order up to 5 Å.

© 2021 The Authors. ChemSusChem published by Wiley-VCH GmbH

ChemSusChem | Full Papers doi.org/10.1002/cssc.202100553 | Chemistry Europe European Chemical Societies Publishing

1864564x, 2021, 11, Downloaded from https://chemistry-europe.onlinelibrary.wiley.com/doi/10.1002/cssc.202100553 by Universitaet Bayreuth, Wiley Online Library on [13/07/2023]. See the Terms and Conditions (https://onlinelibrary.wiley.com/terms-and-conditions) on Wiley Online Library for rules of use; OA articles are governed by the applicable Creative Commons License

nanoparticles. The Co domain size was refined to about 9 nm in comparison to the CoO domain size with about 3 nm (see the Supporting Information Table S3). An average particle diameter of 5.9 nm with a distribution from 3–9 nm was determined by TEM (Figure 1B). This suggests that separate Co and CoO nanoparticles exist rather than Co and CoO domains within one particle.

Optimization of the reaction conditions

In order to determine the optimized reaction conditions, the reductive amination of acetophenone to 1-phenylethylamine was chosen as benchmark reaction. The solvent screening revealed that a concentration of ammonia in water of 32% leads to the best yield of amine product since the high concentration accelerates the imine formation prior to the reduction step. The optimally adjusted reaction parameters could be defined as 3.5 mL aqueous ammonia (32%), 10 bar H_2, 50 °C and 1.5 mol% cobalt. Since water is our preferred solvent, ammonia gas could also be used, which would form ammonia dissolved in water then. We further investigated the influence of varying metal loadings of the catalyst (Table 1). The experiments revealed that the catalyst with theoretically 3 wt% cobalt showed the best activity in the reductive amination. Lowering the pyrolysis temperature to 600 °C led to a significant reduction of yield. Applying a higher temperature (800 °C) led to better results than 600 °C but could not match the superior activity of the catalyst that was pyrolyzed at 700 °C. Pure N-SiC support as well as cobalt nitrate on various commercially available supports showed no conversion of acetophenone.

Table 1. Cobalt catalyst comparison.[a]

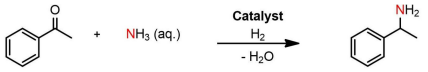

Entry	Metal source	Support	Pyrolysis temperature [°C]	Yield = Conversion [%]
1	Co-nitrate (3 wt% Co)	N-SiC	700	99
2	Co-nitrate	N-SiC	600	3
3	Co-nitrate	N-SiC	800	87
4	Co-nitrate (2 wt% Co)	N-SiC	700	21
5	Co-nitrate (4 wt% Co)	N-SiC	700	91
6	Co-nitrate (5 wt% Co)	N-SiC	700	32
7	Co-nitrate	activated C	700	0
8	Co-nitrate	Al_2O_3	700	0
9	Co-nitrate	TiO_2	700	0
10	Co-nitrate	SiO_2	700	0
11	–	N-SiC	700	0
12[b]	Ni salen complex	Al_2O_3	700	0

[a] Reaction conditions: 1.5 mol% Co (2.24 wt% Co, 0.0075 mmol Co, 0.44 mg Co), 0.5 mmol acetophenone, 50 °C, 20 h, 10 bar H_2, 3.5 mL aq. NH_3-32%. Yields were determined by GC using *n*-dodecane as an internal standard. [b] 2.0 mol% Ni (4.0 wt% Ni).

TEM investigation of these materials revealed inhomogeneously distributed or barely present nanoparticles (see the Supporting Information Figure S4). A highly active Ni/Al_2O_3 catalyst introduced by our group in 2019 also showed no activity when applied under the conditions mentioned above.[6] For this Ni-catalyst, a Ni complex stabilized by a N,O-ligand called salen was used as a metal precursor and the C- and N-atoms of the ligand provide an N-doped carbon matrix in which the Ni nanoparticles are embedded and, so, fixed at the Al_2O_3 support. It might be that the very mild reaction conditions make it very challenging for other supports in combination with inexpensive simple metal precursor Co nitrate. When comparing the activity and selectivity of well-known and commercially available noble metal catalysts to our cobalt system, it can be shown that the latter is outperforming all noble catalysts applying the same reaction conditions. Ru/C and Rh/C are inactive regarding the formation of the primary amine **1**. Other metals (Pd, Pt, and Ir) form the desired product of about 50% and simultaneously side products based on acetophenone hydrogenation mainly 1-phenylethanol (**2**) and 1-phenyl-cyclohexylalcohol (**3**) (Table 2). When compared to the literature where the selective reductive amination of ketones to branched primary amines using ammonia is addressed, all papers except one report harsher conditions in terms of temperature and hydrogen pressure than we have used for our cobalt catalyst system.[10] In 2020, Wang and co-workers reported on palladium nanoparticles for the reductive amination of 16 aromatic ketones with aqueous ammonia under milder conditions.[11] However, extremely high catalyst loadings of 37 mol% Pd were used.

Substrate scope

Since the optimized reaction conditions have been predefined, we were interested in the substrate scope of our highly active/selective catalyst system. The product yields refer to the isolated corresponding hydrochloride salts of the synthesized amines.

Table 2. Reductive amination with noble metal catalysts.[a]

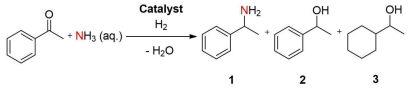

Entry	Catalyst	Yield 1 [%]	Yield 2 [%]	Yield 3 [%]	Other products [%]
13[b]	Pd/C	46	53	–	–
14[c]	Pt/C	48	32	–	19
15[d]	Ru/C	3	58	6	32
16[e]	Rh/C	0	0	48	51
17[f]	Ir/C	49	30	–	20

[a] Reaction conditions: 0.5 mmol acetophenone, 50 °C, 20 h, 10 bar H_2, 3.5 mL aq. NH_3-32%. Yields were determined by GC using *n*-dodecane as an internal standard. [b] 2.0 mol% Pd (10.0 wt% Pd). [c] 2.0 mol% Pt (5.0 wt % Pt). [d] 2.0 mol% Ru (5.0 wt% Ru). [e] 2.0 mol% Rh (5.0 wt% Rh). [f] 2.0 mol% Ir (1.0 wt% Ir).

 © 2021 The Authors. ChemSusChem published by Wiley-VCH GmbH

ChemSusChem | Full Papers doi.org/10.1002/cssc.202100553 | Chemistry Europe European Chemical Societies Publishing

1864564x, 2021, 11, Downloaded from https://chemistry-europe.onlinelibrary.wiley.com/doi/10.1002/cssc.202100553 by Universitaet Bayreuth, Wiley Online Library on [13/07/2023]. See the Terms and Conditions (https://onlinelibrary.wiley.com/terms-and-conditions) on Wiley Online Library for rules of use; OA articles are governed by the applicable Creative Commons License

First, we investigated the reductive amination of aryl-alkyl ketones with various substituents. Substrates with short, moderate and long aliphatic moieties (Scheme 2, products **1**–**3**) could be isolated in very good yields of 84–99%. The conversion of ketones with electron-withdrawing substituents, such as halogens, also worked out well with yields of over 90% for the *para*-substituted derivatives (Scheme 2, products **4**–**6**). The sterically more demanding *meta*-chloroacetophenone (Scheme 2, product **7**) could also be converted with an isolated yield of 90%. The heavily electron-withdrawing trifluoromethyl group (Scheme 2, product **8**) required higher reaction temperatures (60 °C) to be converted into its corresponding primary amine with an excellent yield of 97%. Minor electron-donating substituents, such as methyl groups, could be tolerated very well in *meta*- and *para*-positions of the aromatic ring (Scheme 2, products **9** and **10**). For the *ortho*-substituted acetophenone, we had to increase the temperature to 60 °C to obtain 91% of isolated product (Scheme 2, product **11**). If the electron-donating property of the substituents was increased (e.g., methoxy groups), *meta*- and *para*-substituted ketones (Scheme 2, products **12** and **13**), as well as dimethoxy acetophenone (product **14**) could be converted smoothly into the corresponding primary amines without any need to increase the temperature. The reductive amination of benzophenone (Scheme 2, product **15**) showed that aryl-aryl ketones can also be converted with slightly harsher conditions, which are also needed for the sterically demanding benzyl-4-fluorophenyl ketone (product **18**). The amination of a N-heterocyclic ketone (Scheme 2, product **16**) proceeded smoothly with an isolated yield of 91%. The corresponding amine of 1-indanon could be acquired with a 62% yield (product **17**). For the reductive amination of benzylic aldehydes, higher temperatures were needed to suppress the self-coupling reaction of the primary amine product with unconverted substrate. Therefore 80 °C and a catalyst loading of 1.1 mol% were used. Benzaldehyde (Scheme 2, product **19**), as well as its substituted derivates could be converted in very good yields. Electron-donating substituents such as methyl and methoxy groups (Scheme 2, products **20** and **21**) were tolerated very well with isolated yields of the corresponding amines up to 88%. In addition, the conversion of substituted benzaldehydes containing electron-withdrawing moieties such as halogens was also accomplished with very good yields up to 91% (Scheme 2, products **22** and **23**).

In addition, we investigated the reductive amination of purely aliphatic ketones. Substrates with long and short branched and linear aliphatic chains as well as cyclic ketones could be aminated in moderate to very good yields (36–93%, Scheme 3). Aliphatic ketones with low molecular weight could only be isolated in moderate yields due to their low boiling points, which caused significant losses of product during the workup procedure.

Next, we became interested in the reductive amination of biologically active molecules under very mild conditions. The selective conversion of nabumetone, 4- and 2-methoxyphenylacetone to their corresponding primary amines could be accomplished in isolated yields of up to 90% (Scheme 4). The reductive amination of steroid molecules was rather challenging, due to the poor water solubility of this substance class at 50 °C.

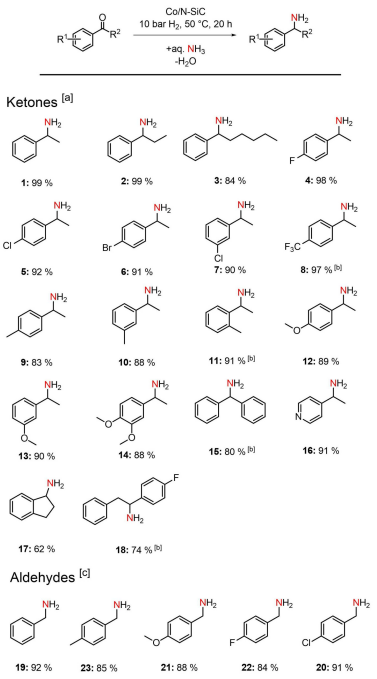

Scheme 2. Reductive amination of aryl substituted ketones and aldehydes to primary amines. [a] Reaction conditions for ketones: 1.5 mol% Co (2.24 wt% Co, 0.0075 mmol Co, 0.44 mg Co), 0.5 mmol ketone, 50 °C, 20 h, 10 bar H_2, 3.5 mL aq. NH_3-32%. [b] 60 °C. [c] Reaction conditions for aldehydes: 1.1 mol% Co, 0.5 mmol aldehyde, 80 °C, 20 h, 10 bar H_2, 3.5 mL aq. NH_3-32%. Isolated yields of the converted hydrochloride salts.

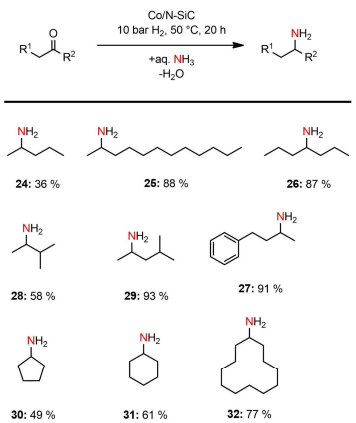

Scheme 3. Reductive amination of purely aliphatic ketones to primary amines. Reaction conditions: 1.5 mol% Co (2.24 wt% Co, 0.0075 mmol Co, 0.44 mg Co), 0.5 mmol ketone, 50 °C, 20 h, 10 bar H_2, 3.5 mL aq. NH_3-32%. Isolated yields of the converted hydrochloride salts.

 © 2021 The Authors. ChemSusChem published by Wiley-VCH GmbH

ChemSusChem | Full Papers doi.org/10.1002/cssc.202100553 | Chemistry Europe European Chemical Societies Publishing

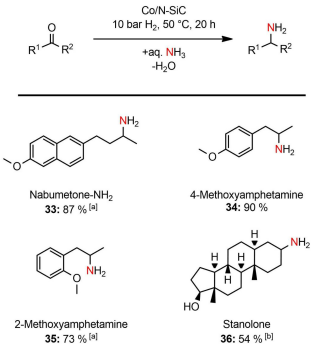

Scheme 4. Reductive amination of biologically active molecules to primary amines. Reaction conditions:1.5 mol% Co (2.24 wt% Co, 0.0075 mmol Co, 0.44 mg Co), 0.5 mmol ketone, 50 °C, 20 h, 10 bar H_2, 3.5 mL aq. NH_3-32%; Isolated yields of the converted hydrochloride salts. [a] 60 °C; [b] 3 mol% Co, 65 °C, 3.2 mL aq. NH_3-32%, 0.3 mL EtOH.

By applying 65 °C and 3 mol% Co as well as adding 0.3 mL of ethanol to enhance the solubility, 54% of Stanolone-NH_2 could be obtained. Attempts to aminated examples carrying an ester, an amide, or a nitro group and a keto acid failed under the given conditions.

Reusability and upscaling

Finally, we examined the reusability and upscaling of our cobalt catalyst system. Five consecutive runs without any loss of activity were performed to confirm the recyclability (see the Supporting Information Figure S1), and the reductive amination of 10 mmol acetophenone, our model substrate, could be accomplished with 95% yield (see the Supporting Information 2.4.3).

Nature of the N-SiC support

The key for the high activity seems to be the N-SiC support, which we analyzed in detail employing solid-state NMR spectroscopy (ssNMR), synchrotron radiation-based powder X-ray diffraction (PXRD)/PDF, Raman spectroscopy, XPS, and acid-base titration. Key results of the NMR spectroscopic and PXRD/PDF investigations are listed in Figure 2. The starting point of the support synthesis is a copolymerization of acrylonitrile with the commercially available polycarbosilane SMP 10 followed by pyrolysis up to 1000 °C. The pyrolyzed material is then treated with a 1 M NaOH solution at 85 °C for 16 h. ^{13}C cross polarization (CP) and ^{29}Si single pulse magic angle spinning (SP MAS) NMR spectra (see the Supporting Information Figure S12 and Figure 2A) suggest that the pyrolyzed material consists of graphitic domains and silicon rich regions with mixed SiC_xO_{4-x} and SiN_xO_{4-x} environments.[9,12] The NaOH treatment leads to a nearly complete removal of the silicon-rich domains. In this process, the specific surface area increases from 6 to 545 $m^2 g^{-1}$ [Ar sorption,

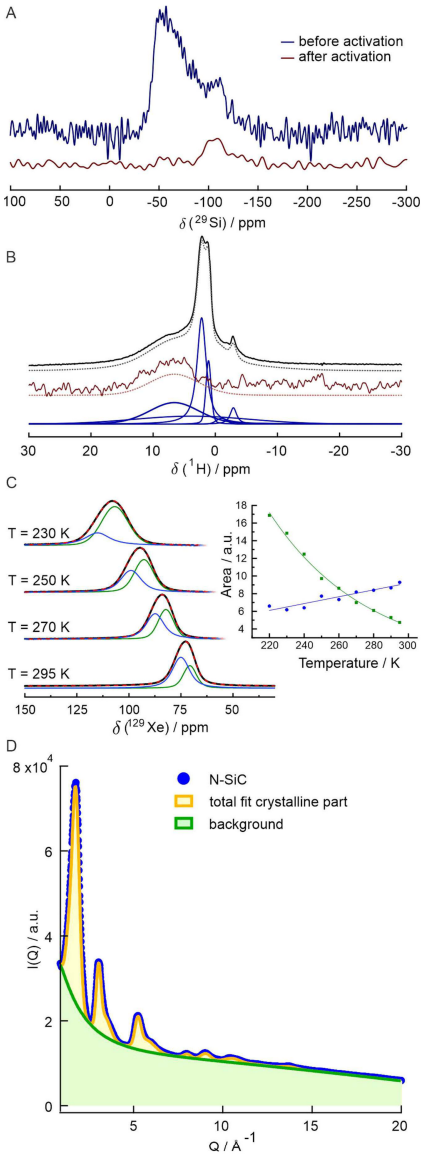

Figure 2. NMR and PXRD/PDF investigations. (A) ^{29}Si SP MAS NMR spectra of the N-SiC support prior (blue) and after (brown) NaOH treatment (activation). (B) Ultrafast ^1H MAS NMR spectra; SP excitation (top) and nitrogen selective ^1H-^{14}N HMQC excitation (brown). Both spectra are deconvoluted with the same set of normal components (blue lines). The resulting lineshapes are depicted by pointed lines beneath the experimental spectra (C) Variable-temperature ^{129}Xe NMR spectra using hyperpolarized ^{129}Xe within the limiting shift region. The inset depicts the intensity trend for the observed two resonances as function of temperature. (D) PXRD data of N-SiC support material (blue) with its fit for the crystalline phase fraction (yellow) of 17% on the big amorphous background (green).

 © 2021 The Authors. ChemSusChem published by Wiley-VCH GmbH

1864564x, 2021, 11, Downloaded from https://chemistry-europe.onlinelibrary.wiley.com/doi/10.1002/cssc.202100553 by Universitaet Bayreuth, Wiley Online Library on [13/07/2023]. See the Terms and Conditions (https://onlinelibrary.wiley.com/terms-and-conditions) on Wiley Online Library for rules of use; OA articles are governed by the applicable Creative Commons License

ChemSusChem | Full Papers doi.org/10.1002/cssc.202100553 | Chemistry Europe European Chemical Societies Publishing

1864564x, 2021, 11, Downloaded from https://chemistry-europe.onlinelibrary.wiley.com/doi/10.1002/cssc.202100553 by Universitaet Bayreuth, Wiley Online Library on [13/07/2023]. See the Terms and Conditions (https://onlinelibrary.wiley.com/terms-and-conditions) on Wiley Online Library for rules of use; OA articles are governed by the applicable Creative Commons License

Brunauer-Emmett-Teller (BET) model, see the Supporting Information Figure S5]. The pore size distribution below 2.3 nm supports a domain structure of the pyrolyzed material, which is turned into a predominantly microporous material by the NaOH treatment. Besides adsorbed mobile water, the ^{1}H NMR spectra obtained with ultrafast MAS and SP (black) as well as nitrogen-selective ^{1}H-^{14}N heteronuclear multiple quantum coherence (HMQC) excitation (brown) (Figure 2B) prove the presence of a substantial amount of NH_x ($x = 1, 2$) functionalities.[13] The latter is also supported by the ^{15}N{^{1}H} CP MAS NMR spectra (see the Supporting Information Figure S14) and the downfield flank within the ^{13}C MAS NMR spectrum supportive for carbon atoms in local $CN_y(NH_x)$ environments also observed for graphitic carbon nitrides.[14] The N 1s XPS spectra (see the Supporting Information Figure S2D) are in agreement with this analysis. Hyperpolarized ^{129}Xe NMR (see Supporting Information Figures S15, S16), and especially the line shape analysis in the high-temperature regime (Figure 2C) reveal that the adsorbed signal consists of two different resonances with a markedly different depolarization behavior. The intensity of the highfield signal increases with decreasing temperature, which is expected for diamagnetic systems due to the larger Xe uptake.[15] In contrast, the intensity of the downfield signal decreases, demonstrating that depolarization dominates as typical for graphite.[16] We thus assign the two ^{129}Xe resonances to domains consisting of graphite and a diamagnetic component (e.g., a carbon nitride like region). In the low loading limit at high temperatures, usually smaller pores are preferentially populated. The depolarization behavior of the adsorbed hyperpolarized ^{129}Xe (Figure 2C) thus suggests that the smaller pores occur predominantly in the graphitic regions. Considering the bimodal pore size distribution with nearly the same pore volume for both pore size ranges (see Supporting Information Figure S5 and Figure 1C [catalyst]), it is suggestive that the region with the larger pores contains the observed NH_x functionalities. A fit of the PXRD data of the N-SiC support material after NaOH treatment (blue) resulted in a crystalline phase fraction of about 17% (total fit yellow, Figure 2D and Supporting Information Figure S9) on a big amorphous background (green). A widened average interlayer distance of 3.57 Å was found by fitting the (002) reflex in PXRD data, alongside a smaller fraction of stronger expanded stacks with an average interlayer distance of 4.52 Å in comparison to hexagonal graphite with an interlayer distance of 3.354 Å (see the Supporting Information 3.8). The multinuclear NMR and Raman spectra (see Figure 2 and Supporting Information Figure S6) are in accordance with a dominantly amorphous graphitic material. The PDF of the N-SiC support (see the Supporting Information Figure S10) indicates hexagonal graphite structure. Below 5 Å, all distances match in-plane carbon–carbon distances in hexagonal carbon rings. Since the PDF decayed to 0 beyond about 20 Å, it can be concluded that the structural coherence of the N-SiC support is about 2 nm. Rather high atomic displacement parameters u_{33} along the *c*-axis corroborate turbostratic disorder in PDF refinements. HRTEM based analysis of the graphitic domains (see the Supporting Information Figure S8) is in accordance and revealed a mean size of the graphitic domains of 1.6 nm and a widened interlayer distance of 3.6 Å. Acid-base titration revealed the presence of 0.42 mmol accessible basic N atom functionalities per gram N-SiC material after activation.

In summary, our N-SiC support is an N doped (≈7 wt%) amorphous carbon material (processed at 1000 °C) having graphitic and nitrogen doped domains smaller than 2 nm with a turbostratic disorder and widened interlayer distances. The material is predominantly microporous with a bimodal size distribution, which might be chemically different. The larger one of them seems to contain the accessible basic NH functionalities most likely formed via hydrolysis of C–N–Si bonds during NaOH treatment.

Conclusion

We report on a highly active 3d-metal catalyst for the selective synthesis of primary amines via reductive amination employing hydrogen, a key reaction in industry and academia. Our catalyst is nanostructured and reusable, has a large scope, and outperforms noble metal catalysts. The key for the high activity seems to be our support: an amorphous N-doped carbon material with small graphitic domains and with pores that carry NH-functionalities. 88% of the basic NH-functionalities are still present or available in the final cobalt catalyst. The accessible NH-functionalities can bind cobalt species during catalyst synthesis or even catalysis and might catalyze the crucial condensation step. Related materials might be suitable for a more rational design of highly active 3d-metal catalysts.

Experimental Section

General considerations

All air- and moisture sensitive reactions were performed under dry argon or nitrogen atmosphere using standard Schlenk and glovebox techniques. All dried solvents were obtained from a solvent purification system (activated alumina cartridges) or purchased from Acros. Deuterated solvents were dried via molecular sieves. All chemicals were acquired from commercial sources with purity over 95% and used without further purification. The precursor SMP-10 was purchased from Starfire Systems, New York, USA. Pyrolysis of the support material was carried out under nitrogen atmosphere in a high temperature furnace (Gero, Berlin, Germany). Pyrolysis and reduction of the catalyst were performed under nitrogen or forming gas (90:10) atmosphere in a ChemBET Pulsar TPR/TPD instrument from Quantachrome. TEM was carried out by using a Variant LEO 9220 (200 kV) and a JEOL JEM 2200FS (200 kV) device. For the sample preparation, the samples were suspended in chloroform and sonicated for 5 min.

Pore characterizations were carried out via nitrogen sorption measurements using a 3P Micro 100 Surface Area and Pore Size Analyzer device. The pore size distribution was computed via DFT calculations (calculation model: Ar at −186.15 °C on cylindrical pore, MDFT equilibrium model). The specific surface area was calculated by using p/p_0 values from 0.005–0.1 (BET).

NMR measurements were performed using a Varian INOVA 300 (300 MHz for 1H, 75 MHz for ^{13}C) and a Bruker Avance III HD 500 (500 MHz for 1H, 125 MHz for ^{13}C) instrument at 296 K.

 © 2021 The Authors. ChemSusChem published by Wiley-VCH GmbH

ChemSusChem | Full Papers doi.org/10.1002/cssc.202100553 | Chemistry Europe European Chemical Societies Publishing

1864564x, 2021, 11, Downloaded from https://chemistry-europe.onlinelibrary.wiley.com/doi/10.1002/cssc.202100553 by Universitaet Bayreuth, Wiley Online Library on [13/07/2023]. See the Terms and Conditions (https://onlinelibrary.wiley.com/terms-and-conditions) on Wiley Online Library for rules of use; OA articles are governed by the applicable Creative Commons License

The hydrogenation experiments were carried out with Parr Instrument stainless-steel autoclavesN-MT5 250 mL equipped with heating mantles and temperature controller.

PXRD data was collected at 65 keV (0.1907 Å) at ID31 at the European Synchrotron Radiation Facility (ESRF) with a CdTe Dectris Pilatus X 2 M detector. NIST cerium oxide standard was used for distance calibration and determination of instrumental resolution ($Q_{damp} = 0.016$; $Q_{broad} = 0.008$). Fits to the PXRD data were conducted with the multipeak fitting option within the software Igor Pro 8.

^{129}Xe, ^{29}Si, ^{15}N and ^{13}C solid-state NMR measurements were performed on a Bruker Avance II NMR spectrometer operating at an external field of 7.05 T corresponding to Larmor frequencies of 83.4, 59.6, 30.4 and 75.5 MHz for the ^{129}Xe, ^{29}Si, ^{15}N and ^{13}C, respectively.

Variable-temperature measurements of hyperpolarized (hp) ^{129}Xe spectra were performed using a wideline 5 mm double-resonance Bruker probe. Hyperpolarized Xenon was supplied by a homebuilt polarizer with a gas composition of 1% *v/v* Xe with natural abundance of the ^{129}Xe isotope, 6% *v/v* N_2 as fluorescence quenching gas and He as buffer gas at a system pressure of 4×10^5 Pa. ^{129}Xe wideline SP NMR spectra were recorded in steps of 10 K with an equilibration time of 3 min before starting the acquisition. The pulse length for the $\pi/2$ pulse was set to 3.25 µs with a nutation frequency of approximately 77 kHz. Two scans were accumulated for each temperature with a temperature dependent recycle delay between 1 s at room temperature and 120 s at 130 K. The chemical shift was referenced to gaseous xenon at zero pressure (0 ppm).

^{13}C NMR spectra were recorded as SP and CP experiments under MAS with a spinning speed of 10 kHz using a Bruker 4 mm triple-resonance MAS probe. SP MAS NMR spectra were accumulated with pulse lengths of 2.3 µs for the $\pi/2$ pulse with a nutation frequency of approximately 110 kHz. Recycle delays were varied between 10 and 300 s after a pre-saturation pulse train.

Catalytic procedures

All catalytic reactions were carried out after the procedure described in the following: A magnetic stirring bar, 0.5 mmol ketone, 3.5 mL aq. NH_3 (32%) and 2 mol% Co catalyst (3.0 wt% Co, 0.01 mmol Co 0.59 mg Co, 19.7 mg catalyst) were filled in a 5 mL glass reaction vial. For aldehydes, 1.5 mol% Co was used. The vial was placed in a 250 mL high-pressure autoclave (Parr Instruments) and flushed three times with 0.5 MPa of hydrogen. The autoclave was pressurized with 1.0 MPa of hydrogen and the reaction was stirred for 20 h at 50 °C for ketones and 80 °C for aldehydes. After cooling to room temperature and release of the hydrogen pressure, the solution was extracted five times with methyl *tert*-butyl ether and dried over Na_2SO_4. The resulting solution was filtered and the solvent was removed under reduced pressure. To obtain the amine hydrochloride salts, 0.5 mL HCl in ether were added. The solvent was removed under reduced pressure and the resulting solid was then further analyzed by NMR spectroscopy.

Acknowledgements

R.K. (KE 756/34-1) and J.S. (SFB 840, C1) thank the DFG for financial support. We thank F. Baier for XPS analysis, Dr. H. Schmalz for Raman measurements and Dr. C. Denner for SEM/EDX measurements. We acknowledge the ERSF for providing beamtime at ID31 as well as local support from Jakub Drnec. Open access funding enabled and organized by Projekt DEAL.

Conflict of Interest

The authors declare no conflict of interest.

Keywords: catalysis · cobalt · ketones · primary amines · reductive amination

[1] a) K. Murugesan, T. Senthamarai, V. G. Chandrashekar, K. Natte, P. C. J. Kamer, M. Beller, R. V. Jagadeesh, *Chem. Soc. Rev.* **2020**, *49*, 6273–6328; b) T. Irrgang, R. Kempe, *Chem. Rev.* **2020**, *120*, 9583–9674.
[2] a) S. A. Lawrence, *Amines: Synthesis, Properties and Applications*, Cambridge University Press, **2004**; b) R. Vardanyan, V. Hruby, *Synthesis of Best-Seller Drugs*, Academic Press, **2016**.
[3] K. Weissermel, H.-J. Arpe, *Industrial Organic Chemistry*, Wiley-VCH, **2008**.
[4] W. S. Emerson, The preparation of amines by reductive alkylation. *Org. React.* **1948**, *4*, 174–202.
[5] a) R. V. Jagadeesh, K. Murugesan, A. S. Alshammari, H. Neumann, M.-M. Pohl, J. Radnik, M. Beller, *Science* **2017**, *358*, 326–332; b) T. Senthamarai, V. G. Chandrashekhar, M. B. Gawande, N. V. Kalevaru, R. Zboril, P. C. J. Kamer, R. V. Jagadeesh, M. Beller, *Chem. Sci.* **2020**, *11*, 2973–2981.
[6] a) G. Hahn, P. Kunnas, N. de Jonge, R. Kempe, *Nat. Catal.* **2019**, *2*, 71–77. For related work of others see: K. Murugesan, M. Beller, R. V. Jagadeesh *Angew. Chem. Int. Ed.* **2019**, *58*, 5064–5068; *Angew. Chem.* **2019**, *131*, 5118–5122.
[7] C. Bäumler, C. Bauer, R. Kempe, *ChemSusChem* **2020**, *13*, 3110–3114.
[8] a) T. Stemmler, F. A. Westerhaus, A.-E. Surkus, M.-M. Pohl, K. Junge, M. Beller, *Green Chem.* **2014**, *16*, 4535–4540; b) F. Mao, D. Sui, Z. Qi, H. Fan, R. Chen, J. Huang, *RSC Adv.* **2016**, *6*, 94068–94073; c) X. Cui, K. Liang, M. Tian, Y. Zhu, J. Ma, Z. Dong, *J. Colloid Interface Sci.* **2017**, *501*, 231–240; d) Z. Yuan, B. Liu, P. Zhou, Z. Zhang, Q. Chi, *J. Catal.* **2019**, *370*, 347–356; e) T. Schönauer, S. L. J. Thomä, L. Kaiser, M. Zobel, R. Kempe, *Chem. Eur. J.* **2021**, *27*, 1609–1614; f) K. Murugesan, Z. Wie, V. G. Chandrashekhar, H. Neumann, A. Spannenberg, H. Jiao, M. Beller, R. V. Jagadeesh, *Nat. Commun.* **2019**, *10*, 5443.
[9] L. Γ. B. Ribiero, O. Γlores, P. Γurtat, C. Gervais, R. Kempe, R. A. Γ. Machado, G. Motz, *J. Mater. Chem. A.* **2017**, *5*, 720–729.
[10] a) G. Liang, A. Wang, L. Li, G. Xu, N. Yan, T. Zhang, *Angew. Chem. Int. Ed.* **2017**, *56*, 3050–3054; *Angew. Chem.* **2017**, *129*, 3096–3100; b) T. Ikenaga, K. Matsushita, J. Shinozawa, S. Yada, Y. Takagi, *Tetrahedron* **2005**, *61*, 2105–2109; c) S. Jiang, W. Ramdani, E. Muller, C. Ma, M. Pera-Titus, F. Jerome, K. De Oliveira Vigiera, *ChemSusChem* **2020**, *13*, 1699–1704; d) D. Chandra, Y. Inoue, M. Sasase, M. Kitano, A. Bhaumik, K. Kamata, H. Hosono, M. Hara, *Chem. Sci.* **2018**, *9*, 5949–5956; e) D. Deng, Y. Kita, K. Kamata, M. Hara, *ACS Sustainable Chem. Eng.* **2019**, *7*, 469–4698.
[11] X. Jv, S. Sun, Q. Zhang, M. Du, L. Wang, B. Wang, *ACS Sustainable Chem. Eng.* **2020**, *8*, 1618–1626.
[12] G. Mera, A. Navrotsky, S. Sen, H.-J. Kleebe, R. Riedel, *J. Mater. Chem. A* **2013**, *1*, 3826–3836.
[13] Z. Gan, J. P. Amoureux, J. Trébosc, *Chem. Phys. Lett.* **2007**, *435*, 163–169.
[14] B. V. Lotsch, M Döblinger, J. Sehnert, L. Seyfarth, J. Senker, O. Oeckler, W. Schnick, *Chem. Eur. J.* **2007**, *13*, 4969–4980.
[15] R. Anedda, D. V. Soldatov, I. L. Moudrakovski, M. Casu, J. A. Ripmeester, *Chem. Mater.* **2008**, *20*, 2908–2920.
[16] S. Xu, X. Li, C. Sun, A. Zheng, W. Zhang, X. Han, X. Liu, X. Bao, *Phys. Chem. Chem. Phys.* **2019**, *21*, 3287–3293.

Manuscript received: March 17, 2021
Revised manuscript received: April 1, 2021
Accepted manuscript online: April 7, 2021
Version of record online: May 6, 2021

 © 2021 The Authors. ChemSusChem published by Wiley-VCH GmbH

WILEY-VCH

SUPPORTING INFORMATION

Supporting Information
©Wiley-VCH 2019
69451 Weinheim, Germany

Co Catalyzed Synthesis of Primary Amines via Reductive Amination employing Hydrogen under very mild Conditions - a Nanostructured 3d Metal Catalyst outperforms Noble Metal Catalysts

Matthias Elfinger,[a] Timon Schönauer,[a] Sabrina Thomä,[b] Robert Stäglich,[c] Markus Drechsler,[d] Mirijam Zobel,[b] Jürgen Senker,[c] Rhett Kempe*[a]

Abstract: Nanostructured and reusable 3d-metal catalysts that operate with high activity and selectivity in important chemical reactions are highly desirable. We report here on a cobalt catalyst for the synthesis of primary amines via reductive amination employing hydrogen as the reducing agent and easy to handle ammonia, dissolved in water, as the nitrogen source. Our catalyst operates under very mild conditions (1.5 mol% catalyst loading, 50 °C and 10 bar H_2 pressure) and outperforms commercially available noble metal catalysts (Pd, Pt, Ru, Rh, Ir). We observe a broad scope and a very good functional group tolerance. The key for the high activity seems to be the used support: an N-doped amorphous carbon material with small and turbostratically disordered graphitic domains. It is hierarchically porous with basic NH functionalities in the pores.

DOI: 10.1002/anie.2016XXXXX

WILEY-VCH

SUPPORTING INFORMATION

Table of contents

1 General considerations....3
2. Experimental procedures....5
2.1 Synthesis of the support material....5
2.2. Synthesis of the catalyst....5
2.3 Catalytic procedures....5
2.4 Catalytic studies....6
2.4.1 Screening of reaction parameters....6
2.4.2 Reusability....8
2.4.3 Upscaling....9
3. Characterization of the catalyst....9
3.1 ICP-OES....9
3.2 XPS....10
3.3 SEM/EDX....11
3.4 TEM....12
3.5 Argon physisorption....13
3.6 Raman spectroscopy and elemental analysis....14
3.7 HR-TEM graphitic domain analysis....15
3.8 PXRD and PDF....16
3.9 Solid State NMR spectroscopy....19
4. Characterization of the isolated products....22
5. NMR Spectra....35
6. References....71

SUPPORTING INFORMATION

1 General considerations

All air- and moisture sensitive reactions were performed under dry argon or nitrogen atmosphere using standard Schlenk and glove box techniques. All dried solvents were obtained from a solvent purification system (activated alumina cartridges) or purchased from Acros. Deuterated solvents were dried via molecular sieves. All chemicals were acquired from commercial sources with purity over 95 % and used without further purification. The precursor SMP-10 was purchased from Starfire Systems, New York, USA. Pyrolysis of the support material was carried out under nitrogen atmosphere in a high temperature furnace (Gero, Berlin, Germany). Pyrolysis and reduction of the catalyst were performed under nitrogen or forming gas (90/10) atmosphere in a ChemBET Pulsar TPR/TPD instrument from Quantachrome. Transmission electron microscopy (TEM) was carried out by using a Variant LEO 9220 (200 kV) and a JEOL JEM 2200FS (200 kV) device. For the sample preparation, the samples were suspended in chloroform and sonicated for 5 min. For analysis, LC200-Cu and CF200-Cu grids were used.

Pore characterizations were carried out via nitrogen sorption measurements using a 3P Micro 100 Surface Area and Pore Size Analyzer device. The pore size distribution was computed via DFT calculations (calculation model: Ar at -186.15 °C on cylindrical pore, MDFT equilibrium model). The specific surface area was calculated by using p/p_0 values from 0.005-0.1 (BET).

The cobalt content was determined by ICP-OES. The fusion of the catalyst was carried out in a Berghof SpeedWave 4 microwave, for the ICP-OES measurement a Varian Vista Pro was used.

X-ray photoelectron spectroscopy (XPS) was performed using a Physical Electronics Phi 5000 Versa Probe III instrument. As X-ray source a monochromatic Al K α with a spot size of 100 µm

(21.1 W) was used. The kinetic pass energy of the photoelectrons was determined with a hemispheric analyzer (45°) set to pass energy of 13 eV for high-resolution spectra.

NMR measurements were performed using a Varian INOVA 300 (300 MHz for ^{1}H, 75 MHz for ^{13}C) and a Bruker Avance III HD 500 (500 MHz for ^{1}H, 125 MHz for ^{13}C) instrument at 296 K. Chemical shifts are reported in ppm relative to the residual solvent signal (DMSO-d6: 2.50 ppm (^{1}H), 39.51 ppm (^{13}C)), coupling constants (J) are reported in Hz.

GC analyses were carried out on an Agilent 6850 GC system equipped with an Optima 17 column (30 m x 0.32 mm x 0.25 µm).

The hydrogenation experiments were carried out with Parr Instrument stainless steel autoclaves N-MT5 250 mL equipped with heating mantles and temperature controller.

Powder X-ray diffraction (PXRD) data was collected at 65 keV (0.1907 Å) at ID31 at the European Synchrotron Radiation Facility (ESRF) with a CdTe Dectris Pilatus X 2M detector. All samples were measured in 1 mm Kapton® capillaries. NIST cerium oxide standard was used for distance calibration and determination of instrumental resolution (Q_{damp} = 0.016; Q_{broad} = 0.008). Masking and distance calibration were done with the software package pyFAI[1]. Azimuthal integration to powder diffraction patterns was performed with xpdtools[2]. Pair Distribution Function (PDF) calculation was done with PDFgetX3[3], using a Q-range of at least 0.9 – 18.0 Å^{-1}. For the support material, an elemental composition of $SiC_{9.36}N_{0.99}O_{1.62}$ derived from elemental analysis (see 3.6) was used while a nominal composition of CoNSiC was employed for the calculation of the difference-PDF of the catalyst using the unloaded support as background. The I(Q) of the support material was rescaled for analysis of the materials in reciprocal space as well as for calculation of the difference-PDF, so that reflexes of Co-containing phases are positive in the difference signal. For PDF modelling we used PDFgui[4]. Cif files for PDF modelling were downloaded from the American Mineralogist Crystal Structure Database (AMCSD)[5] or created from published structures[6] found with the software X'Pert Highscore. Fits to the PXRD data were conducted with the multipeak fitting option within the software Igor Pro 8.

^{129}Xe, ^{29}Si, ^{15}N and ^{13}C solid state NMR measurements were performed on a Bruker Avance II NMR spectrometer operating at an external field of 7.05 T corresponding to Larmor frequencies of 83.4, 59.6, 30.4 and 75.5 MHz for the ^{129}Xe, ^{29}Si, ^{15}N and ^{13}C, respectively.

Variable temperature measurements of hyperpolarized (hp) ^{129}Xe spectra were performed using a wideline 5mm double-resonance Bruker probe. Hyperpolarized Xenon was supplied by a homebuilt polarizer with a gas composition of 1 % v/v Xenon with natural abundance of the ^{129}Xe isotope, 6 % v/v N_2 as fluorescence quenching gas and Helium as buffer gas at a system pressure of $4 \cdot 10^5$ Pa. ^{129}Xe wideline single pulse (SP) NMR spectra were recorded in steps of 10 K with an equilibration time of 3 minutes before starting the acquisition. The pulse length for the π/2 pulse was set to 3.25 µs with a nutation frequency of approximately 77 kHz. Two scans were accumulated for each temperature with a temperature dependent recycle delay between 1 s at room temperature and 120 s at 130 K. The chemical shift was referenced to gaseous xenon at zero pressure (0 ppm).

^{13}C NMR spectra were recorded as SP and cross polarization (CP) experiments under magic angle spinning (MAS) with a spinning speed of 10 kHz using a Bruker 4 mm triple-resonance MAS probe. SP MAS NMR spectra were accumulated with pulse lengths of 2.3 µs for the π/2 pulse with a nutation frequency of approximately 110 kHz. Recycle delays were varied between 10 and 300 s after a pre-saturation pulse train. For the CP MAS NMR spectroscopic measurements an initial π/2 pulse of 2.5 µs with a nutation frequency of 100 kHz for protons was utilized, followed by 5 ms CP contact time with a nutation frequency of 65 kHz on the ^{13}C channel and a linearly ramped pulse from 50 kHz to 100 kHz on the proton channel.[13] Heteronuclear broadband decoupling was performed with a SPINAL-64 sequence[14] using a ^{1}H nutation frequency of 70 kHz with phase increments of 5 degrees. Between 64 to 256 scans were performed for SP MAS NMR spectroscopic measurements and between 3000 to 4000 scans were accumulated for CP MAS NMR spectra. The ^{13}C MAS NMR spectra are referenced indirectly with respect to tetramethylsilane (TMS) using adamantane as secondary reference.

^{29}Si SP NMR spectra were recorded under MAS with a spinning speed of 10 kHz. 2600 (before activation) / 4600 (after activation) scans were accumulated with a recycle delay of 60 s and a pulse length of 3.2 µs for the initial π/2 pulse.

For the ^{15}N CP MAS experiments a 4 mm triple-resonance MAS probe was utilized with a spinning speed of 5 kHz. An initial pulse length for protons of 4.8 µs with a nutation frequency of 52 kHz was used, followed by 500 µs / 1000 µs CP contact time.[13] SPINAL-

64 sequence was utilized for heteronuclear decoupling with a frequency of 55 kHz.[14] with a recycle delay of 1 s a total of 530,000 / 300,000 scans were accumulated.

Solid-state NMR spectroscopic studies of ^{1}H nuclei were performed on a Bruker Avance III HD NMR spectrometer at an external field of 14.1 T, corresponding to a larmor frequency of 600.1 MHz. The measurements were carried out in a 1.3 mm MAS double-resonance wide bore probe with commercial ZrO_2 rotors with a spinning speed of 62.5 kHz. For the acquisition of ^{1}H SP NMR spectra, a nutation frequency of 180 kHz with a pulse length of 1.4 µs, 32 scans and a recycle delay of 3 s were set. The ^{1}H-^{14}N *D*-HMQC[15,16] experiment was performed with a spinning of 50.0 kHz ($\nu_0(^{14}N)$ = 43.4 MHz). The super-cycled symmetry based $SR4_1^2$ sequence[17] was used for the ^{1}H-^{14}N dipolar recoupling. The recoupling time was adjusted to 240 µs. A rotor-synchronized delay was employed between the two ^{14}N pulses. The ^{14}N pulses were set to 28 µs using a B_1 field of approximately 60 kHz.

2. Experimental procedures

2.1 Synthesis of the support material

For the preparation of the N-SiC support material a known literature method was modified.[7]
200 mg SMP-10 (StarPCS™), 0.987 mL (0.800 g, 15.08 mmol) acrylonitrile and 45 mg (0.28 mmol) azobis(isobutyronitrile) were dissolved in 4 mL dimethylformamide and crosslinked for 16 h at 75 °C. After solvent removal under reduced pressure, the obtained greenbody was pyrolyzed using the following program:

$$20\ ^\circ\text{C} \xrightarrow{5\ \text{K/min}} 200\ ^\circ\text{C}\ (0\ \text{h}) \xrightarrow{1\ \text{K/min}} 400\ ^\circ\text{C}\ (0\ \text{h}) \xrightarrow{5\ \text{K/min}} 1000\ ^\circ\text{C}\ (1\ \text{h}) \xrightarrow{10\ \text{K/min}} 20\ ^\circ\text{C}$$

After ball mining for 40 minutes, 400 mg of the ceramic were washed by stirring in solution of 5.3 mL aq. NaOH (1 M) and 4 mL MeOH at 85 °C for 24 h. Afterwards the material was washed until neutrality and dried at room temperature.

2.2. Synthesis of the catalyst

1000 mg N-SiC were impregnated with 148 mg $Co(NO_3)_2 \cdot 6\ H_2O$ in 20 mL H_2O and stirred at 110 °C until the solvent was completely removed. Afterwards, the material was pyrolyzed and reduced using the following program:

$$\text{RT} \xrightarrow[N_2]{2\ \text{K/min}} 300\ ^\circ\text{C} \xrightarrow[N_2]{10\ \text{K/min}} 700\ ^\circ\text{C}\ (0.5\ \text{h}) \xrightarrow[N_2]{20\ \text{K/min}} 100\ ^\circ\text{C} \xrightarrow[N_2/H_2]{5\ \text{K/min}} 550\ ^\circ\text{C}\ (3\ \text{h}) \xrightarrow[N_2/H_2]{20\ \text{K/min}} 40\ ^\circ\text{C}$$

2.3 Catalytic procedures

All catalytic reactions were carried out after the procedure described in the following: A magnetic stirring bar, 0.5 mmol ketone, 3.5 mL aq. NH_3 (32%) and 2 mol % Co catalyst (3.0 wt% Co, 0.01 mmol Co 0.59 mg Co, 19.7 mg catalyst) were filled in a 5 mL glass reaction vial. For aldehydes, 1.5 mol% Co were used. The vial was placed in a 250 mL high pressure autoclave (Parr Instruments) and flushed three times with 0.5 MPa of hydrogen. The autoclave was pressurized with 1.0 MPa of hydrogen and the reaction was stirred for 20 h at 50 °C for ketones and 80 °C for aldehydes. After cooling to room temperature and release of the hydrogen pressure, the solution was extracted five times with methyl *tert*-butyl ether and dried over Na_2SO_4. The resulting solution was filtered and the solvent was removed under reduced pressure. To obtain the amine hydrochloride salts, 0.5 mL HCl in ether were added. The solvent was removed under reduced pressure and the resulting solid was then further analyzed by NMR spectroscopy.

2.4 Catalytic studies

2.4.1 Screening of reaction parameters

Solvent screening of the model substrate acetophenone

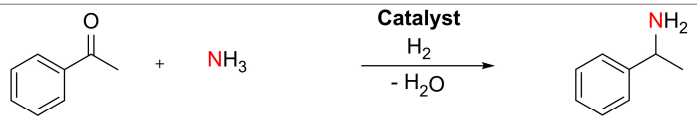

Solvent	Yield / %
NH_3 in Dioxane (0.5 M)	0
NH_3 in EtOH (0.5 M)	0
NH_3 in H_2O (0.5 M)	4
NH_3 in EtOH (2.0 M)	0
NH_3 in H_2O (13.4 M)	16
NH_3 in H_2O (17.2 M)	30

Reaction conditions: 1.5 mol% Co (2.24 wt% Co, 0.0075 mmol Co, 0.44 mg Co), 0.5 mmol acetophenone; 30 °C, 20 h, 1.0 MPa H_2, 3.0 mL solvent; yields were determined by GC using *n*-dodecane as an internal standard.

Screening of the NH_3 amount

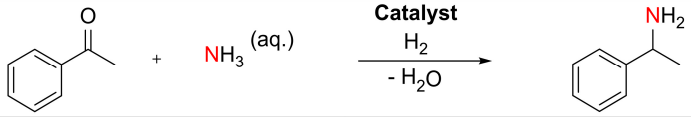

Volume aq. NH_3 (32 %) / mL	Yield / %
1	0
2	0
2.5	14
3	30
3.5	40
4	8
5	4
6	2

Reaction conditions: 1.5 mol% Co (2.24 wt% Co, 0.0075 mmol Co, 0.44 mg Co), 0.5 mmol acetophenone; 30 °C, 20 h, 1.0 MPa H_2, solvent: aq. NH_3 (32 %); yields were determined by GC using *n*-dodecane as an internal standard.

Screening of the metal loading of the catalyst

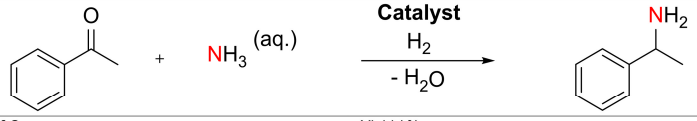

Theoretical wt% of Co	Yield / %
2	5
3	35
4	32
5	22

Reaction conditions: 1.5 mol% Co (2.24 wt% Co, 0.0075 mmol Co, 0.44 mg Co), 0.5 mmol acetophenone; 30 °C, 20 h, 1.0 MPa H_2, 3.5 mL aq. NH_3 (32 %); yields were determined by GC using *n*-dodecane as an internal standard.

SUPPORTING INFORMATION

Screening of the catalyst loading

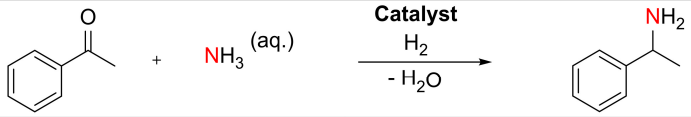

Catalyst loading / mol%	Yield / %
1	8
2	38
3	46
4	73
5	76

Reaction conditions: 1.5 mol% Co (2.24 wt% Co, 0.0075 mmol Co, 0.44 mg Co), 0.5 mmol acetophenone; 30 °C, 20 h, 1.0 MPa H_2, 3.5 mL aq. NH_3 (32 %); yields were determined by GC using *n*-dodecane as an internal standard.

Screening of the reaction temperature

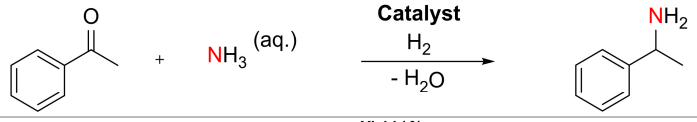

Temperature / °C	Yield / %
30	32
40	42
50	99
60	99

Reaction conditions: 1.5 mol% Co (2.24 wt% Co, 0.0075 mmol Co, 0.44 mg Co), 0.5 mmol acetophenone; 20 h, 1.0 MPa H_2, 3.5 mL aq. NH_3 (32 %); yields were determined by GC using *n*-dodecane as an internal standard.

Temperature screening of the model substrate benzaldehyde

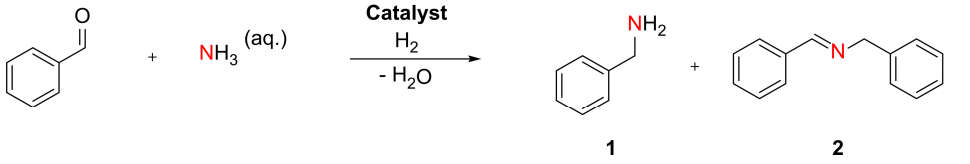

1 **2**

Temperature / °C	Yield 1 / %	Yield 2 / %
40	0	73
50	0	77
60	12	64
70	34	46
80	83	7

Reaction conditions: 1.1 mol% Co (2.24 wt% Co, 0.0055 mmol Co 0.32 mg Co), 0.5 mmol benzaldehyde; 20 h, 1.0 MPa H_2, 3.5 mL aq. NH_3 (32 %); yields were determined by GC using *n*-dodecane as an internal standard.

2.4.2 Reusability

The reusability of the catalyst was investigated using the reductive amination of acetophenone with aqueous ammonia. The reaction was carried out for 13 h under the optimized reaction conditions to obtain 60 % yield of 1-phenylethylamine, which was determined by GC using *n*-dodecane as an internal standard. After each run, the reaction mixture was separated from the catalyst using Pasteur pipettes. This was possible due to the magnetic catalyst, which was attracted to the magnetic stirring bar inside the reaction vial. The catalyst was washed two times with water and used directly for the subsequent run. The procedure was carried out 5 times without a loss of activity (Fig. S1).

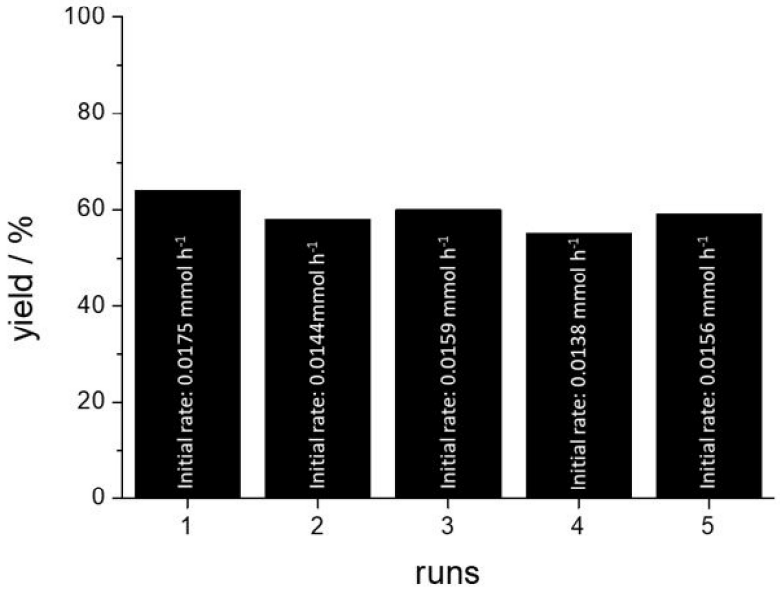

Figure S1: Reusability and initial rates of the Co/N-SiC catalyst for 5 consecutive runs. Reaction conditions for 60 % yield: 1.5 mol% Co (2.24 wt% Co, 0.0075 mmol Co, 0.44 mg Co), 0.5 mmol acetophenone; 13 h, 1.0 MPa H_2, 3.5 mL aq. NH_3 (32 %); yields were determined by GC using *n*-dodecane as an internal standard.

2.4.3 Upscaling

Acetophenone was used as a model substrate to carry out an upscaling experiment. For the reaction, 392 mg Co/N-SiC (3 wt%, 2.0 mol%), 10 mmol acetophenone and 70 mL aq. NH_3-32 % were stirred in a Schott bottle within a 250 mL high pressure autoclave (Parr Instruments) under the optimized reaction conditions (50 °C, 1.0 MPa H_2, 20 h). The workup was identical to the 0.5 mmol reactions. Isolated yield of 1-phenylethanaminium chloride: 1.495 g, 95 %.

3. Characterization of the catalyst

3.1 ICP-OES

25 mg of the sample were solved in 1.5 mL HNO_3 (65 %, distilled), 4.5 mL HCl (32 %, p.a.) and 1 mL HF (40 %) and heated in the microwave at 170 °C for 7 min (80 % power), at 180 °C for 7 min (85 % power) and 195 °C for 20 min (90 % power).

Theoretical Co content: 3 wt%
Measured Co content: 2.24 wt%

3.2 XPS

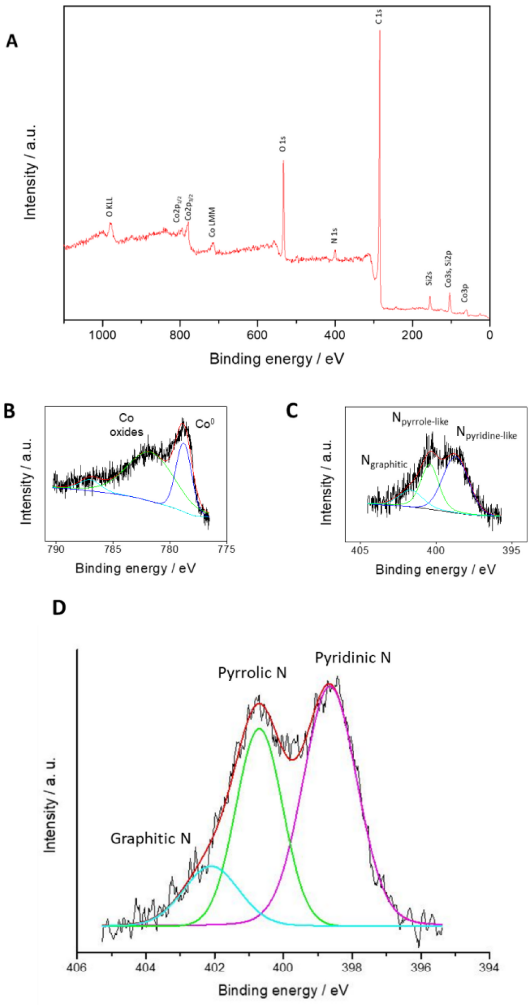

Figure S2: X-ray photoelectron spectra (XPS) of the catalyst. **A**: overview spectrum. **B**: analysis of the Co $2p_{3/2}$ area shows the presence of metallic cobalt (28 %) and cobalt oxide (65 %). **C**: analysis of the nitrogen area suggests different binding modes of nitrogen within the catalyst (graphitc: 16 %, pyrrole-like: 33 %, pyridine-like: 51 %). **D:** High resolution XPS of the N1s region of the catalyst.

The N_{1s} region of the XPS-spectrum (Fig. S2**D**) shows three major peaks, which can be addressed to 16.4 % graphitic nitrogen (401.3 eV), 32.8 % pyrrolic nitrogen (400.5 eV) and 50.8 % pyridinic nitrogen (398.6 eV). The Co and CoO ratios determined by fitting the Co_{2p} region (28 % Co; 65 % CoO) are consistent with those obtained by PDF (23 % Co; 77 % CoO; see 3.8).

3.3 SEM/EDX

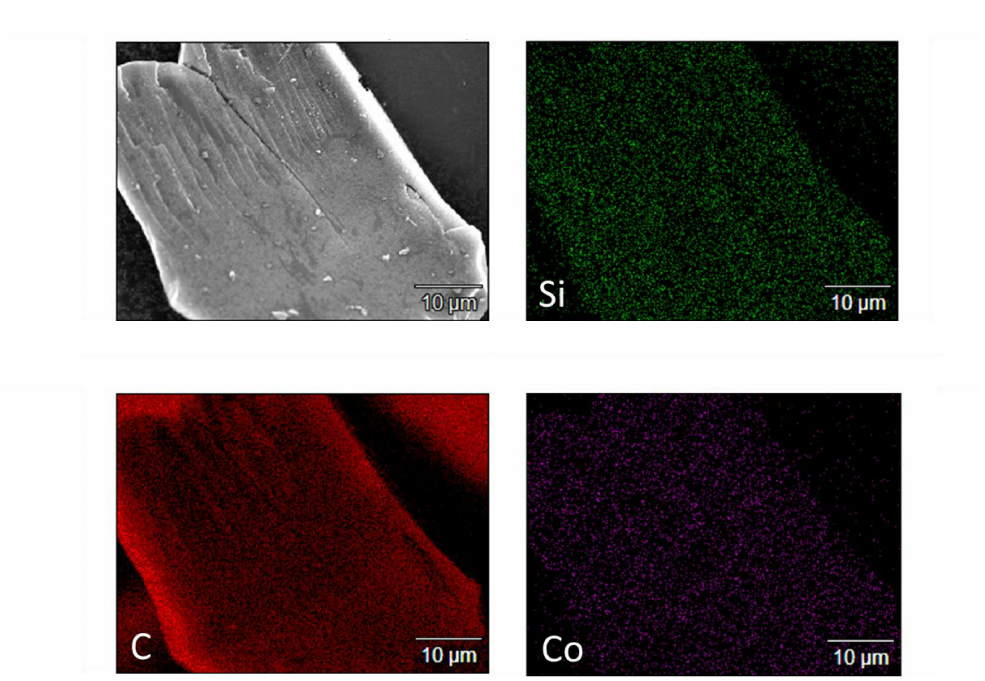

Figure S3: Scanning electron microscopy (SEM) in combination with energy dispersive X-ray (EDX) mapping. The measurements show a homogeneous distribution of all individual elements, including cobalt, on the surface of the support material.

3.4 TEM

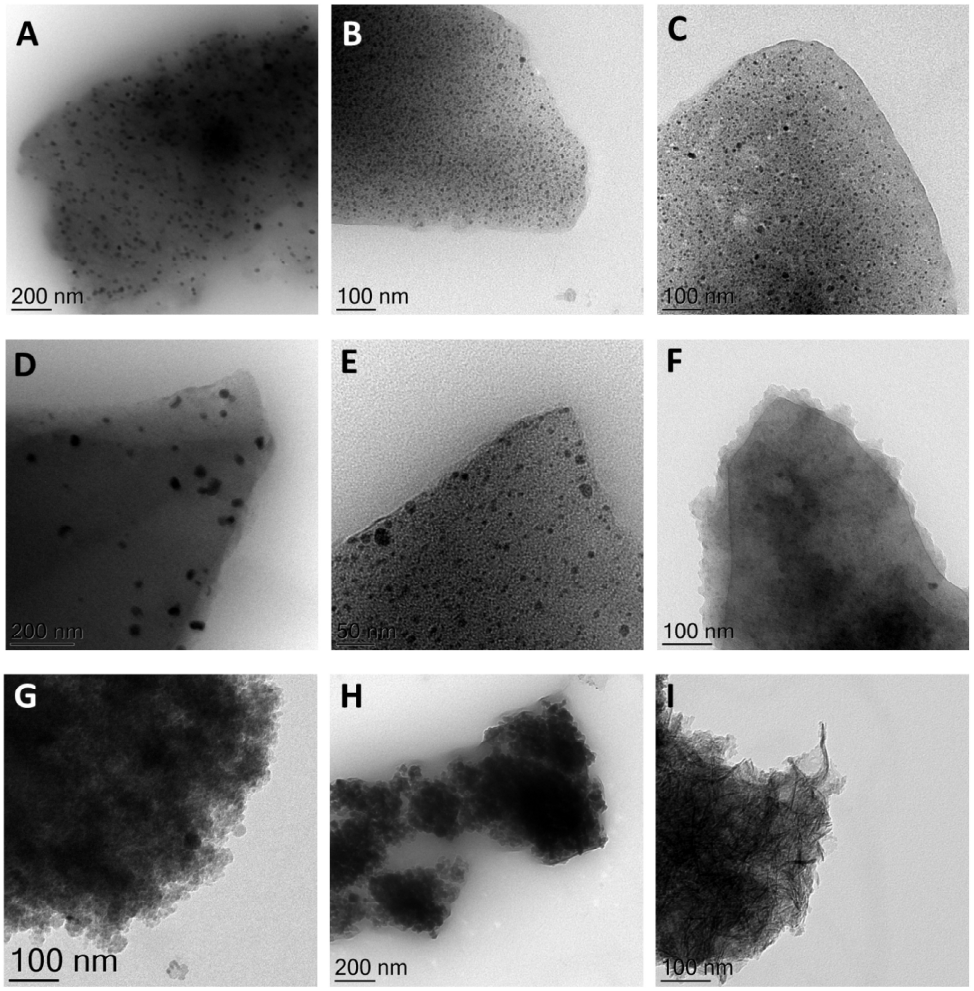

Figure S4: TEM characterization of the catalyst used for the activity screening in the reductive amination of ketones. Variation of the metal content regarding the Co/N-SiC catalyst: A) 2 wt% Co; B) 4 wt% Co; C) 5 wt% Co; Variation of the pyrolysis temperature of the Co/N-SiC catalyst: D) 600 °C; E) 800 °C; Variation of the support material while using $Co(NO_3)_2 \cdot 6\ H_2O$ as metal source: F) Co/activated carbon; G) Co/SiO_2; H) Co/TiO_2; I) Co/Al_2O_3

3.5 Argon physisorption

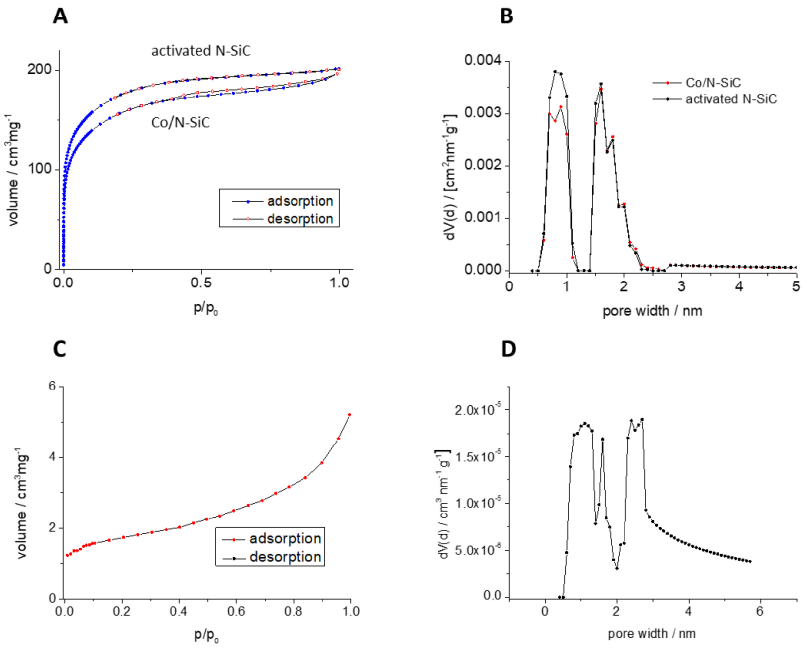

Figure S5: A Surface characterization and **B** pore size distribution of the catalyst and activated N-SiC support via argon physisorption measurements [calculation model: Ar at 87 K on carbon (cylindr. pores, NLDFT equilibrium model)]. The specific surface showed a slight decline from 545 m^2g^{-1} of the activated support material to 491 m^2g^{-1} of the catalyst. **C** surface characterization and pore size distribution **D** of the support material prior to activation. The surface area increases from 6 to 545 m^2g^{-1} after treatment with NaOH solution.

SUPPORTING INFORMATION

3.6 Raman spectroscopy and elemental analysis

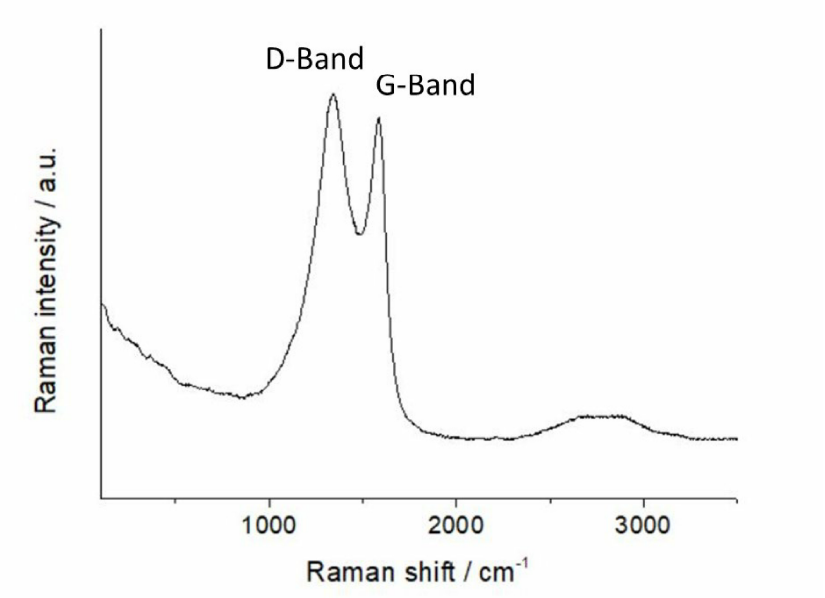

Figure S6: Raman spectrum of the activated support material

The Raman spectrum (Fig. S6) shows the D- and G-peaks, which are the most dominant. The D-peak is caused by disordered structure of graphene, such as structural defects that break the symmetry. The G-peak corresponds to the only allowed Raman transition in the spectrum region of large graphite crystals. It results from a C-C stretching in the longitudinal symmetry axis of the graphite plane.
The presence of NH_x groups in the support material could be verified by titration experiments. The calculation of the addressable amine groups in the liquid phase was done by determining the absolute number of amine groups that could be converted to ammonium chloride functionalities by the uptake of hydrogen chloride. Per 100 mg of support material, 0.04175 mmol HCl were used up. Hence, the presence of $2.514 \cdot 10^{20}$ NH_x groups could be determined. With the elemental analysis of the support material (Fig. S7), the percentage of NH_x groups compared to the whole nitrogen content can be specified.

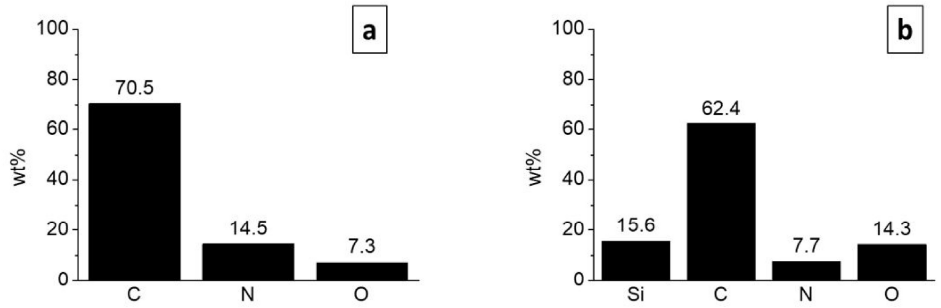

Figure S7: a) Elemental analysis of pure pyrolyzed polyacrylnitrile and **b)** activated N-SiC support material. The silicon content of N-SiC was calculated based on the difference of the measured elements to 100 %.

Based on a total nitrogen content of 7.7 wt% and 0.585 wt% NH_x groups in the support material, an amount of 7,6 % of the total nitrogen content is addressable via titration. Considering that XPS measurements (Fig. S2) are suggesting that 49.2 % of nitrogen within the N-SiC material can possibly be described as NH_x groups (graphitic and pyrrolic N), the accessible amount of NH_x groups in liquid phase seems to be significantly lower. Titration of the Co/N-SiC catalyst revealed an uptake of 0.03685 mmol HCl per 100 g, resulting in $2.219 \cdot 10^{20}$ NHx groups. For the same experiment with used catalyst, 100 mg of it was washed with water two times and dried under vacuum conditions. The titrated amount of NH_x groups didn't show any significant changes in comparison to the unused catalyst.

3.7 HR-TEM graphitic domain analysis

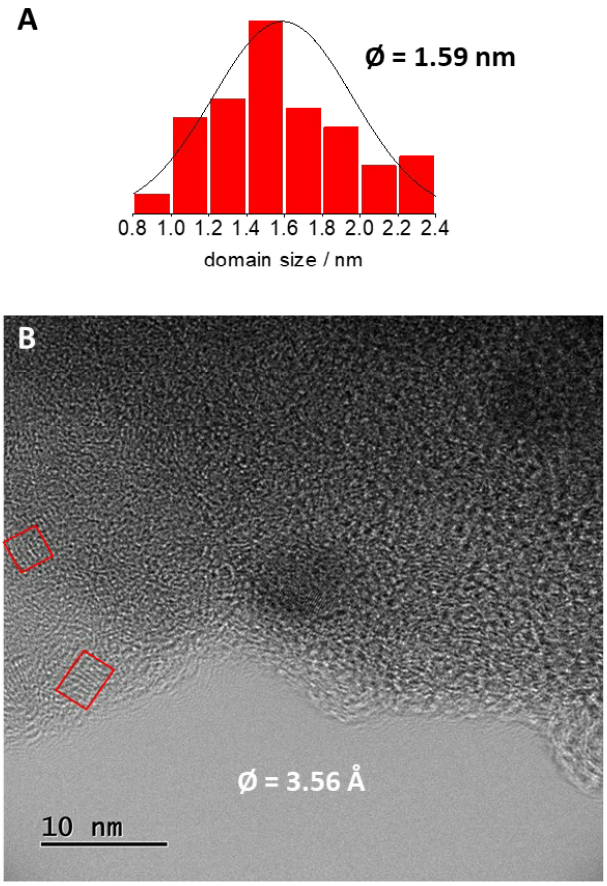

Figure S8: Size analysis of the graphitic domains within the N-SiC support via HR-TEM with a median domain size of 1.59 nm (**A**) and a median interlayer distance of 3.56 Å. Some domains show even further interlayer spacing of up to 4.2 Å (**B**, red markers). These results are in good agreement with PXRD analysis (see 3.8).

3.8 PXRD and PDF

Figure S9 panel A shows the PXRD data of both the N-SiC support and the Co/N-SiC catalyst, together with the respective difference signal catalyst minus support. Evidently the N-SiC support features broad Bragg peaks, which can be indexed by hexagonal graphite. The data shown is already corrected for background scattering of air and empty capillary, and hence the Bragg peaks sit on top of a noticeable amorphous background. To quantify the ratio of amorphous and crystalline phases in the support material we fit a continuous function (polynomial 5th order in log(Q) describes the background best) to the background in the Q-range of 0.9 - 20 Å^{-1}, as well as several Gaussian peaks to the broad Bragg peaks of the hexagonal graphite. The ratio of the integrated areas beneath the individually fitted Gaussians and the background represents the fraction of crystalline graphitic material in the sample. This results in a crystalline phase fraction of 17 % (see Figure 2D).The Bragg peaks in the pink difference curve can be assigned to two different phases based on different widths of reflexes, which were identified to be Co fcc (amcsd code 0011143)[5] and CoO fcc[6]. Additionally, the difference signal features a broad negative feature between 1.6 – 2.2 Å^{-1}, indicating that structural signal is lost in the Co/N-SiC catalyst in comparison to the N-SiC support and that the support restructured due to the Co loading.

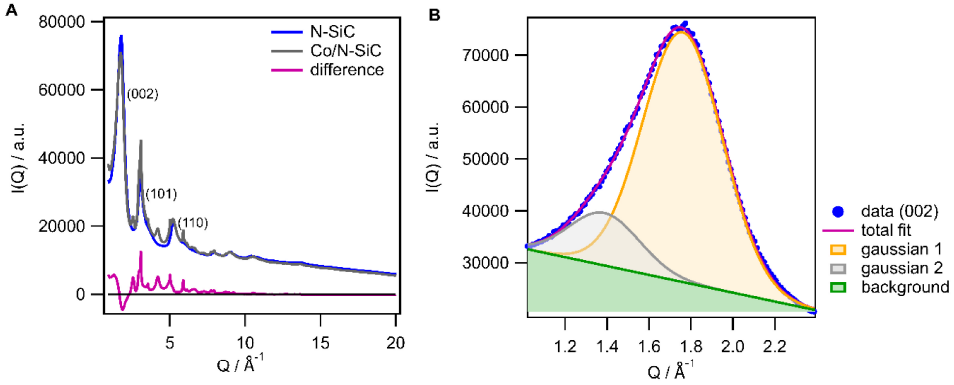

Figure S9: PXRD characterization of the catalyst and support material. A) PXRD data of N-SiC support material (blue), the Co/N-SiC catalyst (grey) and their difference (pink), which is the active catalytic phase. B) The (002) reflex (blue circles) of the N-SiC support material was fitted with two Gaussian peaks (grey and yellow; total fit pink) on a linear baseline (i.e. the amorphous support, green).

To further characterize the support material we fitted the (002) reflex with 2 Gaussians $G(x) = A \cdot e^{-\frac{(x-\mu)^2}{w^2}}$ on top of a linear baseline in the Q-range of 1.0 – 2.4 Å^{-1}, see Figure S9 B and fit results in Table S1: the peak maximum (location μ) corresponds to d-spacing of graphitic domains via d = 2π/Q, the width (w) reflects the distribution of lattice spacings around the respective average, the amplitude (A) describes the height of the peak and defines the peak area representing the corresponding phase fraction. Chi square is the goodness of fit parameter. The data was best described by two Gaussian peaks centered at 1.76 and 1.39 Å^{-1} corresponding to d-spacings of ca. 3.6 and 4.5 Å. This shows, that the majority of the crystalline graphitic domains are in average expanded by ca. 0.25 Å compared to hexagonal graphite (d-spacing of 3.354 Å). This expansion is well explained by the N-doping of graphite, increasing d-spacings. Moreover, 15 % of the graphitic domains are expanded by 1.15 Å compared to hexagonal graphite (derived from areas under peaks, i.e. 4,240/27,600). These results are in good agreement with HR-TEM analysis (see 3.7).

Table S1: Fit parameters of two Gaussian peaks to (002) reflex of PXRD of N-SiC support.

		Location (Å^{-1})	d-spacing (Å)	Amplitude	Width	Area	Total Area	Chi Square
N-SiC	Peak 0	1.39 ± 1.23e-2	4.52	1.01e+4 ± 7.14e+2	2.37e-1 ± 1.36e-2	4.24e+3 ± 5.31e+2	2.76e+4 ± 6.81e+2	1.79e+7
	Peak 1	1.76 ± 3.53e-3	3.57	4.81e+4 ± 3.95e+2	2.73e-1 ± 2.91e-3	2.33e+4 ±4.26e+2		

In order to characterize the local structure of the N-SiC support and the active catalytic species, pair distribution function (PDF) analysis was conducted. The PDF is a histogram of all interatomic distances within the sample. Figure S10 shows the PDF of the N-SiC support and its fit with the hexagonal graphite structure, Table S2 the resulting parameters. Distances < 5 Å are colour-coded in the PDF and the inset of the hexagonal ring structure of graphite: 1.42, 2.43 and 2.88 Å are nearest-neighbor distances within one ring, and 3.73, 4.24 and 4.97 Å are distances to carbon atoms in adjacent rings.

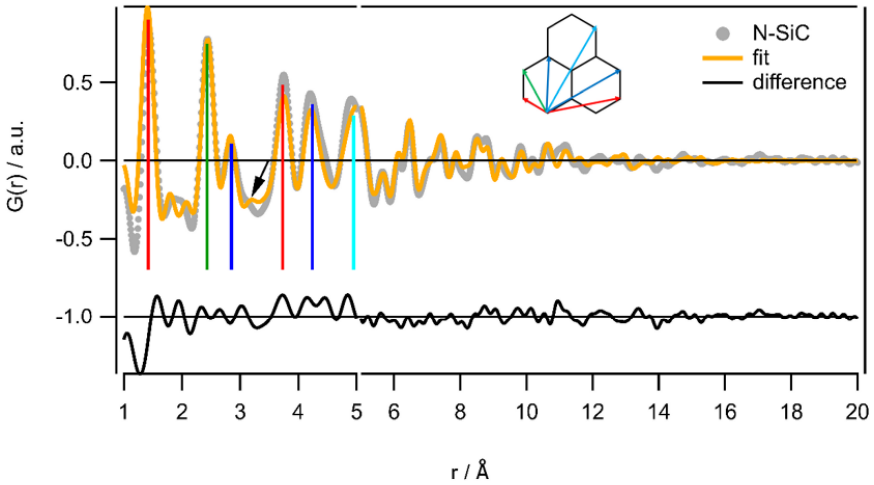

Figure S10: PDF of N-SiC (grey) with its fit (orange, graphite structure) and the resulting difference curve (black, in offset). Nearest-neighbor correlations up to 5 Å are marked in different colours and are assigned in the hexagonal ring structure in the inset. The x-axis is expanded in the region up to 5 Å. The arrow is marking a shoulder at 3.2 Å.

All peaks are fairly symmetric indicating the absence of a large portion of non-hexagonal rings.[8] Yet, the small shoulder at about 3.2 Å (see arrow Figure S10) could point towards the presence of seven-membered rings.[8a, 9]No distance correlation at the interlayer spacing of 3.6 Å is observed, suggesting turbostratic disorder[8].The discrepancies in experimental and fitted intensities of PDF peaks can be reasoned by N-doping, which reflects a 14 % increase in electron density compared to C.
The fit with the graphite structure (amcsd code 0011247)[5] was first carried out over 1-8 Å corresponding to one stack height, to retrieve atomic displacement parameters u_{11}=u_{22}, lattice parameter c and delta2. These parameters were then fixed for refining of the longer range, in order to prevent incorrect modeling of peak broadening according to Poulain et al.[8a]. For all fit ranges, the atomic displacement parameter u_{33} along the c axis was found to be quite high, corroborating the turbostratic disorder. Domain sizes, i.e. structural coherence, was refined to 19 – 23 Å depending on the fit range. Further, it is noteworthy that the lattice parameter a is shortened for the refinement for the whole range up to 20 Å as well as when only modeling the long range of 10 – 20 Å, in comparison to the short range of only up to 8 Å. Consequently, the atoms are systematically closer together in this range than predicted by the model. This indicates curvature of the sheets and implies, that structural coherence is also quite limited in ab-plane and not only along the c-axis.[8a, 10] Moreover, the fit overestimates the experimental data in the first three peaks, which might be a hint for the presence of non-hexagonal rings[11] or might stem from the N-doping. Additionally, we want to note, that the support material also contains a large fraction of amorphous and only very short-range ordered material, as shown with our analysis in reciprocal space (see Figure 2C). The amorphous fraction is not implemented in this model and thus deviations between model and data are expected.

Table S2: Results of PDF refinement of graphite to N-SiC PDF data. a, b, c: unit cell parameter (starting values in brackets); scale factor to match theoretical and experimental PDF data in intensity; u_{11}, u_{22}, u_{33}: isotropic atomic displacement parameters, delta2: parameter to account for correlated atomic motion; particle size and R_w: goodness-of-fit. Parameters, which were fixed during refinement are marked with *.

	Range 1-8	Range 1-15	Range 1-20	Range 10-20
a,b	2.4493 (2.546)	2.4477 (2.546)	2.4478 (2.546)	2.4324 (2.546)
c	6.9221 (7.140)	6.9221 (7.140)*	6.9221 (7.140)*	6.9221 (7.140)*
scale factor	0.1251	0.1327	0.1336	0.1128
u_{11}, u_{22}	0.0044	0.0044*	0.0044*	0.0044*
u_{33}	0.1906	0.2345	0.2319	0.8010
δ2	1.0536	1.0536*	1.0536*	1.0536*
particle size	23.2592	18.9321	18.5636	20.3012
R_w	**0.31**	**0.34**	**0.34**	**0.68**

The difference-PDF (d-PDF) of the Co/N-SiC catalyst, with the N-SiC support already subtracted, was refined with two phases being Co fcc[5] and CoO fcc phase[6], see Table S3 for refined parameters and Figure S11 for the plot..

Table S3: Results from biphasic simultaneous refinement of Co fcc and CoO fcc phases to difference-PDF data of Co/N-SiC.

Co fcc		CoO fcc	
a, b, c	3.5397 (3.548)	a, b, c	4.2319 (4.24)
scale factor	0.0601	scale factor	0.1367
particle size	92.7809	particle size	27.7549
u_{11}, u_{22}, u_{33}	0.0071	Co u_{11}, u_{22}, u_{33}	0.0126
		O u_{11}, u_{22}, u_{33}	0.060
delta 2	5.0759	delta 2	3.9211
R_w	**0.43**		

The biphasic refinement results in phase fractions of 77% CoO and 23% percent Co with respect to mass and of 86% CoO and 14% Co with respect to atoms and is in agreement with XPS results (see 3.2). The goodness of fit parameter R_w of 0.43 is in line with remaining structural signal up to about 8 Å in the difference curve. We hypothesize, that this signal stems from restructured support material. The first peak in this difference at 1.61 Å is not accounted for in the biphasic model. This peak matches well the bond lengths of Si-O as determined with total scattering by Tucker et al.[12]. We conjecture, that the small remaining Si phase after activation of the support forms SiO_2 domains due to heating steps carried out during Co impregnation to build the catalyst from the support.

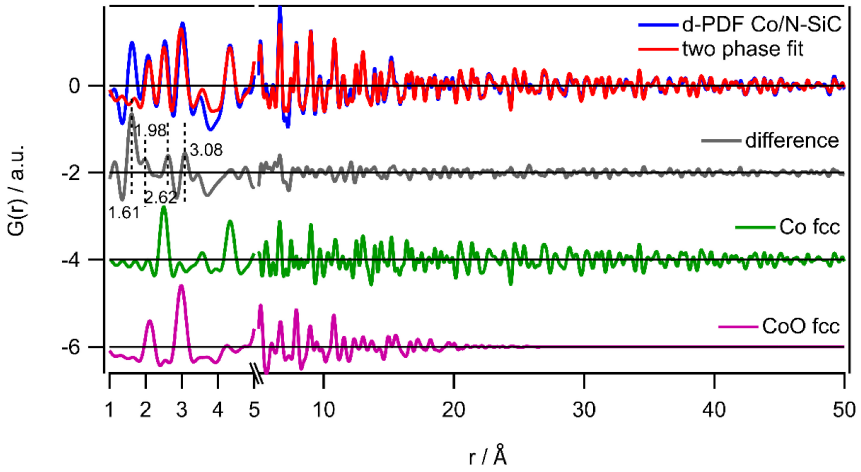

Figure S11: d-PDF of Co/N-SiC catalyst (blue) with its two phase fit (red), the resulting difference curve (grey; in offset), the contributions of Co fcc phase (green) and CoO fcc phase (purple) to the total fit (both in offset). Note that x axis is splitted and the area up to 5 Å is expanded. Distances in the difference curve in this area are labeled.

3.9 Solid State NMR spectroscopy

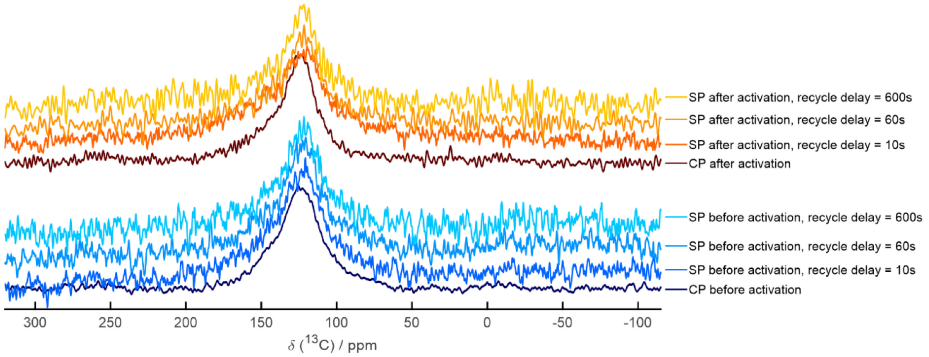

Figure S12: ^{13}C Single Pulse (SP) and Cross Polarization (CP) NMR spectra for samples before and after activation with NaOH. The similar line shapes of the SP and CP ^{13}C NMR spectra before and after activation suggest a regular distribution of proton spin density over the sample.

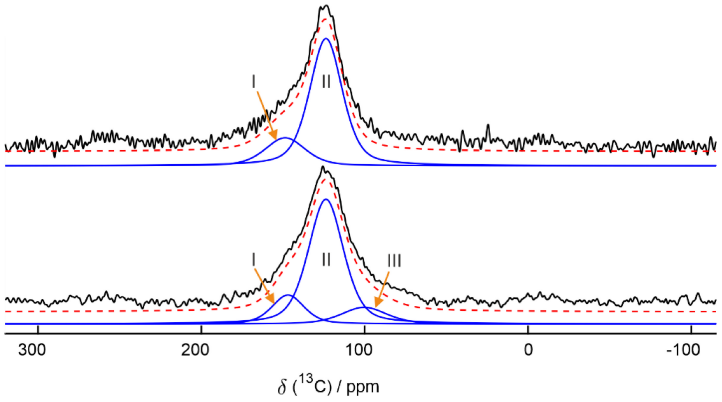

Figure S13: Deconvolution of ^{13}C CP MAS NMR spectra before (bottom) and after (top) activation with NaOH. The spectral regions I, II and III are characteristic for graphitic carbon with nitrogen incorporation, graphitic carbon without nitrogen and graphitic carbon in contact to silicon, respectively. The disappearance of signal region III is in line with the removal of silicon rich domains by activation with NaOH, as pointed out in Figure 2A. The similar intensity ratio for regions I and II show that the graphitic regions are insensitive to the activation procedure.

Table S4: Refinement parameters for deconvolution of ^{13}C CP MAS NMR spectra in Figure S13

	Before Activation			After Activation	
	I	II	III	I	II
δ / ppm	146.9	123.7	100.3	148.7	123.7
Intensity	0.15	0.73	0.12	0.21	0.79
G/L	0.6	0.6	0.6	0.6	0.6
FWHM / ppm	23.1	25.4	32.5	28.8	23.6

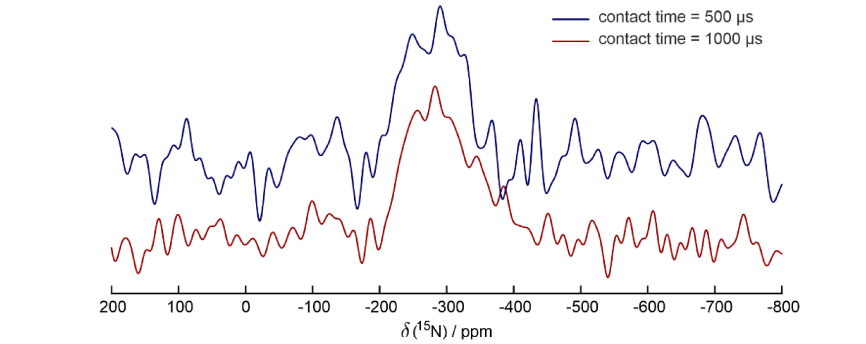

Figure S14: ^{15}N CPMAS NMR spectra with polarization transfer contact times of 500 µs (blue) and 1 ms (red). The similarity of both spectral shapes is indicative for close proton contacts for all nitrogen environments. The broad chemical shift range for the corresponding nitrogen atoms is typical for nitrogen embedded in graphitic domains.

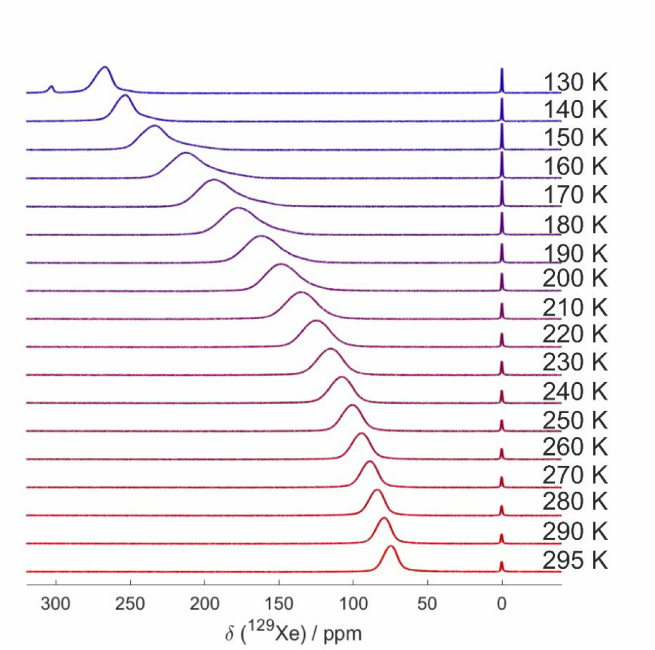

Figure S15: series of hyperpolarized (hp) ^{129}Xe NMR spectra at variable temperatures. The ^{129}Xe chemical shift (CS) in the low loading limit (high temperature range, 260 – 295 K) is typical for isolated xenon atoms in microporous graphitic materials. A detailed analysis of the shift in this region is given in Figure 2C. Towards lower temperatures the ^{129}Xe CS increases, corresponding to a larger xenon uptake, where also Xe-Xe interactions influence the chemical shift.

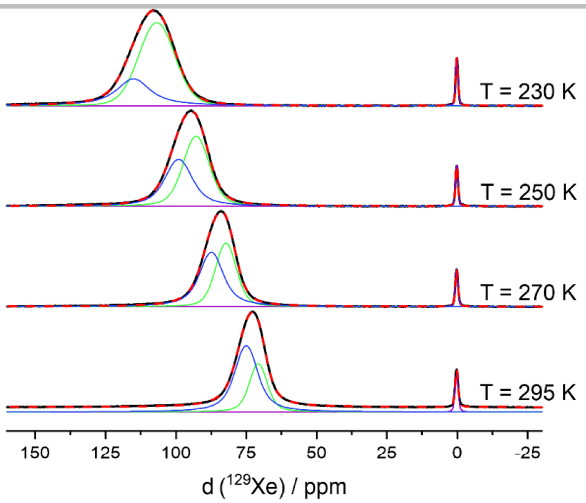

Figure S16: Depiction of the deconvolution of the limiting shift region of hp ^{129}Xe NMR spectra with a larger chemical shift range compared to Figure 2C.

4. Characterization of the isolated products

1-Phenylethanaminium chloride (1)

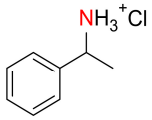

MW = 157.64 g/mol

^{1}H NMR (500 MHz, DMSO-D_6): δ = 8.55 (s, 3 H), 7.55 (d, *J* = 7.55 Hz, 2 H), 7,44-7,32 (m, 3 H), 4.41-4.30 (q, *J* = 4.36, 1 H), 1.52 (d, *J* = 1.55 Hz, 3 H) ppm

^{13}C NMR (126 MHz, DMSO-D_6): δ = 140.15, 129.10, 128.72, 127.31, 50.47, 21.43 ppm

Yield: 99 % (78 mg) as a white solid

1-Phenylpropan-1-aminium chloride (2)

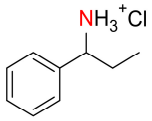

MW = 171.67 g/mol

^{1}H NMR (500 MHz, DMSO-D_6): δ = 8.64 (s, 3 H), 7.53-7.34 (m, 5 H), 4.3 (m, 1 H), 2.23-1.45 (m, 2 H), 0.79-0.70 (t, *J* = 0.75 Hz, 3 H) ppm

^{13}C NMR (126 MHz, DMSO-D_6): δ = 138.24, 129.13, 128.92, 127.96, 56.27, 27.95, 10.49 ppm

Yield: 99 % (85 mg) as a white solid

1-Phenylhexan-1-aminium chloride (3)

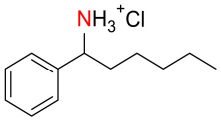

MW = 213.75 g/mol

^{1}H NMR (500 MHz, DMSO-D$_6$): δ = 8.49 (s, 3 H), 7.70-7.35 (m, 5 H), 3.04-2.96 (t, *J* = 3.01 Hz, 1 H), 1.64-1.56 (m, 2 H), 1.34-1.06 (m, 5 H), 0.87-0.77 (m, 3 H) ppm

^{13}C NMR (126 MHz, DMSO-D$_6$): δ = 137.19, 133.48, 129.16, 128.32, 38.35, 31.62, 28.79, 24.25, 22.50, 14.39 ppm

Yield: 84 % (90 mg) as a white solid

1-(4'-Fluorophenyl)ethanaminium chloride (4)

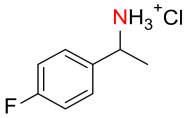

MW = 175.63 g/mol

^{1}H NMR (500 MHz, DMSO-D$_6$): δ = 8.75 (s, 3 H), 7.64-7.59 (q, *J* = 7.62 Hz, 2 H), 7.29-7.22 (t, *J* = 7.26 Hz, 2 H), 4.42-4.37 (q, *J* = 4.40 Hz, 1 H), 1,50 (d, *J* = 1.52 Hz, 3 H) ppm

^{13}C NMR (126 MHz, DMSO-D$_6$): δ = 161.40, 136.20, 129.73, 115.96, 49.76, 21.22 ppm

Yield: 98 % (86 mg) as a white solid

1-(4'-Chlorophenyl)ethanaminium chloride (5)

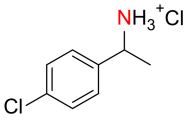

MW = 192.08 g/mol

^{1}H NMR (500 MHz, DMSO-D$_6$): δ = 8.79 (s, 3 H), 7.48 (d, *J* = 7.60 Hz, 2 H), 7.58 (d, *J* = 7.48 Hz, 2 H), 4.38-4.43 (q, *J* = 4.40 Hz, 1 H), 1.51 (d, *J* = 1.51 Hz, 3 H) ppm

^{13}C NMR (126 MHz, DMSO-D$_6$): δ = 138.94, 133.38, 129.44, 129.04, 49.79, 21.14 ppm

Yield: 92 % (88 mg) as a white solid

1-(4‘-Bromophenyl)ethanaminium chloride (6)

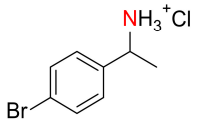

MW = 236.54 g/mol

^{1}H NMR (300 MHz, DMSO-D_6): δ = 8.82 (s, 3 H), 7.87 (d, *J* = 7.87 Hz, 2 H), 7.70 (d, *J* = 7.72 Hz, 2 H), 4.42-4.35 (m, 1 H), 1.52 (d, *J* = 1.52 Hz, 3 H) ppm

^{13}C NMR (75 MHz, DMSO-D_6): δ = 139.30, 132.18, 130.64, 121.99, 49.90, 27.17 ppm

Yield: 91 % (108 mg) as a white solid

1-(3‘-Chloropheny)lethanaminium chloride (7)

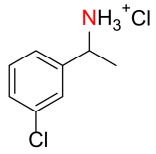

MW = 192.08 g/mol

^{1}H NMR (500 MHz, DMSO-D_6): δ = 8.75 (s, 3 H), 7.96-7.41 (m, 4 H), 4.46-4.39 (m, 1 H), 1.53 (d, *J* = 1.52 Hz, 3 H) ppm

^{13}C NMR (126 MHz, DMSO-D_6): δ = 142.36, 133.37, 131.20, 128.29, 127.44, 49.90, 27.35 ppm

Yield: 90 % (86 mg) as a white solid

1-(4-(Trifluoromethyl)phenyl)ethanaminium chloride (8)

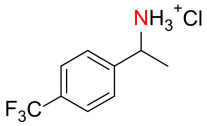

MW = 225.64 g/mol

^{1}H NMR (300 MHz, DMSO-D_6): δ = 8.85 (s, 3 H), 7.87-7.77 (s, 4 H), 4.63-4.45 (m, 1 H), 1.53 (d, *J* = 1.53 Hz, 3 H) ppm

^{13}C NMR (75 MHz, DMSO-D_6): δ = 144.53, 128.35, 126.03, 125.98, 50.00, 21.10 ppm

Yield: 97 % (109 mg) as a white solid

1-(4‘-Methylphenyl)ethanaminium chloride (9)

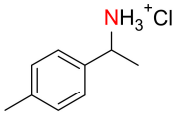

MW = 171.67 g/mol

^{1}H NMR (500 MHz, DMSO-D_6): δ = 8.66 (s, 3 H), 7.42 (d, J = 7.41 Hz, 2 H), 7.22 (d, J = 7.22 Hz, 2 H), 4.33-4,27 (q, J = 4.32 Hz, 1 H), 2.28 (s, 3 H), 1.50 (d, J = 1.54 Hz, 3 H) ppm

^{13}C NMR (126 MHz, DMSO-D_6): δ = 138.09, 136.95, 129.60, 127.24, 50.19, 21.26, 21.16 ppm

Yield: 83 % (71 mg) as a white solid

1-(3‘-Methylphenyl)ethanaminium chloride (10)

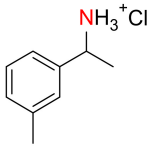

MW = 171.67 g/mol

^{1}H NMR (500 MHz, DMSO-D_6): δ = 8.74 (s, 3 H), 7.44-7.16 (m, 5 H), 4.34-4.29 (m, 1 H), 2.3 (s, 3 H), 1.53 (d, *J* = 1.51 Hz, 3 H) ppm

^{13}C NMR (126 MHz, DMSO-D_6): δ = 139.93, 138.25, 129.04, 127.91, 124.32, 50.45, 21.51, 21.32 ppm

Yield: 88 % (76 mg) as a white solid

1-(2‘-Methylphenyl)ethanaminium chloride (11)

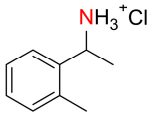

MW = 171.67 g/mol

^{1}H NMR (300 MHz, DMSO-D_6): δ = 8.74 (s, 3 H), 7.70-7.62 (m, 1 H), 7.35-7.21 (m, 3 H) 4.62-4.45 (m, 1 H), 2.34 (s, 3 H), 1.53 (d, *J* = 1.51 Hz, 3 H) ppm

^{13}C NMR (75 MHz, DMSO-D_6): δ = 138.34, 135.52, 130.96, 128.48, 126.94, 125.93, 46.65, 20.84, 19.27 ppm

Yield: 88 % (76 mg) as a white solid

1-(4‘-Methoxyphenyl)ethanaminium chloride (12)

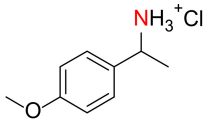

MW = 187.67 g/mol

^{1}H NMR (300 MHz, DMSO-D_6): δ = 8.58 (s, 3 H), 7.95 (d, J = 7.45 Hz, 2 H), 7.02 (d, J = 7.19 Hz, 2 H), 4.33-4.27 (m, 1 H), 3.85 (s, 3 H), 1.50 (d, J = 1.54 Hz, 3 H) ppm

^{13}C NMR (75 MHz, DMSO-D_6): δ = 163.56, 159.66, 130.95, 114.40, 55.99, 49.92, 26.88 ppm

Yield: 89 % (84 mg) as a white solid

1-(3‘-Methoxyphenyl)ethanaminium chloride (13)

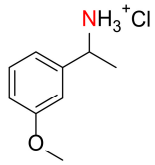

MW = 187.67 g/mol

^{1}H NMR (500 MHz, DMSO-D_6): δ = (500 MHz, DMSO-D_6): δ = 8.68 (s, 3 H), 7.36-7.29 (m, 1 H), 7.22-7.17 (m, 1 H), 7.08 (d, J = 7.52, 1 H), 6.95 (d, J = 7.56, 1 H), 4.34-4.29 (m, 1 H), 3.72 (s, 3 H), 1.53 (d, *J* = 1.56 Hz, 3 H) ppm

^{13}C NMR (126 MHz, DMSO-D_6): δ = 159.89, 141.53, 130.24, 119.31, 114.20, 113.05, 55.69, 50.44, 21.34 ppm

Yield: 90 % (84 mg) as a white solid

1-(3',4'-dimethoxyphenyl)ethanaminium chloride (14)

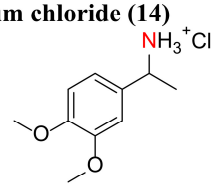

MW = 217.69 g/mol

^{1}H NMR (300 MHz, DMSO-D_6): δ = 8.51 (s, 3 H), 7.30-7.26 (m, 1 H), 7.06-6.97 (m, 2 H), 4.42-4.27 (m, 1 H), 3,82 (s, 3 H), 3.77 (s, 3 H), 1,48 (d, J = 7.5 Hz, 3 H) ppm

^{13}C NMR (75 MHz, DMSO-D_6): δ = 149.25, 132.16, 119.52, 112.15, 111.37, 56.11, 50.33, 21.21 ppm

Yield: 88 % (96 mg) as a white solid

diphenylmethanaminium chloride (15)

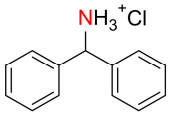

MW = 219.71 g/mol

^{1}H NMR (300 MHz, DMSO-D_6): δ = 9.26 (s, 3 H), 7.94-7.37 (m, 10 H), 5.77-5.50 (m, 1 H) ppm

^{13}C NMR (75 MHz, DMSO-D_6): δ = 138.84, 135.72, 132.19, 131.39, 129.60, 129.22, 128.73, 127.84, 57.55 ppm

Yield: 80 % (88 mg) as a white solid

1-(Pyridin-4-yl)ethanaminium chloride (16)

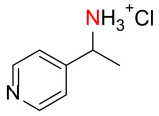

MW = 158.63 g/mol

^{1}H NMR (300 MHz, DMSO-D_6): δ = 9.22 (s, 3 H), 9.04-8,98 (d, *J* = 6.9, 2 H), 8.22 (d, *J* = 6.8, 2 H), 4.86-4.59 (m, 1 H), 1.58 (d, J = 7.5 Hz, 3 H) ppm

^{13}C NMR (75 MHz, DMSO-D_6): δ = 159.05, 142.32, 125.89, 49.57, 20.62 ppm

Yield: 91 % (72 mg) as a yellow solid

2,3-dihydro-1H-inden-1-aminium chloride (17)

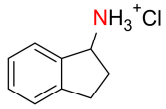

MW = 169.65 g/mol

^{1}H NMR (300 MHz, DMSO-D_6): δ = 8.65 (s, 3 H), 7.69 (d, *J* = 6.8, 2 H), 7.40-7.25 (m, 3 H), 4.78-4.63 (m, 1 H), 3.19-3.02 (m, 1 H), 2.97-2.81 (m, 1 H), 2.51-2.40 (m, 1 H), 2.12-1.92 (m, 1 H) ppm

^{13}C NMR (75 MHz, DMSO-D_6): δ = 144.39, 139.86, 129.39, 127.08, 125.51, 125.33, 55.04, 30.77, 30.31 ppm

Yield: 62 % (53 mg) as a white solid

1-(4-fluorophenyl)-benzeneethanaminium chloride (18)

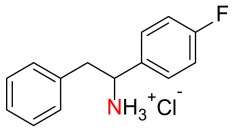

MW = 251.73 g/mol

^{1}H NMR (300 MHz, DMSO-D_6): δ = 8.78 (s, 3 H), 7.58-7.46 (m, 2 H), 7.29-7.14 (m, 5 H), 7.12-7.05 (m, 2 H), 4.63-4.48 (m, 1 H), 3.51-3.39 (m, 1 H), 3.20-3.06 (m, 1 H) ppm

^{13}C NMR (75 MHz, DMSO-D_6): δ = 160.82, 136.55, 133.80, 130.65, 130.54, 129.72, 128.79, 127.15, 115.91, 115.63, 55.45 ppm

Yield: 74 % (93 mg) as a white solid

Phenylmethanaminium chloride (19)

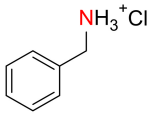

MW = 143.61 g/mol

^{1}H NMR (300 MHz, DMSO-D_6): δ = 8.71 (s, 3 H), 7.59-7.51 (m, 2 H), 7.47-7.36 (m, 3 H), 4.01 (s, 2 H) ppm

^{13}C NMR (75 MHz, DMSO-D_6): δ = 134.62, 129.46, 128.98, 128.81, 52.56 ppm

Yield: 92 % (66 mg) as a white solid

p-tolylmethanaminium chloride (20)

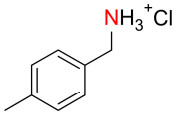

MW = 157.64 g/mol

^{1}H NMR (300 MHz, DMSO-D_6): δ = 8.54 (s, 3 H), 7.40 (d, *J* = 7.5 Hz, 2 H), 7.24 (d, *J* = 7.5 Hz, 2 H), 4.04-3.91 (m, 2 H), 2.32 (s, 3 H) ppm

^{13}C NMR (75 MHz, DMSO-D_6): δ = 138.22, 131.54, 129.57, 129.39, 42.38, 21.23 ppm

Yield: 85 % (67 mg) as a white solid

(4-Methoxyphenyl)methanaminium chloride (21)

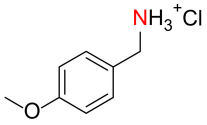

MW = 173.64 g/mol

^{1}H NMR (300 MHz, DMSO-D_6): δ = 8.51 (s, 3 H), 7.47 (d, *J* = 7.5 Hz, 2 H), 6.98 (d, *J* = 7.5 Hz, 2 H), 4.01-3.88 (m, 2 H), 3.79-3.77 (s, 3 H) ppm

^{13}C NMR (75 MHz, DMSO-D_6): δ = 159.79, 131.04, 126.48, 114.35, 55.69, 42.09 ppm

Yield: 88 % (76 mg) as a white solid

(4-Fluorophenyl)methanaminium chloride (22)

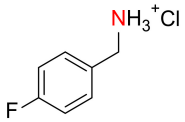

MW = 161.6 g/mol

^{1}H NMR (300 MHz, DMSO-D_6): δ = 8.67 (s, 3 H), 7.65-7.57 (m, 2 H), 7.30-7.23 (m, 2 H), 4.07-3.97 (s, 2 H) ppm

^{13}C NMR (75 MHz, DMSO-D_6): δ = 164.16, 131.92, 131.81, 130.92, 115.94, 115.66, 41.83 ppm

Yield: 84 % (68 mg) as a white solid

(4-Chlorophenyl)methanaminium chloride (23)

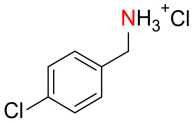

MW = 178.06 g/mol

^{1}H NMR (300 MHz, DMSO-D_6): δ = 8.75 (s, 3 H), 7.63-7.56 (m, 2 H), 7.52-7.45 (m, 2 H), 4.08-3.98 (s, 2 H) ppm

^{13}C NMR (75 MHz, DMSO-D_6): δ = 133.62, 133.53, 131.51, 128.91, 41.83 ppm

Yield: 91 % (81 mg) as a white solid

Pentan-aminium chloride (24)

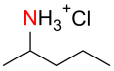

MW = 123.62 g/mol

^{1}H NMR (500 MHz, DMSO-D_6): δ = 8.12 (s, 3 H), 3.16-3.08 (m, 1 H), 1.60-1.11 (m, 7 H), 0.92-0.84 (t, J = 0.88, 3 H) ppm

^{13}C NMR (126 MHz, DMSO-D_6): δ = 46.95, 36.70, 18.57, 14.16 ppm

Yield: 36 % (22 mg) as a white solid

Dodean-2-aminium chloride (25)

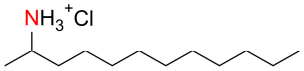

MW = 221.81 g/mol

^{1}H NMR (500 MHz, DMSO-D_6): δ = 8.00 (s, 3 H), 3.20-3.05 (m, 1 H), 1.62-1.15 (m, 21 H), 0.88-0.82 (t, *J* = 0.86, 3 H) ppm

^{13}C NMR (126 MHz, DMSO-D_6): δ = 47.19, 34.56, 31.77, 29.47, 29.41, 29.32, 29.24, 29.18, 25.23, 22.58, 18.58, 14.44 ppm

Yield: 88 % (98 mg) as a white solid

Heptan-4-aminium chloride (26)

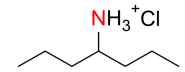

MW = 151.68 g/mol

^{1}H NMR (500 MHz, DMSO-D_6): δ = 8.24 (s, 3 H), 3.06-2.97 (m, 1 H), 1.56-1.28 (m, 8 H), 0.88-0.83 (m, 6 H) ppm

^{13}C NMR (126 MHz, DMSO-D_6): δ = 50.66, 34.54, 18.28, 14.25 ppm

Yield: 87 % (66 mg) as a white solid

3-Methyl-2-Butylaminium chloride (27)

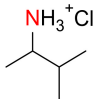

MW = 123.62 g/mol

^{1}H NMR (500 MHz, DMSO-D_6): δ = 7.99 (s, 3 H), 3.04-2.98 (m, 1 H), 1.86-1.77 (m, 1 H), 1.11 (d, J = 1.12 Hz, 3 H), 0.94-0.84 (m, 6 H) ppm

^{13}C NMR (126 MHz, DMSO-D_6): δ = 52.15, 31.28, 19.21, 17.43, 15.10 ppm

Yield: 58 % (36 mg) as a white solid

4-Methyl-2-Pentylaminium chloride (28)

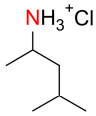

MW = 137.65 g/mol

^{1}H NMR (500 MHz, DMSO-D_6): δ = 8.08 (s, 3 H), 3.21-3.10 (m, 1 H), 1.71-1.62 (m, 1 H), 1.50-1.42 (m, 1 H), 1.34-1.28 (m, 1 H), 1.19-1.14 (d, J = 1.18 Hz, 3 H), 0.91-0.84 (m, 6 H) ppm

^{13}C NMR (126 MHz, DMSO-D_6): δ = 45.46, 43.72, 24.27, 23.33, 22.23, 18.80 ppm

Yield: 93 % (64 mg) as a white solid

1-Methylbenzylpropylaminium chloride (29)

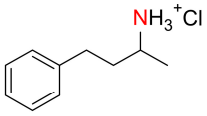

MW = 185.70 g/mol

^{1}H NMR (500 MHz, DMSO-D_6): δ = 8.26 (s, 3 H), 7.32-7.16 (m, 5 H), 3.16-3.07 (m, 1 H), 2.72-2.58 (m, 2 H), 1.97-1.88 (m, 1 H), 1.99-1.91 (m, 1 H), 1.24 (d, *J* = 1.23 Hz, 3 H) ppm

^{13}C NMR (126 MHz, DMSO-D_6): δ = 141.50, 128.88, 128.70, 126.45, 46.84, 44.60, 30.22, 18.49 ppm

Yield: 91 % (85 mg) as a white solid

Cyclopentylaminium chloride (30)

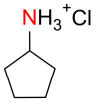

MW = 121.61 g/mol

^{1}H NMR (500 MHz, DMSO-D_6): δ = δ = 8.08 (s, 3 H), 3.48-3.40 (m, 1 H), 1.94-1.83 (m, 2 H), ppm 1.72-1.63 (m, 2 H), 1.59-1.44 (m, 2 H) ppm

^{13}C NMR (126 MHz, DMSO-D_6): δ = 51.58, 31.08, 23.91 ppm

Yield: 49 % (30 mg) as a white solid

Cyclohexylaminium chloride (31)

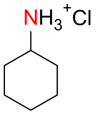

MW = 135.64 g/mol

^{1}H NMR (500 MHz, DMSO-D_6): δ = 8.18 (s, 3 H), 2.95-2.87 (m, 1 H), 1.94-1.04 (m, 11 H) ppm

^{13}C NMR (126 MHz, DMSO-D_6): δ = 49.69, 30.72, 24.21, 24.18 ppm

Yield: 61 % (41 mg) as a white solid

Cyclododecylaminium chloride (32)

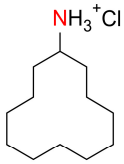

MW = 219.80 g/mol

^{1}H NMR (500 MHz, DMSO-D$_6$): δ = 8,17 (s, 3 H), 2,46-2,39 (m, 4 H), 1,66-1,58 (m, 4 H), 1,33-1,11 (m, 16 H) ppm

^{13}C NMR (126 MHz, DMSO-D$_6$): δ = 65.40, 48.24, 28.02, 24.68, 24.60, 24.22, 22.45 ppm

Yield: 77 % (85 mg) as a white solid

Nabumetone-NH$_3^+$Cl$^-$ (33)

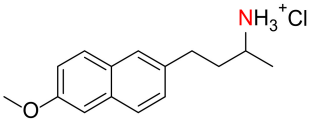

MW = 265.78 g/mol

^{1}H NMR (300 MHz, DMSO-D$_6$): δ = 8,22 (s, 3 H), 7.82-7.65 (m, 3 H), 7.40-7.27 (m, 2 H), 7.19-7.13 (m, 1 H), 3.88 (s, 3 H), 3.23-3.12 (m, 1 H), 2.92-2.70 (m, 1 H), 2.12-1.76 (m, 2 H), 1.32-1.29 (d, *J* = 6 Hz, 3 H) ppm

^{13}C NMR (75 MHz, DMSO-D$_6$): δ = 157.32, 136.54, 133.30, 129.27, 129.05, 128.04, 127.35, 126.43, 119.06, 106.30, 46.91, 36.28, 31.27, 15.57 ppm

Yield: 87 % (116 mg) as a white solid

1-(4-methoxyphenyl)propan-2-aminium chloride (34)

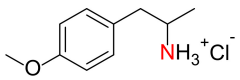

MW = 201.69 g/mol

^{1}H NMR (300 MHz, DMSO-D$_6$): δ = 8.19 (s, 3 H), 7.19 (d, *J* = 7.5 Hz, 2 H), 6.92 (d, *J* = 7.5 Hz, 2 H), 7.19-7.13 (m, 1 H), 3.77 (s, 3 H), 3.39-3.26 (m, 1 H), 3.08-2.94 (m, 1 H), 2.69-2.57 (m, 1 H), 1.12 (d, *J* – 6 Hz, 3 H) ppm

^{13}C NMR (75 MHz, DMSO-D$_6$): δ = 158.58, 130.75, 129.11, 114.46, 55.53, 48.63, 17.92 ppm

Yield: 90 % (91 mg) as a white solid

1-(2-methoxyphenyl)propan-2-aminium chloride (35)

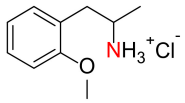

MW = 201.69 g/mol

^{1}H NMR (300 MHz, DMSO-D_6): δ = 8.21 (s, 3 H), 7.32-6.91 (m, 4 H), 3.81 (s, 3 H), 3.47-3.39 (m, 1 H), 3.10-2.95 (m, 1 H), 2.81-2.65 (m, 1 H), 1.10 (d, *J* = 6 Hz, 3 H) ppm

^{13}C NMR (75 MHz, DMSO-D_6): δ =157.77, 131.40, 128.86, 125.04, 120.87, 111.42, 55.84, 47.18, 35.38, 18.19 ppm

Yield: 73 % (74 mg) as a white solid

Stanolone-$NH_3^+Cl^-$ (36)

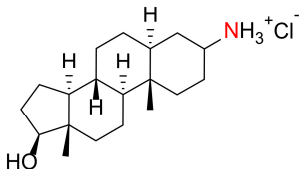

MW = 327.94 g/mol

^{1}H NMR (300 MHz, DMSO-D_6): δ = 8.14 (s, 3 H), 2.09-0.75 (m, 25 H), 0.63 (s, 3 H) ppm

^{13}C NMR (75 MHz, DMSO-D_6): δ = 80.55, 53.85, 51.31, 46.80, 44.71, 43.07, 38.57, 36.04, 35.57, 31.62, 31.31, 31.07, 30.39, 28.26, 23.52, 20.45, 11.78, 11.57 ppm

Yield: 54 % (89 mg) as a white solid

Further experiments with electron withdrawing substituents and α-keto acids:

The reductive amination of 4-nitro acetophenone couldn't be accomplished due to the reduction of the nitro group to an amine group. The reductive amination of 4-acetamidoacetophenone, Methyl-4-acetylbenzoate and phenylglyoxylic acid delivered hardly any yield.

5. NMR Spectra

1:

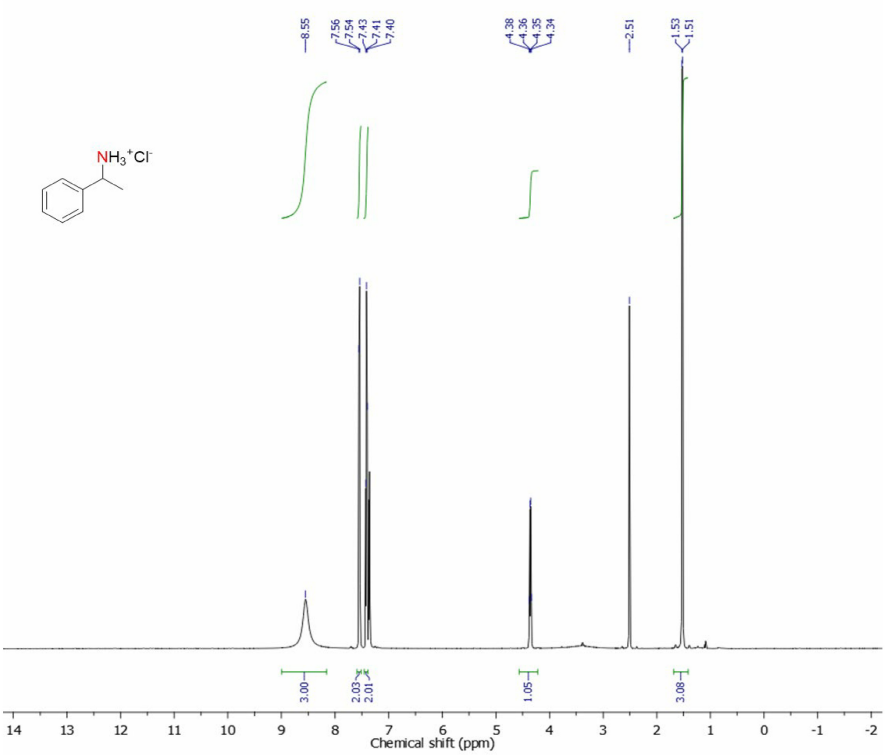

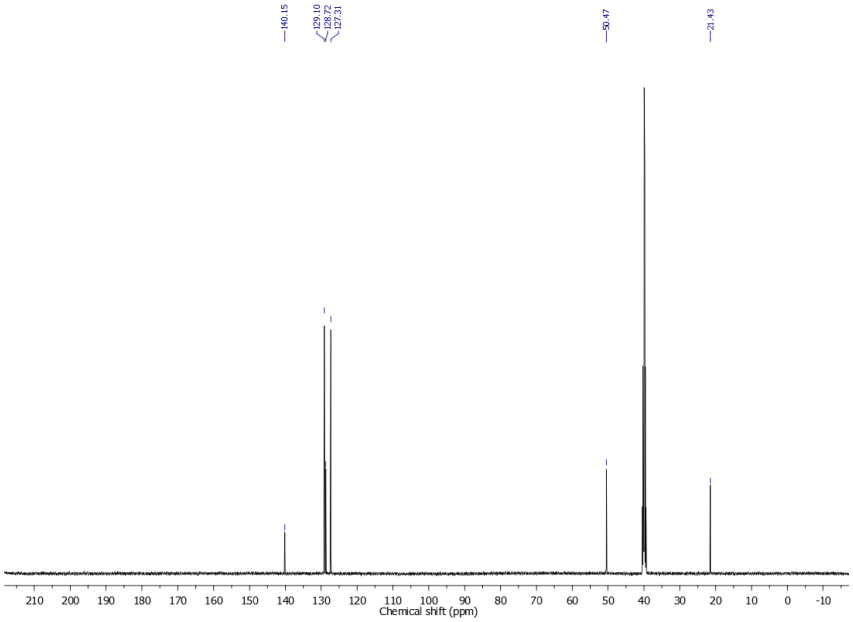

2:

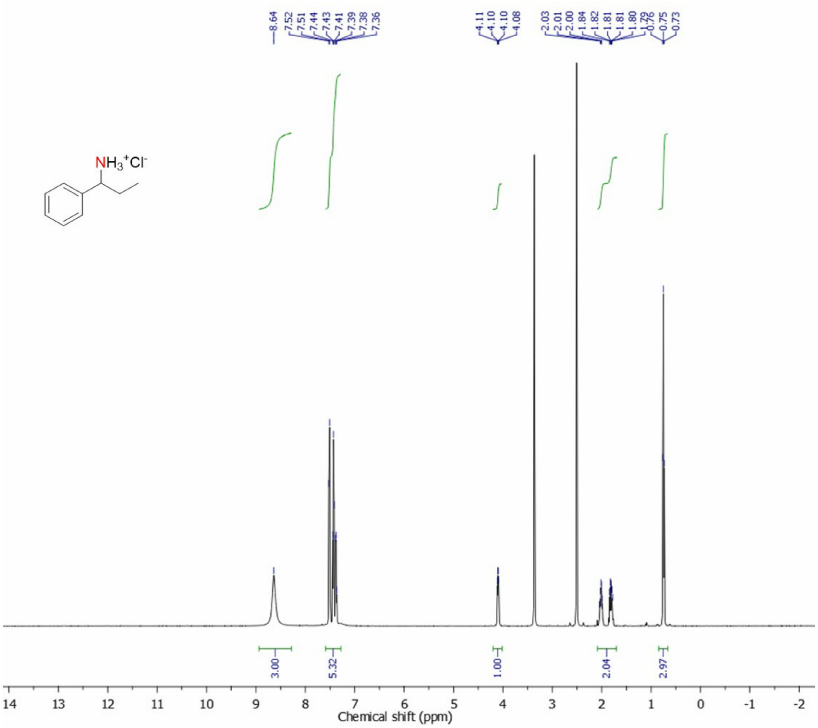
8.64
7.52
7.51
7.44
7.43
7.41
7.39
7.38
7.36
4.11
4.10
4.10
4.08
2.03
2.01
2.00
1.84
1.82
1.81
1.81
1.80
1.78
0.76
0.75
0.73
NH3+Cl-
3.00
5.32
1.00
2.04
2.97
Chemical shift (ppm)

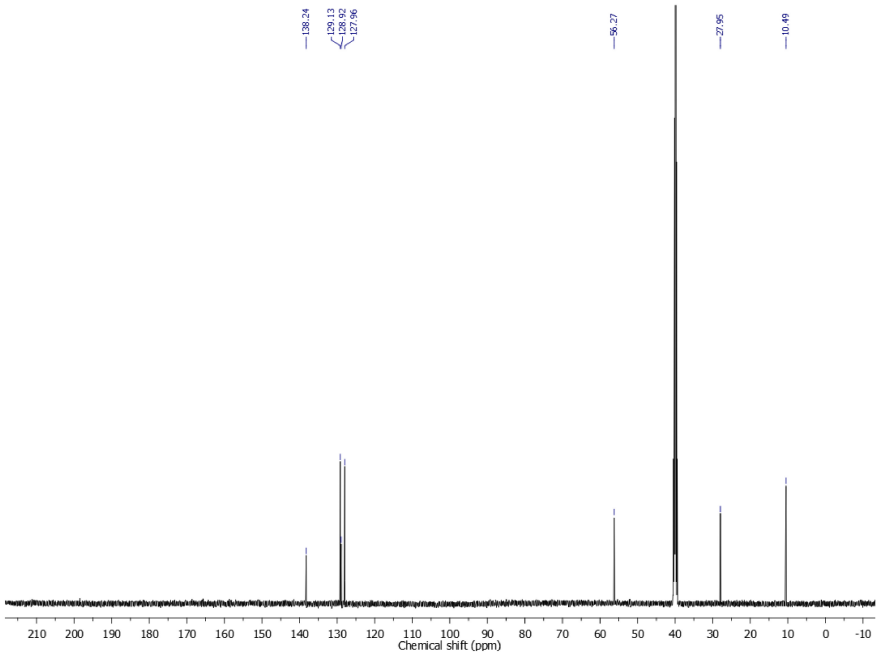
138.24
129.13
128.92
127.96
56.27
27.95
10.49
Chemical shift (ppm)

3:

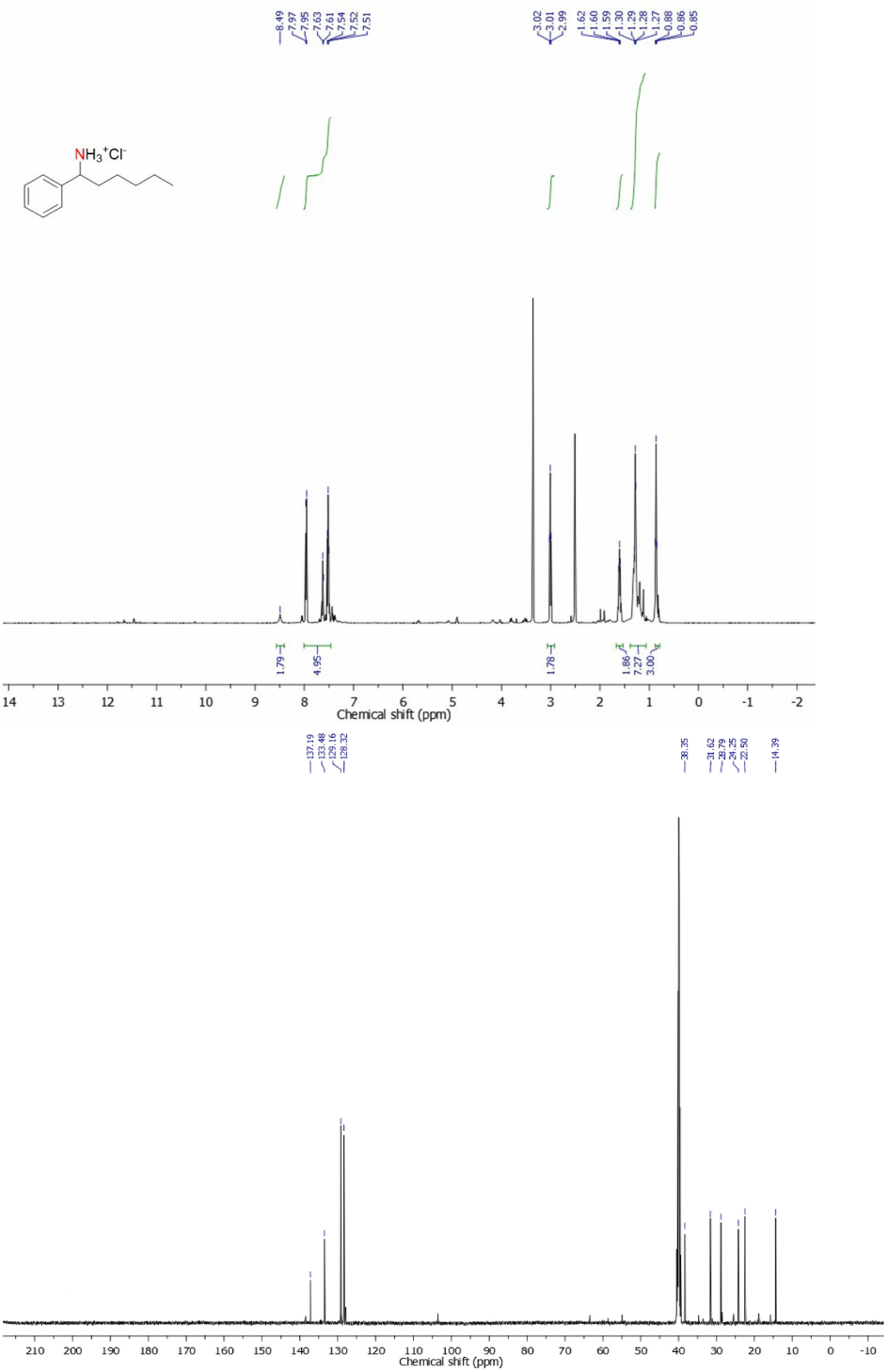
8.49
7.97
7.95
7.63
7.61
7.54
7.52
7.51
3.02
3.01
2.99
1.62
1.60
1.59
1.30
1.29
1.28
1.27
0.88
0.86
0.85
NH3+Cl-
1.79
4.95
1.78
1.86
7.27
3.00
Chemical shift (ppm)
137.19
133.48
129.16
128.32
38.35
31.62
26.79
24.25
22.50
14.39
Chemical shift (ppm)

4:

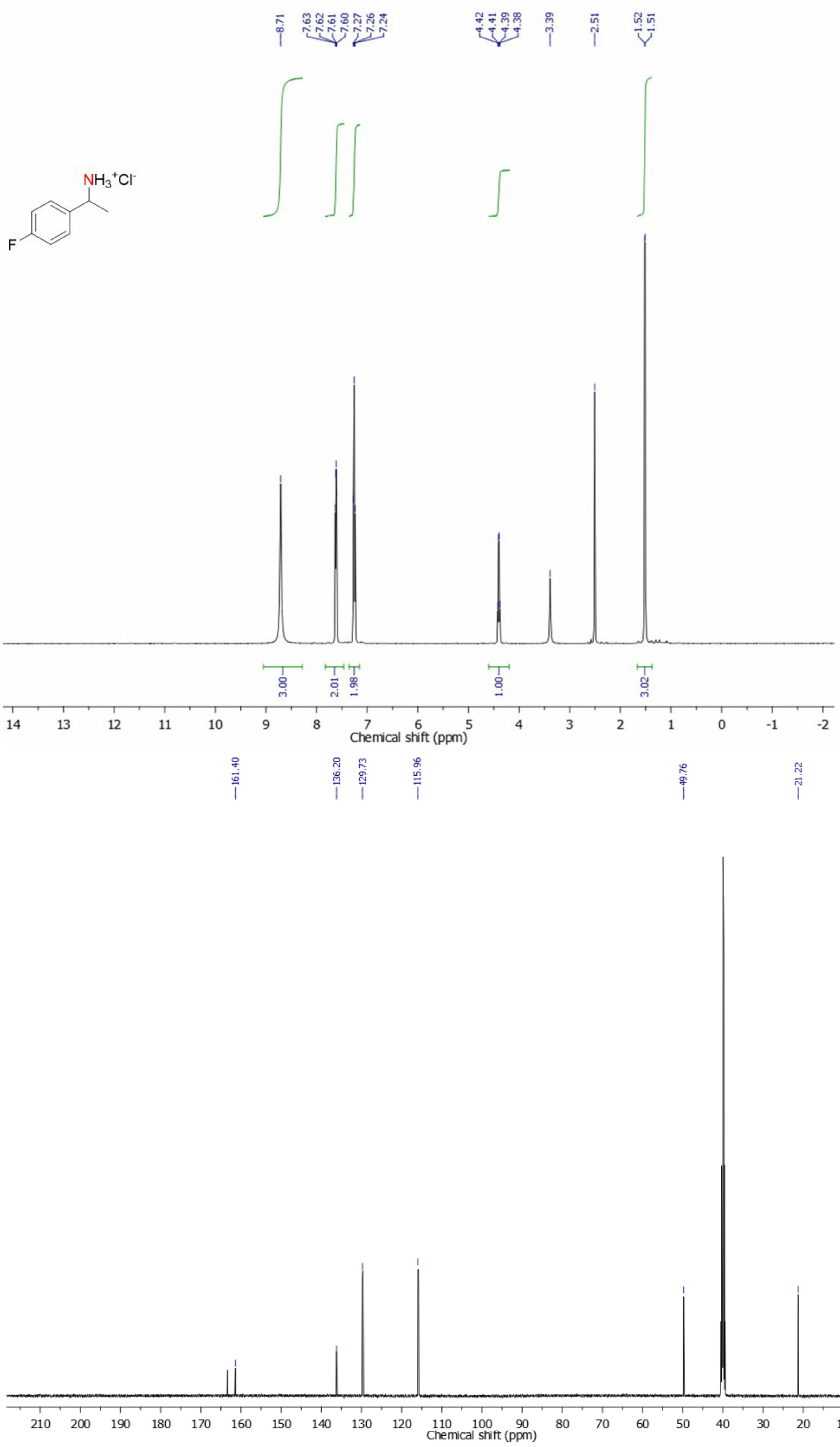
8.71
7.63
7.62
7.61
7.60
7.27
7.26
7.24
4.42
4.41
4.39
4.38
3.39
2.51
1.52
1.51
NH3+Cl-
F
3.00
2.01
1.98
1.00
3.02
Chemical shift (ppm)
161.40
136.20
129.73
115.96
49.76
21.22
Chemical shift (ppm)

5:

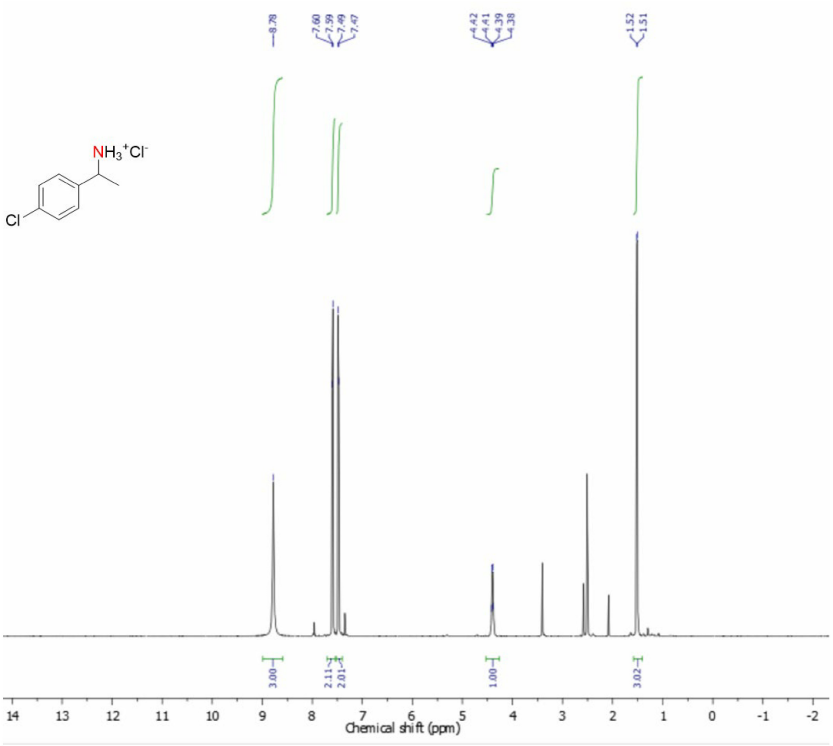
8.78
7.60
7.59
7.49
7.47
4.42
4.41
4.39
4.38
1.52
1.51
NH3+Cl-
Cl
3.00
2.11
2.01
1.00
3.02
14 13 12 11 10 9 8 7 6 5 4 3 2 1 0 -1 -2
Chemical shift (ppm)

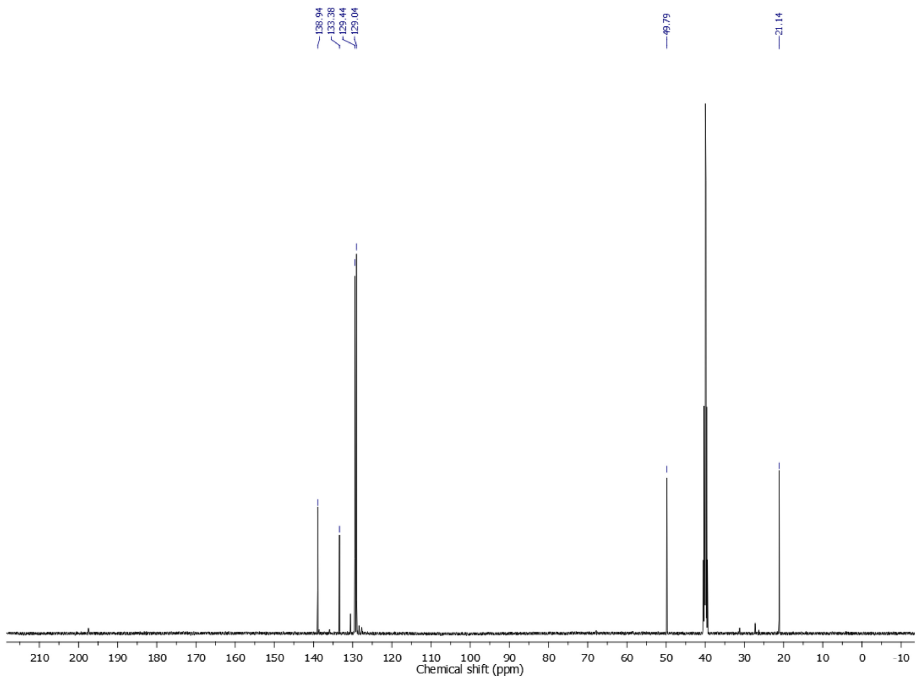
138.94
133.38
129.44
129.04
49.79
21.14
210 200 190 180 170 160 150 140 130 120 110 100 90 80 70 60 50 40 30 20 10 0 -10
Chemical shift (ppm)

6:

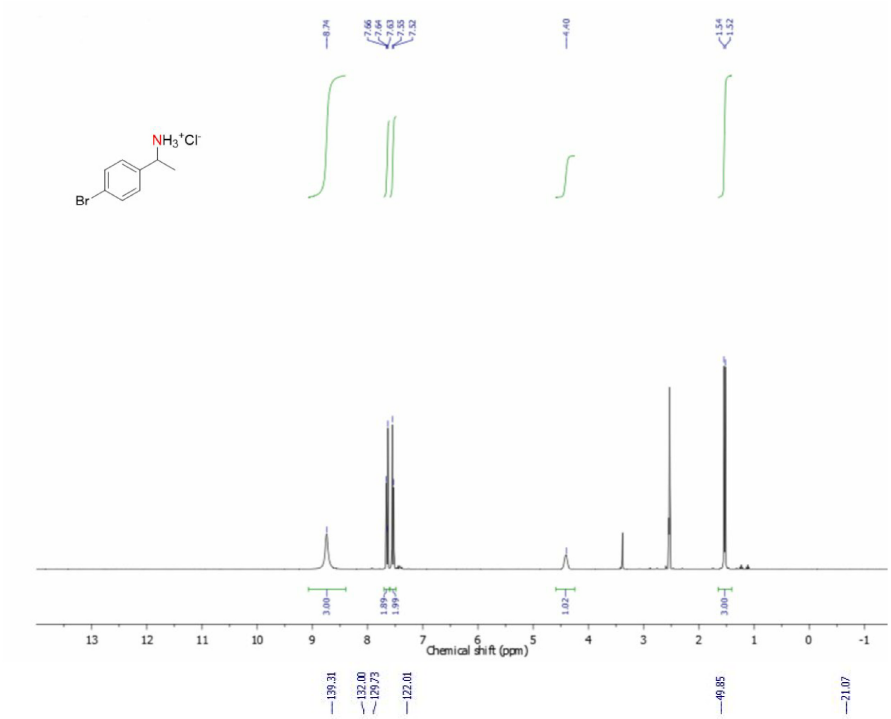

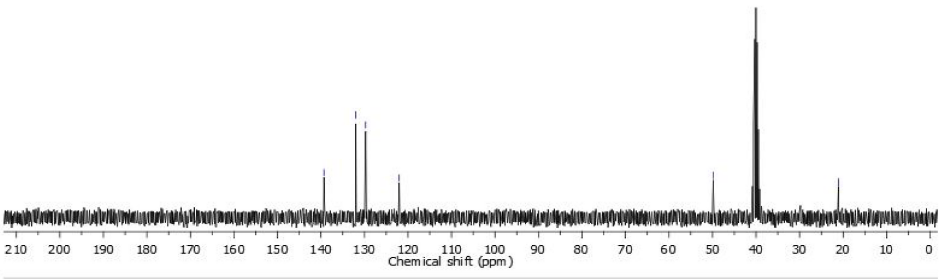

7:

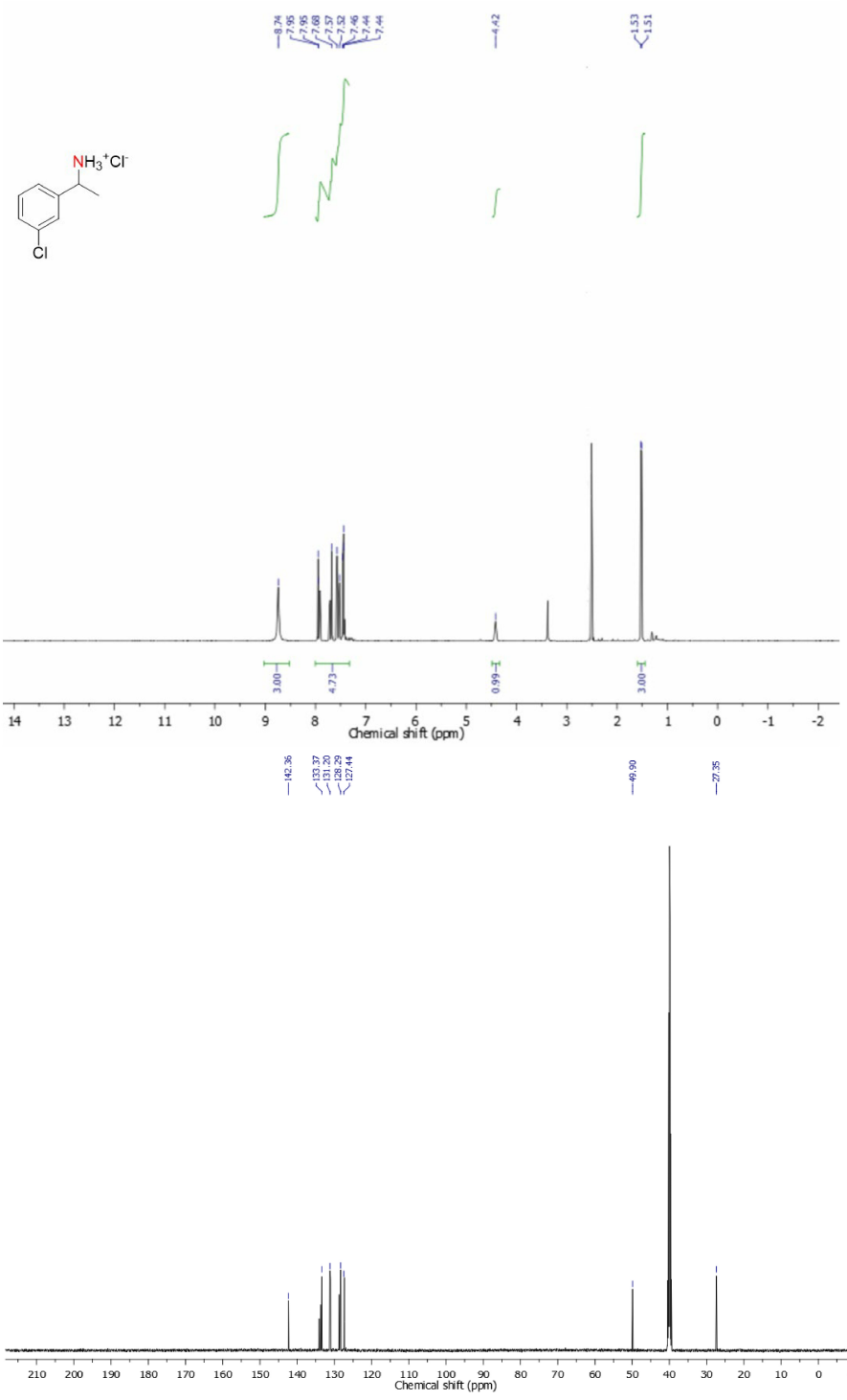
NH3+Cl-
Cl
8.74
7.95
7.95
7.68
7.57
7.52
7.46
7.44
7.44
4.42
1.53
1.51
3.00
4.73
0.99
3.00
Chemical shift (ppm)
142.36
133.37
131.20
128.29
127.44
49.90
27.35
Chemical shift (ppm)

8:

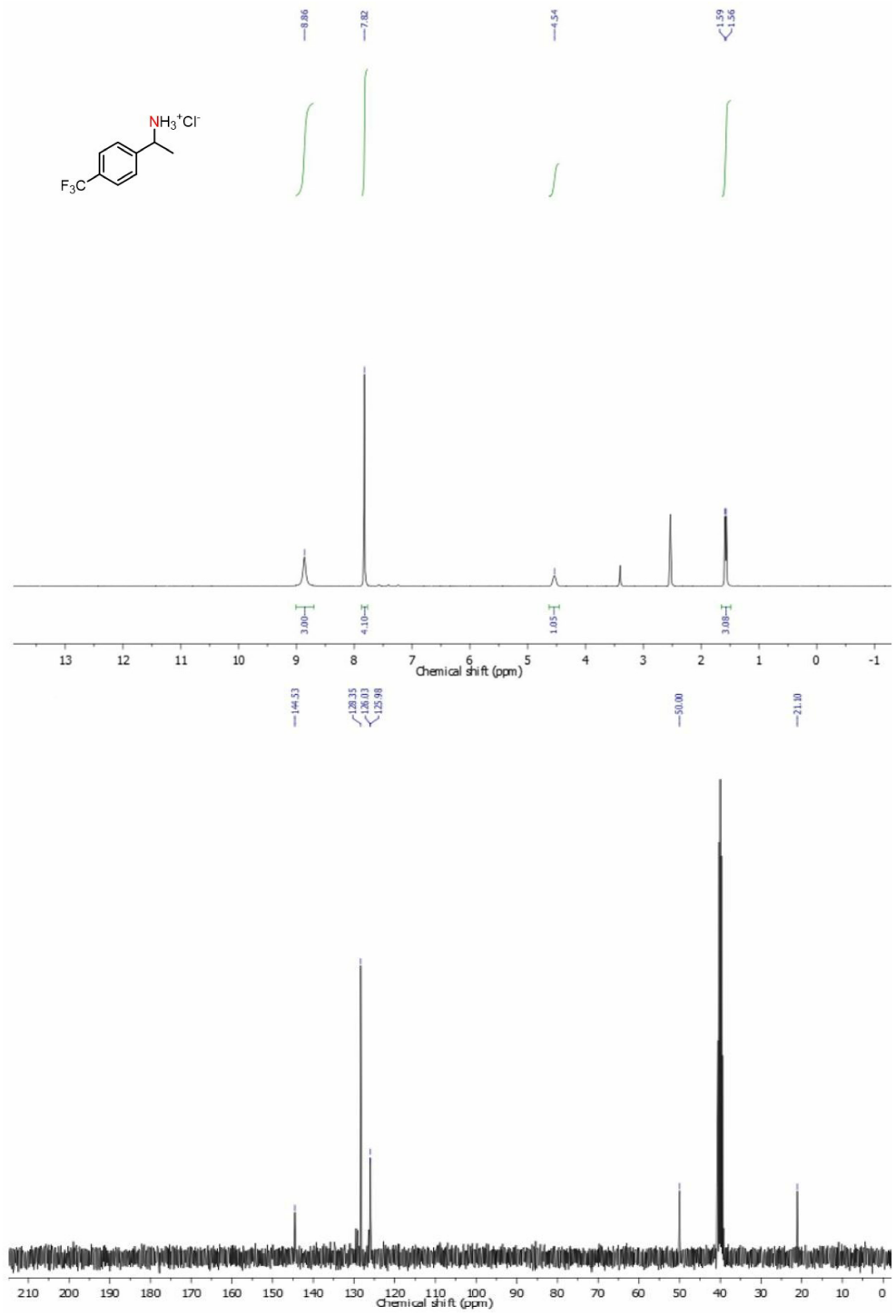
NH3+Cl-
F3C
8.86
7.82
4.54
1.59
1.56
3.00
4.10
1.05
3.08
Chemical shift (ppm)
144.53
128.35
126.03
125.98
50.00
21.10
Chemical shift (ppm)

9:

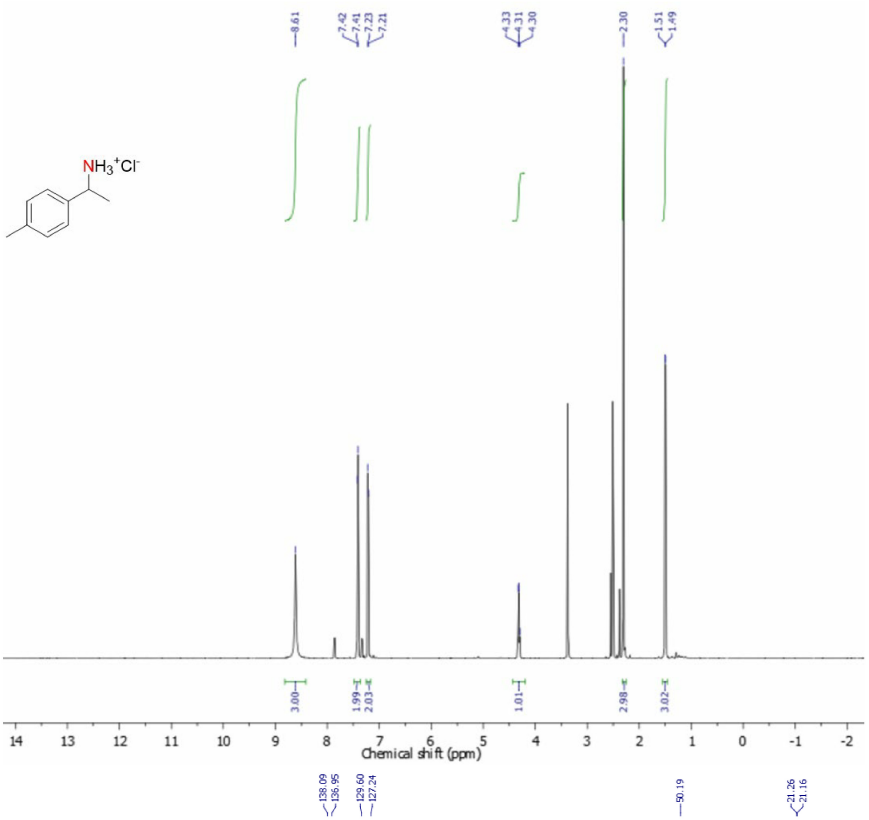
8.61
7.42
7.41
7.23
7.21
4.33
4.31
4.30
2.30
1.51
1.49
NH3+Cl-
3.00
1.99
2.03
1.01
2.98
3.02
Chemical shift (ppm)

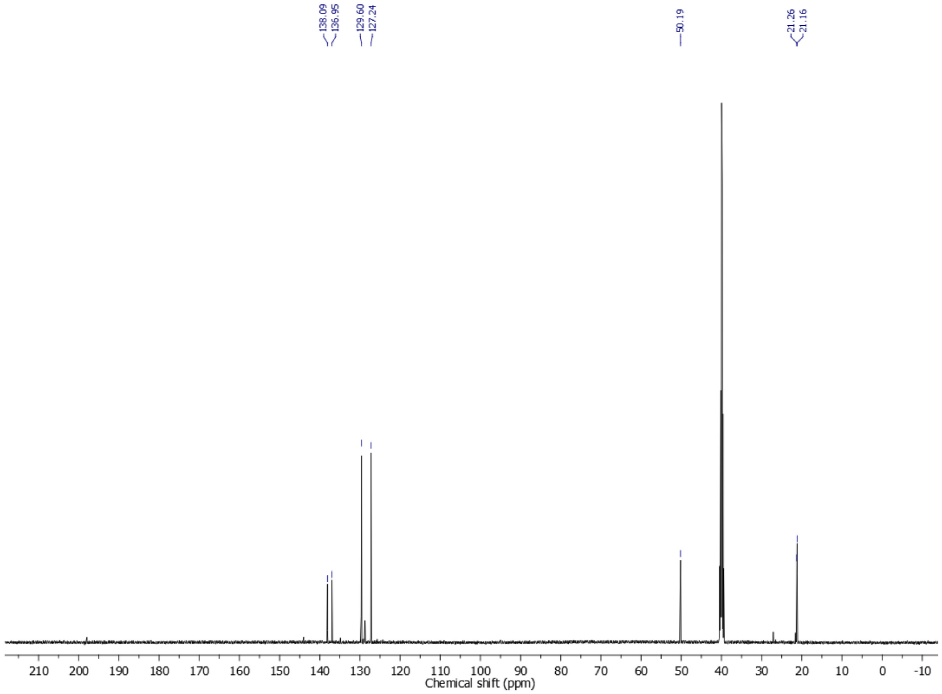
138.09
136.95
129.60
127.24
50.19
21.26
21.16
Chemical shift (ppm)

10:

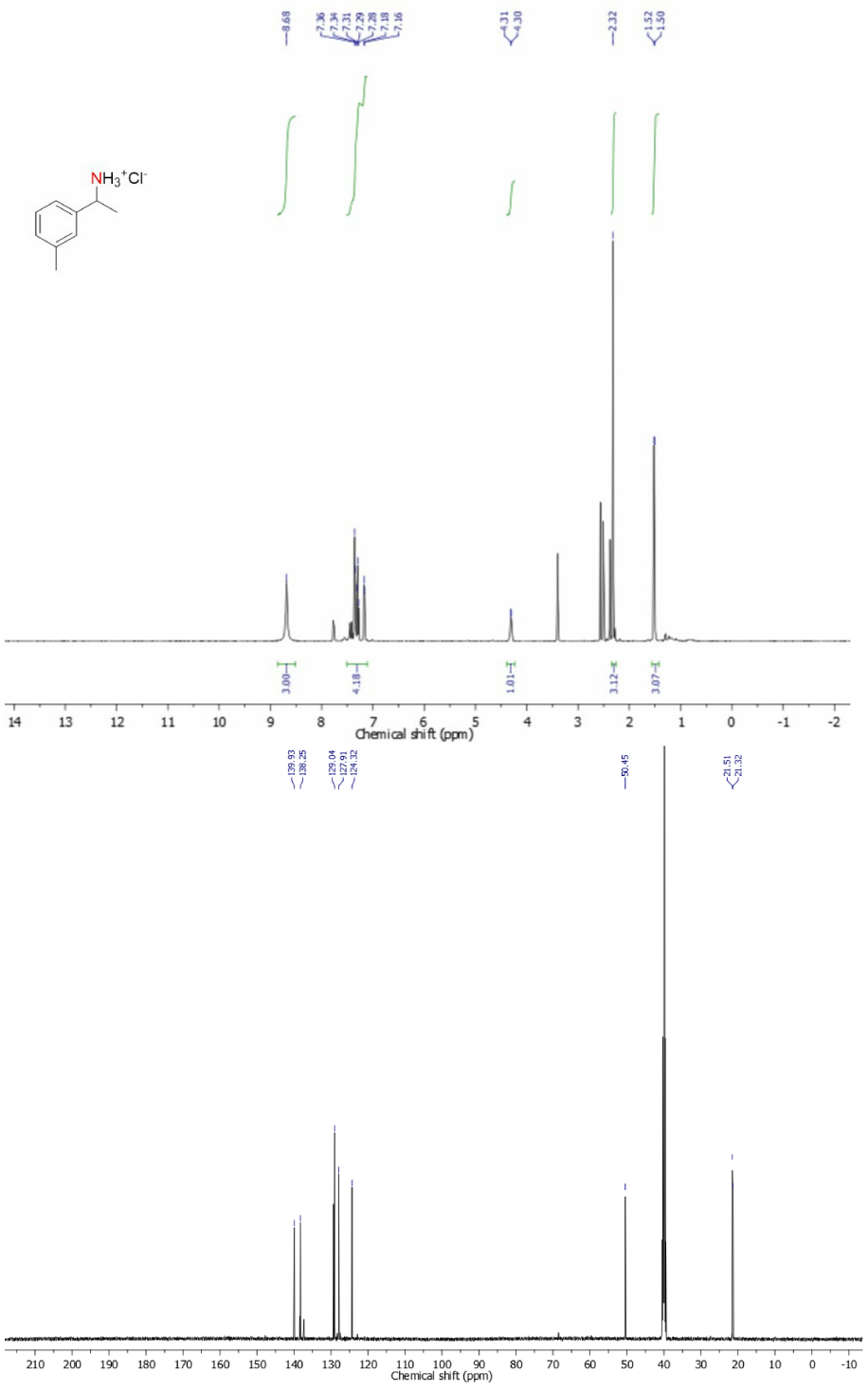
NH3+Cl-
8.68
7.36
7.34
7.31
7.29
7.28
7.18
7.16
4.31
4.30
2.32
1.52
1.50
3.00
4.18
1.01
3.12
3.07
Chemical shift (ppm)
139.93
138.25
129.04
127.91
124.32
50.45
21.51
21.32
Chemical shift (ppm)

11:

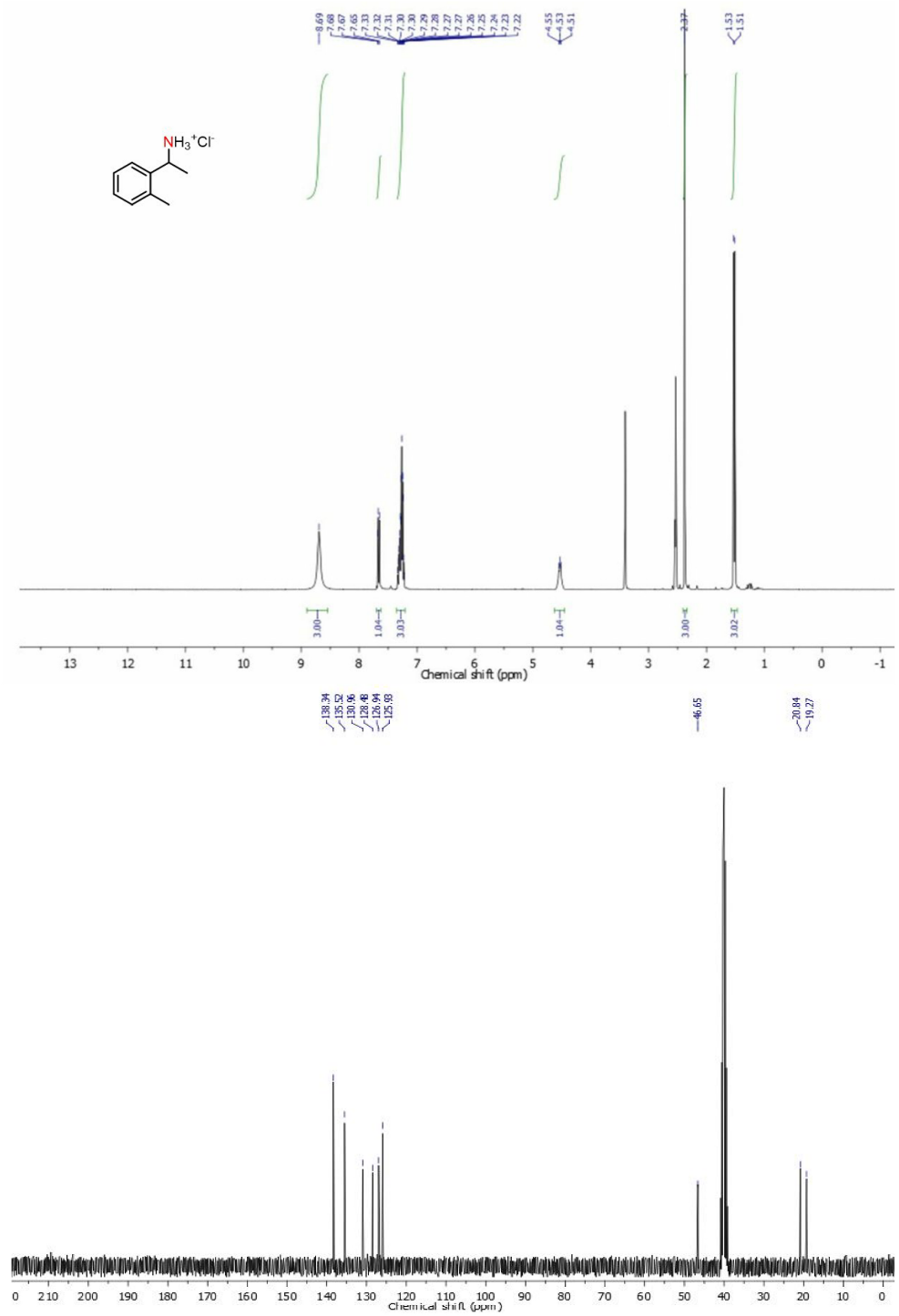

12:

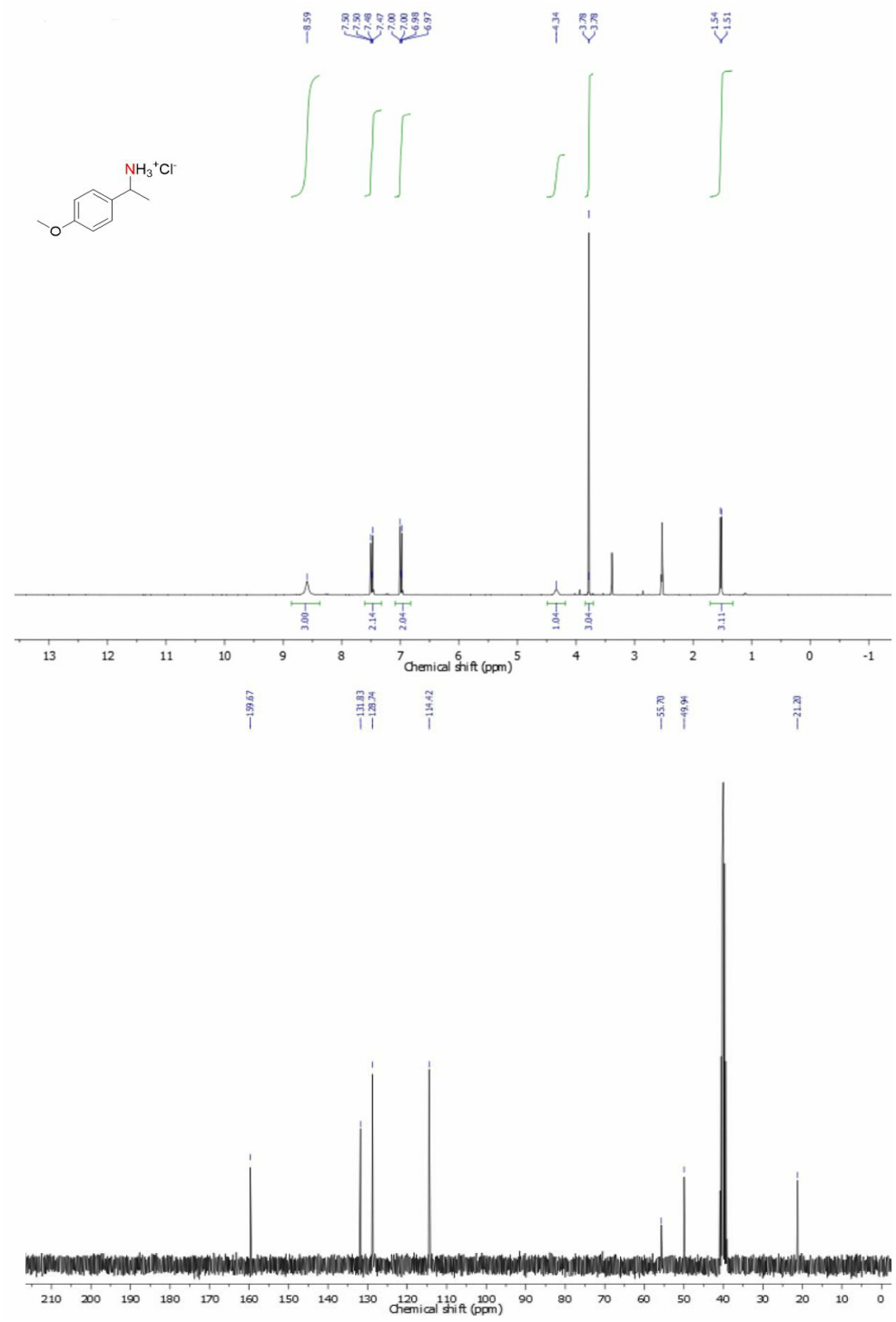

13:

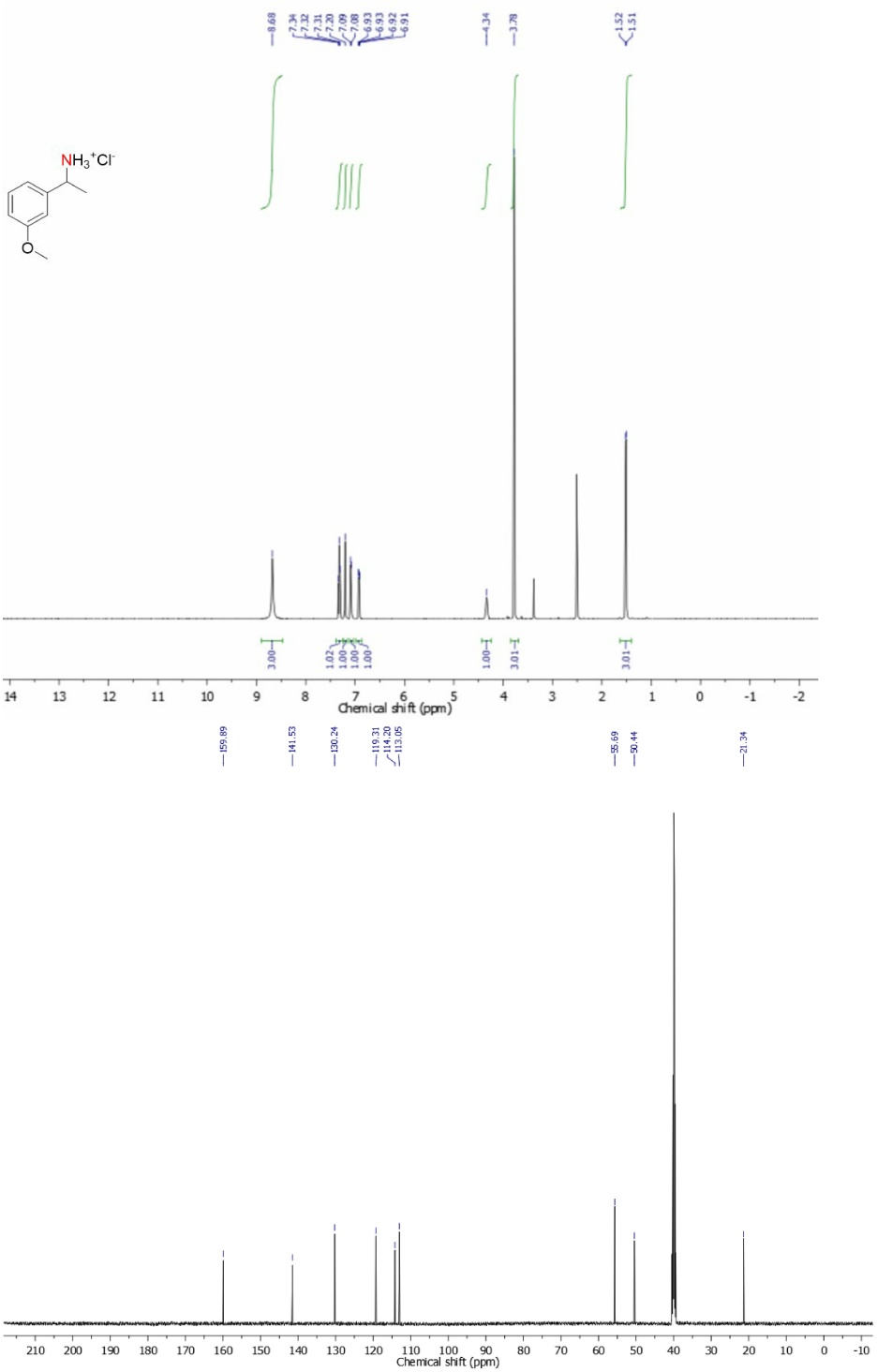
NH3+Cl-
O
8.68
7.34
7.32
7.31
7.20
7.09
7.08
6.93
6.92
6.91
4.34
3.78
1.52
1.51
3.00
1.02
1.00
1.00
1.00
1.00
3.01
3.01
Chemical shift (ppm)
159.89
141.53
130.24
119.31
114.20
113.05
55.69
50.44
21.34
Chemical shift (ppm)

14:

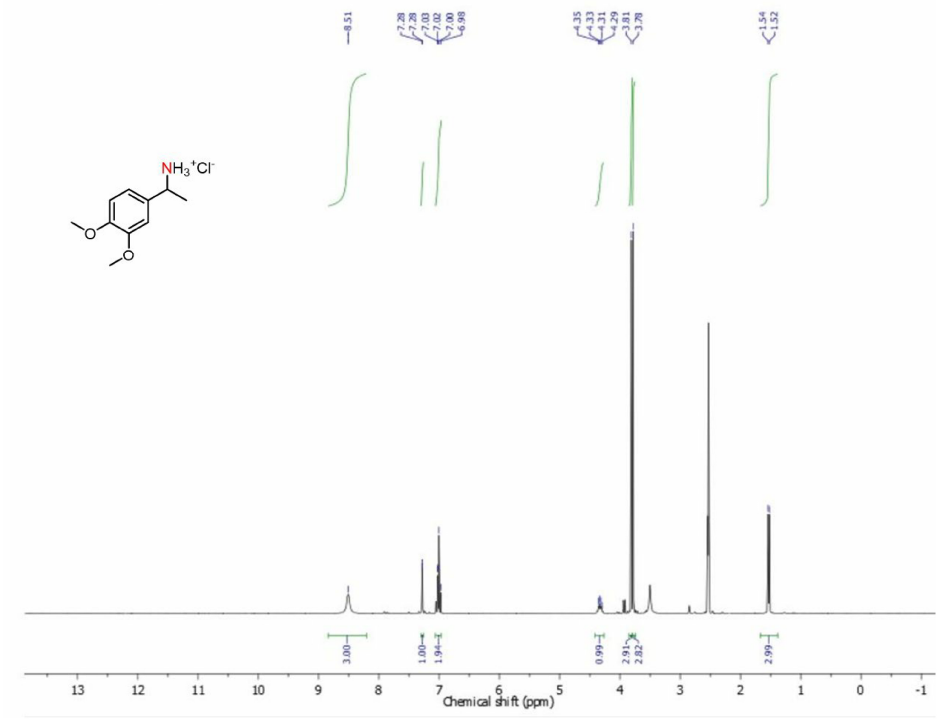
NH3+Cl-
Chemical shift (ppm)

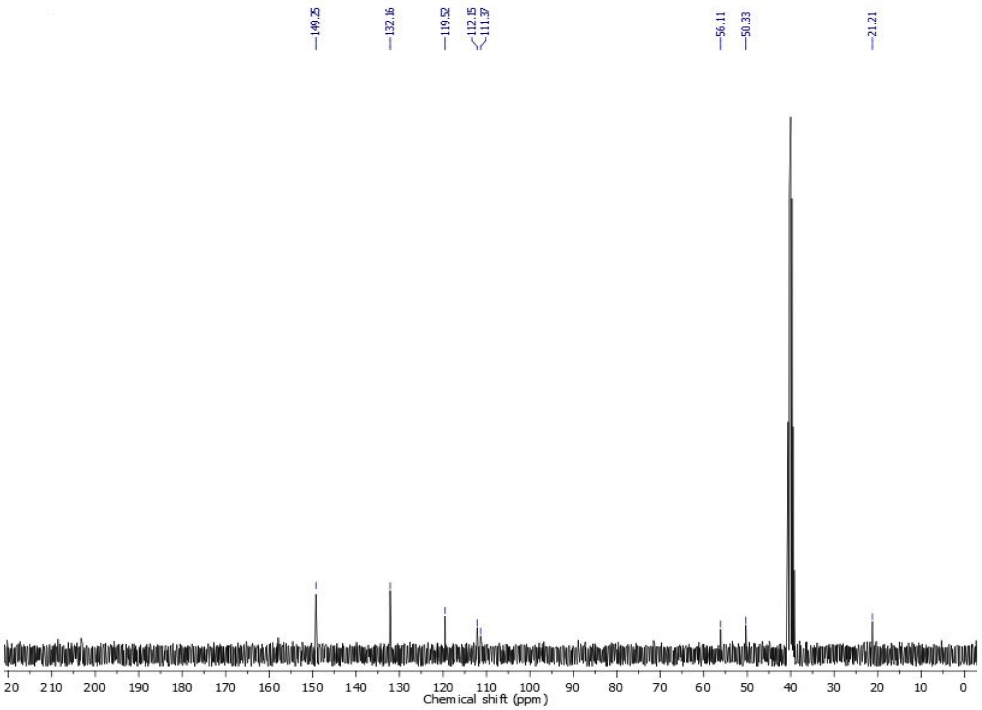
149.25
132.16
119.92
112.15
111.37
56.11
50.33
21.21
Chemical shift (ppm)

15:

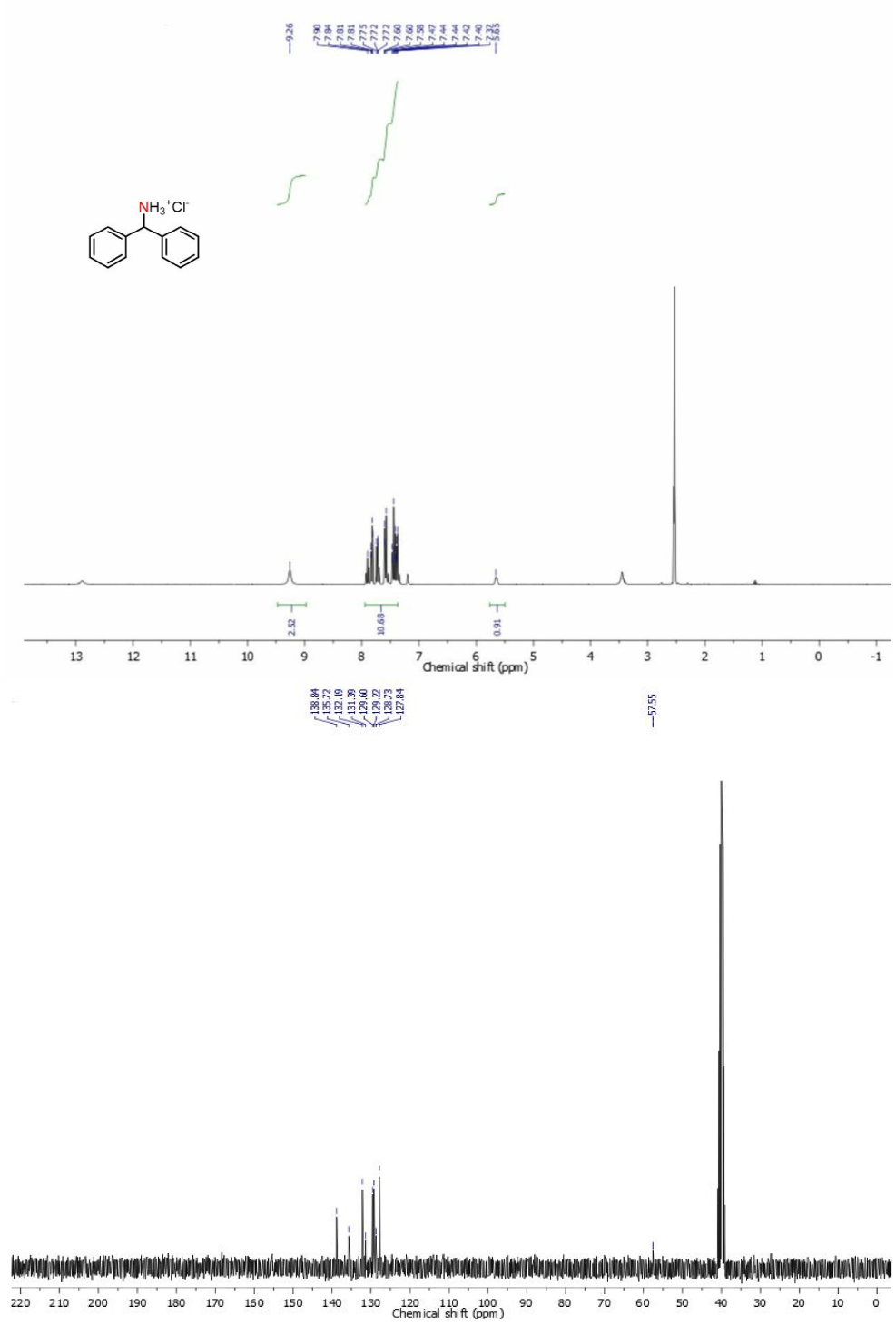

16:

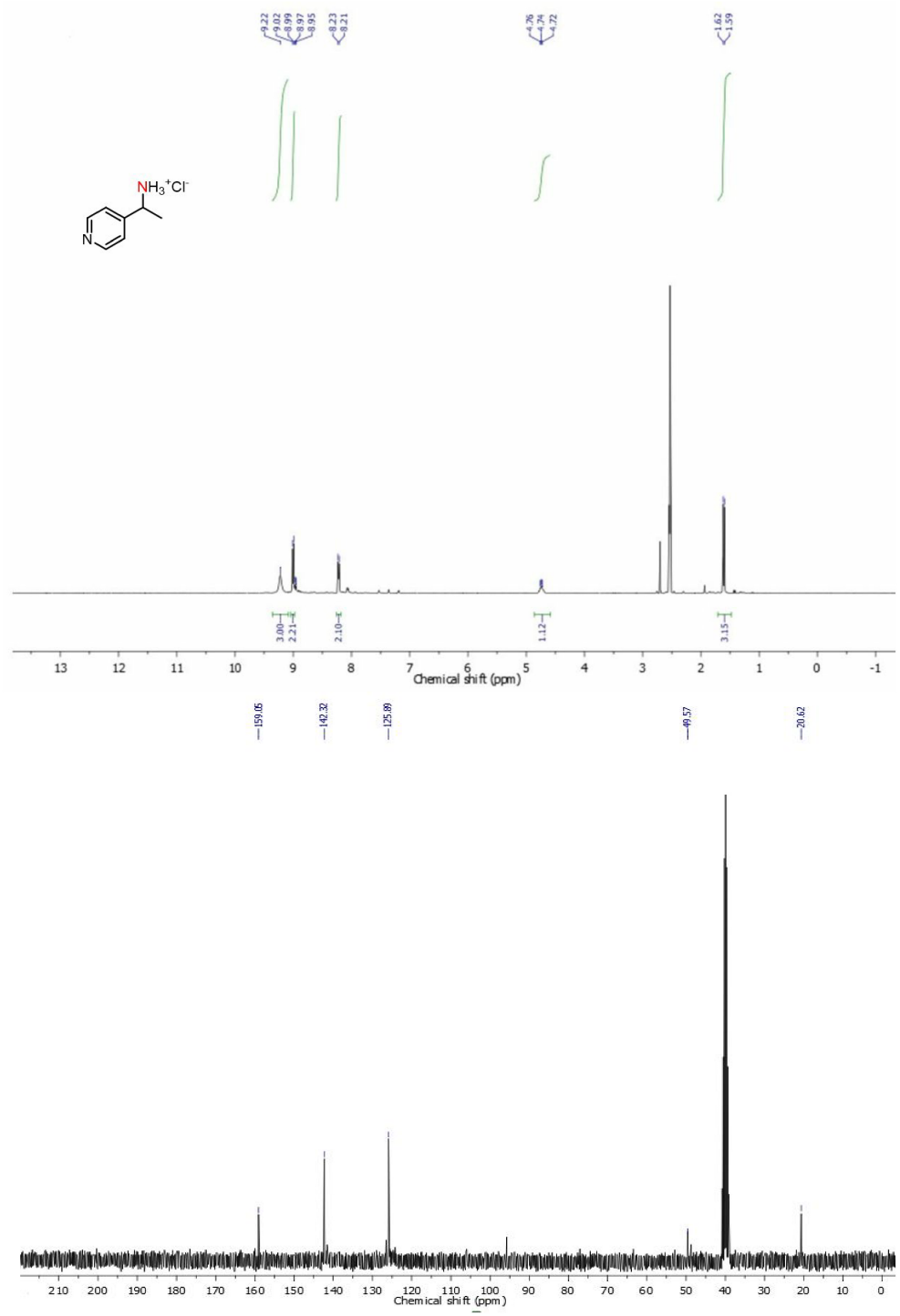
NH3+Cl-
N
9.22
9.02
8.99
8.97
8.95
8.23
8.21
4.76
4.74
4.72
1.62
1.59
3.00
2.21
2.10
1.12
3.15
Chemical shift (ppm)
159.05
142.32
125.89
49.57
20.62
Chemical shift (ppm)

17:

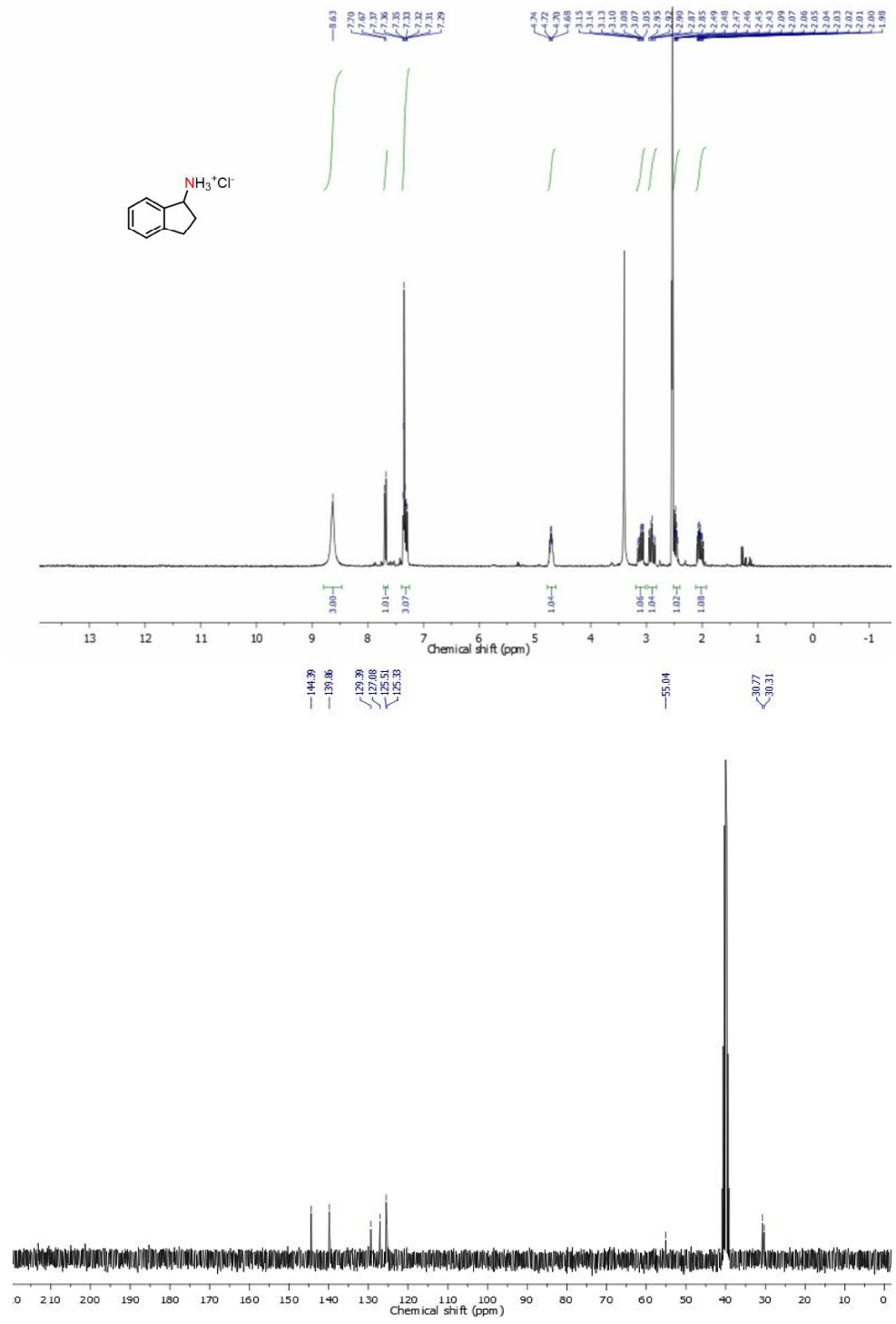

18:

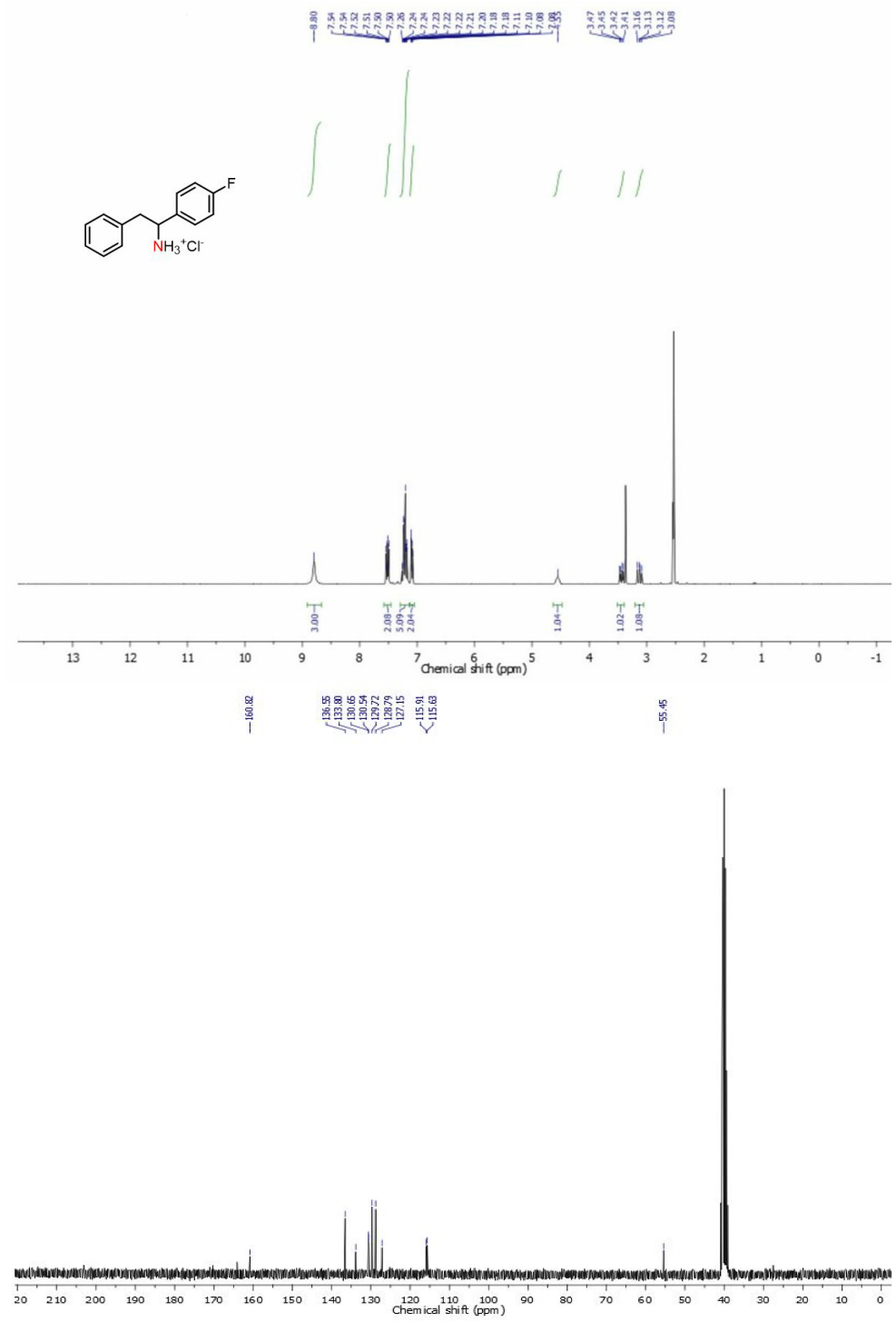

19:

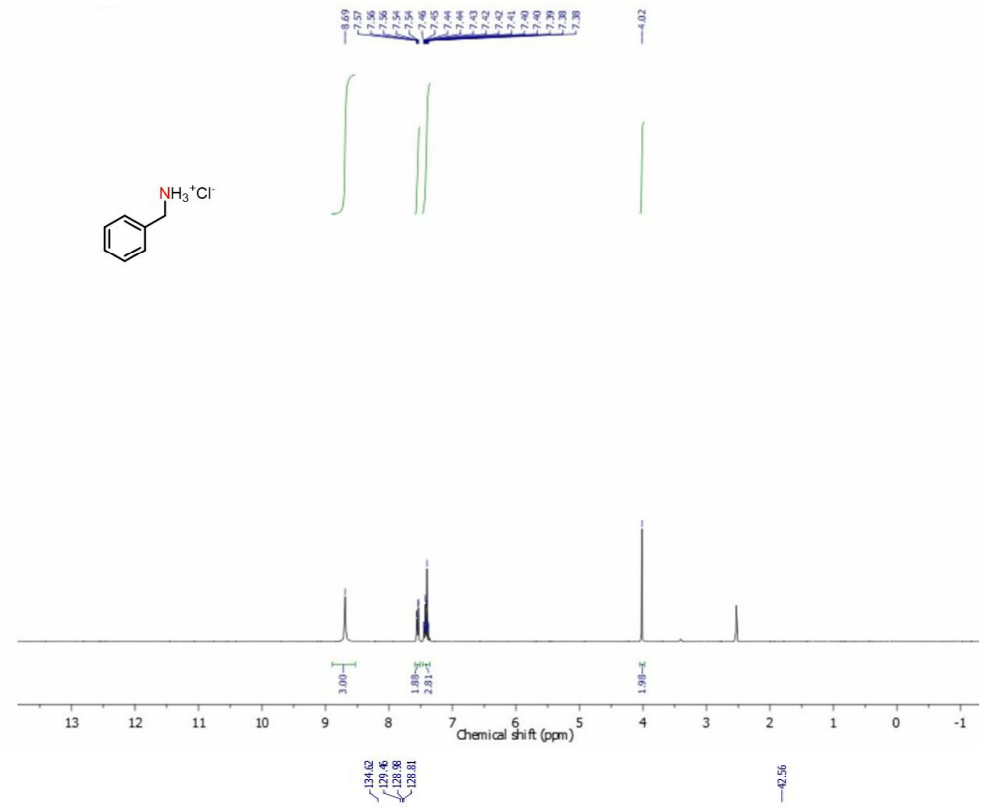

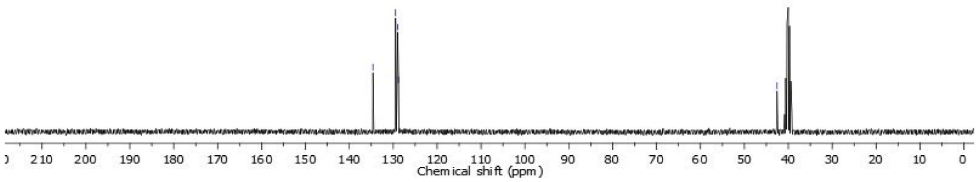

20:

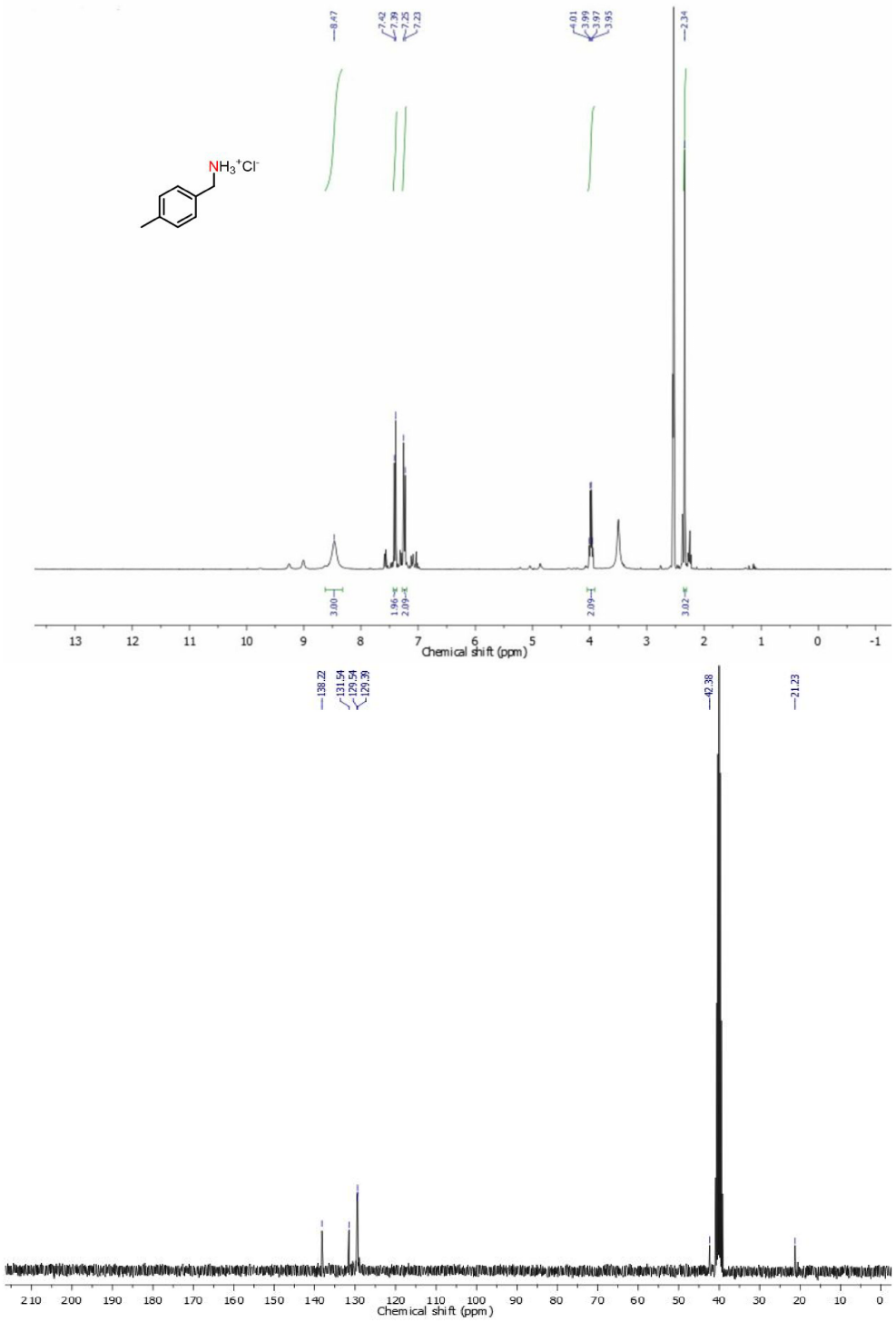
NH3+Cl-
8.47
7.42
7.38
7.25
7.23
4.01
3.99
3.97
3.95
2.34
3.00
1.96
2.09
2.09
3.02
Chemical shift (ppm)
138.22
131.54
129.54
129.39
42.38
21.23
Chemical shift (ppm)

21:

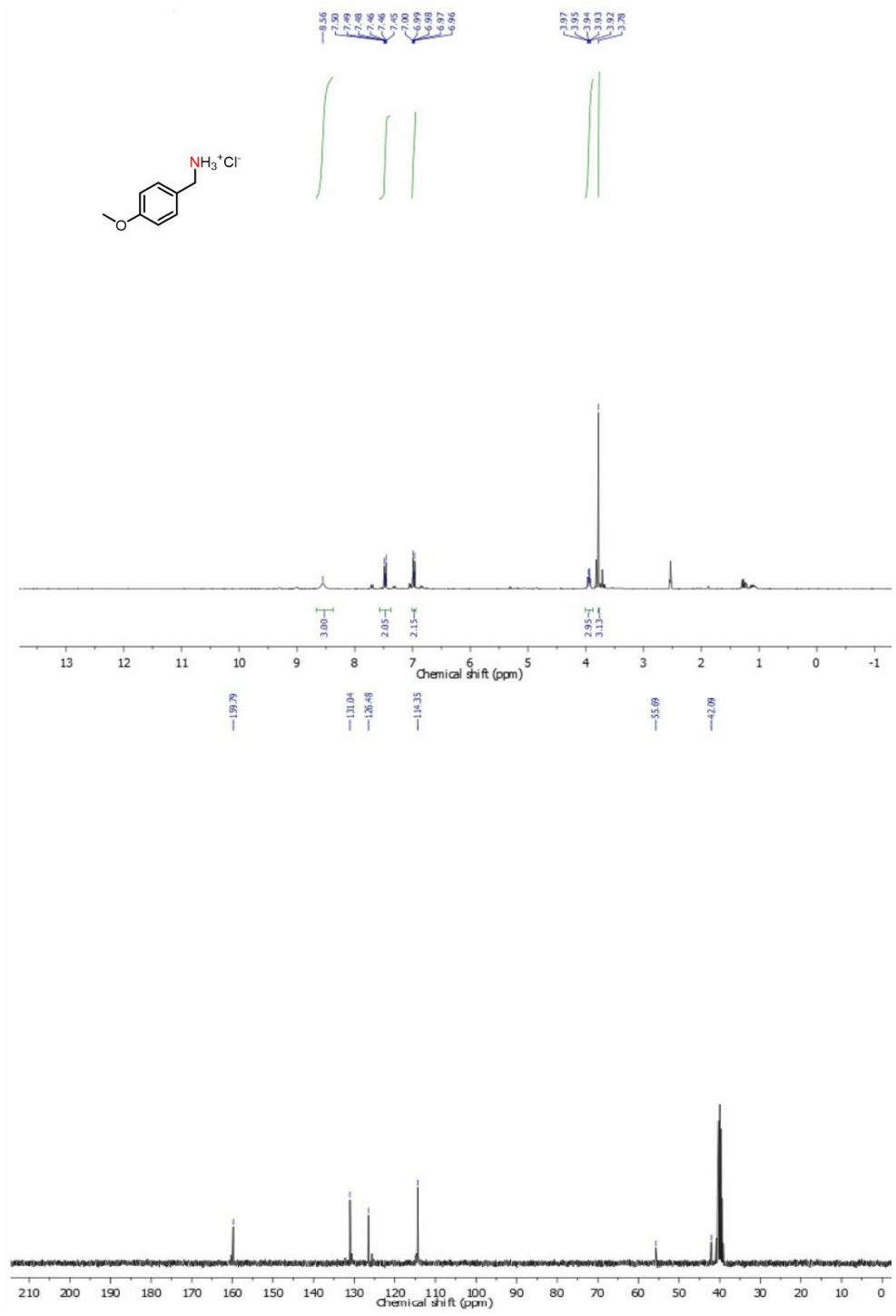

22:

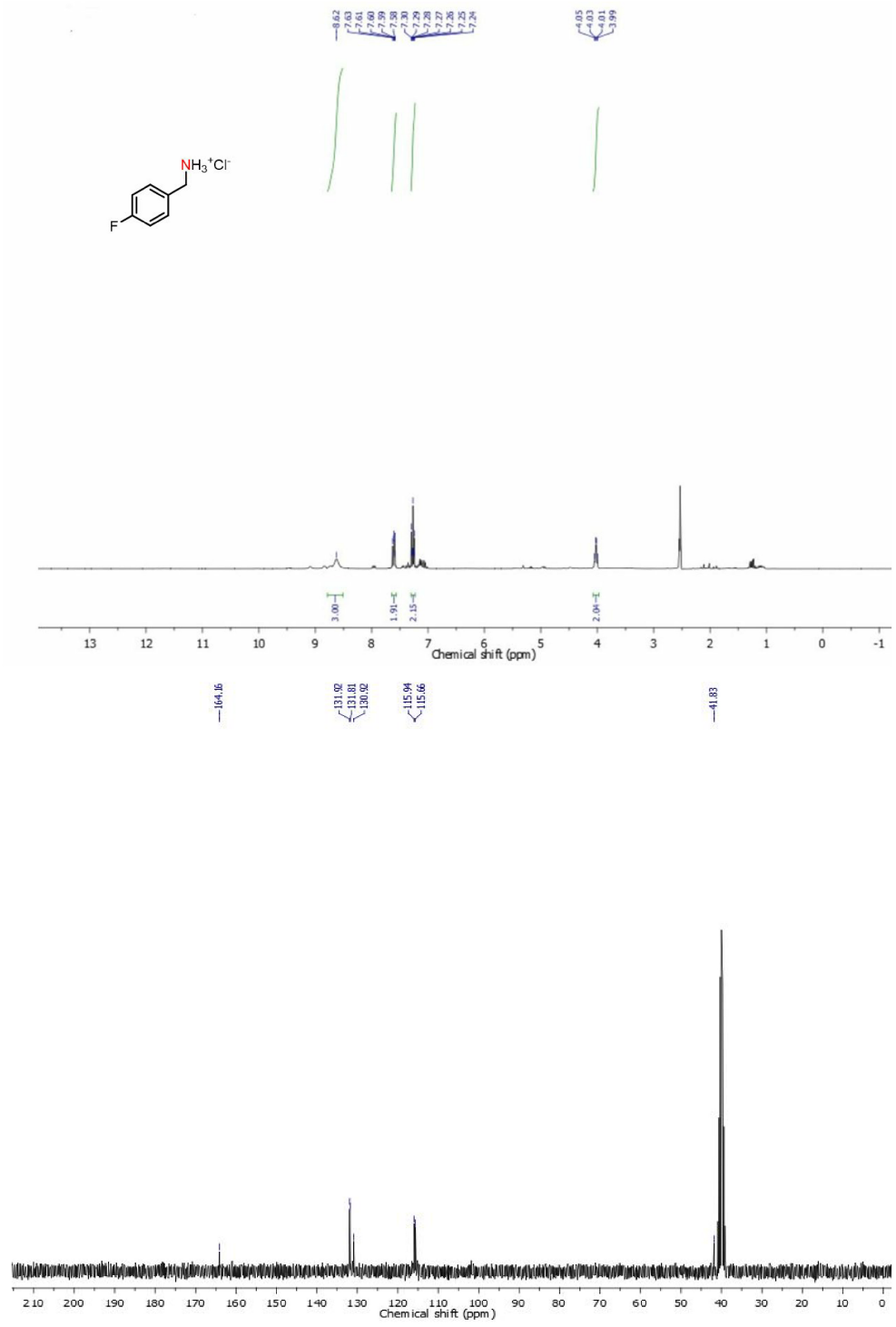

23:

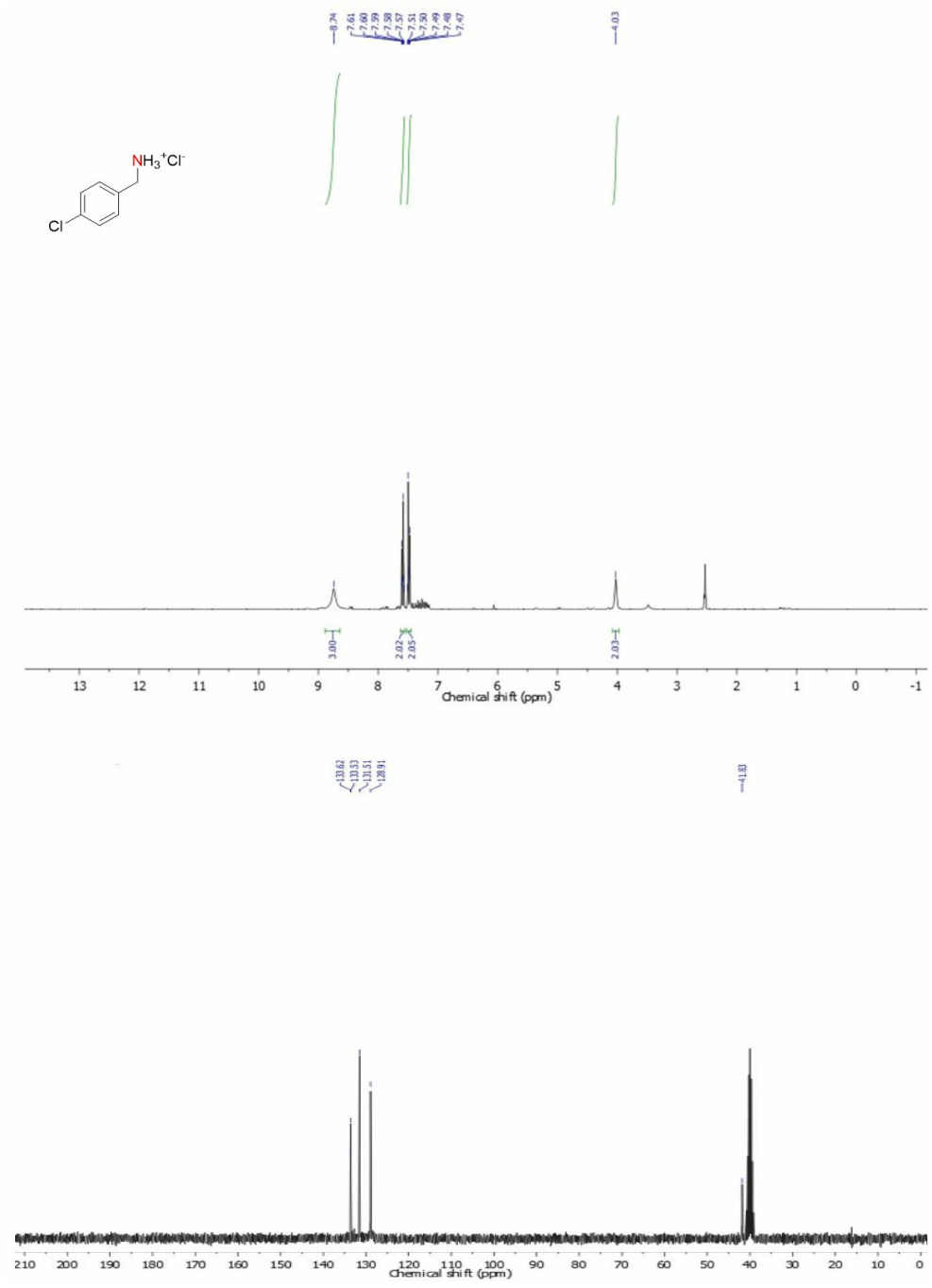

24:

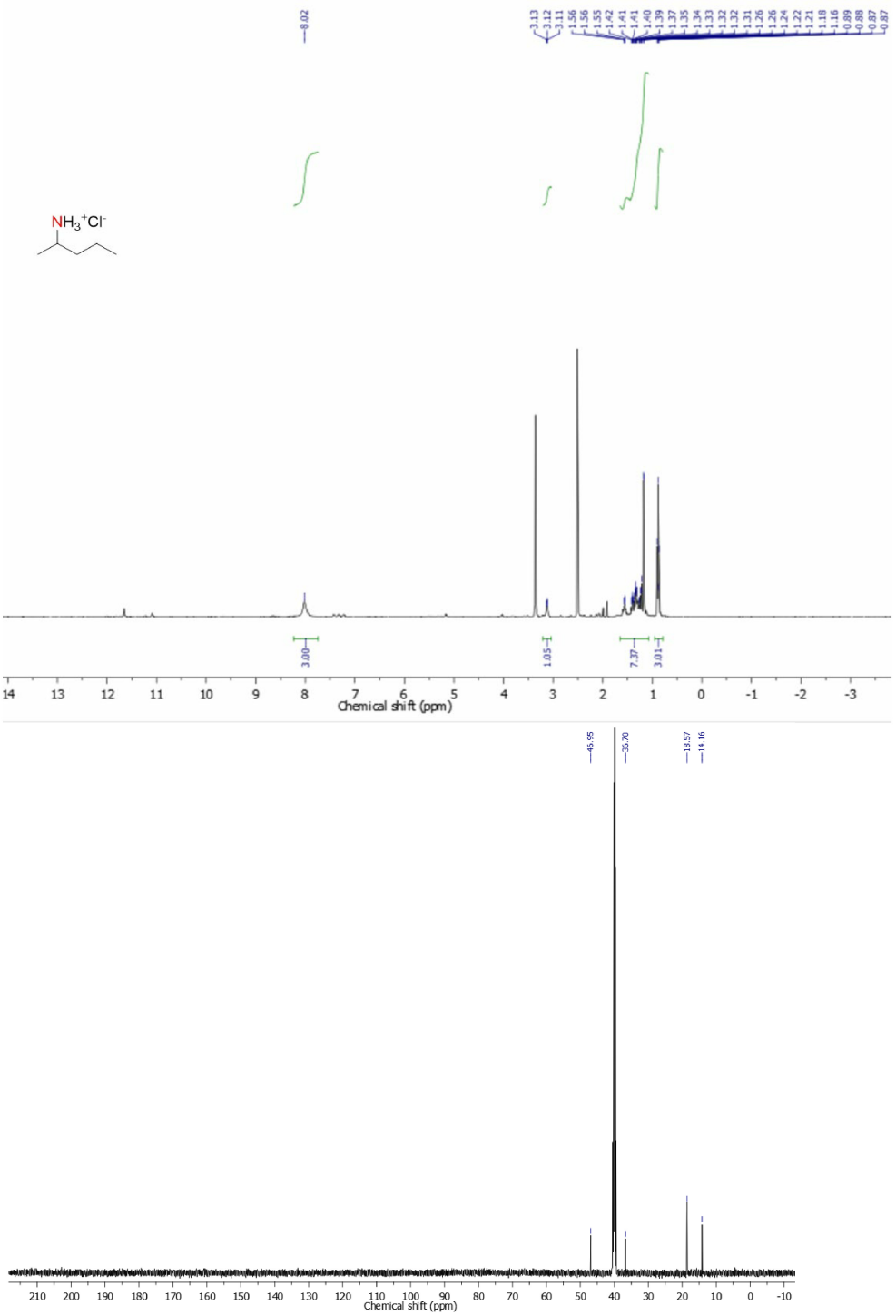

25:

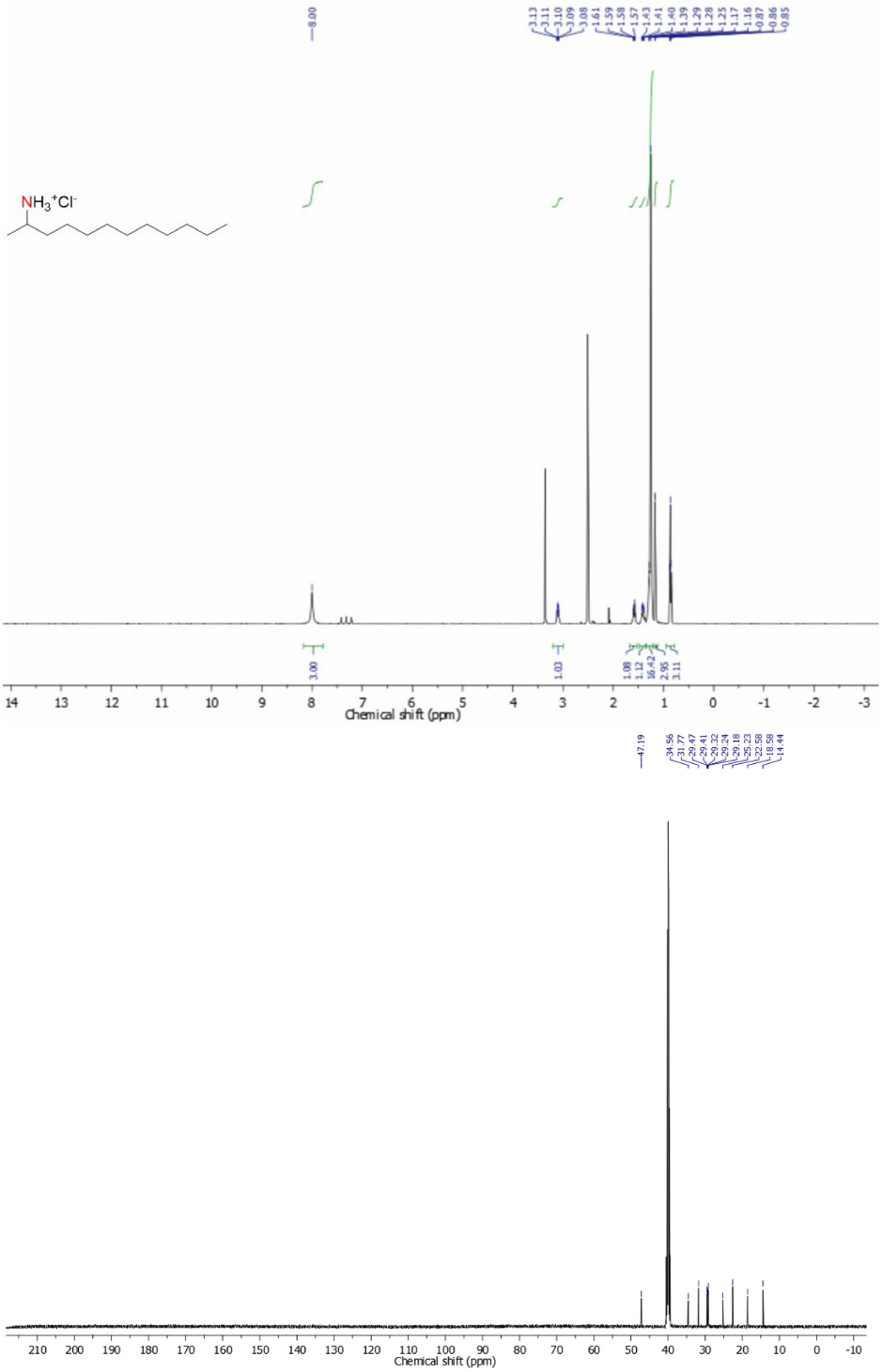

26:

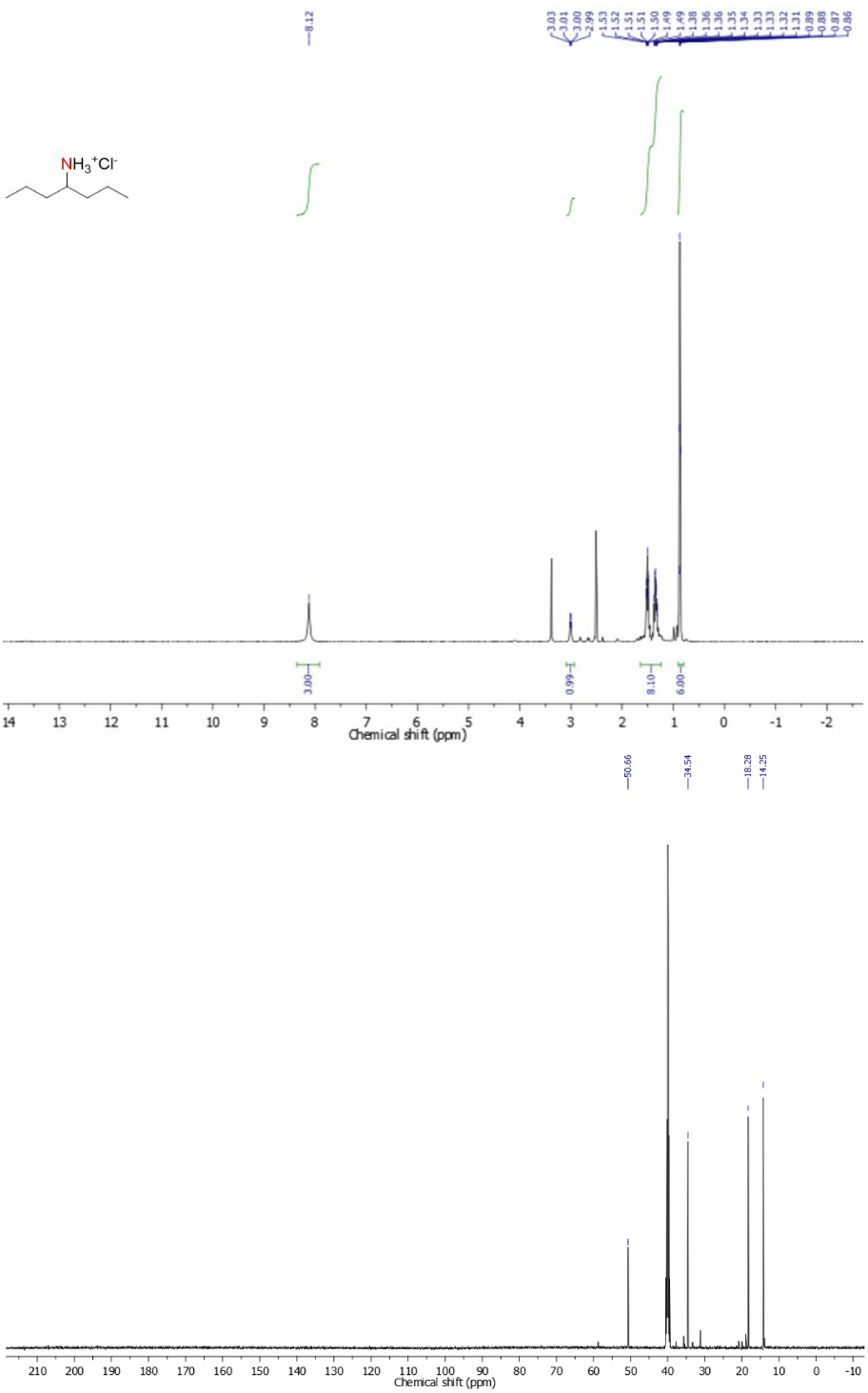
NH3+Cl-
8.12
3.03
3.01
3.00
2.99
1.53
1.52
1.51
1.51
1.50
1.49
1.49
1.38
1.36
1.36
1.35
1.34
1.33
1.33
1.32
1.31
0.89
0.88
0.87
0.86
3.00
0.99
8.10
6.00
14 13 12 11 10 9 8 7 6 5 4 3 2 1 0 -1 -2
Chemical shift (ppm)
50.66
34.54
18.28
14.25
210 200 190 180 170 160 150 140 130 120 110 100 90 80 70 60 50 40 30 20 10 0 -10
Chemical shift (ppm)

27:

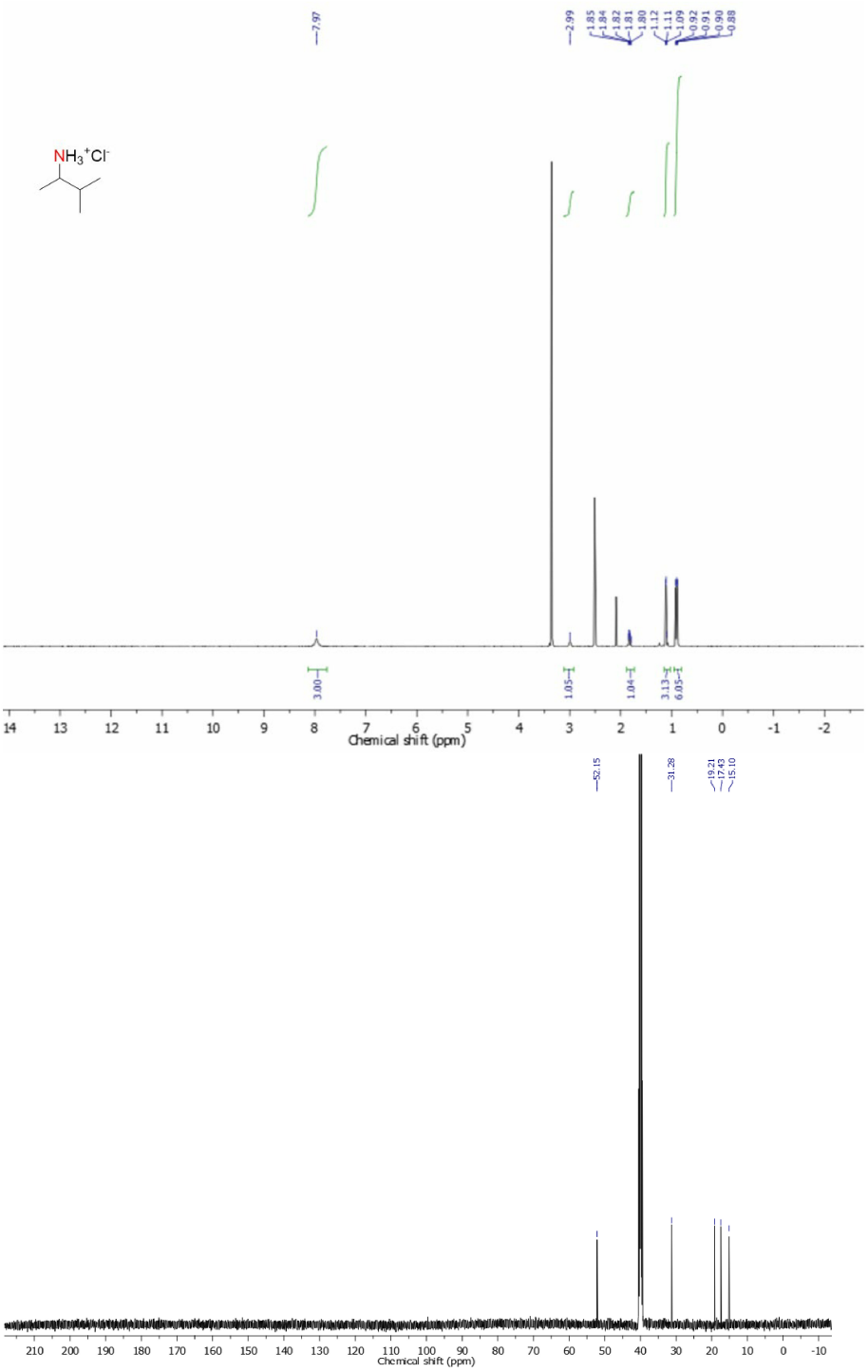
NH3+Cl-
7.97
2.99
1.85
1.84
1.82
1.81
1.80
1.12
1.11
1.09
0.92
0.91
0.90
0.88
3.00
1.05
1.04
3.13
6.05
Chemical shift (ppm)
52.15
31.28
19.21
17.43
15.10
Chemical shift (ppm)

28:

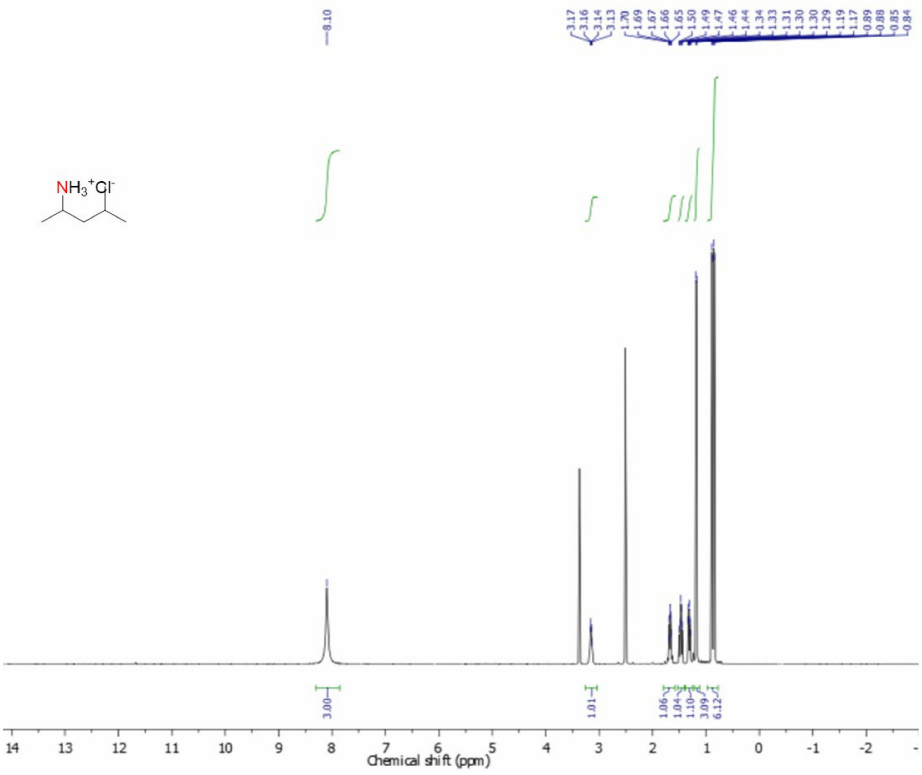

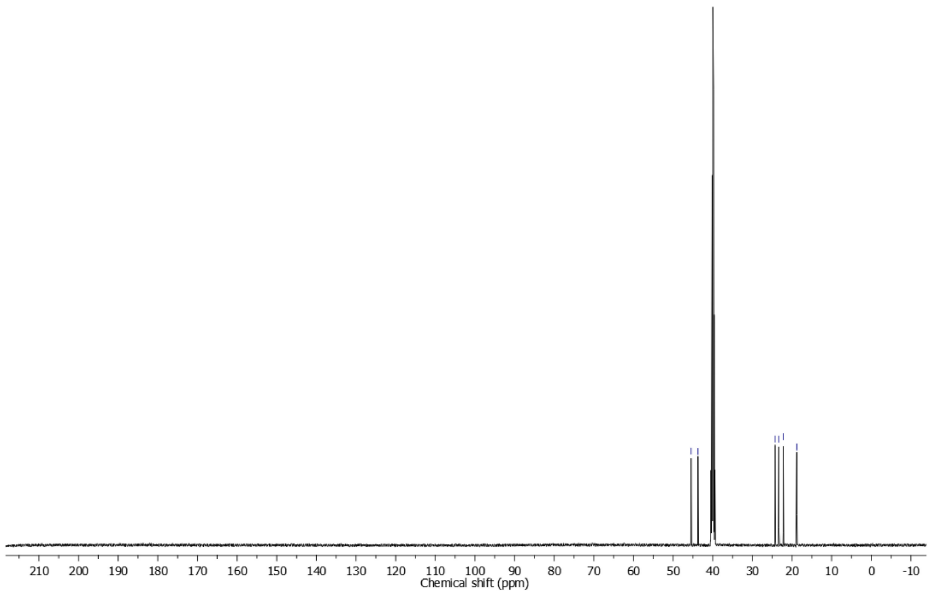

29:

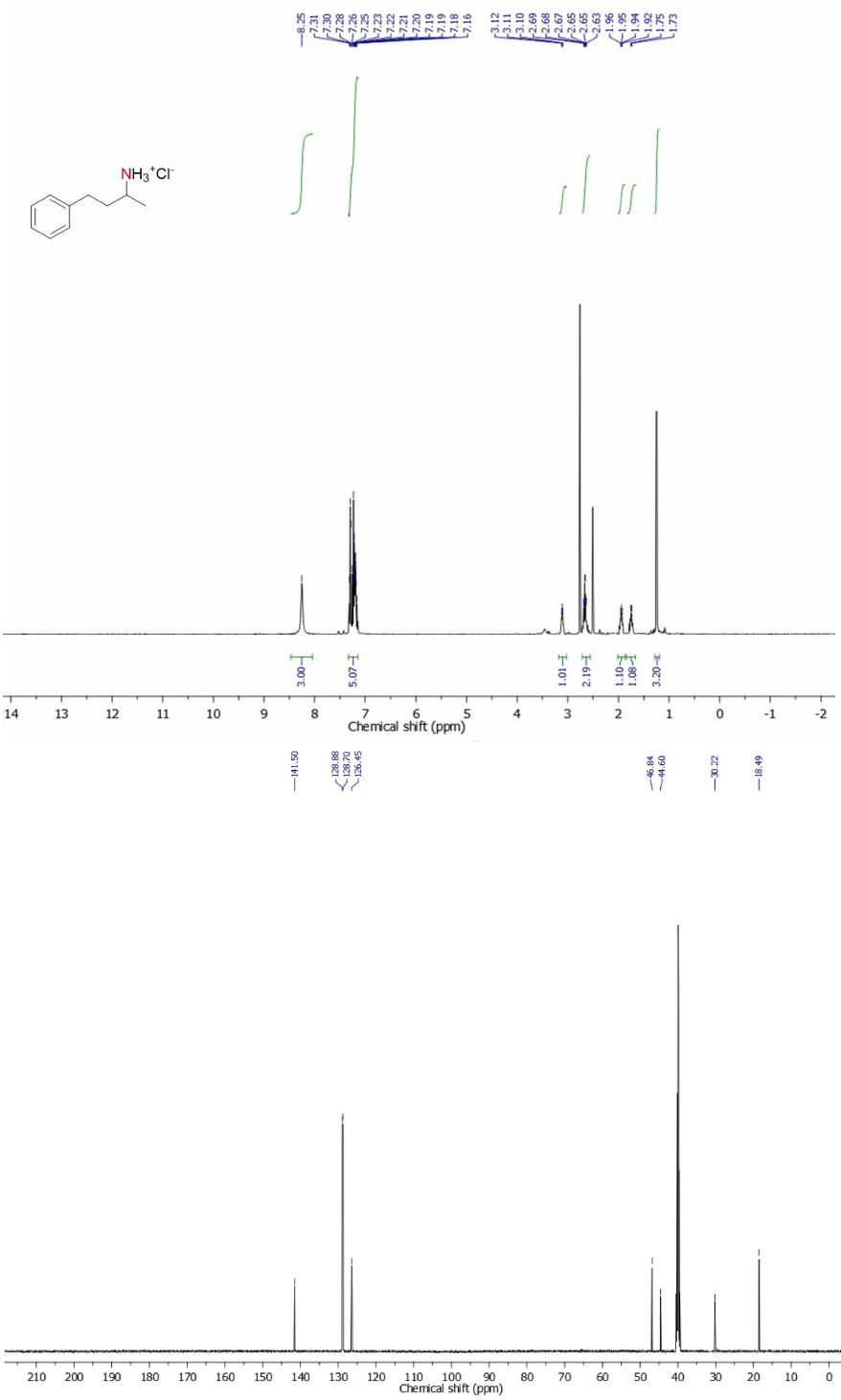

30:

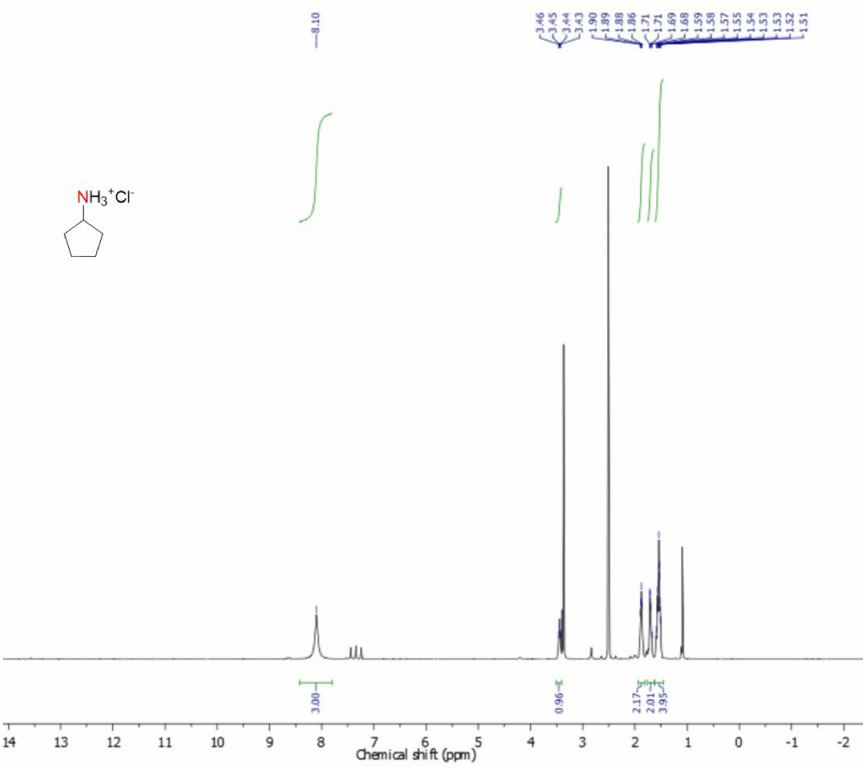
NH3+Cl-
8.10
3.46
3.45
3.44
3.43
1.90
1.89
1.88
1.86
1.71
1.71
1.69
1.68
1.59
1.58
1.57
1.55
1.54
1.53
1.53
1.52
1.51
3.00
0.96
2.17
2.01
3.95
14 13 12 11 10 9 8 7 6 5 4 3 2 1 0 -1 -2
Chemical shift (ppm)

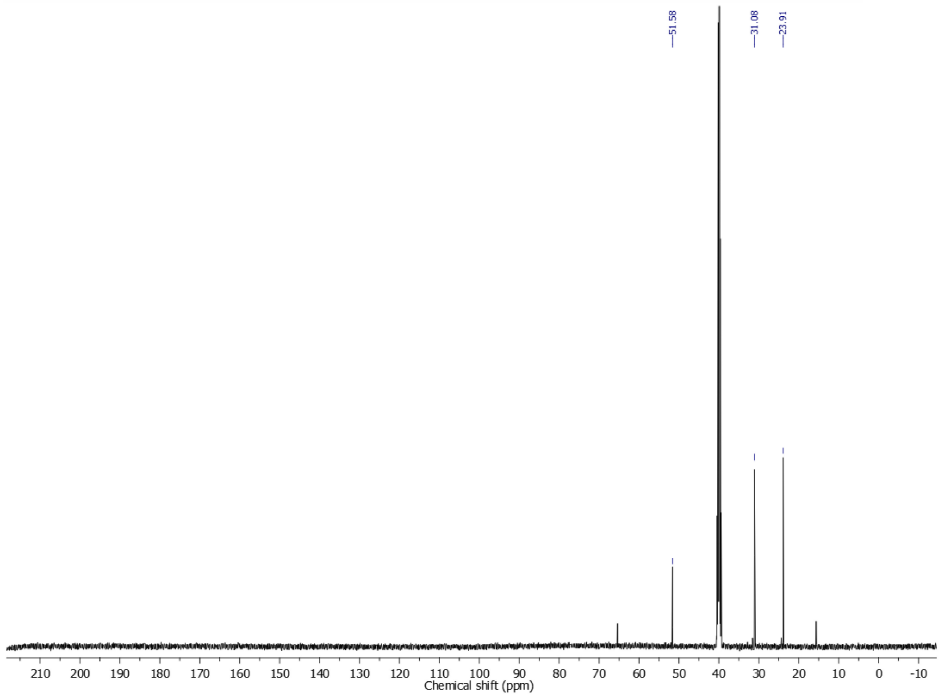
51.58
31.08
23.91
210 200 190 180 170 160 150 140 130 120 110 100 90 80 70 60 50 40 30 20 10 0 -10
Chemical shift (ppm)

31:

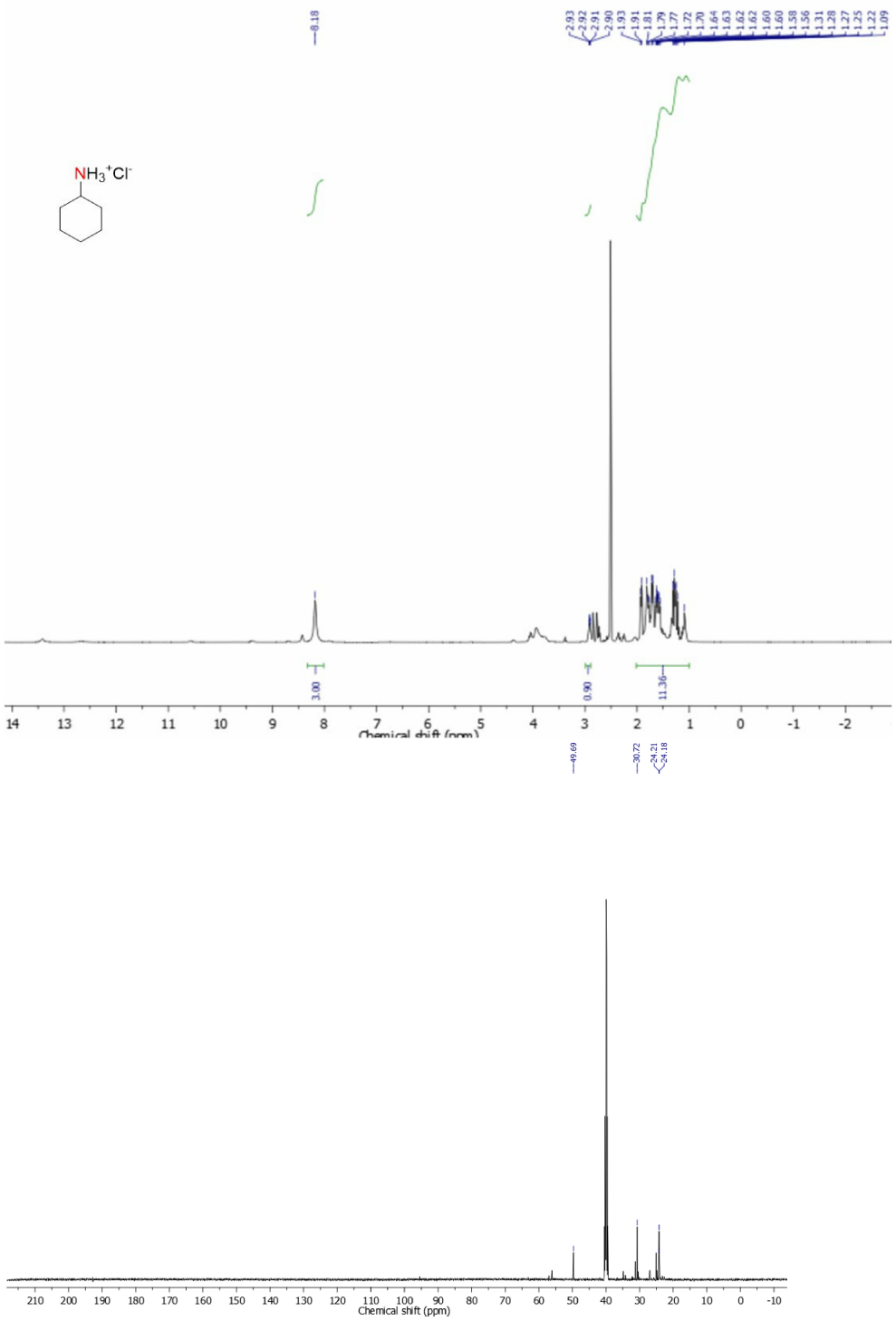

32:

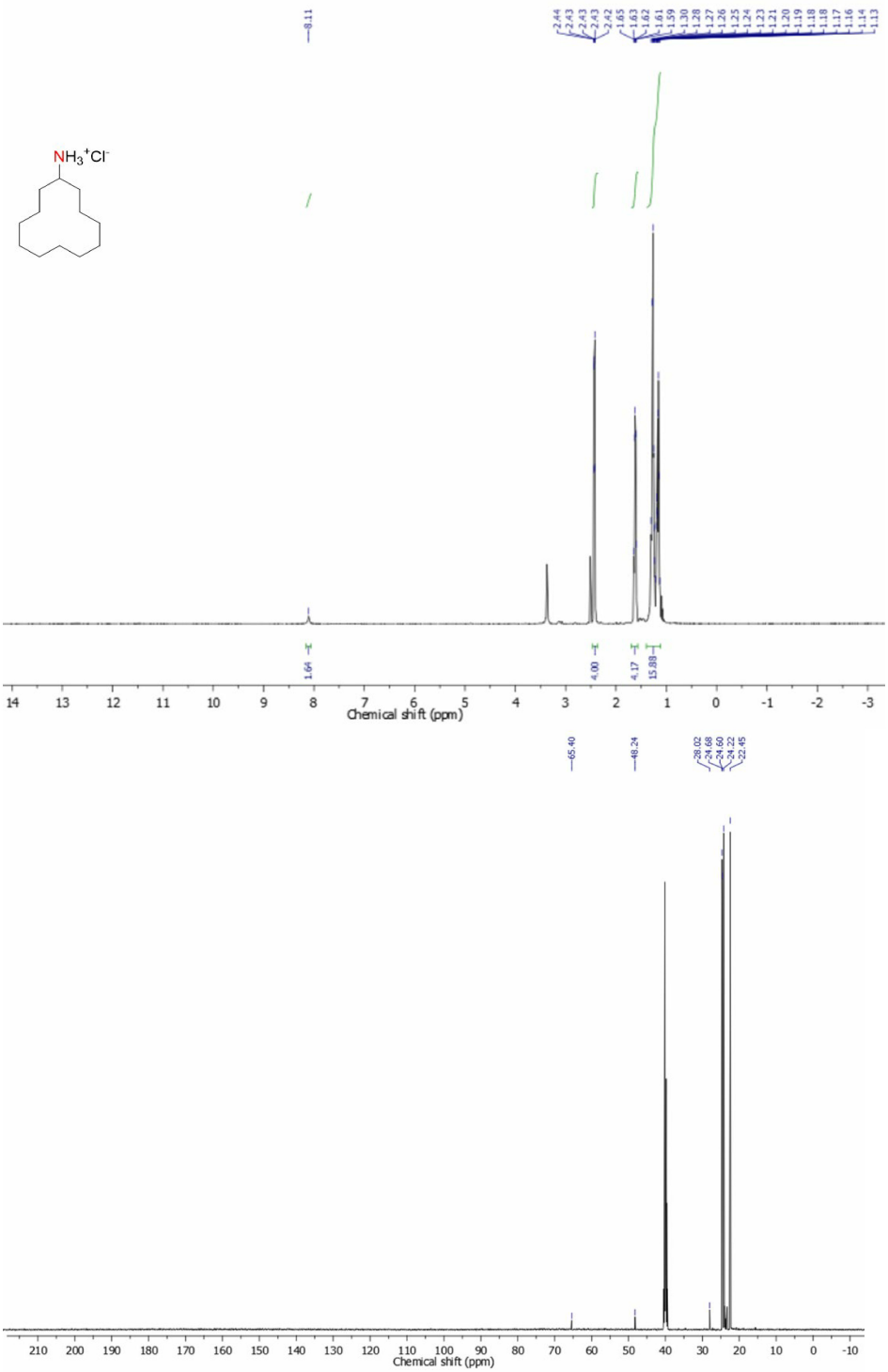

33:

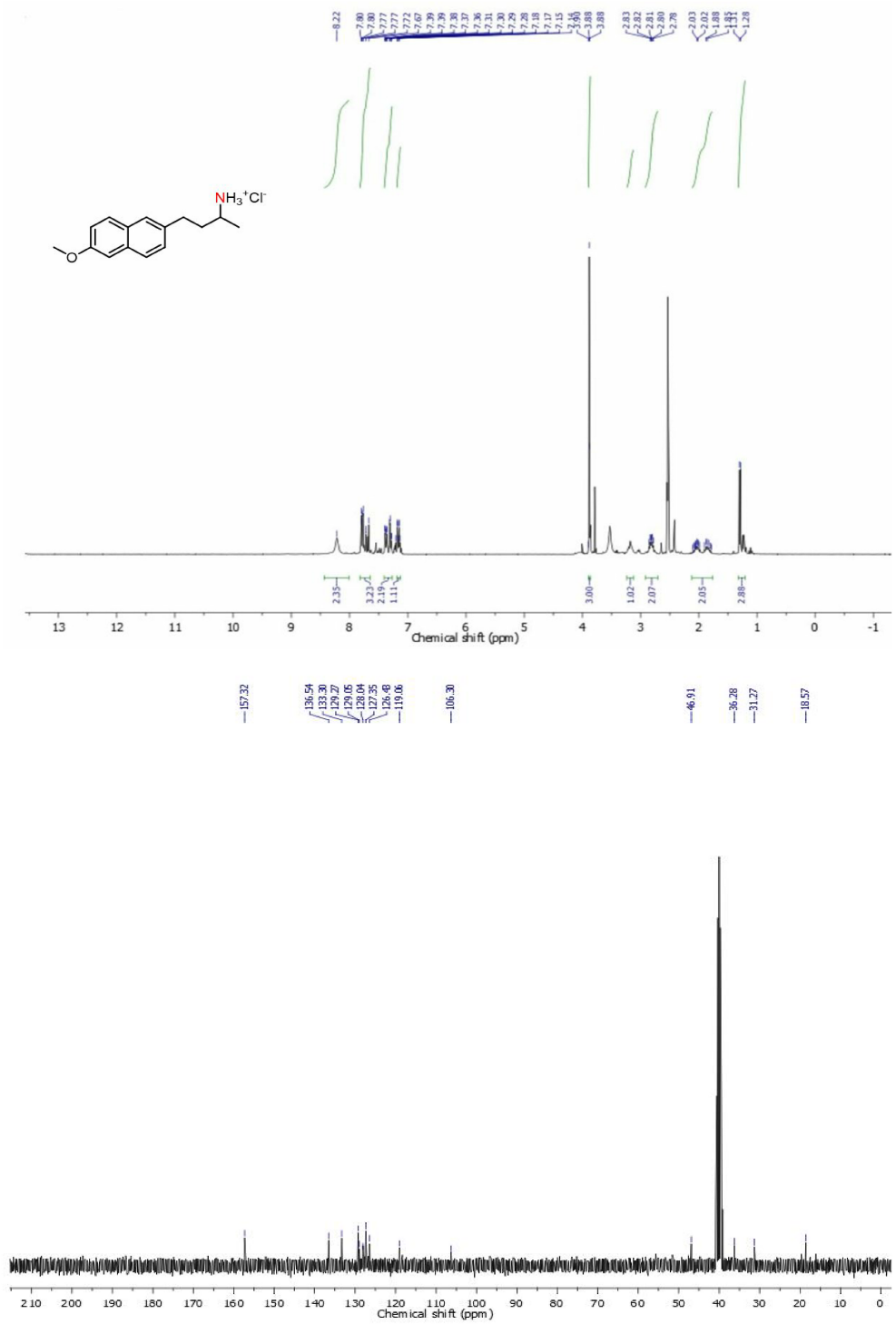

34:

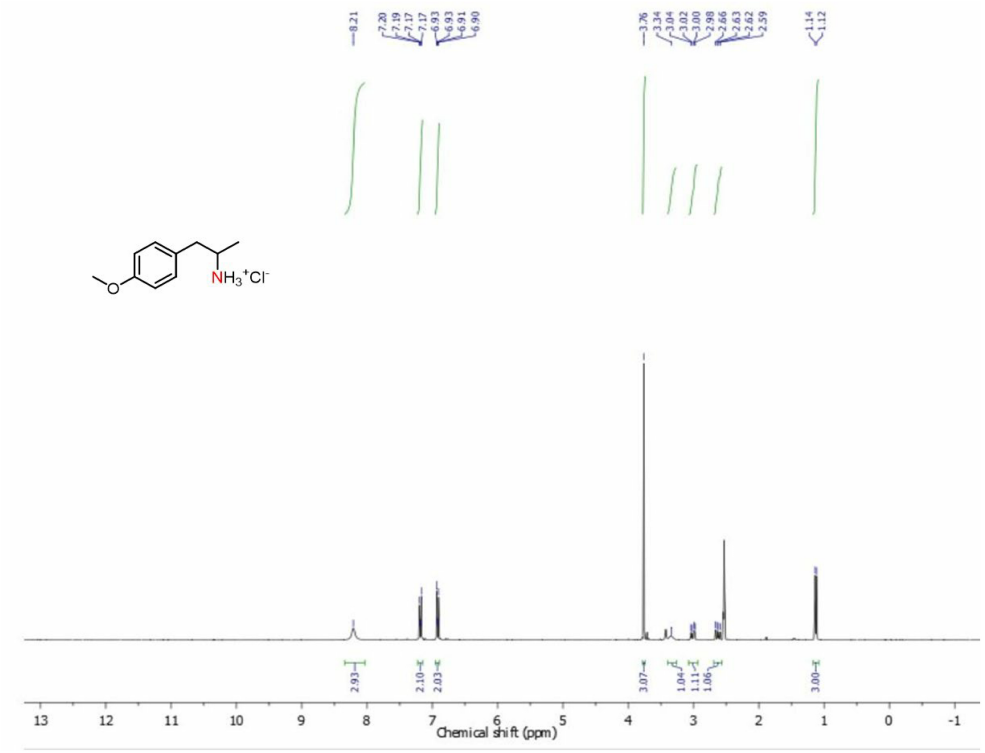
8.21
7.20
7.19
7.17
7.17
6.93
6.93
6.91
6.90
3.76
3.34
3.34
3.02
3.00
2.98
2.66
2.63
2.62
2.59
1.14
1.12
NH3+Cl-
2.93
2.10
2.03
3.07
1.04
1.11
1.06
3.00
Chemical shift (ppm)

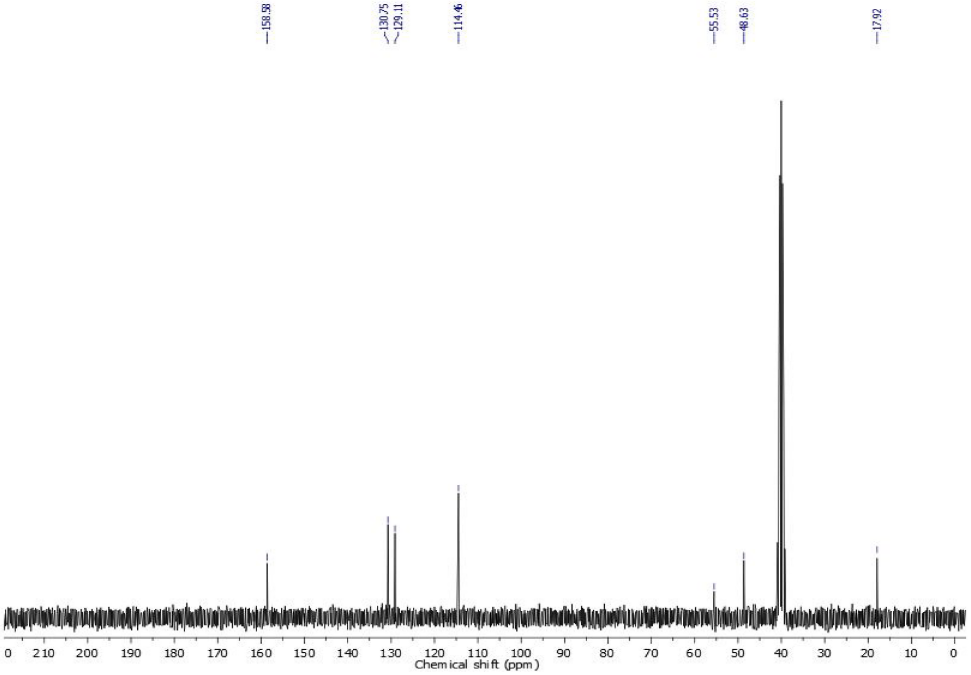
158.98
130.75
129.11
114.46
55.53
48.63
17.92
Chemical shift (ppm)

35:

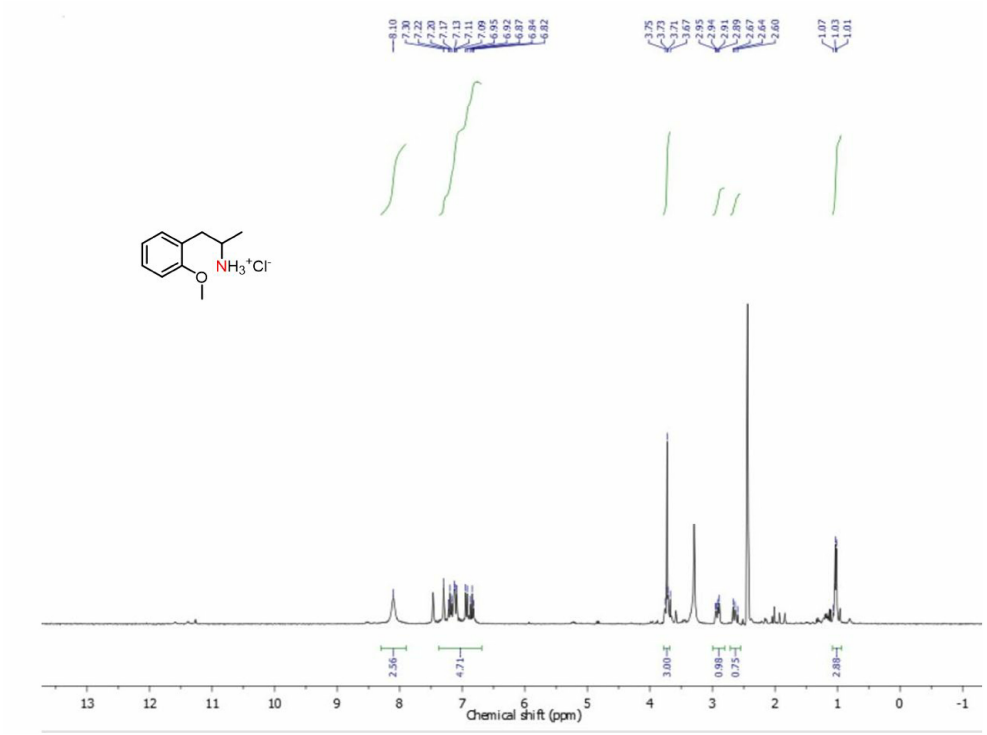
NH3+Cl-
Chemical shift (ppm)

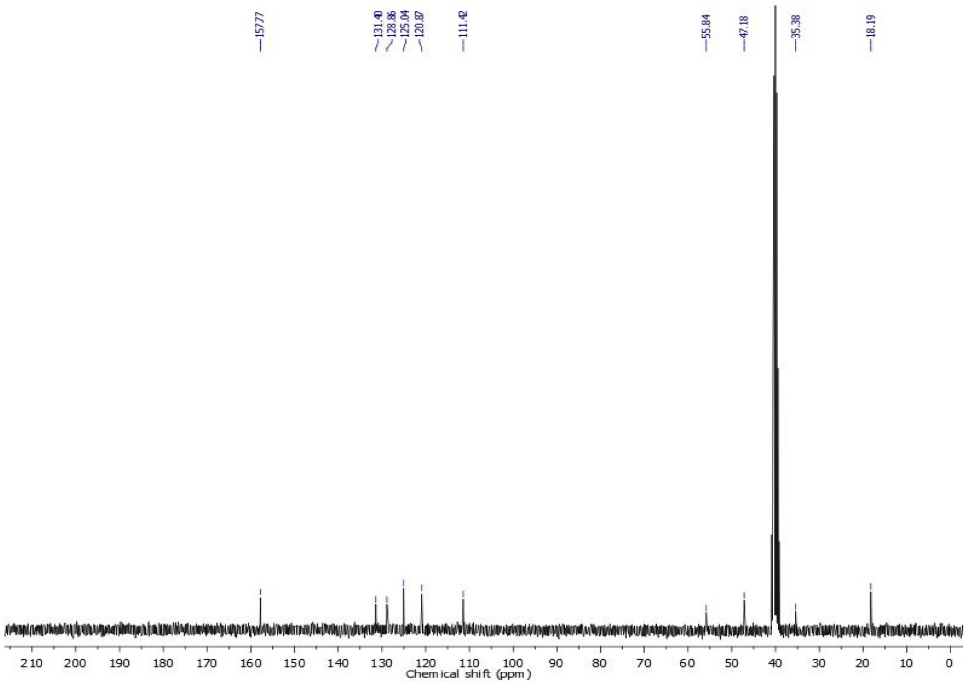
157.77
131.40
128.86
125.04
120.87
111.42
55.84
47.18
35.38
18.19
Chemical shift (ppm)

36:

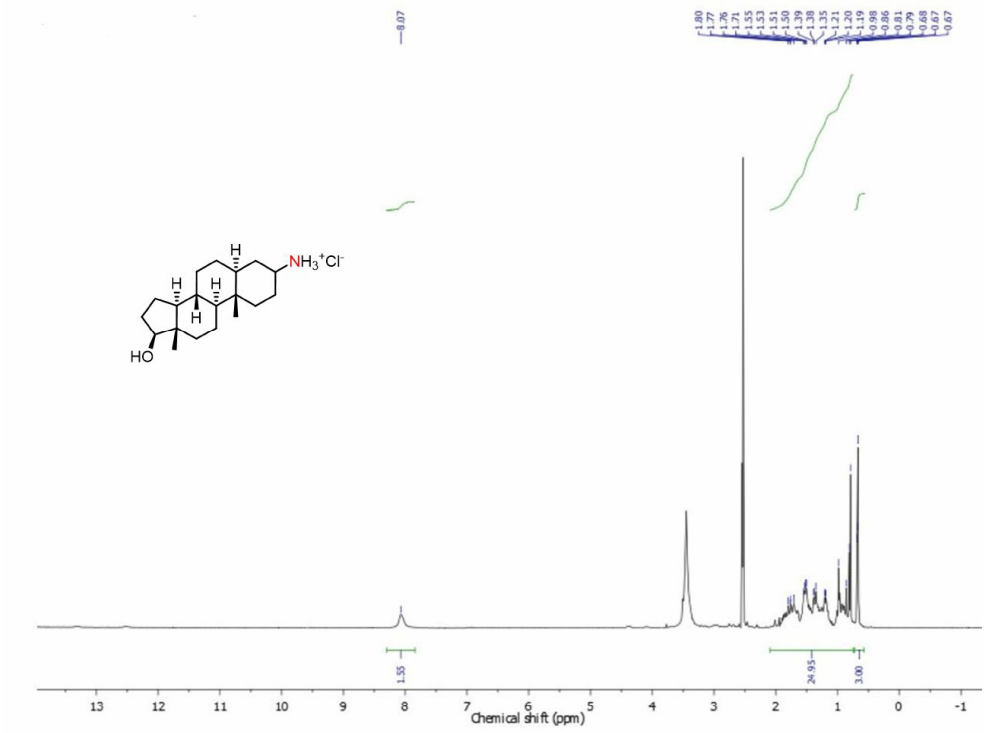

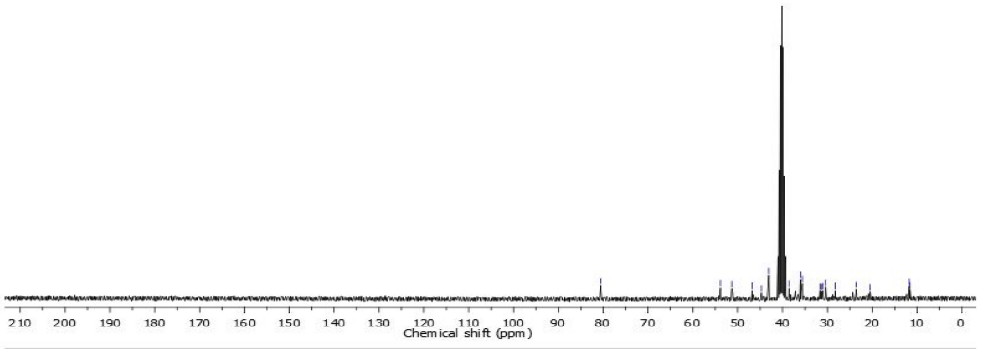

6. References

[1] G. Ashiotis, A. Deschildre, Z. Nawaz, J. P. Wright, D. Karkoulis, F. E. Picca, J. Kieffer, *J. Appl. Crystallogr.* **2015**, *48*, 510-519.
[2] xpdtools.
[3] P. Juhás, T. Davis, C. L. Farrow, S. J. L. Billinge, *J. Appl. Crystallogr.* **2013**, *46*, 560-566.
[4] C. L. Farrow, P. Juhas, J. W. Liu, D. Bryndin, E. S. Bozin, J. Bloch, T. Proffen, S. J. Billinge, *J. Phys. Condens. Matter.* **2007**, *19*, 335219.
[5] J. Zemann, *Acta Crystallographica* **1965**, *18*, 139-139.
[6] J. D. Hanawalt, H. W. Rinn, L. K. Frevel, *Ind. Eng. Chem. Res.* **1938**, *10*, 457-512.
[7] L. F. B. Ribeiro, O. Flores, P. Furtat, C. Gervais, R. Kempe, R. A. F. Machado, G. Motz, *J. Mater. Chem. A* **2017**, *5*, 720-729.
[8] a) A. Poulain, C. Dupont, P. Martinez, C. Guizani, J. Drnec, *J. Appl. Crystallogr.* **2019**, *52*, 60-71; b) V. Petkov, R. G. Difrancesco, S. J. L. Billinge, M. Acharya, H. C. Foley, *Philosophical Magazine B* **2009**, *79*, 1519-1530.
[9] A. C. Forse, C. Merlet, P. K. Allan, E. K. Humphreys, J. M. Griffin, M. Aslan, M. Zeiger, V. Presser, Y. Gogotsi, C. P. Grey, *Chem. Mater.* **2015**, *27*, 6848-6857.
[10] J. M. Stratford, P. K. Allan, O. Pecher, P. A. Chater, C. P. Grey, *Chem. Commun.* **2016**, *52*, 12430-12433.
[11] C. Bommier, T. W. Surta, M. Dolgos, X. Ji, *Nano Lett.* **2015**, *15*, 5888-5892.
[12] M. G. Tucker, M. T. Dove, D. A. Keen, *J. Phys. Condens. Matter.* **2000**, *12*, L425-L430.
[13] A. Pines, M. G. Gibby, J. S. Waugh, *J. Chem. Phys.* **1972**, *56*, 1776
[14] B. M. Fung, A. K. Khitrin, K. Ermolaev, *J. Magn. Reson.* **2000**, *142*, 97-101
[15] Z. Gan, *J. Am. Chem. Soc.* **2006**, *128*, 6040-6041
[16] S. Cavadini, A. Lupulescu, S. Antonijevic, G. Bodenhausen, *J. Am. Chem. Soc.* **2006**, *128*, 7706-7707
[17] A. Brinkmann, A. P. M. Kentgens, *J. Am. Chem. Soc.* **2006**, *128*, 14758-14759

Author Contributions

M. E. carried out the catalyst synthesis, catalytic reactions and catalyst characterization. S. L. J. T. and M. Z. performed XRD analyses and PDF refinement. T. S. and M. E. co-developed the catalyst. R. S. and J. S. carried out solid state NMR analyses. M. D. recorded the 'TEM images. M. E. and R. K. co-wrote the manuscript.

5 Synthesis of Secondary Amines via Borrowing Hydrogen employing a Nanostructured Bimetallic 3d-Metal Catalyst

Matthias Elfinger, Marie Bergmann, Rhett Kempe

Synthesis of Secondary Amines via Borrowing Hydrogen employing a Nanostructured Bimetallic 3d-Metal Catalyst

To be submitted.

Synthesis of Secondary Amines via Borrowing Hydrogen employing a Nanostructured Bimetallic 3d-Metal Catalyst

Matthias Elfinger,[a] Marie Bergmann[a] and Rhett Kempe[a,*]

[a] Sustainable Chemistry Centre, University of Bayreuth, Universitätsstraße 30, 95440 Bayreuth

Abstract

Abstract: Secondary amines are an important class of compounds in pharmaceutical and chemical industries due to their diverse applications in medicine and materials science. Here, we report the efficient synthesis of secondary amines from alcohols employing an already developed heterogeneous 3d metal catalyst. The catalyst, composed of our in house developed N-SiC support material, as well as cobalt and scandium, shows excellent catalytic activity towards the conversion of primary alcohols and aromatic amines under mild conditions with catalytic amounts of base. The catalyst is easily recoverable and reusable, providing a green and sustainable approach to the synthesis of secondary amines. We observe a broad scope and a very good functional group tolerance.

Introduction

The alkylation of amines by alcohols following the borrowing hydrogen or the hydrogen autotransfer (BH HA) concept is a green or sustainable way for the selective synthesis of alkyl amines (Scheme 1).[1] The reaction was first discovered by Winans and Adkins in 1932.[2] In recent years, numerous 3d-metal catalysts mostly molecular catalysts have been disclosed.[3] A Fe catalyst was introduced by Feringa and Barta and coworkers,[4] we disclosed a Co[5] and a Cr[6] catalyst and the group of Beller the first Mn catalyst.[7] Unfortunately, many of the homogeneous catalysts require an up to stoichiometric amount of base to catalyze the alkylation of amines lowering the degree of sustainability of the overall reaction significantly especially since the reaction can be mediated by bases alone.[8] Heterogeneous 3d metal catalysts with a broad scope are extremely rare. Recently, Beller/Jagadeesh and coworkers disclosed a nanostructured Co catalyst[9] and we showed that the combination of Co and Sc is beneficial for a combination for BH HA and reductive amination.[10]

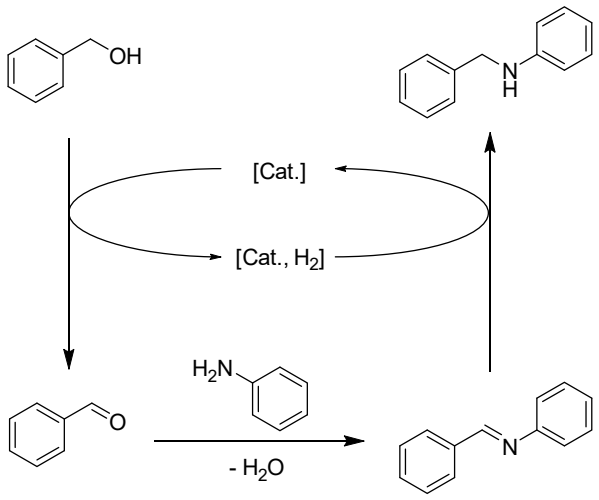

Scheme 1: borrowing hydrogen / hydrogen autotransfer reaction of benzyl alcohol and aniline.

Herein we report on a heterogeneous, bimetallic 3d metal catalyst developed by us employed for the BH HA-synthesis of secondary amines under mild conditions with catalytical amount of base.

Results and discussion

To obtain the catalyst, a literature known procedure was applied.[11] First the commercially available polycarbosilane precursor SMP-10 is copolymerized with acrylonitrile in dimethylformamide, initiated by azobis-isobutyronitrile. To obtain the support material, pyrolysis at 1000°C under inert atmosphere is needed. To increase the surface area, base activation with 1M NaOH is performed at 85 °C for 16 h. Afterwards, the two metal salts were distributed over the support material via co-evaporation of 2 wt% $Co(NO_3)_2 \cdot 6\ H_2O$ and 2 wt% $Sc(NO_3)_3 \cdot 5\ H_2O$ dissolved in water as well as the activated support itself. The last step includes pyrolysis (700°C, N_2) and reduction (550°C, N_2/H_2). An overview is shown in Figure 1.

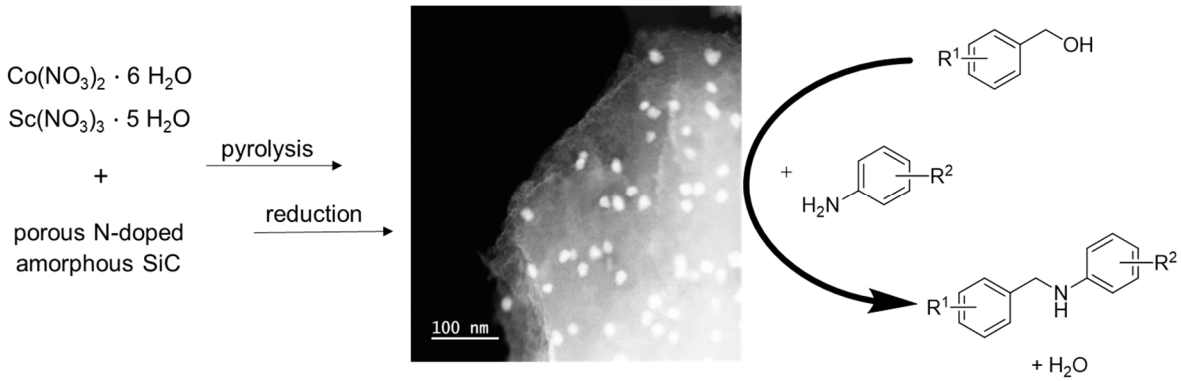

Figure 1: Synthesis of the cobalt-scandium catalyst (left) with HAADF-STEM image (middle) and the borrowing hydrogen reaction scheme (right).

Next, we optimized the reaction conditions by exploring the reaction between benzyl alcohol and aniline. In every step, the yield of amine and imine as side product is monitored. First, we discovered that 0.5 mL of toluene is the best solvent for the reaction (see Supporting Information Tables 1 and 2). The reaction temperature was set to 120 °C for quantitative yield of the desired product (see SI Table 3). We intentionally used an alcohol amount of 2 equivalents which proved to be the optimal quantity (see SI Table 4). Lastly KOH could be identified as the best base, delivering 96 % yield with only 0.5 equivalents (see SI Tables 5 and 6). The catalyst loading wasn't changed from our previous works. Thus, the optimized reaction conditions are 1.0 mol% Co, 0.33 mol% Sc, 120 °C, 0.5 mmol amine, 1.0 mmol alcohol, 0.25 mmol KOH and 0.5 mL toluene.
Subsequently we became interested in the functional group tolerance of our catalyst and investigated the substrate scope. The variation of the aniline is shown in Scheme 2.

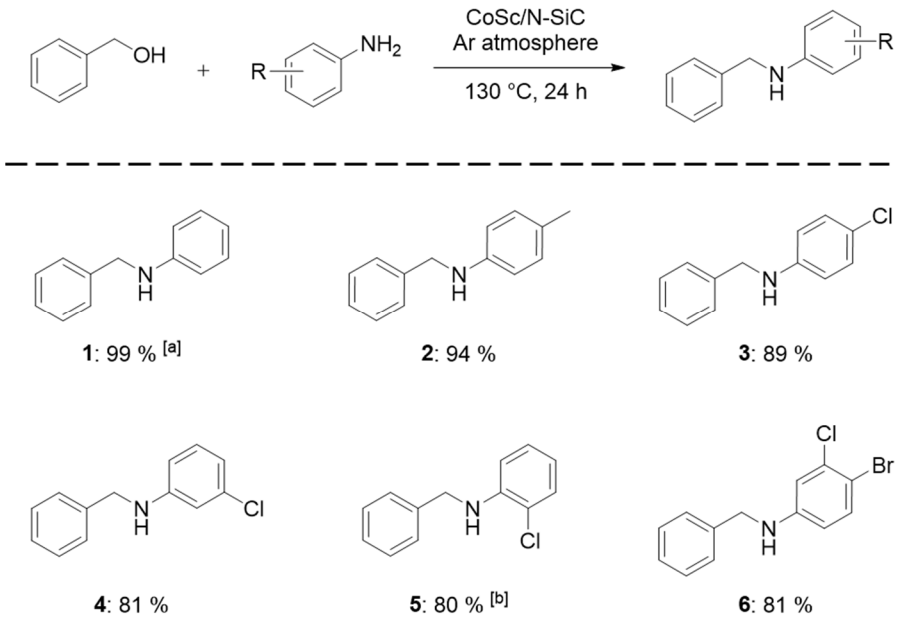

Scheme 2: Variation of the aromatic amine. Reaction conditions: 1.0 mmol benzyl alcohol, 0.5 mmol amine, 1.0 mol% Co, 0.33 mol% Sc, 0.5 mL toluene, 0.25 mmol KOH, 130 °C, 24 h, argon atmosphere. [a] 120 °C, [b] 140 °C. Isolated yields of the converted hydrochloride salts.

The model substrate (**1**) could be isolated in quantitative amounts using the optimal reaction conditions determined before. For all other substrates an increase in temperature was needed. *N*-Benzyl-4-methylaniline (**2**) could be synthesized with a yield of 94 % at 130 °C. Chloride as substituent could be tolerated in all ring positions (**3-5**) with very good yields of up to 89 %. However, for the ortho substituted aniline a temperature increase to 140 °C was needed. Even a sterically more demanding doubly halogenated aniline derivate could be used as an educt, leading to 81 % yield of the corresponding amine **6**.

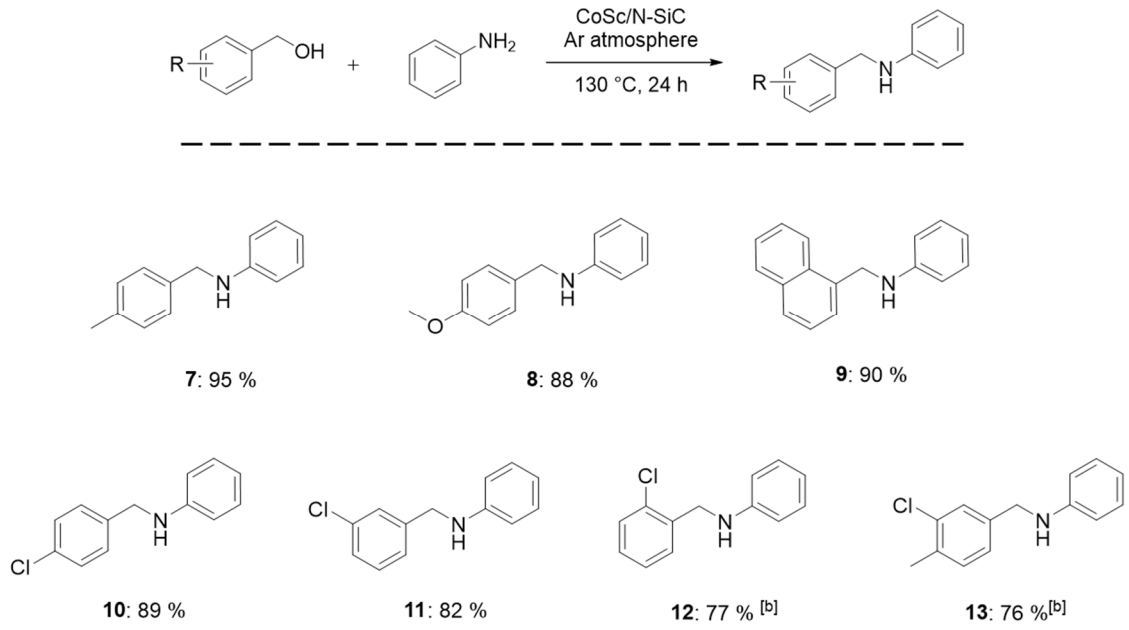

Scheme 3: Variation of the benzyl alcohol. Reaction conditions: [a] 1.0 mmol benzyl alcohol, 0.5 mmol aniline, 1.0 mol% Co, 0.33 mol% Sc, 0.5 mL toluene, 0.25 mmol KOH, 130 °C, 24 h, argon atmosphere. [b] 140 °C. Isolated yields of the converted hydrochloride salts.

By varying the benzyl alcohol part (Scheme 3) seven additional substrates could be synthesized. Electron donating groups such as methyl (**7**) and methoxy (**8**) could be tolerated well with 95 % and 88 % yield respectively for the corresponding secondary amine. The bulkier 1-naphtalene methanol could be converted smoothly without any temperature increases needed (**9**). Electron withdrawing groups like chloride could be tolerated in all ring positions (**10-12**) with the ortho substituted derivate requiring a temperature increase to 140 °C. The latter conditions also allowed the synthesis of a secondary amine with an electron donating and an electron withdrawing residue on the aromatic ring (**13**).

Conclusion

We were able to employ an already synthesized bimetallic Co/Sc-catalyst for the synthesis of secondary amines via borrowing hydrogen / hydrogen autotransfer methodology. The catalyst manages to operate under mild conditions and only requires catalytical amounts of base.

References

[1] a) G. Guillena, D. J Ramón, M. Yus, *Chem. Rev.* **2010**, *110*, 1611; b) A. J. A. Watson, J. M. J. Williams, *Science (New York, N.Y.)* **2010**, *329*, 635.

[2] C. F. Winans, H. Adkins, *J. Am. Chem. Soc.* **1932**, *54*, 306.

[3] T. Irrgang, R. Kempe, *Chem. Rev.* **2019**, *119*, 2524.

[4] T. Yan, B. L. Feringa, K. Barta, *Nat. Commun.* **2014**, *5*, 5602.

[5] S. Rösler, M. Ertl, T. Irrgang, R. Kempe, *Angew. Chem. Int. Ed.* **2015**, *54*, 15046.

[6] F. Kallmeier, R. Fertig, T. Irrgang, R. Kempe, *Angew. Chem. Int. Ed.* **2020**, *59*, 11789.

[7] M. Peña-López, P. Piehl, S. Elangovan, H. Neumann, M. Beller, *Angew. Chem.* **2016**, *128*, 15191.

[8] A. S. Kozlov, O. I. Afanasyev, D. Chusov, *J. Catal.* **2022**, *413*, 1070.

[9] Z. Ma, B. Zhou, X. Li, R. G. Kadam, M. B. Gawande, M. Petr, R. Zbořil, M. Beller, R. V. Jagadeesh, *Chem. Sci.* **2021**, *13*, 111.

[10] M. Elfinger, J. Schmauch, M. Moritz, C. Wichmann, C. Papp, R. Kempe, *Angew. Chem.* ***2023*** (submitted).

[11] L. F. B. Ribeiro, O. Flores, P. Furtat, C. Gervais, R. Kempe, R. A. F. Machado, G. Motz, *J. Mater. Chem. A* **2017**, *5*, 720.

Supporting Information

General considerations

All air- and moisture sensitive reactions were performed under dry argon or nitrogen atmosphere using standard Schlenk and glove box techniques. All dried solvents were obtained from a solvent purification system (activated alumina cartridges) or purchased from Acros. Deuterated solvents were dried via molecular sieves. All chemicals were acquired from commercial sources with purity over 95 % and used without further purification. The precursor SMP-10 was purchased from Starfire Systems, New York, USA. Pyrolysis of the support material was carried out under nitrogen atmosphere in a high temperature furnace (Gero, Berlin, Germany). Pyrolysis and reduction of the catalyst were performed under nitrogen or forming gas (90/10) atmosphere in a ChemBET Pulsar TPR/TPD instrument from Quantachrome. For the STEM investigations a JEOL JEM-ARM 200F with cold FEG emission gun was used equipped with a CEOS Cs corrector and a HAADF detector.
NMR measurements were performed using a Varian INOVA 300 (300 MHz for 1H, 75 MHz for ^{13}C) at 296 K. Chemical shifts are reported in ppm relative to the residual solvent signal (DMSO-d6: 2.50 ppm (^{1}H), 39.51 ppm (^{13}C)), coupling constants (J) are reported in Hz.
GC analyses were carried out on an Agilent 6850 GC system equipped with an Optima 17 column (30 m x 0.32 mm x 0.25 µm) with *n*-dodecane as an internal standard.
The borrowing hydrogen reactions were carried out in 20 mL Schlenk flasks under argon atmosphere.

Experimental procedures

Synthesis of the support material

For the preparation of the N-SiC support material a known literature method was modified.[7]
200 mg SMP-10 (StarPCS™), 0.987 mL (0.800 g, 15.08 mmol) acrylonitrile and 45 mg (0.28 mmol) azobis(isobutyronitrile) were dissolved in 4 mL dimethylformamide and crosslinked for 16 h at 75 °C. After solvent removal under reduced pressure, the obtained greenbody was pyrolyzed using the following program:

$$20\ °C \xrightarrow{5\ K/min} 200\ °C\ (0\ h) \xrightarrow{1\ K/min} 400\ °C\ (0\ h) \xrightarrow{5\ K/min} 1000\ °C\ (1\ h) \xrightarrow{10\ K/min} 20\ °C$$

After ball mining for 40 minutes, 400 mg of the ceramic were washed by stirring in solution of 5.3 mL aq. NaOH (1 M) and 4 mL MeOH at 85 °C for 24 h. Afterwards the material was washed until neutrality and dried at room temperature.

Synthesis of the catalyst

1000 mg N-SiC were impregnated with 98,75 mg $Co(NO_3)_2 \cdot 6\,H_2O$ and 143 mg $Sc(NO_3)_2 \cdot 5\,H_2O$ in 20 mL H_2O and stirred at 110 °C until the solvent was completely removed. Afterwards, the material was pyrolyzed and reduced using the following program:

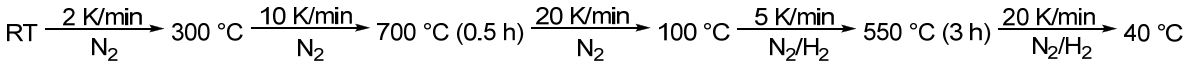

Catalytic procedures

The catalytic reaction (borrowing hydrogen/hydrogen autotransfer) was carried out after the procedure described in the following: A magnetic stirring bar, 1.0 mmol alcohol, 0.5 mmol amine, 0.5 mL toluene (freeze pumped), 0.25 mmol KOH (14 mg) and 28.8 mg of cobalt/scandium-catalyst (2.0 wt% Co, 1.0 mol% Co, 0.58 mg Co, 2.0 wt% Sc, 0.33 mol% Sc, 0.58 mg Sc) were filled directly into a 20 mL Schlenk flask under argon flow. The flask was evacuated and kept under argon before. The flask was heated to the desired temperature for the desired time. Afterwards, the reaction mixture was allowed to cool to room temperature. To obtain the amine hydrochloride salts, the remaining solution was filtrated into a round bottom flask to remove the catalyst. After the addition of 30 mL of diethyl ether and 0.5 mL HCl in ether (2 M) the precipitate was filtrated, dried under reduced pressure and the resulting solid was then further analyzed by NMR spectroscopy.

Table 1: Catalyst screening for borrowing hydrogen.

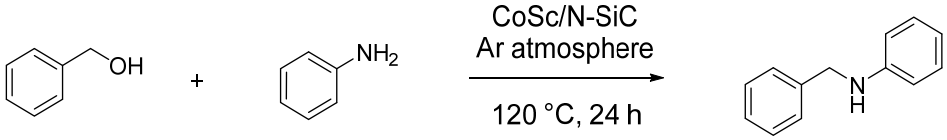

Entry	Metal source	Catalyst	Yield Amine / %	Yield Imine / %
1[a]	Co nitrate	Co/N-SiC	21	15
2[a]	Ni nitrate	Ni/N-SiC	14	16
3[a]	Cu acetate	Cu/N-SiC	31	9
4[a]	Ce nitrate	Ce/N-SiC	22	10
5[a]	Co/Ce nitrate	CoCe/N-SiC	78	13
6[a]	Co/La nitrate	CoLa/N-SiC	91	9
7[a]	Cu acetate, La nitrate	CuLa/N-SiC	17	3
8[a]	Co/Pr nitrate	CoPr/N-SiC	71	27

9[a]	Co/Nd nitrate	CoNd/N-SiC	73	18
10[a]	Co nitrate, Eu chloride	CoEu/N-SiC	53	19
11[a]	**Co/Gd nitrate**	**CoGd/N-SiC**	**99**	**-**
12[a]	**Co/Yb nitrate**	**CoYb/N-SiC**	**99**	**-**
13[a]	**Co/Lu nitrate**	**CoLu/N-SiC**	**99**	**-**
14[b]	Co/Gd nitrate	CoGd/N-SiC	63	4
15[b]	**Co/Yb nitrate**	**CoYb/N-SiC**	**99**	**-**
16[b]	**Co/Lu nitrate**	**CoLu/N-SiC**	**99**	**-**
17[c]	Co/Yb nitrate	CoYb/N-SiC	24	14
18[c]	Co/Lu nitrate	CoLu/N-SiC	59	24
19[c]	**Co/Sc nitrate**	**CoSc/N-SiC**	**99**	**-**
20[c]	Co nitrate	Co/N-SiC	16	11
21[c]	Sc nitrate	Sc/N-SiC	44	-

Reaction conditions: [a] 1.0 mmol benzyl alcohol, 0.5 mmol aniline, 2 wt% Co; 2 wt% rare earth metal, 0.5 mL solvent, 0.5 mmol KOH, 120 °C, 16 h, Ar. [b] 0.5 mol% first metal, 0.22 mol% second metal [c] 0.5 mol% first metal, 0.22 mol% second metal, 115 °C.

Table 2: Solvent screening. Reaction conditions: 1.0 mmol benzyl alcohol, 0.5 mmol aniline, 1 mol% Co, 0.44 mol% Sc, 2 mL solvent, 0.5 mmol KOH, 140 °C, 16 h, Ar.

Solvent	Yield amine / %	Yield imine / %
Xylene	52	22
THF	28	19
Toluene	**99**	**-**

Table 3: Solvent amount screening. Reaction conditions: 1.0 mmol benzyl alcohol, 0.5 mmol aniline, 1 mol% Co, 0.44 mol% Sc, toluene, 0.5 mmol KOH, 120 °C, 16 h, Ar.

Solvent amount / mL	Yield amine / %	Yield imine / %
0.5	**99**	**-**
1	83	13
2	65	22
3	39	30
4	12	22
5	7	21

Characterization of the isolated products

***N*-phenyl-benzenmethanamine hydrochloride (1)**

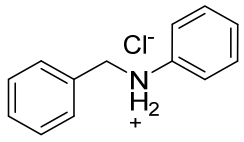

MW: 219.71 g/mol

^{1}H NMR (300 MHz, DMSO-d_6): δ = 11.07 (s, 2 H), 7.51-7.28 (m, 10 H), 4.49 (s, 2 H) ppm

^{13}C NMR (75 MHz, $(CD_3)_2SO$)): δ = 137.93, 133.18, 130.54, 129.92, 129.00, 128.82, 127.44, 122.57, 53.06 ppm.

Yield: 99 % as a white solid.

***N*-(4-methylphenyl)-benzenmethanamine hydrochloride (2)**

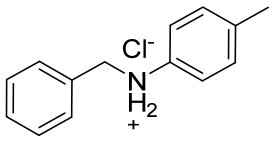

MW: 233.74 g/mol

^{1}H NMR (300 MHz, DMSO-d_6): δ = 11.03 (s, 2H), 7.51 – 7.20 (m, 9 H), 4.45 (s, 2 H), 2.27 (s, 3 H)

^{13}C NMR (75 MHz, $(CD_3)_2SO$)): δ = 134.93, 132.83, 130.39, 130.17, 128.88, 128.67, 123.46, 122.43, 53.11, 20.80 ppm.

Yield: 94 % as a white solid.

***N*-(4-chlorophenyl)-benzenmethanamine hydrochloride (3)**

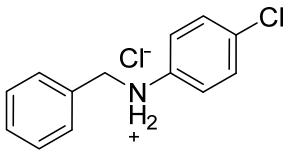

MW = 254.15 g/mol

^{1}H NMR (500 MHz, DMSO-d_6): δ = 10.81 (s, 2 H), 7.52 – 7.03 (m, 9 H), 4.39 (s, 2 H) ppm.

^{13}C NMR (125 MHz, $(CD_3)_2SO$)): δ = 135.66, 130.20, 129.70, 129.55, 129.07, 128.88, 128.42, 127.84, 125.31, 119.61, 49.92 ppm.

Yield: 89 % as a white solid.

***N*-(3-chlorophenyl)-benzenmethanamine hydrochloride (4)**

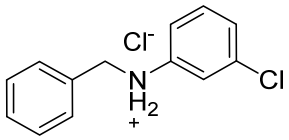

MW = 254.15 g/mol

^{1}H NMR (300 MHz, DMSO-d_6): δ = 10.20 (s, 2 H), 7.51 – 6.71 (m, 9 H), 4.32 (s, 2 H) ppm.

^{13}C NMR (75 MHz, $(CD_3)_2SO$)): δ = 147.14, 137.76, 133.58, 130.57, 128.41, 128.00 127.30, 114.37, 113.77, 47.88 ppm.

Yield: 81 % as a white solid.

***N*-(2-chlorophenyl)-benzenmethanamine hydrochloride (5)**

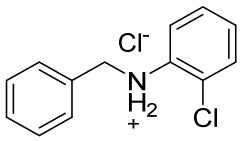

MW = 254.15 g/mol

^{1}H NMR (300 MHz, DMSO-d_6): δ = 8.53 (s, 1H), 7.43 – 7.00 (m, 7 H), 6.58-6.53 (m, 2 H), 4.45 (dd, *J* = 28.5 Hz, 8.5 Hz, 2 H) ppm.

^{13}C NMR (75 MHz, $(CD_3)_2SO$)): δ = 143.68, 139.64, 130.26, 129.56, 129.03, 128.42, 128.40, 127.87, 126.92, 126.76, 118.03, 116.76, 111.97, 46.11 ppm.

Yield: 80 % as a white solid.

***N*-(3-chloro-4-bromophenyl)-benzenmethanamine hydrochloride (6)**

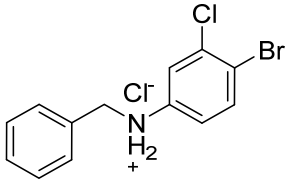

MW = 333.05 g/mol

^{1}H NMR (300 MHz, DMSO-d_6): δ = 7.89 (s, 2 H), 7.37 – 7.26 (m, 6 H), 6.83 (t, *J* = 3 Hz, 1 H), 6.56 (dd, *J* = 8.8 Hz, 2.7 Hz, 1 H), 4.31 (d, *J* = 18 Hz, 2 H) ppm.

^{13}C NMR (75 MHz, $(CD_3)_2SO$)): δ = 148.64, 138.85, 133.60, 133.19, 128.43, 128.04, 127.40, 126.99, 113.76, 106.17, 46.51 ppm.

Yield: 81 % as a white solid.

4-methyl-*N*-phenyl-benzenmethanamine hydrochloride (7)

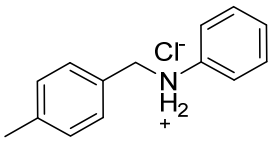

MW = 233.74 g/mol

^{1}H NMR (300 MHz, DMSO-d_6): δ = 10.75 (s, 2 H), 7.40 – 7.12 (m, 9 H), 4.42 (s, 2 H), 2.27 (s, 3 H) ppm

^{13}C NMR (75 MHz, $(CD_3)_2SO$)): δ = 137.42, 129.97, 129.49, 129.14, 128.64, 125.80, 121.02, 51.63, 20.50 ppm.

Yield: 95 % as a white solid.

4-methoxy-*N*-phenyl-benzenmethanamine hydrochloride (8)

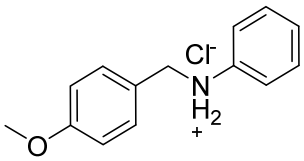

MW = 249.74 g/mol

^{1}H NMR (300 MHz, DMSO-d_6): δ = 10.81 (s, 2 H), 7.49 – 6.87 (m, 9 H), 4.40 (s, 2 H), 3.72 (d, *J* = 3 Hz, 3 H) ppm.

^{13}C NMR (75 MHz, $(CD_3)_2SO$)): δ = 159.03, 159.03, 131.08, 129.16, 123.06, 121.26, 113.44, 54.84, 51.69 ppm.

Yield: 88 % as a white solid.

_N_-phenyl-naphtalenemethanamine hydrochloride (9)

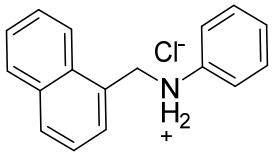

MW = 269.77 g/mol

^{1}H NMR (300 MHz, DMSO-d_6): δ = 10.21 (s, 2 H), 8.18-8.14 (m, 1 H), 7.98-7.92 (m, 2 H), 7.70 (d, *J* = 7.0 Hz, 1 H), 7.59-7.56 (m, 2 H), 7.50 (t, *J* = 7.5 Hz, 1 H), 7.29 (t, J = 7.6 Hz, 2 H), 7.17-7.04 (m, 3 H), 4.89 (s, 2 H) ppm.

^{13}C NMR (75 MHz, $(CD_3)_2SO$)): δ = 133.29, 131.24, 130.80, 129.73, 129.32, 128.57, 127.80, 126.46, 125.99, 125.34, 123.72, 123.44, 118.81, 48.23 ppm.

Yield: 90 % as a white solid.

4-chloro-_N_-phenyl-benzenmethanamine hydrochloride (10)

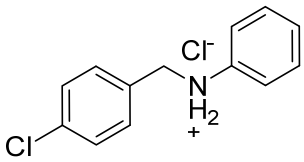

MW = 254.15 g/mol

^{1}H NMR (300 MHz, DMSO-d_6): δ = 9.64 (s, 2 H), 7.52 – 7.13 (m, 9 H), 4.45 (s, 2 H) ppm.

^{13}C NMR (75 MHz, $(CD_3)_2SO$)): δ = 132.92, 131.50, 129.41, 128.33, 125.16, 120.21, 50.67 ppm.

Yield: 89 % as a white solid.

3-chloro-*N*-phenyl-benzenmethanamine hydrochloride (11)

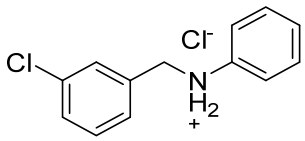

MW = 245.15 g/mol

^{1}H NMR (300 MHz, DMSO-d_6): δ = 10.63 (s, 2H), 7.60 (s, 1 H), 7.50 – 7.07 (m, 8 H), 4.46 (d, *J* = 15 Hz, 2 H) ppm.

^{13}C NMR (75 MHz, $(CD_3)_2SO$)): δ = 137.38, 132.97, 130.25, 129.93, 129.75, 129.49, 129.41, 129.12, 128.41, 129.12, 128.41, 1228.03, 123.42, 119.63, 50.15 ppm.

Yield: 82 % as a white solid.

2-chloro-*N*-phenyl-benzenmethanamine hydrochloride (12)

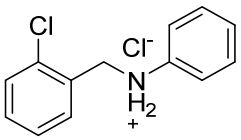

MW = 254.15 g/mol

^{1}H NMR (300 MHz, DMSO-d_6): δ = 9.11 (s, 2 H), 7.50 – 7.15 (m, 7 H), 6.81 (d, *J* = 6 Hz, 2 H), 4.44 (d, J = 18 Hz, 2H) ppm.

^{13}C NMR (75 MHz, $(CD_3)_2SO$)): δ = 132.81, 131.93, 129.96, 129.78, 129.60, 129.46, 129.32, 129.16, 128.59, 128.38, 127.40, 123.52, 46.70 ppm.

Yield: 77 % as a white solid.

4-methyl-3-chloro-*N*-phenyl-benzenmethanamine hydrochloride (13)

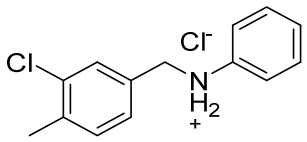

MW = 268.18 g/mol

^{1}H NMR (300 MHz, DMSO-d_6): δ = 7.89 (s, 2H), 7.55 – 7.10 (m, 8 H), 4.42 (s, 2 H), 2.30 (s, 3 H) ppm.

^{13}C NMR (75 MHz, $(CD_3)_2SO$)): δ = 148.64, 138.85, 133.60, 133.19, 128.43, 128.04, 127.40, 126.99, 113.76, 106.17, 46.51 ppm.

Yield: 76 % as a white solid.

NMR Spectra

1:

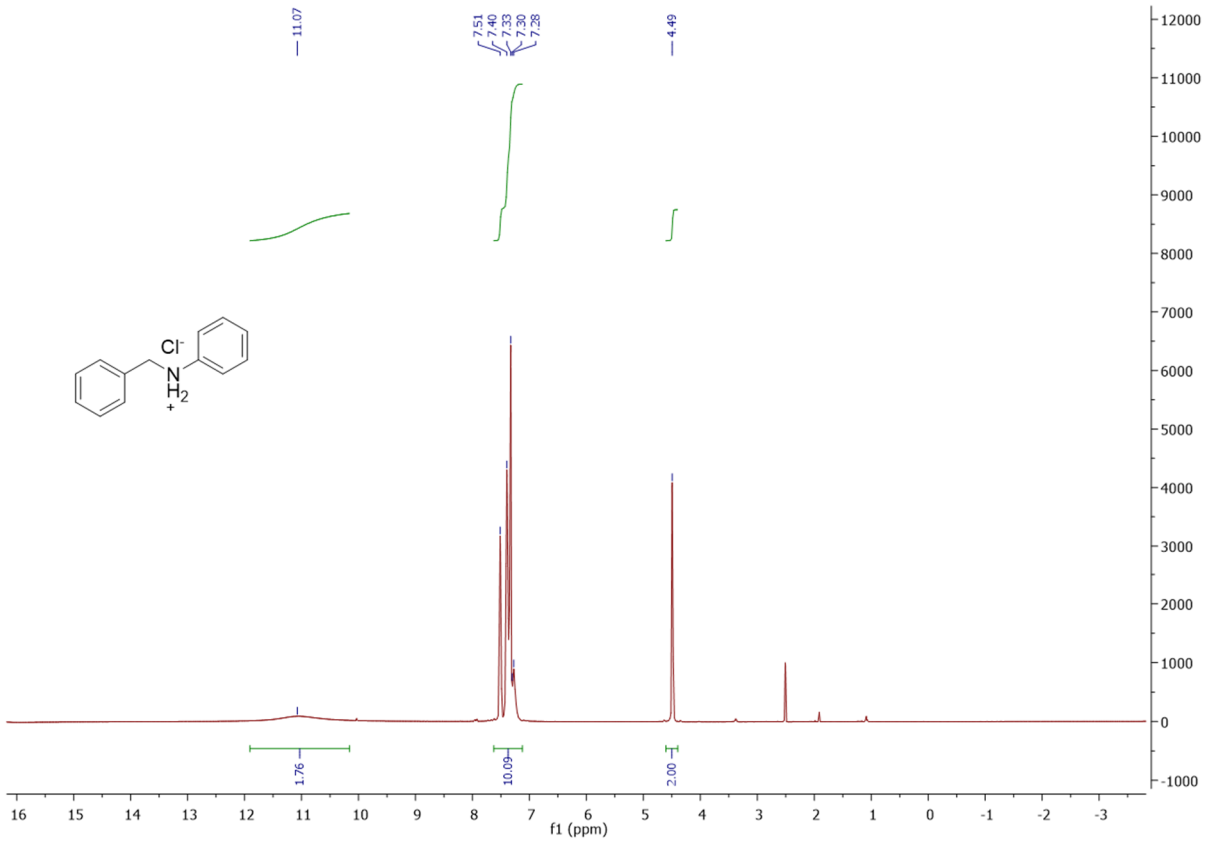

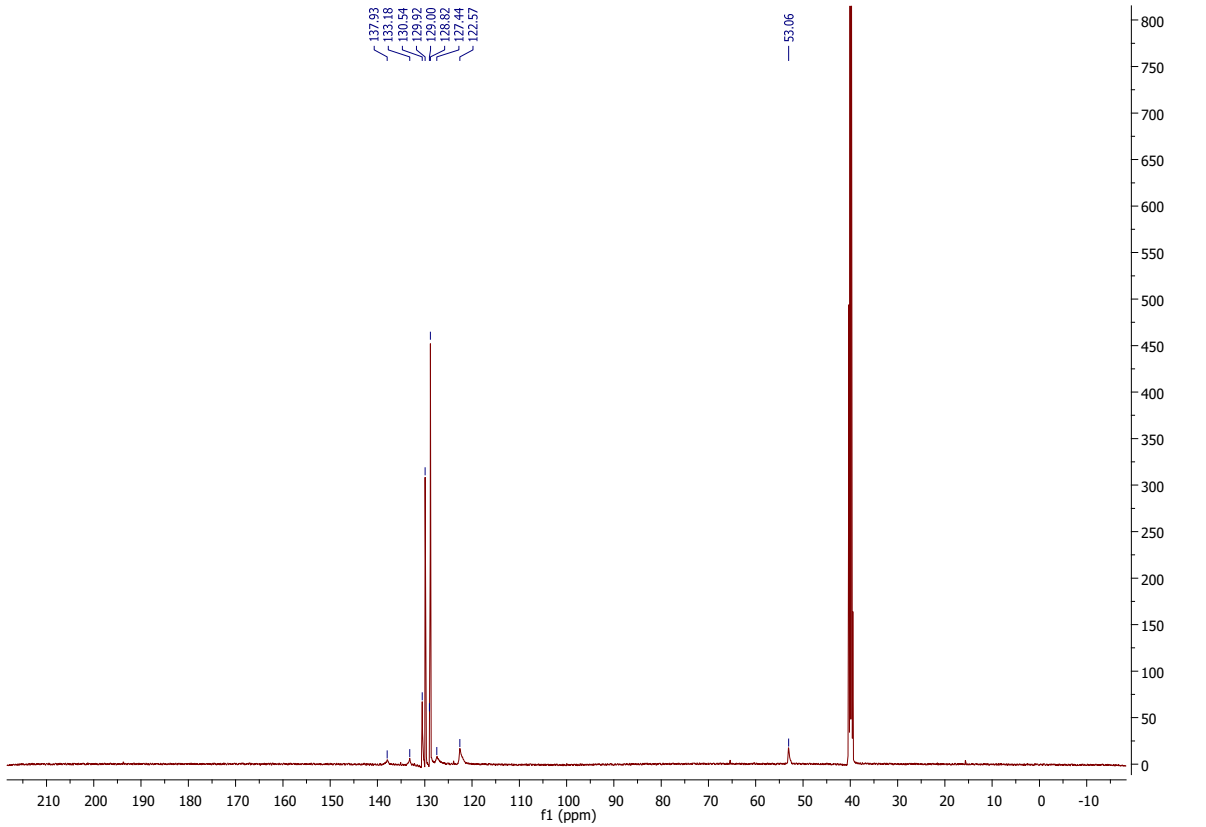

2:

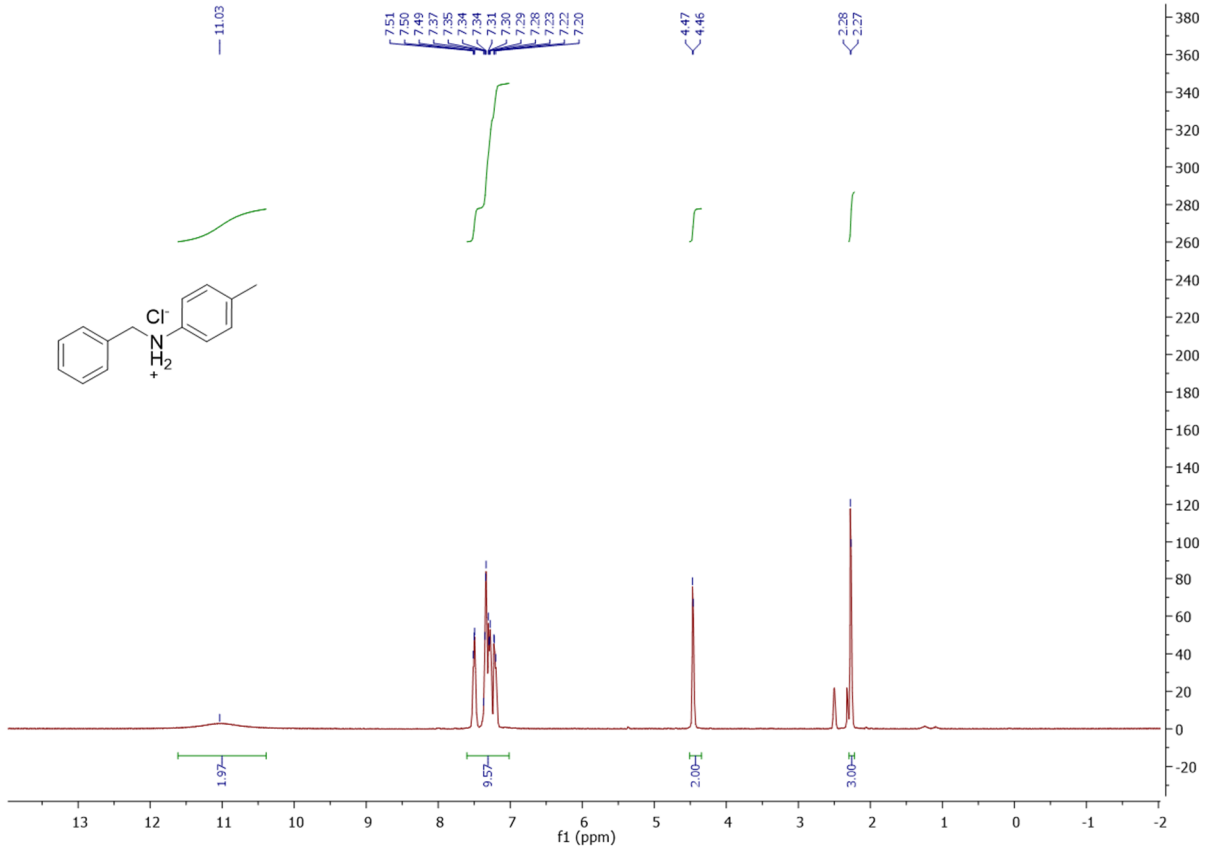
11.03
7.51
7.50
7.49
7.37
7.35
7.34
7.34
7.31
7.30
7.29
7.28
7.23
7.22
7.20
4.47
4.46
2.28
2.27
Cl⁻
N
H2
+
1.97
9.57
2.00
3.00
f1 (ppm)

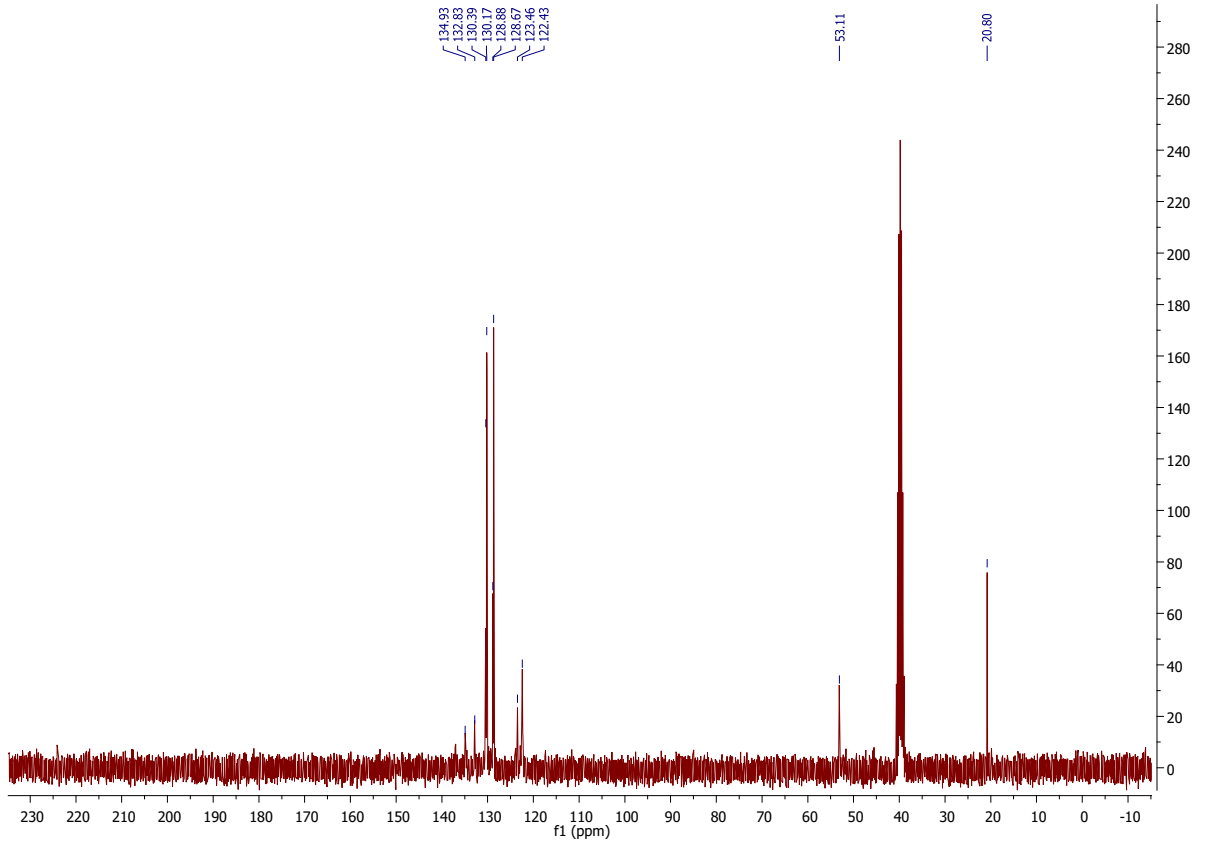
134.93
132.83
130.39
130.17
128.88
128.67
123.46
122.43
53.11
20.80
f1 (ppm)

3:

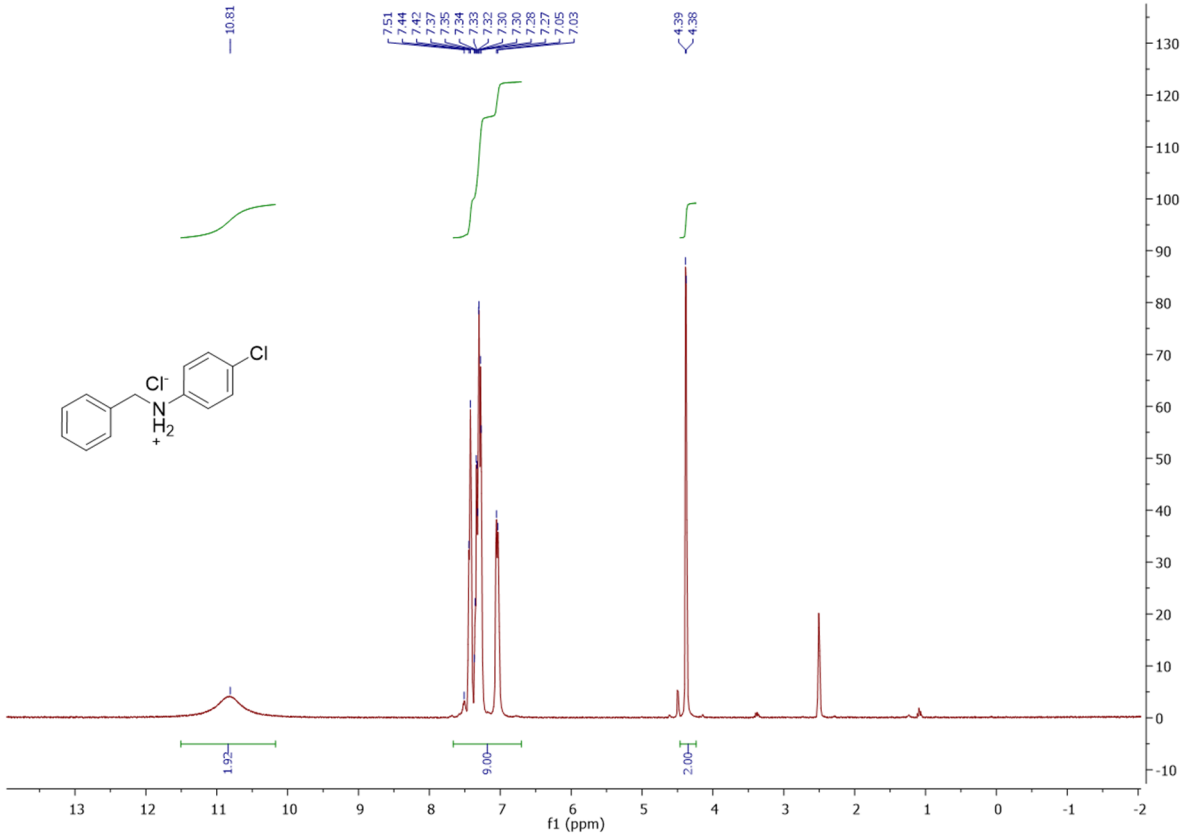
10.81
7.51
7.44
7.42
7.37
7.35
7.34
7.33
7.32
7.30
7.28
7.27
7.05
7.03
4.39
4.38
Cl
Cl⁻
N
H2
+
1.92
9.00
2.00
f1 (ppm)

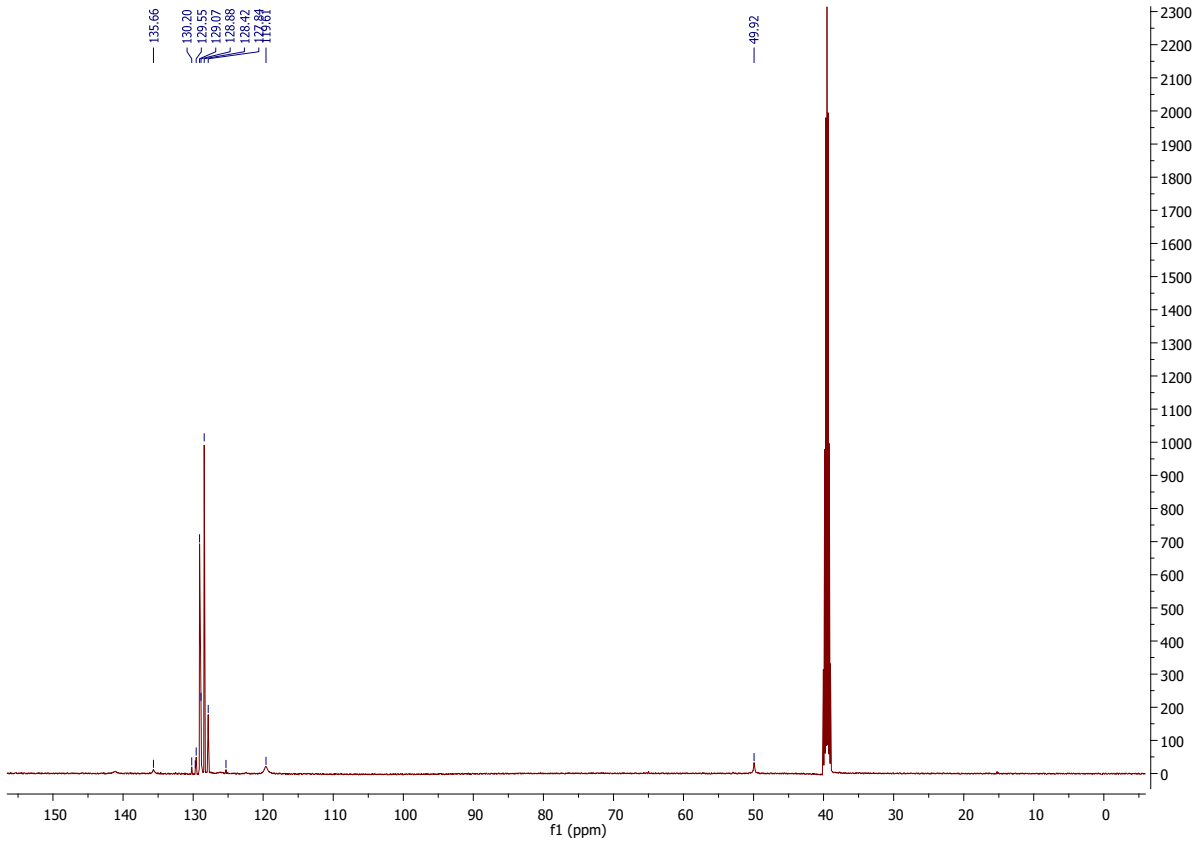
135.66
130.20
129.55
129.07
128.88
128.42
49.92
f1 (ppm)

4:

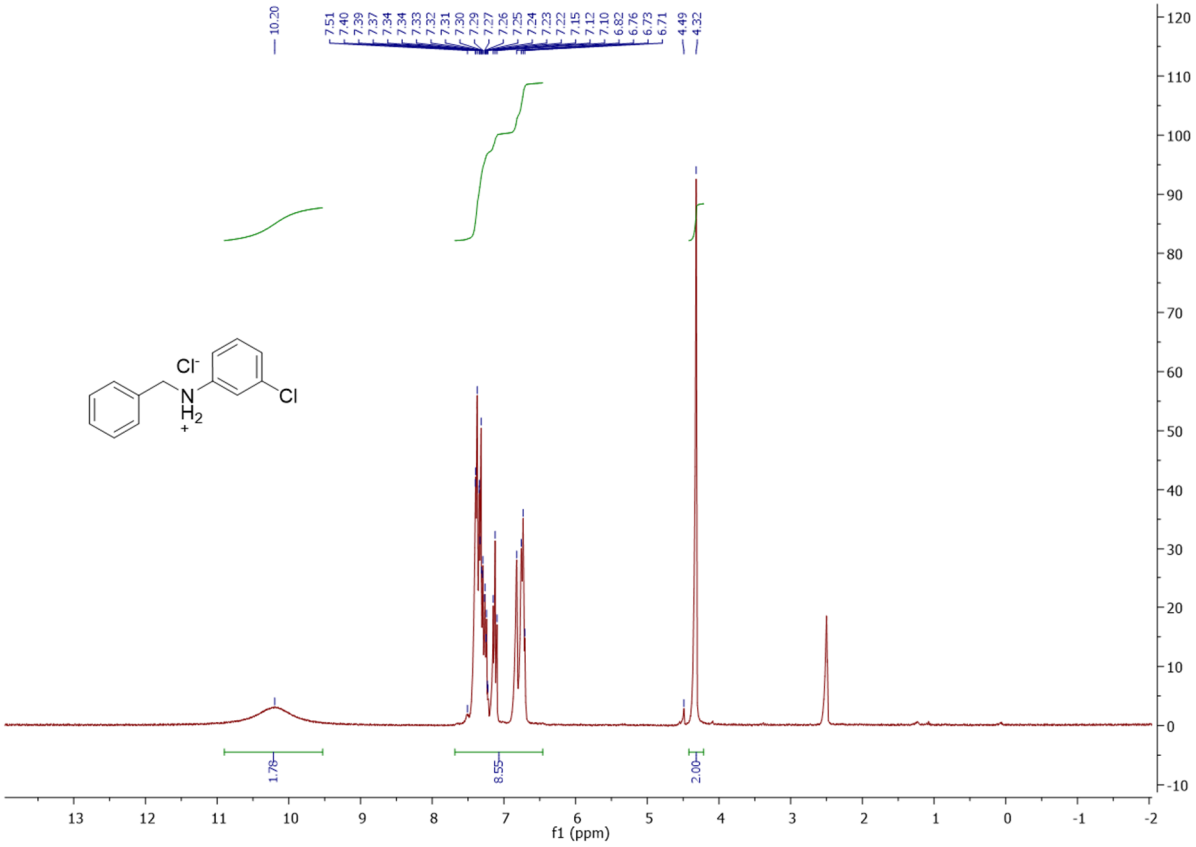
10.20
7.51
7.40
7.39
7.37
7.34
7.34
7.33
7.32
7.31
7.30
7.29
7.27
7.26
7.25
7.24
7.23
7.22
7.15
7.12
7.10
6.82
6.76
6.73
6.71
4.49
4.32
Cl⁻
N
H2
+
Cl
1.78
8.55
2.00
f1 (ppm)

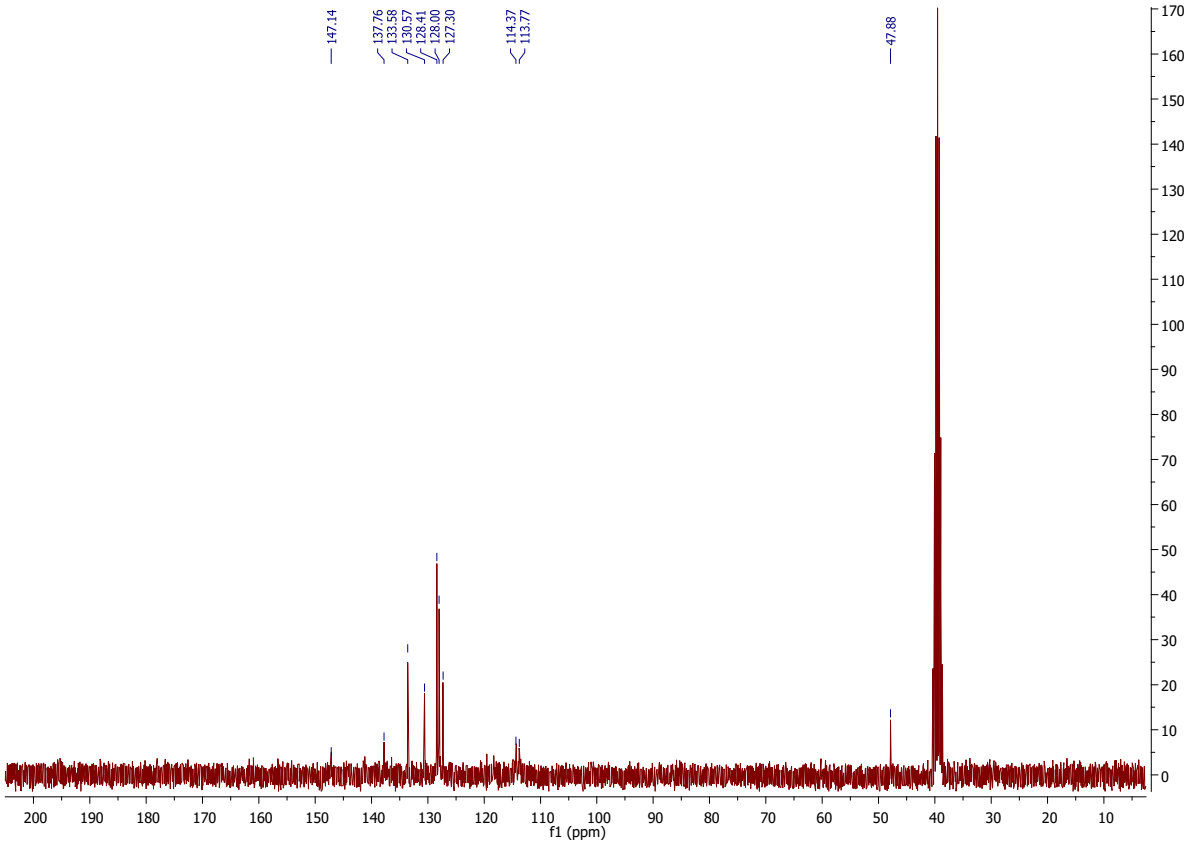
147.14
137.76
133.58
130.57
128.41
128.00
127.30
114.37
113.77
47.88
f1 (ppm)

5:

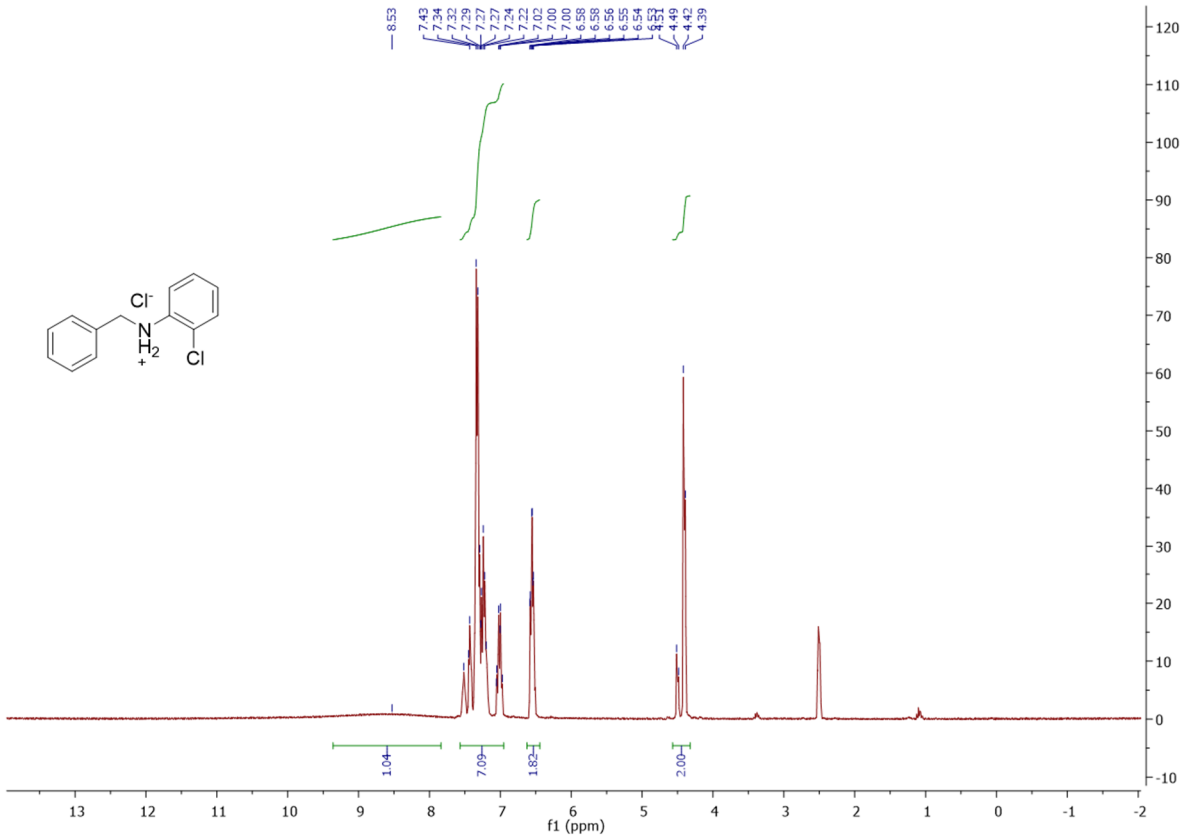
8.53
7.43
7.34
7.32
7.29
7.27
7.27
7.24
7.22
7.02
7.00
7.00
6.58
6.56
6.55
6.54
4.51
4.49
4.42
4.39
Cl⁻
N
H2
+
Cl
1.04
7.09
1.82
2.00
f1 (ppm)

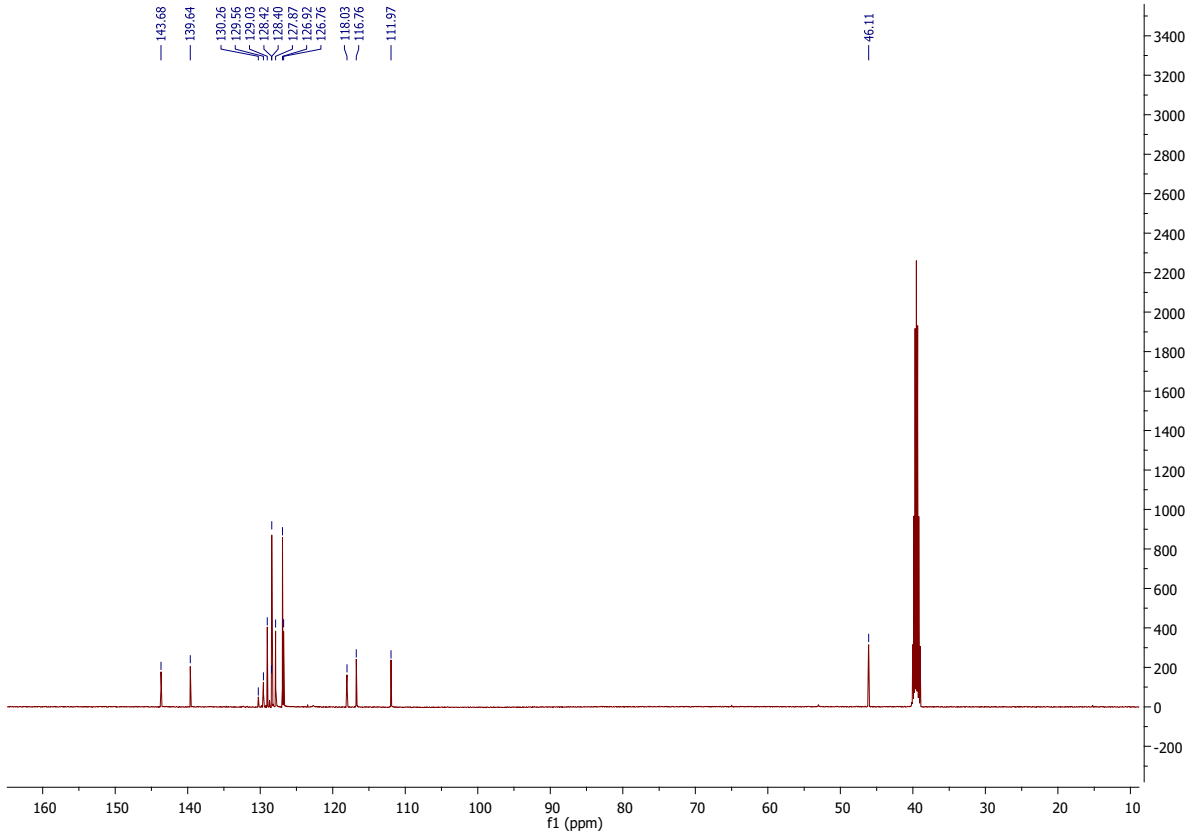
143.68
139.64
130.26
129.56
129.03
128.42
128.40
127.87
126.92
126.76
118.03
116.76
111.97
46.11
f1 (ppm)

6:

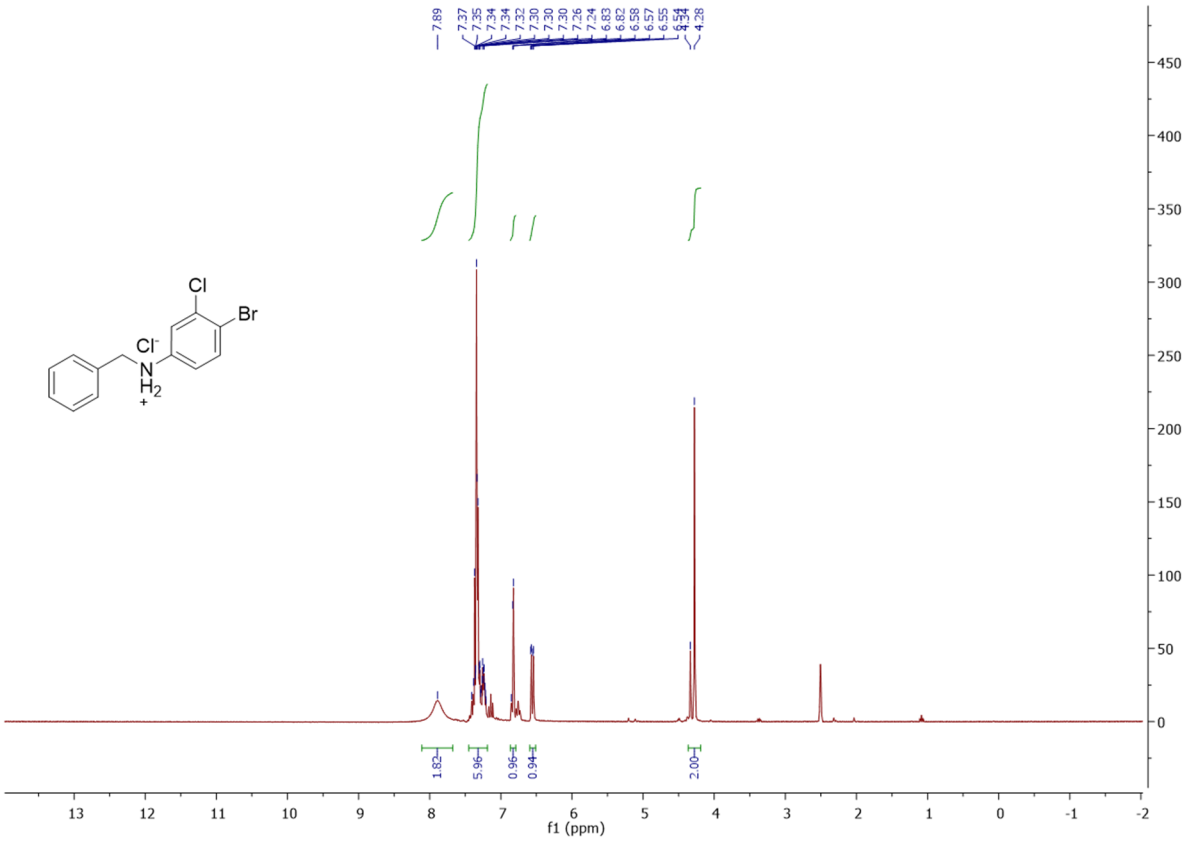
7.89
7.37
7.35
7.34
7.34
7.32
7.30
7.30
7.30
7.26
7.24
6.83
6.82
6.58
6.57
6.55
4.28
Cl
Br
Cl⁻
N
H2
+
1.82
5.96
0.96
0.94
2.00
f1 (ppm)

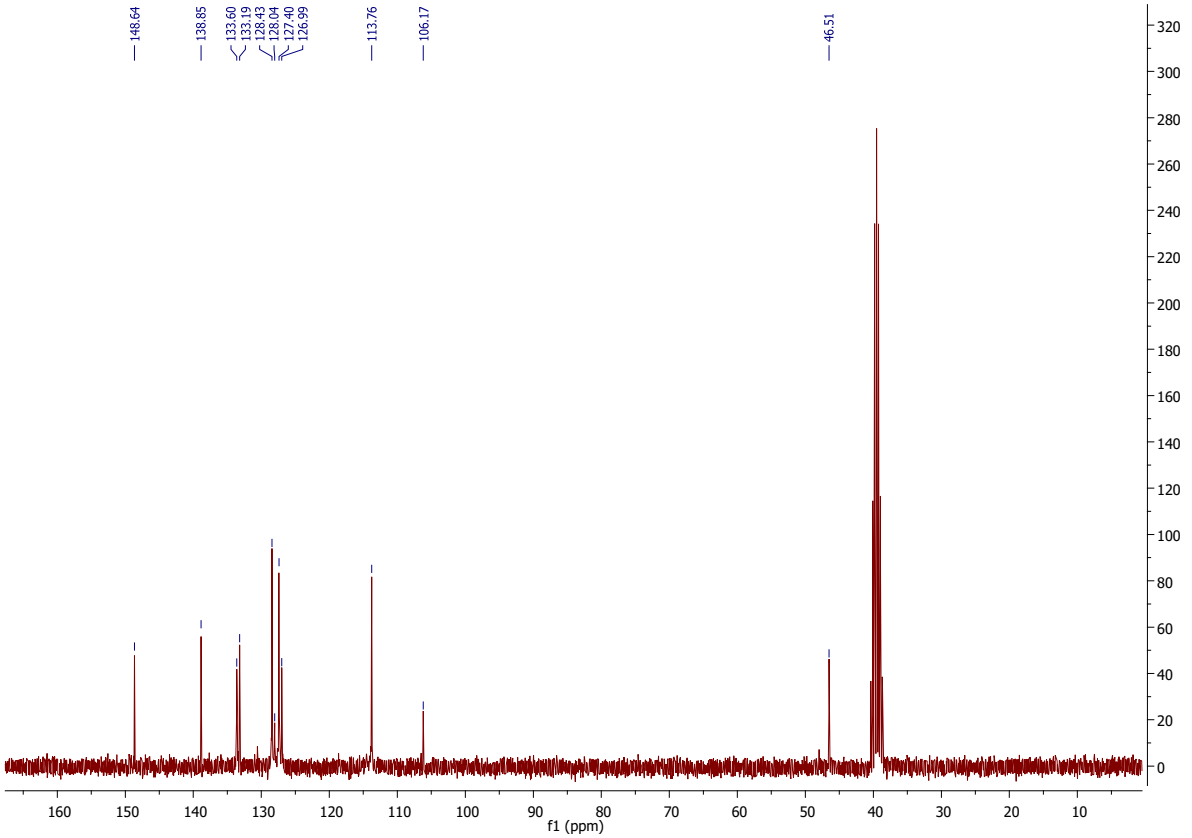
148.64
138.85
133.60
133.19
128.43
128.04
127.40
126.99
113.76
106.17
46.51
f1 (ppm)

7:

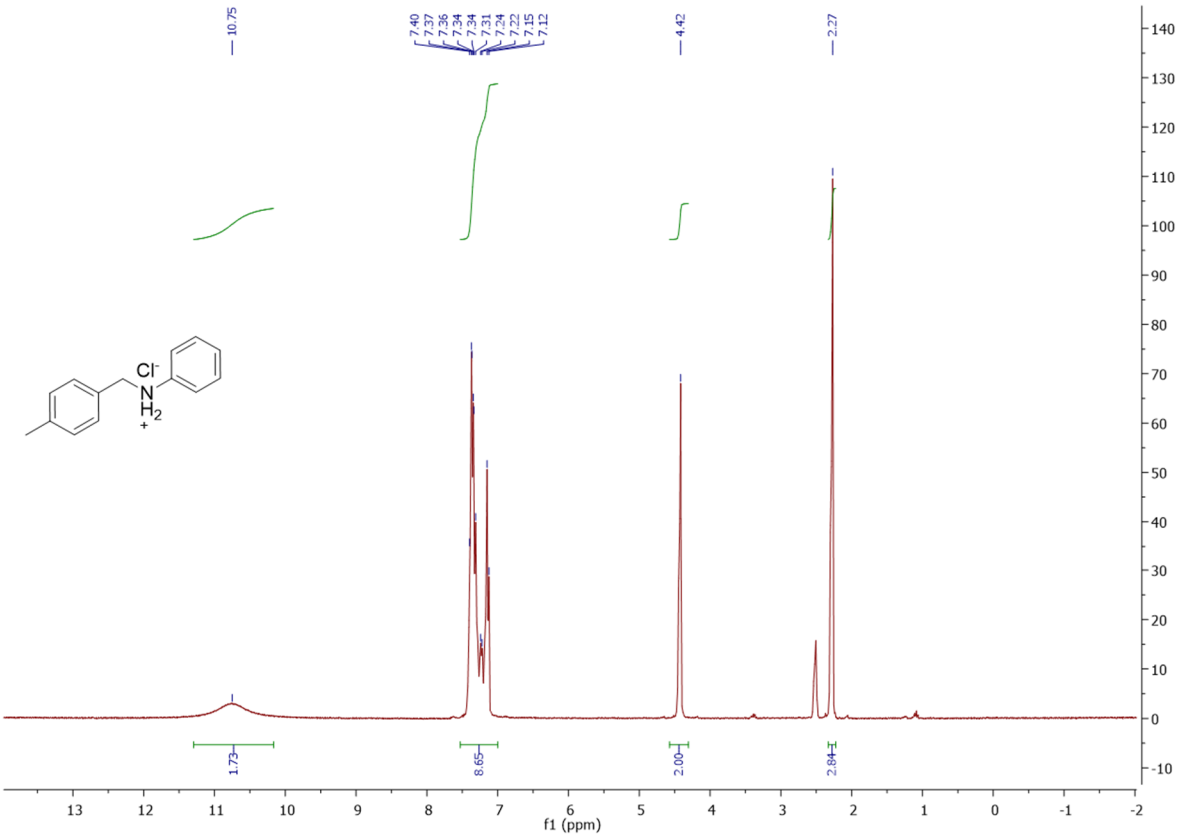
10.75
7.40
7.37
7.36
7.34
7.34
7.31
7.24
7.22
7.15
7.12
4.42
2.27
Cl⁻
NH2
+
1.73
8.65
2.00
2.84
f1 (ppm)

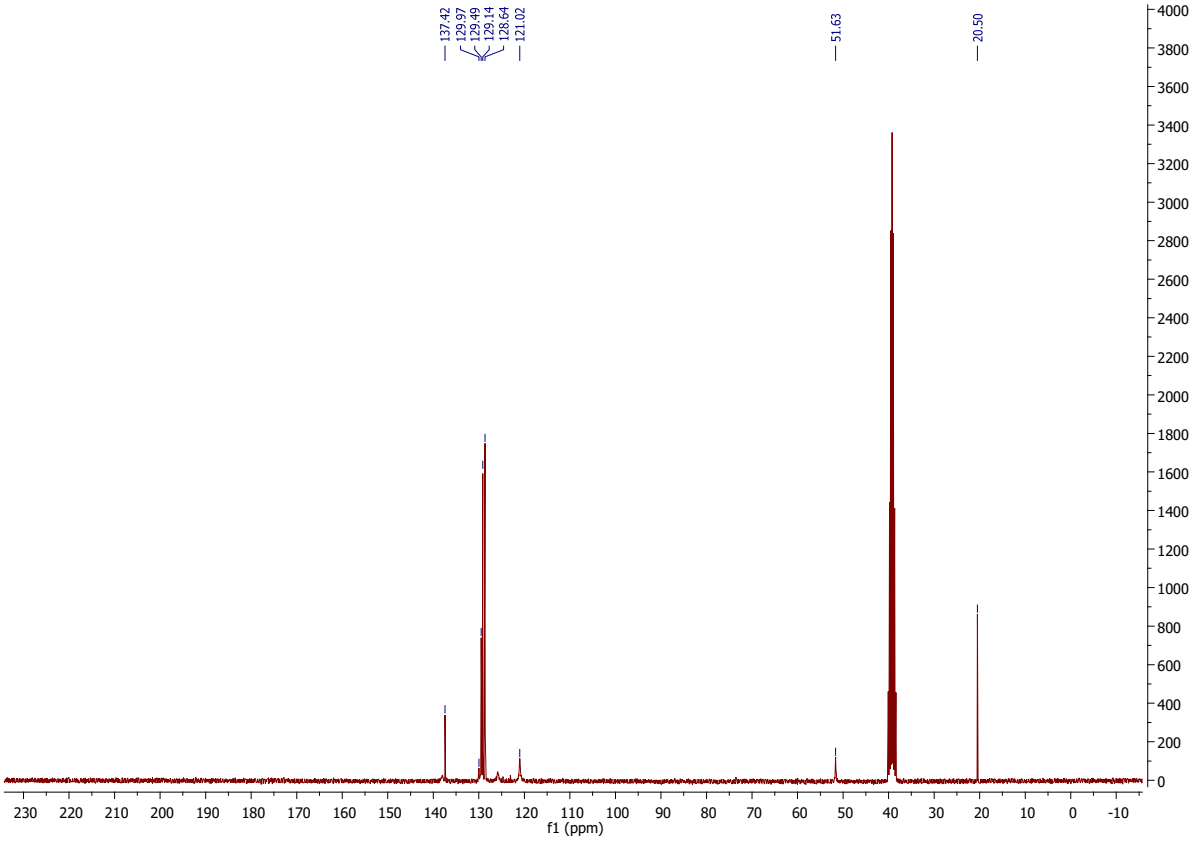
137.42
129.97
129.49
129.14
128.64
121.02
51.63
20.50
f1 (ppm)

8:

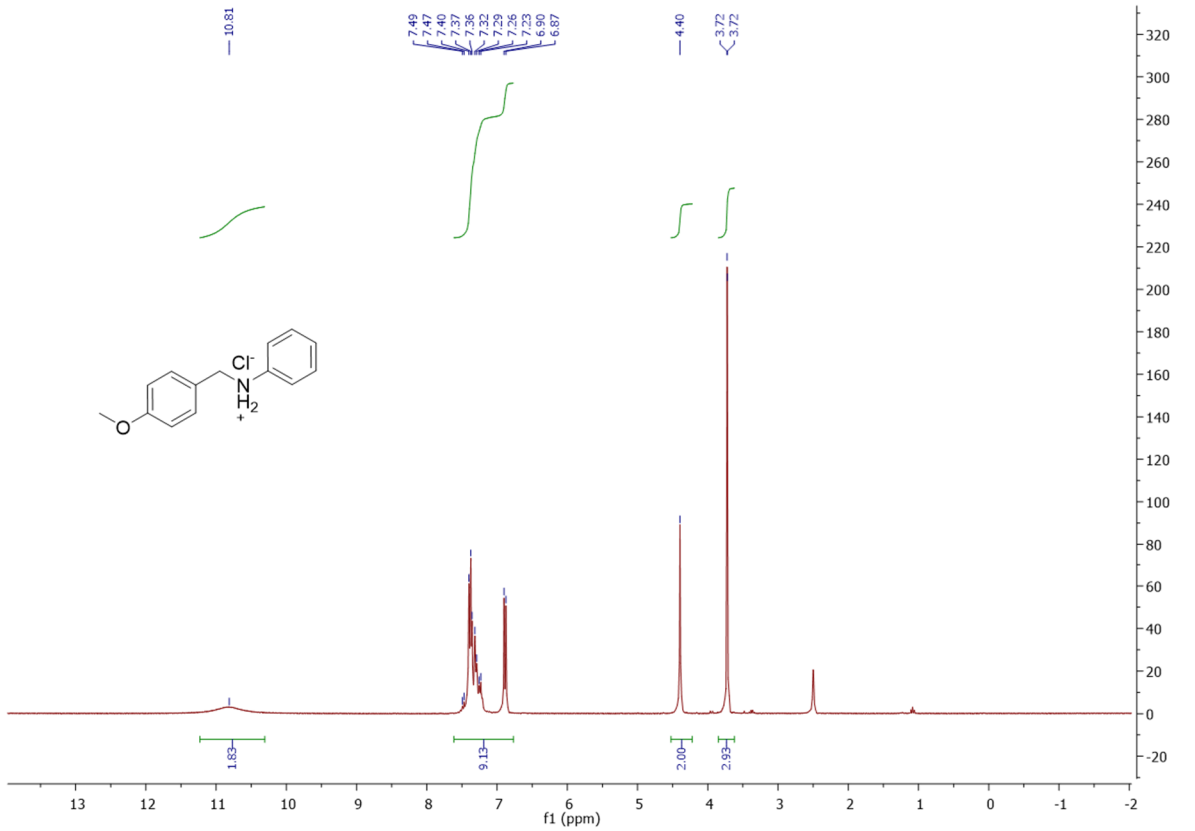
10.81
7.49
7.47
7.40
7.37
7.36
7.32
7.29
7.26
7.23
6.90
6.87
4.40
3.72
3.72
Cl⁻
N
H2
+
O
1.83
9.13
2.00
2.93
f1 (ppm)

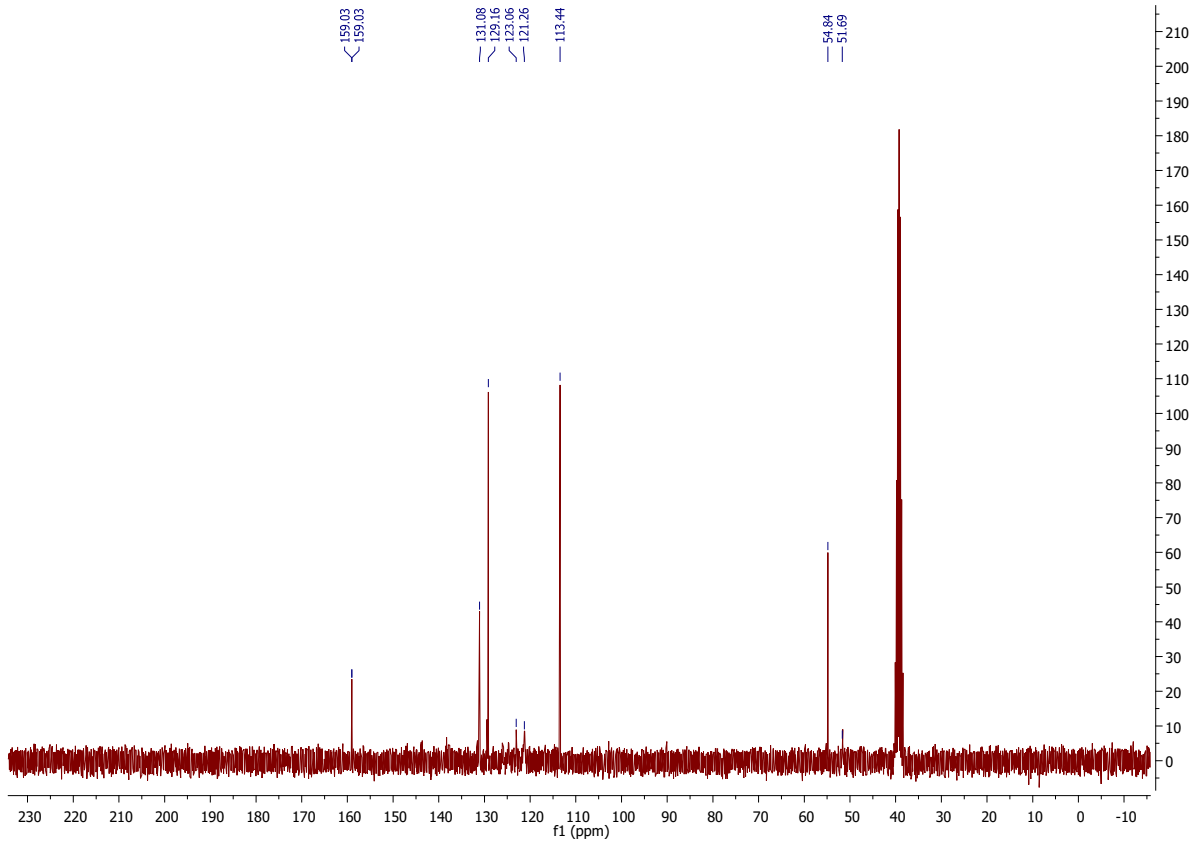
159.03
159.03
131.08
129.16
123.06
121.26
113.44
54.84
51.69
f1 (ppm)

9:

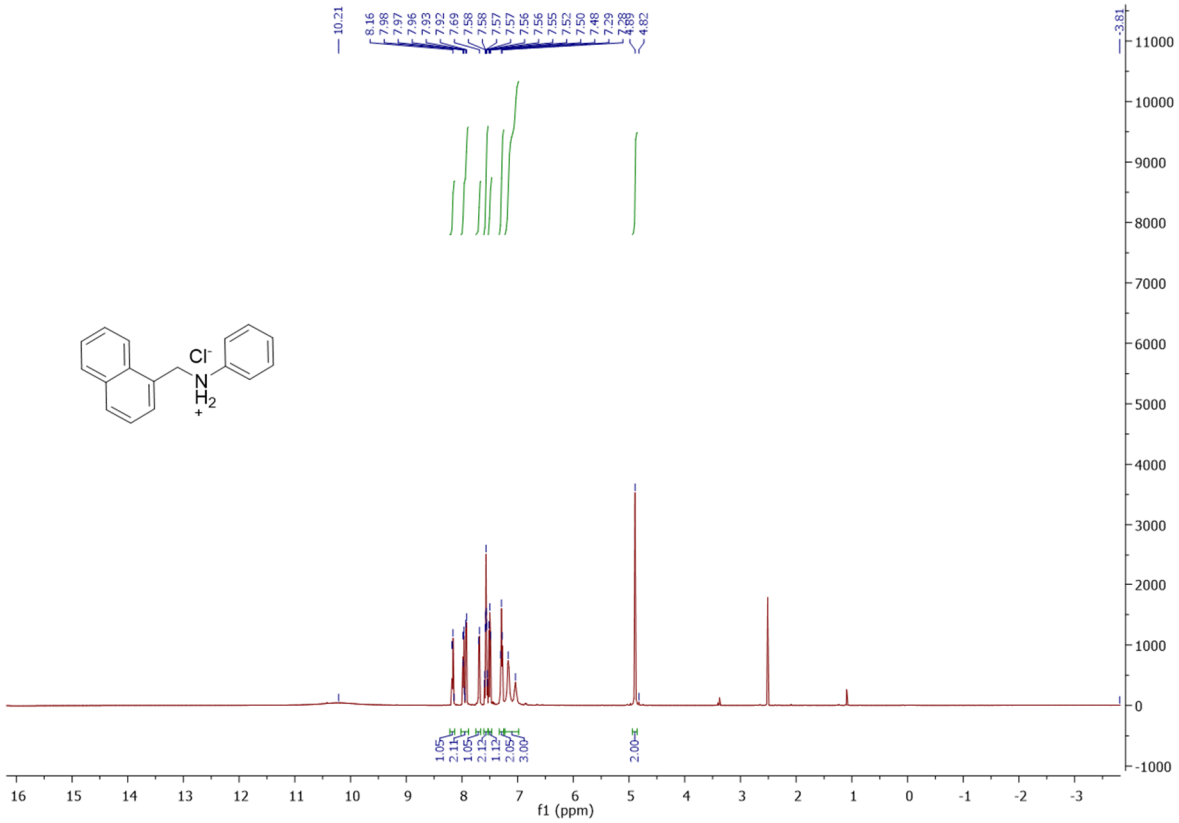
10.21
8.16
7.98
7.97
7.96
7.93
7.92
7.69
7.58
7.58
7.57
7.57
7.56
7.56
7.55
7.52
7.50
7.48
7.29
7.28
4.89
4.82
3.81
Cl⁻
N
H2
+
1.05
2.11
1.05
2.13
1.12
2.05
3.00
2.00
f1 (ppm)

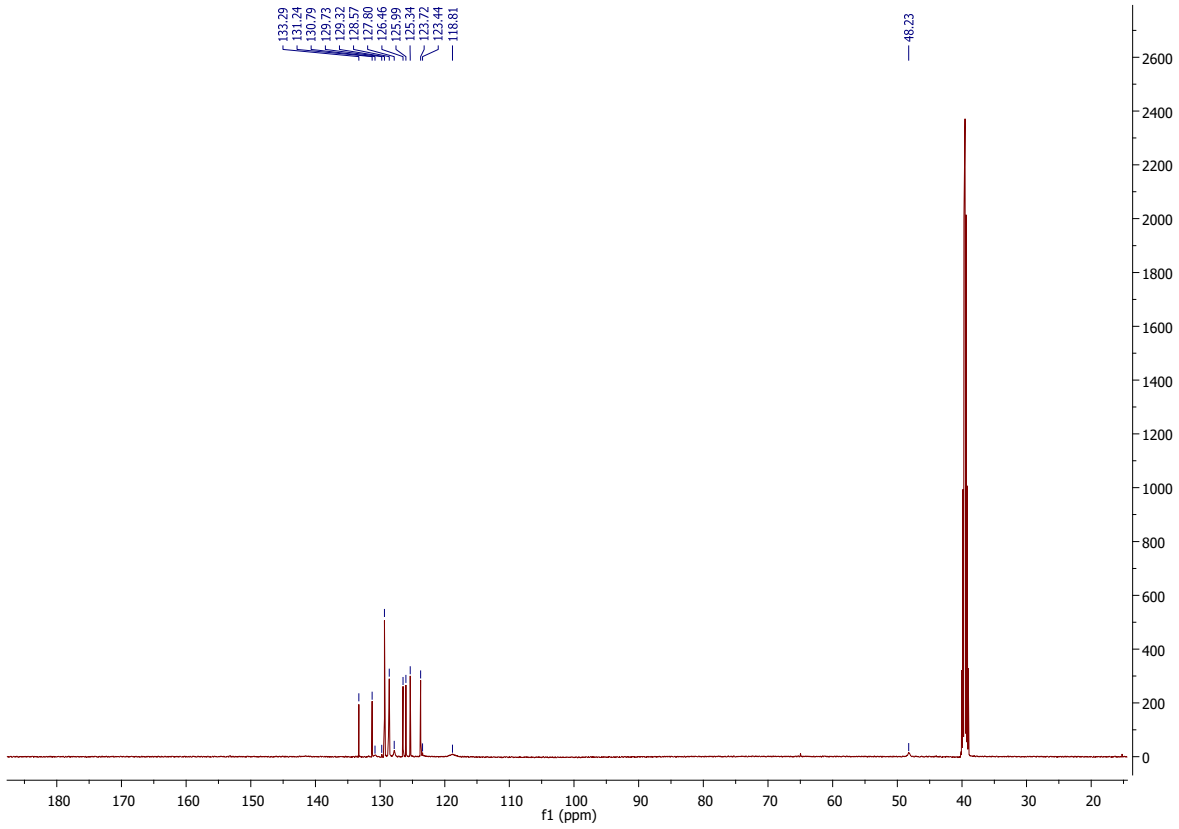
133.29
131.24
130.79
129.73
129.32
128.57
127.80
126.46
125.99
125.34
123.72
123.44
118.81
48.23
f1 (ppm)

10:

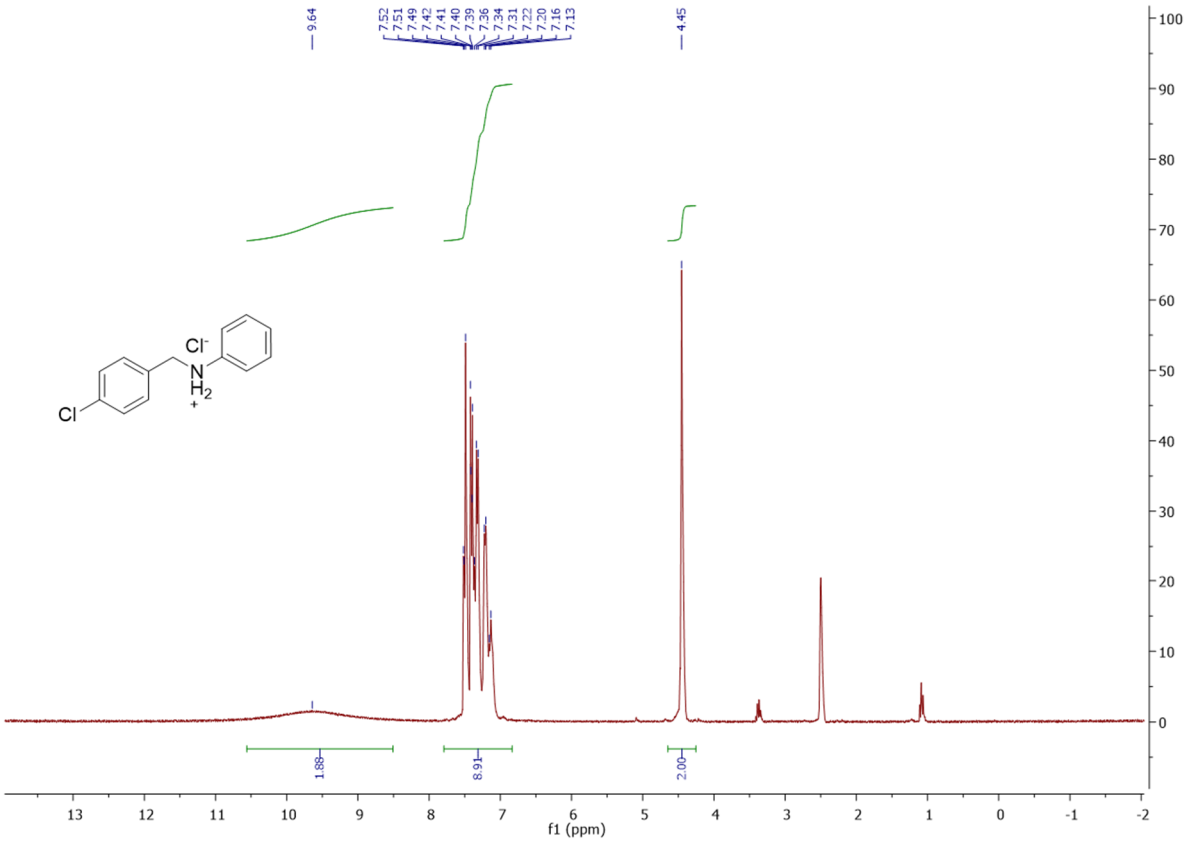
9.64
7.52
7.51
7.49
7.42
7.41
7.40
7.39
7.36
7.34
7.31
7.22
7.20
7.16
7.13
4.45
Cl
N
H2
Cl
1.88
8.91
2.00
f1 (ppm)

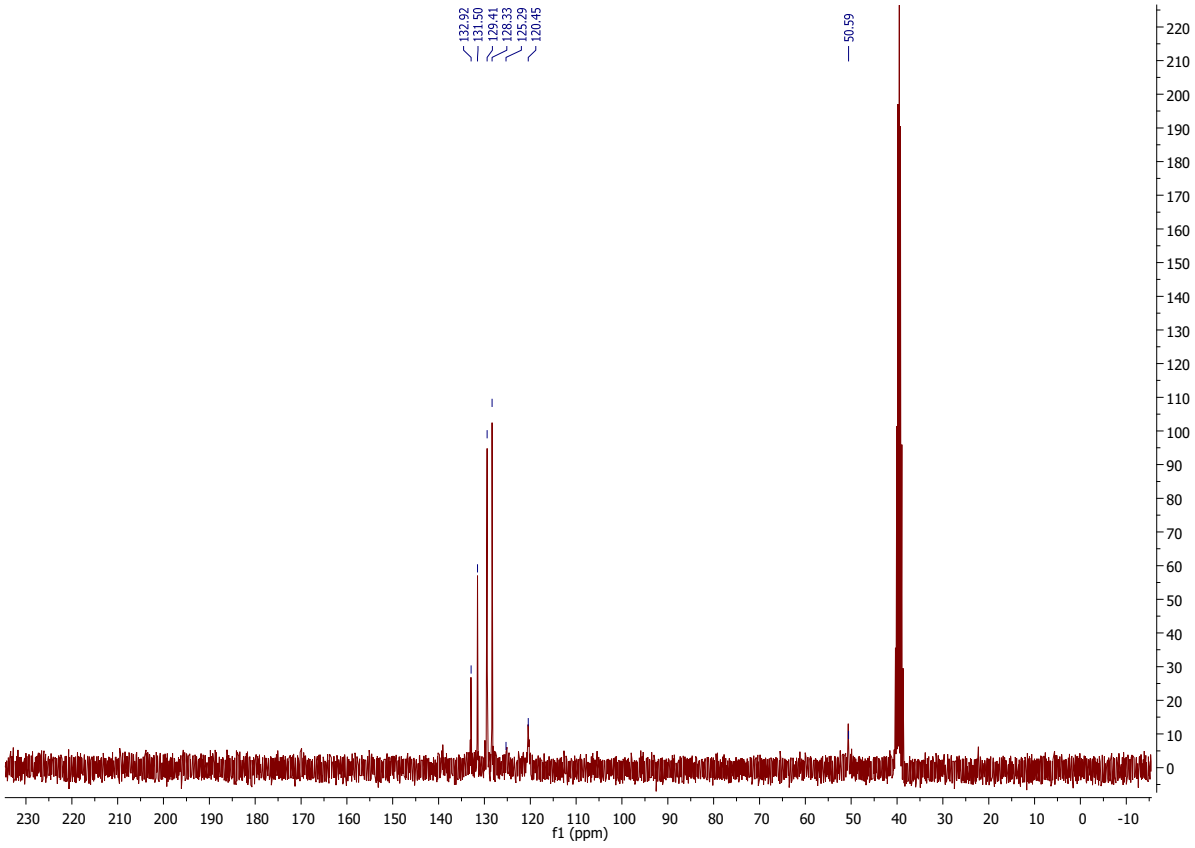
132.92
131.50
129.41
128.33
125.29
120.45
50.59
f1 (ppm)

11:

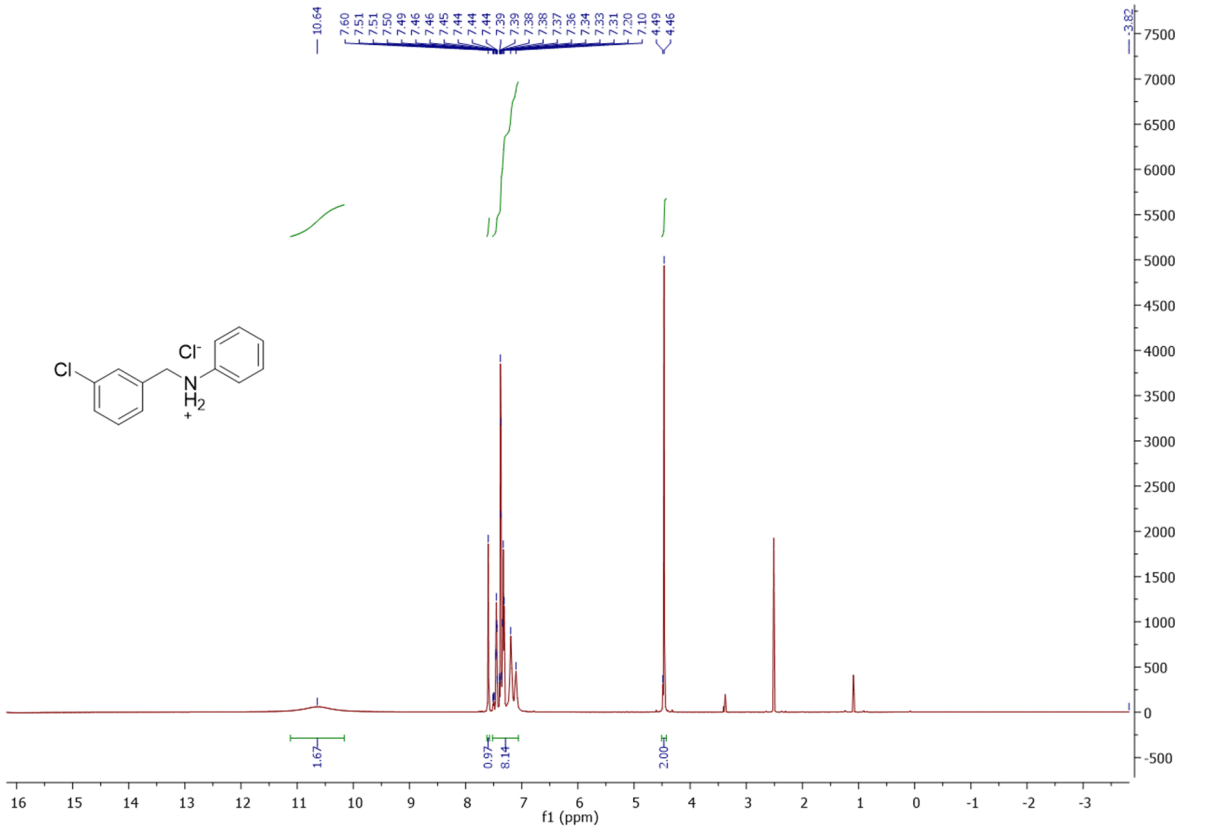
10.64
7.60
7.51
7.51
7.50
7.49
7.46
7.46
7.45
7.44
7.44
7.44
7.39
7.39
7.38
7.38
7.37
7.36
7.34
7.33
7.31
7.20
7.10
4.49
4.46
3.82
Cl
Cl⁻
N
H2
+
1.67
0.97
8.14
2.00
f1 (ppm)

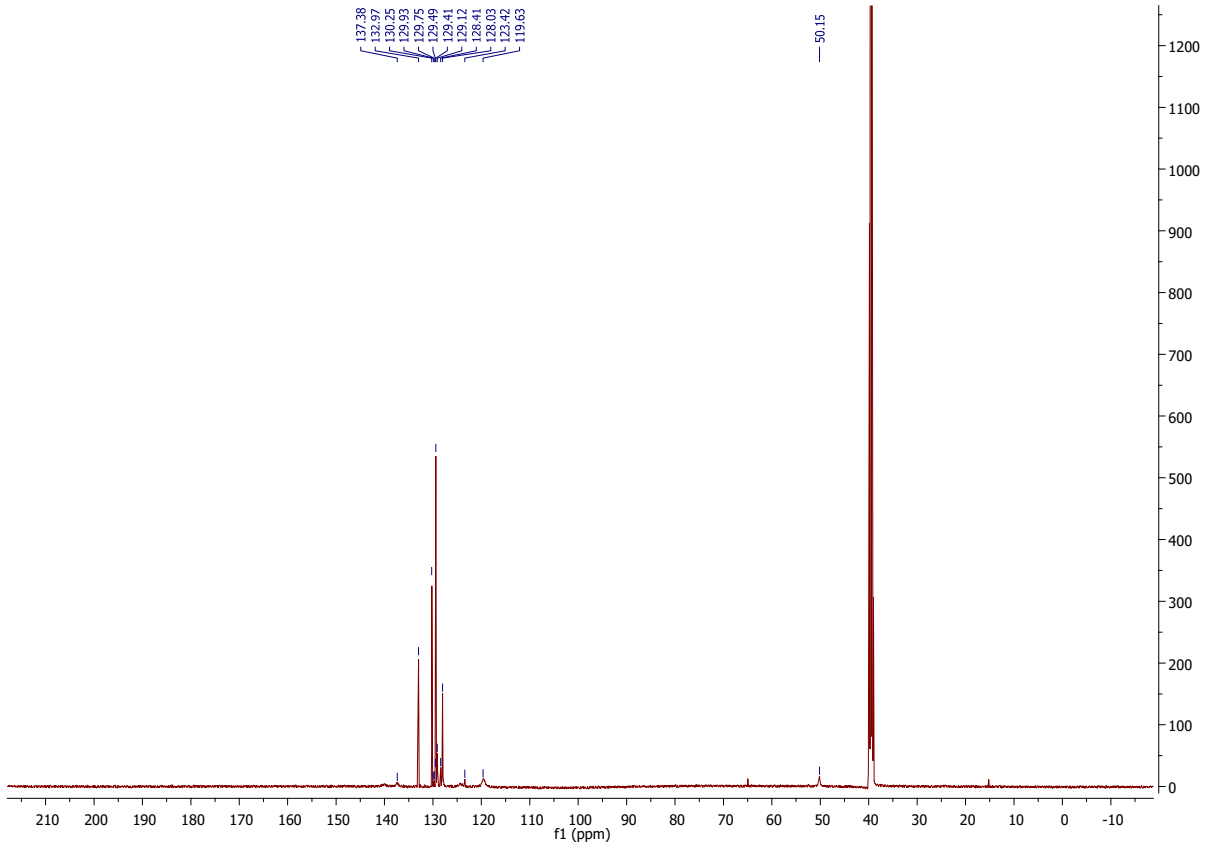
137.38
132.97
130.25
129.93
129.75
129.49
129.41
129.12
128.41
128.03
123.42
119.63
50.15
f1 (ppm)

12:

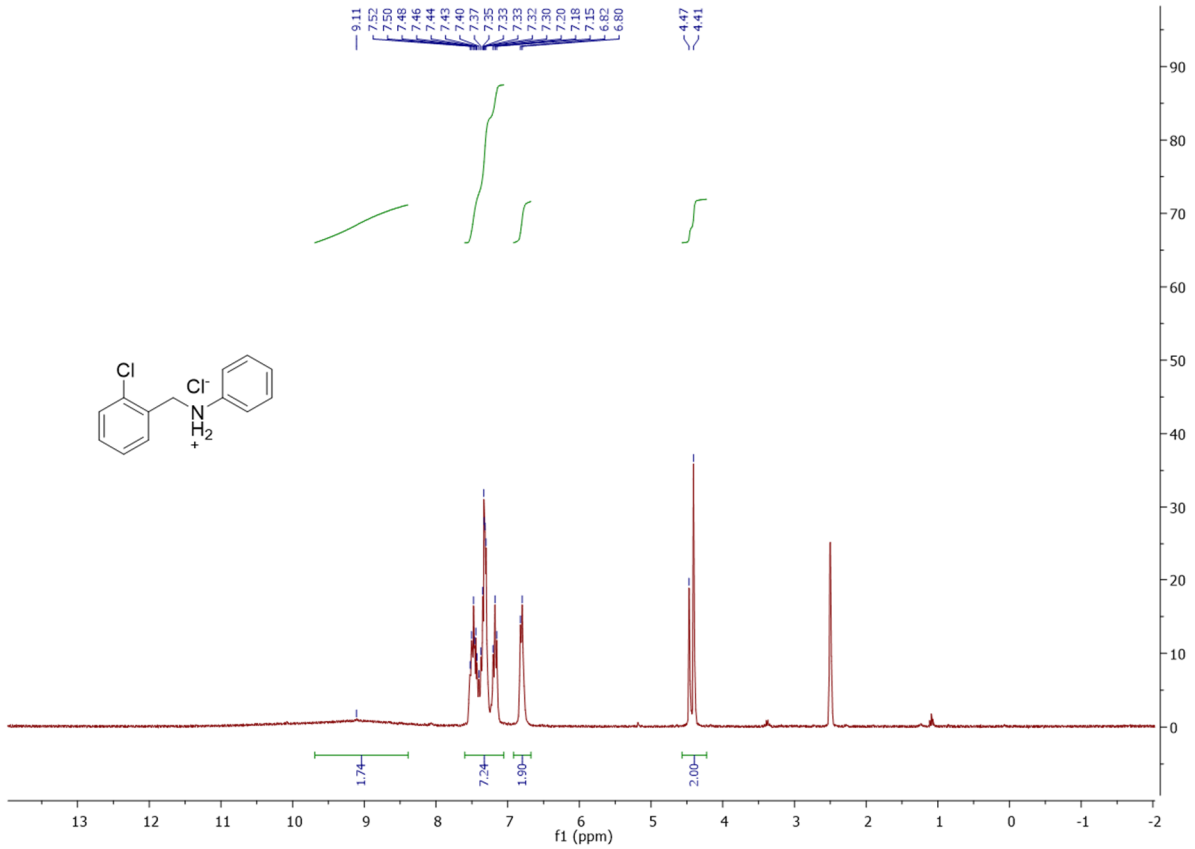
9.11
7.52
7.50
7.48
7.46
7.44
7.43
7.40
7.37
7.35
7.33
7.33
7.32
7.30
7.20
7.18
7.15
6.82
6.80
4.47
4.41
Cl
Cl-
N
H2
+
1.74
7.24
1.90
2.00
f1 (ppm)

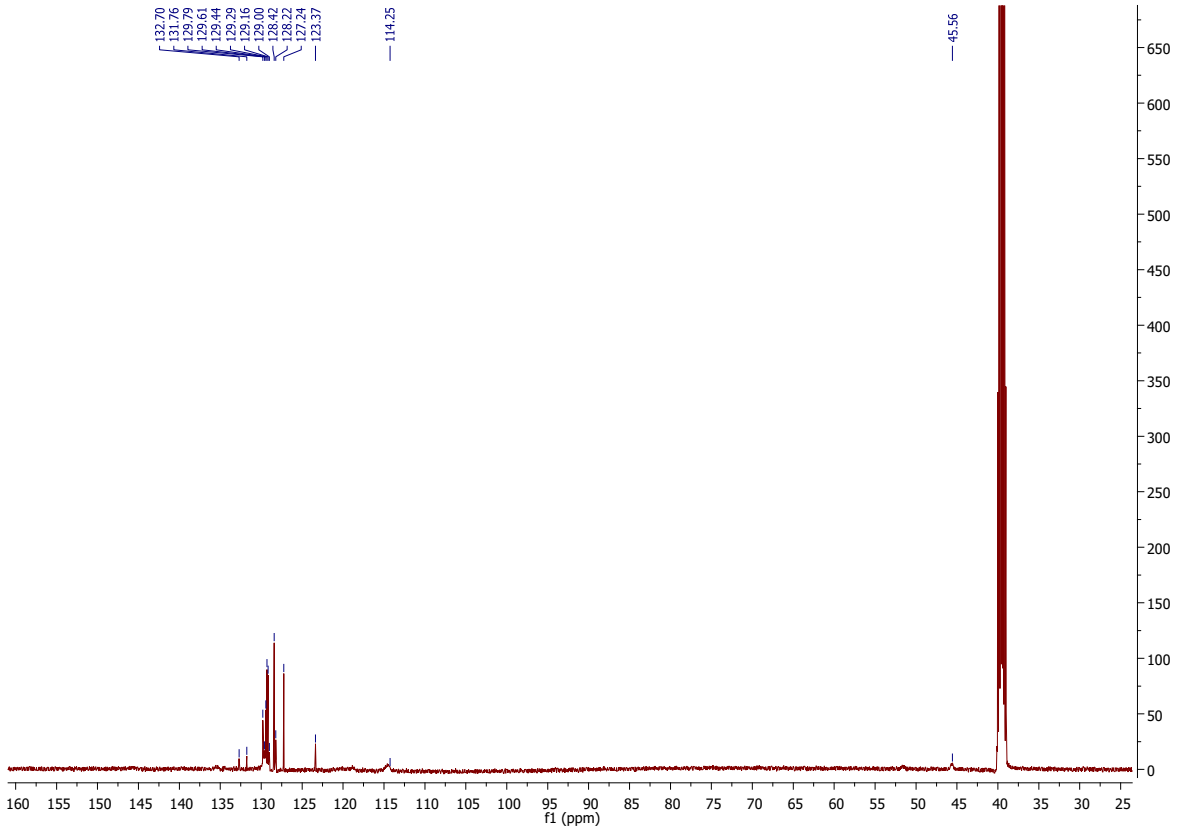
132.70
131.76
129.79
129.61
129.44
129.29
129.16
129.00
128.42
128.22
127.24
123.37
114.25
45.56
f1 (ppm)

13:

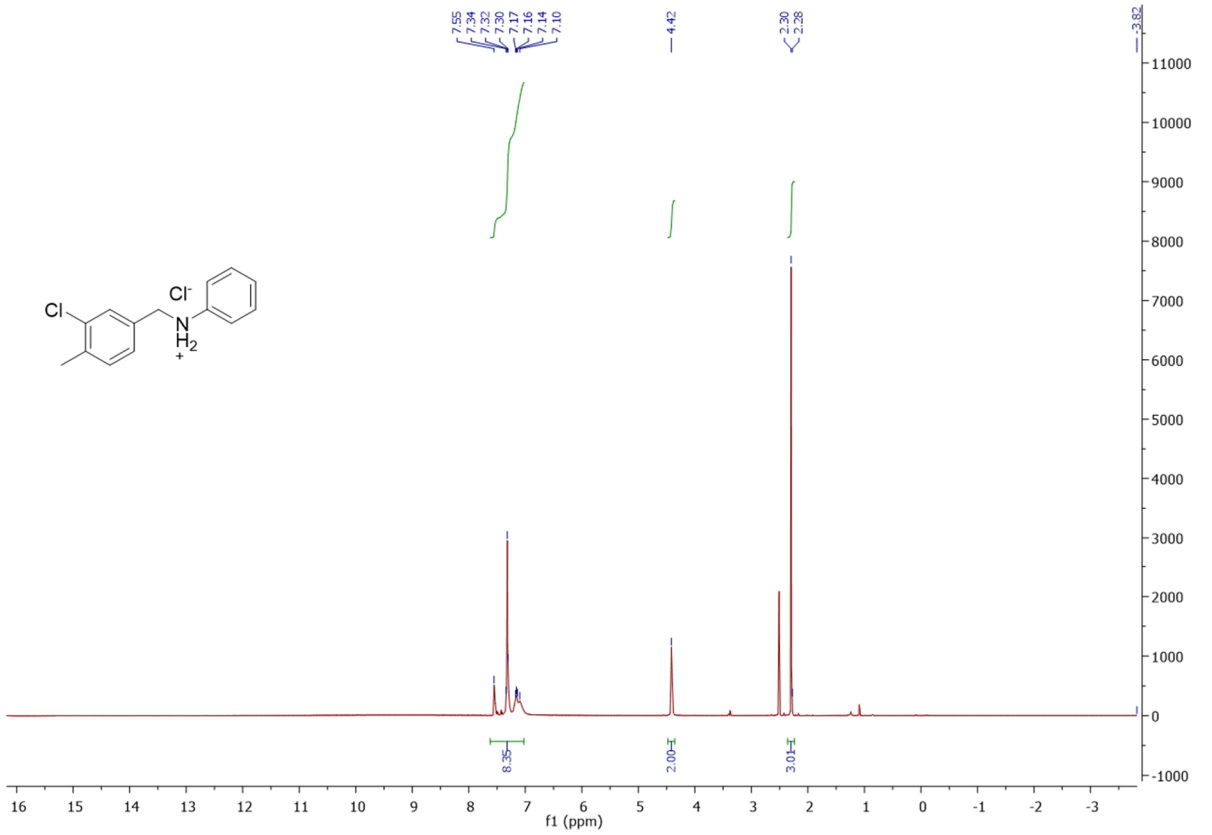
7.55
7.34
7.32
7.30
7.17
7.16
7.14
7.10
4.42
2.30
2.28
3.82
Cl
Cl⁻
N
H2
+
8.35
2.00
3.01
f1 (ppm)

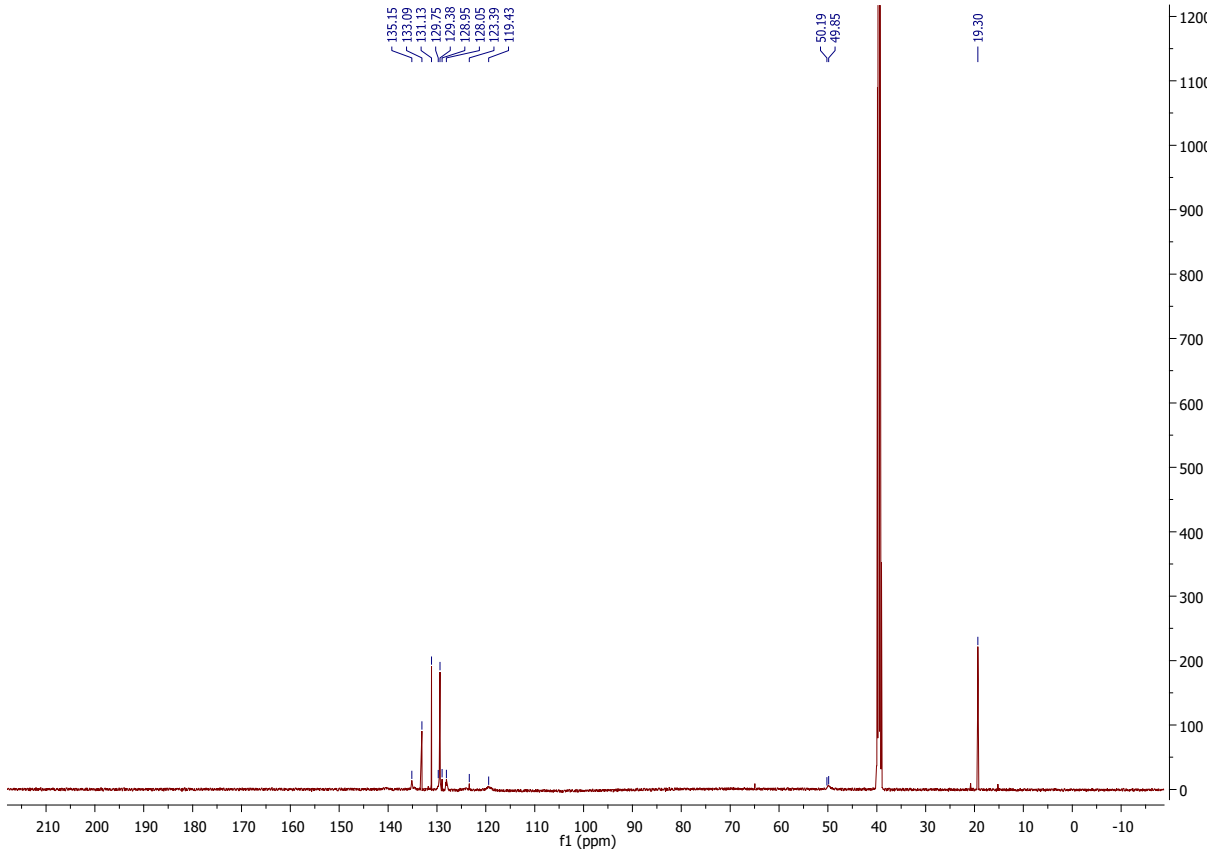
135.15
133.09
131.13
129.75
129.38
128.95
128.05
123.39
119.43
50.19
49.85
19.30
f1 (ppm)

Author Contributions

Matthias Elfinger carried out the catalyst synthesis, catalytic reactions and catalyst characterization. Marie Bergmann carried out some substrate syntheses. Matthias Elfinger and Rhett Kempe co-wrote the manuscript.

6 General Synthesis of Alkyl Amines via Borrowing Hydrogen and Reductive Amination

Matthias Elfinger, Christof Bauer, Jörg Schmauch, Michael Moritz, Christoph Wichmann, Christian Papp, Rhett Kempe

General Synthesis of Alkyl Amines via Borrowing Hydrogen and Reductive Amination

Adv. Synth. Catal. **2023**, *365*, 4654-4661

Copyright Wiley-VCH GmbH.
Reproduced with permission (https://creativecommons.org/licences/by/4.0/).

RESEARCH ARTICLE doi.org/10.1002/adsc.202301179

General Synthesis of Alkyl Amines via Borrowing Hydrogen and Reductive Amination

Matthias Elfinger,[a] Christof Bauer,[a] Jörg Schmauch,[b] Michael Moritz,[c] Christoph Wichmann,[c, d] Christian Papp,[c] and Rhett Kempe[a,*]

[a] Inorganic Chemistry II – Catalyst Design, Sustainable Chemistry Centre
University of Bayreuth
95440 Bayreuth, Germany
E-mail: kempe@uni-bayreuth.de
[b] Department of Experimental Physics
Saarland University, Campus D2 2
66123 Saarbrücken, Germany
[c] Department of Physical Chemistry II
Friedrich-Alexander-University Erlangen-Nürnberg
91058 Erlangen, Germany
[d] Department of Physical and Theoretical Chemistry
Free University of Berlin
14195 Berlin, Germany

Manuscript received: October 16, 2023; Revised manuscript received: October 30, 2023;
Version of record online: November 21, 2023

Supporting information for this article is available on the WWW under https://doi.org/10.1002/adsc.202301179

© 2023 The Authors. Advanced Synthesis & Catalysis published by Wiley-VCH GmbH. This is an open access article under the terms of the Creative Commons Attribution License, which permits use, distribution and reproduction in any medium, provided the original work is properly cited.

Abstract: Amines are a very important class of compounds and the selective synthesis of differently substituted primary, secondary and tertiary alkyl amines is challenging. Here we present the synthesis of primary, secondary, and tertiary alkyl amines from ammonia and alcohols, aldehydes, ketones and hydrogen by combining borrowing hydrogen or hydrogen autotransfer and reductive amination with hydrogen. The key is a nanostructured, bimetallic Co/Sc catalyst able to mediate both reactions or concepts efficiently. We observe a broad product scope, a very good functional group tolerance, upscaling is easily accomplished and our catalyst is reusable.

Keywords: amines; borrowing hydrogen; cobalt; reductive amination; scandium

Introduction

Amines are one of the most important classes of chemical compounds and are present in many bulk and fine chemicals,[1] drugs,[2] agro chemicals and materials.[3] The selective synthesis of differently substituted primary, secondary and tertiary alkyl amines is especially challenging since the alkylated product amine is a better nucleophile and more reactive than the amine or ammonia starting material. Two broadly applied and green or sustainable and selective methods have been developed a century ago namely the reductive amination[4] (Scheme 1A) introduced by Mignonac in 1921[5] and the borrowing hydrogen[6] or the hydrogen auto-transfer[7] (BH HA) concepts[8] (Scheme 1B) introduced by Winans and Adkins in 1932.[9] Both methods have strengths and weaknesses in comparison to each other. The BH HA approach is highly selective in the first alkylation step while an already alkylated primary or secondary amine is challenging to be modified. The reductive amination is rather unselective in the primary alkylation step if ammonia is employed but selective and efficient regarding the introduction of an already alkylated

© 2023 The Authors. Advanced Synthesis & Catalysis published by Wiley-VCH GmbH

RESEARCH ARTICLE asc.wiley-vch.de Advanced Synthesis & Catalysis

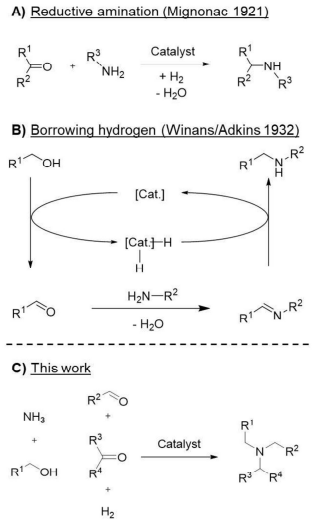

Scheme 1. Combination of reductive amination employing hydrogen (A) and borrowing hydrogen (B) permits the general synthesis of alkyl amines (C).

amine. We concluded that a catalyst mediating both reactions would permit to use the one or the other reaction or concept if they are strong and could give rise to a general catalytic access to primary, secondary, and tertiary alkyl amines. We have introduced the first Co[10] and Cr[11] catalyst for BH HA and highly efficient and selective nanostructured catalysts for the synthesis of primary amines via reductive amination employing hydrogen.[12,13] A nanostructured Co catalyst for the synthesis of alkyl amines via BH HA has been introduced by Beller and Jagadeesh and coworkers recently.[14] No potential use of that catalyst in reductive amination employing hydrogen has been reported. Furthermore, nanostructured Co catalysts for the general synthesis of primary alkyl amines via reductive amination from carbonyl compounds and ammonia employing hydrogen as the reducing agent have been disclosed.[13,15] Here, the potential use as catalysts in BH HA based amine alkylation has not been disclosed. Furthermore, Beller and Jagadeesh and coworkers introduced a general alkyl amine synthesis namely the nickel mediated hydrogenative coupling of nitriles and amines recently.[16] We report here on the synthesis of primary, secondary, and tertiary alkyl amines from ammonia and alcohols, aldehydes, and ketones with hydrogen as a reducing agent for the amination step (Scheme 1C). The key is a nanostructured, bimetallic Co/Sc catalyst able to mediate BH HA and reductive amination with hydrogen efficiently. Our catalyst is based on 3d metals with a high abundancy in the earth's crust with Sc being more abundant than Co.[17] Our catalyst is easy to synthesize and based on a N-doped and Si-doped porous carbon support developed by us.[18] While numerous catalysts that mediate reductive amination employing hydrogen or borrowing hydrogen-based amine alkylation are known, the combination of both approaches seems not been reported yet. We observe a broad product scope, a very good functional group tolerance, upscaling is easily accomplished and our catalyst is reusable.

Results and Discussion

Catalyst Synthesis and Characterization

The synthesis of the catalyst support follows an already published procedure, based on the crosslinking of the commercially available polycarbosilane precursor SMP-10 and acrylonitrile applying azobisisobutyronitrile as an initiator.[13,18] The resulting greenbody was pyrolyzed at 1000 °C under nitrogen atmosphere (see Supporting Information 2.1). By means of this process a microphase separated, silicon rich NC-material is created. To obtain the final N–SiC support material, an activation step is required. By treatment with 1 M NaOH at 85 °C overnight, a significant percentage of the Si rich domains are washed out and thus creating free C–N–H_x groups.[13] The metal nanoparticles could be introduced via wet impregnation of the N–SiC support and the two metal salts $Co(NO_3)_2 \cdot 6\ H_2O$ and $Sc(NO_3)_3 \cdot 5\ H_2O$ in water, pyrolysis (700 °C, N_2) and subsequent reduction (550 °C, N_2/H_2). The measured metal content, identified via inductively coupled plasma optical emission spectroscopy (ICP-OES) analysis, showed no significant deviation from the theoretical metal content of 2 wt% for Sc and Co. Scanning transmission electron microscopy in combination with high-angle annular dark-field imaging (HAADF-STEM) analysis (Figure 1A and B) revealed homogeneously distributed Co nanoparticles with an average particle size of 13.9 nm. In combination with electron energy loss spectroscopy (EELS, Figure 1C), the STEM analysis could also show that the scandium particles are smaller by orders of magnitude than the cobalt ones with the former finely distributed over the support material. Scanning electron microscopy (SEM) in combination with energy dispersive X-ray spectroscopy (EDX) also confirmed the homogeneously distributed cobalt nanoparticles and revealed, that the remaining silicon, which was not removed from the support material, is allocated in the same way as the scandium particles (see Supporting Information Figure S2). To further explore the nature of our catalyst material, X-ray Photoelectron Spectroscopy (XPS) was performed. The spectra of the support without metal particles (black) and the metal particles on the support (green) are shown in Figure 2. In Figure 2A, a wide

© 2023 The Authors. Advanced Synthesis & Catalysis published by Wiley-VCH GmbH

16154169, 2023, 24, Downloaded from https://onlinelibrary.wiley.com/doi/10.1002/adsc.202301179 by CochraneAustria, Wiley Online Library on [10/03/2024]. See the Terms and Conditions (https://onlinelibrary.wiley.com/terms-and-conditions) on Wiley Online Library for rules of use; OA articles are governed by the applicable Creative Commons License

RESEARCH ARTICLE asc.wiley-vch.de Advanced Synthesis & Catalysis

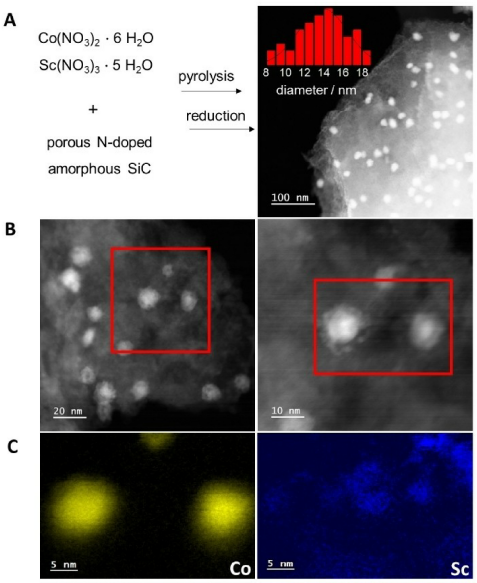

Figure 1. Synthesis and characterization of the Co catalyst: (**A**) Synthesis of the crosslinked material, followed by pyrolysis and NaOH treatment to obtain the support material; wet impregnation, pyrolysis and reduction led to the active Co/Sc catalyst. (**B**) HAADF-STEM analysis of the nanoparticles combined with STEM-EELS analysis (**C**) revealed the size difference of cobalt and scandium particles with the latter being significantly smaller and finely distributed over the support material.

scan with the expected signals for both, the support material (Si 2p, N 1s, C 1s, O 1s) and the supported catalyst particles (Si 2p, C 1s, O 1s, Sc 2p, Co 2p) and carbon and oxygen impurities, are shown. Additional ghost signals, originating from Ga Lα radiation and shifted by 155.7 eV, are marked with a "*". In Figure 2B, the Co $2p_{3/2}$ region is shown. For the support, as expected, no signals are visible. For the supported Sc/Co catalyst, a broad signal arises at 780 eV. Two binding energies at 780.6 and 786.4 eV for Co oxides and their shake-ups, respectively, are indicated.[19] The splitting is characteristic for Co_2O_3 and/or $Co(OH)_2$. Additionally, a third energy at 777.3 eV for metallic Co is indicated.[17,20] The binding energies suggest that the surface Co is oxidized. The Sc 2s region is shown in Figure 2C. A single species with a binding energy of 501.1 eV is found, indicating oxidized Sc when considering the literature binding energy for metallic Sc of 499 eV.[18] Comparing the corrected signal areas of the Co 2p and the Sc 2s region, the amount of Sc detected by XPS is 10 times higher than that of Co (9.6 : 1.3 at%, Sc : Co), albeit the same concentration is expected from ICP-OES results. Because of the high surface sensitivity of XPS and additional information from microscopy; we conclude that Sc is finely dispersed on the outer layer, while Co is present as or inside of bigger particles. We assume that the close proximity of the Co and Sc oxide centres are beneficial for the combination of (de)hydrogenation and condensation steps needed in both catalytic reactions - reductive amination and BH HA.

Optimization of the Reaction Conditions

To determine the optimal reaction conditions, the BH HA reaction of benzyl alcohol with gaseous ammonia has been selected as a benchmark for all screenings (see Supporting Information 2.4). The solvent screening revealed that toluene was the most suitable. The toluene amount was set to 2.0 mL since this delivered the maximum yield of benzyl amine. Furthermore, potassium hydroxide in equimolar amounts as well as a temperature of 160 °C were determined. The ammonia pressure was kept at 20 bar. For the comparison to other catalysts, the rare earth metal was varied (Table 1). It could be shown that the selectivity of the catalyst is higher the smaller the used rare earth metal is, which led us to Sc as the most active. Neither Co nor Sc as monometallic catalysts could deliver the

Table 1. Catalyst Screening.[a]

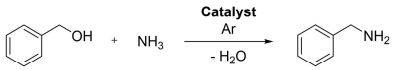

Entry	Metal(s)	Support	Yield/%
1	Co/La	N–SiC	5
2	Co/Gd	N–SiC	9
3	Co/Lu	N–SiC	54
4	**Co/Sc**	**N–SiC**	**99**
5	Fe/Sc	N–SiC	7
6	Ni/Sc	N–SiC	33
7[b]	Fe	N–SiC	0
8[b]	Ni	N–SiC	12
9[b]	Co	N–SiC	16
10[b]	Sc	N–SiC	32
11	Co/Sc	Activated C	67
12	Co/Sc	Al_2O_3	2
13	Co/Sc	TiO_2	0
14	Co/Sc	SiO_2	0
15	–	N–SiC	0

[a] Reaction conditions: 1.5 mol% Co/Fe/Ni, 0.85 mol% La, 0.74 mol% Gd, 0.66 mol% Lu, 0.49 mol% Sc, pyrolyzed at 700 °C, 0.5 mmol benzyl alcohol, 2.0 mL toluene, 0.5 mmol KOH, 160 °C, 44 h, 20 bar NH_3. Yields were determined by GC using *n*-dodecane as an internal standard.
[b] 1.5 mol% Fe/Ni/Co/Sc.

© 2023 The Authors. Advanced Synthesis & Catalysis published by Wiley-VCH GmbH

16154169, 2023, 24, Downloaded from https://onlinelibrary.wiley.com/doi/10.1002/adsc.202301179 by CochraneAustria, Wiley Online Library on [10/03/2024]. See the Terms and Conditions (https://onlinelibrary.wiley.com/terms-and-conditions) on Wiley Online Library for rules of use; OA articles are governed by the applicable Creative Commons License

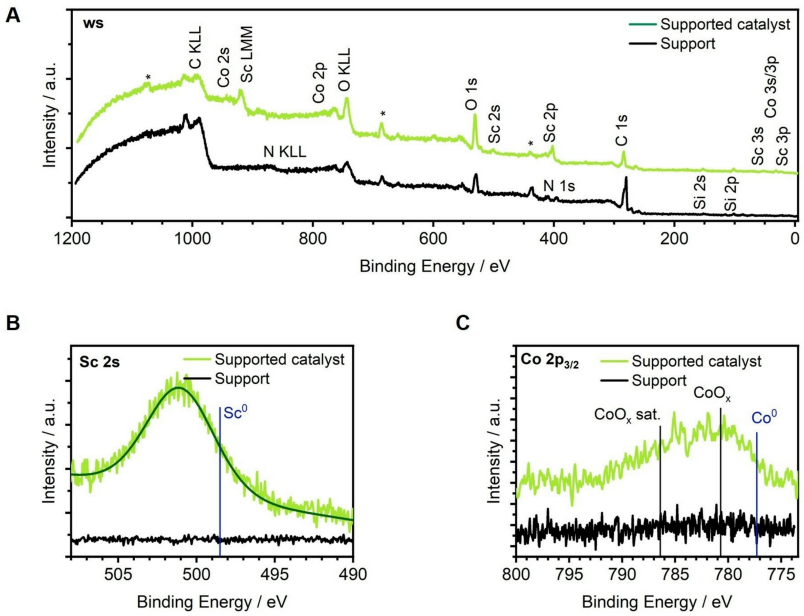

Figure 2. XPS spectra: (**A**) wide scan (ghost peaks from Ga Lα excitation (*)), (**B**) Co 2p, (**C**) Sc 2s.

outstanding activity of the bimetallic material. The variation of the support material revealed that only activated carbon could show a decent activity while Al_2O_3, TiO_2, SiO_2 and N–SiC without a metal loading indicated little to no conversion of benzyl alcohol. The superiority of the N–SiC material as a catalyst support is based on its unique structure with free C–N–H_x functionalities and an Si coating.[13]

Substrate Scope

After the optimized reaction conditions have been determined, we became interested in the applicability of our catalyst system and investigated the substrate scope. The product yields are given for the isolated corresponding hydrochloride salts of the synthesized amines. For better clarity, we split the substrate scope in three parts, one for primary, secondary, and tertiary amines each. First, we wanted to show that the catalyst permits the synthesis of different primary amines (Scheme 2). We discovered that as soon as the aromatic ring of the benzyl alcohol derivate was substituted, we had to raise the reaction temperature from 160 to 180 °C. With that done, several electron donating substituents in various ring positions (products **2**–**5**) as well as electron withdrawing substituents (**6**, **7**) could be tolerated. Unfortunately, there is too much steric hindrance to the reaction if the CF_3 group is placed in the ortho position. NO_2, CN and $CONR_2$ groups were also not tolerated due to numerous side reactions. A second amine function within the alcohol did not pose any problem (**8**). To further show the applicability of our catalyst we synthesized two completely aliphatic amines (products **9** and **10**) from ketones like we did in our previous work with a single metal Co/N–SiC catalyst employed in the reductive amination.[13] The conversion of three biologically active molecules (**11**–**13**) could also be accomplished. As it can be seen, the bimetallic CoSc/N–SiC catalyst could also mediate the reductive amination of these ketones with aqueous ammonia. Next, we explored the synthesis of secondary amines. Since we already showed above that the catalyst can permit the reductive amination of carbonyl compounds, we combined borrowing hydrogen and reductive amination as a consecutive reaction to give rise to more complex amine structures. The same catalyst is reused for the second step and beside neutralization, 0.8 mmol carbonyl compound was added (Scheme 3). The reductive amination part then proceeds at 100 °C and 40 bars of hydrogen pressure. Under these conditions, short, medium and long aliphatic moieties could be introduced (Scheme 3, substrates **14**–**16**). The presence of a terminal hydroxy group on the carbonyl compound

© 2023 The Authors. Advanced Synthesis & Catalysis published by Wiley-VCH GmbH

16154169, 2023, 24, Downloaded from https://onlinelibrary.wiley.com/doi/10.1002/adsc.202301179 by CochraneAustria, Wiley Online Library on [10/03/2024]. See the Terms and Conditions (https://onlinelibrary.wiley.com/terms-and-conditions) on Wiley Online Library for rules of use; OA articles are governed by the applicable Creative Commons License

RESEARCH ARTICLE asc.wiley-vch.de Advanced Synthesis & Catalysis

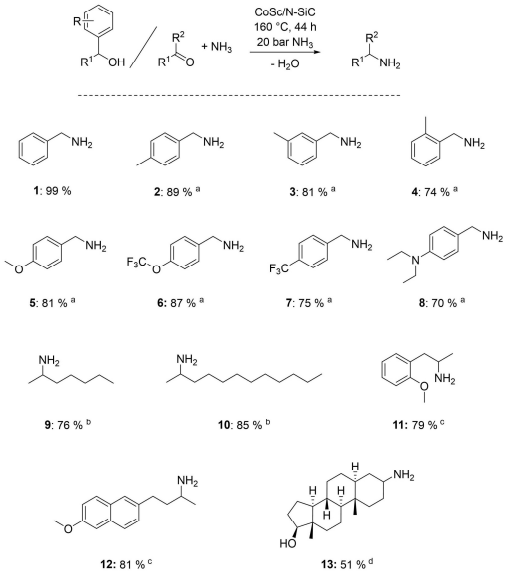

Scheme 2. Synthesis of primary amines employing a Co/Sc-catalyst. Isolated yields of the converted hydrochloride salts. Reaction conditions: 1.5 mol% Co, 0.49 mol% Sc, 0.5 mmol alcohol, 2.0 mL toluene, 0.5 mmol KOH, 160 °C, 44 h, 20 bar NH_3. [a] 180 °C. [b] 0.5 mmol ketone, 50 °C, 20 h, 10 bar H_2, 3.5 mL aq. NH_3 32%. [c] 0.5 mmol ketone, 60 °C, 20 h, 15 bar H_2, 3.5 mL aq. NH_3 32%. [d] 0.25 mmol ketone, 65 °C, 20 h, 15 bar H_2, 3.2 mL aq. NH_3 32%, 0.3 mL EtOH.

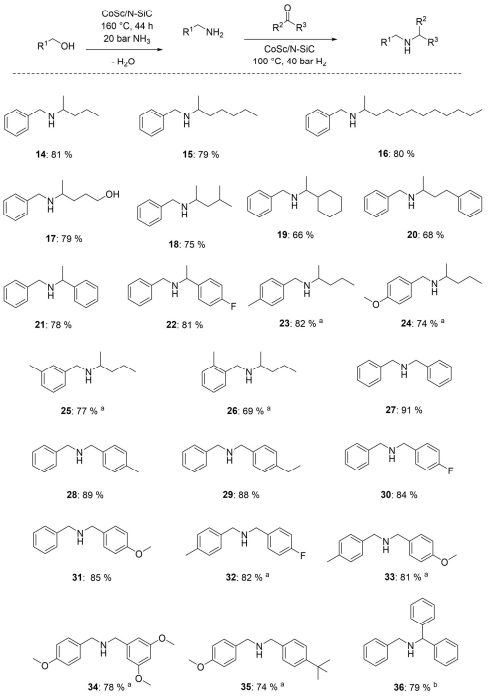

Scheme 3. One pot synthesis of secondary amines employing a Co/Sc-catalyst. Isolated yields of the converted hydrochloride salts. Reaction conditions for first step: 1.5 mol% Co, 0.49 mol% Sc, 0.5 mmol alcohol, 2.0 mL toluene, 0.5 mmol KOH, 160 °C, 44 h, 20 bar NH_3. [a] 180 °C. Reaction conditions for second step: 1.5 mol% Co, 0.49 mol% Sc, 0.8 mmol carbonyl compound, 2.0 mL toluene, 100 °C, 20 h, 40 bar H_2, 0.05 mL 32% HCl. [b] 150 °C.

did not present any difficulties for our catalyst (**17**). Even double branched (**18**) or alicyclic ketones (**19**) could be tolerated in good to median yields. Combining an aliphatic part with a terminal aromatic ring led to substrate **20**. Furthermore, acetophenone and its fluoro-substituted derivative could be employed in the reductive amination step (**21** and **22**). Note that the difficulty to introduce halogenide substituted educts in the borrowing hydrogen step due to dehalogenation under these harsh conditions could thus be compensated. When varying the benzyl alcohol side of the amine (**23**–**26**), the temperature had to be raised to 180 °C again. Hence, a methyl group in all ring positions as well as a methoxy group could be tolerated. Moving forward, we switched the carbonyl compound of the reductive amination step from ketones to aldehydes. Besides dibenzyl amine (**27**), its methyl- (**28**), ethyl- (**29**), fluoro- (**30**) and methoxy-substituted (**31**) derivatives could be synthesized with very good yields. Varying both sides was also possible at 180 °C for the first step and gave rise to multiple products (**32**–**35**) with small to more bulkier substituents. Lastly, the addition of benzophenone as an educt could also be accomplished by increasing the temperature of the second step from 100 to 150 °C (**36**). To complete our work, we studied the synthesis of (differently substituted) tertiary amines, which presented a major challenge overall. For the synthesis of tertiary amines with three benzylic alkyl substituents (Scheme 4, upper half), we extended our consecutive synthesis by a third step, which involves the addition of 1.0 mmol of a further aldehyde as well as an increase in temperature to 140 °C. The addition of 0.05 mL concentrated hydrochloric acid was necessary since it supports the tertiary imine formation of the secondary amine with the aldehyde. Utilizing this three-step synthesis protocol we were able to synthesize three tertiary amines with one, two and three different moieties in good to very good yields (**37**–**39**). Next, we established a workaround approach (Scheme 4, lower half). For the borrowing hydrogen

© 2023 The Authors. Advanced Synthesis & Catalysis published by Wiley-VCH GmbH

16154169, 2023, 24, Downloaded from https://onlinelibrary.wiley.com/doi/10.1002/adsc.202301179 by CochraneAustria, Wiley Online Library on [10/03/2024]. See the Terms and Conditions (https://onlinelibrary.wiley.com/terms-and-conditions) on Wiley Online Library for rules of use; OA articles are governed by the applicable Creative Commons License

RESEARCH ARTICLE asc.wiley-vch.de Advanced Synthesis & Catalysis

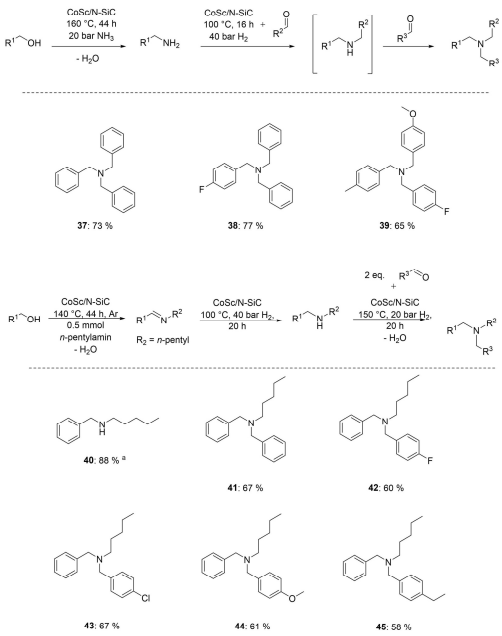

Scheme 4. One pot synthesis of tertiary amines employing a Co/Sc-catalyst. Isolated yields of the converted hydrochloride salts. Substrates 37–39: Reaction conditions for first step: 1.5 mol% Co, 0.49 mol% Sc, 0.5 mmol alcohol, 2.0 mL toluene, 0.5 mmol KOH, 160 °C, 44 h, 20 bar NH_3. Reaction conditions for second step: 1.5 mol% Co, 0.49 mol% Sc, 0.8 mmol aldehyde, 2.0 mL toluene, 100 °C, 20 h, 40 bar H_2, 0.05 mL 32% HCl. Reaction conditions for third step: 1.5 mol% Co, 0.49 mol% Sc, 1.0 mmol aldehyde, 2.0 mL toluene, 140 °C, 20 h, 40 bar H_2, 0.05 mL 32% HCl. Substrates 40–45: Reaction conditions for first step: 2.0 mol% Co, 0.65 mol% Sc, 0.5 mmol alcohol, 0.5 mmol *n*-pentylamine, 2.0 mL toluene, 0.5 mmol KOH, 140 °C, 44 h, Ar atmosphere. Reaction conditions for second step: 2.0 mol% Co, 0.65 mol% Sc, 2.0 mL toluene, 100 °C, 20 h, 40 bar H_2. Reaction conditions for third step: 2.0 mol% Co, 0.65 mol% Sc, 1.0 mmol aldehyde, 2.0 mL toluene, 150 °C, 20 h, 20 bar H_2, 0.05 mL 32% HCl. [a] Product isolated after second step.

step we switched the gaseous ammonia with *n*-pentylamine. By increasing the catalyst loading to 2.0 mol% Co and lowering the temperature to 140 °C under argon atmosphere, the catalyst was able to generate the imine, but not to hydrogenate it further to the corresponding amine. Thus, we had to implement an extra hydrogenation step by applying 40 bars of hydrogen pressure at 100 °C for 20 h, which led to the desired product (**40**). By then adding 1.0 mmol aldehyde and 0.05 mL of concentrated hydrochloric acid as well as slightly adjusting the reaction conditions (150 °C, 20 bar H_2), five more tertiary amines could be isolated (**41**–**45**) with products **39** and **42**–**45** not yet known to literature. Unfortunately, the synthesis of tertiary alkyl amines carrying one branched alkyl substituent (resulting from a ketone educt) failed due to steric overloading. For the synthesis of such secondary alkyl amines, see Scheme 3. Although our reaction protocol alone confirms the reusability of our bimetallic catalyst system, we investigated it further for five consecutive runs of the first reaction step - the borrowing hydrogen reaction of our model substrate benzyl alcohol. Five consecutive runs without any loss of activity could be accomplished (see Supporting Information 2.4.3). Furthermore, we confirmed the upscaling capabilities of our catalyst by carrying out the above reaction and the consecutive reductive amination to give rise to product **14** (Scheme 3) again - but this time with ten times the amount of all compounds involved. This led to 76% yield of the isolated product (see Supporting Information 2.4.4). Finally, a hot filtration test was performed and the filtrate did not show any catalytic activity (see Supporting Information 2.4.5). In addition, competition experiments have been conducted for BH HA and the reductive amination (see Supporting Information 2.4.6).

Conclusion

In conclusion, we report on the synthesis of primary, secondary, and tertiary alkyl amines combining the borrowing hydrogen or hydrogen auto-transfer concept and the concept of reductive amination employing hydrogen. We use green or sustainable starting materials namely ammonia and alcohols or aldehydes and ketones and hydrogen for our amine synthesis. The key is a nanostructured, bimetallic Co/Sc catalyst able to mediate both reactions or concepts. Both metals are of high abundance in the Earth's crust with Sc being the more abundant 3d metal. We observe a broad product scope with five examples not known to literature yet, a very good functional group tolerance, upscaling is easily accomplished and our catalyst is reusable.

Experimental Section

Synthesis of the Support Material

For the preparation of the N–SiC support material 0.200 g SMP-10 (StarPCS™), 0.987 mL (0.800 g, 15.08 mmol) acrylonitrile and 45 mg (0.28 mmol) azobis(isobutyronitrile) were dissolved in 4 mL dimethylformamide and crosslinked for 16 h at 75 °C. After solvent removal under reduced pressure, the obtained greenbody was pyrolyzed at 1000 °C under nitrogen flow. After ball mining for 40 min, 0.400 g of the ceramic were washed by stirring in solution of 5.3 mL aq. NaOH (1 M) and 4 mL MeOH at 85 °C for 24 h. Afterwards the material was washed until neutrality and dried at room temperature.

© 2023 The Authors. Advanced Synthesis & Catalysis published by Wiley-VCH GmbH

16154169, 2023, 24, Downloaded from https://onlinelibrary.wiley.com/doi/10.1002/adsc.202301179 by CochraneAustria, Wiley Online Library on [10/03/2024]. See the Terms and Conditions (https://onlinelibrary.wiley.com/terms-and-conditions) on Wiley Online Library for rules of use; OA articles are governed by the applicable Creative Commons License

RESEARCH ARTICLE asc.wiley-vch.de Advanced Synthesis & Catalysis

Synthesis of the Catalyst

1000 mg N–SiC were impregnated with 98.75 mg $Co(NO_3)_2 \cdot 6 H_2O$ and 143 mg $Sc(NO_3)_2 \cdot 5 H_2O$ in 20 mL H_2O and stirred at 110 °C until the solvent was completely removed. Afterwards, the material was pyrolyzed at 700 °C under nitrogen atmosphere and reduced at 550 °C under forming gas (90:10, N_2:H_2).

Catalytic Procedures

The first step of the catalytic reaction (borrowing hydrogen/hydrogen autotransfer) of benzyl alcohol and its derivates was carried out after the procedure described in the following: A magnetic stirring bar, 0.5 mmol alcohol, 2.0 mL toluene (freeze pumped), 0.5 mmol KOH (28 mg) and 28.8 mg of cobalt/scandium-catalyst (2.0 wt% Co, 1.5 mol% Co, 0.58 mg Co, 2.0 wt% Sc, 0.49 mol% Sc, 0.58 mg Sc) were placed directly into a 130 mL high pressure autoclave (Parr Instruments) and flushed with argon for 10 seconds. The autoclave was placed in a liquid nitrogen bath for 5 min whereafter gaseous ammonia was condensed inside for 5 s. The autoclave was then heated to the desired temperature and the reaction was stirred for 44 h. After cooling to room temperature and release of the ammonia pressure, the autoclave was opened and 0.8 mmol of the carbonyl compound as well as one drop of concentrated hydrochloric acid for the neutralization of the remaining ammonia was added. The autoclave was then flushed three times with 10 bars of H_2, pressurized with 40 bars of H_2 and heated to 100 °C for 20 h. In case of the synthesis of tertiary amines, the autoclave was opened again after cooldown and pressure release and 1.0 mmol of aldehyde as well as one drop of concentrated hydrochloric acid were added. The autoclave was flushed again three times with 10 bars of H_2, pressurized with 20 bars of H_2 and heated to 140 °C. To obtain the amine hydrochloride salts, the remaining solution was filtrated into a round bottom flask to remove the catalyst. After the addition of 30 mL of diethyl ether and 0.5 mL HCl in ether (2 M) the precipitate was filtrated, dried under reduced pressure and the resulting solid was then further analyzed by NMR spectroscopy. This was carried out after every step from which the product should be obtained for characterization. For the synthesis of amines with a non-branched aliphatic moiety a slightly different method was used. For the first step, a magnetic stirring bar, 0.5 mmol benzyl alcohol or its derivates and 0.5 mmol of *n*-pentylamine together with 0.5 mmol of KOH (28 mg), 2 mL of freeze pumped toluene and 38.4 mg of cobalt/scandium-catalyst (2.0 wt% Co, 2.0 mol% Co, 0.77 mg Co, 2.0 wt% Sc, 0.65 mol% Sc, 0.77 mg Sc) were placed inside a pressure tube and flushed with argon. The tube was heated to 140 °C for 44 h. After cooling, the whole content was transferred to an autoclave, flushed with 10 bars of H_2 three times and pressurized with 40 bars of H_2 to hydrogenate the remaining double bond. After cooldown, 1.0 mmol of aldehyde as well as one drop of concentrated hydrochloric acid were added. The autoclave was flushed with 10 bars of H_2 three times, pressurized with 20 bars of H_2 and heated to 150 °C for 20 h. To obtain the amine hydrochloride salts, the remaining solution was filtrated into a round bottom flask to remove the catalyst. After the addition of 30 mL of diethyl ether and 0.5 mL HCl in ether (2 M) the precipitate was filtrated, dried under reduced pressure and the resulting solid was then further analyzed by NMR spectroscopy.

Acknowledgements

R. Kempe thanks the DFG for financial support: KE 756/34-1. M. Moritz, C. Wichmann and C. Papp acknowledge the SFB 1452 CLINT from the DFG for financial support and we thank C. Denner for SEM/EDX measurements. J. Schmauch thanks the Leibniz Institute for New Materials, Saarbrücken, for the access to the Jeol ARM200 STEM. Open Access funding enabled and organized by Projekt DEAL.

References

[1] H.-J. Arpe, *Industrial organic chemistry*, Wiley-VCH, Weinheim, **2010**.
[2] R. Vardanyan, V. Hruby, *Synthesis of best-seller drugs*, Academic Press, London, **2016**.
[3] S. A. Lawrence, *Amines. Synthesis, properties, and applications*, Cambridge University Press, Cambridge, **2004**.
[4] a) T. Irrgang, R. Kempe, *Chem. Rev.* **2020**, *120*, 9583; b) K. Murugesan, T. Senthamarai, V. G. Chandrashekhar, K. Natte, P. C. J. Kamer, M. Beller, R. V. Jagadeesh, *Chem. Soc. Rev.* **2020**, *49*, 6273.
[5] G. Mignonac, *Compt. Rend.* **1921**, *172*, 223–226.
[6] A. J. A. Watson, J. M. J. Williams, *Science* **2010**, *329*, 635.
[7] G. Guillena, D. J. Ramón, M. Yus, *Chem. Rev.* **2010**, *110*, 1611.
[8] a) A. Corma, J. Navas, M. J. Sabater, *Chem. Rev.* **2018**, *118*, 1410; b) T. Irrgang, R. Kempe, *Chem. Rev.* **2019**, *119*, 2524.
[9] C. F. Winans, H. Adkins, *J. Am. Chem. Soc.* **1932**, *54*, 306.
[10] S. Rösler, M. Ertl, T. Irrgang, R. Kempe, *Angew. Chem. Int. Ed.* **2015**, *54*, 15046.
[11] F. Kallmeier, R. Fertig, T. Irrgang, R. Kempe, *Angew. Chem. Int. Ed.* **2020**, *59*, 11789.
[12] a) G. Hahn, P. Kunnas, N. de Jonge, R. Kempe, *Nat. Catal.* **2019**, *2*, 71; b) C. Bäumler, C. Bauer, R. Kempe, *ChemSusChem* **2020**, *13*, 3110.
[13] M. Elfinger, T. Schönauer, S. L. J. Thomä, R. Stäglich, M. Drechsler, M. Zobel, J. Senker, R. Kempe, *ChemSusChem* **2021**, *14*, 2360.
[14] a) Z. Ma, B. Zhou, X. Li, R. G. Kadam, M. B. Gawande, M. Petr, R. Zbořil, M. Beller, R. V. Jagadeesh, *Chem. Sci.* **2022**, *13*, 111.
[15] a) R. V. Jagadeesh, K. Murugesan, A. S. Alshammari, H. Neumann, M.-M. Pohl, J. Radnik, M. Beller, *Science* **2017**, *358*, 326–332; b) B. Zheng, J. Xu, J. Song, H. Wu, X. Mei, K. Zhang, W. Han, W. Wu, M. He, B. Han, *Chem. Sci.* **2022**, *13*, 9047; c) M. Sheng, S. Fujita, S. Yamaguchi, J. Yamasaki, K. Nakajima, S. Yamazoe, T. Mizugaki, T. Mitsudome, *JACS Au* **2021**, *1*, 501; d) K. Kato, D. Deng, Y. Kita, K. Kamata, M. Hara, *Catal. Sci.*

© 2023 The Authors. Advanced Synthesis & Catalysis published by Wiley-VCH GmbH

16154169, 2023, 24, Downloaded from https://onlinelibrary.wiley.com/doi/10.1002/adsc.202301179 by CochraneAustria, Wiley Online Library on [10/03/2024]. See the Terms and Conditions (https://onlinelibrary.wiley.com/terms-and-conditions) on Wiley Online Library for rules of use; OA articles are governed by the applicable Creative Commons License

Technol. **2022**, *12*, 5425; c) T. Senthamarai, V. G. Chandrashekar, M. B. Gawande, N. V. Kalevaru, R. Zboril, P. C. J. Kamer, R. V. Jagadeesh, M. Beller, *Chem. Sci.* **2020**, *11*, 2973–2981.
[16] V. G. Chandrashekhar, W. Baumann, M. Beller, R. V. Jagadeesh, *Science* **2022**, *376*, 1433.
[17] U. S. Geological Survey Fact Sheet, **2002**, 087–02.
[18] L. F. B. Ribeiro, O. Flores, P. Furtat, C. Gervais, R. Kempe, R. A. F. Machado, G. Motz, *J. Mater. Chem. A* **2017**, *5*, 720.
[19] B. J. Tan, K. J. Klabunde, P. M. A. Sherwood, *J. Am. Chem. Soc.* **1991**, *113*, 855.
[20] J. F. Moulder, J. Chastain (Eds.) *Handbook of X-ray photoelectron spectroscopy. A reference book of standard spectra for identification and interpretation of XPS data*, Perkin-Elmer Corporation, Eden Prairie, Minn., **1992**.

© 2023 The Authors. Advanced Synthesis & Catalysis published by Wiley-VCH GmbH

16154169, 2023, 24, Downloaded from https://onlinelibrary.wiley.com/doi/10.1002/adsc.202301179 by CochraneAustria, Wiley Online Library on [10/03/2024]. See the Terms and Conditions (https://onlinelibrary.wiley.com/terms-and-conditions) on Wiley Online Library for rules of use; OA articles are governed by the applicable Creative Commons License



Supporting Information

General Synthesis of Alkyl Amines via Borrowing Hydrogen and Reductive Amination

Matthias Elfinger, Christof Bauer, Jörg Schmauch, Michael Moritz, Christoph Wichmann, Christian Papp, and Rhett Kempe*© 2023 The Authors. Advanced Synthesis & Catalysis published by Wiley-VCH GmbH. This is an open access article under the terms of the Creative Commons Attribution License, which permits use, distribution and reproduction in any medium, provided the original work is properly cited.

WILEY-VCH

SUPPORTING INFORMATION

General Synthesis of Alkyl Amines via Borrowing Hydrogen and Reductive Amination

Matthias Elfinger,[a] Christof Bauer,[a] Jörg Schmauch,[b] Michael Moritz,[c] Christoph Wichmann,[c,d] Christian Papp[c] and Rhett Kempe*[a]

Abstract: Amines are a very important class of compounds and the selective synthesis of differently substituted primary, secondary and tertiary alkyl amines is challenging. We introduce here the synthesis of primary, secondary, and tertiary alkyl amines from ammonia and alcohols, aldehydes, and ketones with hydrogen as a reducing agent for the amination step. The key is a nanostructured, bimetallic Co/Sc catalyst able to mediate borrowing hydrogen or hydrogen autotransfer and reductive amination with hydrogen efficiently. We observe a broad product scope, a very good functional group tolerance, upscaling is easily accomplished and our catalyst is reusable.

WILEY-VCH

SUPPORTING INFORMATION

Table of Contents

1 General considerations ... 3

2. Experimental procedures ... 4

2.1 Synthesis of the support material ... 4

2.2. Synthesis of the catalyst ... 4

2.3 Catalytic procedures ... 4

2.4 Catalytic studies ... 6

2.4.1 Screening of reaction parameters for the Borrowing Hydrogen/Hydrogen Autotransfer step ... 6

2.4.2 Screening of reaction parameters for the Reductive Amination step ... 7

2.4.3 Reusability ... 9

2.4.5 Hot filtration test ... 10

2.4.6 Competition experiments ... 10

3. Characterization of the catalyst ... 12

3.1 ICP-OES ... 12

3.2 SEM/EDX ... 12

3.3 Argon physisorption ... 13

4. Characterization of the isolated products ... 14

5. NMR and IR spectra ... 37

6 References ... 138

Author Contributions ... 140

SUPPORTING INFORMATION

1 General considerations

All air- and moisture sensitive reactions were performed under dry argon or nitrogen atmosphere using standard Schlenk and glove box techniques. All dried solvents were obtained from a solvent purification system (activated alumina cartridges) or purchased from Acros. Deuterated solvents were dried via molecular sieves. All chemicals were acquired from commercial sources with purity over 95 % and used without further purification. The precursor SMP-10 was purchased from Starfire Systems, New York, USA. Pyrolysis of the support material was carried out under nitrogen atmosphere in a high temperature furnace (Gero, Berlin, Germany). Pyrolysis and reduction of the catalyst were performed under nitrogen or forming gas (90/10) atmosphere in a ChemBET Pulsar TPR/TPD instrument from Quantachrome. For the STEM investigations a JEOL JEM-ARM 200F with cold FEG emission gun was used equipped with a CEOS Cs corrector, a HAADF detector and a GATAN EELS spectrometer. The EELS mapping was carried out with a collecting semi-angel of 120 mrad and a dispersion of 1 ev/ch.

IR spectra were collected on a JASCO FT/IR-6100 apparatus in a measuring range from 4000-400 cm^{-1}.

Pore characterizations were carried out via argon sorption measurements using a 3P Micro 100 Surface Area and Pore Size Analyzer device. The pore size distribution was computed via DFT calculations (calculation model: Ar at -186.15 °C on cylindrical pore, MDFT equilibrium model). The specific surface area was calculated by using p/p_0 values from 0.005-0.1 (BET).

The cobalt and scandium contents was determined by ICP-OES. The fusion of the catalyst was carried out in a Berghof SpeedWave 4 microwave, for the ICP-OES measurement a Varian Vista Pro was used.

X-ray photoelectron spectroscopy measurements were conducted in a dedicated instrument described in detail elsewhere.[1] The instrument is equipped with a non-monochromatized Specs XR 50 NAP dual Al/Mg anode for X-ray generation. The spectra in this work were attained in Mg mode. A modified Omicron EA 125 hemispherical analyzer was used. The catalyst particles were glued onto vacuum copper tape and introduced to the vacuum right after opening. The data was signal to 101.9 eV.[2] For the fitting of non-metallic signals, a Gaussian-Lorentzian function was chosen (GL(30) as implemented in Casa XPS). For quantification, the intensities of the respective regions were divided by theoretically derived sensitivity factors.[3]

NMR measurements were performed using a Varian INOVA 300 (300 MHz for ^{1}H, 75 MHz for ^{13}C) or a Bruker Avance III HD 500 (500 MHz for ^{1}H, 125.7 MHz for ^{13}C, 376 MHz for ^{19}F) instruments at 296 K. Chemical shifts are reported in ppm relative to the residual solvent signal (DMSO-d6: 2.50 ppm (^{1}H), 39.51 ppm (^{13}C)), coupling constants (J) are reported in Hz. Estimated ^{1}H and ^{13}C NMR spectra were simulated (DMSO-d_6, 300 MHz) using ChemDraw Professional Version 21.0.0.28.

GC analyses were carried out on an Agilent 6850 GC system equipped with an Optima 17 column (30 m x 0.32 mm x 0.25 µm).

Unknown substrates with incomplete spectroscopic literature data were additionally analyzed via liquid chromatography high resolution mass spectra (LC-HRMS). LC-HRMS were obtained from a Thermo Fisher scientific Q-Exactive instrument with a hybrid quadrupole orbitrap analyzer in ESI+ mode.

The hydrogenation as well as ammonia experiments were carried out with Parr Instrument stainless steel autoclaves N-MT5 250 mL and 130 mL respectively equipped with heating mantle and temperature controller.

SUPPORTING INFORMATION

2. Experimental procedures

2.1 Synthesis of the support material

For the preparation of the N-SiC support material a known literature method was modified.[4] 200 mg SMP-10 (StarPCS™), 0.987 mL (0.800 g, 15.08 mmol) acrylonitrile and 45 mg (0.28 mmol) azobis(isobutyronitrile) were dissolved in 4 mL dimethylformamide and crosslinked for 16 h at 75 °C. After solvent removal under reduced pressure, the obtained greenbody was pyrolyzed using the following program:

$$20\ ^\circ\mathrm{C} \xrightarrow{5\ \mathrm{K/min}} 200\ ^\circ\mathrm{C}\ (0\ \mathrm{h}) \xrightarrow{1\ \mathrm{K/min}} 400\ ^\circ\mathrm{C}\ (0\ \mathrm{h}) \xrightarrow{5\ \mathrm{K/min}} 1000\ ^\circ\mathrm{C}\ (1\ \mathrm{h}) \xrightarrow{10\ \mathrm{K/min}} 20\ ^\circ\mathrm{C}$$

After ball mining for 40 minutes, 400 mg of the ceramic were washed by stirring in solution of 5.3 mL aq. NaOH (1 M) and 4 mL MeOH at 85 °C for 24 h. Afterwards the material was washed until neutrality and dried at room temperature.

2.2. Synthesis of the catalyst

1000 mg N-SiC were impregnated with 98,75 mg $Co(NO_3)_2 \cdot 6\ H_2O$ and 143 mg $Sc(NO_3)_2 \cdot 5\ H_2O$ in 20 mL H_2O and stirred at 110 °C until the solvent was completely removed. Afterwards, the material was pyrolyzed and reduced using the following program:

$$\mathrm{RT} \xrightarrow[N_2]{2\ \mathrm{K/min}} 300\ ^\circ\mathrm{C} \xrightarrow[N_2]{10\ \mathrm{K/min}} 700\ ^\circ\mathrm{C}\ (0.5\ \mathrm{h}) \xrightarrow[N_2]{20\ \mathrm{K/min}} 100\ ^\circ\mathrm{C} \xrightarrow[N_2/H_2]{5\ \mathrm{K/min}} 550\ ^\circ\mathrm{C}\ (3\ \mathrm{h}) \xrightarrow[N_2/H_2]{20\ \mathrm{K/min}} 40\ ^\circ\mathrm{C}$$

2.3 Catalytic procedures

The first step of the catalytic reaction (borrowing hydrogen/hydrogen autotransfer) of benzyl alcohol and its derivates was carried out after the procedure described in the following: A magnetic stirring bar, 0.5 mmol alcohol, 2.0 mL toluene (freeze pumped), 0.5 mmol KOH (28 mg) and 28.8 mg of cobalt/scandium-catalyst (2.0 wt% Co, 1.5 mol% Co, 0.58 mg Co, 2.0 wt% Sc, 0.49 mol% Sc, 0.58 mg Sc) were placed directly into a 130 mL high pressure autoclave (Parr Instruments) and flushed with argon for 10 seconds. The autoclave was placed in a liquid nitrogen bath for 5 minutes whereafter gaseous ammonia was condensed inside for 5 seconds. The autoclave was then heated to the desired temperature (160 °C for benzyl alcohol and 180 °C for derivates) and the reaction was stirred for 44 h. After cooling to room temperature and release of the ammonia pressure, the autoclave was opened and 0.8 mmol of the carbonyl compound as well as one drop of concentrated hydrochloric acid for the neutralization of the remaining ammonia was added. The autoclave was then flushed three times with 10 bars of hydrogen, pressurized with 40 bars of hydrogen and heated to 100 °C for 20 h. In case of the synthesis of tertiary amines, the autoclave was opened again after cooldown and pressure release and 1.0 mmol of aldehyde as well as one drop of concentrated hydrochloric acid were added. The autoclave was flushed again three times with 10 bars of hydrogen, pressurized with 20 bars of hydrogen and heated to 140 °C. To obtain the amine hydrochloride salts, the remaining solution was filtrated into a round bottom flask to remove the catalyst. After the addition of 30 mL of diethyl ether and 0.5 mL HCl in ether (2 M) the

precipitate was filtrated, dried under reduced pressure and the resulting solid was then further analyzed by NMR spectroscopy. This was carried out after every step from which the product should be obtained for characterization.

For the synthesis of amines with a non-branched aliphatic moiety (substrates numbers **40-45**), a slightly different method was used. For the first step, a magnetic stirring bar, 0.5 mmol benzyl alcohol or its derivates and 0.5 mmol of *n*-pentylamine together with 0.5 mmol of KOH (28 mg), 2 mL of freeze pumped toluene and 38.4 mg of cobalt/scandium-catalyst (2.0 wt% Co, 2.0 mol% Co, 0.77 mg Co, 2.0 wt% Sc, 0.65 mol% Sc, 0.77 mg Sc) were placed inside a pressure tube and flushed with argon. The tube was heated to 140 °C for 44 h. After cooling, the whole content was transferred to an autoclave (130 mL, Parr Instruments), flushed with 10 bars of hydrogen three times and pressurized with 40 bars of hydrogen to hydrogenate the remaining double bond. After cooldown, 1.0 mmol of aldehyde as well as one drop of concentrated hydrochloric acid were added. The autoclave was flushed with 10 bars of hydrogen three times, pressurized with 20 bars of hydrogen and heated to 150 °C for 20 h. To obtain the amine hydrochloride salts, the remaining solution was filtrated into a round bottom flask to remove the catalyst. After the addition of 30 mL of diethyl ether and 0.5 mL HCl in ether (2 M) the precipitate was filtrated, dried under reduced pressure and the resulting solid was then further analyzed by NMR spectroscopy.

2.4 Catalytic studies

2.4.1 Screening of reaction parameters for the Borrowing Hydrogen/Hydrogen Autotransfer step

Solvent screening of the model substrate benzyl alcohol

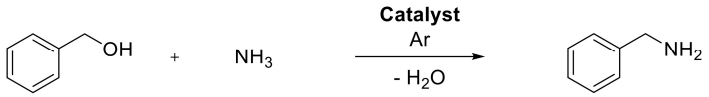

Solvent	Yield / %
Xylene	52
THF	28
Toluene	99

Reaction conditions: 0.5 mmol benzyl alcohol, 1.5 mol% cobalt; 0.49 mol% scandium, 2.0 mL solvent, 0.5 mmol KOH, 160 °C, 44 h, 20 bar NH_3. Yields determined by GC using *n*-dodecane as an internal standard.

Screening of the toluene amount

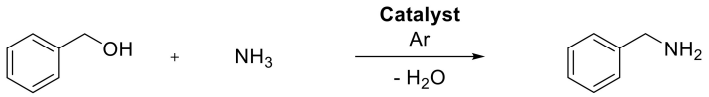

Volume toluene / mL	Yield / %
0.5	94
1	95
2	99
5	77

Reaction conditions: 0.5 mmol benzyl alcohol, 1.5 mol% cobalt; 0.49 mol% scandium, 0.5 mmol KOH, 160 °C, 44 h, 20 bar NH_3. Yields determined by GC using *n*-dodecane as an internal standard.

Base screening

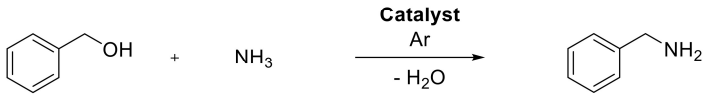

Base	Yield / %
KOtBu	64
NaOH	4
KOH	99
Amberlyst A-26	9

Reaction conditions: 0.5 mmol benzyl alcohol, 1.5 mol% cobalt; 0.49 mol% scandium, 2 mL toluene, 0.5 mmol base, 160 °C, 44 h, 20 bar NH_3. Yields determined by GC using *n*-dodecane as an internal standard.

Screening of the KOH amount

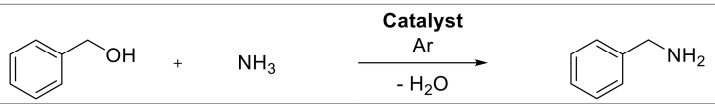

KOH amount / eq.	Yield / %
0	-
0.5	59
1	99
2	99

Reaction conditions: 0.5 mmol benzyl alcohol, 1.5 mol% cobalt; 0.49 mol% scandium, 2 mL toluene, 160 °C, 44 h, 20 bar NH_3. Yields determined by GC using *n*-dodecane as an internal standard.

Screening of the reaction temperature

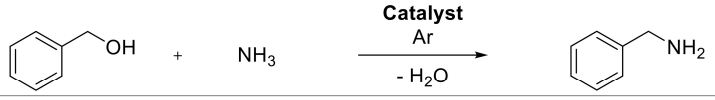

Temperature / °C	Yield / %
120	-
140	78
160	99

Reaction conditions: 0.5 mmol benzyl alcohol, 1.5 mol% cobalt; 0.49 mol% scandium, 0.5 mmol KOH, 2 mL toluene, 44 h, 20 bar NH_3. Yields determined by GC using *n*-dodecane as an internal standard.

2.4.2 Screening of reaction parameters for the Reductive Amination step

The only parameters varied here are temperature, hydrogen pressure and reaction time since all other parameters are predetermined due to the consecutive nature of the reaction. As a model substrate, the reductive amination of 2-pentanone with benzyl amine was used.

Screening of the reaction temperature

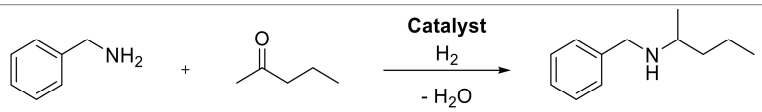

Temperature / °C	Yield / %
60	35
80	71
90	91
100	99

Reaction conditions: 1.5 mol% Co (2.24 wt% Co, 0.0075 mmol Co, 0.44 mg Co), 0.5 mmol benzyl amine; 0.8 mmol 2-pentanone, 20 h, 40 bar H_2, 2 mL toluene; yields were determined by GC using *n*-dodecane as an internal standard.

SUPPORTING INFORMATION

Screening of the hydrogen pressure

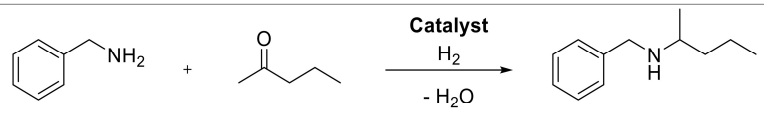

H_2 pressure / °bar	Yield / %
20	53
30	84
40	99

Reaction conditions: 1.5 mol% Co (2.24 wt% Co, 0.0075 mmol Co, 0.44 mg Co), 0.5 mmol benzyl amine; 0.8 mmol 2-pentanone, 100 °C, 20 h, 2 mL toluene; yields were determined by GC using *n*-dodecane as an internal standard.

Screening of the reaction time

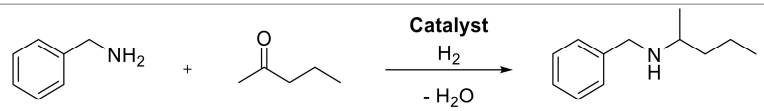

Reaction time / h	Yield / %
16	92
20	99

Reaction conditions: 1.5 mol% Co (2.24 wt% Co, 0.0075 mmol Co, 0.44 mg Co), 0.5 mmol benzyl amine; 0.8 mmol 2-pentanone, 100 °C, 40 bar H_2, 2 mL toluene; yields were determined by GC using *n*-dodecane as an internal standard.

2.4.3 Reusability

The reusability of the catalyst was investigated using the borrowing hydrogen reaction of benzyl alcohol with gaseous ammonia. The reaction was carried out for 24 h under the optimized reaction conditions to obtain 60 % yield of benzyl amine, which was determined by GC using n-dodecane as an internal standard. After each run, the reaction mixture was centrifuged and separated from the catalyst using Pasteur pipettes. The catalyst was washed two times with toluene and used directly for the subsequent run. The procedure was carried out 5 times without a significant loss of activity (Fig. S1). The turnover number (TON) for each run is given in the figure below. It was calculated via the mmol amount of obtained product divided by the mmol amount of metal in the catalyst used.

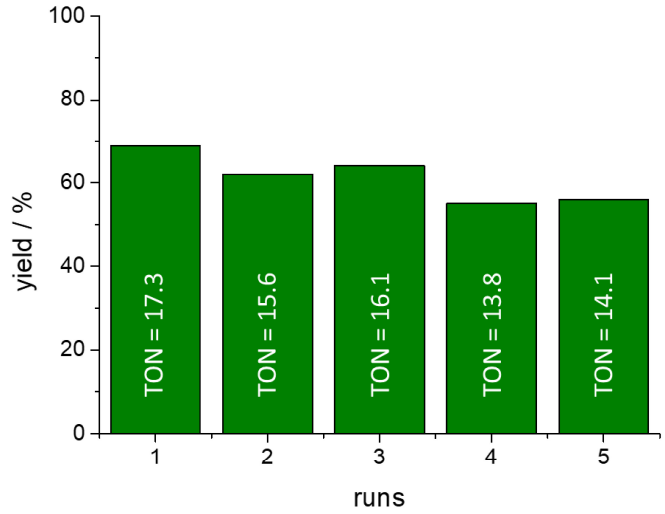

Figure S1: Reusability of the CoSc/N-SiC catalyst for 5 consecutive runs. Reaction conditions for approximately 60 % yield: 1.5 mol% Co, 0.49 mol% Sc, 0.5 mmol benzyl alcohol; 20 h, 20 bar NH_3; yields were determined by GC using *n*-dodecane as an internal standard. The turnover number for each run is given in the respective column.

2.4.4 Up-scaling

The borrowing hydrogen reaction of benzyl alcohol to benzyl amine and subsequent reductive amination with 2-pentanone to the corresponding amine was performed as up-scaling experiment. For the reaction, 288 mg CoSC/N-SiC (1.5 mol% Co, 0.49 mol% Sc), 5 mmol benzyl alcohol (320 µl), 5 mmol KOH (280 mg) and 20 mL toluene were put into a 250 mL high pressure autoclave (Parr Instruments) and pressurized with 20 bar NH_3 via condensation. The reaction was carried out under the optimized reaction conditions (160 °C, 44 h). After 44 h, the autoclave was cooled to room temperature, opened and 10 drops of aq. HCl (32 %) as well as 8 mmol 2-pentanone were added. The autoclave was then closed again, pressurized with 40 bar H_2 and heated to 100 °C for 24 h. The yield of *N*-(1-Methylbutyl)-benzenemethanamine was 76 % and determined by GC using *n*-dodecane as an internal standard.

2.4.5 Hot filtration test

To assess the heterogenicity of the catalyst, a hot filtration test was performed. For this, a magnetic stirring bar, 0.5 mmol benzyl alcohol, 2.0 mL toluene (freeze pumped), 0.5 mmol KOH (28 mg) and 28.8 mg of cobalt/scandium-catalyst (2.0 wt% Co, 1.5 mol% Co, 0.58 mg Co, 2.0 wt% Sc, 0.49 mol% Sc, 0.58 mg Sc) were placed directly into a 130 mL high pressure autoclave (Parr Instruments) and flushed with argon for 10 seconds. The autoclave was placed in a liquid nitrogen bath for 5 minutes whereafter gaseous ammonia was condensed inside for 5 seconds. The autoclave was then heated to 160 °C and the reaction was stirred for 18 h to obtain 30 % yield of benzylamine. After cooling to approx. 80 °C, the reaction mixture was filtrated hot to remove the catalyst and re-added to the autoclave. After the addition of 0.5 mmol of benzyl alcohol, the reaction was carried out again, following the procedure above. After 44 h, no further formation of benzylamine could be observed. The yield of the product was monitored via GC using *n*-dodecane as an internal standard.

2.4.6 Competition experiments

To check the selectivity of the catalyst, two different competition experiments were conducted. First, the borrowing hydrogen step was carried out as described above (section 2.3) with the exception, that 0.5 mmol benzyl alcohol were switched for a combination of benzyl alcohol, 4-methyl-benzyl alcohol and 4-trifluoromethyl-benzyl alcohol (0.167 mmol each). After the reaction time was over, the resulting solution was analyzed via GC with *n*-dodecane as an internal standard. The results are shown in Table S9.

Table S9: Borrowing hydrogen competition experiment.

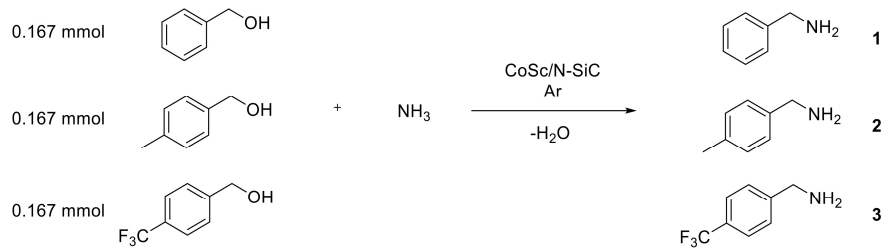

Product	Yield / %
1	43
2	27
3	14

Reaction conditions: 1.5 mol% Co, 0.49 mol% Sc, 2.0 mL toluene, 0.5 mmol KOH, 160 °C, 44 h, 20 bar NH_3. Yields were determined by GC using *n*-dodecane as an internal standard.

It can be seen that at 160 °C the selectivity of the catalyst is highest towards the formation of benzylamine and lowest towards the formation of 4-trifluoromethyl-benzyl amine. The remaining 15 % of product could be determined as various coupling products of the various benzyl amines with the intermediate aldehyde products.
To check the selectivity of the catalyst in the reductive amination step, 0.5 mmol of benzyl amine were used and 0.167 mmol each of benzaldehyde, 4-methyl-benzaldehyde and 4-fluoro-benzaldehyde were added. The reaction was carried out as described at point 2.3. GC analyses revealed the results in Table S10.

Table S10: Reductive amination competition experiment.

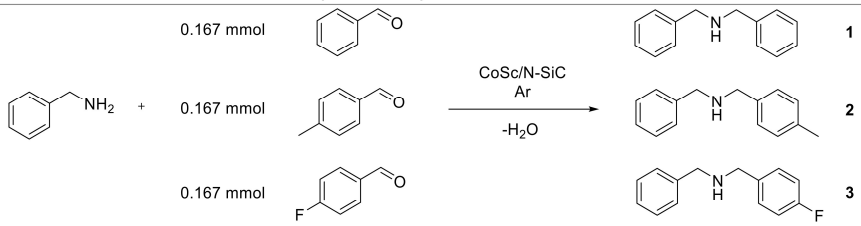

Product	Yield / %
1	56
2	34
3	4

Reaction conditions: 1.5 mol% Co, 0.49 mol% Sc, 2.0 mL Toluene, 100 °C, 20 h, 40 bar H_2. Yields were determined by GC using *n*-dodecane as an internal standard.

The selectivity of the catalyst is highest towards the formation of product **1** and lowest towards the formation of product **3**. The remaining 5 % of product are the hydrogenated aldehydes.

3. Characterization of the catalyst

3.1 ICP-OES

The elemental amounts were determined via a microwave digestion in a MARS 6 from CEM followed by ICP-OES analysis in a SPECTRO ARCOS device from Spectro.

Theoretical Co content:	2.00 wt%
Measured Co content:	2.06 wt%
Theoretical Sc content:	2.00 wt%
Measured Sc content:	2.09 wt%

Since the differences of theoretical and measured contents are insignificant and most likely caused by measuring errors, we continued to use the theoretical values.

3.2 SEM/EDX

SEM/EDX measurements were performed to determine the distribution of the individual elements of the support material. As shown in Figure S3, all studied elements can be described as homogeneously distributed.

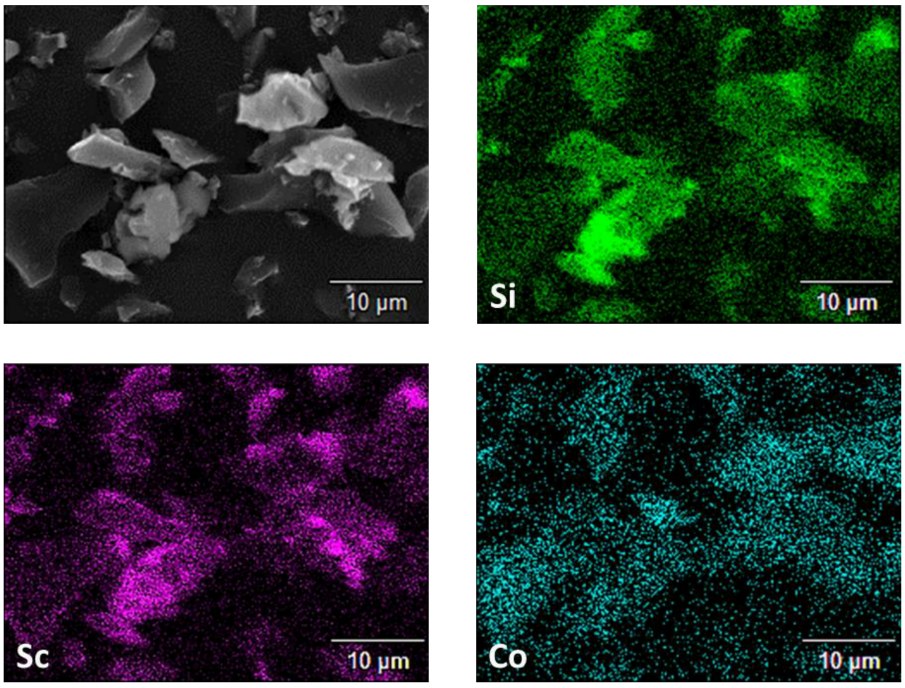

Figure S2: Scanning electron microscopy (SEM) in combination with energy dispersive X-ray (EDX) mapping. The measurements show the distribution of the elements on the sample surface.

3.3 Argon physisorption

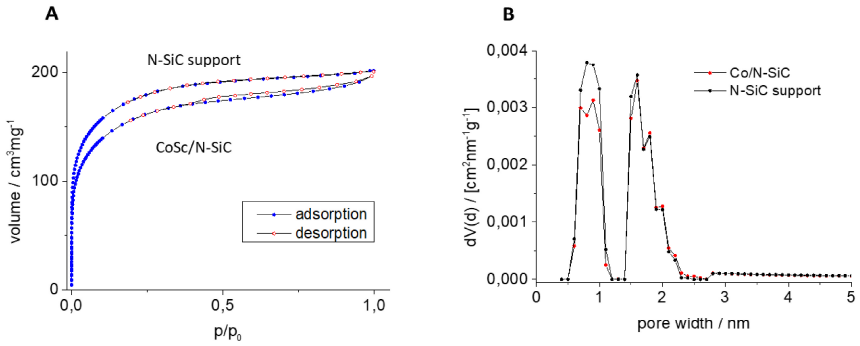

Figure S3: **A** Surface characterization and **B** pore size distribution of the catalyst and activated N-SiC support via argon physisorption measurements. Calculation model: Ar at 87 K on carbon (cylindr. pores, NLDFT equilibrium model). The specific surface showed a slight decline from 545 m^2/g of the activated support material to 468 m^2/g of the catalyst.

4. Characterization of the isolated products

Phenylmethanaminium chloride (1)

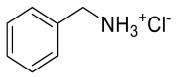

MW = 143.61 g/mol

^{1}H NMR (300 MHz, DMSO-D_6): δ = 8.70 (s, 3 H), 7.56-7.36 (m, 5 H), 4.01 (q, *J* = 5.8 Hz, 2 H) ppm

^{13}C NMR (75 MHz, DMSO-D_6): δ = 134.6, 129.5, 129.0, 128.8, 42.5 ppm

Yield: 99 % (71 mg) as a white solid.

The spectroscopic data match those reported in literature.[5] (CAS Number: 3287-99-8)

p-tolylmethanaminium chloride (2)

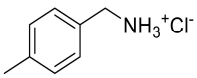

MW = 157.64 g/mol

^{1}H NMR (300 MHz, DMSO-D_6): δ = 8.54 (s, 3 H), 7.40 (d, *J* = 7.8 Hz, 2 H), 7.24 (d, *J* = 7.8 Hz, 2 H), 4.04-3.91 (m, 2 H), 2.32 (s, 3 H) ppm

^{13}C NMR (75 MHz, DMSO-D_6): δ = 138.2, 131.5, 129.6, 129.4, 42.4, 21.2 ppm

Yield: 89 % (70 mg) as a white solid.

The spectroscopic data match those reported in literature.[6] (CAS Number: 26177-45-7)

m-tolylmethanaminium chloride (3)

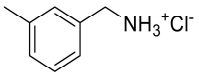

MW = 157.64 g/mol

^{1}H NMR (300 MHz, DMSO-D_6): δ = 8.59 (s, 3 H), 7.33-7.29 (m, 3 H), 7.18 (d, *J* = 6.9 Hz, 2 H), 3.95 (s, 2 H), 2.31 (s, 3 H) ppm

^{13}C NMR (75 MHz, DMSO-D_6): δ = 138.1, 134.5, 130.0, 129.4, 128.9, 126.5, 42.5, 21.4.

Yield: 81 % (64 mg) as a white solid.

The spectroscopic data match those reported in literature.[6] (CAS Number: 42365-50-4)

o-tolylmethanaminium chloride (4)

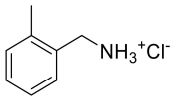

MW = 157.64 g/mol

^{1}H NMR (300 MHz, DMSO-D_6): δ = 8.58 (s, 3 H), 7.42-7.40 (m, 1 H), 7.24-7.18 (m, 3 H), 3.95 (q, *J* = 5.5 Hz, 2 H), 2.32 (s, 3 H) ppm

^{13}C NMR (75 MHz, DMSO-D_6): δ = 136.7, 132.4, 130.3, 129.2, 128.4, 126.0, 39.4, 18.9 ppm

Yield: 74 % (58 mg) as a white solid.

The spectroscopic data match those reported in literature.[6] (CAS Number: 14865-38-4)

(4-Methoxyphenyl)methanaminium chloride (5)

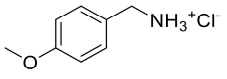

MW = 173.64 g/mol

^{1}H NMR (300 MHz, DMSO-D_6): δ = 8.51 (s, 3 H), 7.47 (m, 2 H), 6.98 (m, 2 H), 4.01-3.88 (m, 2 H), 3.79-3.77 (s, 3 H) ppm

^{13}C NMR (75 MHz, DMSO-D_6): δ = 159.8, 131.0, 126.5, 114.4, 55.7, 42.1 ppm

Yield: 81 % (70 mg) as a white solid.

The spectroscopic data match those reported in literature.[6] (CAS Number: 14865-38-4)

(4-Trifluoromethoxy)methanaminium chloride (6)

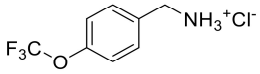

MW = 227.61 g/mol

^{1}H NMR (500 MHz, DMSO-D_6): δ = 8.67 (s, 3 H), 7.68 (d, *J* = 8.5 Hz, 2 H), 7.42 (d, *J* = 8.3 Hz, 2 H), 4.05 (s, 2 H) ppm

^{13}C NMR (126 MHz, DMSO-D_6): δ = 148.7, 134.2, 131.7, 123.6, 121.6, 119.5, 117.4, 41.7 ppm

^{19}F NMR (376 MHz, DMSO-D6): δ = -59.9 ppm

Yield: 87 % (99 mg) as a white solid.

The spectroscopic data match those reported in literature.[7] (CAS Number: 403841-98-5)

(4-Trifluoromethyl)methanaminium chloride (7)

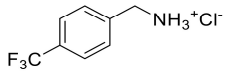

MW = 211.61 g/mol

^{1}H NMR (500 MHz, DMSO-D_6): δ = 8.63 (s, 3 H), 7.70 (dd, J_1 = 8.2 Hz, J_2 = 23.9 Hz, 4 H), 4.06 (s, 2 H) ppm

^{13}C NMR (126 MHz, DMSO-D_6): δ = 138.9, 129.8, 125.4, 125.3, 122.8, 41.56 ppm

^{19}F NMR (376 MHz, DMSO-D6): δ = -61.1 ppm

Yield: 87 % (99 mg) as a white solid.

The spectroscopic data match those reported in literature.[8] (CAS Number: 3047-99-2)

(4-Diethylamino)methanaminium chloride (8)

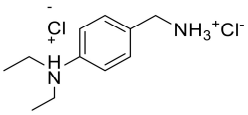

MW = 214.74 g/mol

^{1}H NMR (300 MHz, DMSO-D_6): δ = 13.20 (s, 1 H), 8.76 (s, 2 H), 7.89-7.77 (m, 3 H), 4.03 (s, 2 H), 3.50 (s, 4 H), 0.99 (t, J = 7.1 Hz, 6 H) ppm

^{13}C NMR (75 MHz, DMSO-D_6): δ = 137.9, 135.9, 132.0, 130.7, 130.4, 123.2, 52.2, 41.4, 9.94 ppm

Yield: 70 % (88 mg) as a white solid.

Not all the protons of the amino group are visible due to the exchange of deuterium with the NMR solvent. The spectroscopic data match those reported in literature.[9] (CAS Number: 104566-33-8)

Heptan-2-aminium chloride (9)

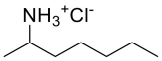

MW = 151.68 g/mol

^{1}H NMR (300 MHz, DMSO-D_6): δ = 8.10 (s, 3 H), 3.07-3.02 (m, 1 H), 1.59-1.52 (m, 1 H), 1.39-1.32 (m, 1 H), 1.26-1.20 (m, 6 H), 0.82 (t, *J* = 7.0 Hz, 3 H) ppm

^{13}C NMR (75 MHz, DMSO-D_6): δ = 47.1, 34.4, 31.4, 24.8, 22.3, 18.5, 14.3 ppm

Yield: 76 % (58 mg) as a white solid.

The spectroscopic data match those reported in literature.[10] (CAS Number: 6159-35-9)

Dodecan-2-aminium chloride (10)

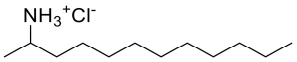

MW = 221.81 g/mol

^{1}H NMR (300 MHz, DMSO-D_6): δ = 8.54 (s, 3 H), 3.21 (s, 1 H), 1.74 (s, 1 H), 1.49-1.21 (m, 20 H), 0.91-0.87 (m, 3 H) ppm

^{13}C NMR (75 MHz, DMSO-D_6): δ = 61.9, 31.8, 29.5, 29.5, 29.3, 29.3, 29.2, 22.6, 18.4, 14.5 ppm

Yield: 85 % (94 mg) as a white solid.

Not all the protons of the amino group are visible due to the exchange of deuterium with the NMR solvent. The spectroscopic data match those reported in literature.[6] (CAS Number: 205746-45-8)

1-(2-methoxyphenyl)propan-2-aminium chloride (11)

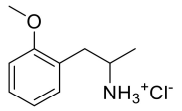

MW = 201.69 g/mol

^{1}H NMR (500 MHz, DMSO-D_6): δ = 8.29 (s, 3H), 7.23 (dd, J = 10.8, 4.8 Hz, 1H), 7.15 (dd, J = 7.4, 1.5 Hz, 1H), 6.98 (d, J = 8.2 Hz, 1H), 6.89 (t, J = 7.4 Hz, 1H), 3.77 (s, 3H), 3.37 (s, 1H), 3.01 (dd, J = 13.1, 5.1 Hz, 1H), 2.70 (dd, J = 13.0, 9.3 Hz, 1H), 1.08 (d, J = 6.5 Hz, 3H) ppm

^{13}C NMR (126 MHz, DMSO-D_6): δ = 157.7, 131.3, 128.8, 125.0, 120.8, 111.3, 55.7, 47.1, 35.3, 18.1 ppm

Yield: 79 % (80 mg) as a white solid.

The spectroscopic data match those reported in literature.[6] (CAS Number: 72739-03-8)

Nabumetone-$NH_3^+Cl^-$ (12)

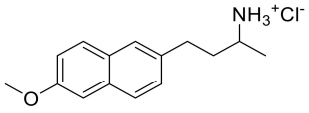

MW = 265.78 g/mol

^{1}H NMR (500 MHz, DMSO-D_6): δ = 8.17 (s, 3 H), 7.71 (dd, J_1 = 8.7 Hz, J_2 = 3.1 Hz, 2 H), 7.59 (s, 1 H), 7.30 (dd, J_1 = 8.4 Hz, J_2 = 1.7 Hz, 1 H), (d, J = 2.5 Hz, 1 H), (dd, J_1 = 8.9 Hz, J_2 = 2.6 Hz, 1 H), 3.8 (s, 3 H), 3.1 (s, 1 H), 2.77-2.71 (m, 2 H), 2.00-1.94 (m, 1 H), 1.80-1.76 (m, 1 H), 1.22 (d, J = 6.5 Hz, 3 H) ppm

^{13}C NMR (126 MHz, DMSO-D_6): δ = 157.2, 136.5, 133.2, 129.2, 129.0, 128.0, 127.3, 126.4, 119.0, 106.2, 55.5, 46.8, 36.2, 31.2, 19.6, 18.5 ppm

Yield: 81 % (107 mg) as a white solid.

The spectroscopic data match those reported in literature.[6] (CAS Number: 2247686-16-2)

Stanolone-$NH_3^+Cl^-$ (13)

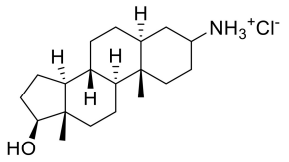

MW = 327.94 g/mol

^{1}H NMR (500 MHz, MEOH-D_4): δ = 7.84 (s, 3 H), 3.55-3.48 (m, 2 H), 1.95-1.15 (m, 20 H), 1.02-0.84 (m, 6 H), 0.7 (s, 3 H) ppm

^{13}C NMR (126 MHz, MEOH-D_4): δ = 81.0, 54.2, 53.9, 50.9, 50.8, 50.3, 44.7, 42.6, 38.9, 36.5, 36.3, 35.7, 35.4, 35.3, 35.1, 32.5, 31.3, 31.2, 31.1, 30.6, 29.2, 28.0, 27.8, 26.1, 25.8, 23.9, 22.8, 22.8, 20.4, 20.0, 11.1, 10.3, 10.2 ppm

Yield: 51 % (42 mg) as a white solid (diastereomeric mixture).

Not all the protons of the amino group are visible due to the exchange of deuterium with the NMR solvent. The spectroscopic data match those reported in literature.[11] (CAS Number: 2365462-75-3)

***N*-(1-methylbutyl)-benzenemethanamine hydrochloride (14)**

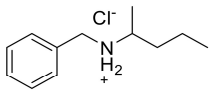

MW = 213.75 g/mol

^{1}H NMR (300 MHz, DMSO-D_6): δ = 9.29 (s, 2 H), 7.64-7.62 (m, 2 H), 7.45-7-40 (m, 3 H), 4.13 (q, *J* = 13.2 Hz, 2 H), 3.08 (s, 1 H), 1.82-1.79 (m, 1 H), 1.53-1.50 (m, 1 H), 1.40-1.38 (m, 1 H), 1.29-1.24 (m, 4 H), 0.9 (t, *J* = 7.3 Hz, 3 H) ppm

^{13}C NMR (75 MHz, DMSO-D_6): δ = 132.8, 130.5, 129.2, 129.1, 53.3, 47.4, 34.5, 18.7, 15.9, 14.2 ppm

Yield: 81 % (87 mg) as a white solid.

The spectroscopic data match those reported in literature.[12] (CAS Number: 2103392-27-2)

***N*-(1-methylhexyl)-benzenemethanamine hydrochloride (15)**

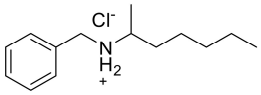

MW = 241.80 g/mol

^{1}H NMR (300 MHz, DMSO-D_6): δ = 9.44 (d, J = 43.5 Hz, 2H), 7.70 – 7.59 (m, 2H), 7.46 – 7.34 (m, 3H), 4.11 (s, 2H), 3.05 (s, 1H), 1.90 – 1.77 (m, 1H), 1.59 – 1.45 (m, 1H), 1.35 – 1.18 (m, 9H), 0.86 (t, J = 6.8 Hz, 3H).

^{13}C NMR (75 MHz, DMSO-D_6): δ = 132.8, 130.6, 129.2, 129.0, 53.4, 47.4, 32.3, 31.4, 25.0, 22.4, 15.9, 14.3 ppm

Yield: 79 % (96 mg) as a white solid.

The spectroscopic data match those reported in literature.[13] (CAS Number: 92330-45-5)

***N*-(1-methylundecyl)-benzenemethanamine hydrochloride (16)**

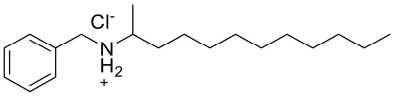

MW = 311.94 g/mol

^{1}H NMR (300 MHz, DMSO-D_6): δ = 9.44 (s, 1 H), 9.30 (s, 1 H), 7.67-7.64 (m, 2 H), 7.48-7.41 (m, 3 H), 4.17-4.12 (m, 2 H), 3.08 (s, 1 H), 1.91-1.79 (m, 1 H), 1.57-1.42 (m, 1 H), 1.33-1.26 (m, 19 H), 0.88 (m, 3 H) ppm

^{13}C NMR (75 MHz, DMSO-D_6): δ = 132.2, 130.0, 128.7, 128.5, 52.9, 46.8, 31.8, 31.2, 28.9, 28.6, 24.7, 22.0, 15.4, 13.9 ppm

Yield: 79 % (123 mg) as a white solid.

The spectroscopic data match those reported in literature.[13] (CAS Number: 1427378-88-8)

4-[(Phenylmethyl)amino]-1-pentanol hydrochloride (17)

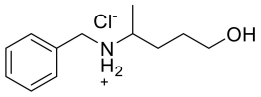

MW = 229.75 g/mol

^{1}H NMR (300 MHz, DMSO-D_6): δ = 9.51 (s, 1 H), 9.36 (s, 1 H), 7.66-7.63 (m, 2 H), 7.40-7.37 (m, 3 H), 4.90 (s, 2 H), 4.11 (s, 2 H), 3.43-3.38 (t, *J* = 6.2 Hz, 2 H), 1.98-1.88 (m, 1 H), 1.65-1.54 (d, J = 6.5 Hz, 3 H) ppm

^{13}C NMR (75 MHz, DMSO-D_6): δ = 132.7, 130.5, 129.1, 128.9, 60.8, 53.7, 47.6, 29.5, 28.80, 16.1 ppm

Yield: 75 % (86 mg) as a white solid.

No spectroscopic data in the literature but known substrate. (CAS Number: 1514217-60-7)

***N*-(1,3-dimethylbutyl)-benzenemethanamine hydrochloride (18)**

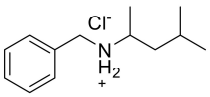

MW = 227.78 g/mol

^{1}H NMR (300 MHz, DMSO-D_6): δ = 9.40 (s, 2 H), 7.68-7.65 (m, 2 H), 7.46-7.41 (m, 3 H), 4.15 (s, 2 H), 3.16-3.09 (m, 1 H), 1.31 (d, *J* = 6.5 Hz, 3 H), 1.70-1.65 (m, 2 H), 1.52-1.46 (m, 1 H), 0.91 (d, *J* = 9 Hz, 3 H), 0.81 (d, *J* = 9 Hz, 3 H) ppm

^{13}C NMR (75 MHz, DMSO-D_6): δ = 132.8, 130.6, 129.2, 129.0, 51.9, 47.3, 24.5, 24.0, 21.4, 16.2 ppm

Yield: 75 % (85 mg) as a white solid.

The spectroscopic data match those reported in literature.[14] (CAS Number: 2375135-37-6)

***N*-(1-cyclohexylethyl)-benzenemethanamine hydrochloride (19)**

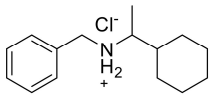

MW = 253.81 g/mol

^{1}H NMR (300 MHz, DMSO-D_6): δ = 9.57 (s, 1 H), 9.10 (s, 1 H), 7.71-7.68 (m, 2 H), 7.47-7.42 (m, 3 H), 4.19-4.12 (m, 2 H), 2.92 (s, 1 H), 1.82-1.53 (m, 6 H), 1.24-1.02 (m, 8 H), ppm

^{13}C NMR (75 MHz, DMSO-D_6): δ = 132.5, 130.8, 129.3, 129.0, 57.5, 48.0, 29.7, 26.3, 26.2, 25.8, 12.1 ppm

Yield: 66 % (84 mg) as a white solid.

The spectroscopic data match those reported in literature.[15] (CAS Number: 177721-69-6)

α-methyl-*N*-(phenylmethyl)-benzenepropanamine hydrochloride (20)

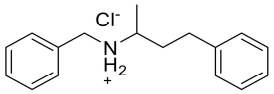

MW = 275.82 g/mol

^{1}H NMR (300 MHz, DMSO-D_6): δ = 9.49 (d, *J* = 7.8 Hz, 2 H), 7.66-7.22 (m, 10 H), 4.156 (s, 2 H), 3.10 (s, 1 H), 2.76-2.57 (m, 2 H), 2.24-2.19 (m, 1 H), 1.89-1.85 (m, 1 H), 1.39 (d, *J* = 6.5 Hz, 3 H) ppm

^{13}C NMR (75 MHz, DMSO-D_6): δ = 140.7, 132.2, 130.1, 128.7, 128.5, 128.4, 128.2, 126.0, 52.5, 46.8, 33.7, 30.8, 15.4 ppm

Yield: 68 % (94 mg) as a white solid.

The spectroscopic data match those reported in literature.[16] (CAS Number: 1158736-70-9)

α-methyl-*N*-(phenylmethyl)-benzenemethanamine hydrochloride (21)

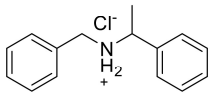

MW = 247.77 g/mol

^{1}H NMR (300 MHz, DMSO-D_6): δ = 10.48 (s, 1 H), 9.90 (s, 1 H), 7.69-7.39 (m, 10 H), 4.35 (s, 1 H), 3.99 (s, 1 H), 3.80 (s, 1 H), 1.68 (d, *J* = 6.4 Hz, 3 H) ppm

^{13}C NMR (75 MHz, DMSO-D_6): δ = 137.8, 132.4, 130.6, 129.4, 129.3, 129.2, 129.0, 128.5, 57.7, 48.8, 20.3 ppm

Yield: 78 % (97 mg) as a white solid.

The spectroscopic data match those reported in literature.[17] (CAS Number: 49746-32-9)

4-fluoro-α-methyl-*N*-(phenylmethyl)-benzenepropanamine hydrochloride (22)

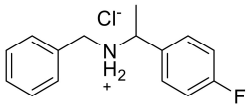

MW = 265.76 g/mol

^{1}H NMR (300 MHz, DMSO-D_6): δ = 10.42 (s, 1 H), 9.92 (s, 1 H), 7.77-7.72 (m, 2 H), 7.56-7.53 (m, 2 H), 7.42-7.28 (m, 5 H), 4.40 (s, 1 H), 4.00 (s, 1 H), 3.80 (s, 1 H), 1.67 (d, *J* = 6.5 Hz, 3 H) ppm

^{13}C NMR (75 MHz, DMSO-D_6): δ = 162.6 (d, $J_{C\text{-}F}$ = 245.1 Hz), 134.0, 134.0, 132.4, 130.9 (d, $J_{C\text{-}F}$ = 8.4 Hz), 130.6, 129.2, 129.0, 116.2 (d, $J_{C\text{-}F}$ = 8.4 Hz), 57.0, 48.7, 20.2 ppm

^{19}F NMR (376 MHz, DMSO-D6): δ = -113.1 ppm

Yield: 81 % (108 mg) as a white solid.

The spectroscopic data match those reported in literature.[18] (CAS Number: 820245-52-1)

4-methyl-*N*-(1-methylbutyl)-benzenemethanamine hydrochloride (23)

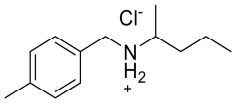

MW = 227.78 g/mol

^{1}H NMR (300 MHz, DMSO-D_6): δ = 9.52 (s, 1 H), 9.38 (s, 1 H), 7.55 (d, J = 8.0 Hz, 2 H), 7.24 (d, J = 7.8 Hz, 2 H), 4.08 (s, 2 H), 3.04 (s, 1 H), 2.33 (s, 3 H), 1.87-1.77 (m, 1 H), 1.57-1.21 (m, 6 H), 0.88 (t, *J* = 7.3 Hz, 3 H) ppm

^{13}C NMR (75 MHz, DMSO-D_6): δ = 138.6, 130.6, 129.6, 129.5, 52.9, 47.0, 34.4, 21.3, 18.7, 15.8, 14.2.ppm

Yield: 82 % (93 mg) as a white solid.

No spectroscopic data in the literature but known substrate. (CAS Number: 1020964-62-8)

4-methoxy-*N*-(1-methylbutyl)-benzenemethanamine hydrochloride (24)

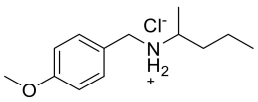

MW = 243.78 g/mol

^{1}H NMR (300 MHz, DMSO-D_6): δ = 9.27 (s, 2 H), 7.59-7.56 (m, 2 H), 7.01-6.98 (m, 2 H), 4.08 (s, 2 H), 3.79 (s, 3 H), 3.06 (s, 1 H), 1.87-1.77 (m, 1 H), 1.56-1.21 (m, 6 H), 0.90 (t, *J* = 0.89 Hz, 3 H) ppm

^{13}C NMR (75 MHz, DMSO-D_6): δ = 132.1, 124.5, 114.4, 55.7, 52.9, 46.8, 34.5, 18.7, 15.9, 14.2 ppm

Yield: 81 % (84 mg) as a white solid.

No spectroscopic data in the literature but known substrate. (CAS Number: 1019472-43-5)

3-methyl-*N*-(1-methylbutyl)-benzenemethanamine hydrochloride (25)

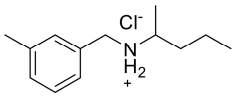

MW = 227.78 g/mol

^{1}H NMR (300 MHz, DMSO-D_6): δ = 9.32 (s, 2 H), 7.47-7.22 (m, 4 H), 4.10 (s, 2 H), 3.09 (s, 1 H), 2,35 (s, 3 H), 1.87-1.78 (m, 1 H), 1.57-1.21 (m, 6 H), 0.90 (t, *J* = 6.8 Hz, 3 H) ppm

^{13}C NMR (75 MHz, DMSO-D_6): δ = 138.3, 132.6, 131.1, 129.8, 129.0, 127.6, 53.3, 47.4, 34.5, 31.2, 21.4, 18.7, 16.0, 14.2 ppm

Yield: 77 % (88 mg) as a white solid.

No spectroscopic data in the literature but known substrate. (CAS Number: 1019491-23-6)

2-methyl-*N*-(1-methylbutyl)-benzenemethanamine hydrochloride (26)

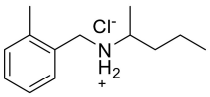

MW = 227.78 g/mol

^{1}H NMR (300 MHz, DMSO-D_6): δ = 9.37 (d, *J* = 9.5 Hz, 2 H), 7.65-7.62 (m, 1 H), 7.30-7.22 (m, 3 H), 4.10 (t, *J* = 6.8 Hz, 2 H), 3.23 (s, 1 H), 2,40 (s, 3 H), 1.87-1.78 (m, 1 H), 1.57-1.21 (m, 6 H), 0.90 (t, *J* = 7.2 Hz, 3 H) ppm

^{13}C NMR (75 MHz, DMSO-D_6): δ = 138.0, 131.4, 131.3, 130.8, 129.3, 126.4, 54.3, 44.7, 19.7, 18.9, 15.9, 14.2 ppm

Yield: 69 % (79 mg) as a white solid.

No spectroscopic data in the literature but known substrate. (CAS Number: 1019545-40-4)

_N_-(phenylmethyl)-benzenemethanamine hydrochloride (27)

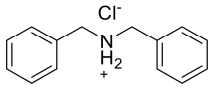

MW = 233.74 g/mol

^{1}H NMR (300 MHz, DMSO-D_6): δ = 10.06 (s, 1 H), 7.63-7.41 (m, 10 H), 4.14-4.11 (m, 4 H) ppm

^{13}C NMR (75 MHz, DMSO-D_6): δ = 132.4, 130.7, 129.3, 129.0, 50.0 ppm

^{19}F NMR (376 MHz, DMSO-D6): δ = -113.1 ppm

Yield: 91 % (106 mg) as a white solid.

The spectroscopic data match those reported in literature.[19] (CAS Number: 20455-68-9)

4-methyl-_N_-(phenylmethyl)-benzenemethanamine hydrochloride (28)

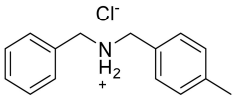

MW = 247.77 g/mol

^{1}H NMR (300 MHz, DMSO-D_6): δ = 9.91 (s, 1 H), 7.62-7.24 (m, 9 H), 4.18-4.07 (m, 4 H), 2.34 (s, 3 H) ppm

^{13}C NMR (75 MHz, DMSO-D_6): δ = 138.8, 138.2, 131.9, 131.4, 130.1, 129.1, 129.1, 129.0, 128.8, 128.5, 128.5, 126.8, 49.4, 49.3, 20.7 ppm

Yield: 89 % (110 mg) as a white solid.

The spectroscopic data match those reported in literature.[17] (CAS Number: 1158274-26-0)

4-ethyl-*N*-(phenylmethyl)-benzenemethanamine hydrochloride (29)

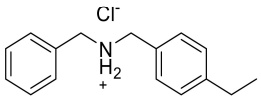

MW = 261.79 g/mol

^{1}H NMR (300 MHz, DMSO-D_6): δ = 9.93 (s, 1 H), 7.63-7.27 (m, 9 H), 4.13-4.09 (m, 4 H), 2.64 (q, *J* = 6.2 Hz, 2 H), 1.20 (t, *J* = 7.0 Hz, 3 H) ppm

^{13}C NMR (75 MHz, DMSO-D_6): δ = 144.5, 131.9, 130.1, 129.1, 128.8, 128.5, 127.9, 127.8, 49.5, 49.3, 27.9, 15.6 ppm

Yield: 88 % (115 mg) as a white solid.

No spectroscopic data in the literature but known substrate. (CAS Number: 1158454-56-8)

4-fluor-*N*-(phenylmethyl)-benzenemethanamine hydrochloride (30)

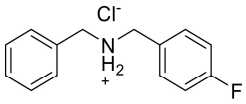

MW = 251.73 g/mol

^{1}H NMR (300 MHz, DMSO-D_6): δ = 9.97 (s, 1 H), 7.70-7.60 (m, 4 H), 7.46-7.43 (m, 3 H), 7.31-7.26 (m, 2 H), 4.15 (q, *J* = 6.8 Hz, 4 H) ppm.

^{13}C NMR (75 MHz, DMSO-D_6): δ = 162.8 (d, *J* = 245.1 Hz), 133.2, 132.4, 130.6, 129.3, 129.0, 116.0, 115.7, 50.1, 49.4 ppm.

^{19}F NMR (376 MHz, DMSO-D6): δ = -113.1 (dq, J_1 = 8.9 Hz, J_2 = 5.5 Hz) ppm

Yield: 84 % (106 mg) as a white solid.

The spectroscopic data match those reported in literature.[17] (CAS Number: 55097-55-7)

4-methoxy-*N*-(phenylmethyl)-benzenemethanamine hydrochloride (31)

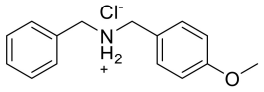

MW = 263.77 g/mol

^{1}H NMR (300 MHz, DMSO-D_6): δ = 9.81 (s, 1 H), 7.61-7.43 (m, 7 H), 7.01-6.98 (m, 2 H), 4.18-4.08 (m, 4 H), 3.80 (s, 3 H) ppm

^{13}C NMR (75 MHz, DMSO-D_6): δ = 159.65, 133.04, 132.02, 131.82, 131.29, 130.17, 128.83, 128.73, 128.58, 123.67, 121.64, 113.91, 55.21, 49.35, 49.15 ppm

Yield: 85 % (106 mg) as a white solid.

Not all the protons of the amino group are visible due to the exchange of deuterium with the NMR solvent. The spectroscopic data match those reported in literature.[17] (CAS Number: 58405-57-5)

4-fluoro-*N*-[(4-methyl]phenylmethyl)-benzenemethanamine hydrochloride (32)

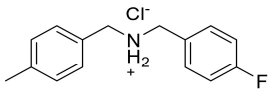

MW = 265.76 g/mol

^{1}H NMR (300 MHz, DMSO-D_6): δ = 10.06 (s, 1 H), 7.73-7.68 (m, 2 H), 7.52 (d, *J* = 7.8 Hz, 2 H), 7.26-7.16 (m, 4 H), 4.11 (d, *J* = 6.8 Hz, 3 H) ppm

^{13}C NMR (75 MHz, DMSO-D_6): δ = 163.6, 160.4, 137.8, 132.2, 132.1, 129.7, 128.7, 128.6, 128.4, 127.8, 115.0, 114.7, 49.0, 48.4, 20.3 ppm

^{19}F NMR (376 MHz, DMSO-D6): δ = -113.1 (m) ppm

Yield: 82 % (118 mg) as a white solid.

Not all the protons of the amino group are visible due to the exchange of deuterium with the NMR solvent. The spectroscopic data match those reported in literature.[20] (CAS Number: 774554-55-1)

4-methoxy-*N*-[(4-methyl]phenylmethyl)-benzenemethanamine hydrochloride (33)

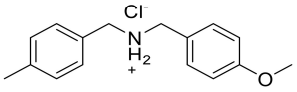

MW = 277.79 g/mol

^{1}H NMR (300 MHz, DMSO-D_6): δ = 10.00 (s, 1 H), 7.63-7.50 (m, 4 H), 7.22 (d, *J* = 7.8 Hz, 2 H), 6.99-6.94 (m, 2 H), 4.15 (s, 2 H), 4.06 (s, 2 H), 3.80 (s, 3 H), 2.34 (s, 3 H) ppm

^{13}C NMR (75 MHz, DMSO-D_6): δ = 159.4, 137.7, 132.5, 131.3, 130.8, 129.7, 128.7, 128.6, 128.5, 123.4, 113.7, 113.6, 55.2, 54.9, 48.8, 20.3 ppm

Yield: 81 % (112 mg) as a white solid.

Not all the protons of the amino group are visible due to the exchange of deuterium with the NMR solvent. The spectroscopic data match those reported in literature.[21] (CAS Number: 1158430-76-2)

3,5-dimethoxy-*N*-[(4-methoxy]phenylmethyl)-benzenemethanamine hydrochloride (34)

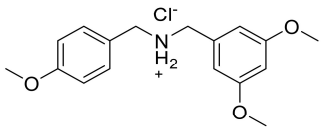

MW = 323.82 g/mol

^{1}H NMR (300 MHz, DMSO-D_6): δ = 9.85 (s, 1 H), 7.54-7.51 (m, 2 H), 7.01-6.98 (m, 2 H), 6.84 (d, *J* = 6.8 Hz, 2 H), 6.54-6.53 (t, *J* = 6.6 Hz, 1 H), 4.04 (s, 4 H), 3.80-3.77 (m, 9 H) ppm

^{13}C NMR (75 MHz, DMSO-D_6): δ = 160.4, 159.6, 134.0, 131.8, 123.6, 113.8, 107.8, 100.5, 55.4, 55.3, 55.1, 49.3, 49.0 ppm

Yield: 78 % (126 mg) as a white solid.

The spectroscopic data match those reported in literature.[22] (CAS Number: 356093-54-4)

4-tertbutyl-*N*-[(4-methoxy]phenylmethyl)-benzenemethanamine hydrochloride (35)

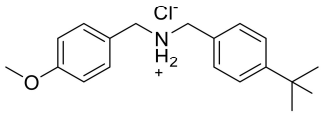

MW = 319.87 g/mol

^{1}H NMR (300 MHz, DMSO-D_6): δ = 9.75 (s, 1 H), 7.52-7.41 (m, 6 H), 6.99-6.93 (m, 2 H), 4.15-4.00 (m, 4 H), 3.76 (s, 3 H), 1.27 (s, 9 H) ppm

^{13}C NMR (75 MHz, DMSO-D_6): δ = 160.1, 151.8, 132.2, 130.4, 129.5, 125.8, 124.1, 114.4, 55.7, 49.7, 49.5, 34.9, 31.5 ppm

Yield: 74 % (123 mg) as a white solid.

The spectroscopic data match those reported in literature.[23] (CAS Number: 2245774-03-0)

α-phenyl-*N*-(phenylmethyl)-benzenepropanamine hydrochloride (36)

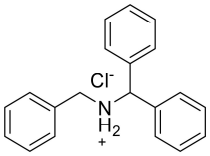

MW = 309.84 g/mol

^{1}H NMR (300 MHz, DMSO-D_6): δ = 10.62 (s, 2 H), 7.72 (d, *J* = 7.4 Hz, 4 H), 7.46-7.31 (m, 11 H), 5.46 (s, 1 H), 4.09-4.00 (m, 2 H) ppm

^{13}C NMR (75 MHz, DMSO-D_6): δ = 137.2, 131.7, 131.0, 129.4, 129.1, 129.0, 128.5, 65.1, 49.8 ppm

Yield: 79 % (122 mg) as a white solid.

Not all the protons of the amino group are visible due to the exchange of deuterium with the NMR solvent. The spectroscopic data match those reported in literature.[17] (CAS Number: 23934-60-3)

_N_,_N_-bis(phenylmethyl)-benzenemethanamine hydrochloride (37)

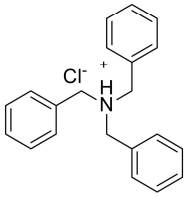

MW = 323.86 g/mol

^{1}H NMR (300 MHz, $CDCl_3$): δ = 11.53 (s, 1 H), 7.62-7.61 (m, 6 H), 7.43-7.42 (m, 9 H) 4.20-4.19 (d, *J* = 7.5 Hz, 6 H) ppm

^{13}C NMR (75 MHz, $CDCl_3$): δ = 131.4, 129.9, 129.4, 128.8, 56.0 ppm

Yield: 73 % (118 mg) as a white solid.

The spectroscopic data match those reported in literature.[24] (CAS Number: 7673-07-6)

4-fluoro-_N_,_N_-bis(phenylmethyl)-benzenemethanamine hydrochloride (38)

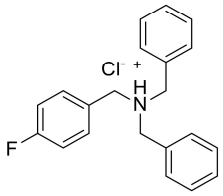

MW = 341.85 g/mol

^{1}H NMR (300 MHz, DMSO-D_6): δ = 11.82 (s, 1 H), 7.67 (d, *J* = 32 Hz, 6 H), 7.41 (s, 6 H), 7.23 (t, *J* = 7.8 Hz, 2 H), 4.25-4.22 (m, 6 H) ppm

^{13}C NMR (75 MHz, DMSO-D_6): δ = 163.0 (d, *J* = 246.5 Hz), 134.5, 134.3, 131.9, 130.5, 129.8, 129.1, 126.8, 126.8, 116.1, 115.8, 56.7, 56.0 ppm

^{19}F NMR (376 MHz, DMSO-D6): δ = -112.2 ppm

Yield: 77 % (132 mg) as a white solid.

The spectroscopic data match those reported in literature.[25] (CAS Number: 359445-99-1)

_N_-(4-fluorobenzyl)-_N_-(4-methoxybenzyl)-1-(_p_-tolyl)methanamine hydrochloride (39)

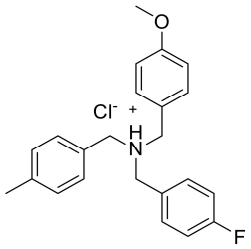

MW = 385.91 g/mol

^{1}H NMR (300 MHz, DMSO-D_6): δ = 11.30 (s, 1 H), 7.68-6.95 (m, 12 H), 4.22-4.13 (m, 6 H), 3.77 (s, 3 H), 2.3 (s, 3 H) ppm

^{13}C NMR (75 MHz, DMSO-D_6): δ = 164.6, 160.9 (d, *J* = 72.8 Hz), 139.3, 134.3, 134.3, 134.2, 133.5, 131.9, 131.8, 129.8, 127.4, 126.8, 122.0, 116.2, 115.9, 114.5, 56.5, 56.1, 55.7, 55.4, 21.3 ppm

^{19}F NMR (376 MHz, DMSO-D6): δ = -112.2 ppm

HRMS (ESI$^+$) Calculated for $C_{23}H_{25}OFN$: 350.1915; found: 350.1904

Yield: 65 % (125 mg) as a colorless oil.

Unknown substrate with incomplete spectroscopic literature data was additionally analyzed via LC-HRMS.

_N_-pentyl-benzenemethanamine hydrochloride (40)

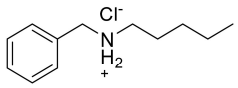

MW = 199.72 g/mol

^{1}H NMR (300 MHz, DMSO-D_6): δ = 9.46 (s, 2H), 7.63 – 7.54 (m, 2H), 7.45 – 7.36 (m, 3H), 4.09 (s, 2H), 2.80 (dd, J = 18.0, 9.9 Hz, 2H), 1.70 – 1.54 (m, 2H), 1.26 (d, J = 4.0 Hz, 2H), 0.88 – 0.83 (m, 3H) ppm

^{13}C NMR (75 MHz, DMSO-D_6): δ = 132.6, 130.6, 129.3, 129.0, 50.2, 46.8, 28.6, 25.3, 22.1, 14.2 ppm

Yield: 88 % (89 mg) as a white solid.

The spectroscopic data match those reported in literature.[17] (CAS Number: 90389-36-9)

***N,N*-dibenzylpentan-1-aminium chloride (41)**

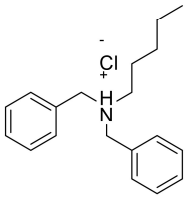

MW = 303.87 g/mol

^{1}H NMR (300 MHz, DMSO-D_6): δ = 11.60 (s, 1 H), 7.76-7.41 (m, 10 H), 4.33-4.12 (m, 4 H), 2.85-2.81 (m, 2 H), 1.78-1.73 (m, 2 H), 1.29-1.09 (m, 4 H), 0.81 (m, 3 H) ppm

^{13}C NMR (75 MHz, DMSO-D_6): δ = 131.9, 130.6, 129.8, 129.2, 56.4, 51.3, 28.7, 22.5, 21.9, 14.1 ppm

Yield: 67 % (102 mg) as a colorless oil.

Not all the protons of the amino group are visible due to the exchange of deuterium with the NMR solvent. The spectroscopic data match those reported in literature.[25] (CAS Number: 79865-95-5)

***N*-benzyl-*N*-(4-fluorobenzyl)pentan-1-aminium chloride (42)**

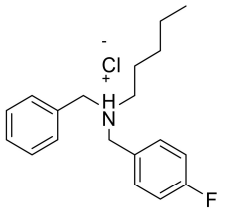

MW = 321.86 g/mol

^{1}H NMR (300 MHz, DMSO-D_6): δ = 11.55 (s, 1 H), 7.79-7.68 (m, 4 H), 7.42-7.40 (m, 2 H), 7.25 (td, J_1 = 8.8 Hz, J_2 = 1.7 Hz, 3 H) 4.30-4.24 (m, 4 H), 2.80-2.77 (m, 2 H), 1.73-1.69 (m, 2 H), 1.18-1.04 (m, 4 H), 0.78-0.75 (m, 3 H) ppm

^{13}C NMR (75 MHz, DMSO-D_6): δ = 164.2, 161.8, 134.3, 134.2, 130.6, 129.7, 129.1, 126.9, 126.9, 116.1, 115.9, 56.3, 55.6, 51.2, 28.7, 22.5, 21.9, 14.1 ppm

^{19}F NMR (376 MHz, DMSO-D6): δ = -112.1 (m) ppm

HRMS (ESI$^+$) Calculated for $C_{19}H_{25}FN$: 286.1966; found: 286.1954

Yield: 60 % (96 mg) as a colorless oil.

Not all the protons of the amino group are visible due to the exchange of deuterium with the NMR solvent. Unknown substrate with incomplete spectroscopic literature data was additionally analyzed via LC-HRMS.

***N*-benzyl-*N*-(4-chlorobenzyl)pentan-1-aminium chloride (43)**

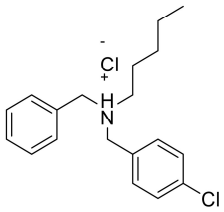

MW = 338.32 g/mol

^{1}H NMR (300 MHz, DMSO-D_6): δ = 11.72 (s, 1 H), 7.78-7.46 (m, 9 H), 4.34-4.28 (m, 4 H), 2.96-2.82 (m, 2 H), 1.81-1.73 (m, 2 H), 1.25-1.09 (m, 4 H), 0.87-0.79 (m, 3 H) ppm

^{13}C NMR (75 MHz, DMSO-D_6): δ = 134.1, 133.3, 131.3, 130.0, 129.1, 129.0, 128.6, 128.6, 55.0, 50.8, 28.1, 22.0, 21.4, 13.5 ppm

HRMS (ESI$^+$) Calculated for $C_{19}H_{25}ClN$: 302.1670; found: 302.1658

Yield: 67 % (105 mg) as a colorless oil.

Not all the protons of the amino group are visible due to the exchange of deuterium with the NMR solvent. Unknown substrate with incomplete spectroscopic literature data was additionally analyzed via LC-HRMS.

***N*-benzyl-*N*-(4-methoxybenzyl)pentan-1-aminium chloride (44)**

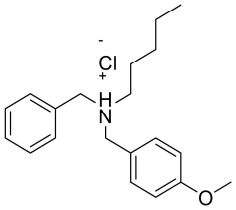

MW = 333.90 g/mol

^{1}H NMR (300 MHz, DMSO-D_6): δ = 11.45 (d, J = 60.4 Hz, 1H), 7.73 (s, 1H), 7.63 (d, J = 8.2 Hz, 3H), 7.41 (s, 1H), 6.96 (d, J = 8.3 Hz, 4H), 4.21 (dd, J = 18.0, 6.8 Hz, 4H), 3.76 (s, 3H), 2.76 (s, 2H), 1.71 (s, 2H), 1.14 (d, J = 6.7 Hz, 2H), 1.06 (d, J = 6.5 Hz, 2H), 0.77 (dd, J = 9.3, 4.8 Hz, 3H) ppm

^{13}C NMR (75 MHz, DMSO-D_6): δ = 159.8, 132.9, 131.3, 130.3, 129.2, 128.7, 121.8, 114.0, 55.2, 55.1, 50.4, 50.0, 28.3, 22.1, 21.5, 13.6 ppm

HRMS (ESI$^+$) Calculated for $C_{20}H_{28}NO$: 298.2165; found: 298.2153

Yield: 61 % (97 mg) as a colorless oil.

Unknown substrate with incomplete spectroscopic literature data was additionally analyzed via LC-HRMS.

***N*-benzyl-*N*-(4-ethylbenzyl)pentan-1-aminium chloride (45)**

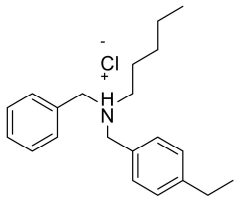

MW = 331.91 g/mol

^{1}H NMR (300 MHz, DMSO-D_6): δ = 11.42 (s, 1 H), 7.76-7.17 (m, 9 H), 4.31-4.17 (m, 4 H), 2.83-2.80 (m, 2 H), 2.67-2.60 (m, 4 H), 1.80-1.75 (m, 2 H), 1.22-1.09 (m, 5 H), 0.80 (t, J = 7.1 Hz, 3 H) ppm

^{13}C NMR (75 MHz, DMSO-D_6): δ = 145.5, 131.9, 130.7, 129.2, 128.6, 128.5, 127.8, 127.8, 56.1, 51.1, 28.7, 28.4, 22.6, 21.9, 15.8, 14.1 ppm

HRMS (ESI$^+$) Calculated for $C_{21}H_{30}N$: 296.2373; found: 296.2361

Yield: 58 % (91 mg) as a colorless oil.

Unknown substrate with incomplete spectroscopic literature data was additionally analyzed via LC-HRMS.

5. NMR and IR spectra

1:

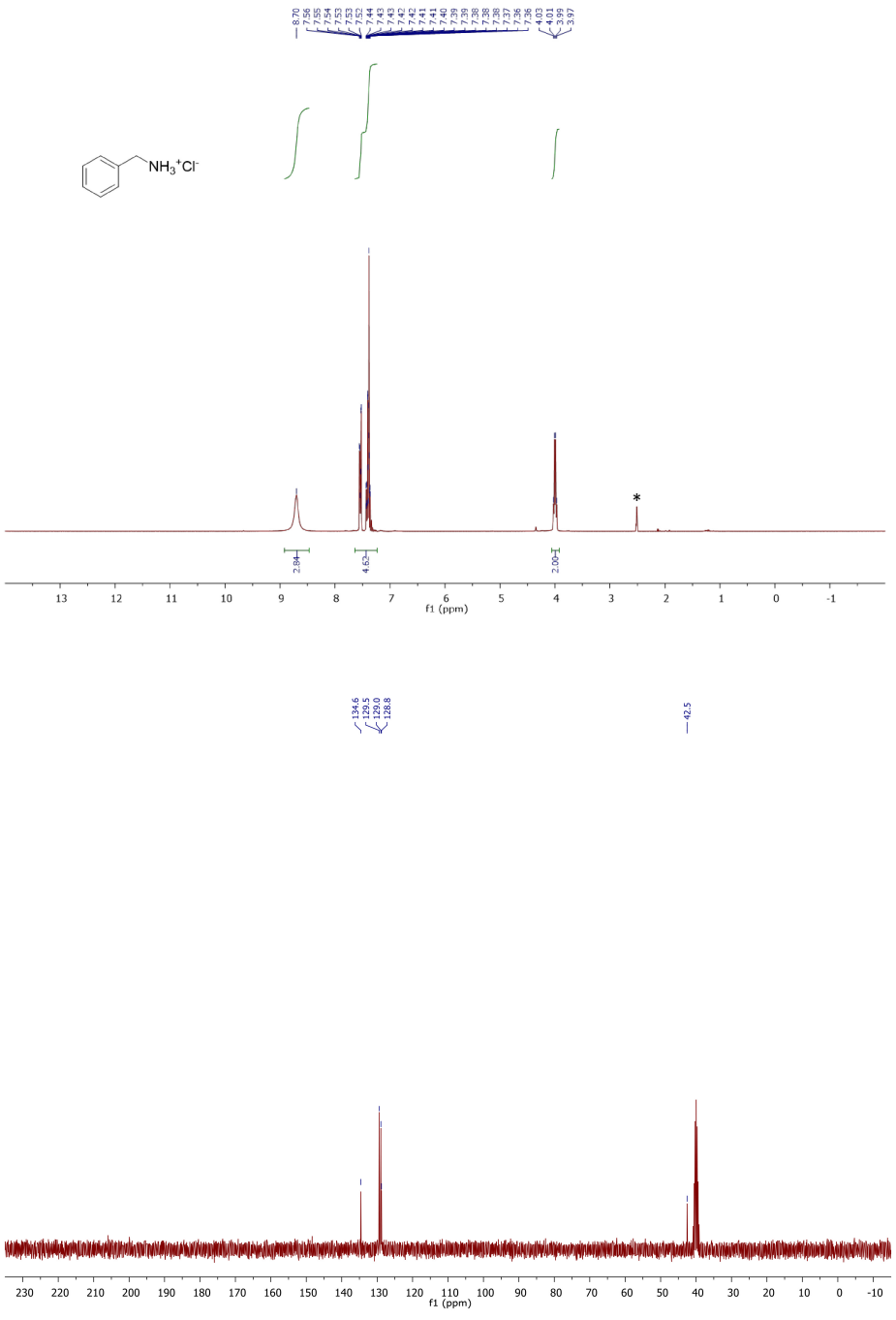

SUPPORTING INFORMATION

ChemNMR ^{1}H Estimation

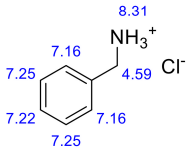

Estimation quality is indicated by color: good, medium, rough

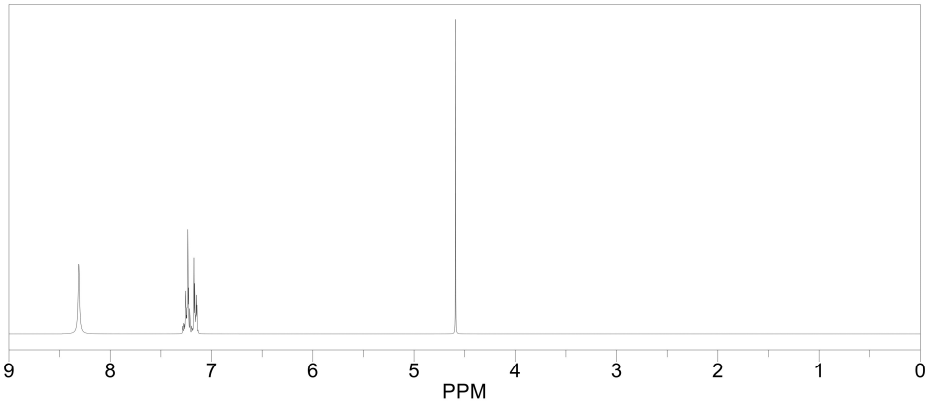

ChemNMR ^{13}C Estimation

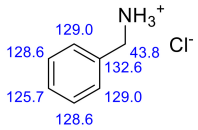

Estimation quality is indicated by color: good, medium, rough

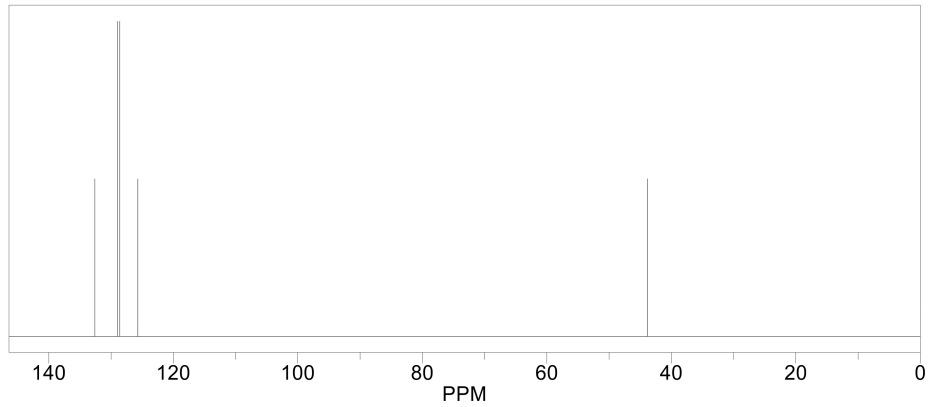

2:

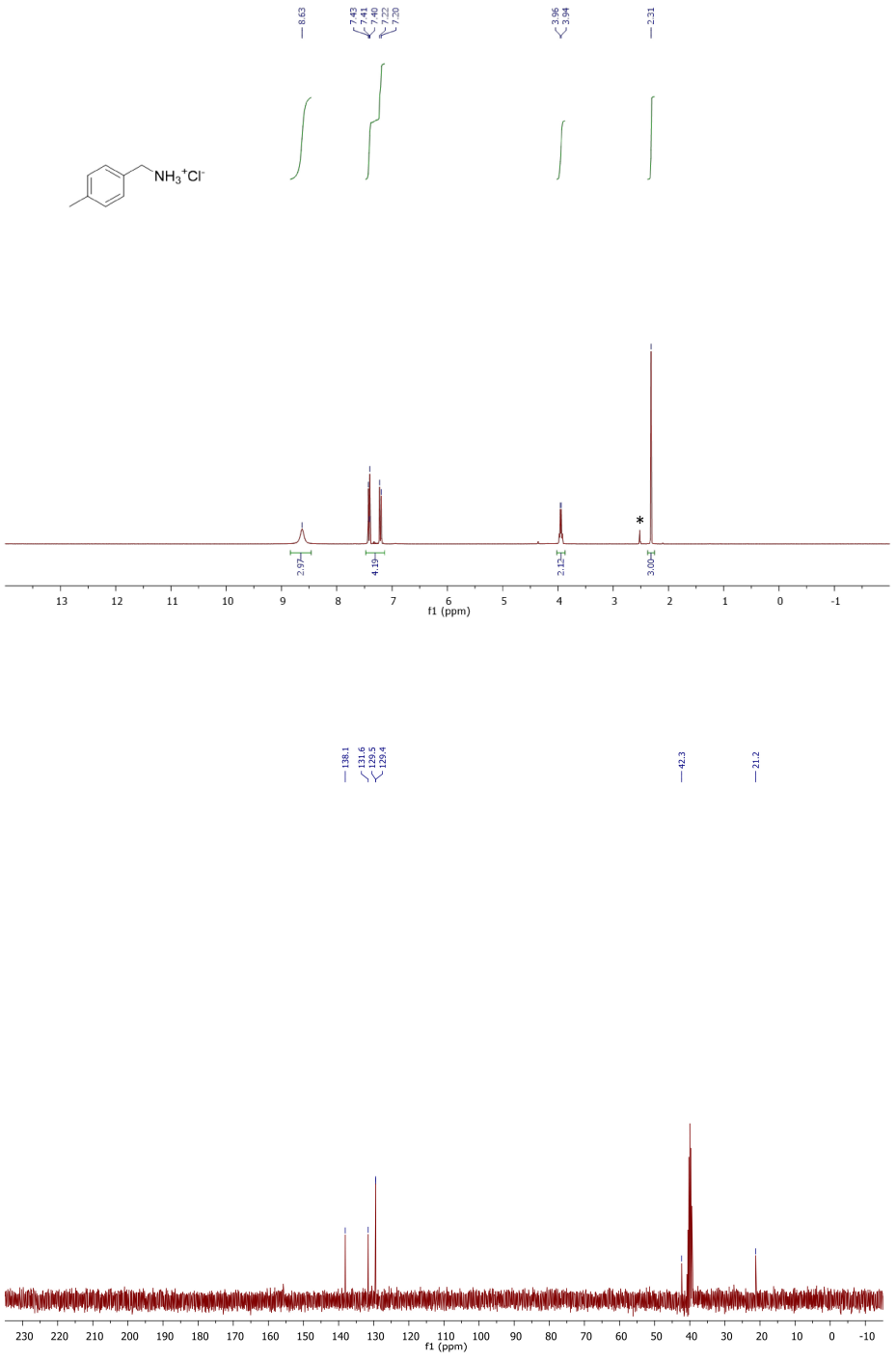
8.63
7.43
7.41
7.40
7.22
7.20
3.96
3.94
2.31
NH3+Cl-
2.97
4.19
2.10
3.00
*
f1 (ppm)
138.1
131.6
129.5
129.4
42.3
21.2
f1 (ppm)

ChemNMR ^{1}H Estimation

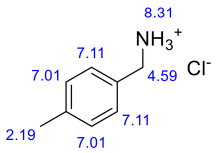

Estimation quality is indicated by color: good, medium, rough

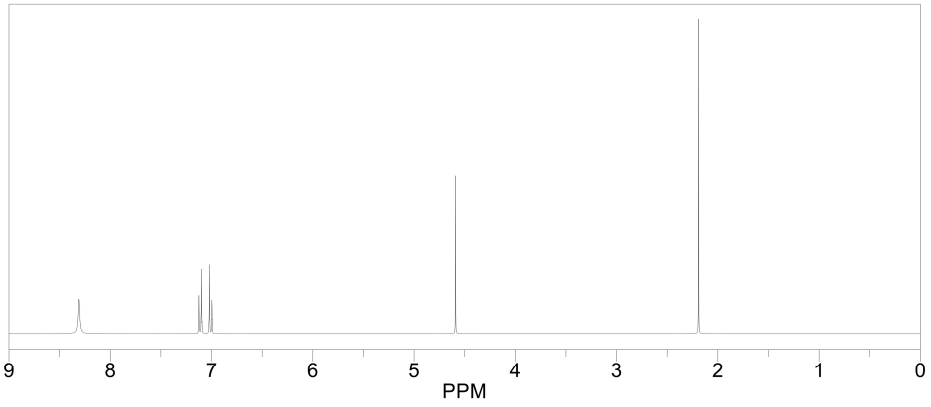

ChemNMR ^{13}C Estimation

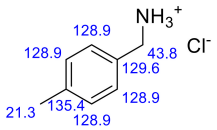

Estimation quality is indicated by color: good, medium, rough

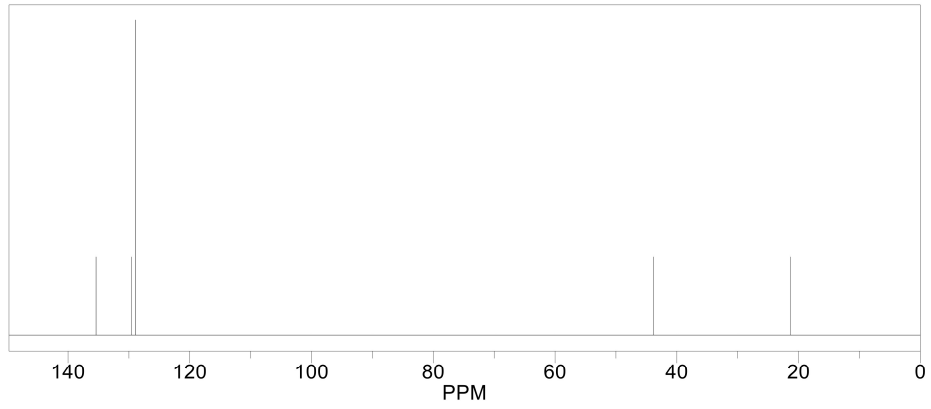

3:

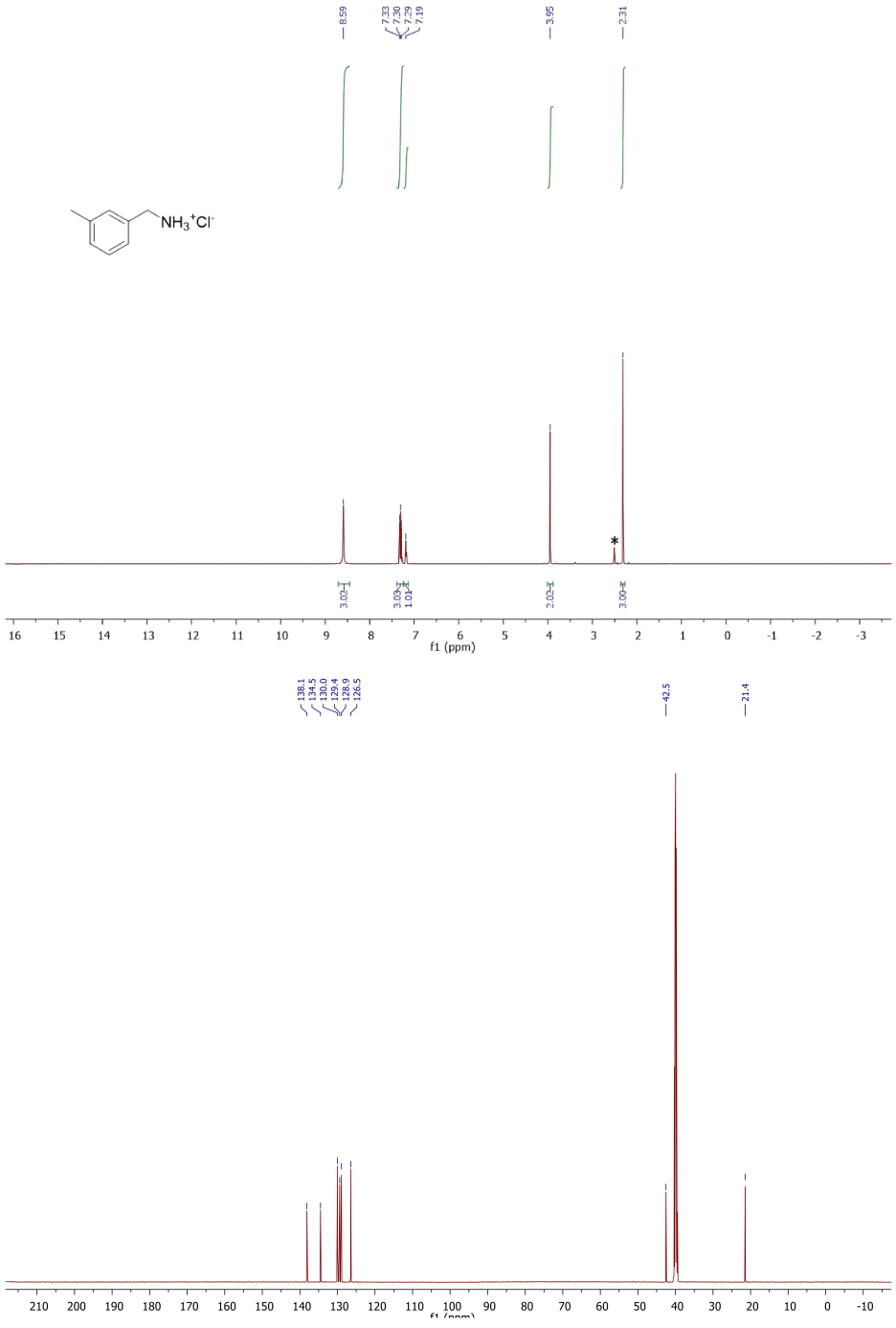
8.59
7.33
7.30
7.29
7.19
3.95
2.31
NH3+Cl-
*
3.02
3.03
1.01
2.02
3.00
f1 (ppm)
138.1
134.5
130.0
129.4
128.9
126.5
42.5
21.4

ChemNMR ^{1}H Estimation

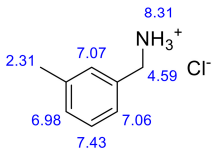

Estimation quality is indicated by color: good, medium, rough

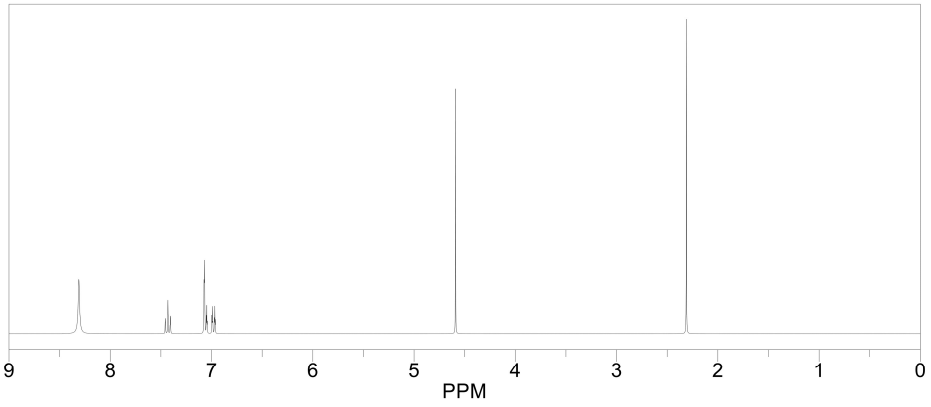

ChemNMR ^{13}C Estimation

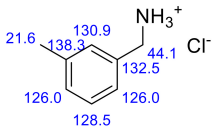

Estimation quality is indicated by color: good, medium, rough

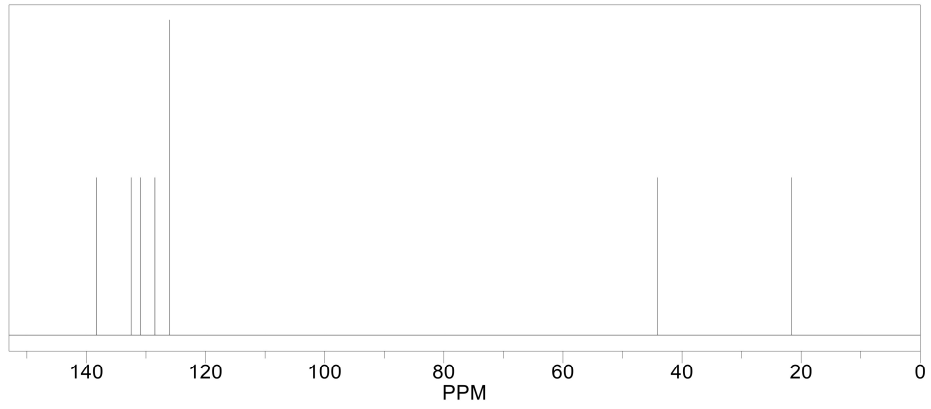

4:

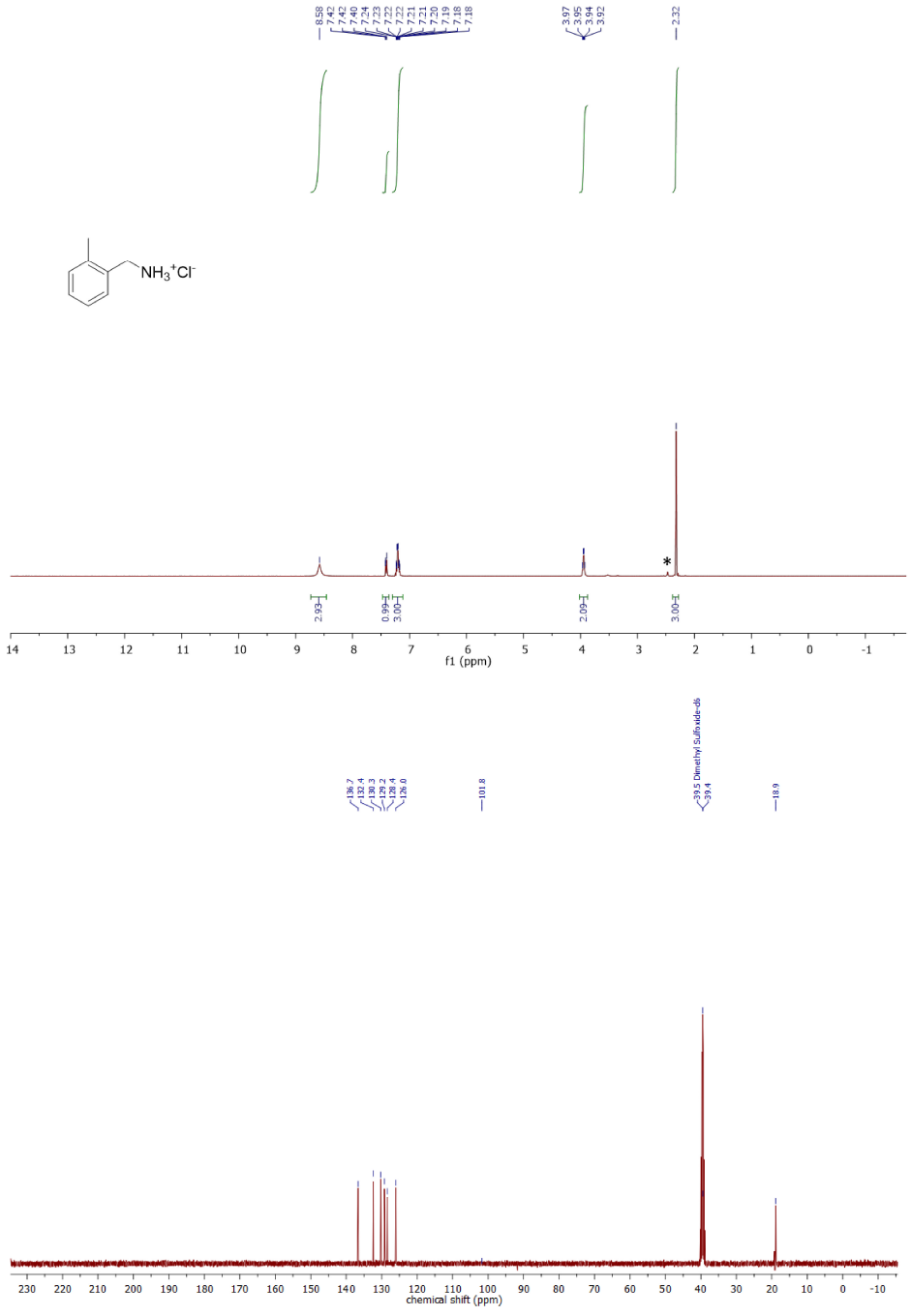
8.58
7.42
7.42
7.40
7.24
7.23
7.22
7.22
7.21
7.21
7.20
7.19
7.18
7.18
3.97
3.95
3.94
3.92
2.32
NH3+Cl-
2.93
0.99
3.00
2.09
3.00
f1 (ppm)
136.7
130.4
130.3
129.2
128.4
126.0
101.8
39.5 Dimethyl Sulfoxide-d6
39.4
18.9
chemical shift (ppm)

SUPPORTING INFORMATION

ChemNMR ^{1}H Estimation

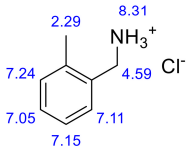

Estimation quality is indicated by color: good, medium, rough

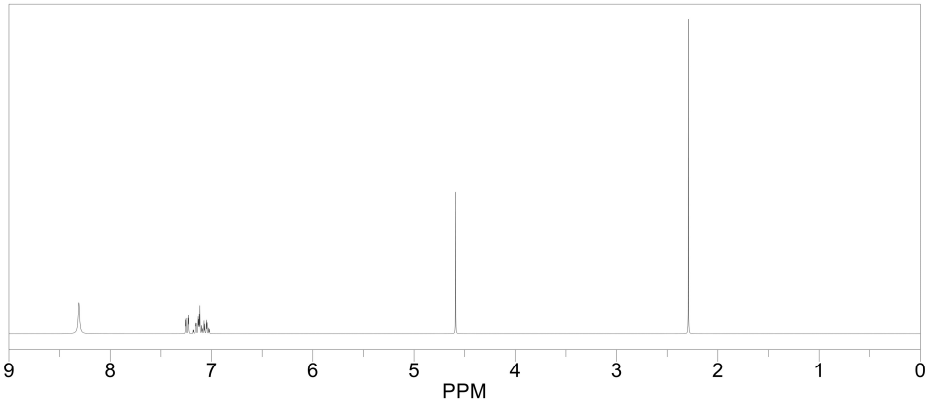

ChemNMR ^{13}C Estimation

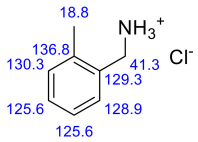

Estimation quality is indicated by color: good, medium, rough

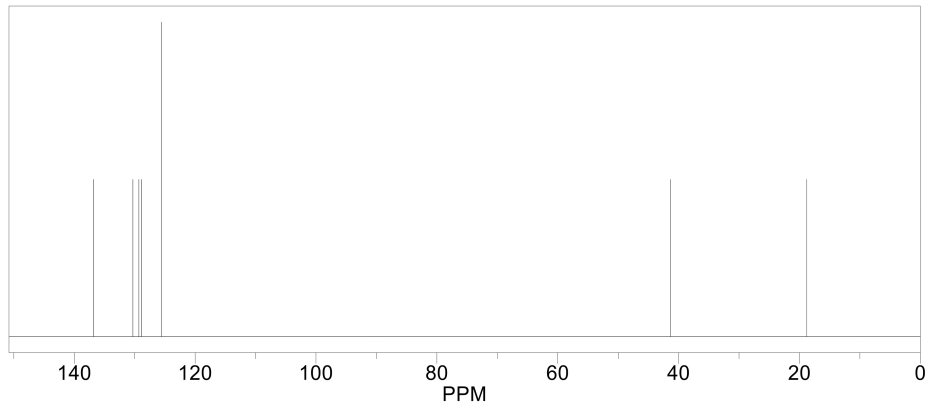

5:

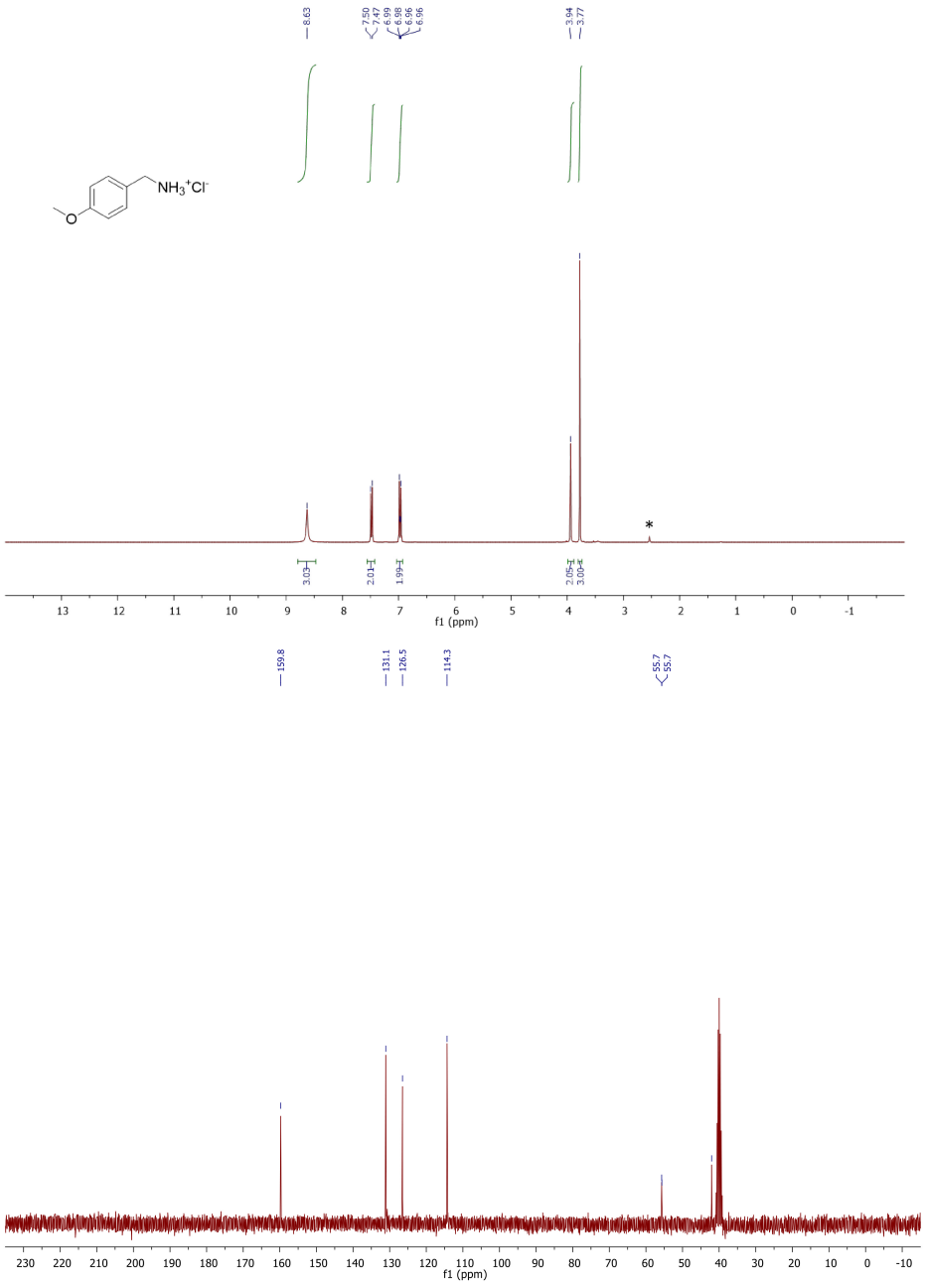
8.63
7.50
7.47
6.99
6.98
6.96
6.96
3.94
3.77
NH3+Cl-
O
*
3.03
2.01
1.99
2.05
3.00
f1 (ppm)
159.8
131.1
126.5
114.3
55.7
55.7
f1 (ppm)

SUPPORTING INFORMATION

ChemNMR ^{1}H Estimation

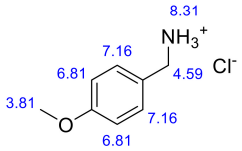

Estimation quality is indicated by color: good, medium, rough

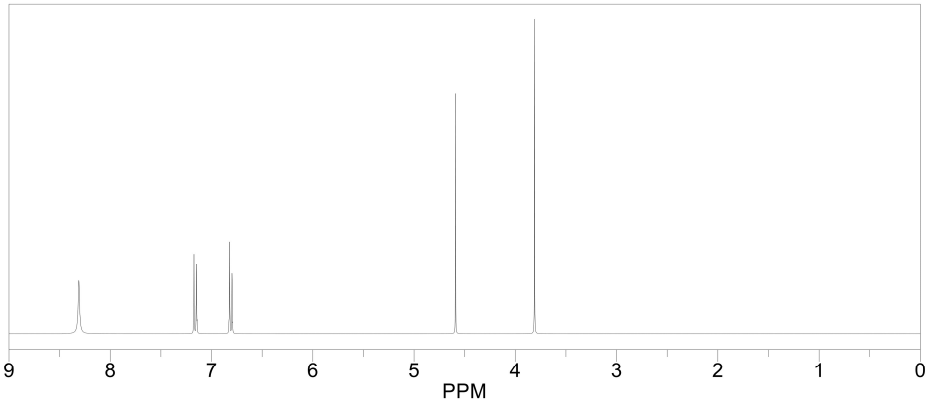

ChemNMR ^{13}C Estimation

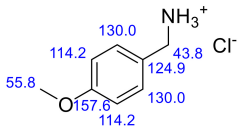

Estimation quality is indicated by color: good, medium, rough

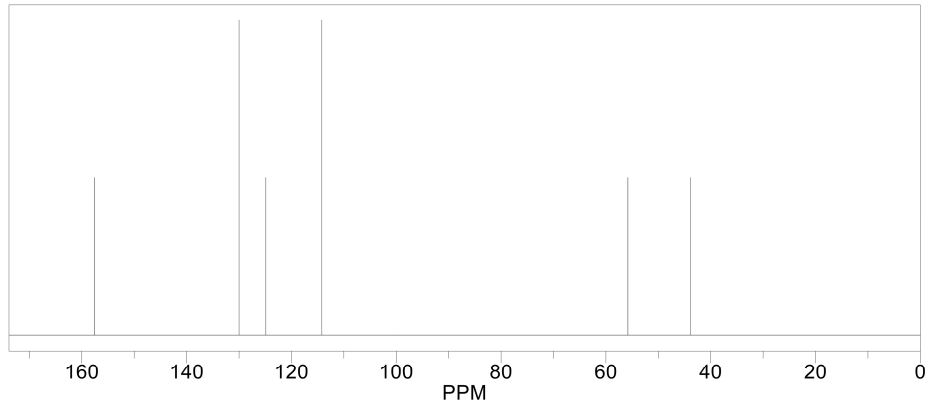

6:

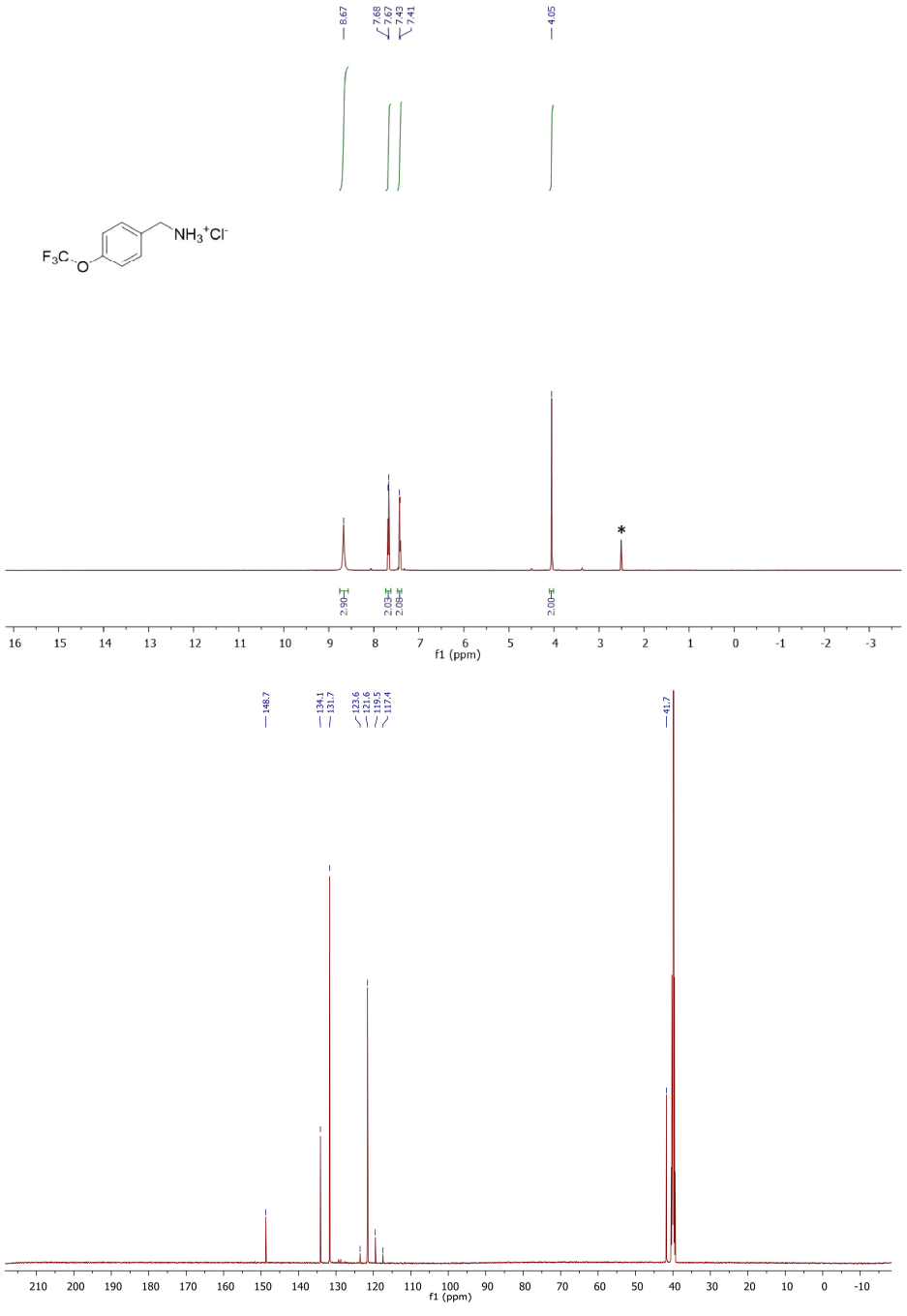
8.67
7.68
7.67
7.43
7.41
4.05
NH3+Cl-
F3C
O
*
2.90
2.03
2.08
2.00
f1 (ppm)
148.7
134.1
131.7
123.6
121.6
119.5
117.4
41.7
f1 (ppm)

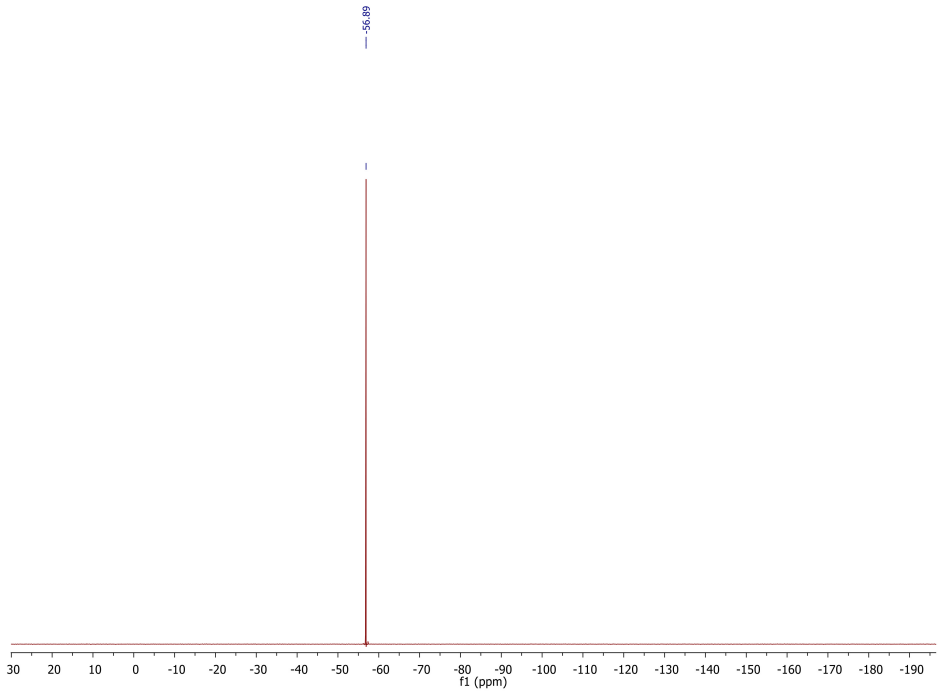
-56.89
30 20 10 0 -10 -20 -30 -40 -50 -60 -70 -80 -90 -100 -110 -120 -130 -140 -150 -160 -170 -180 -190
f1 (ppm)

ChemNMR ^{1}H Estimation

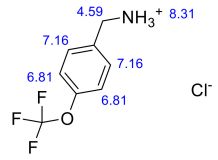

Estimation quality is indicated by color: good, medium, rough

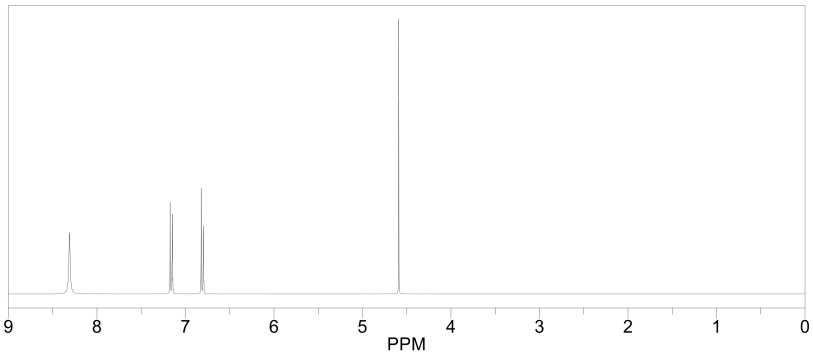

ChemNMR ^{13}C Estimation

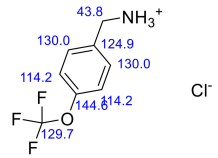

Estimation quality is indicated by color: good, medium, rough

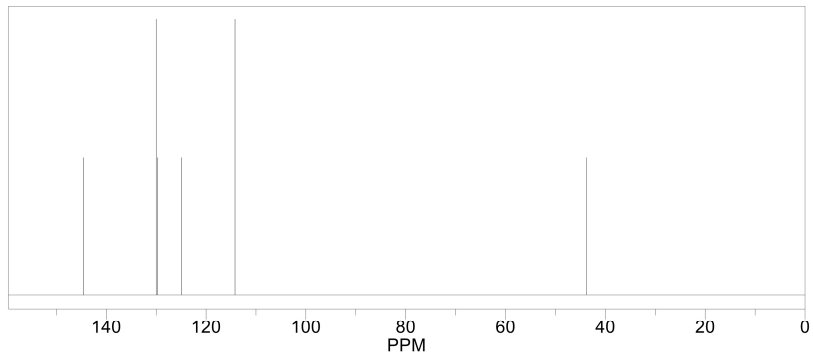

7:

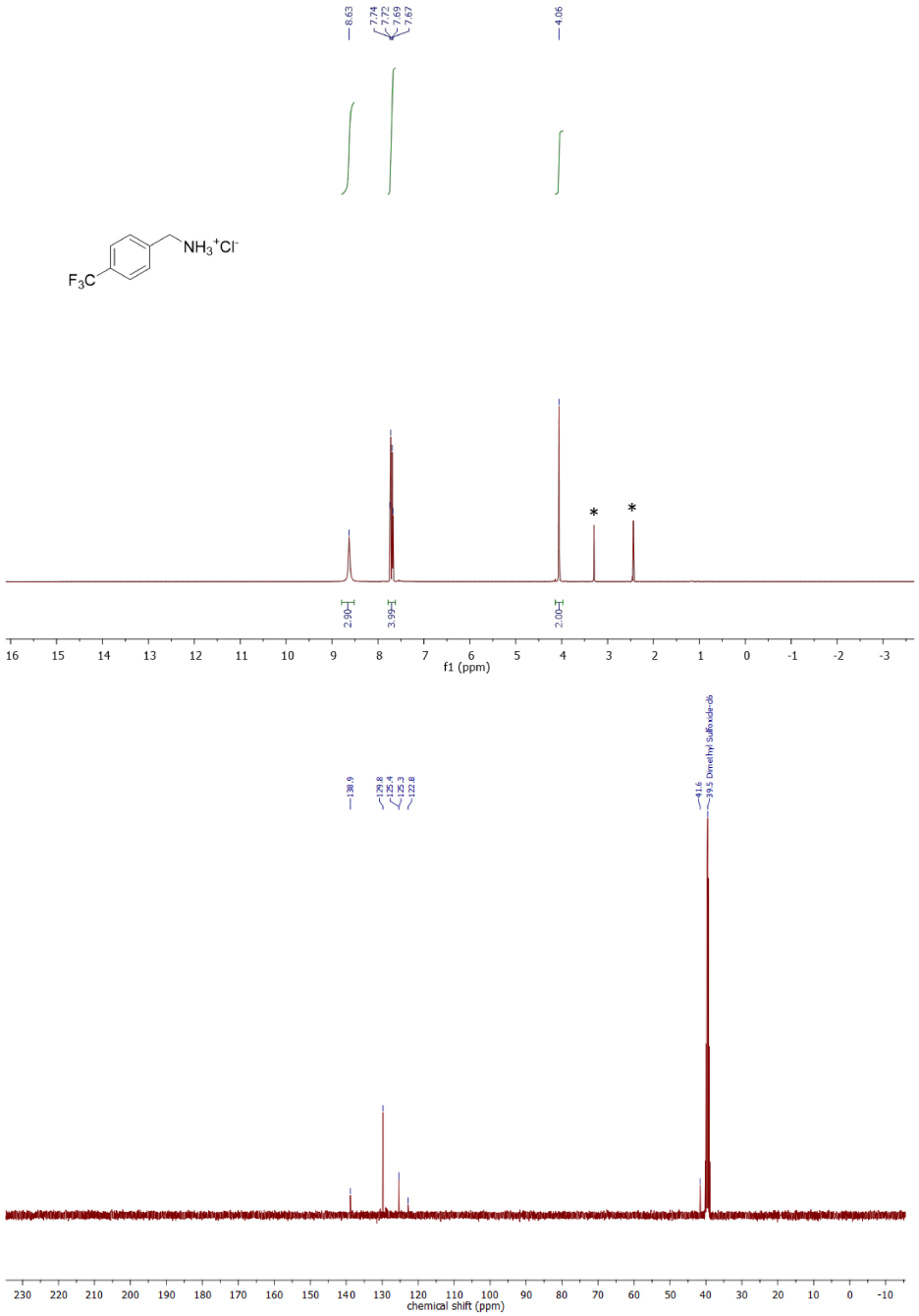
8.63
7.74
7.72
7.69
7.67
4.06
NH3+Cl-
F3C
2.90
3.99
2.00
f1 (ppm)
138.9
129.8
125.4
125.3
122.8
41.6
39.5 Dimethyl Sulfoxide-d6
chemical shift (ppm)

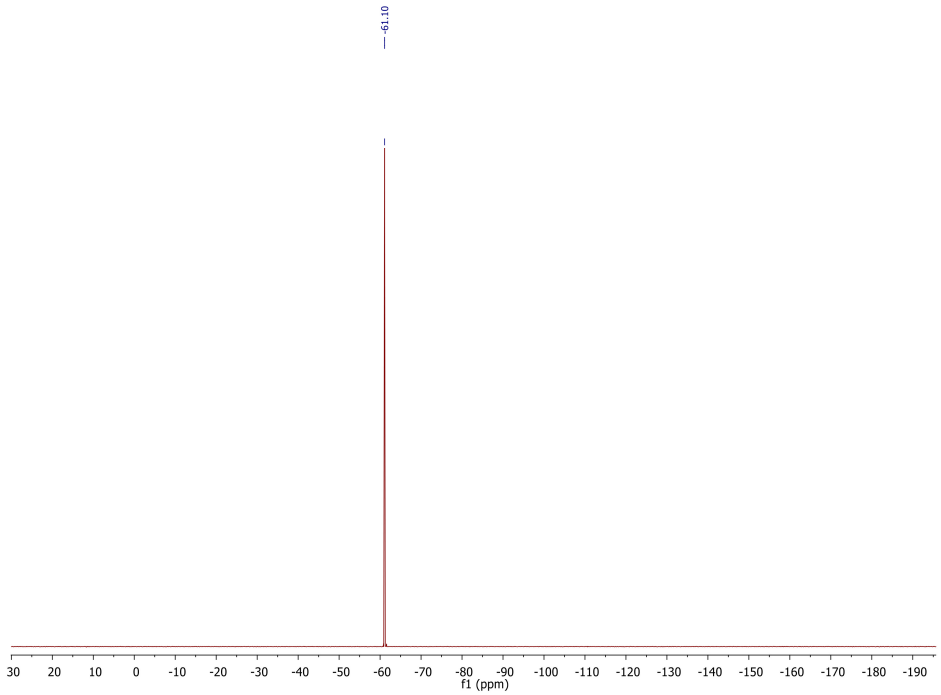
-61.10
30 20 10 0 -10 -20 -30 -40 -50 -60 -70 -80 -90 -100 -110 -120 -130 -140 -150 -160 -170 -180 -190
f1 (ppm)

ChemNMR ^{1}H Estimation

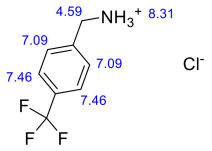

Estimation quality is indicated by color: good, medium, rough

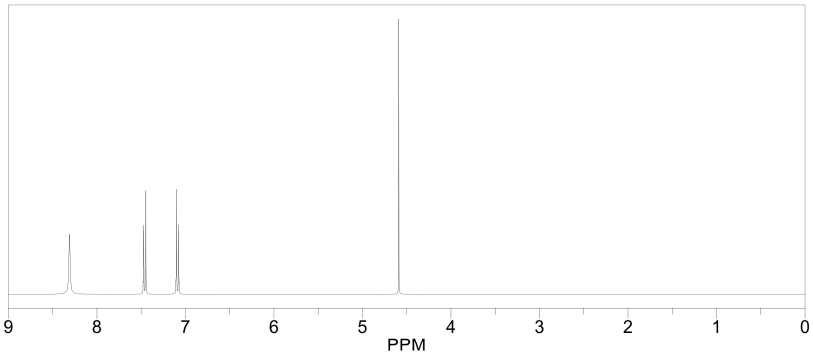

ChemNMR ^{13}C Estimation

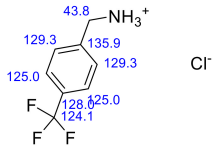

Estimation quality is indicated by color: good, medium, rough

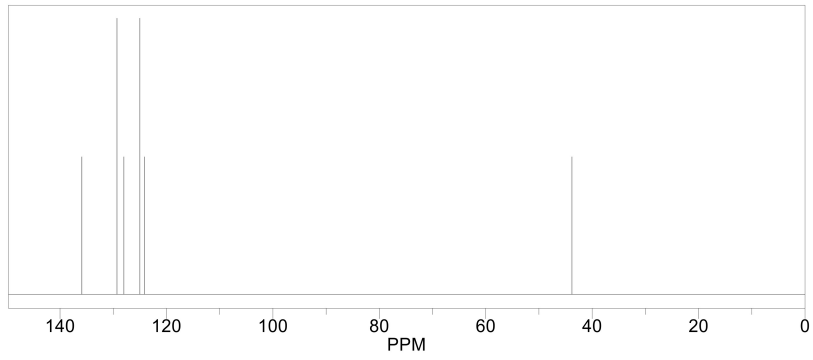

8:

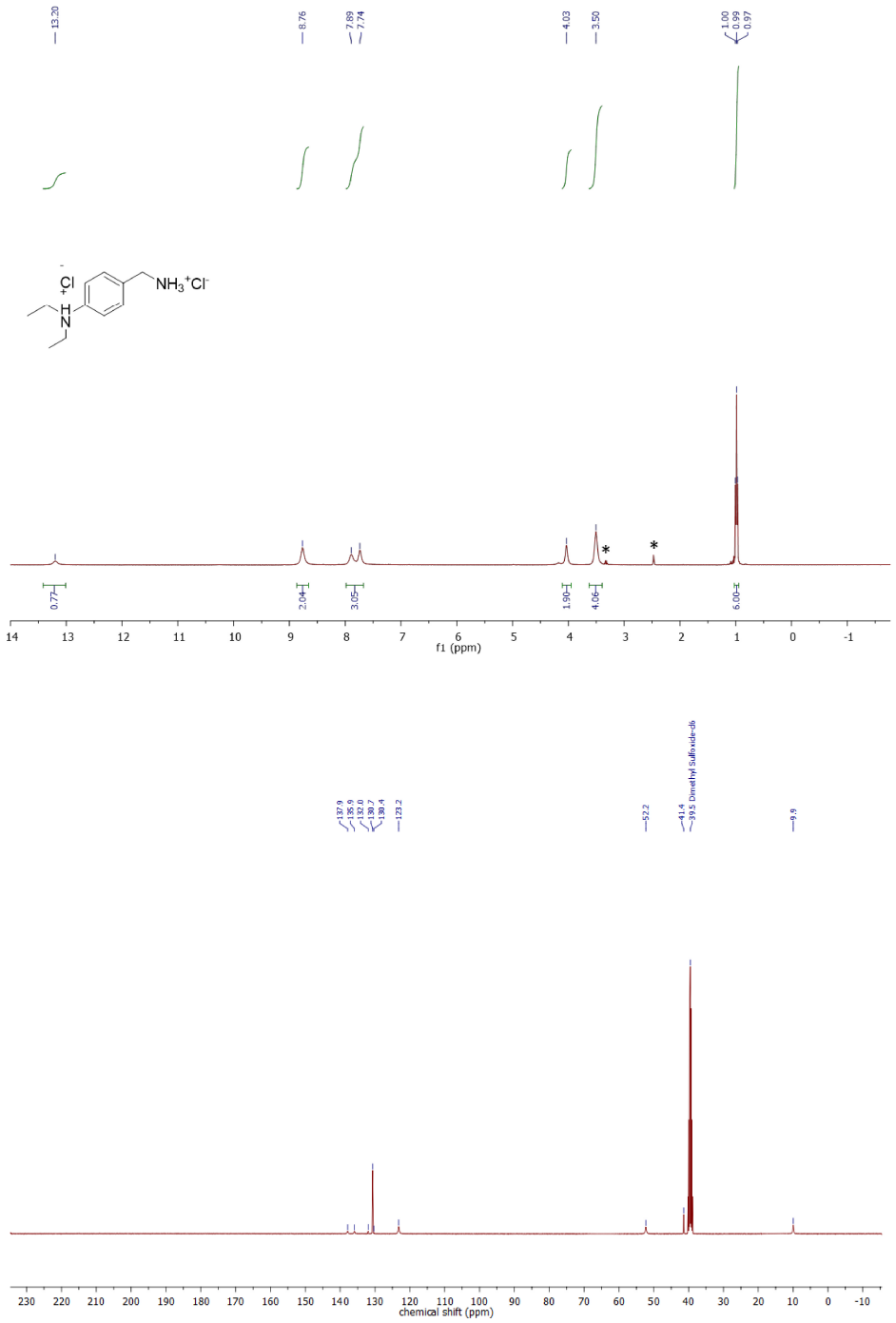
13.20
8.76
7.89
7.74
4.03
3.50
1.00
0.99
0.97
Cl
H
N
NH3+Cl-
0.77
2.04
3.05
1.90
4.06
6.00
f1 (ppm)
137.9
135.9
132.0
130.7
130.4
123.2
52.2
41.4
39.5 Dimethyl Sulfoxide-d6
19.9
chemical shift (ppm)

SUPPORTING INFORMATION

ChemNMR ^{1}H Estimation

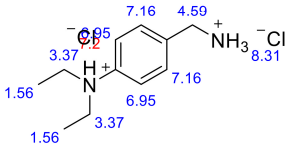

Estimation quality is indicated by color: good, medium, rough

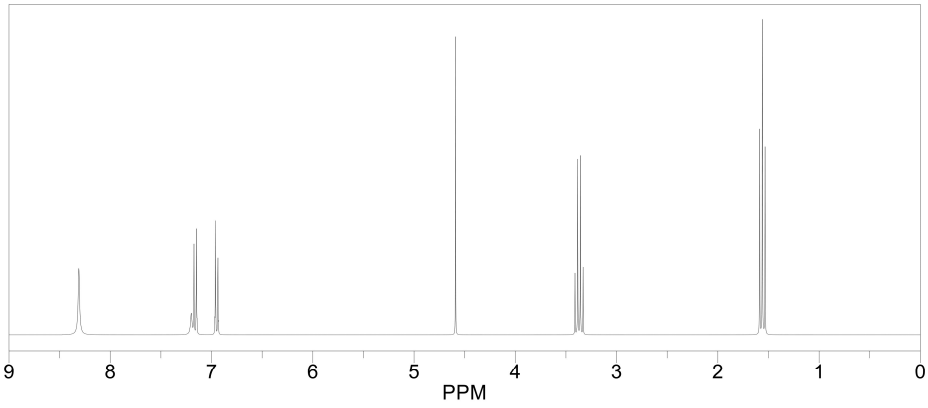

ChemNMR ^{13}C Estimation

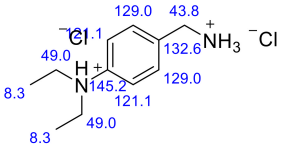

Estimation quality is indicated by color: good, medium, rough

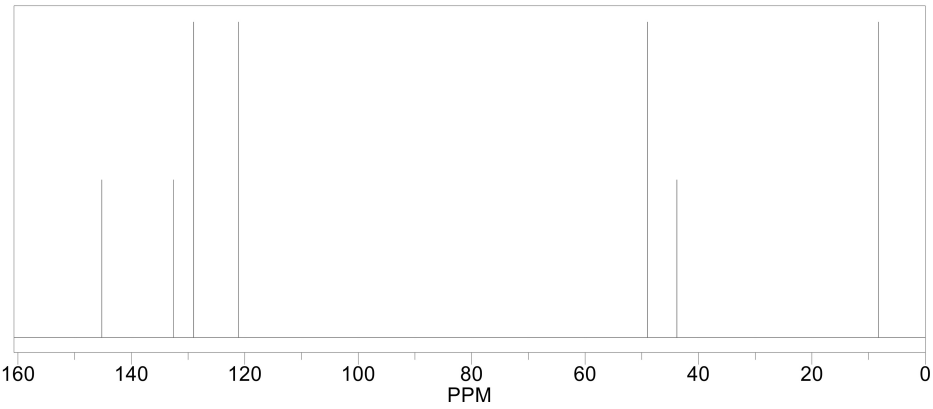

54

9:

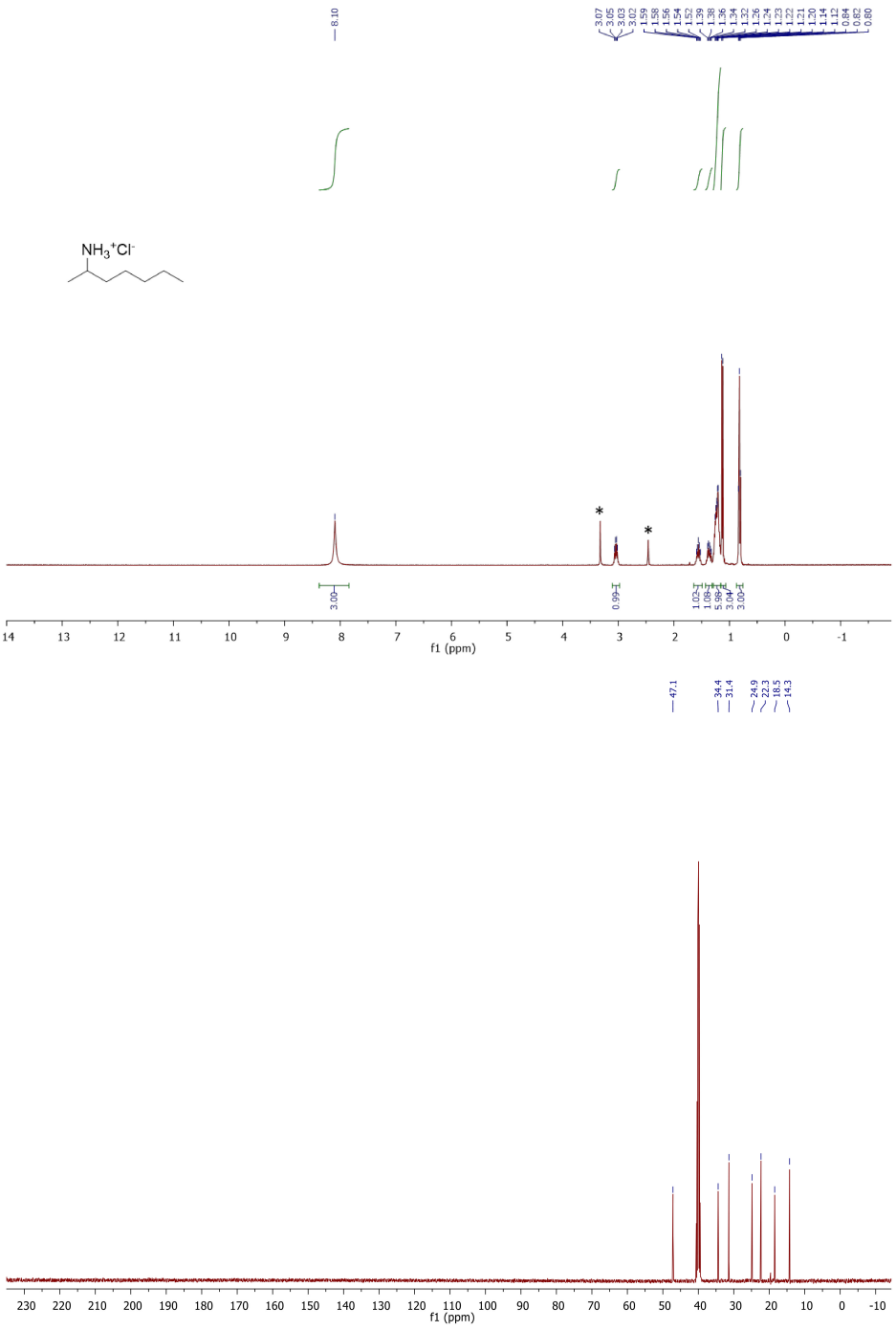
8.10
3.07
3.05
3.03
3.02
1.59
1.58
1.56
1.54
1.53
1.39
1.38
1.36
1.34
1.32
1.26
1.24
1.23
1.22
1.21
1.20
1.14
1.12
0.84
0.82
0.80
NH3+Cl-
3.00
0.99
1.02
1.08
5.99
3.04
3.00
14 13 12 11 10 9 8 7 6 5 4 3 2 1 0 -1
f1 (ppm)
47.1
34.4
31.4
24.9
22.3
18.5
14.3
230 220 210 200 190 180 170 160 150 140 130 120 110 100 90 80 70 60 50 40 30 20 10 0 -10
f1 (ppm)

SUPPORTING INFORMATION

ChemNMR ^{1}H Estimation

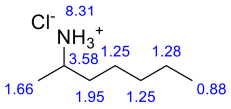

Estimation quality is indicated by color: good, medium, rough

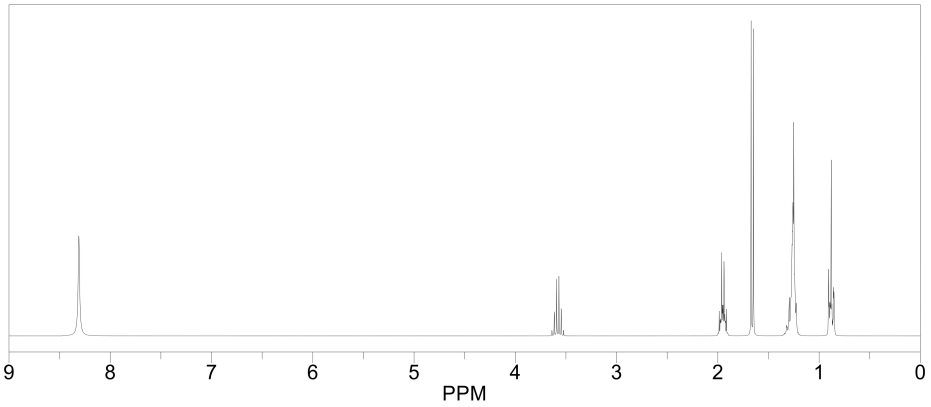

ChemNMR ^{13}C Estimation

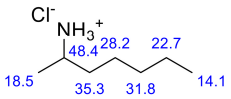

Estimation quality is indicated by color: good, medium, rough

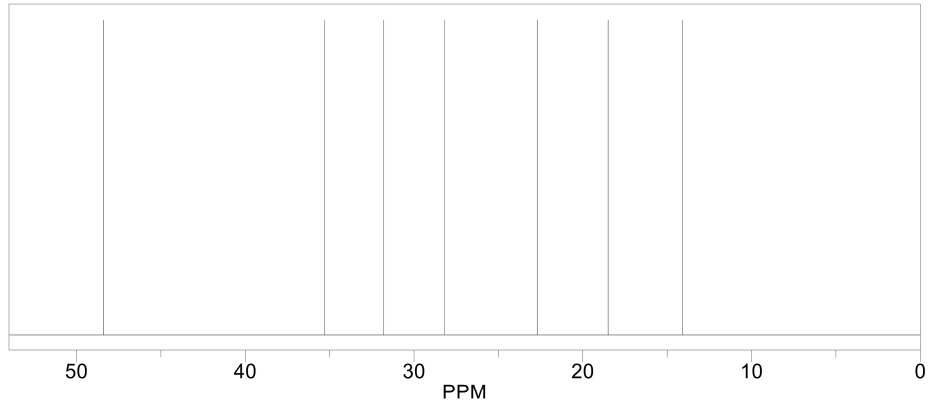

10:

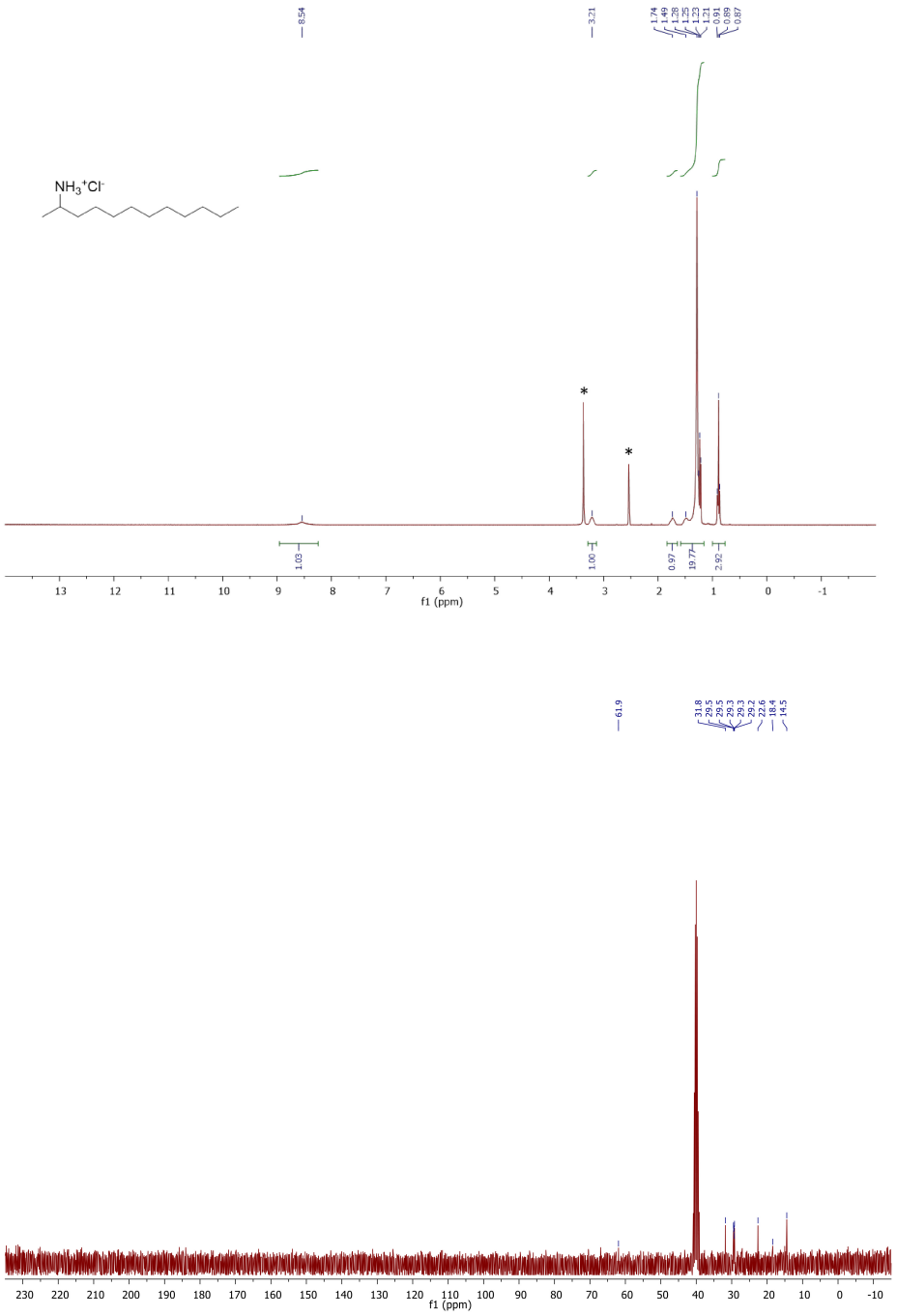
8.54
3.21
1.74
1.49
1.38
1.25
1.23
1.21
0.91
0.89
0.87
NH3+Cl-
*
*
1.03
1.00
0.97
19.77
2.92
f1 (ppm)
61.9
31.8
29.5
29.5
29.3
29.3
29.2
22.6
18.4
14.5
f1 (ppm)

ChemNMR ^{1}H Estimation

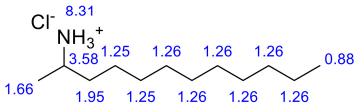

Estimation quality is indicated by color: good, medium, rough

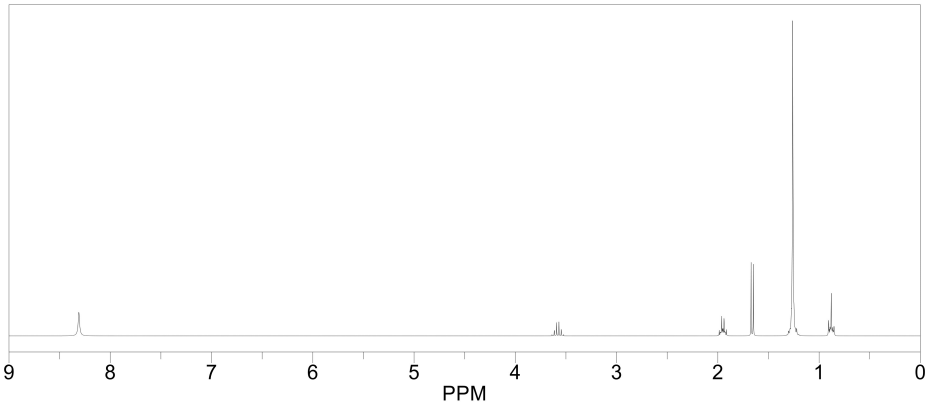

ChemNMR ^{13}C Estimation

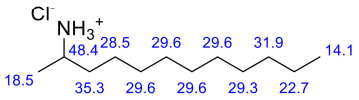

Estimation quality is indicated by color: good, medium, rough

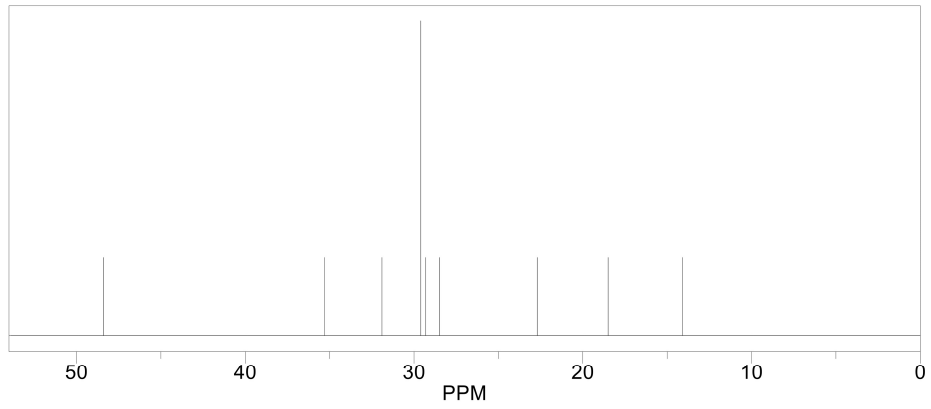

11:

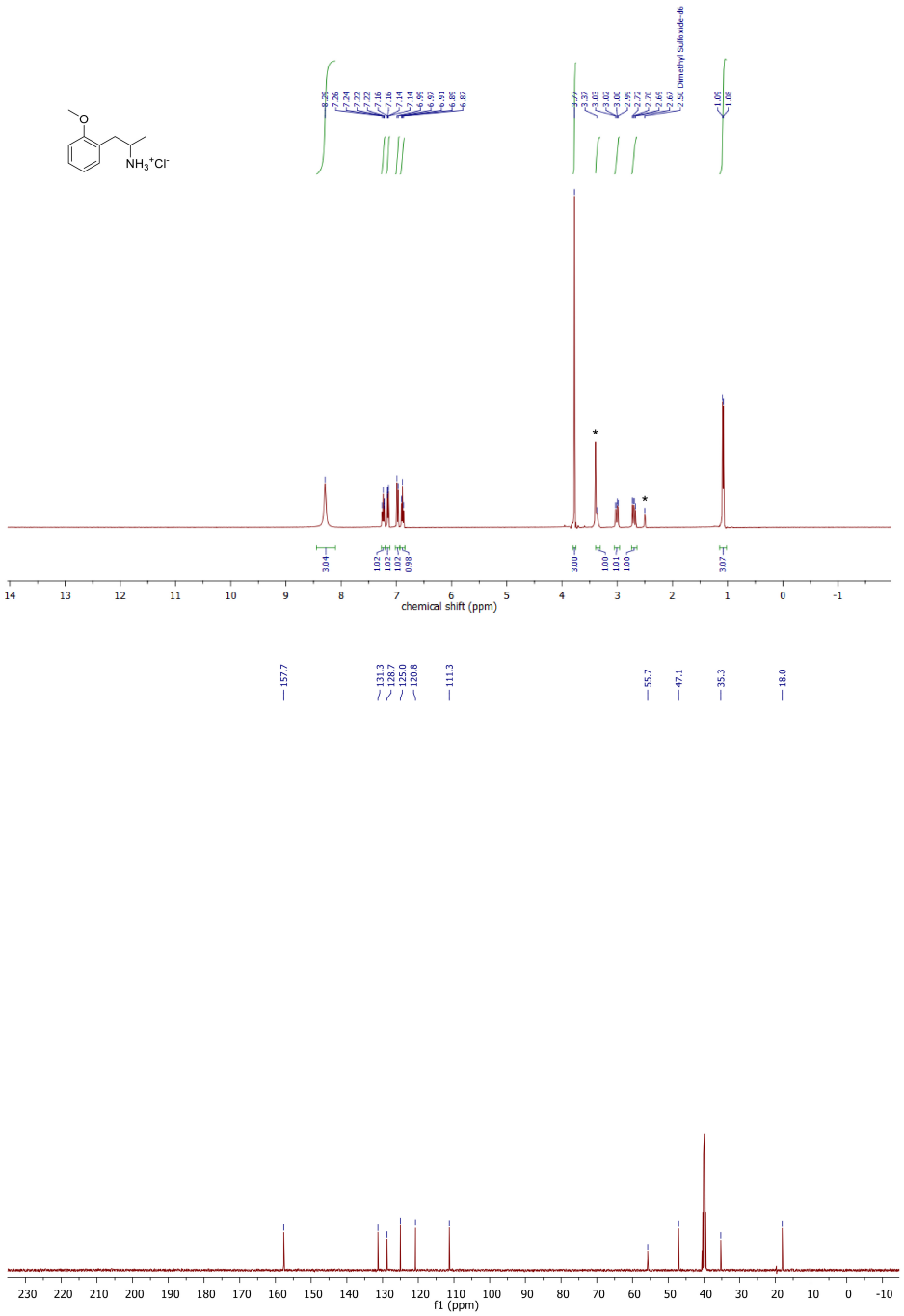

SUPPORTING INFORMATION

ChemNMR ^{1}H Estimation

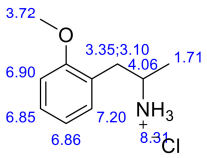

Estimation quality is indicated by color: good, medium, rough

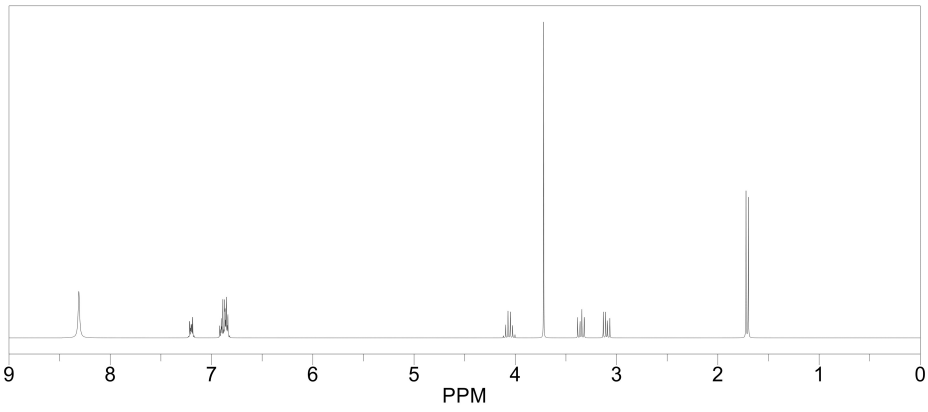

ChemNMR ^{13}C Estimation

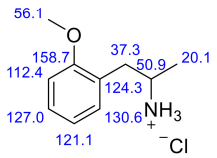

Estimation quality is indicated by color: good, medium, rough

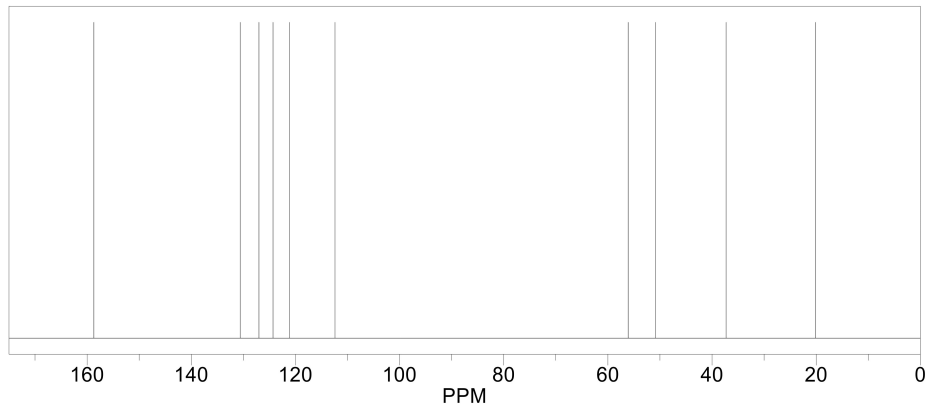

60

12:

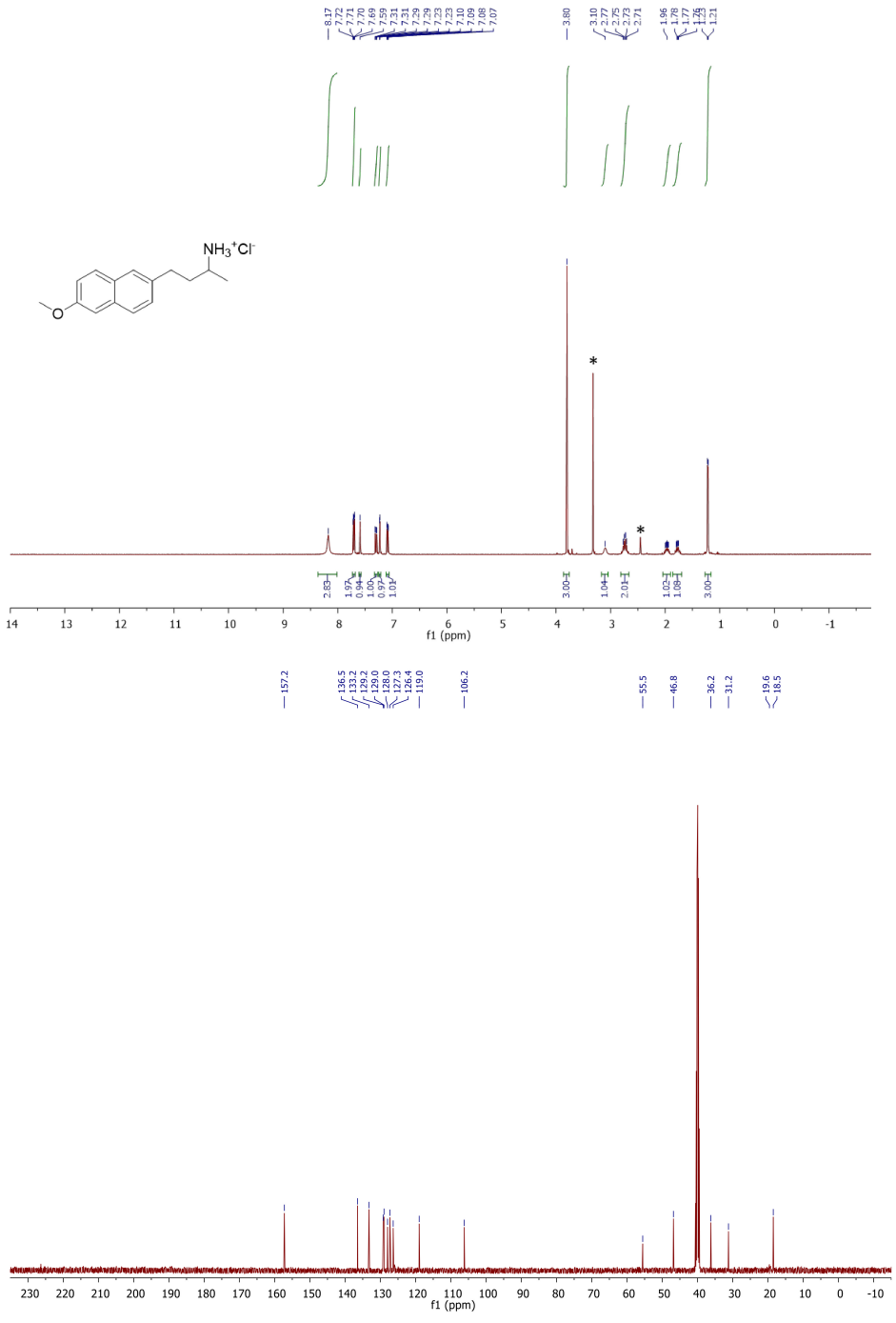

SUPPORTING INFORMATION

ChemNMR ^{1}H Estimation

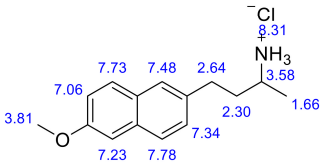

Estimation quality is indicated by color: good, medium, rough

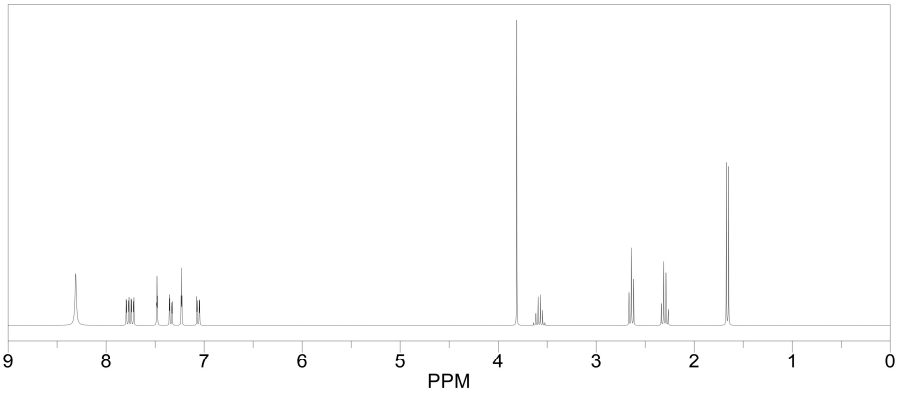

ChemNMR ^{13}C Estimation

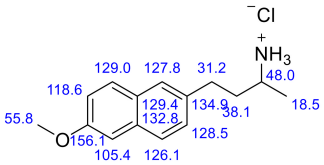

Estimation quality is indicated by color: good, medium, rough

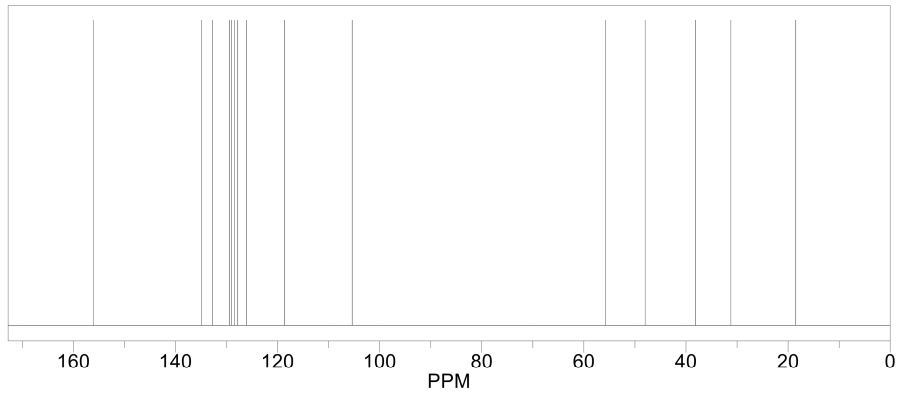

13:

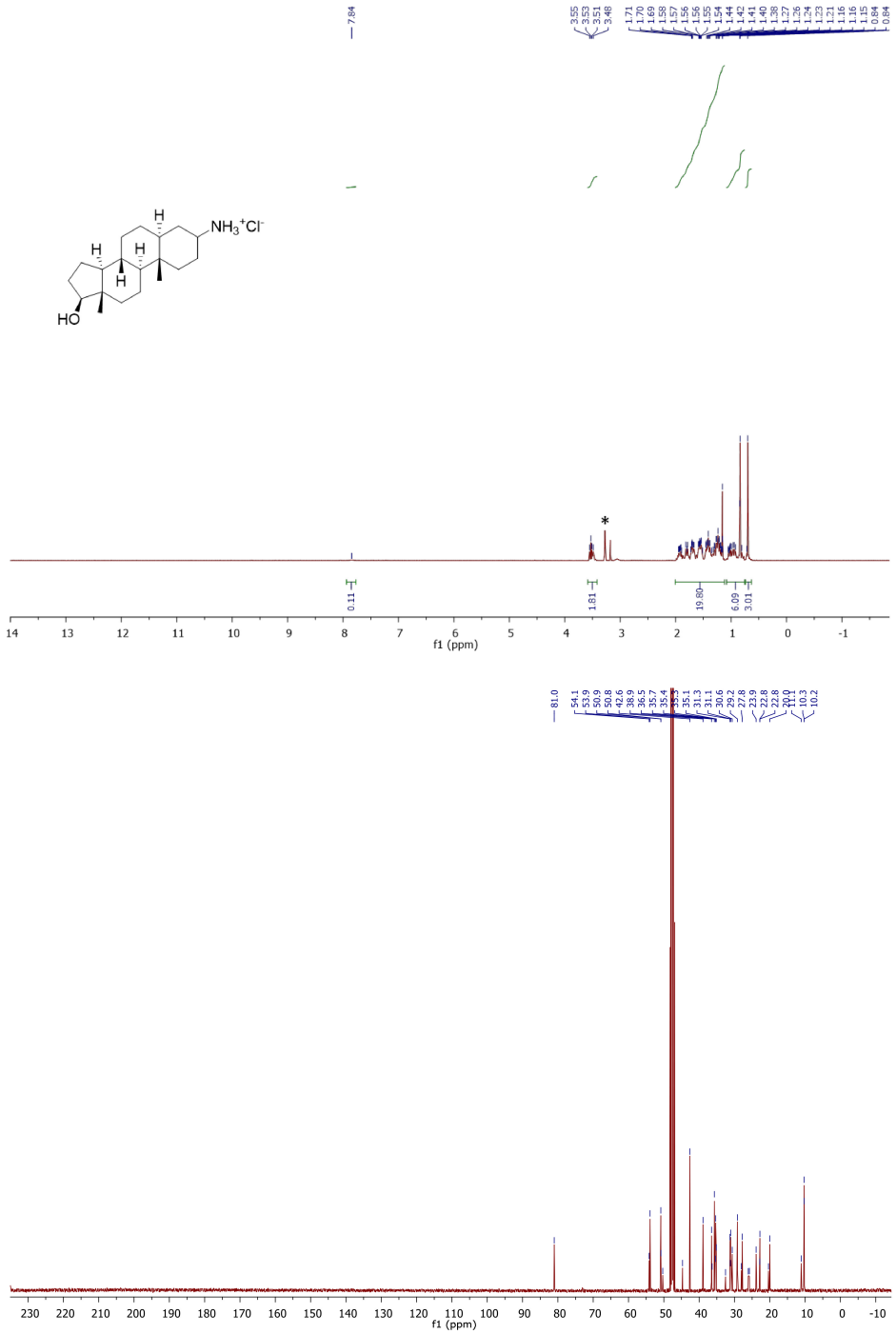

SUPPORTING INFORMATION

ChemNMR ^{1}H Estimation

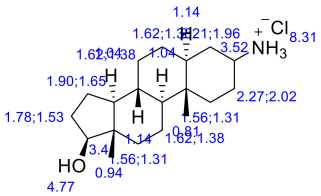

Estimation quality is indicated by color: good, medium, rough

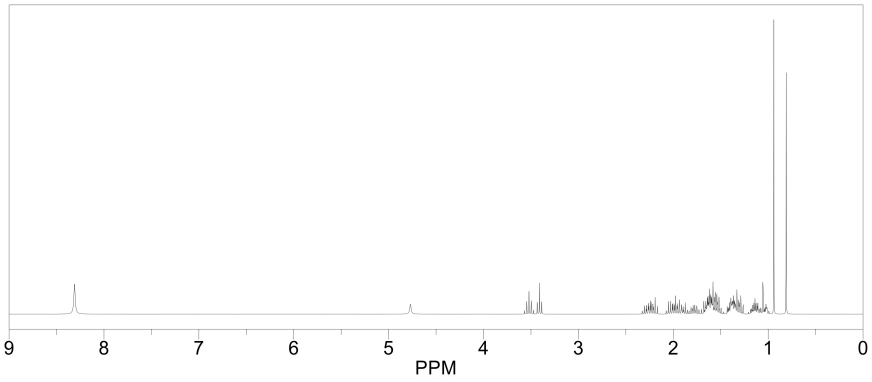

ChemNMR ^{13}C Estimation

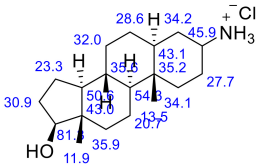

Estimation quality is indicated by color: good, medium, rough

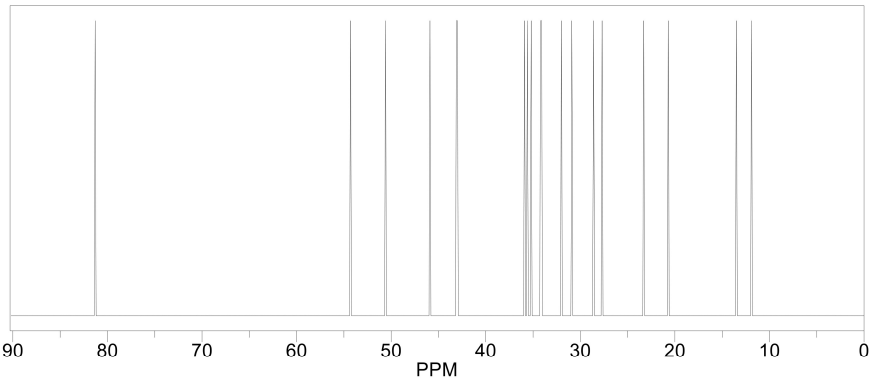

14:

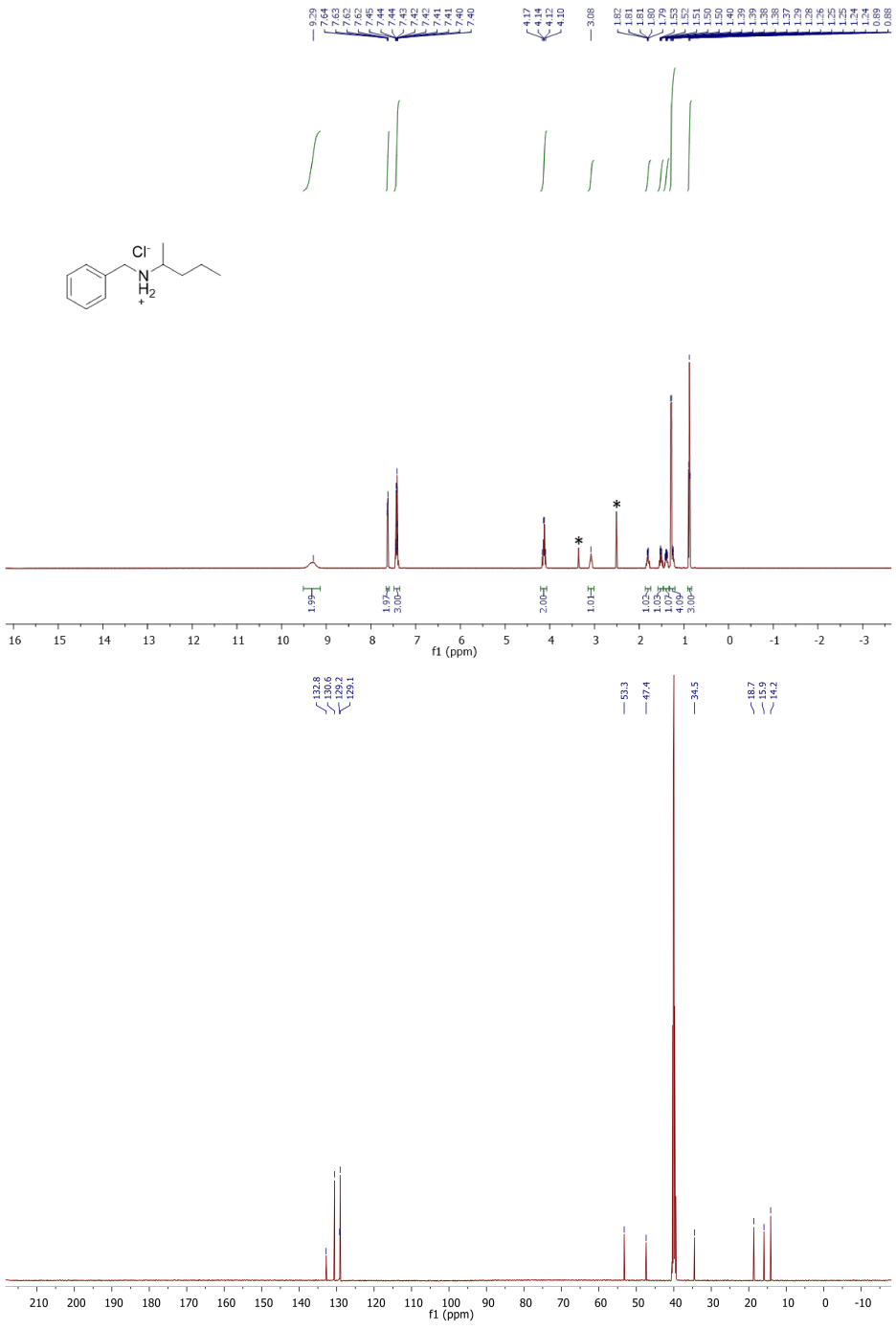

SUPPORTING INFORMATION

ChemNMR ^{1}H Estimation

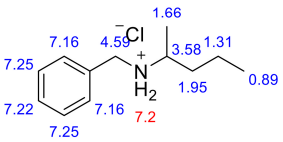

Estimation quality is indicated by color: good, medium, rough

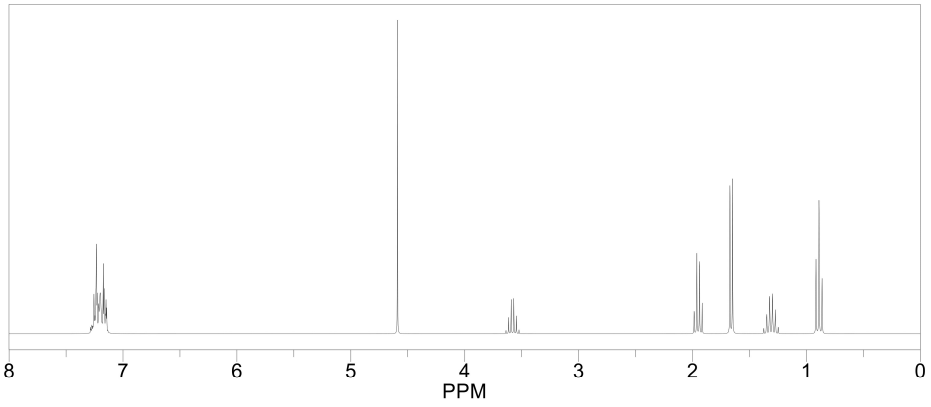

ChemNMR ^{13}C Estimation

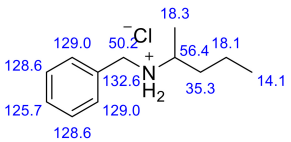

Estimation quality is indicated by color: good, medium, rough

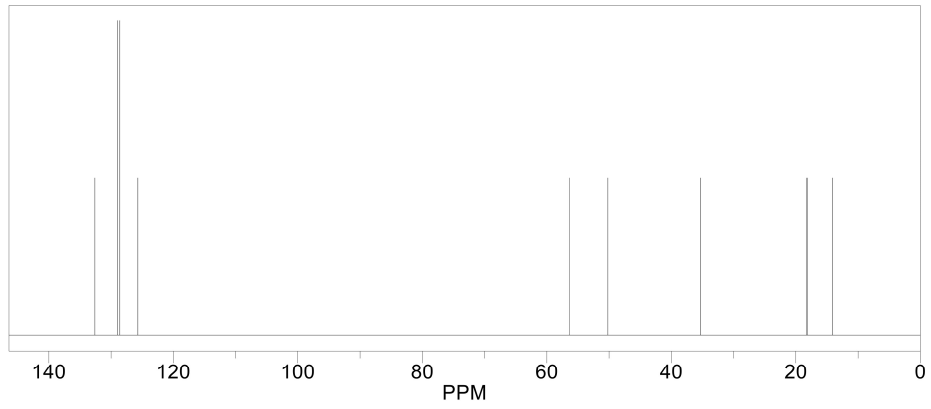

15:

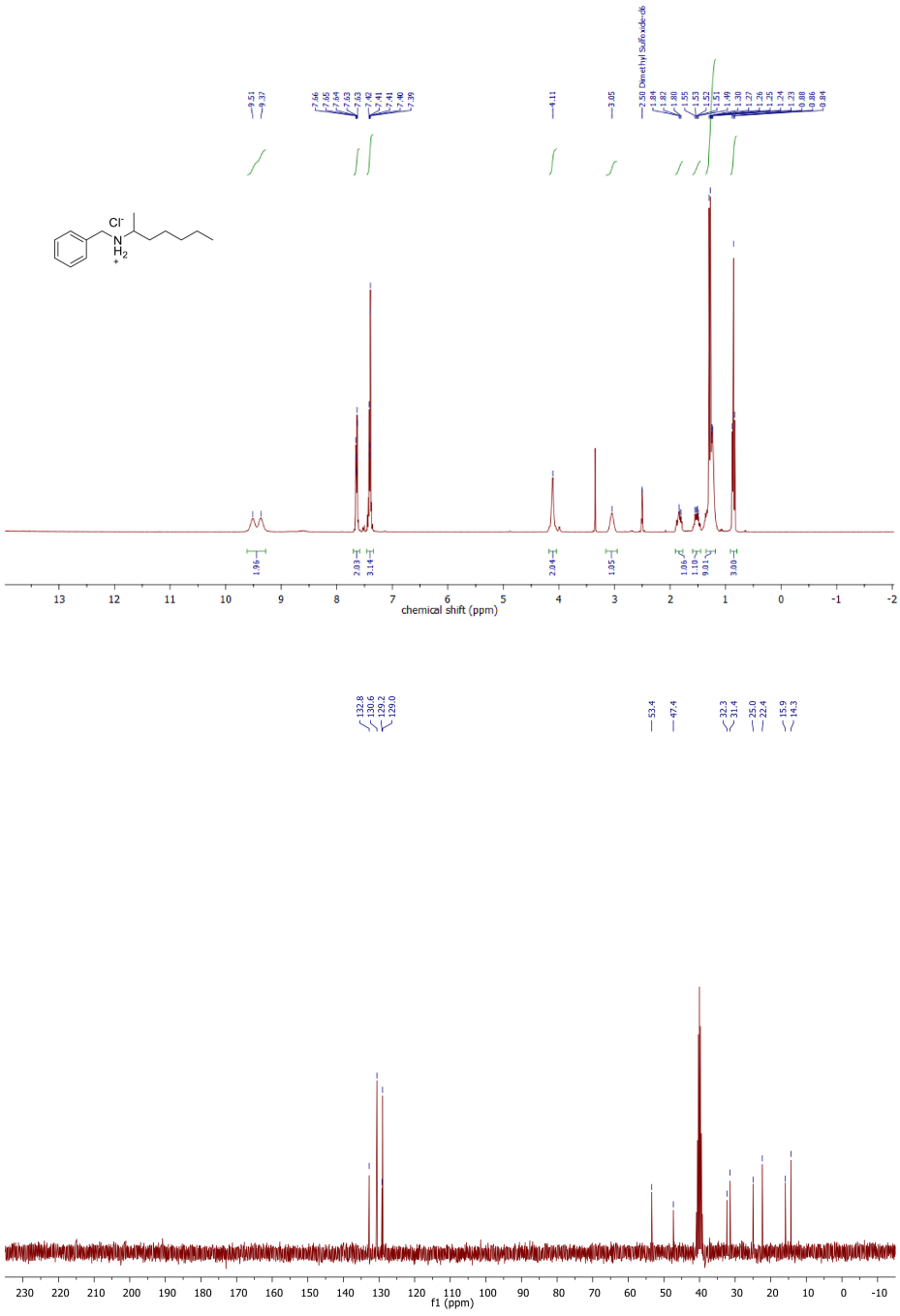
9.51
9.37
7.66
7.65
7.64
7.63
7.63
7.42
7.41
7.41
7.40
7.39
4.11
3.05
2.50 Dimethyl Sulfoxide-d6
1.84
1.82
1.80
1.55
1.53
1.52
1.51
1.49
1.30
1.27
1.26
1.25
1.24
1.23
0.88
0.86
0.84
Cl⁻
NH2
1.96
2.03
3.14
2.04
1.05
1.06
1.10
9.01
3.00
chemical shift (ppm)
132.8
130.6
129.2
129.0
53.4
47.4
32.3
31.4
25.0
22.4
15.9
14.3
f1 (ppm)

SUPPORTING INFORMATION

ChemNMR ^{1}H Estimation

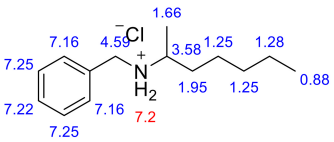

Estimation quality is indicated by color: good, medium, rough

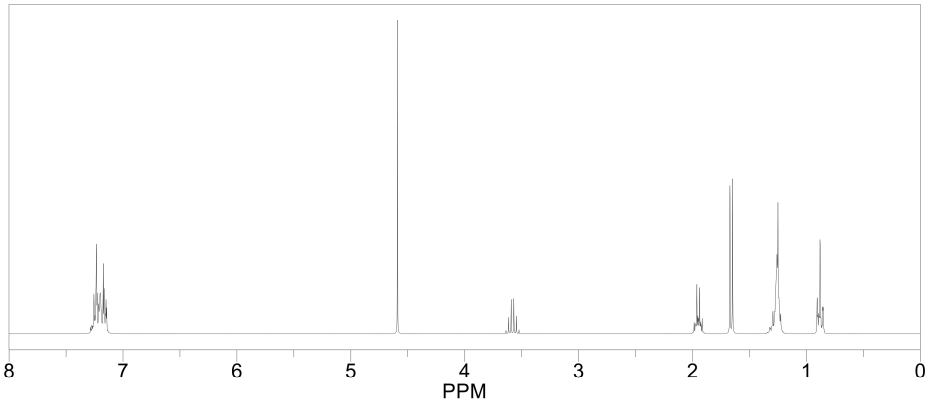

ChemNMR ^{13}C Estimation

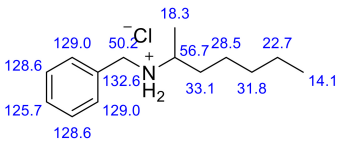

Estimation quality is indicated by color: good, medium, rough

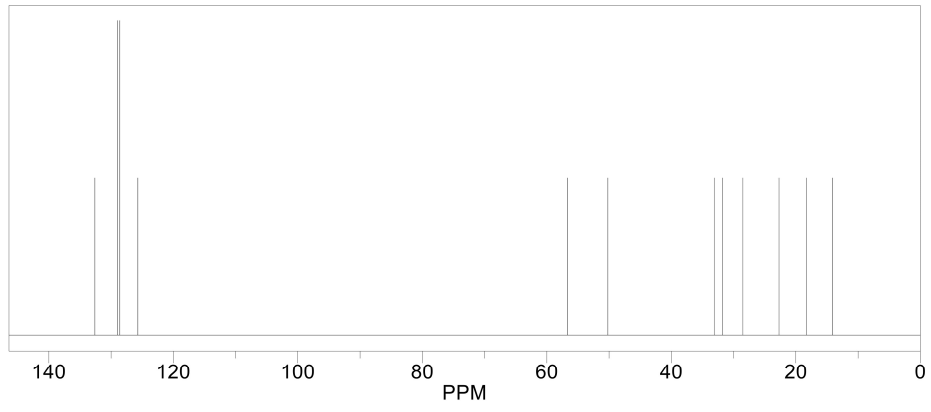

16:

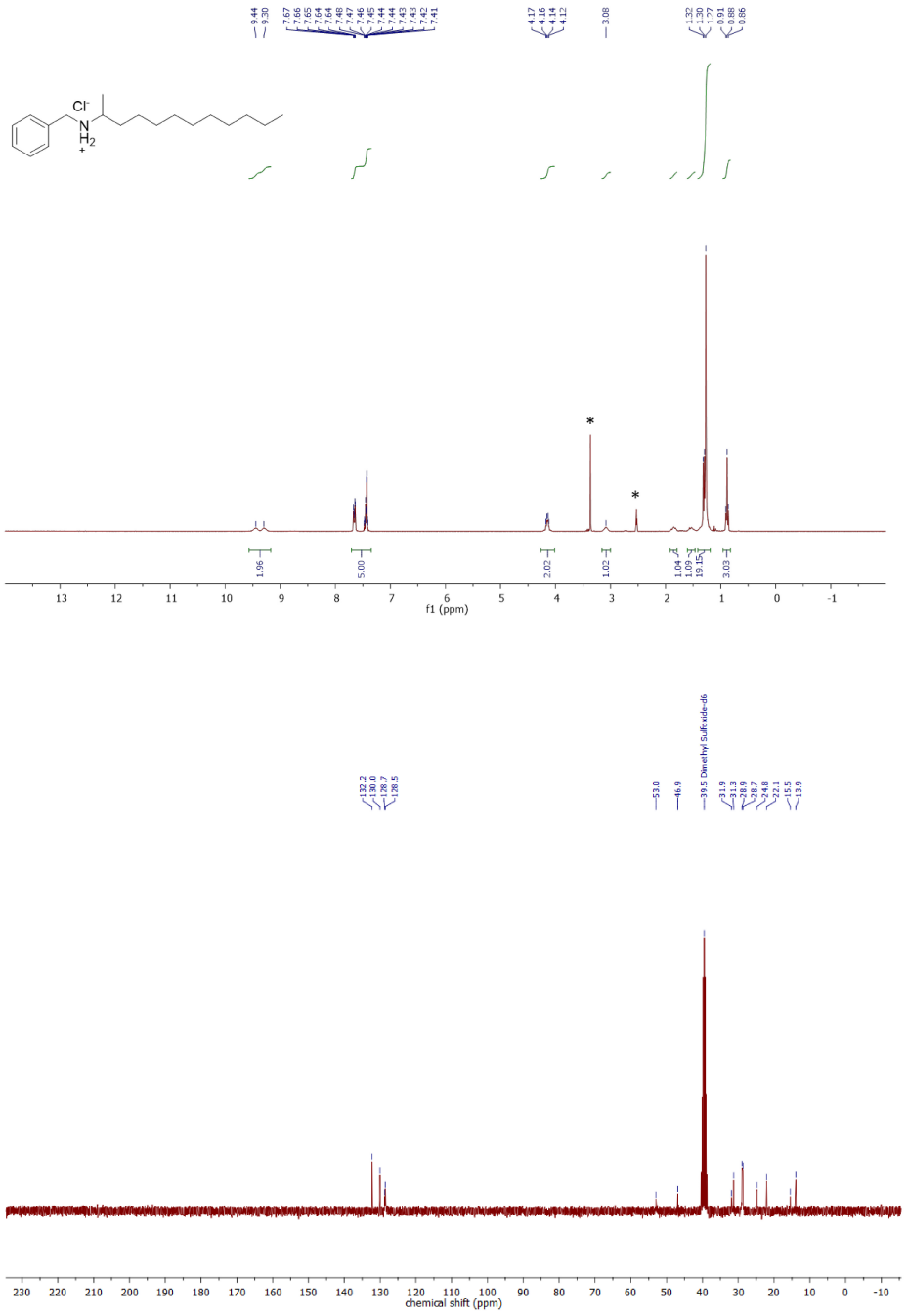

SUPPORTING INFORMATION

ChemNMR ^{1}H Estimation

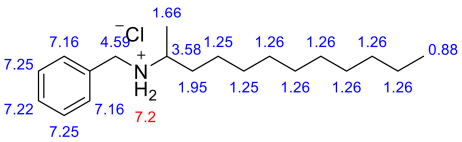

Estimation quality is indicated by color: good, medium, rough

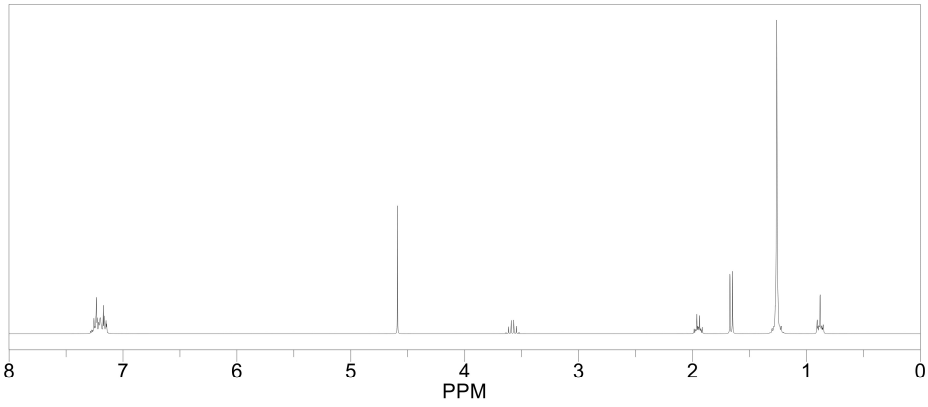

ChemNMR ^{13}C Estimation

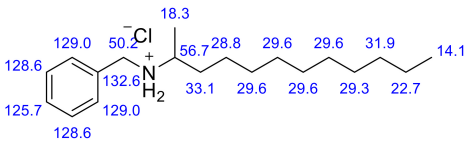

Estimation quality is indicated by color: good, medium, rough

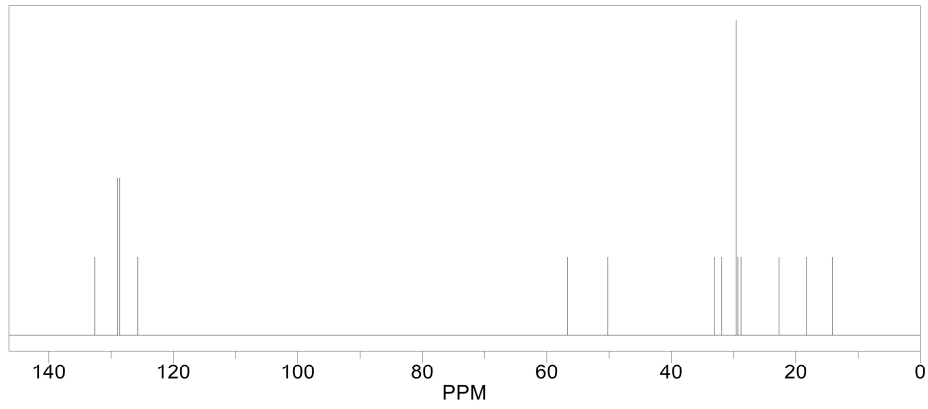

70

17:

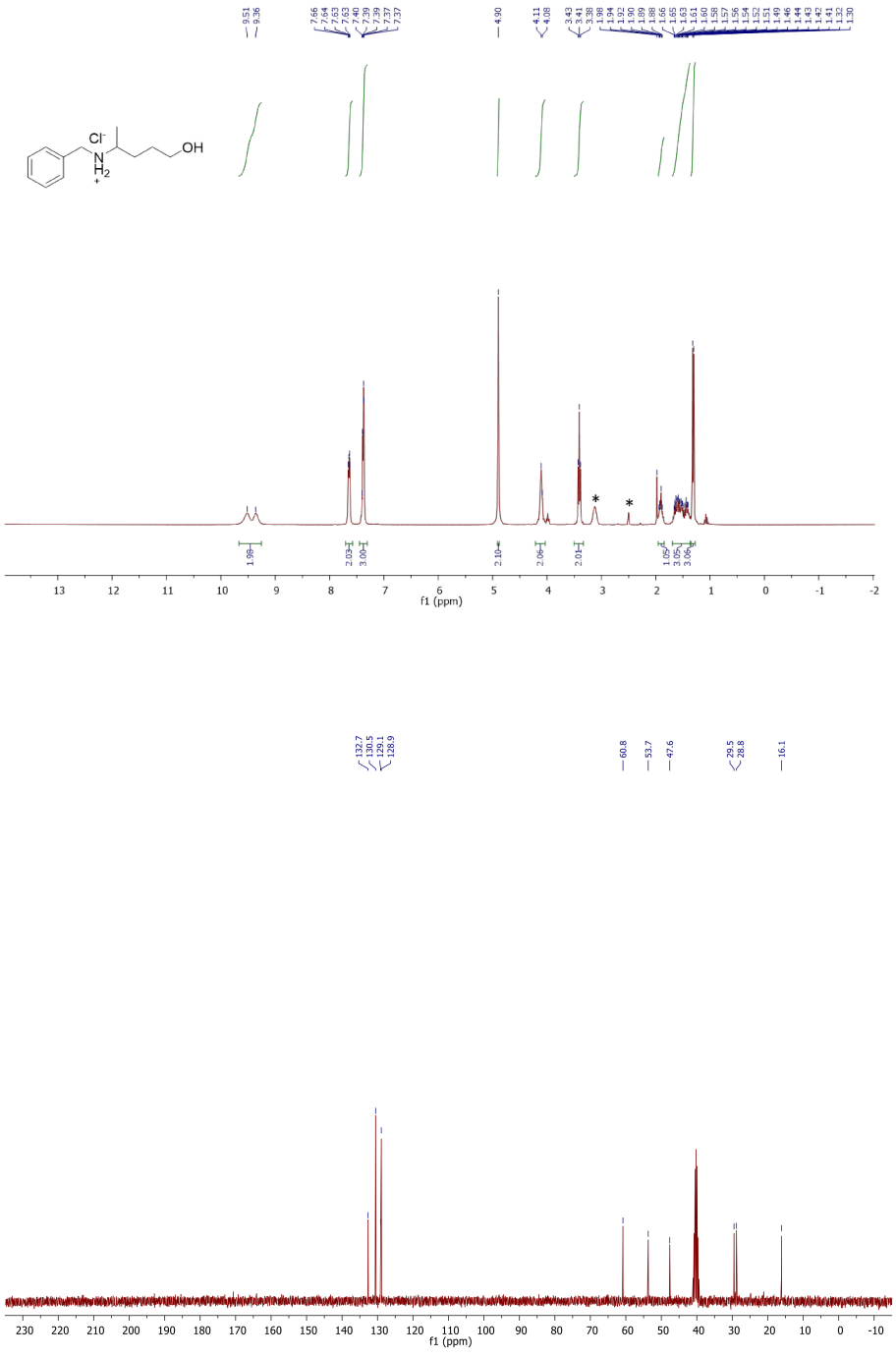

ChemNMR ^{1}H Estimation

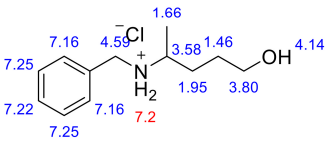

Estimation quality is indicated by color: good, medium, rough

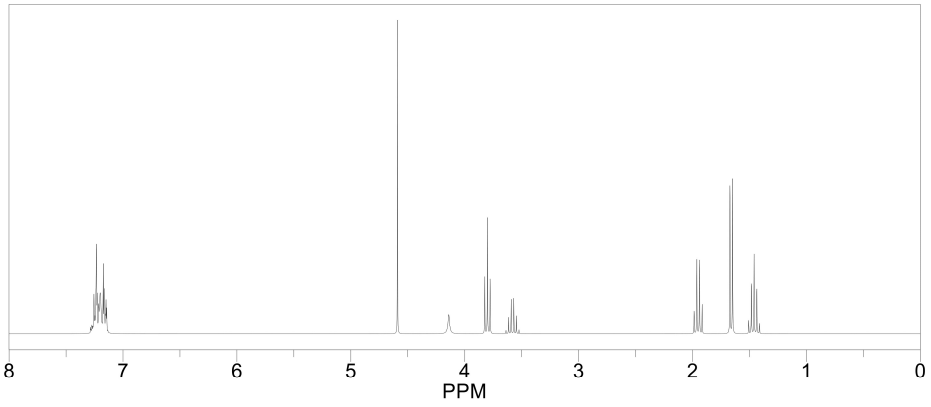

ChemNMR ^{13}C Estimation

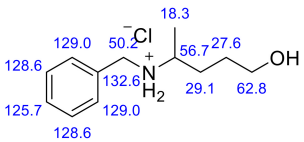

Estimation quality is indicated by color: good, medium, rough

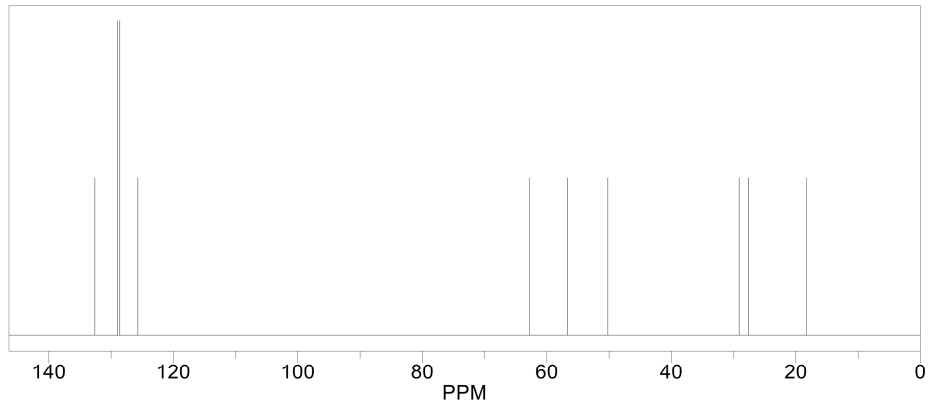

18:

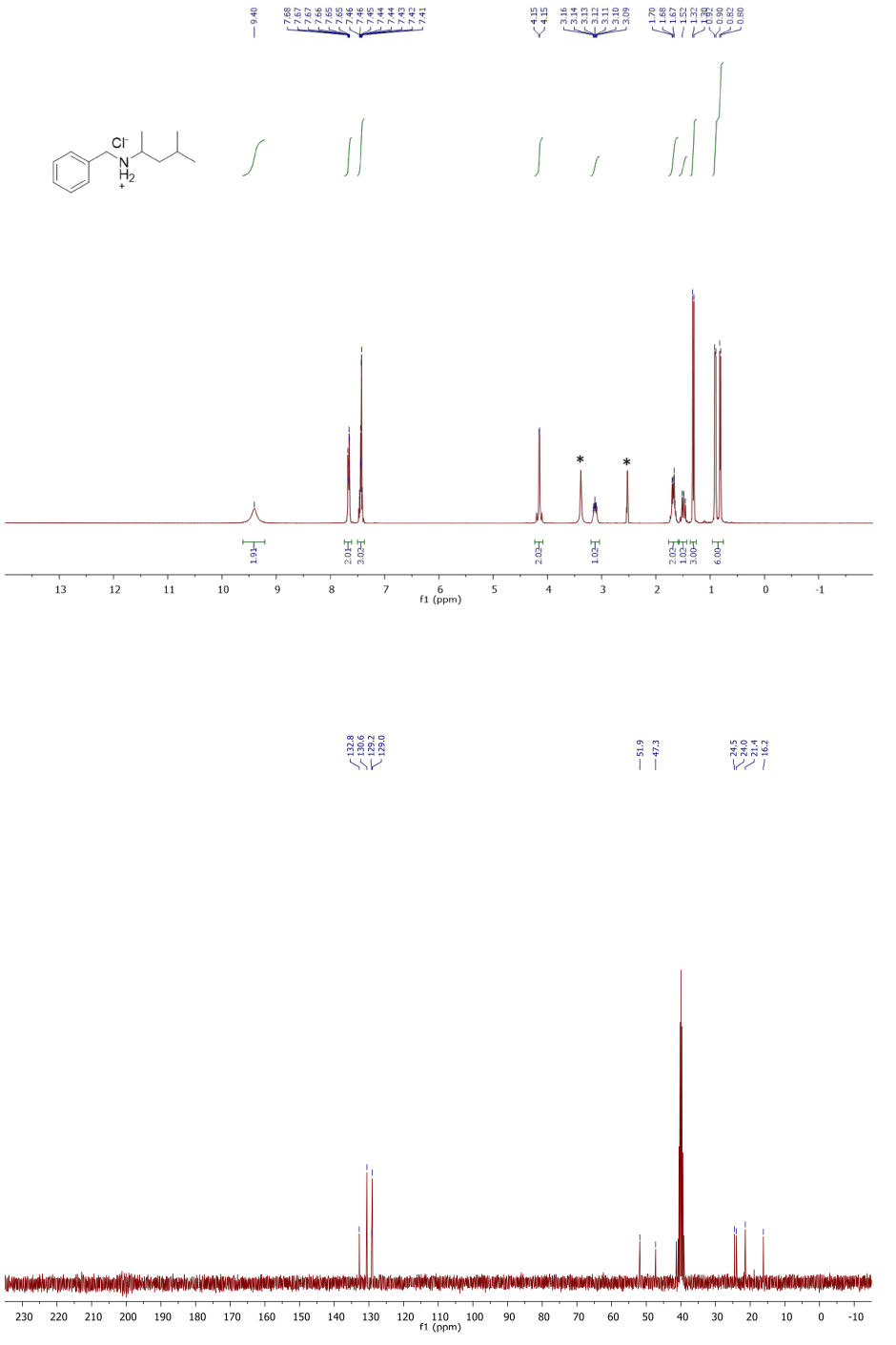
9.40
7.68
7.67
7.67
7.66
7.65
7.65
7.46
7.45
7.44
7.44
7.43
7.42
7.41
4.15
4.15
3.16
3.14
3.13
3.12
3.11
3.10
3.09
1.70
1.68
1.67
1.52
1.32
0.92
0.90
0.82
0.80
Cl⁻
N
H2
+
1.9
2.0
3.0
2.0
1.0
2.0
1.0
3.0
6.0
f1 (ppm)
132.8
130.6
129.2
129.0
51.9
47.3
24.5
24.0
21.4
16.2
f1 (ppm)

73

SUPPORTING INFORMATION

ChemNMR ^{1}H Estimation

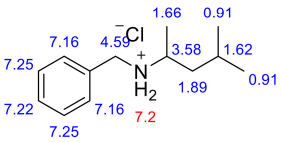

Estimation quality is indicated by color: good, medium, rough

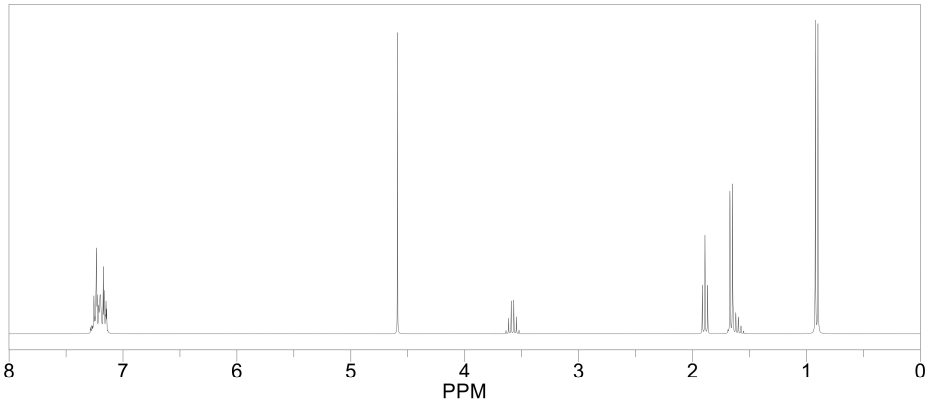

ChemNMR ^{13}C Estimation

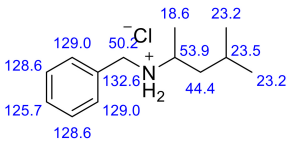

Estimation quality is indicated by color: good, medium, rough

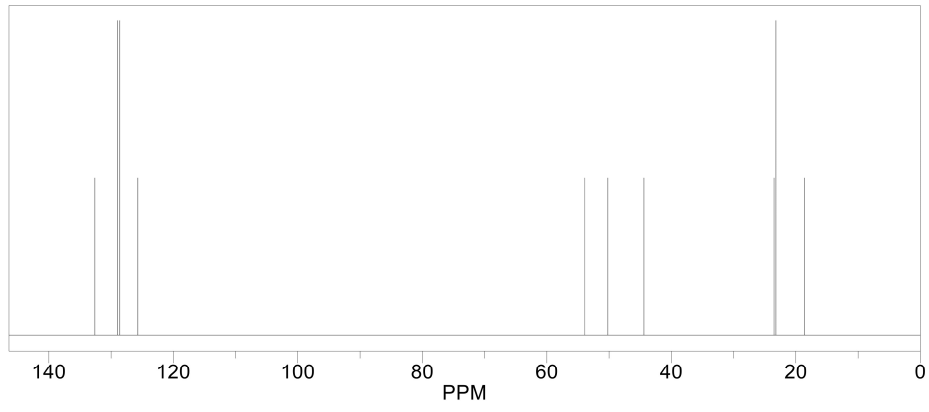

19:

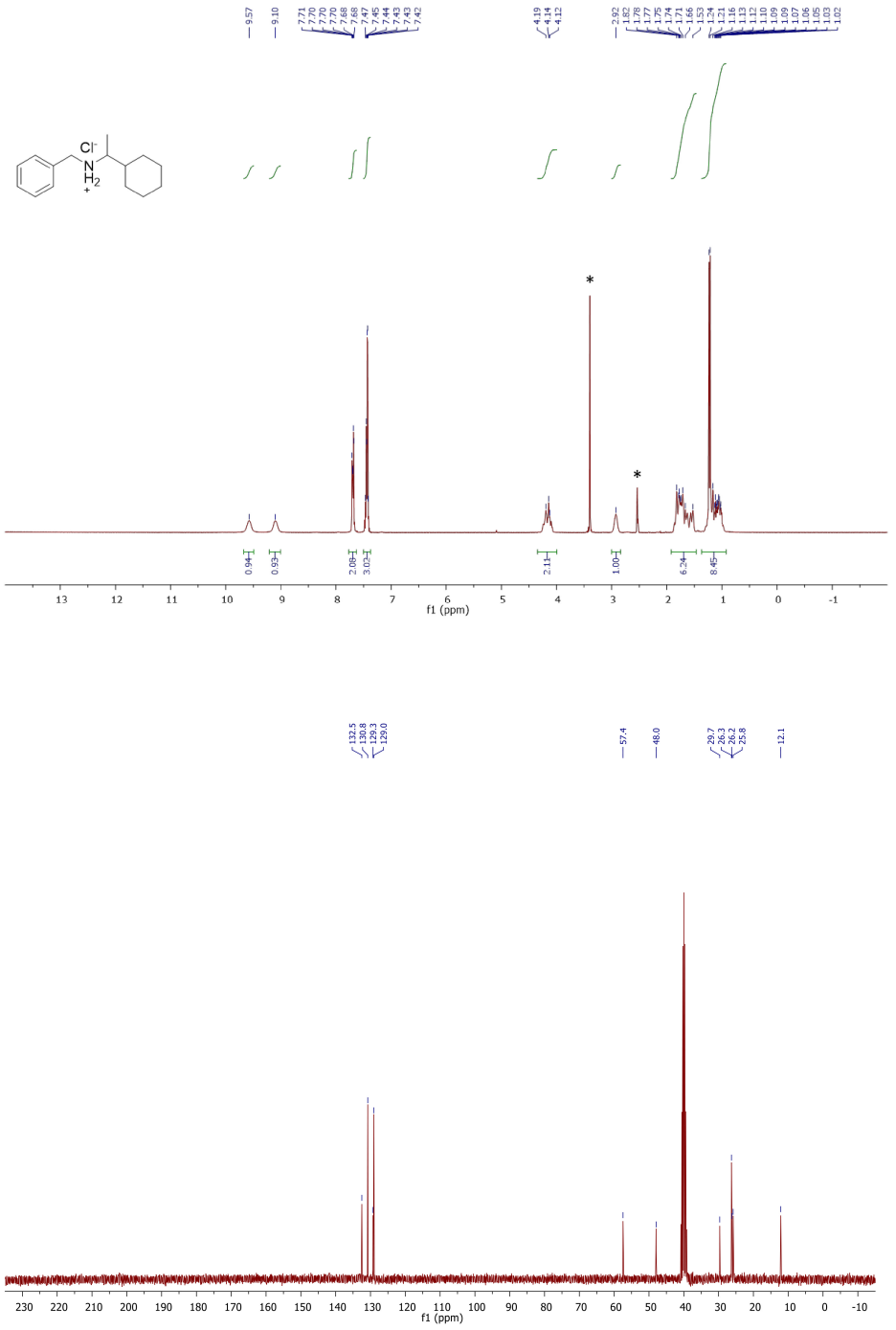
9.57
9.10
7.71
7.70
7.70
7.70
7.68
7.68
7.47
7.45
7.44
7.43
7.43
7.42
4.19
4.14
4.12
2.92
1.82
1.78
1.77
1.75
1.74
1.71
1.66
1.55
1.34
1.21
1.16
1.13
1.12
1.10
1.09
1.09
1.07
1.06
1.05
1.03
1.02
Cl⁻
N
H2
+
*
*
0.94
0.93
2.00
3.02
2.11
1.00
6.24
8.46
13 12 11 10 9 8 7 6 5 4 3 2 1 0 -1
f1 (ppm)
132.5
130.8
129.3
129.0
57.4
48.0
29.7
26.3
26.2
25.8
12.1
230 220 210 200 190 180 170 160 150 140 130 120 110 100 90 80 70 60 50 40 30 20 10 0 -10
f1 (ppm)

SUPPORTING INFORMATION

ChemNMR ^{1}H Estimation

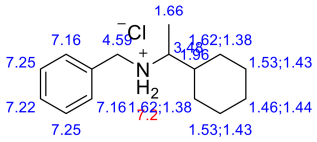

Estimation quality is indicated by color: good, medium, rough

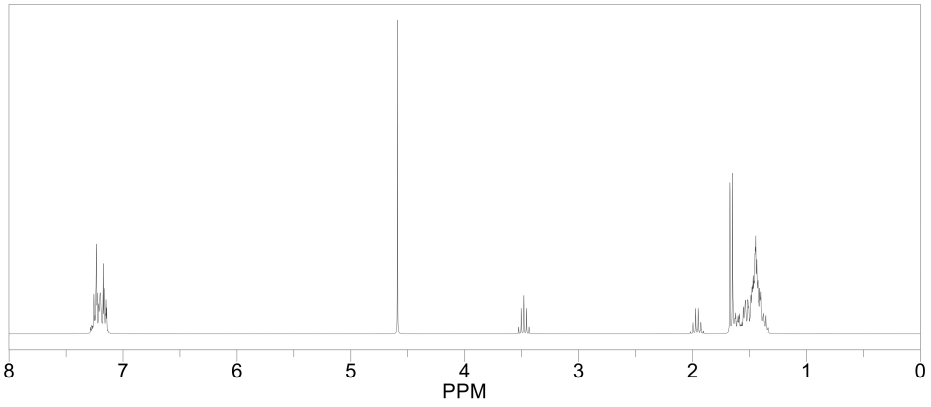

ChemNMR ^{13}C Estimation

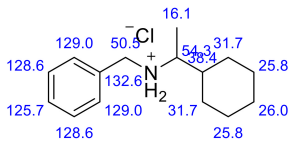

Estimation quality is indicated by color: good, medium, rough

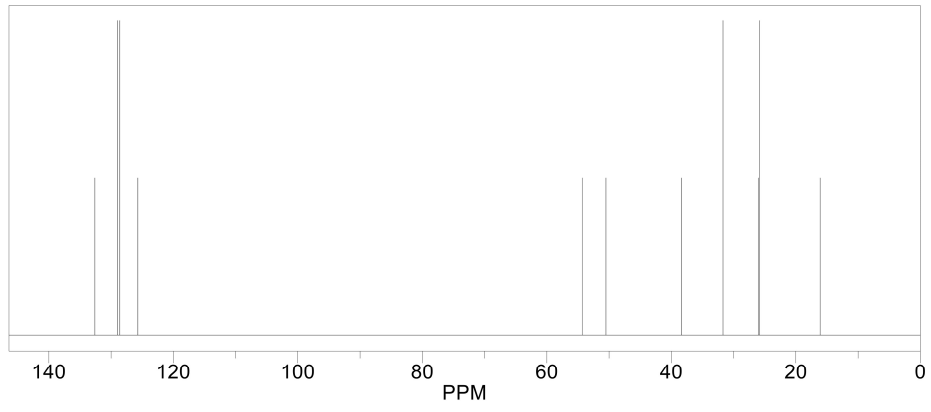

20:

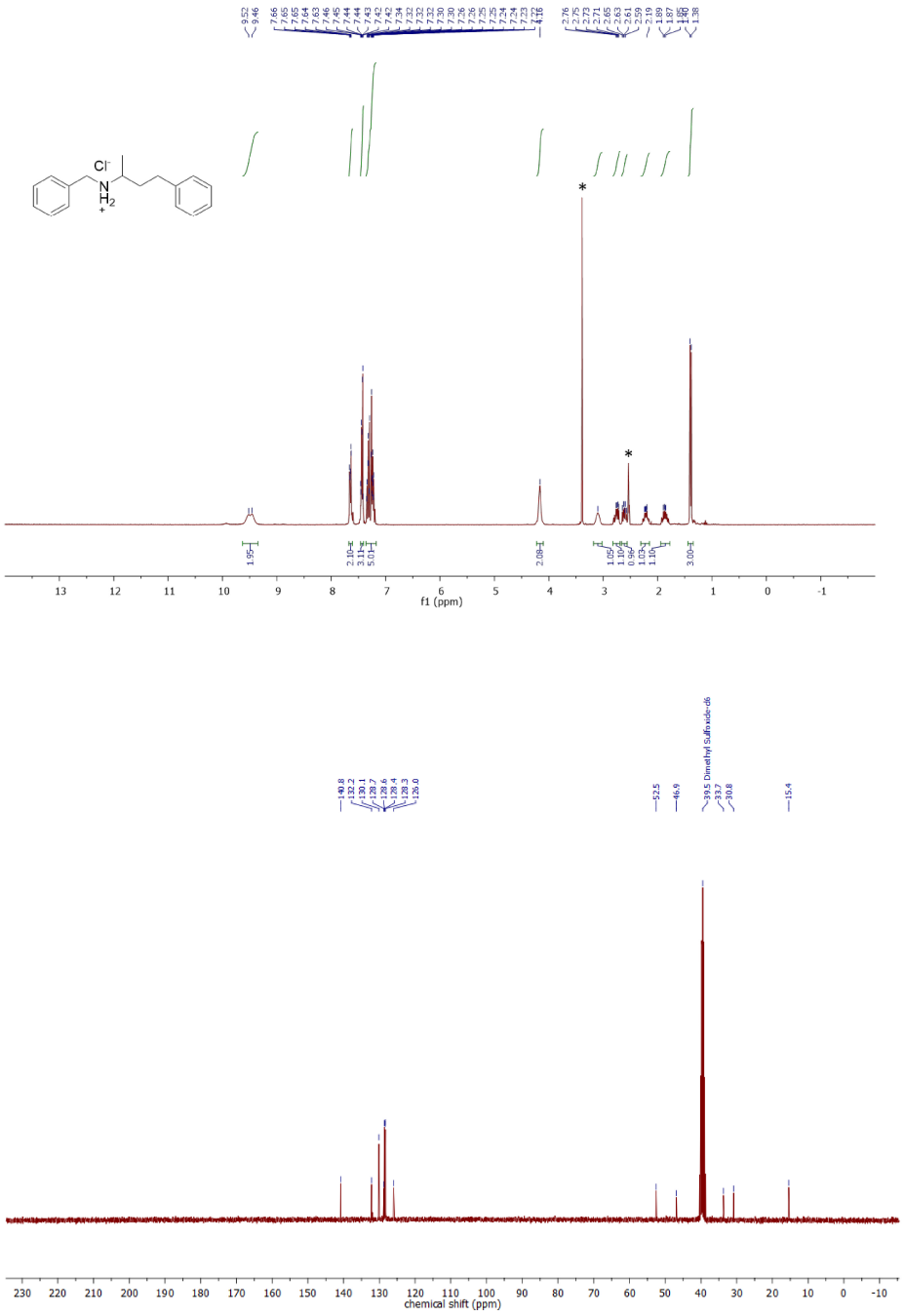

SUPPORTING INFORMATION

ChemNMR ^{1}H Estimation

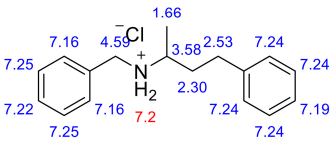

Estimation quality is indicated by color: good, medium, rough

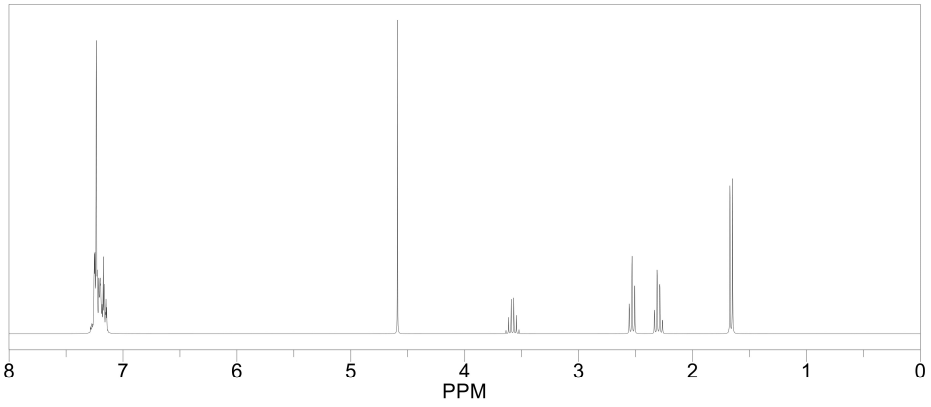

ChemNMR ^{13}C Estimation

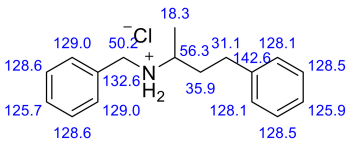

Estimation quality is indicated by color: good, medium, rough

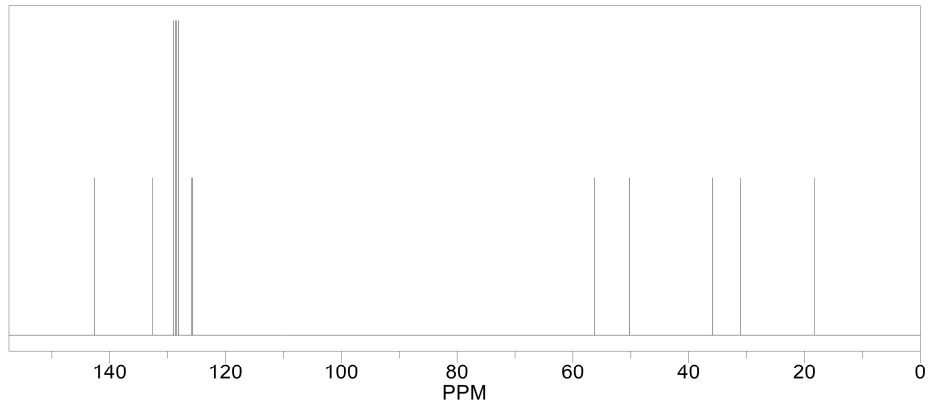

78

21:

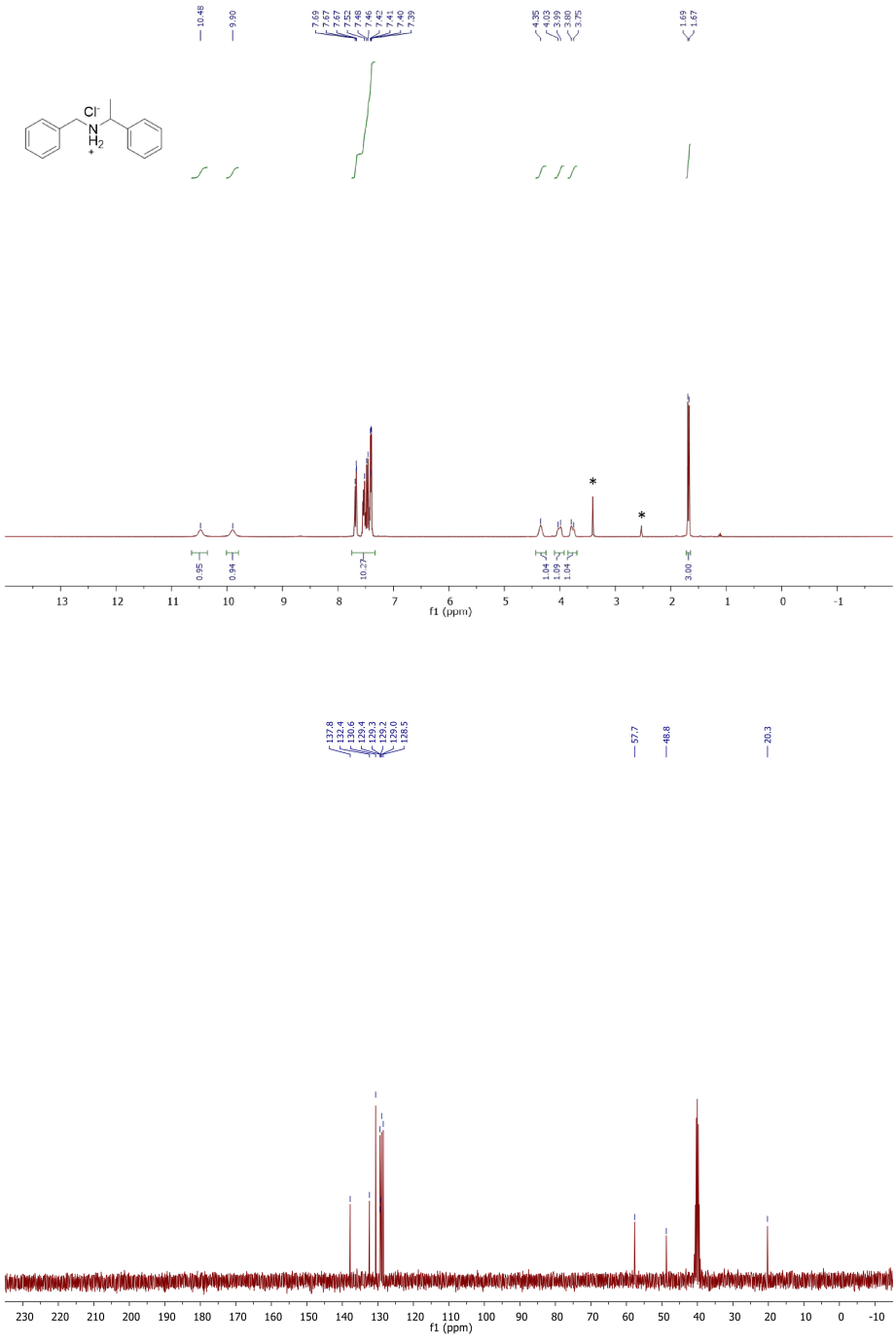
10.48
9.90
7.69
7.67
7.67
7.52
7.48
7.46
7.42
7.41
7.40
7.39
4.35
4.03
3.99
3.80
3.75
1.69
1.67
Cl⁻
N
H2
+
0.95
0.94
10.27
1.04
1.09
1.04
3.00
f1 (ppm)
137.8
132.4
130.6
129.4
129.3
129.2
129.0
128.5
57.7
48.8
20.3
f1 (ppm)

SUPPORTING INFORMATION

ChemNMR ^{1}H Estimation

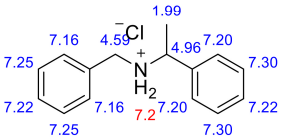

Estimation quality is indicated by color: good, medium, rough

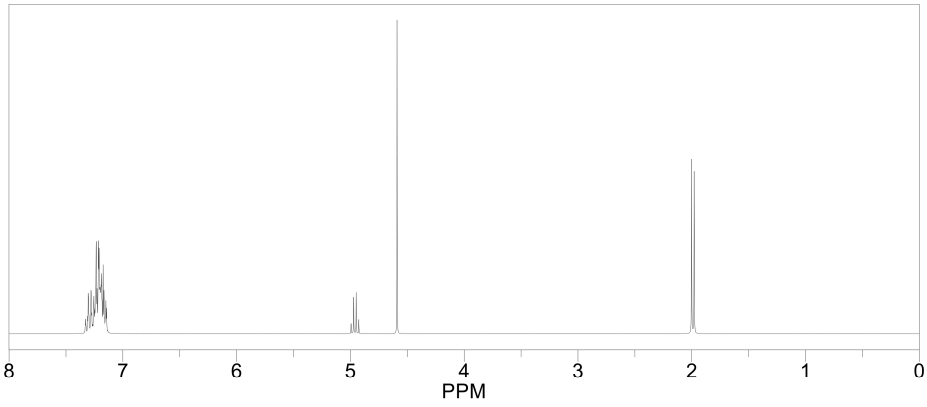

ChemNMR ^{13}C Estimation

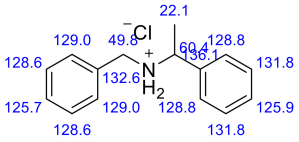

Estimation quality is indicated by color: good, medium, rough

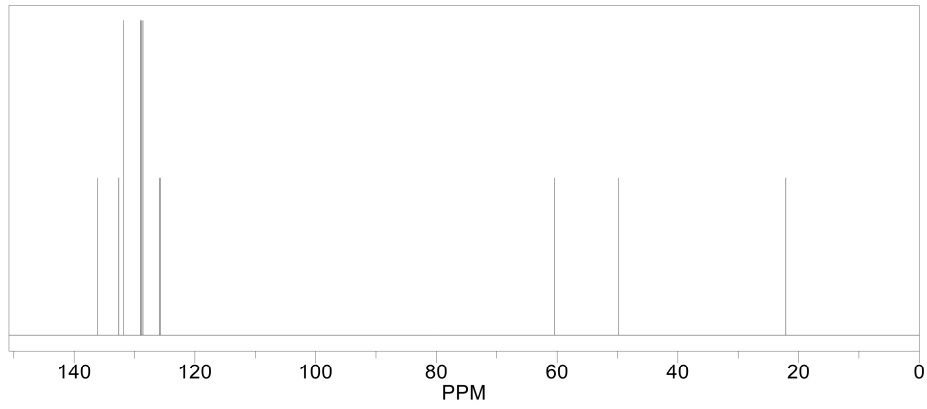

22:

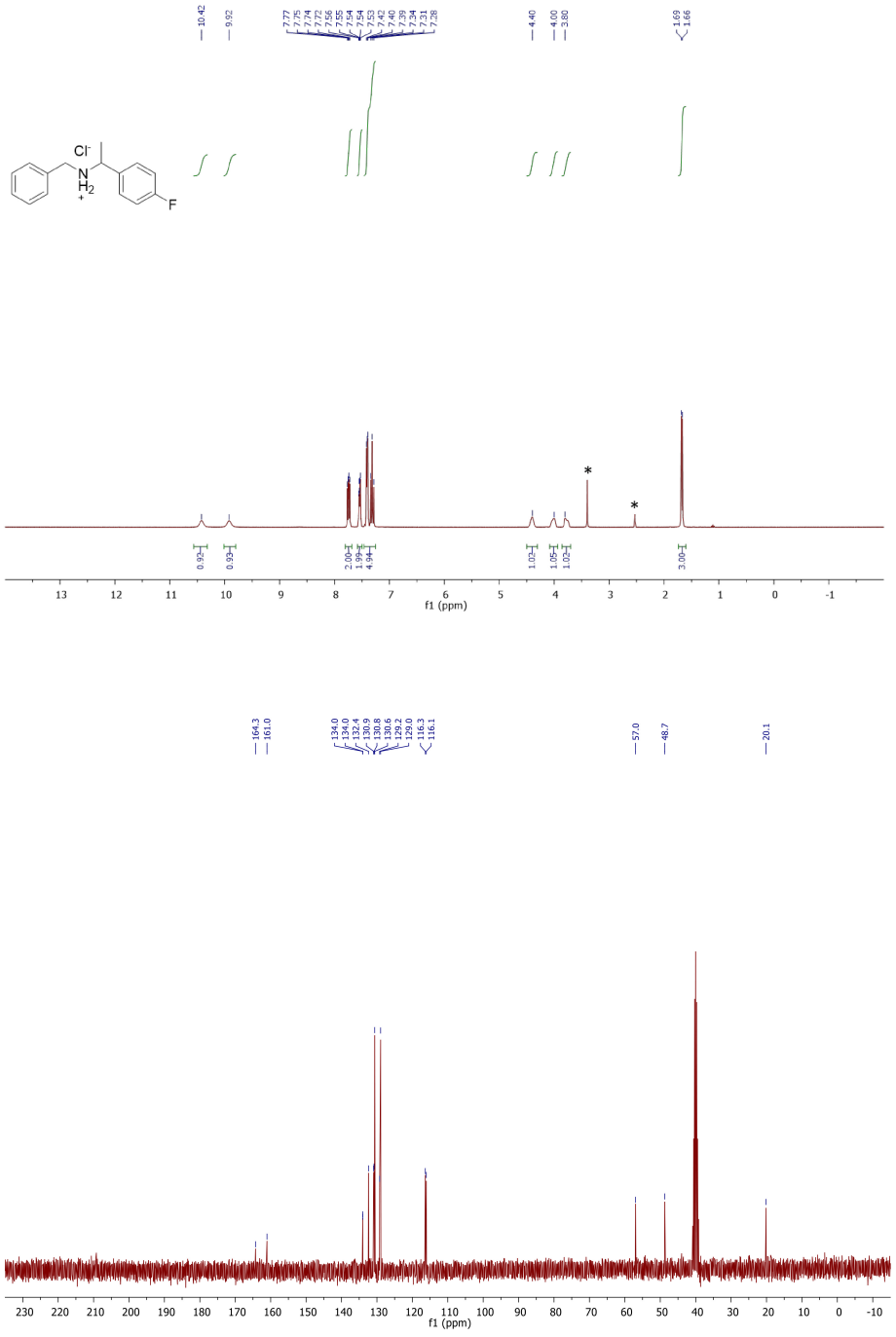
10.42
9.92
7.77
7.75
7.74
7.72
7.56
7.55
7.54
7.53
7.42
7.40
7.39
7.34
7.31
7.28
4.40
4.00
3.88
1.69
1.66
Cl⁻
N
H2
+
F
0.95
0.99
2.00
1.95
4.94
1.03
1.05
1.02
3.00
f1 (ppm)
164.3
161.0
134.0
134.0
132.4
130.9
130.8
130.6
129.2
129.0
116.3
116.1
57.0
48.7
20.1
f1 (ppm)

81

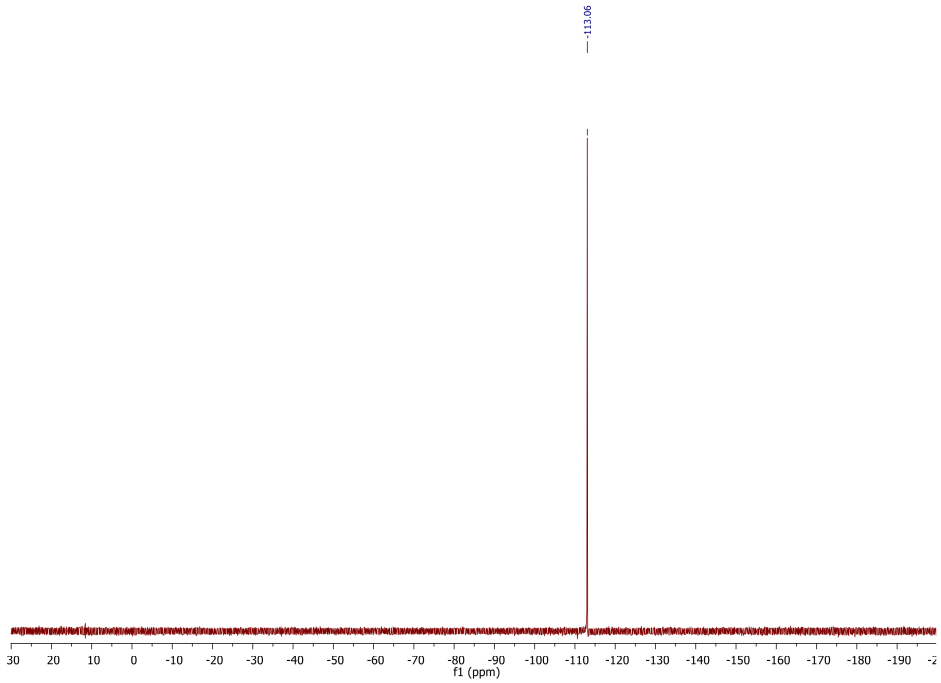
-113.06
30 20 10 0 -10 -20 -30 -40 -50 -60 -70 -80 -90 -100 -110 -120 -130 -140 -150 -160 -170 -180 -190
f1 (ppm)

ChemNMR ^{1}H Estimation

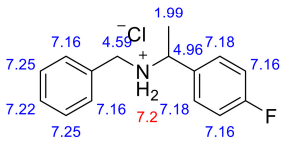

Estimation quality is indicated by color: good, medium, rough

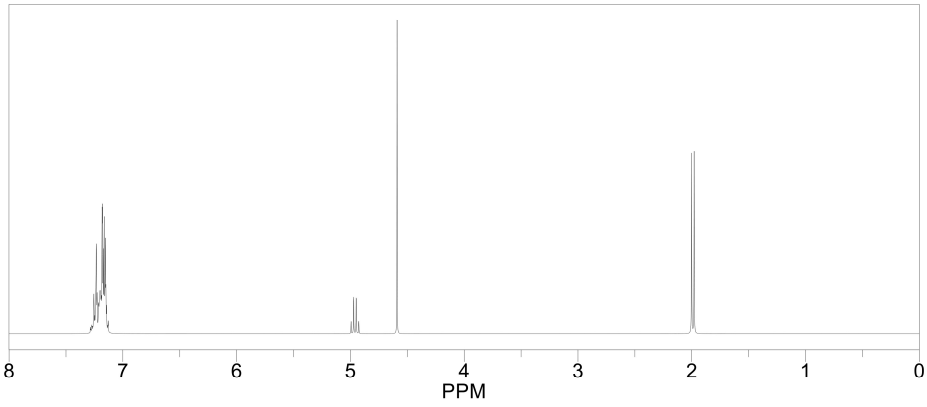

ChemNMR ^{13}C Estimation

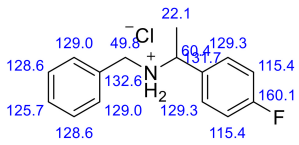

Estimation quality is indicated by color: good, medium, rough

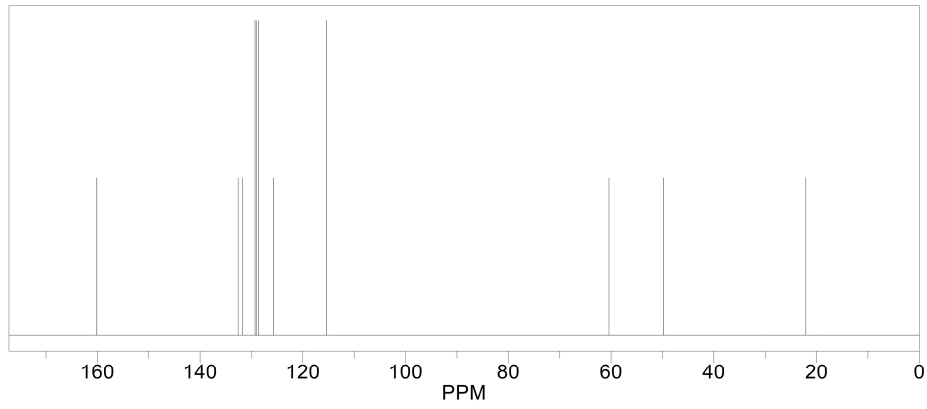

23:

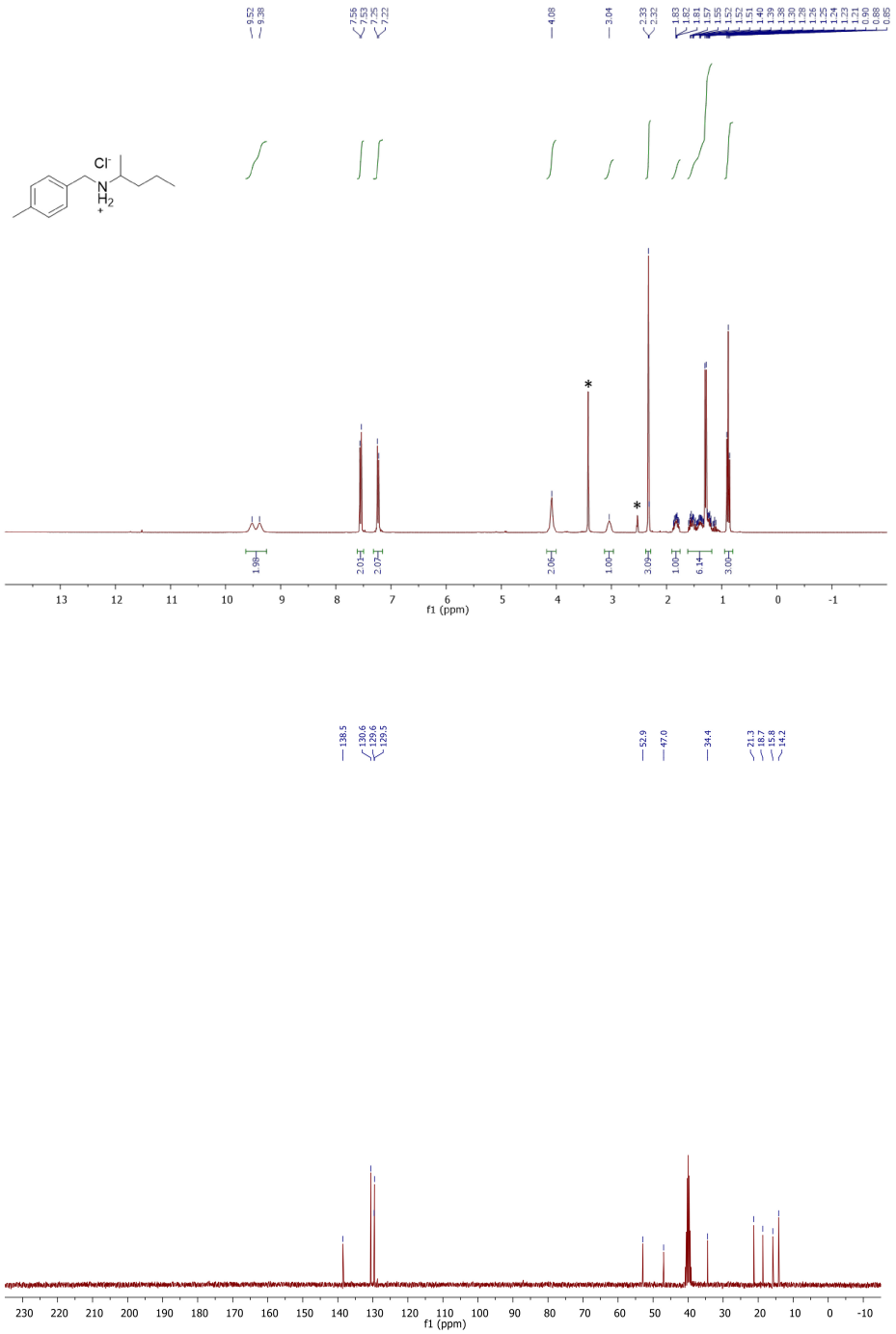

ChemNMR ^{1}H Estimation

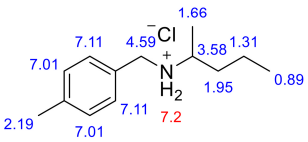

Estimation quality is indicated by color: good, medium, rough

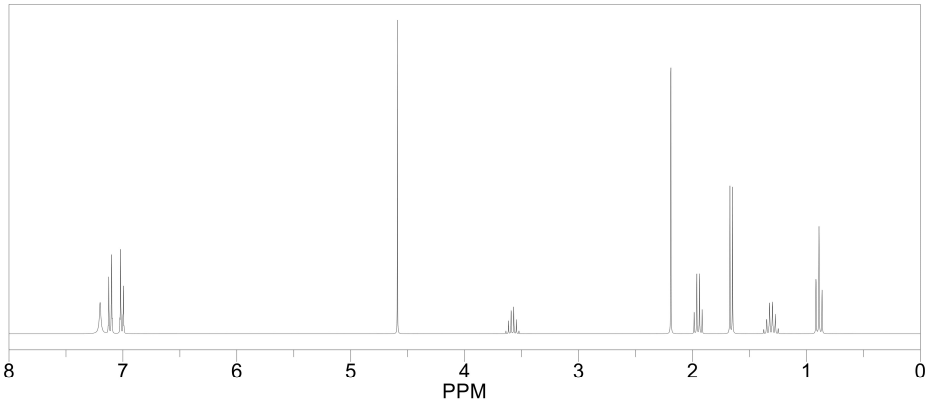

ChemNMR ^{13}C Estimation

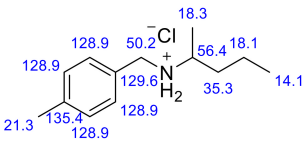

Estimation quality is indicated by color: good, medium, rough

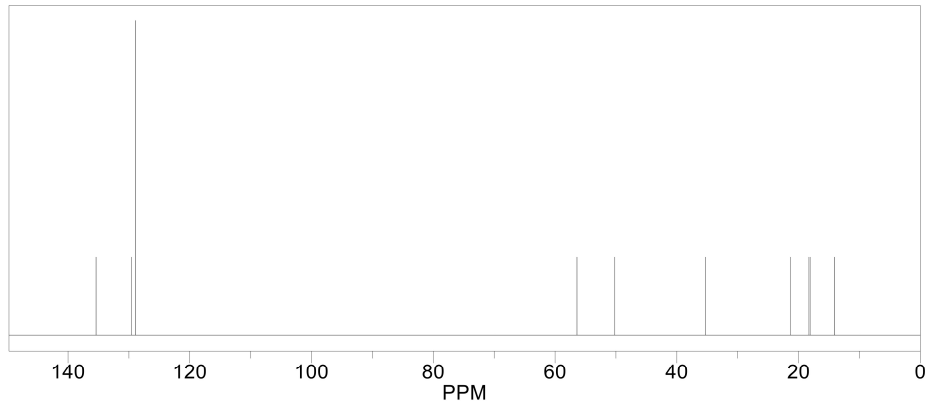

24:

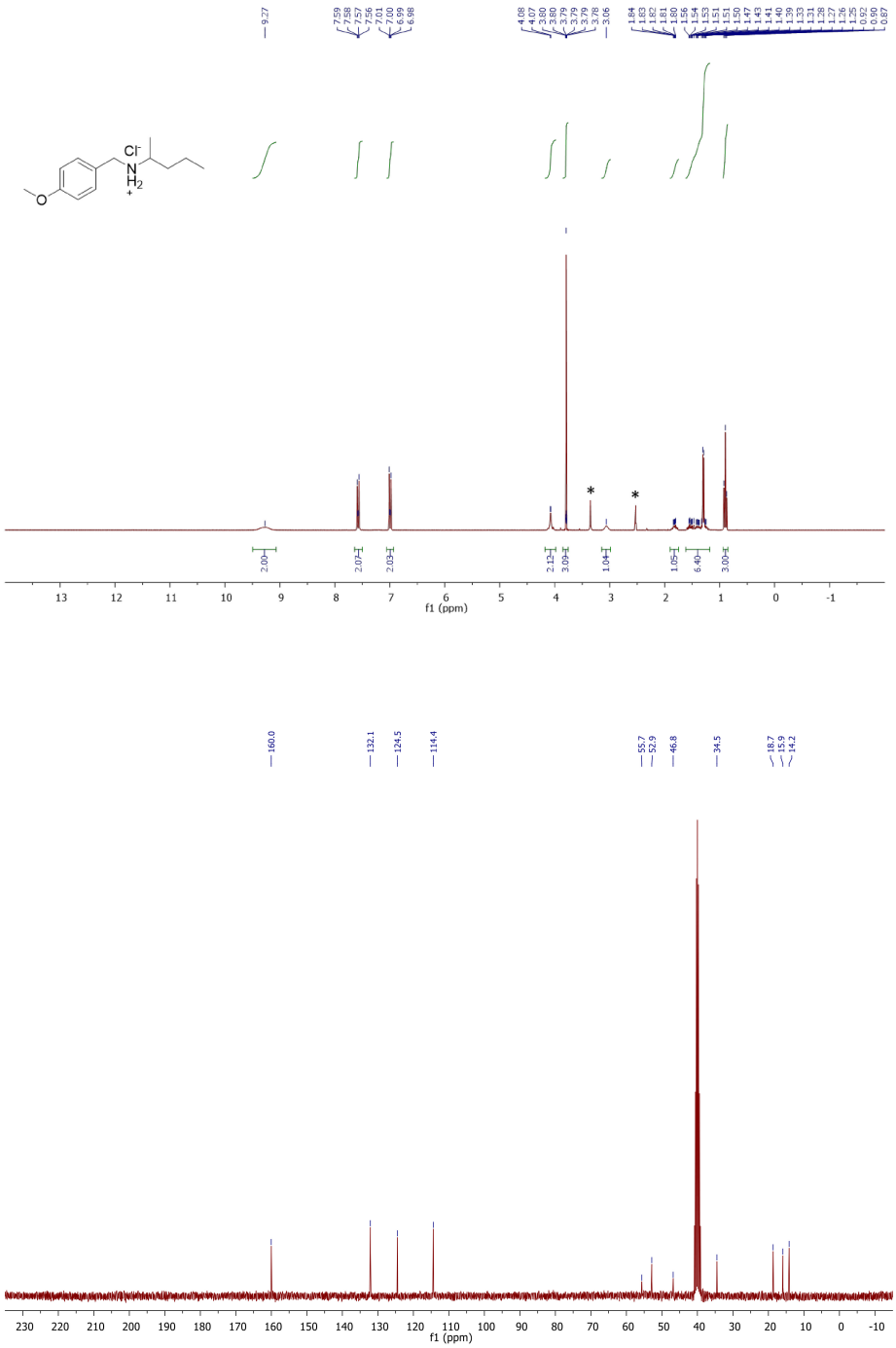

SUPPORTING INFORMATION

ChemNMR ^{1}H Estimation

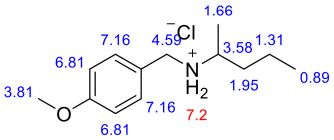

Estimation quality is indicated by color: good, medium, rough

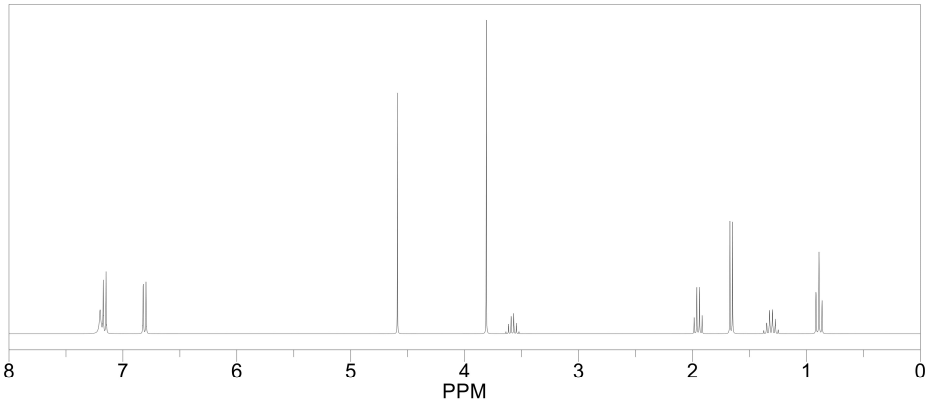

ChemNMR ^{13}C Estimation

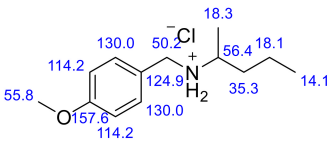

Estimation quality is indicated by color: good, medium, rough

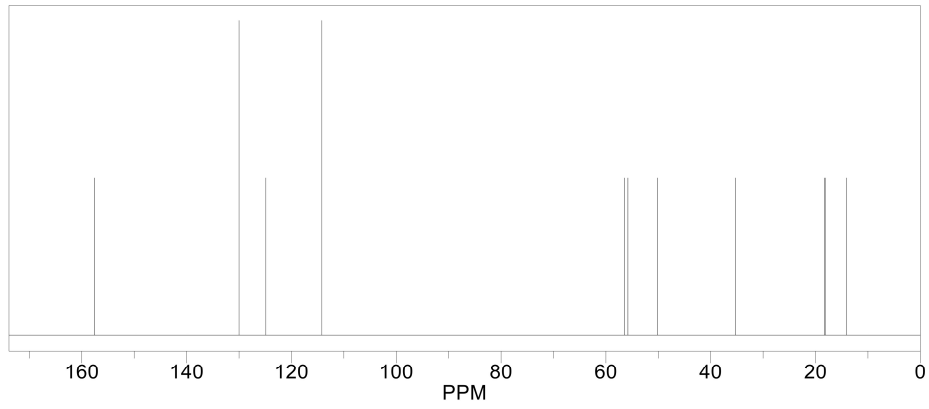

25:

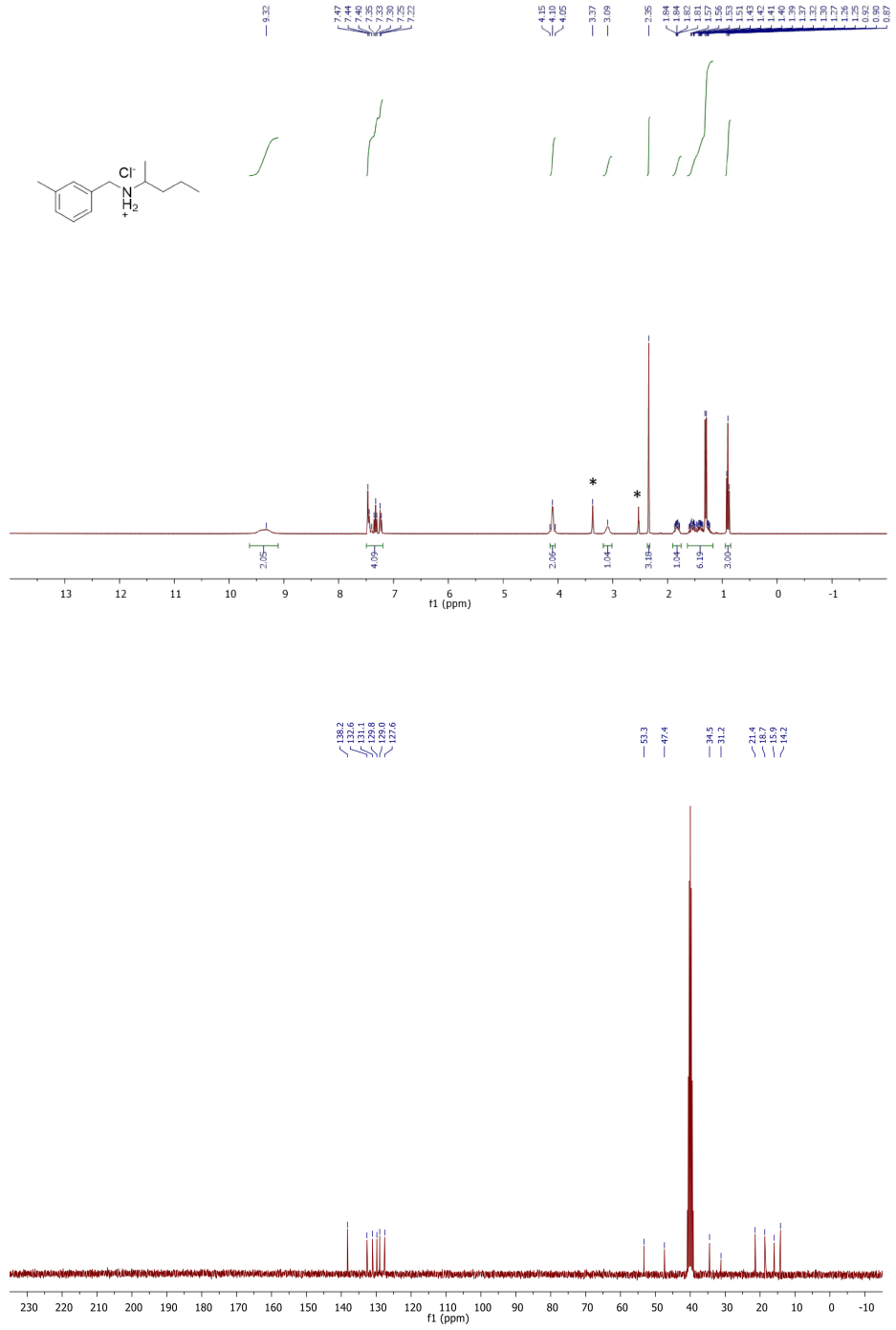

SUPPORTING INFORMATION

ChemNMR ^{1}H Estimation

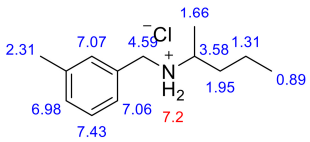

Estimation quality is indicated by color: good, medium, rough

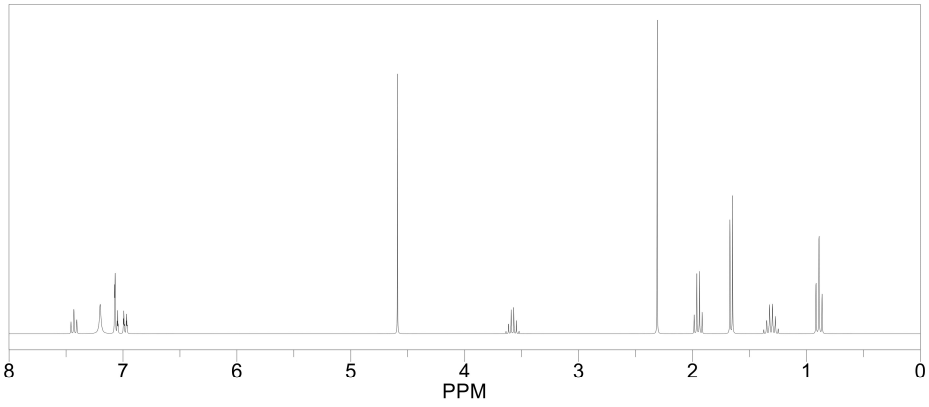

ChemNMR ^{13}C Estimation

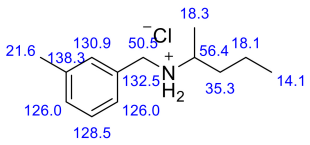

Estimation quality is indicated by color: good, medium, rough

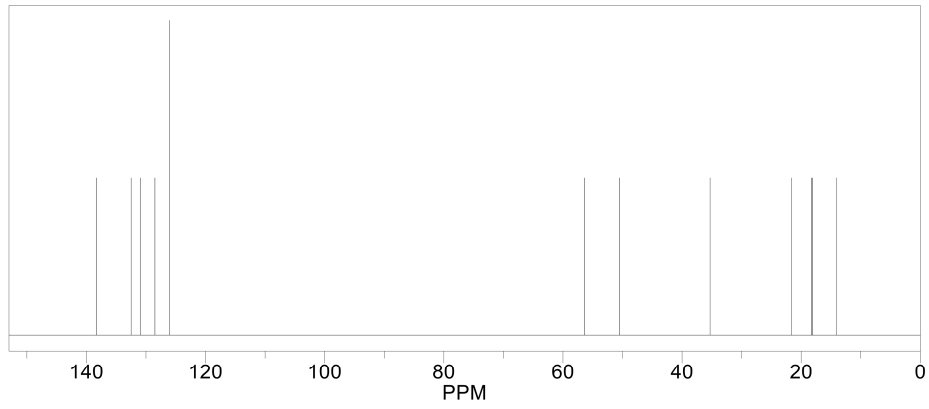

89

26:

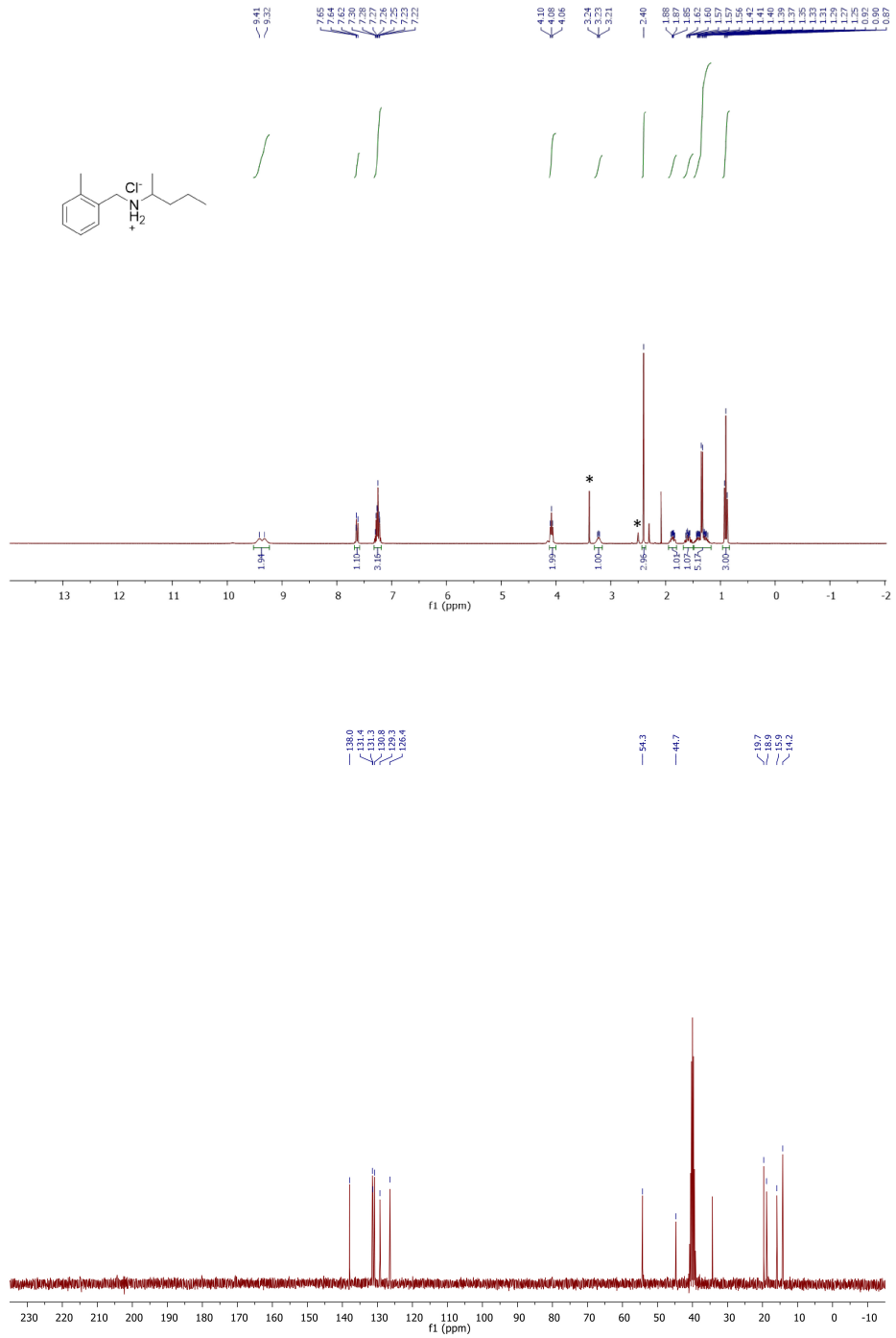

SUPPORTING INFORMATION

ChemNMR ^{1}H Estimation

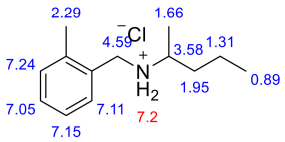

Estimation quality is indicated by color: good, medium, rough

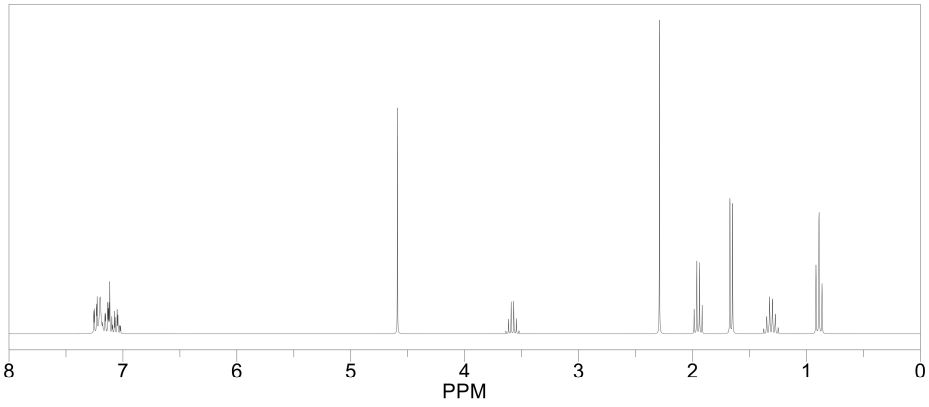

ChemNMR ^{13}C Estimation

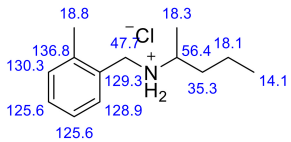

Estimation quality is indicated by color: good, medium, rough

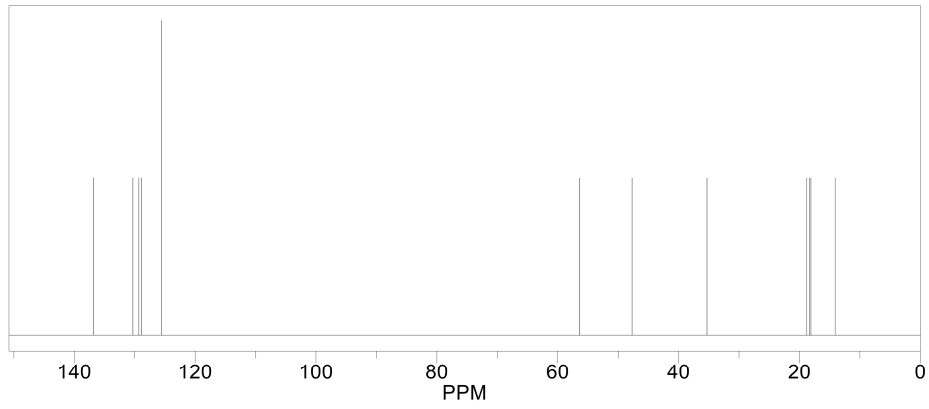

27:

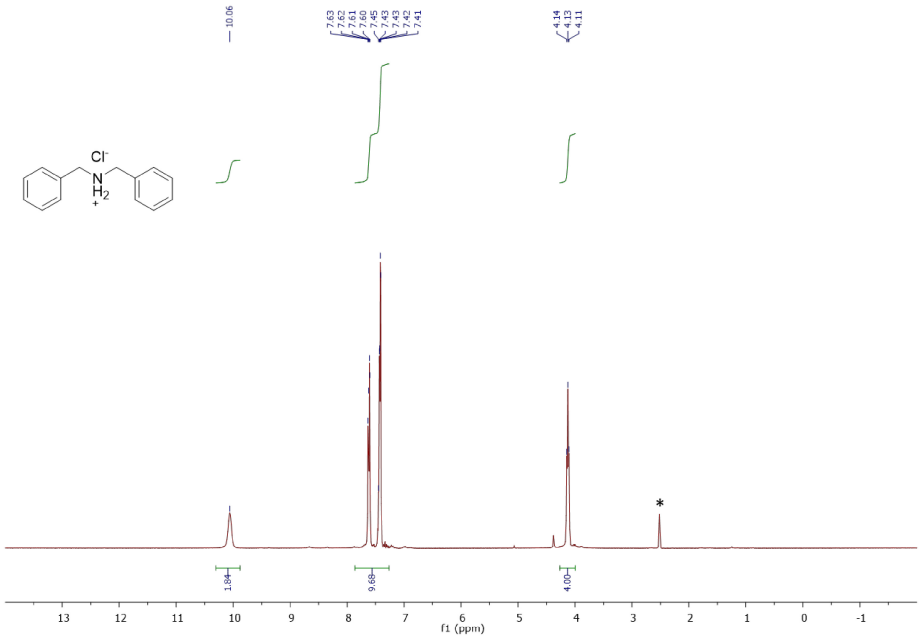
10.06
7.63
7.62
7.61
7.60
7.45
7.43
7.43
7.42
7.41
4.14
4.13
4.11
Cl⁻
N
H2
+
*
1.84
9.68
4.00
13
12
11
10
9
8
7
6
5
4
3
2
1
0
-1
f1 (ppm)

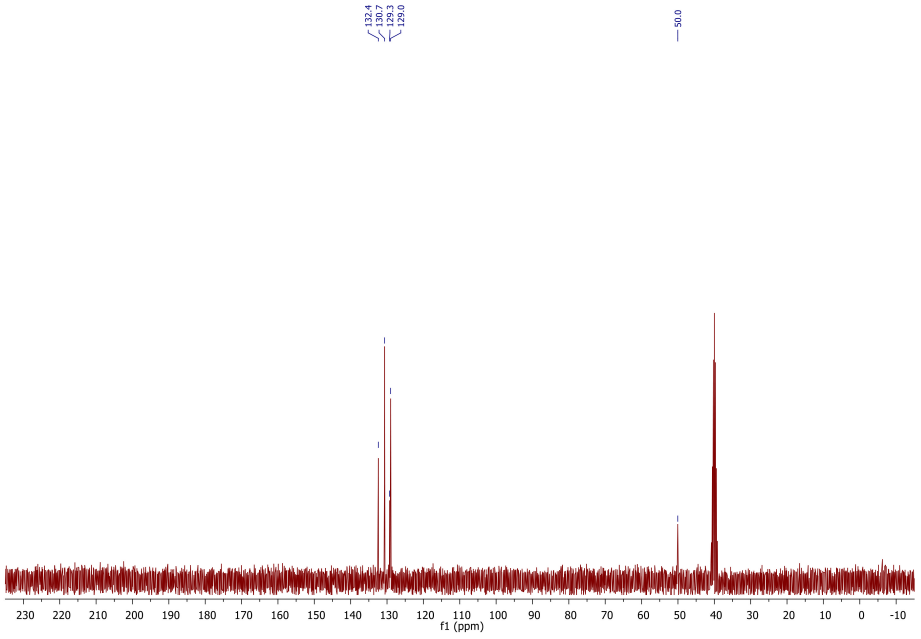
132.4
130.7
129.3
129.0
50.0
230
220
210
200
190
180
170
160
150
140
130
120
110
100
90
80
70
60
50
40
30
20
10
0
-10
f1 (ppm)

SUPPORTING INFORMATION

ChemNMR ^{1}H Estimation

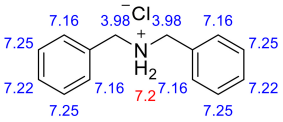

Estimation quality is indicated by color: good, medium, rough

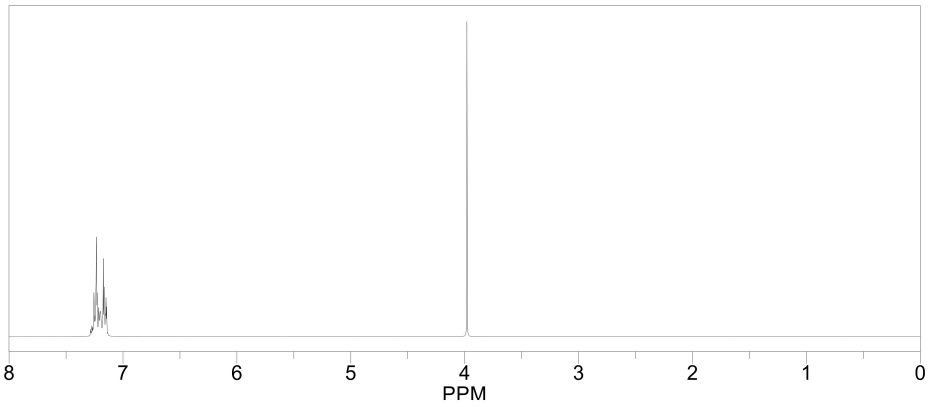

ChemNMR ^{13}C Estimation

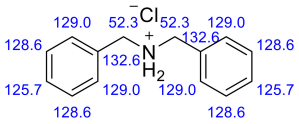

Estimation quality is indicated by color: good, medium, rough

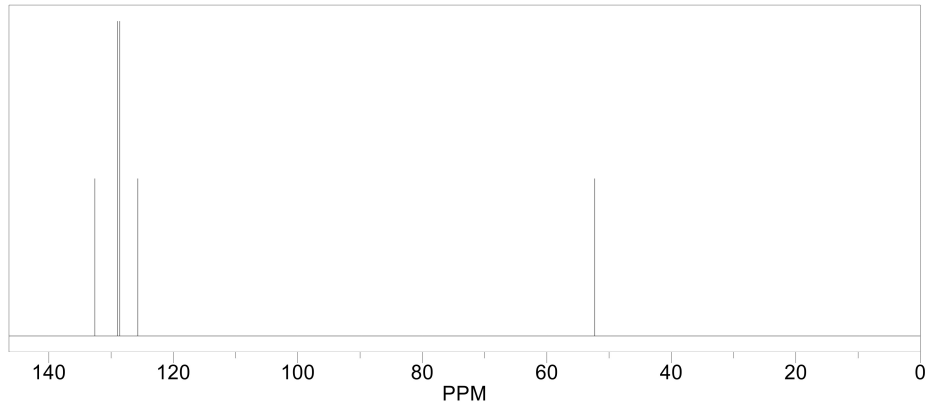

28:

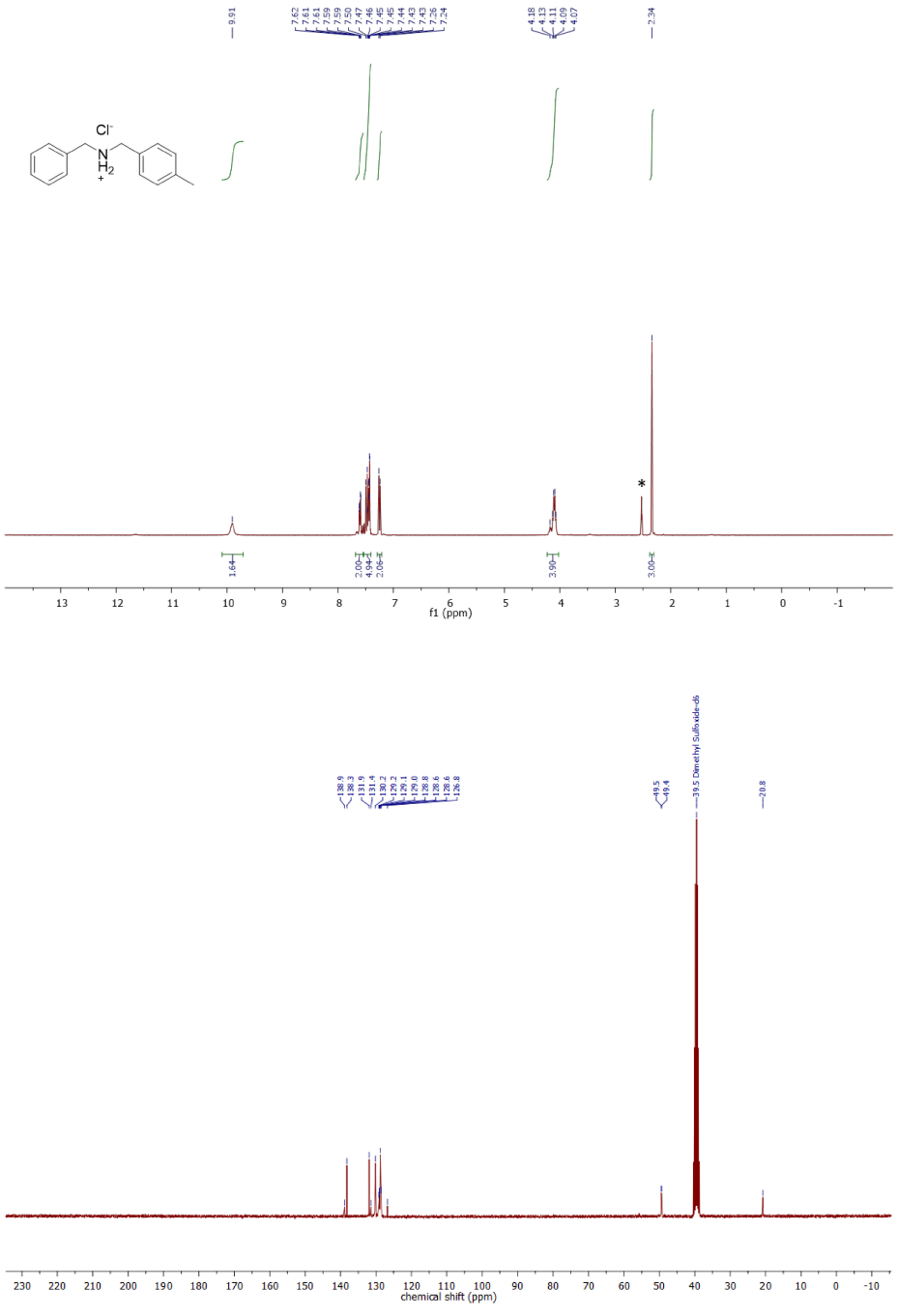
9.91
7.62
7.61
7.61
7.59
7.59
7.50
7.47
7.46
7.45
7.45
7.44
7.43
7.43
7.36
7.24
4.18
4.13
4.11
4.09
4.07
2.34
Cl⁻
N
H2
+
1.64
2.00
4.94
2.06
3.90
3.00
*
f1 (ppm)
138.9
138.3
131.9
131.4
130.2
129.2
129.1
129.0
128.8
128.6
128.6
126.8
49.5
49.4
39.5 Dimethyl Sulfoxide-d6
20.8
chemical shift (ppm)

SUPPORTING INFORMATION

ChemNMR ^{1}H Estimation

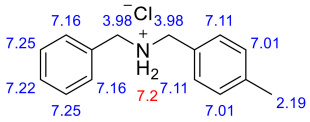

Estimation quality is indicated by color: good, medium, rough

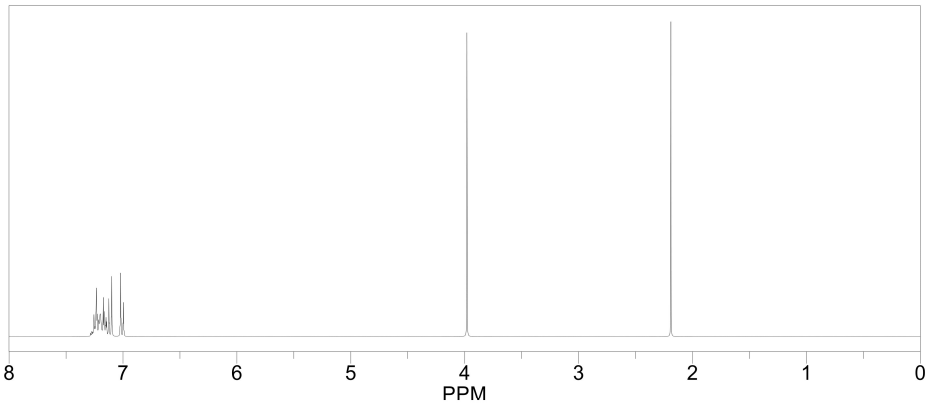

ChemNMR ^{13}C Estimation

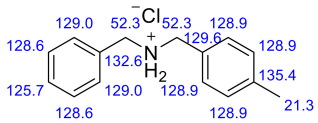

Estimation quality is indicated by color: good, medium, rough

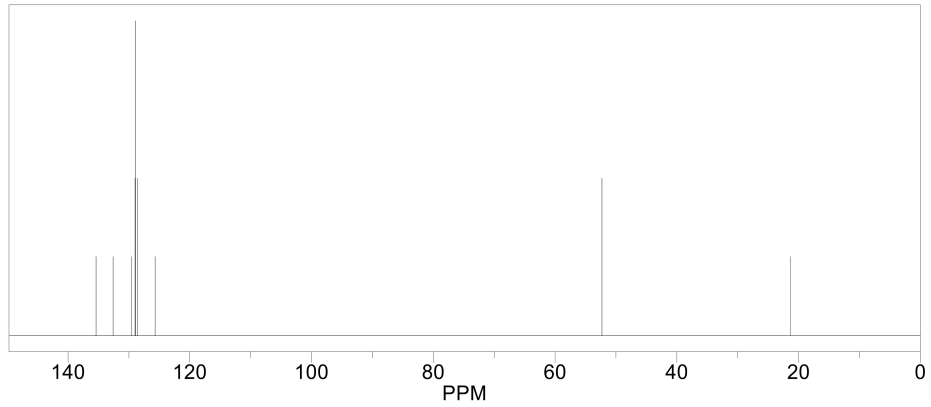

29:

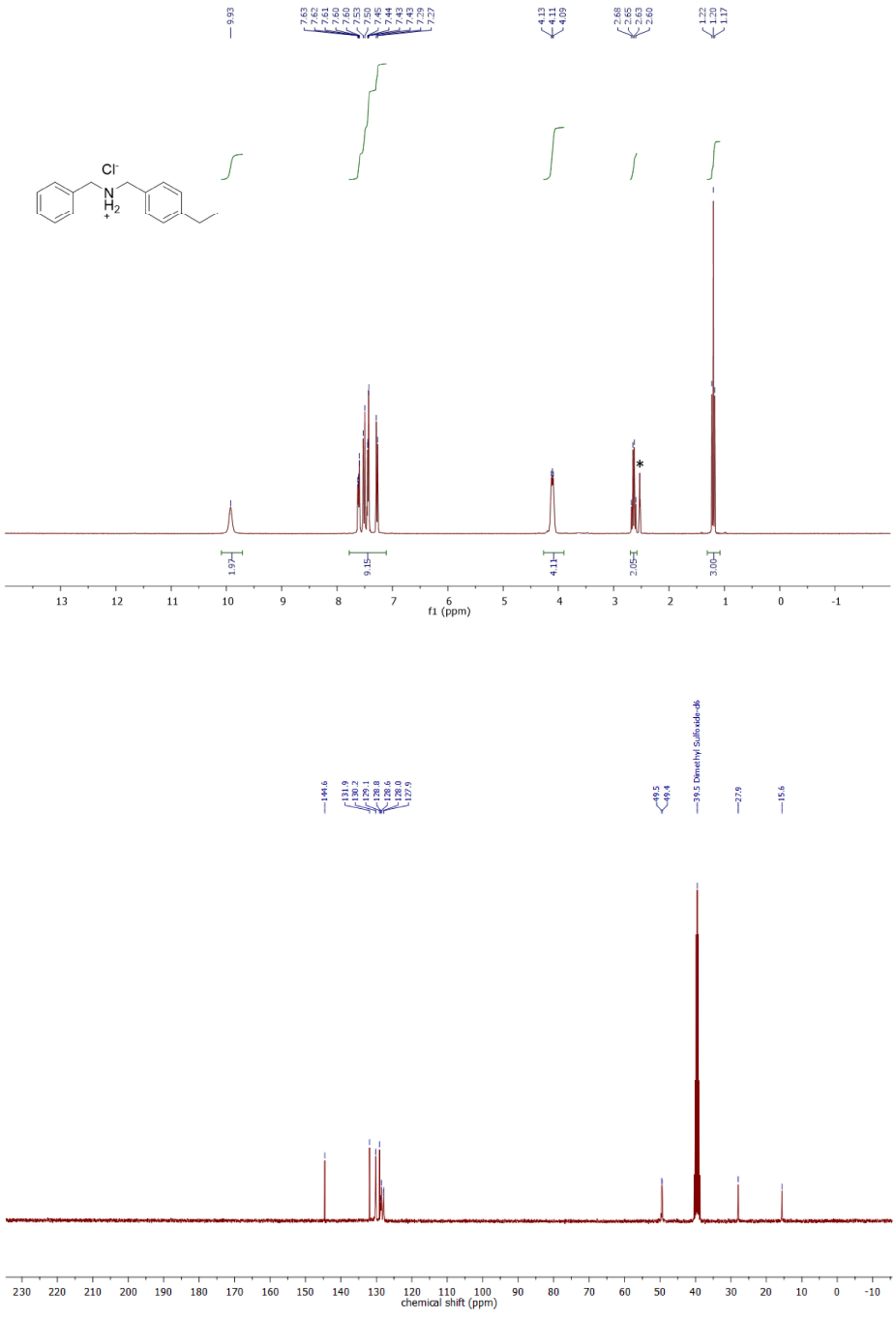
9.93
7.63
7.62
7.61
7.60
7.53
7.50
7.45
7.44
7.43
7.40
7.39
7.27
4.13
4.11
4.09
2.68
2.65
2.63
2.60
1.22
1.20
1.17
Cl⁻
N
H2
+
*
1.97
9.15
4.11
2.05
3.00
f1 (ppm)
144.6
131.9
130.2
129.1
128.8
128.6
128.0
127.9
49.5
49.4
39.5 Dimethyl Sulfoxide-d6
27.9
15.6
chemical shift (ppm)

SUPPORTING INFORMATION

ChemNMR ^{1}H Estimation

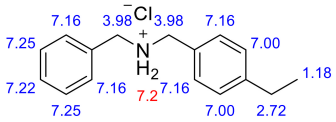

Estimation quality is indicated by color: good, medium, rough

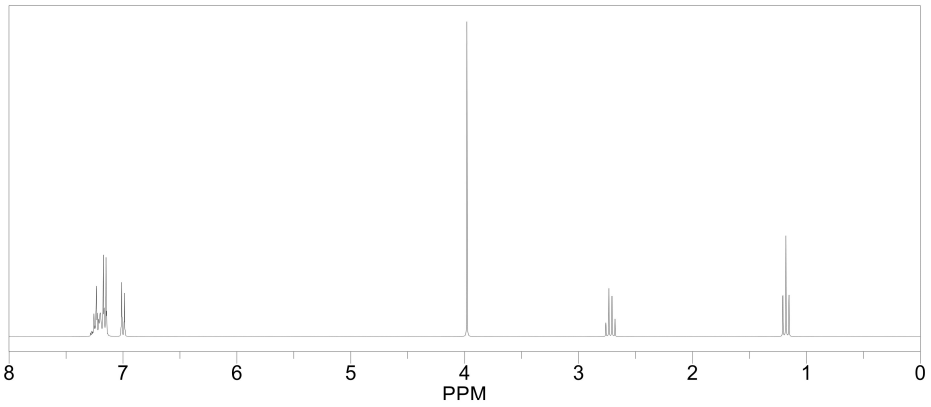

ChemNMR ^{13}C Estimation

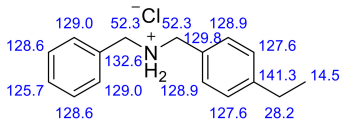

Estimation quality is indicated by color: good, medium, rough

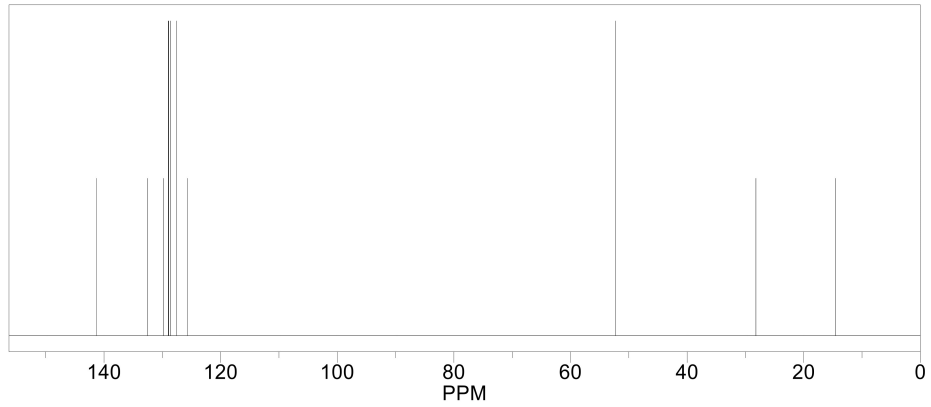

30:

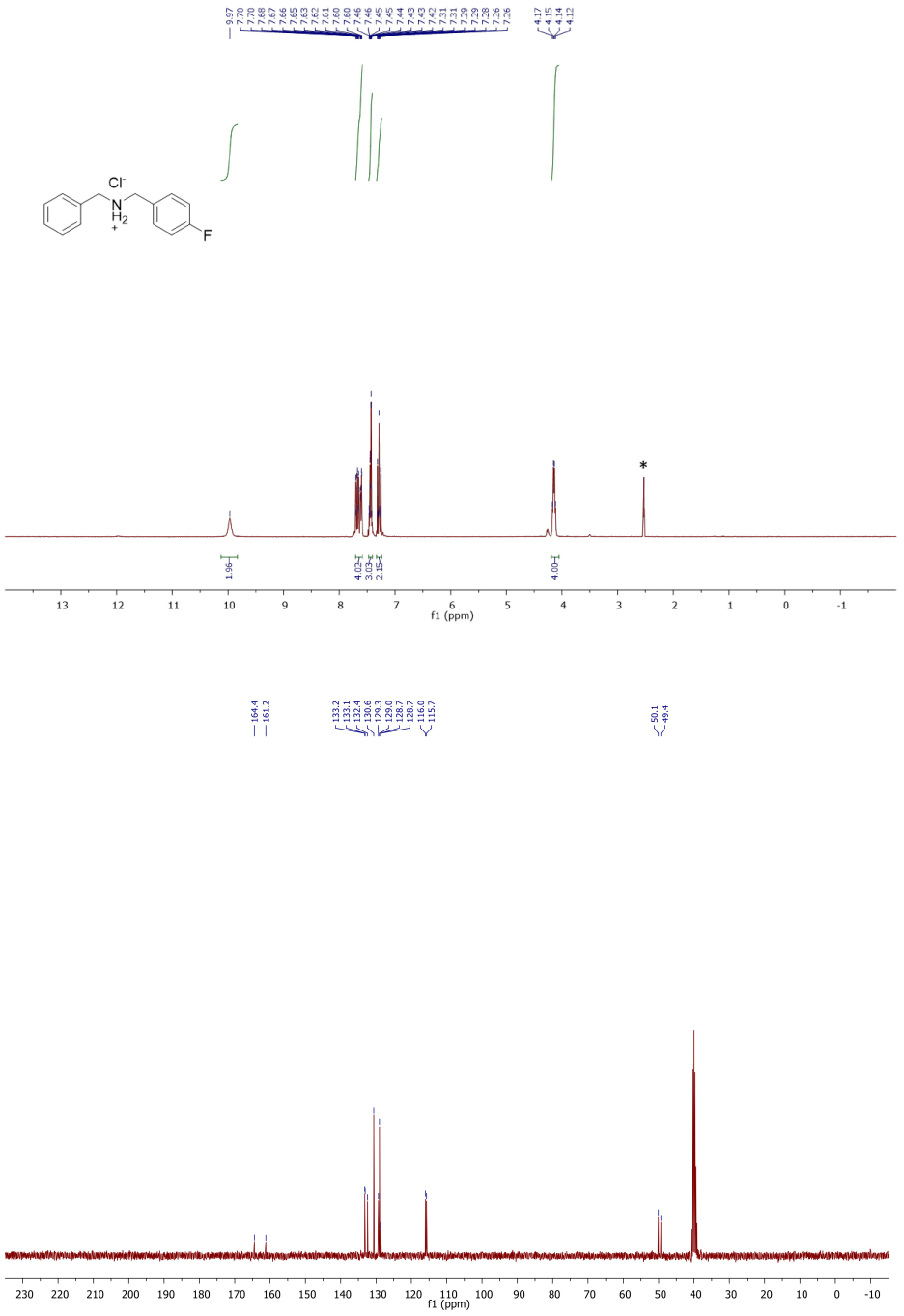
Cl⁻
N
H2
+
F
9.97
7.70
7.70
7.68
7.67
7.66
7.65
7.63
7.62
7.61
7.60
7.60
7.46
7.46
7.45
7.45
7.44
7.43
7.43
7.42
7.31
7.31
7.29
7.29
7.28
7.26
7.26
4.17
4.15
4.14
4.12
*
1.96
4.03
3.01
2.15
4.00
13 12 11 10 9 8 7 6 5 4 3 2 1 0 -1
f1 (ppm)
164.4
161.2
133.2
133.1
132.4
130.6
129.3
129.0
128.7
128.7
116.0
115.7
50.1
49.4
230 220 210 200 190 180 170 160 150 140 130 120 110 100 90 80 70 60 50 40 30 20 10 0 -10
f1 (ppm)

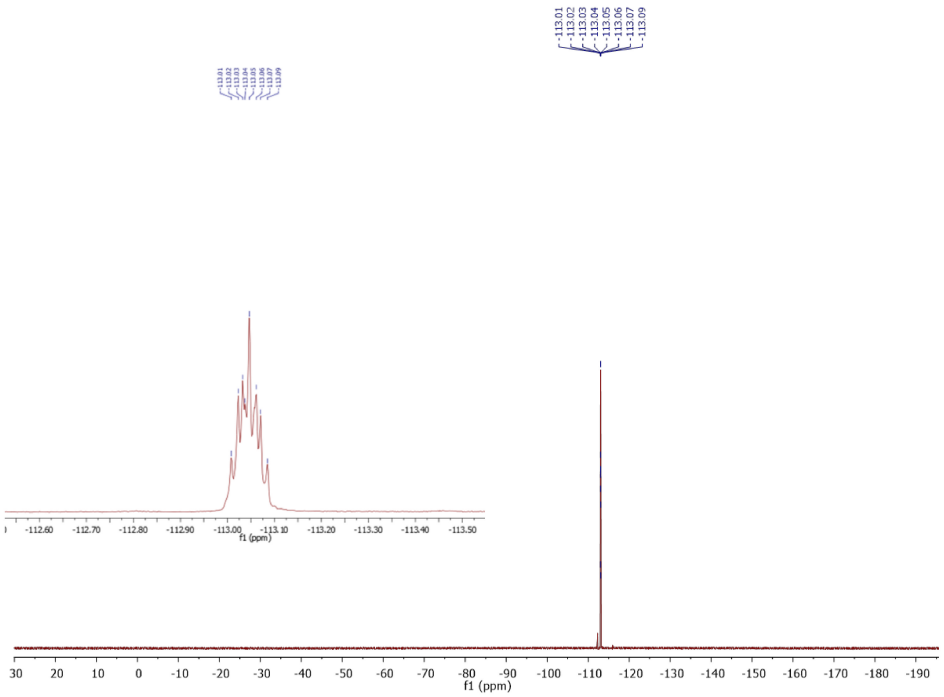
-113.01
-113.02
-113.03
-113.04
-113.05
-113.06
-113.07
-113.09
-112.60
-112.70
-112.80
-112.90
-113.00
-113.10
-113.20
-113.30
-113.40
-113.50
f1 (ppm)
30
20
10
0
-10
-20
-30
-40
-50
-60
-70
-80
-90
-100
-110
-120
-130
-140
-150
-160
-170
-180
-190
f1 (ppm)

SUPPORTING INFORMATION

ChemNMR ^{1}H Estimation

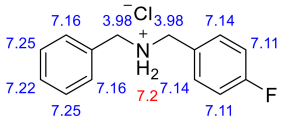

Estimation quality is indicated by color: good, medium, rough

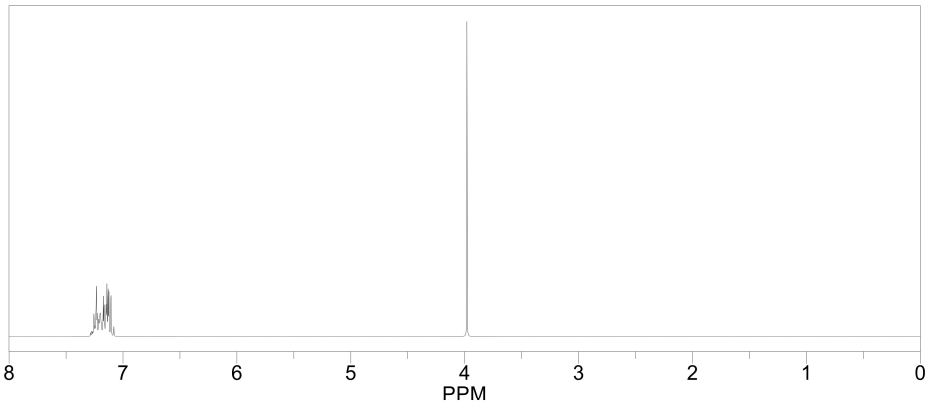

ChemNMR ^{13}C Estimation

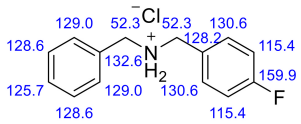

Estimation quality is indicated by color: good, medium, rough

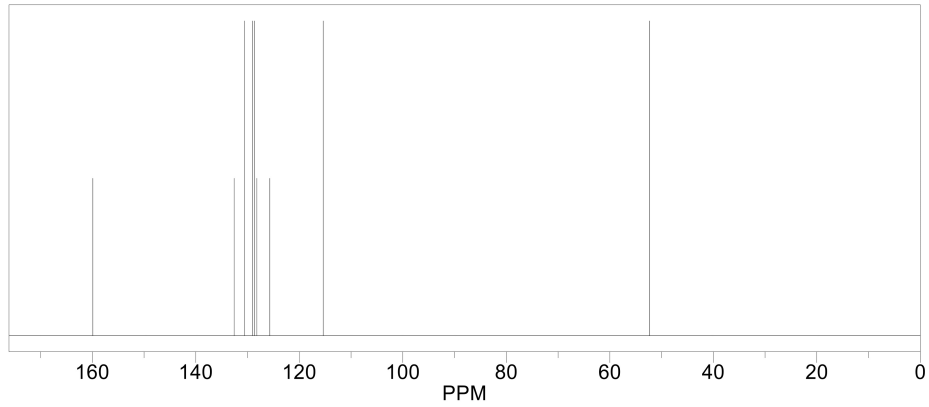

31:

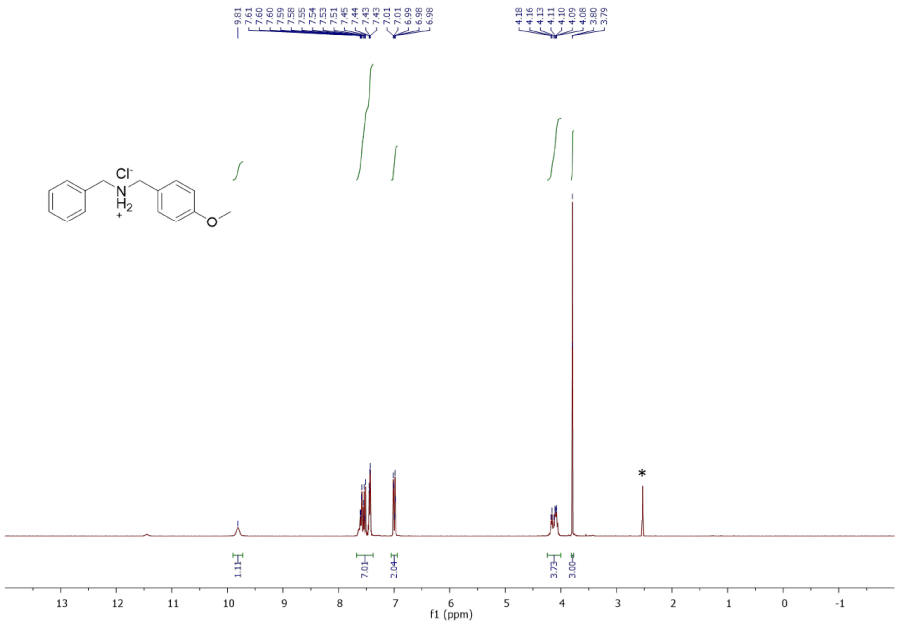
9.81
7.61
7.60
7.60
7.59
7.58
7.55
7.54
7.53
7.51
7.45
7.44
7.43
7.43
7.01
7.01
6.99
6.98
6.98
4.18
4.16
4.13
4.11
4.10
4.09
4.08
3.80
3.79
Cl⁻
N
H2
+
O
*
1.11
7.01
2.04
3.79
3.00
13
12
11
10
9
8
7
6
5
4
3
2
1
0
-1
f1 (ppm)

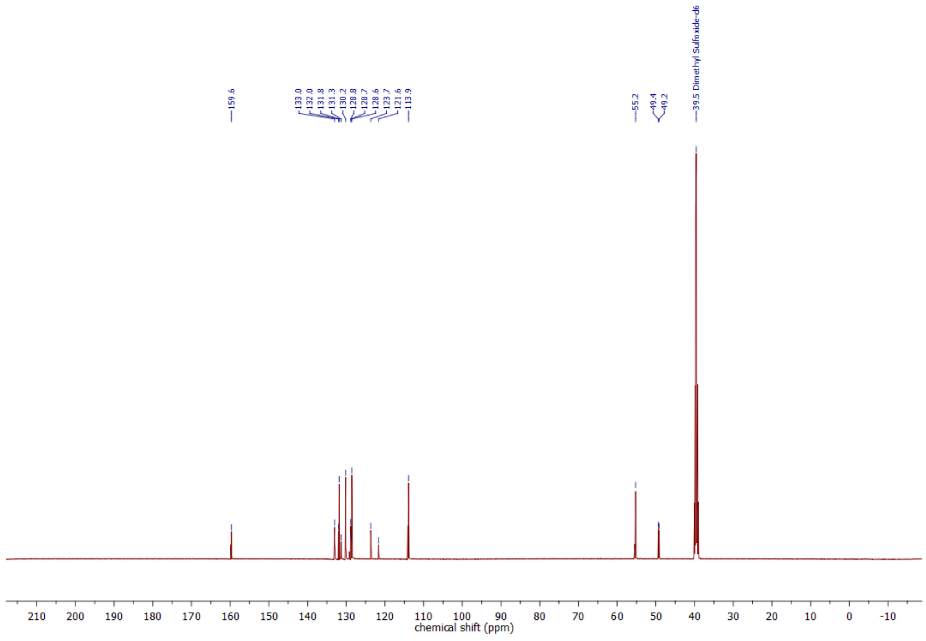
159.6
133.0
132.0
131.8
131.3
130.3
128.8
128.7
128.6
123.7
113.6
113.9
55.2
49.4
49.2
39.5 Dimethyl Sulfoxide-d6
210
200
190
180
170
160
150
140
130
120
110
100
90
80
70
60
50
40
30
20
10
0
-10
chemical shift (ppm)

SUPPORTING INFORMATION

ChemNMR ^{1}H Estimation

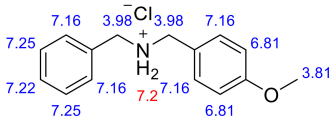

Estimation quality is indicated by color: good, medium, rough

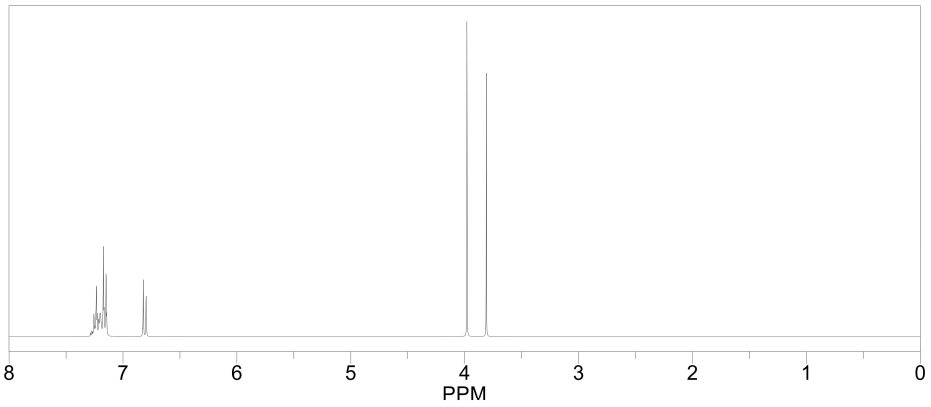

ChemNMR ^{13}C Estimation

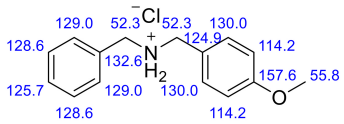

Estimation quality is indicated by color: good, medium, rough

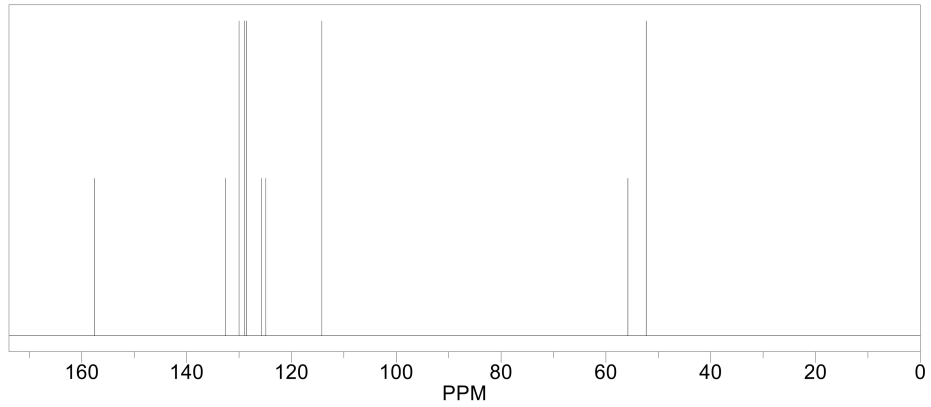

32:

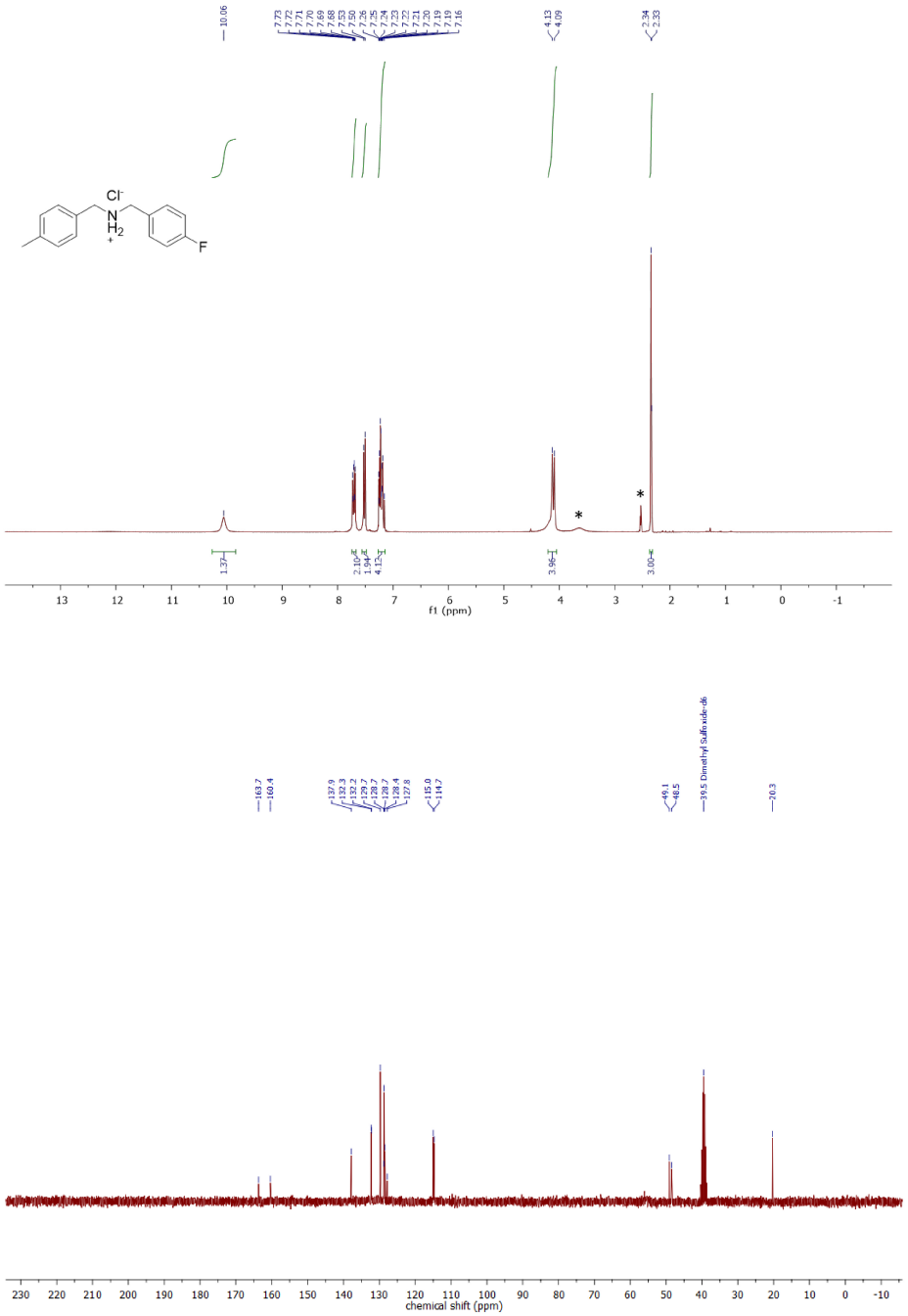
10.06
7.73
7.72
7.71
7.70
7.69
7.68
7.53
7.50
7.36
7.35
7.24
7.23
7.22
7.21
7.20
7.19
7.19
7.16
4.13
4.09
2.34
2.33
Cl⁻
N
H2
+
F
*
*
1.37
2.10
1.94
4.15
3.96
3.00
f1 (ppm)
163.7
160.4
137.9
132.3
132.2
129.7
129.7
128.7
128.4
127.8
115.0
114.7
49.1
48.5
39.5 Dimethyl Sulfoxide-d6
20.3
chemical shift (ppm)

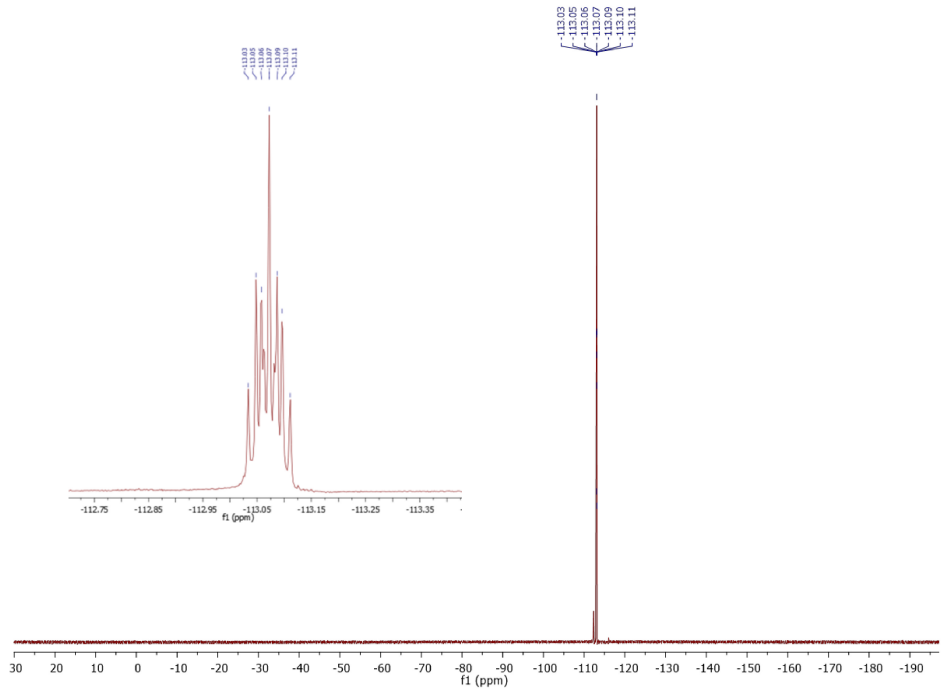
-113.03
-113.05
-113.06
-113.07
-113.09
-113.10
-113.11
-112.75
-112.85
-112.95
-113.05
-113.15
-113.25
-113.35
f1 (ppm)
30 20 10 0 -10 -20 -30 -40 -50 -60 -70 -80 -90 -100 -110 -120 -130 -140 -150 -160 -170 -180 -190
f1 (ppm)

ChemNMR ^{1}H Estimation

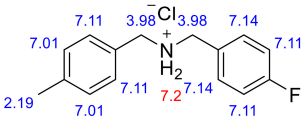

Estimation quality is indicated by color: good, medium, rough

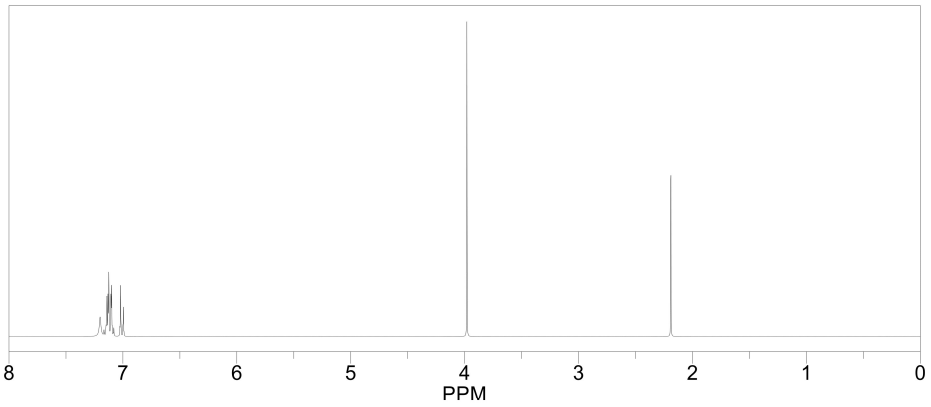

ChemNMR ^{13}C Estimation

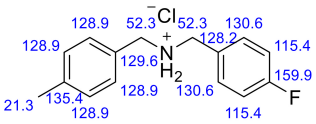

Estimation quality is indicated by color: good, medium, rough

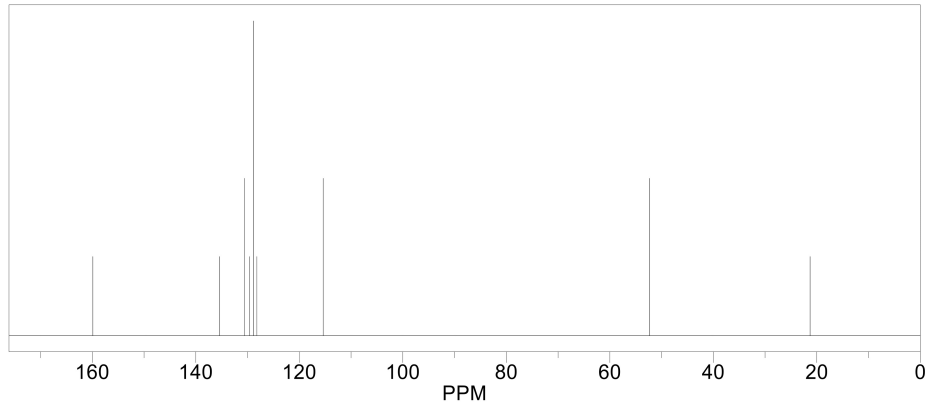

33:

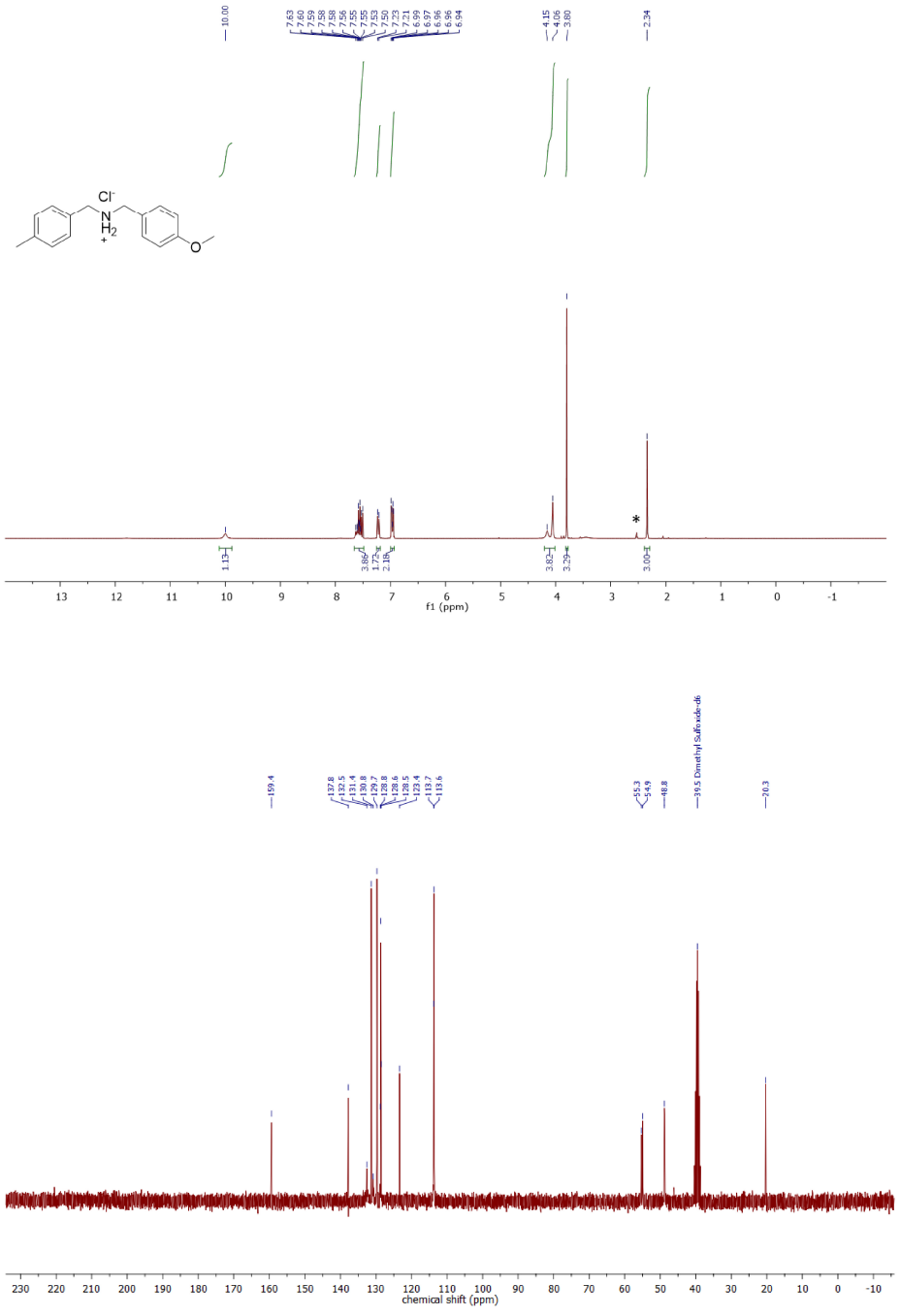

SUPPORTING INFORMATION

ChemNMR ^{1}H Estimation

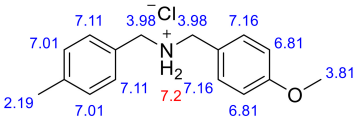

Estimation quality is indicated by color: good, medium, rough

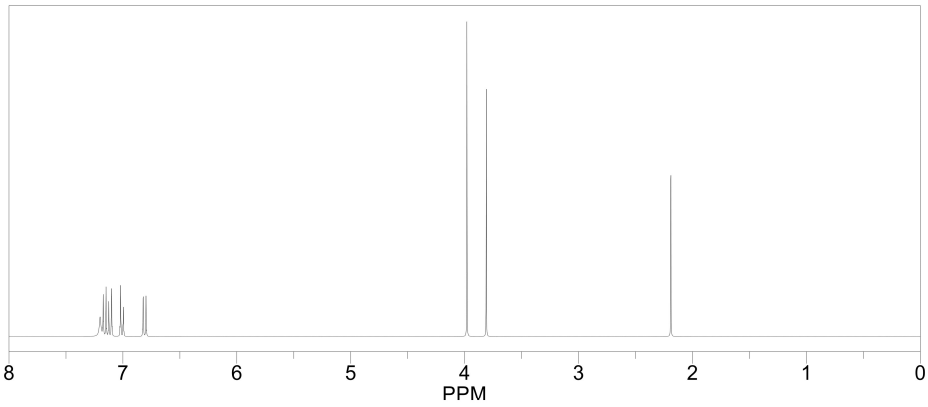

ChemNMR ^{13}C Estimation

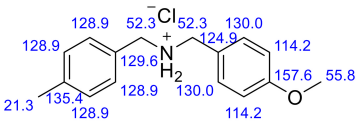

Estimation quality is indicated by color: good, medium, rough

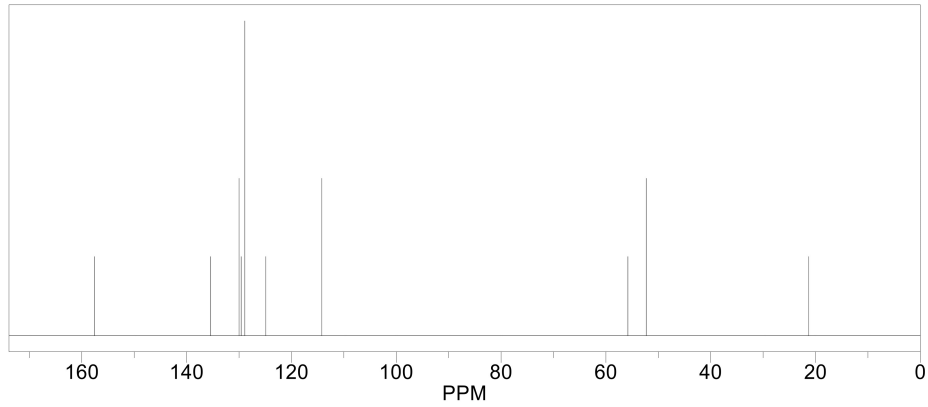

34:

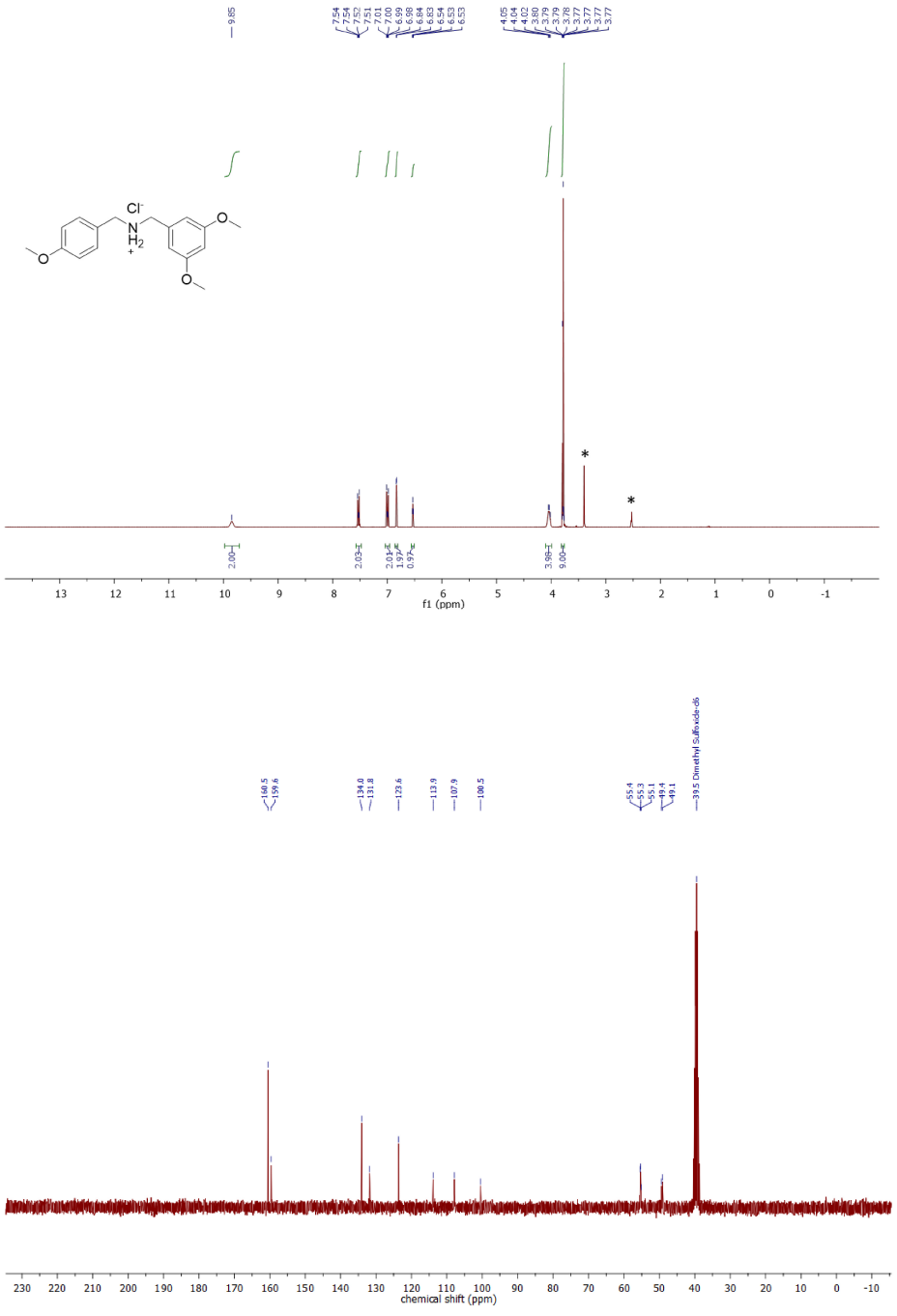

SUPPORTING INFORMATION

ChemNMR ^{1}H Estimation

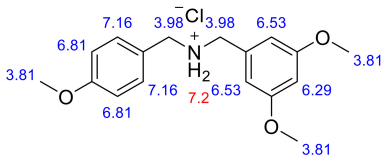

Estimation quality is indicated by color: good, medium, rough

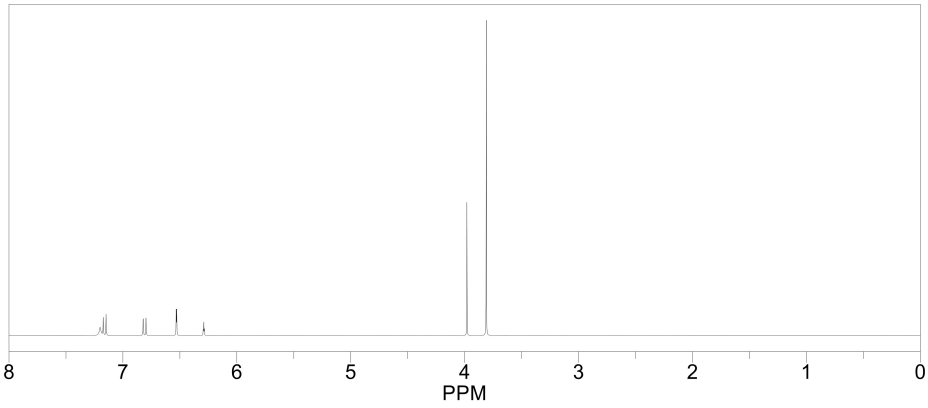

ChemNMR ^{13}C Estimation

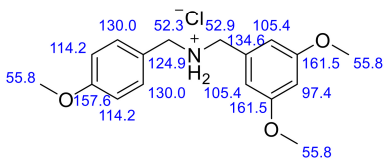

Estimation quality is indicated by color: good, medium, rough

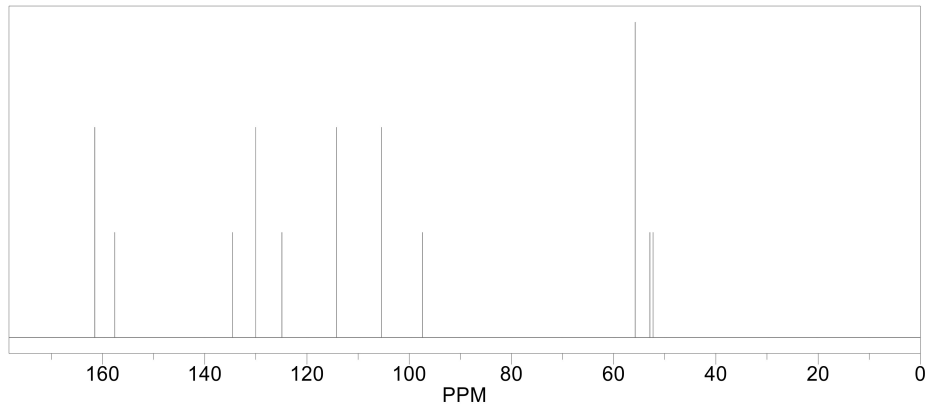

35:

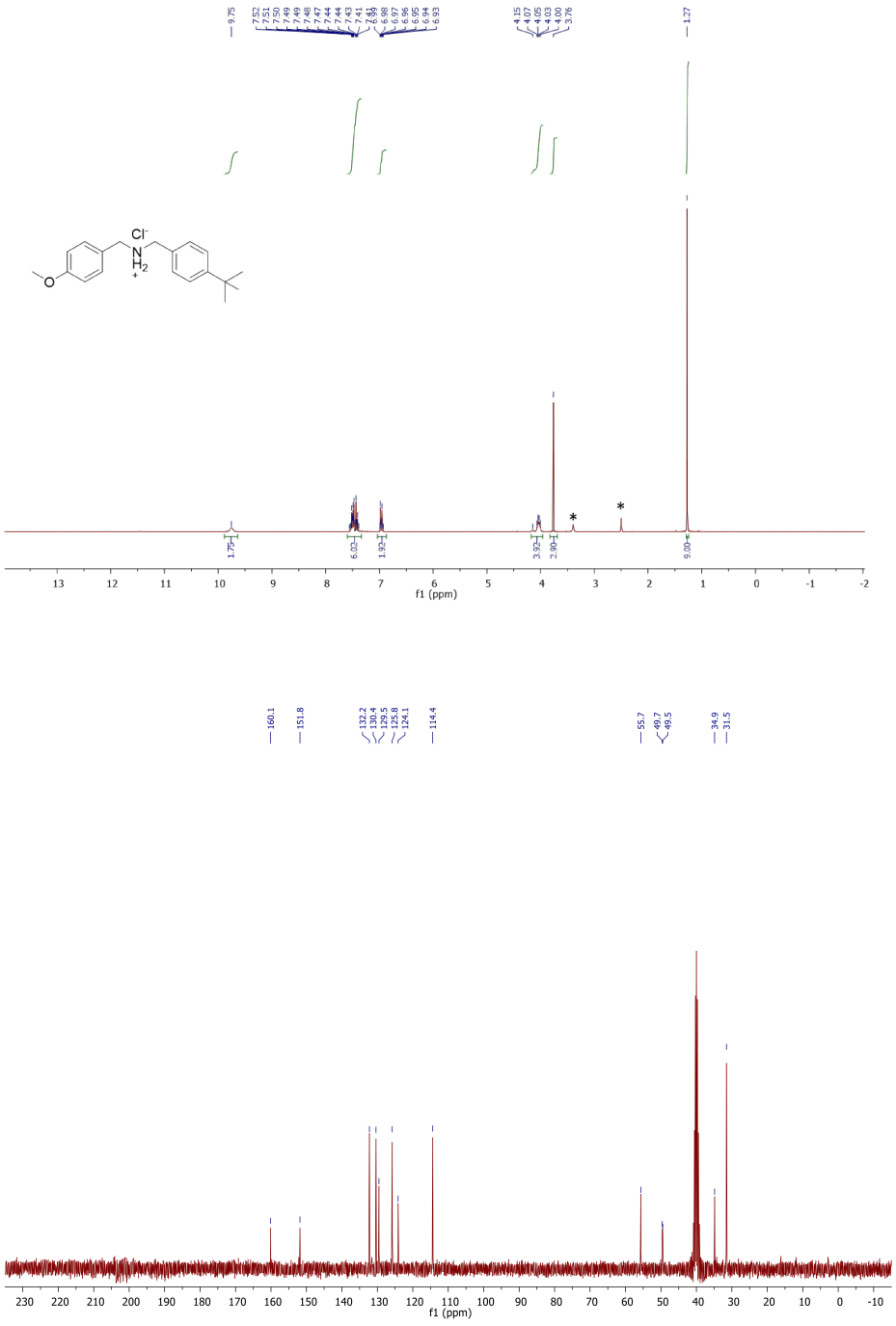
9.75
7.52
7.51
7.50
7.49
7.49
7.48
7.47
7.44
7.44
7.43
7.41
7.41
6.98
6.97
6.96
6.95
6.94
6.93
4.15
4.07
4.05
4.03
4.00
3.76
1.27
Cl⁻
N
H2
+
O
1.75
6.02
1.92
3.92
2.90
9.00
f1 (ppm)
160.1
151.8
132.2
130.4
130.5
125.8
124.1
114.4
55.7
49.7
49.5
34.9
31.5
f1 (ppm)

110

SUPPORTING INFORMATION

ChemNMR ^{1}H Estimation

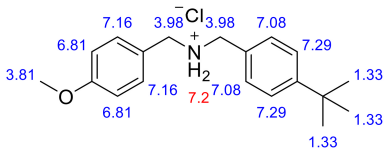

Estimation quality is indicated by color: good, medium, rough

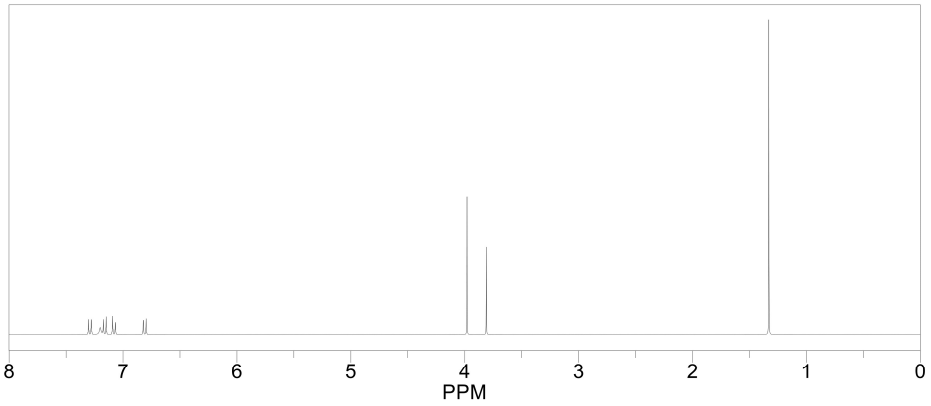

ChemNMR ^{13}C Estimation

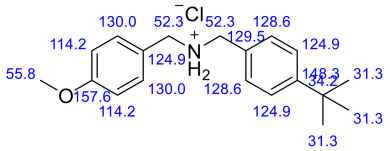

Estimation quality is indicated by color: good, medium, rough

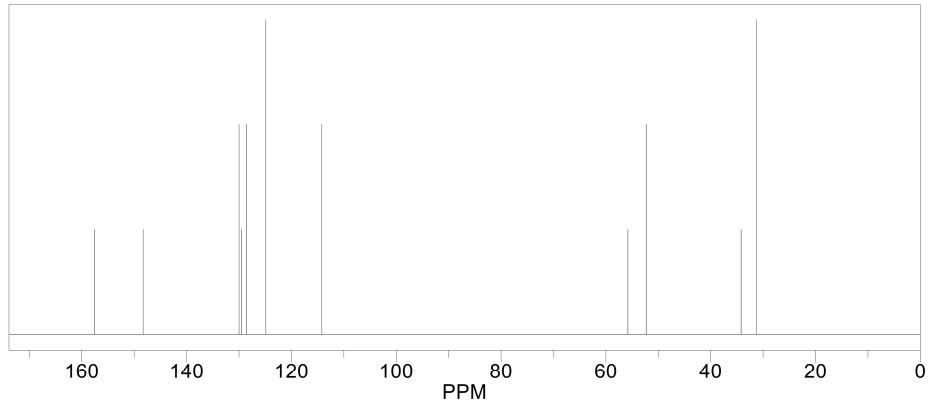

36:

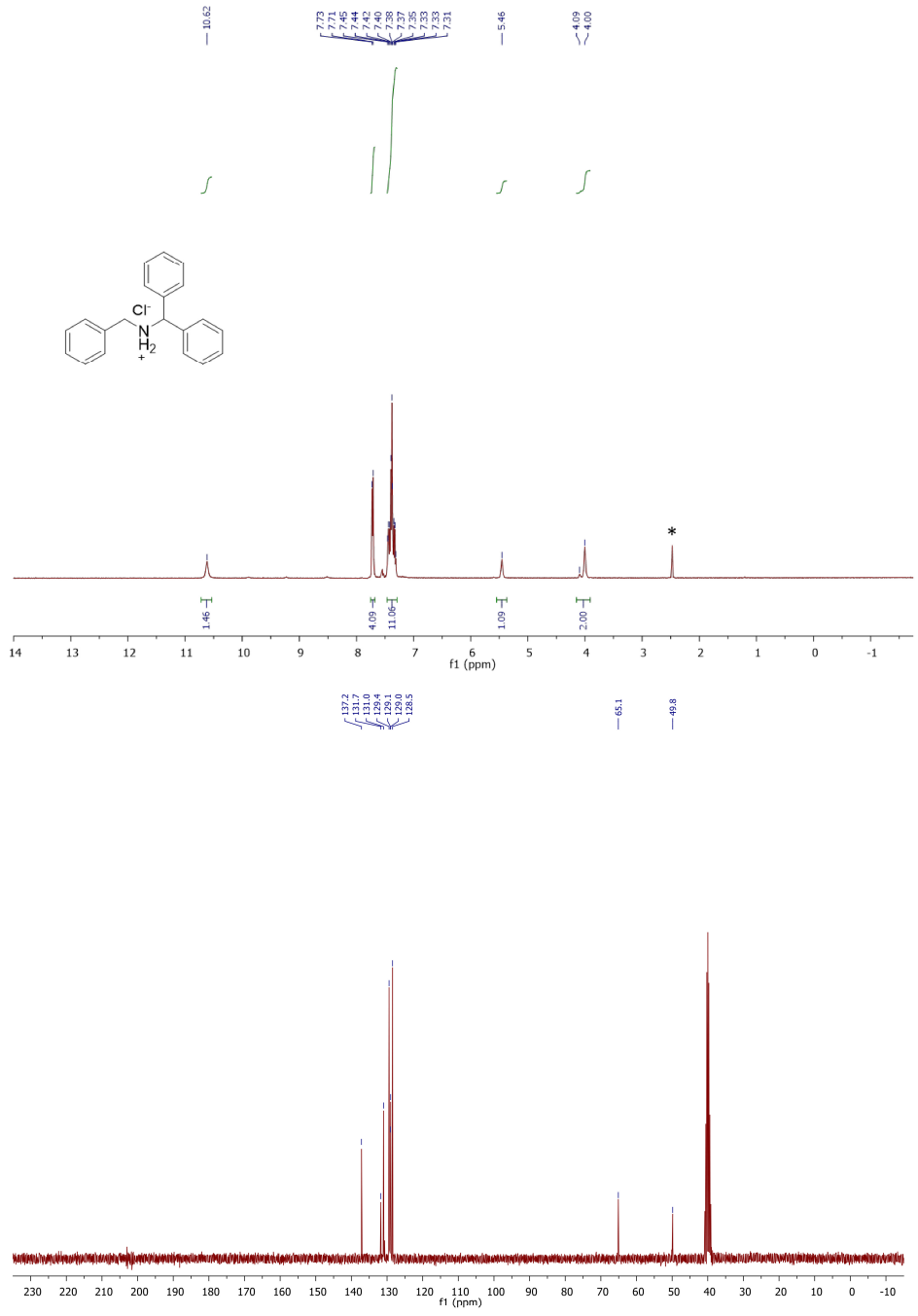
10.62
7.73
7.71
7.45
7.44
7.42
7.40
7.38
7.37
7.35
7.33
7.33
7.31
5.46
4.09
4.00
Cl⁻
N
H2
+
*
1.46
4.09
11.06
1.09
2.00
f1 (ppm)
137.2
131.7
131.0
129.4
129.1
129.0
128.5
65.1
49.8
f1 (ppm)

ChemNMR ^{1}H Estimation

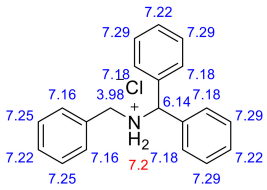

Estimation quality is indicated by color: good, medium, rough

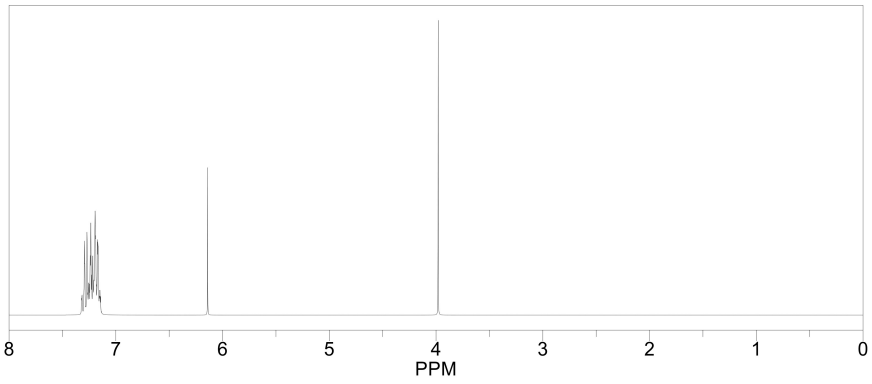

ChemNMR ^{13}C Estimation

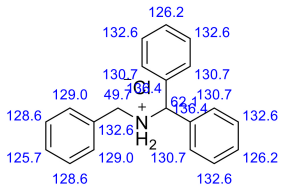

Estimation quality is indicated by color: good, medium, rough

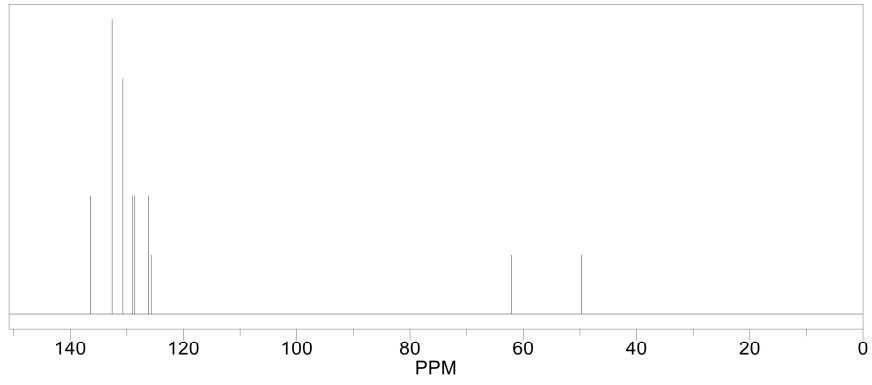

37:

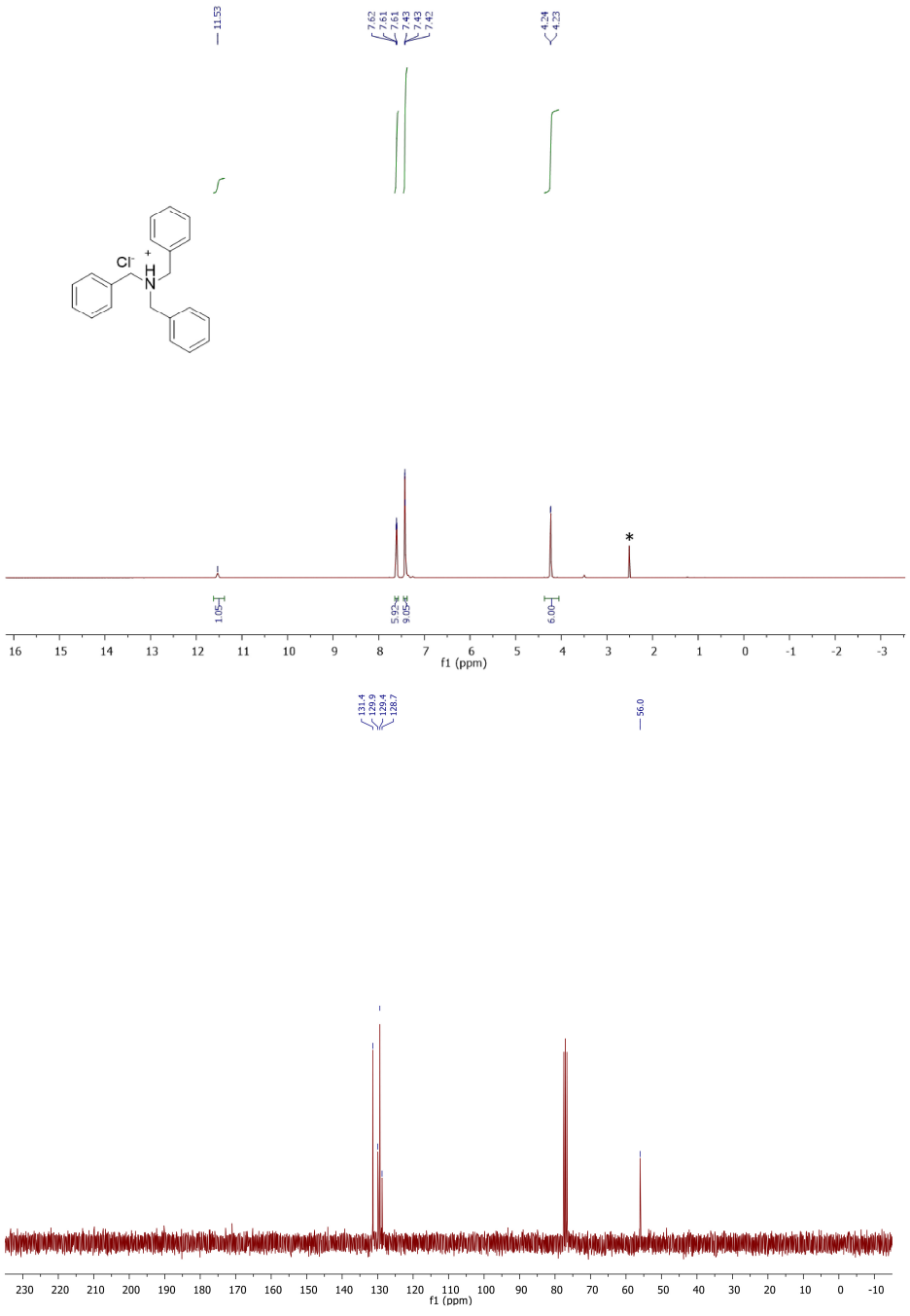
11.53
7.62
7.61
7.61
7.43
7.43
7.42
4.24
4.23
Cl⁻
+
NH
*
1.00
5.92
9.05
6.00
f1 (ppm)
131.4
129.9
129.4
128.7
56.0
f1 (ppm)

ChemNMR ^{1}H Estimation

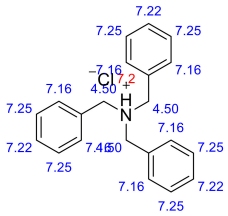

Estimation quality is indicated by color: good, medium, rough

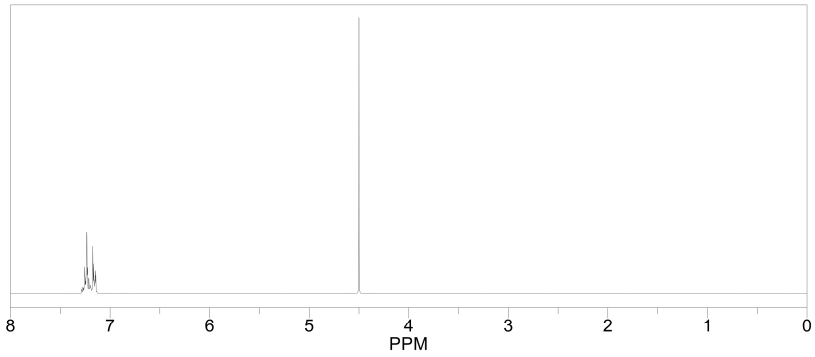

ChemNMR ^{13}C Estimation

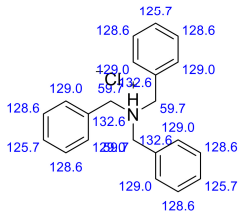

Estimation quality is indicated by color: good, medium, rough

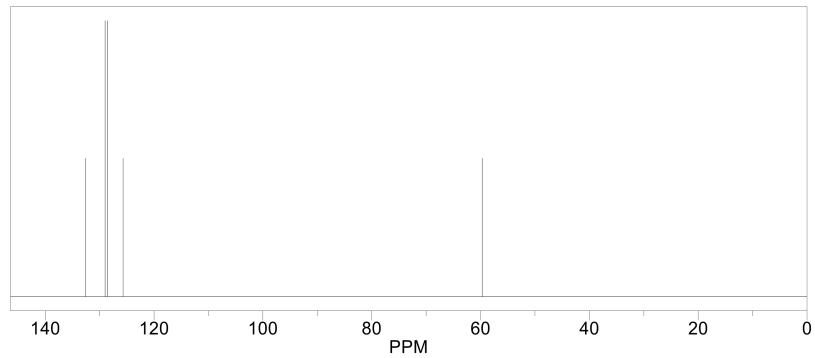

38:

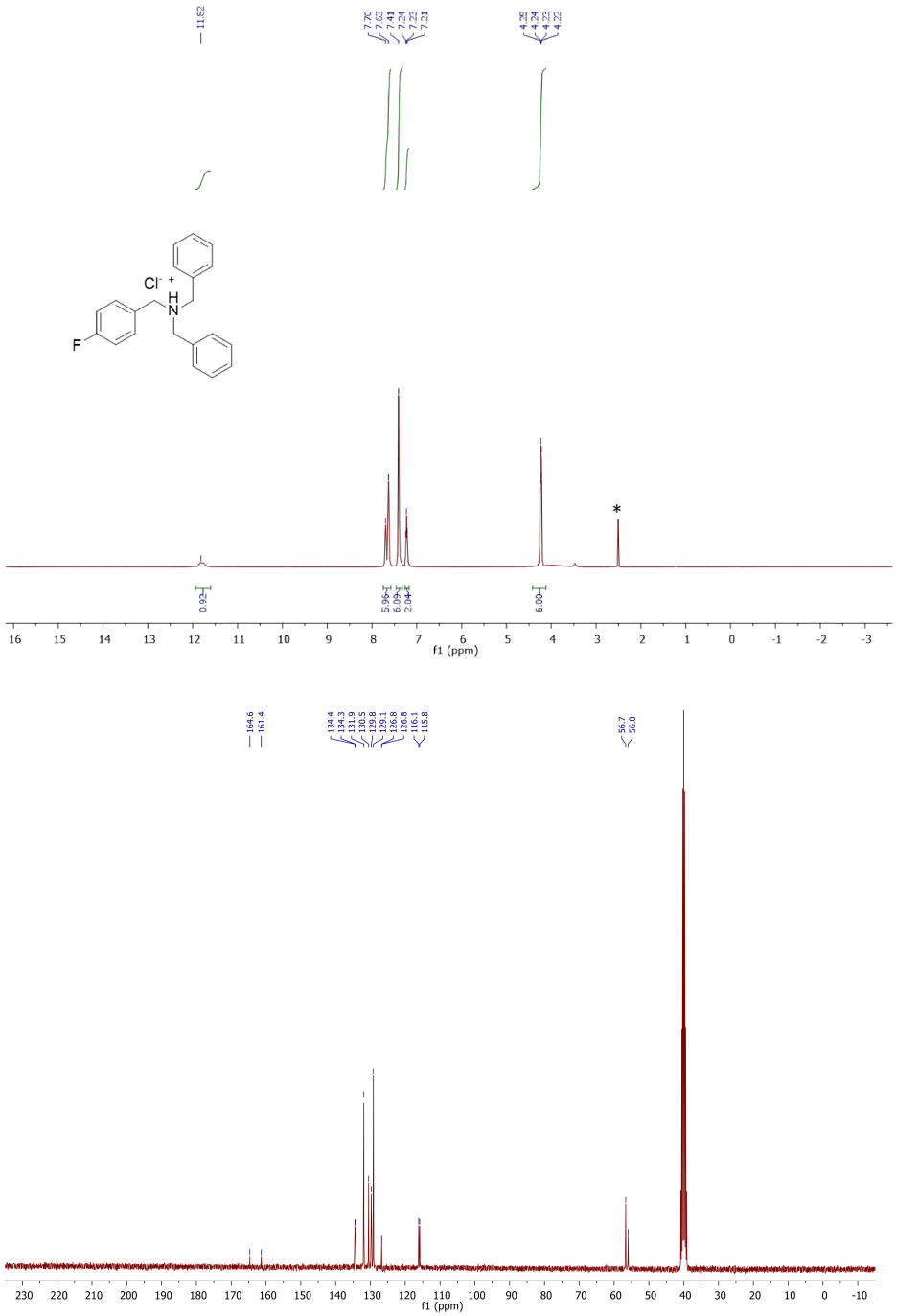
11.82
7.70
7.63
7.41
7.24
7.23
7.21
4.25
4.24
4.23
4.22
Cl⁻ +
H
N
F
*
0.92
5.96
6.09
2.04
6.00
f1 (ppm)
164.6
161.4
134.4
134.3
131.9
130.5
129.8
129.7
126.1
126.8
116.1
115.8
56.7
56.0
f1 (ppm)

116

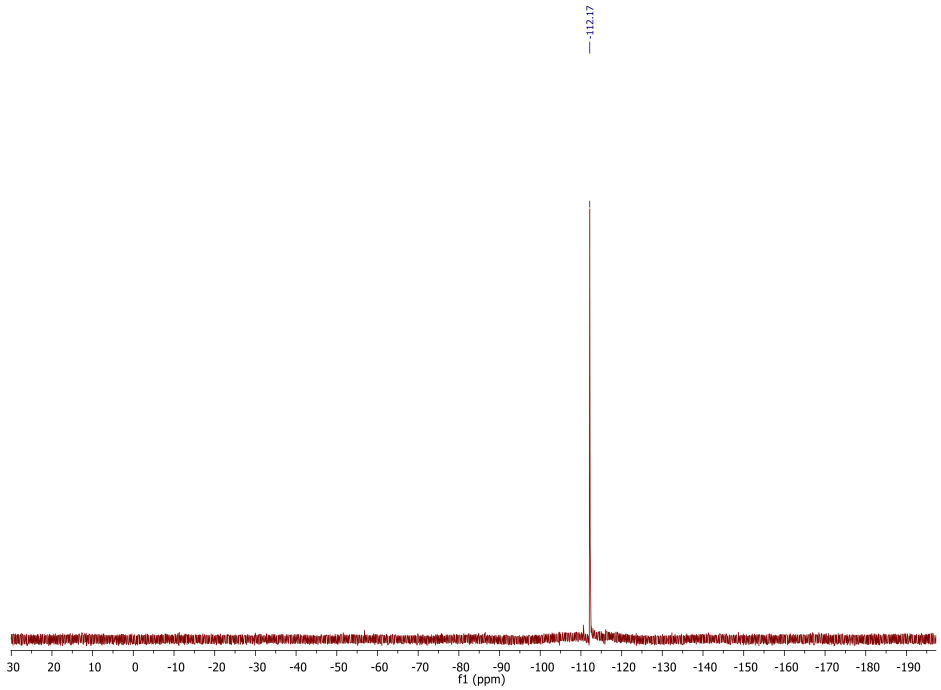
-112.17
30 20 10 0 -10 -20 -30 -40 -50 -60 -70 -80 -90 -100 -110 -120 -130 -140 -150 -160 -170 -180 -190
f1 (ppm)

SUPPORTING INFORMATION

ChemNMR ^{1}H Estimation

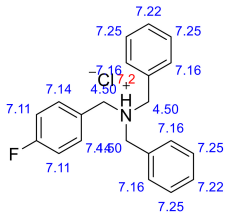

Estimation quality is indicated by color: good, medium, rough

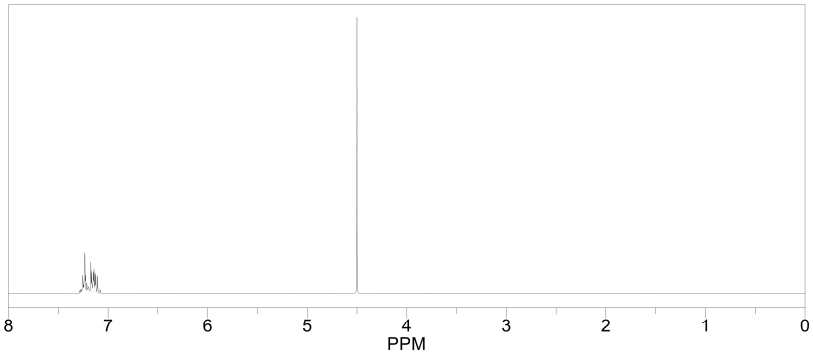

ChemNMR ^{13}C Estimation

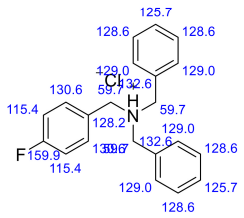

Estimation quality is indicated by color: good, medium, rough

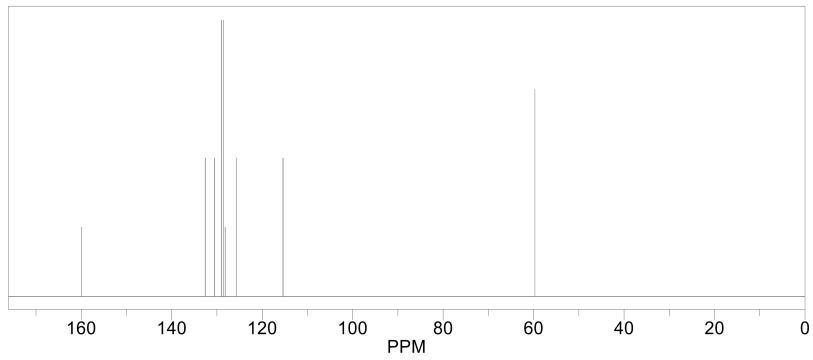

39:

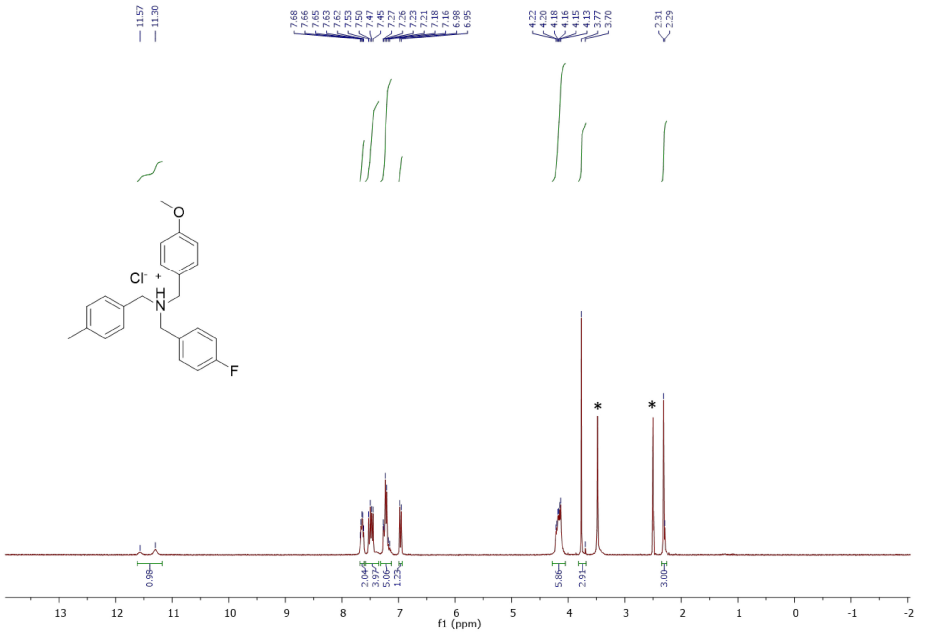
11.57
11.30
7.68
7.66
7.65
7.63
7.62
7.53
7.50
7.47
7.45
7.27
7.26
7.23
7.21
7.18
7.16
6.98
6.95
4.22
4.20
4.18
4.16
4.15
4.13
3.77
3.70
2.31
2.29
O
Cl⁻
+
H
N
F
*
*
0.98
2.04
3.97
5.06
1.25
5.86
2.91
3.00
13 12 11 10 9 8 7 6 5 4 3 2 1 0 -1 -2
f1 (ppm)

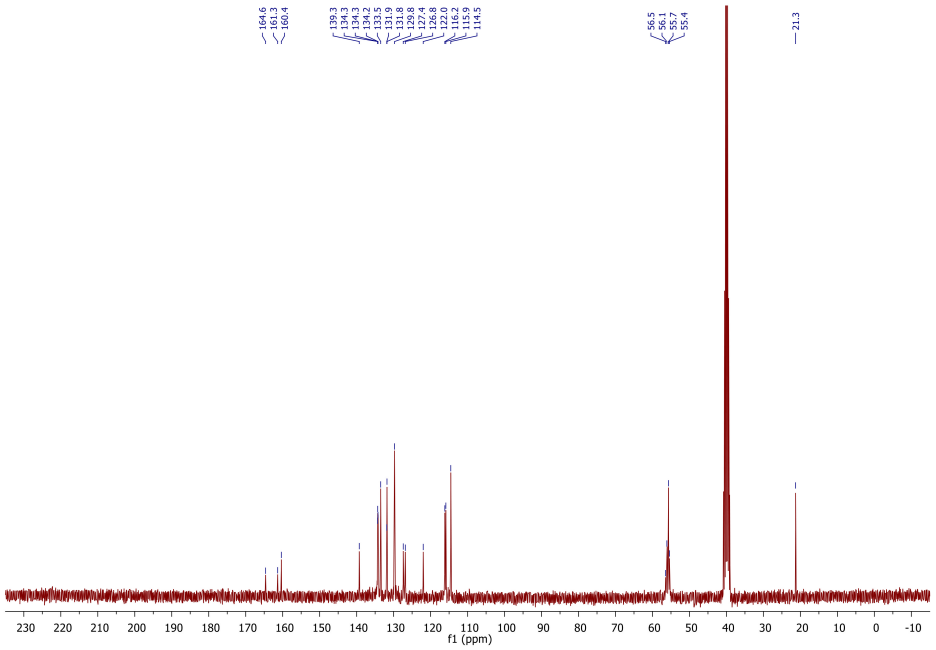
164.6
161.3
160.4
139.3
134.3
134.3
134.2
133.5
131.9
131.8
130.8
127.4
126.8
122.0
116.2
115.9
114.5
56.5
56.1
55.7
55.4
21.3
230 220 210 200 190 180 170 160 150 140 130 120 110 100 90 80 70 60 50 40 30 20 10 0 -10
f1 (ppm)

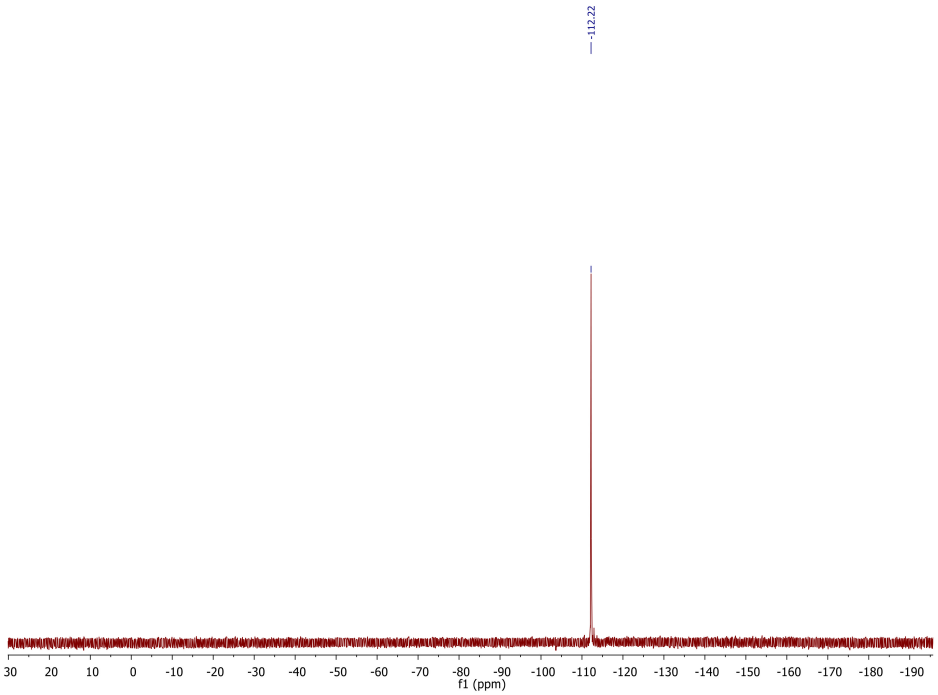
-112.22
30 20 10 0 -10 -20 -30 -40 -50 -60 -70 -80 -90 -100 -110 -120 -130 -140 -150 -160 -170 -180 -190
f1 (ppm)

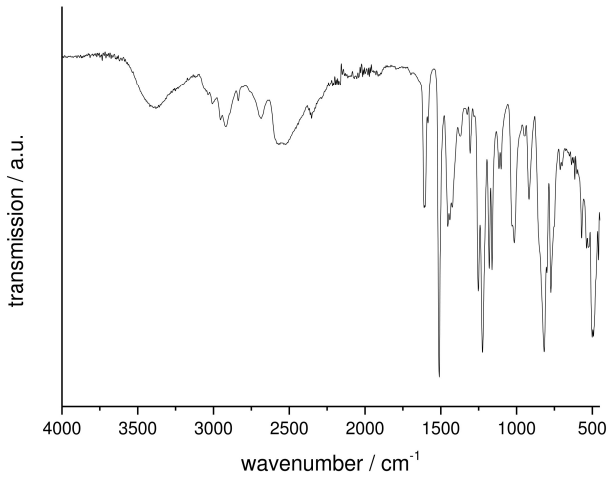
transmission / a.u.
4000 3500 3000 2500 2000 1500 1000 500
wavenumber / cm-1

120

ChemNMR ^{1}H Estimation

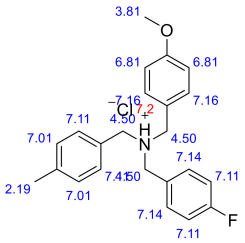

Estimation quality is indicated by color: good, medium, rough

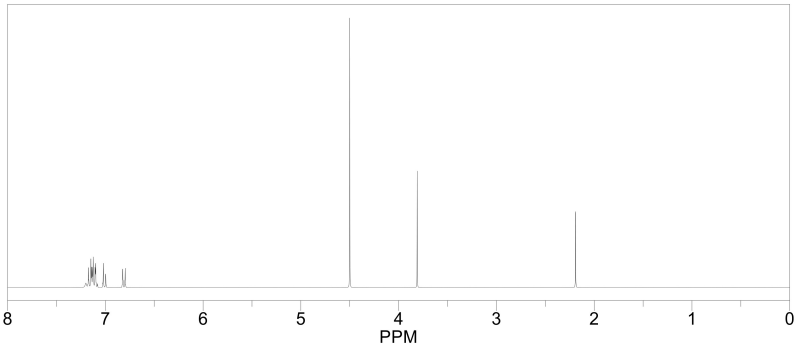

ChemNMR ^{13}C Estimation

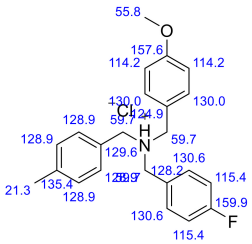

Estimation quality is indicated by color: good, medium, rough

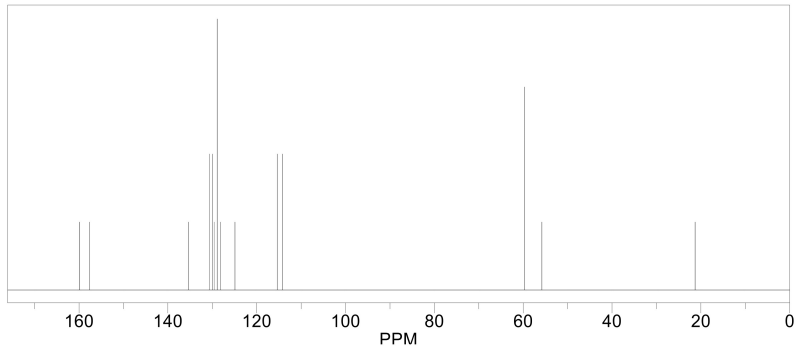

121

40:

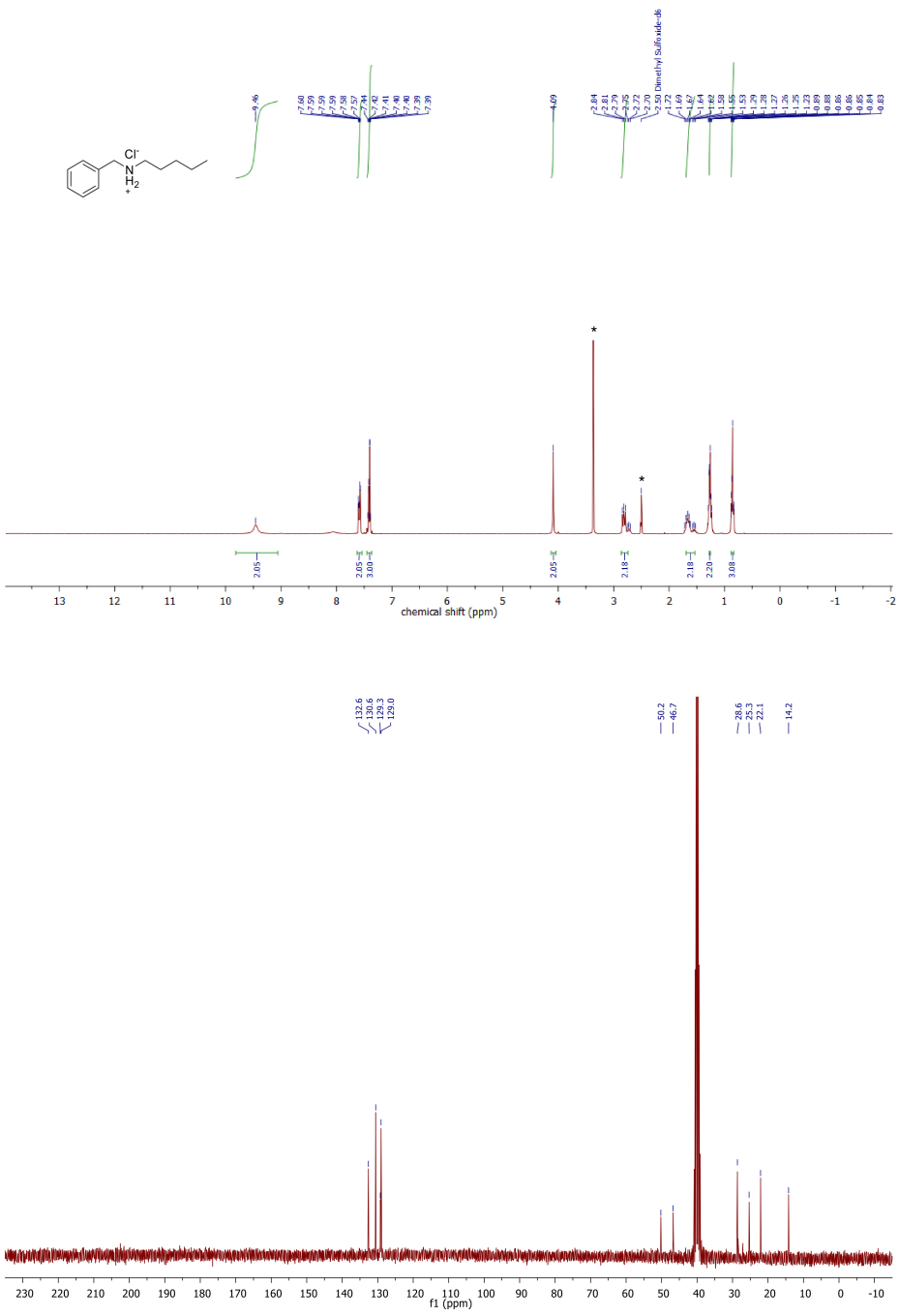

SUPPORTING INFORMATION

ChemNMR ^{1}H Estimation

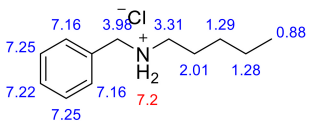

Estimation quality is indicated by color: good, medium, rough

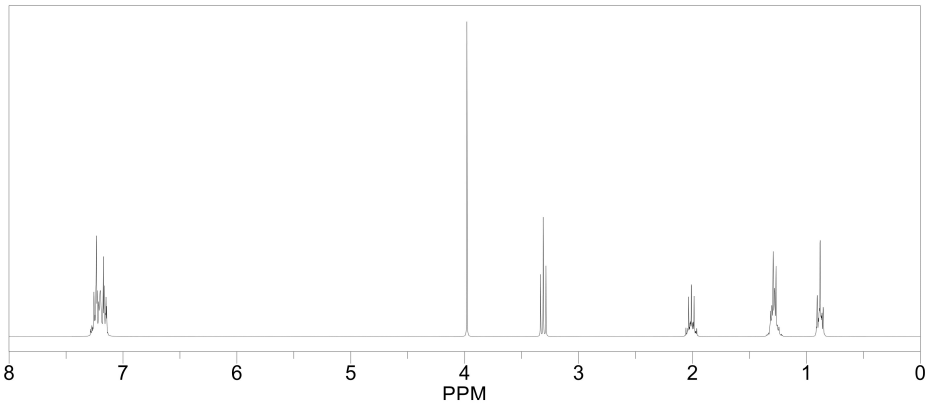

ChemNMR ^{13}C Estimation

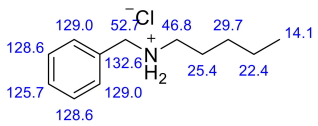

Estimation quality is indicated by color: good, medium, rough

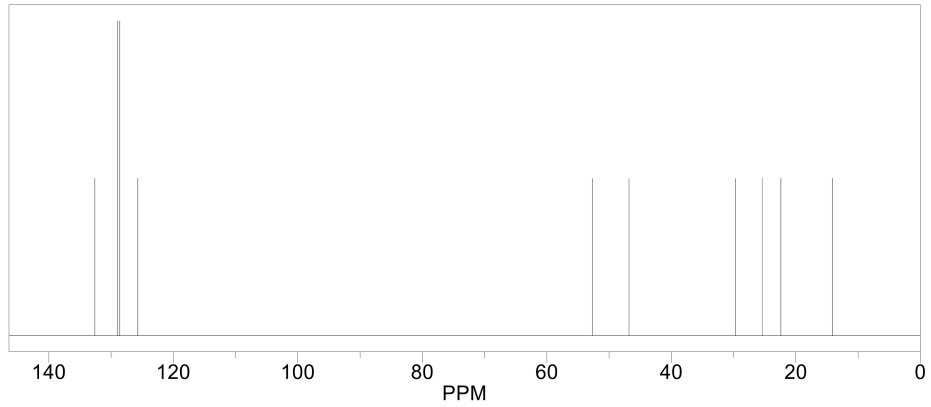

41:

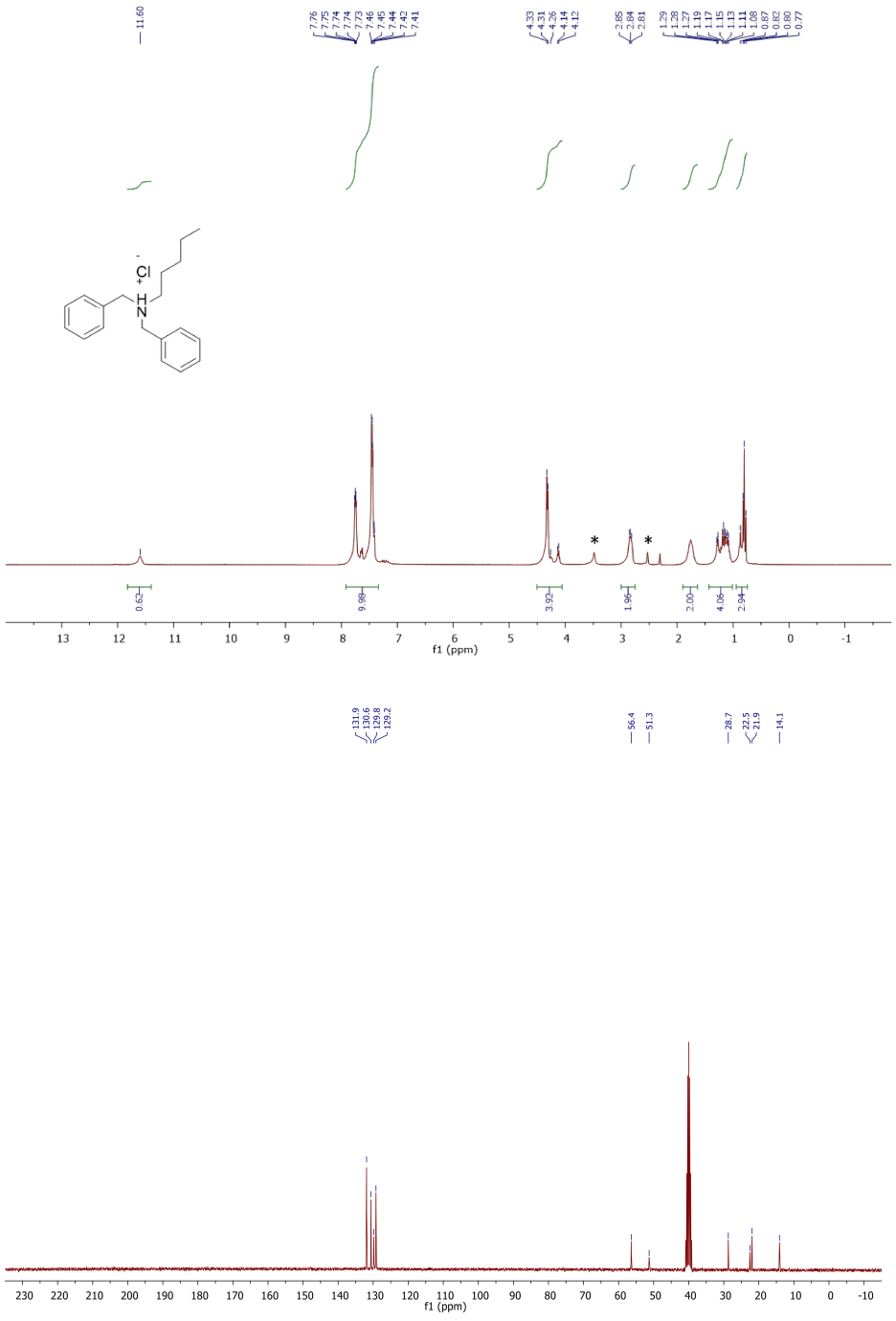
11.60
7.76
7.75
7.74
7.74
7.73
7.46
7.45
7.44
7.42
7.41
4.33
4.31
4.26
4.14
4.12
2.85
2.84
2.81
1.29
1.28
1.27
1.19
1.17
1.15
1.13
1.11
1.08
0.87
0.82
0.80
0.77
Cl
H
N
0.62
9.98
3.92
1.96
2.00
4.06
2.94
f1 (ppm)
131.9
130.6
129.8
129.2
56.4
51.3
28.7
22.5
21.9
14.1
f1 (ppm)

124

SUPPORTING INFORMATION

ChemNMR ^{1}H Estimation

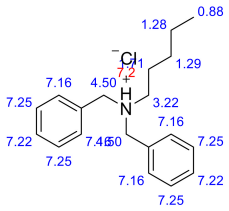

Estimation quality is indicated by color: good, medium, rough

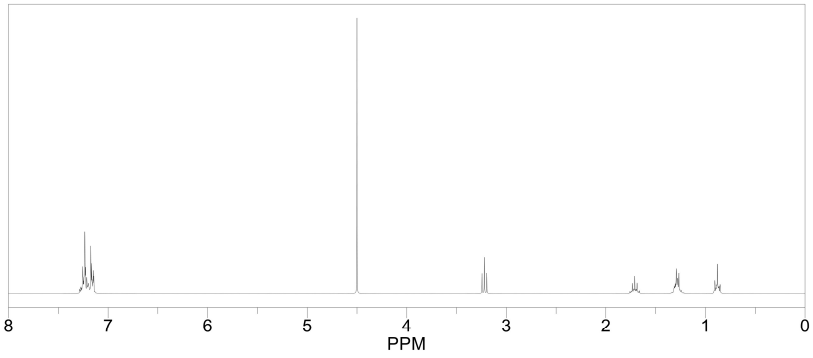

ChemNMR ^{13}C Estimation

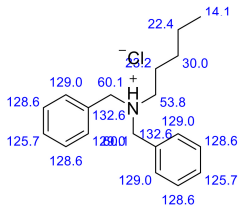

Estimation quality is indicated by color: good, medium, rough

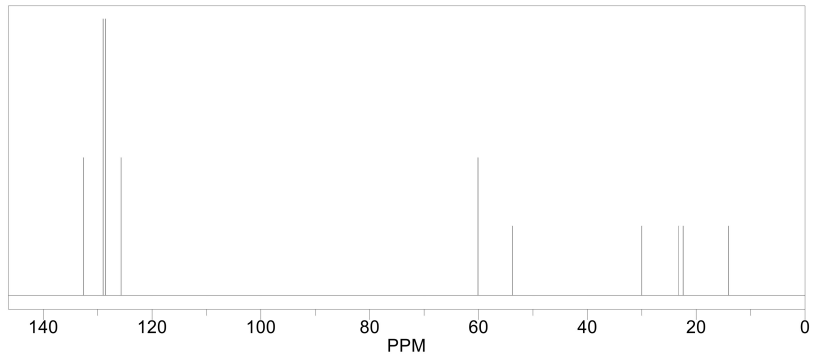

125

42:

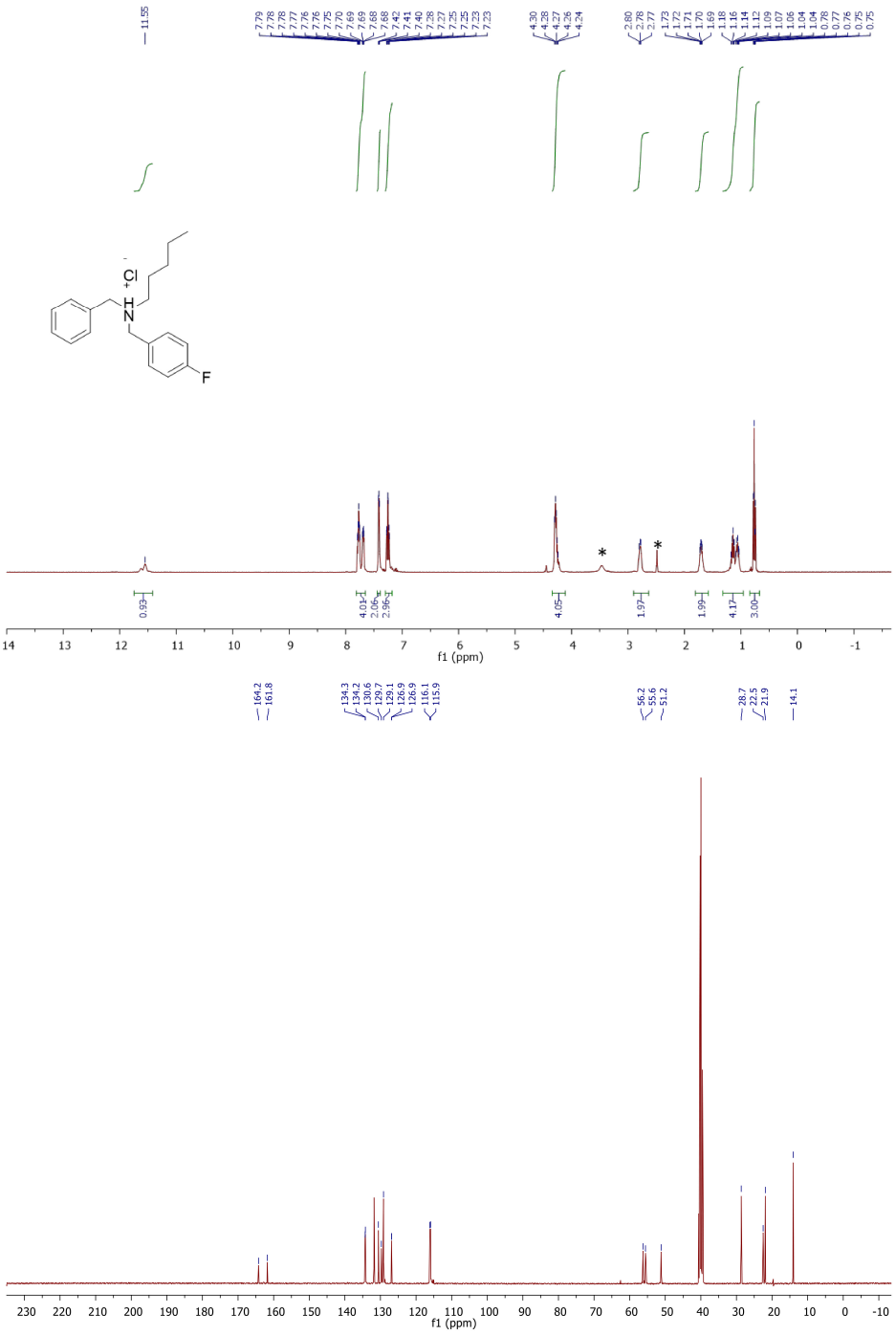

126

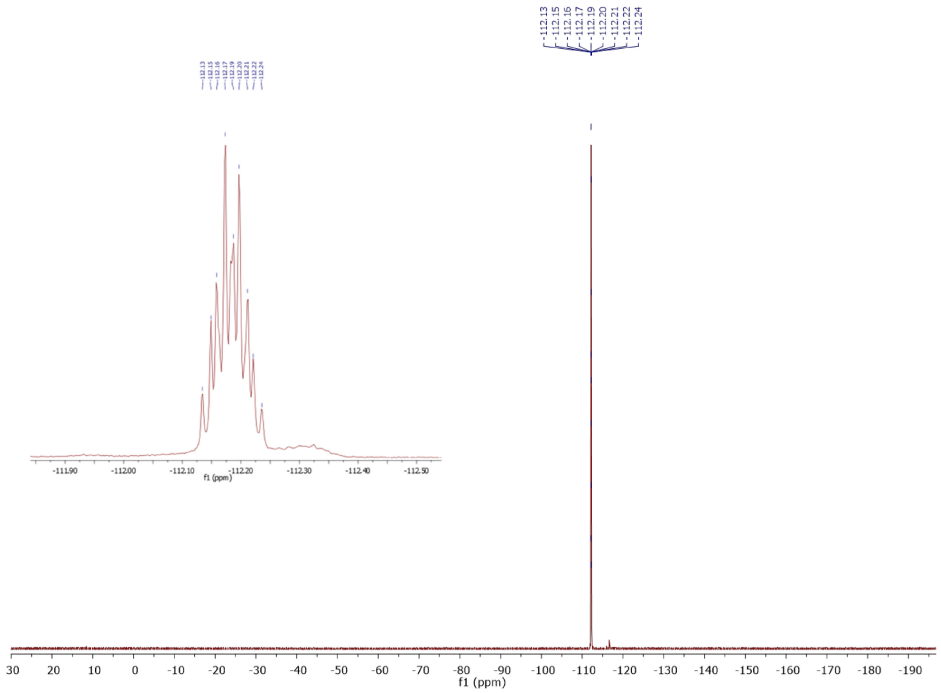

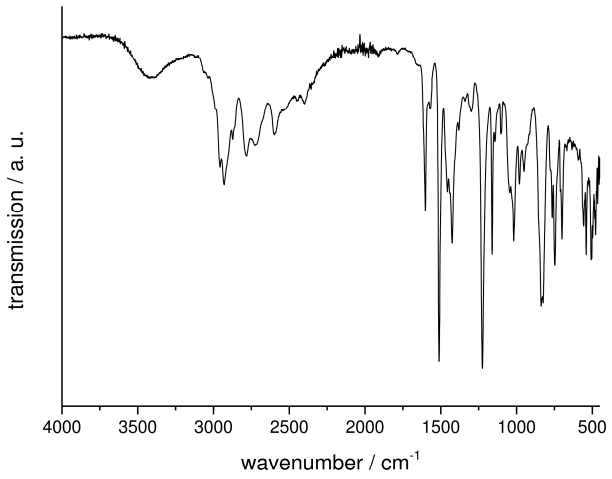

127

SUPPORTING INFORMATION

ChemNMR ^{1}H Estimation

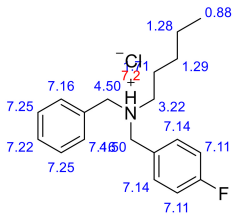

Estimation quality is indicated by color: good, medium, rough

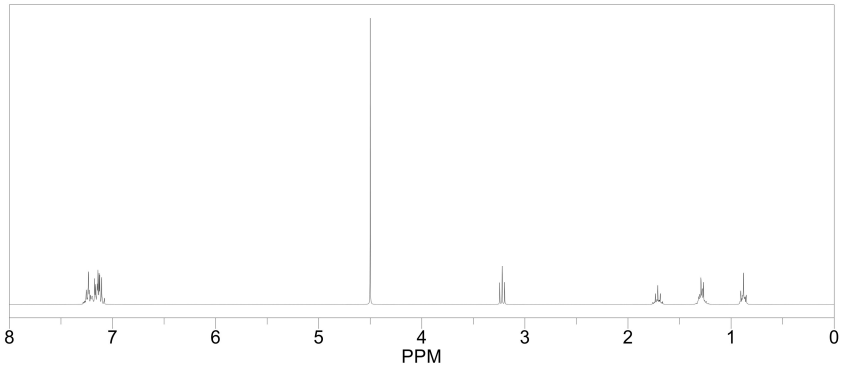

ChemNMR ^{13}C Estimation

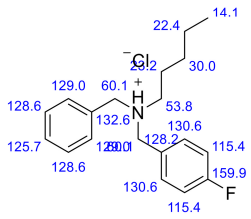

Estimation quality is indicated by color: good, medium, rough

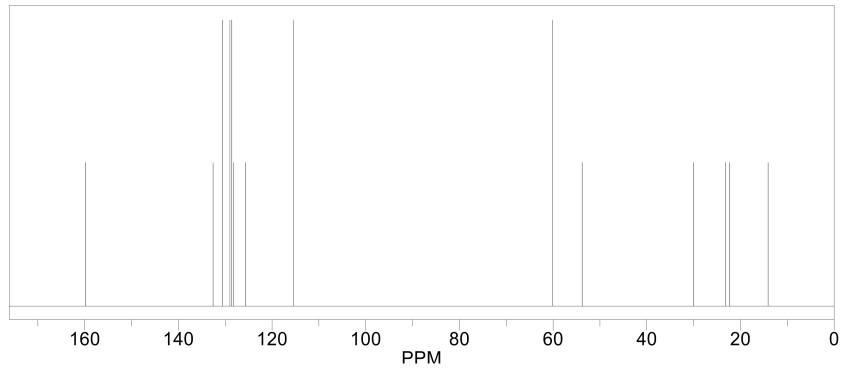

43:

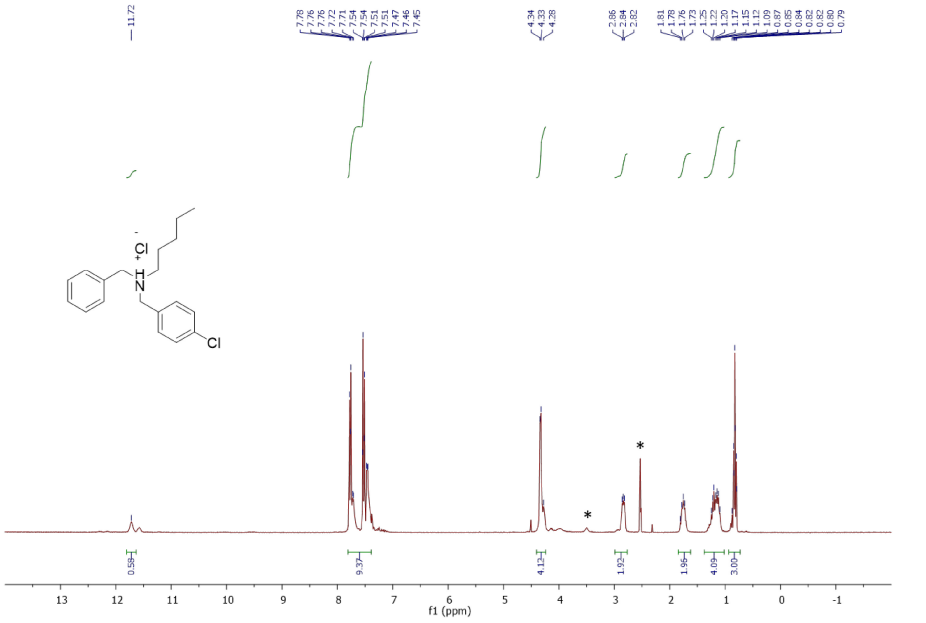
11.72
7.78
7.76
7.76
7.72
7.71
7.54
7.54
7.51
7.51
7.47
7.46
7.45
4.34
4.33
4.28
2.86
2.84
2.82
1.81
1.78
1.76
1.73
1.25
1.22
1.20
1.17
1.15
1.15
1.12
1.09
0.87
0.86
0.84
0.82
0.82
0.80
0.79
Cl
N
H
Cl
*
*
0.55
9.37
4.12
1.92
1.95
4.09
3.00
13
12
11
10
9
8
7
6
5
4
3
2
1
0
-1
f1 (ppm)

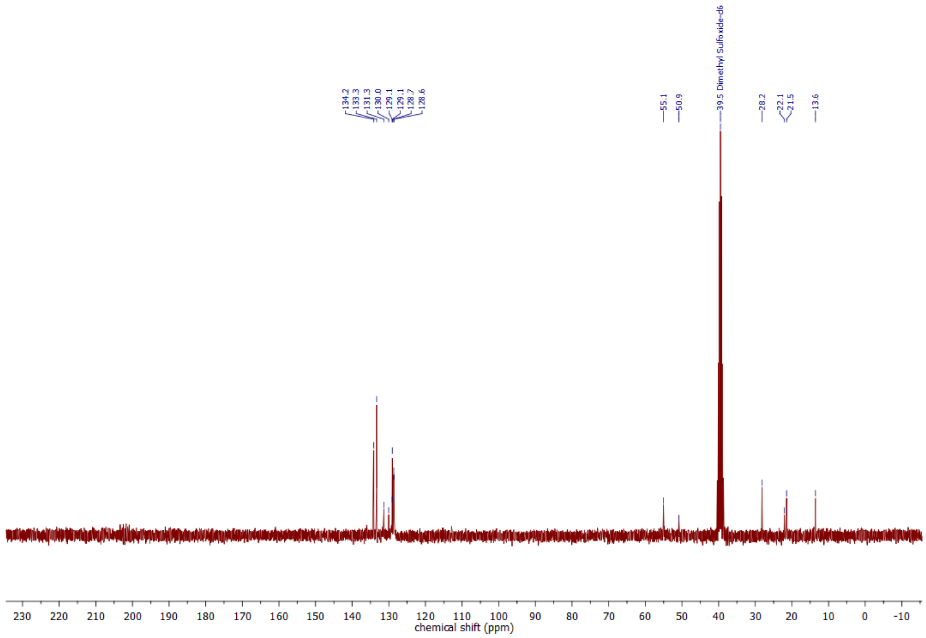
134.2
133.3
131.3
130.0
129.1
129.1
128.7
128.6
55.1
50.9
39.5 Dimethyl Sulfoxide-d6
28.2
22.1
21.5
13.6
230
220
210
200
190
180
170
160
150
140
130
120
110
100
90
80
70
60
50
40
30
20
10
0
-10
chemical shift (ppm)

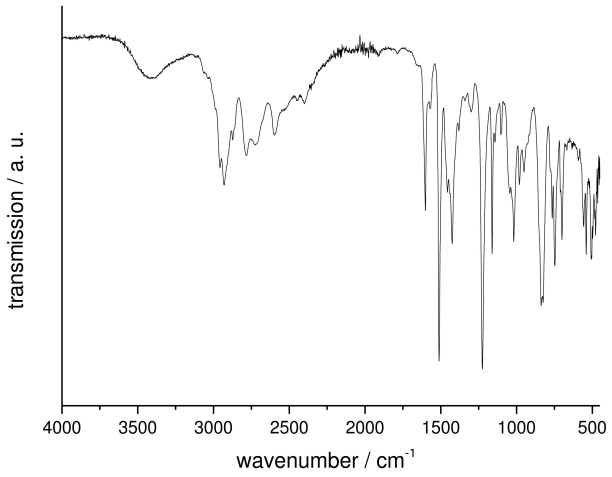
transmission / a. u.
4000
3500
3000
2500
2000
1500
1000
500
wavenumber / cm-1

SUPPORTING INFORMATION

ChemNMR ^{1}H Estimation

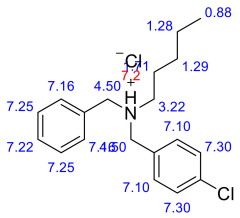

Estimation quality is indicated by color: good, medium, rough

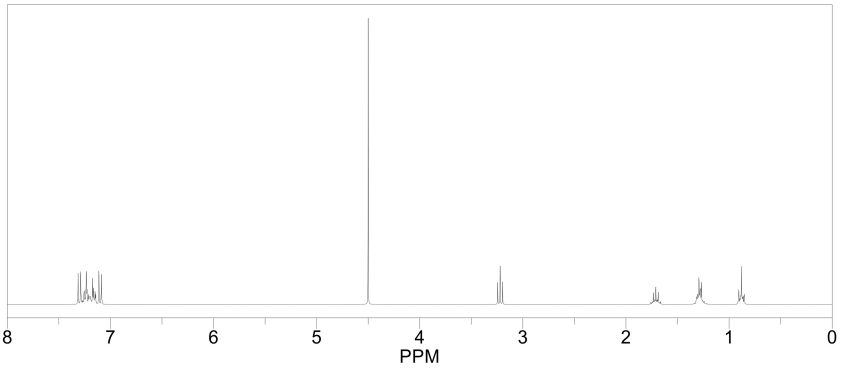

ChemNMR ^{13}C Estimation

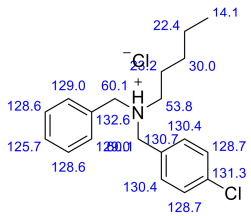

Estimation quality is indicated by color: good, medium, rough

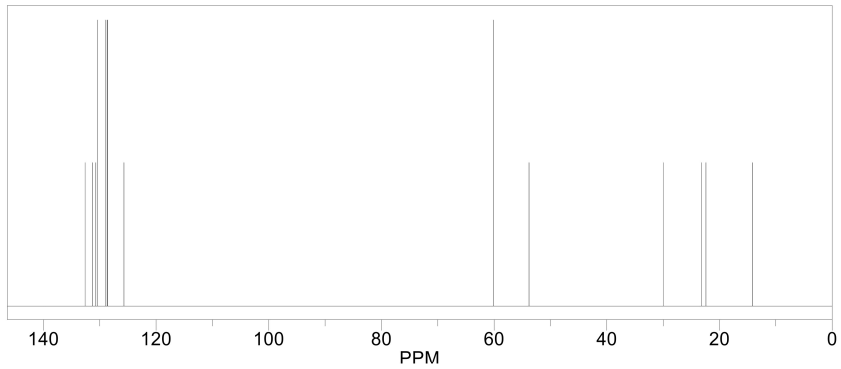

131

44:

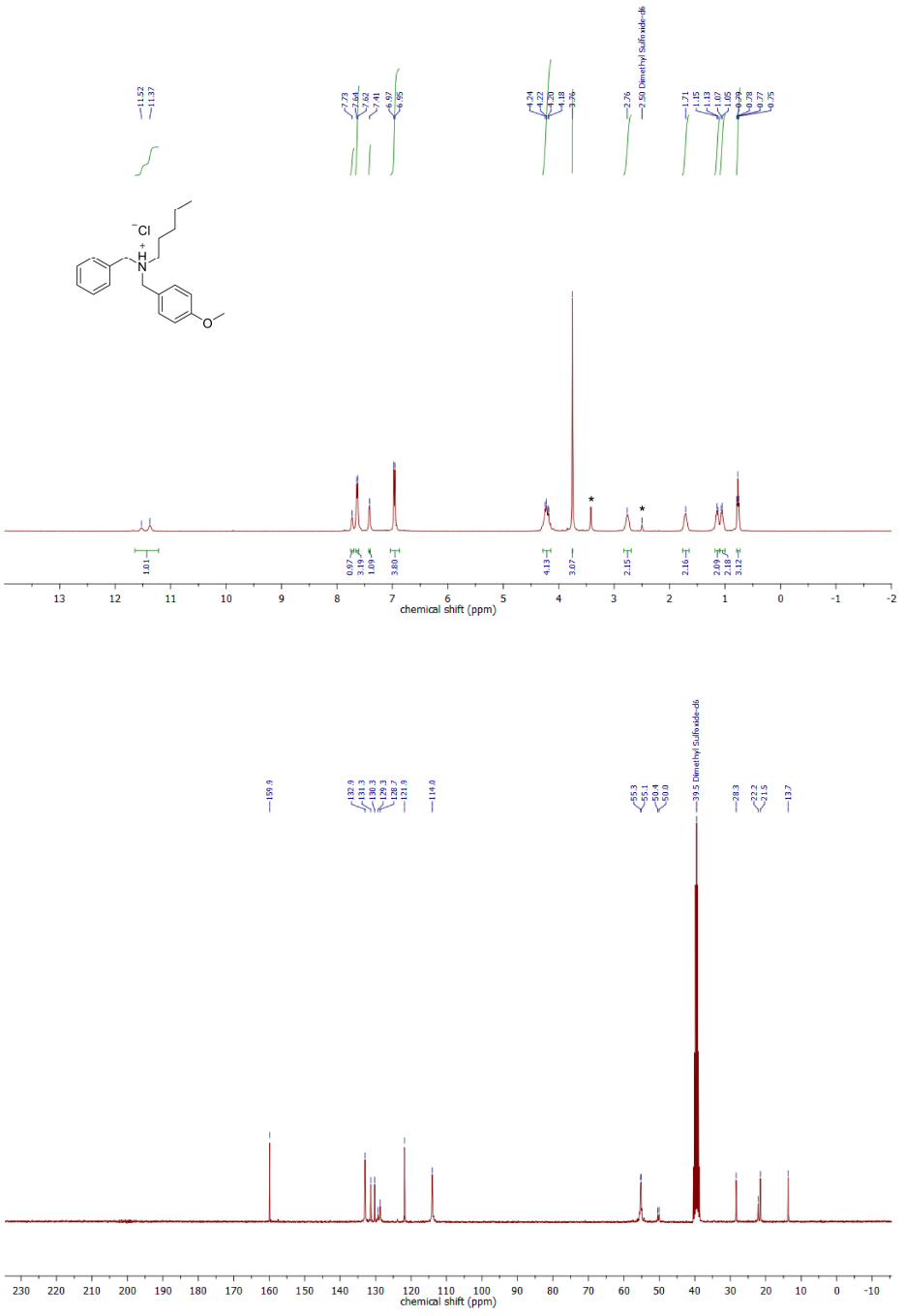

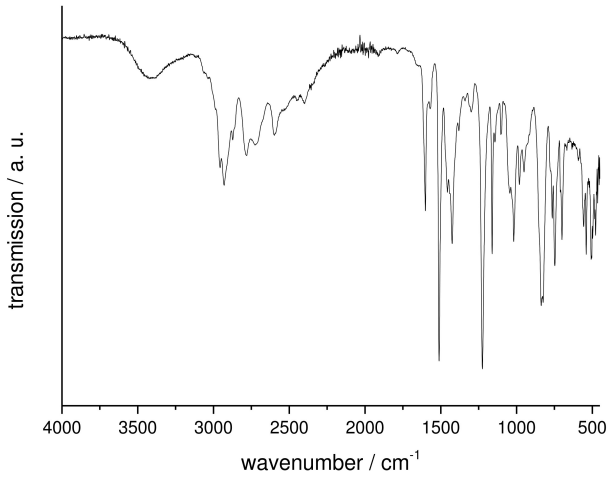
transmission / a. u.
4000
3500
3000
2500
2000
1500
1000
500
wavenumber / cm-1

SUPPORTING INFORMATION

ChemNMR ^{1}H Estimation

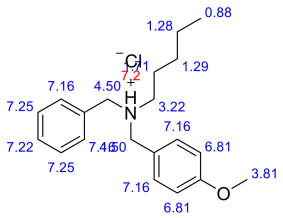

Estimation quality is indicated by color: good, medium, rough

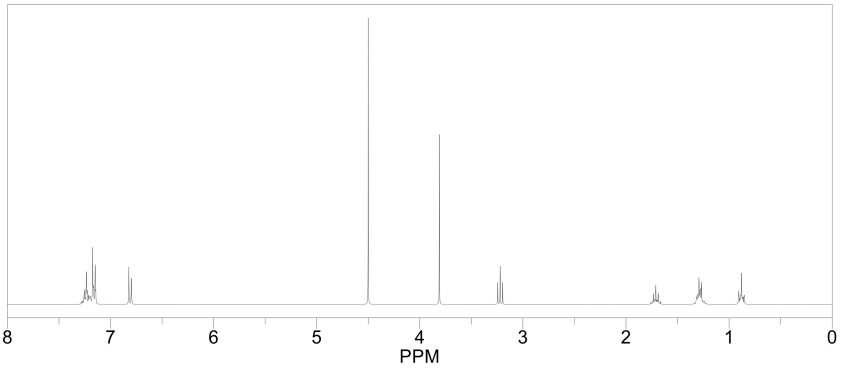

ChemNMR ^{13}C Estimation

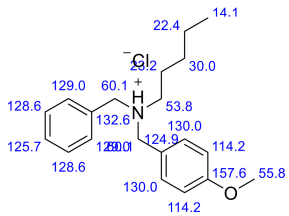

Estimation quality is indicated by color: good, medium, rough

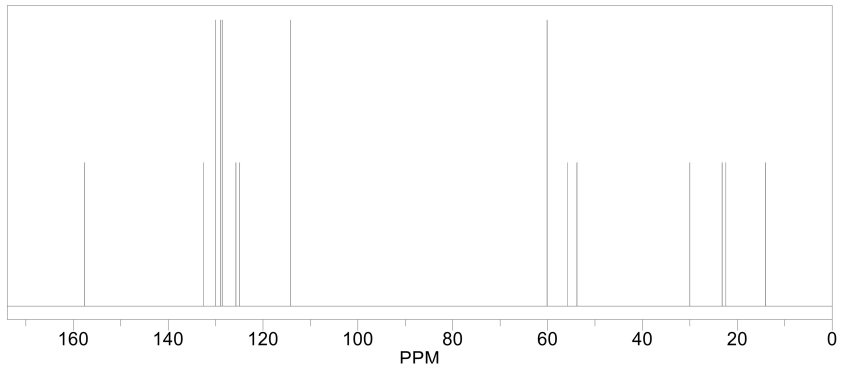

134

45:

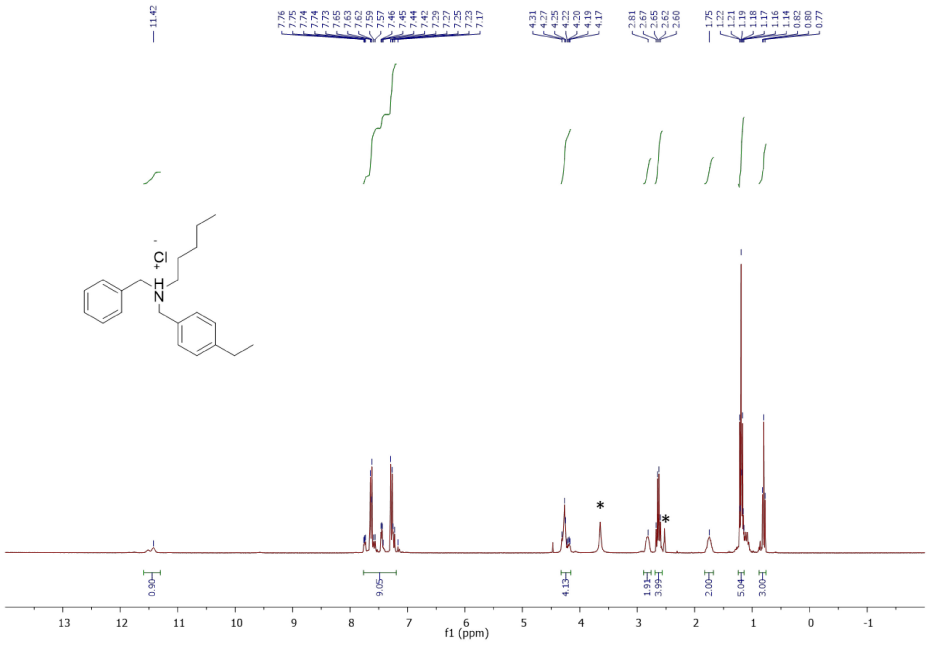
11.42
7.76
7.75
7.74
7.73
7.70
7.65
7.63
7.62
7.59
7.57
7.46
7.45
7.44
7.42
7.29
7.27
7.25
7.23
7.17
4.31
4.27
4.25
4.22
4.20
4.19
4.17
2.81
2.67
2.65
2.62
2.60
1.75
1.22
1.21
1.19
1.18
1.17
1.16
1.14
0.82
0.80
0.77
0.90
9.05
4.13
1.91
3.99
2.00
5.04
3.05
f1 (ppm)

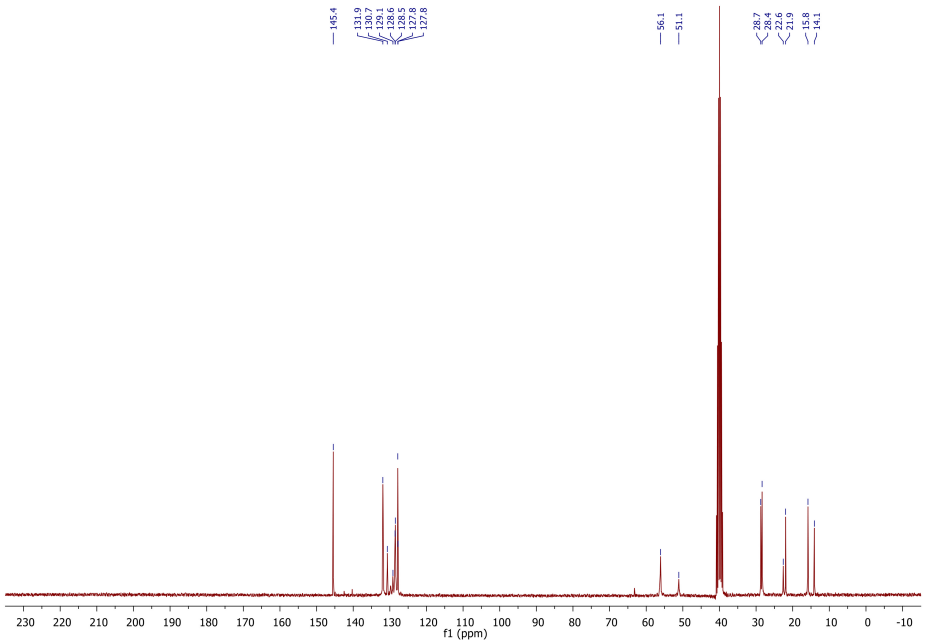
145.4
131.9
130.7
129.1
128.6
128.5
127.8
127.8
56.1
51.1
28.7
28.4
22.6
21.9
15.8
14.1
f1 (ppm)

135

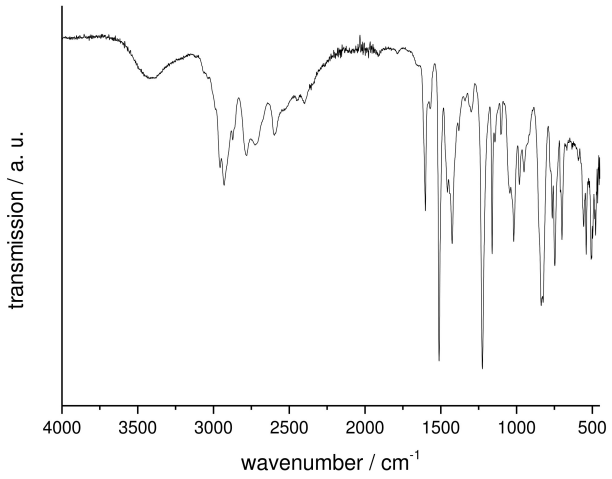
transmission / a. u.
4000
3500
3000
2500
2000
1500
1000
500
wavenumber / cm-1

SUPPORTING INFORMATION

ChemNMR ^{1}H Estimation

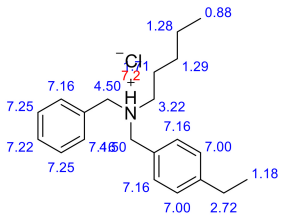

Estimation quality is indicated by color: good, medium, rough

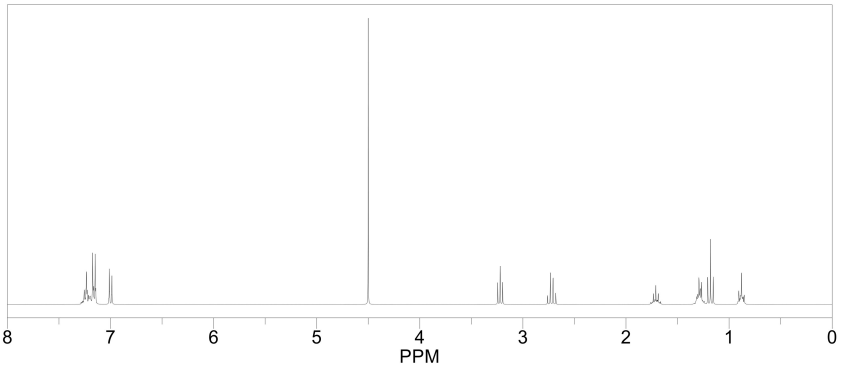

ChemNMR ^{13}C Estimation

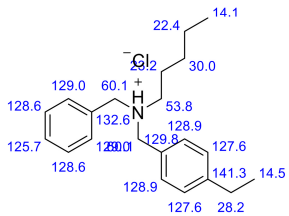

Estimation quality is indicated by color: good, medium, rough

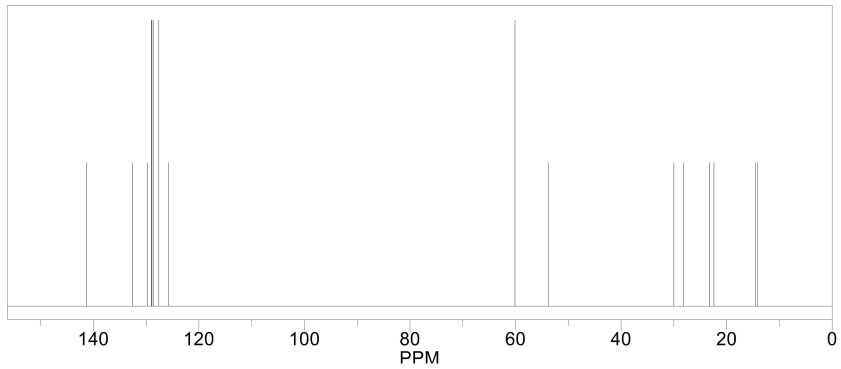

6 References

[1] J. Pantförder, S. Pöllmann, J. F. Zhu, D. Borgmann, R. Denecke, H.-P. Steinrück, *Rev. Sci. Instrum.* **2005**, *76*.

[2] A. Ermolieff, P. Bernard, S. Marthon, J. Da Camargo Costa, *J. Appl. Phys.* **1986**, *60*, 3162–3166.

[3] a) C. R. Brundle, B. V. Crist, *J. Vac. Sci. Technol.* **2020**, *38*; b) W. S. M. Werner, W. Smekal, C. J. Powell, *Simulation of electron spectra for surface analysis (SESSA) version 2.2.0 user s guide*, National Institute of Standards and Technology (U.S.), Gaithersburg, MD, **2021**.

[4] L. F. B. Ribeiro, O. Flores, P. Furtat, C. Gervais, R. Kempe, R. A. F. Machado, G. Motz, *J. Mater. Chem. A* **2017**, *5*, 720–729.

[5] C. Bäumler, C. Bauer, R. Kempe, *ChemSusChem* **2020**, *13*, 3110–3114.

[6] G. Hahn, P. Kunnas, N. de Jonge, R. Kempe, *Nat. Catal.* **2019**, *2*, 71–77.

[7] K. Murugesan, M. Beller, R. V. Jagadeesh, *Angew. Chem. Int. Ed.* **2019**, *58*, 5064–5068.

[8] K. Tokmic, B. J. Jackson, A. Salazar, T. J. Woods, A. R. Fout, *J. Am. Chem. Soc.* **2017**, *139*, 13554–13561.

[9] E. S. Reckzeh, G. Karageorgis, M. Schwalfenberg, J. Ceballos, J. Nowacki, M. C. M. Stroet, A. Binici, L. Knauer, S. Brand, A. Choidas et al., *Cell Chem. Biol.* **2019**, *26*, 1214-1228.e25.

[10] E. Rohrmann, H. A. Shonle, *J. Am. Chem. Soc.* **1944**, *66*, 1516–1520.

[11] R. V. Jagadeesh, K. Murugesan, A. S. Alshammari, H. Neumann, M.-M. Pohl, J. Radnik, M. Beller, *Science* **2017**, *358*, 326–332.

[12] M. S. Kwon, S. Kim, S. Park, W. Bosco, R. K. Chidrala, J. Park, *J. Org. Chem.* **2009**, *74*, 2877–2879.

[13] C. Wang, A. Pettman, J. Basca, J. Xiao, *Angew. Chem. Int. Ed.* **2010**, *49*, 7548–7552.

[14] S. Sato, T. Sakamoto, E. Miyazawa, Y. Kikugawa, *Tetrahedron* **2004**, *60*, 7899–7906.

[15] A. F. Abdel-Magid, K. G. Carson, B. D. Harris, C. A. Maryanoff, R. D. Shah, *J. Org. Chem.* **1996**, *61*, 3849–3862.

[16] Q. Lei, Y. Wei, D. Talwar, C. Wang, D. Xue, J. Xiao, *Chem. Eur. J.* **2013**, *19*, 4021–4029.

[17] R. Kempe, T. Schönauer, S. L. J. Thomä, L. Kaiser, M. Zobel, *Chem. Eur. J.* **2020**.

[18] S. Liang, P. Monsen, G. B. Hammond, B. Xu, *Org. Chem. Front.* **2016**, *3*, 505–509.

[19] L. Xing, C. Cheng, R. Zhu, B. Zhang, X. Wang, Y. Hu, *Tetrahedron* **2008**, *64*, 11783–11788.

[20] T. Yan, B. L. Feringa, K. Barta, *ACS Catal.* **2016**, *6*, 381–388.

[21] K. Sarkar, K. Das, A. Kundu, D. Adhikari, B. Maji, *ACS Catal.* **2021**, *11*, 2786–2794.

[22] L. H. S. Smith, T. T. Nguyen, H. F. Sneddon, D. J. Procter, *Chem. Commun.* **2011**, *47*, 10821–10823.

[23] S. Mizuta, K. Watanabe, N. Nishida, T. Hamada, T. Ishikawa, Y. Tanaka, H. Otaki, J. Yasuda, S. Urata, WO2018181892A1, **2018**.

[24] M. Ruiz‐Castañeda, A. M. Rodríguez, A. H. Aboo, B. R. Manzano, G. Espino, J. Xiao, F. A. Jalón, *Appl. Organometal. Chem.* **2020**, *34*.

[25] P. Ye, Y. Shao, X. Ye, F. Zhang, R. Li, J. Sun, B. Xu, J. Chen, *Org. Lett.* **2020**, *22*, 1306–1310.

WILEY-VCH

SUPPORTING INFORMATION

Author Contributions

Matthias Elfinger carried out the catalyst synthesis, catalytic reactions and catalyst characterization. Jörg Schmauch carried out the STEM-EELS measurements. Michael Moritz measured the XPS samples, Michael Moritz, Christian Papp and Christoph Wichmann performed XPS data analysis and evaluation. Matthias Elfinger and Rhett Kempe co-wrote the manuscript. Christof Bauer revised the manuscript and supporting information and corrected the data and carried out the necessary experiments as well as co-wrote the manuscript.

7 List of Publications

The following publications were published or are to be submitted during the work on this thesis:

1. M. Elfinger, T. Schönauer, S. L. J. Thomä, R. Stäglich, M. Drechsler, M. Zobel, J. Senker, R. Kempe, *ChemSusChem* **2021**, *14*, 2360-2366.
   "*Co-Catalyzed Synthesis of Primary Amines via Reductive Amination employing Hydrogen under very mild Conditions*"

2. M. Elfinger, M. Bergmann, R. Kempe, to be submitted.
   "*Synthesis of Secondary Amines via Borrowing Hydrogen employing a Nanostructured Bimetallic 3d-Metal Catalyst*"

3. M. Elfinger, C. Bauer, J. Schmauch, M. Moritz, C. Wichmann, C. Papp, R. Kempe, *Adv. Synth. Catal.* **2023**, *365*, 4654-4661.
   "*General Synthesis of Alkyl Amines via Borrowing Hydrogen and Reductive Amination*"

8 Acknowledgement

In the first place, I want to thank my academic supervisor,

Prof. Dr. Rhett Kempe,

for giving me the opportunity to do my PhD on this very interesting topic. I am very grateful for his confidence, which enabled me to work under great scientific freedom. Also, I would like to thank him for his constant interest in the progress of the work and for the numerous constructive scientific discussions.

I want to thank Dr. Christine Denner for the excellent supervision over the last years, the SEM and EDX measurements and for her very friendly, positive and professional support, especially during the much-needed coffee breaks.

Big thanks go to all my former and current lab-mates Timon Schönauer, Dr. Christoph Bäumler, Anna-Lena Wolff, Dr. Mara Klarner, Barbara Klausfelder, Sandra Bieger, Christof Bauer and Christoph Maier as well as the other group members Andre Dickert, Christian Heber, Fabian Lukas, Alexander Goller, Christoph Unger, Tobias Seifert, Niko Sila, Felix Leowsky-Künstler, Martin Schlagbauer, Max Leinert Johannes Porschke, Dr. Winfried Kretschmer and Dr. Torsten Irrgang for the ongoing support, coffee breaks and fruitful discussions, as well as drinking after-work beers and lots of good BBQs.
Thanks to all my students, Monika Müller, Marie Bergmann and Cedric Kraus for their support in the lab and contribution to this thesis.
A special thanks goes to Heidi Maisel, Tina Fell, Sandra Keller and Dana Dopheide for all administrative tasks and helping hands with various technical problems.

Without my circle of friends in Bayreuth, who accompanied me in numerous activities, holiday trips, honorless boozings and countless relaxed evenings - with good food, dissolvable ice tea and even better discussions - this time would not have been the same. Thank you, guys!

Finally, and above all, my greatest thanks go to my family for the never-ending support, blind trust and numerous cash injections. Without the support of my parents and grandparents this work would have never been possible.

9 (Eidesstattliche) Versicherungen und Erklärungen

(§ 8 Satz 2 Nr. 3 PromO Fakultät)

Hiermit versichere ich eidesstattlich, dass ich die Arbeit selbstständig verfasst und keine anderen als die von mir angegebenen Quellen und Hilfsmittel benutzt habe (vgl. Art. 64 Abs. 1 Satz 6 BayHSchG).

(§ 8 Satz 2 Nr. 3 PromO Fakultät)

Hiermit erkläre ich, dass ich die Dissertation nicht bereits zur Erlangung eines akademischen Grades eingereicht habe und dass ich nicht bereits diese oder eine gleichartige Doktorprüfung endgültig nicht bestanden habe.

(§ 8 Satz 2 Nr. 4 PromO Fakultät)

Hiermit erkläre ich, dass ich Hilfe von gewerblichen Promotionsberatern bzw. –vermittlern oder ähnlichen Dienstleistern weder bisher in Anspruch genommen habe noch künftig in Anspruch nehmen werde.

(§ 8 Satz 2 Nr. 7 PromO Fakultät)

Hiermit erkläre ich mein Einverständnis, dass die elektronische Fassung der Dissertation unter Wahrung meiner Urheberrechte und des Datenschutzes einer gesonderten Überprüfung unterzogen werden kann.

(§ 8 Satz 2 Nr. 8 PromO Fakultät)

Hiermit erkläre ich mein Einverständnis, dass bei Verdacht wissenschaftlichen Fehlverhaltens Ermittlungen durch universitätsinterne Organe der wissenschaftlichen Selbstkontrolle stattfinden können.

Bayreuth, 01.05.2024 ……

Ort, Datum

…….

Matthias Elfinger